IDŐJÁRÁS

QUARTERLY JOURNAL
OF THE HUNGARIAN METEOROLOGICAL SERVICE

Special Issue: Climate change and impacts from global processes to local effects

Guest Editor: **Mónika Lakatos**

CONTENTS

VOL. 120 * NO. 1 * JANUARY – MARCH 2016

IDŐJÁRÁS

Quarterly Journal of the Hungarian Meteorological Service

Editorial Office: Kitaibel P.u. 1, H-1024 Budapest, Hungary
P.O. Box 38, H-1525 Budapest, Hungary
E-mail: journal.idojaras@met.hu
Fax: (36-1) 346-4669

Indexed and abstracted in Science Citation Index Expanded™ and Journal Citation Reports/Science Edition
Covered in the abstract and citation database SCOPUS®

Subscription by mail:
IDŐJÁRÁS, P.O. Box 38, H-1525 Budapest, Hungary
E-mail: journal.idojaras@met.hu

Editorial

Special Issue: Climate change and impacts from global processes to local effects

Climate is changing and will continue to change in the future as more and more greenhouse gases are emitted to the atmosphere by human activities. The heat-trapping greenhouse gases in the atmosphere reached new record levels in 2015. Carbon dioxide crossed the barrier of 400 ppm during the northern hemisphere spring in average.

The most obvious revealing of the changes are the rising temperatures, disrupting the natural pattern of the seasons, increasing the frequency and intensity of certain extreme weather events, such as heatwaves, heavy rainfall, and droughts in many regions.

The effects of climate change are different from region to region. The climate change is expected to result in significant changes in the Carpathian Region to affect ecosystems and human activities. The 40th Meteorological Scientific Days addressed the presenting of the recent results available in research of climate change, impact, vulnerability, and adaptation in Hungary. This Special Issue of the jubilee academical event emphasizes that improved scientific research is needed to a better understanding of the human induced climate change at national and regional levels, its impacts, and solutions for adaptation.

In December 2015, the world's governments unanimously adopted the Paris Agreement, providing for rapid and deep cuts in greenhouse gas emissions. This historic agreement commits all countries to undertake ambitious efforts to respond to the urgent threat of climate change. On the chance of success I wish the readers exciting exploration of this issue.

Mónika Lakatos
Guest Editor

IDŐJÁRÁS

Quarterly Journal of the Hungarian Meteorological Service
Vol. 120, No. 1, January – March, 2016, pp. 1–40

The anthropogenic climate change hazard: role of precedents and the increasing science-policy gap[1]

Tibor Faragó

Doctoral School of Environmental Sciences, Eötvös Loránd University,
Budapest, Pázmány Péter sétány 1/A, H-1117, Hungary
E-mail: Tibor_Farago@t-online.hu

(Manuscript received in final form January 12, 2016)

Abstract—There are some parallelisms and similarities since the 1960s in the identification, attribution, scientific communication, and the subsequent initial policy setting processes of the acidification, ozone layer depletion, and climate change hazards. The anthropogenic factors behind the latter one were hypothesized well before the discovery of the cause-effect relations of the two other problems; nevertheless, later on the policy approaches to address the "acid rain" and "ozone shield" issues served to some extent as precedents for building up the international climate policy mechanisms. The analysis of these knowledge and policy development cases is of particular interest in light of the widening climate change science-policy gap, whilst efficient international policy and legal regimes have been built up for tackling the acidification and ozone depleting phenomena. Concerning the global climate policy regime, the consideration of its progress covers the time period since the early 1970s by 2015 when its most recent building block was adopted.

Key-words: acidification, ozone layer depletion, climate change, environmental precedence, science-policy gap

"*Let us suppose that the climate changes by one degree during a century, which anyway could be considered as a tremendous change, but nowadays would we be able to detect such a change?*" (*Róna*, 1909)

"*The globally averaged combined land and ocean surface temperature data as calculated by a linear trend, show a warming of 0.85 [0.65 to 1.06] °C, over the period 1880 to 2012.*" (*IPCC*, 2013–2014)

[1] This paper is the extended and updated version of the author's presentation at the Hungarian Academy of Sciences.

1. Introduction

Phases. Various factors were leading to the almost simultaneous intensification of the scientific research activities and the first general international policy reflections by the late 1970s on emerging large-scale atmospheric hazards, namely, the acidification, the ozone layer depletion, and the climate change problems. The formulation of the evidence-based hypotheses on their anthropogenic drivers, sources of the atmospheric emissions, and possible implications was relatively shortly followed by ascertaining the cause-effect relations and the adoption of increasingly rigorous international agreements only for the acidification and ozone depletion problems. It has happened differently for the climate change issue. In general, the earlier chronologies of these scientific and policy-making processes were segmented and separately analyzed from different perspectives (e.g., in the case of acidification by *Levy*, 1995; the ozone layer policy history by *Morrisette*, 1989; the development of climate change policy regime by *Gupta*, 1997 and *Bodansky*, 2001). The parallel and partially interlinked science-driven policy-making for these three atmospheric problems is studied in this paper through the following phases: (i) the "*inception phase*" by the late 1970s associated with the detection of these hazards, the scientific search for their cause-effect relations, and the initial political reactions; (ii) the verification and the "*international policy setup phase*" by about the turn of the 20th century, which is characterized by reaching much higher confidence level in the attribution of these hazardous phenomena to certain anthropogenic factors affecting the natural mechanisms and also by the development of the relevant international policy regimes; and (iii) the following "*divergent phase*", when the effective solution of the acidification and ozone layer hazards was already on track, meanwhile the science-policy gap was widening for the global climate change problem. The "inception phase" is actually coincides with the birth of a new and prosperous branch of atmospheric sciences, namely the air chemistry (*Mészáros*, 1981), which is *inter alia* dedicated to the subjects of those atmospheric processes, the interrelated science-policy aspects of which are considered in this paper. More generally, the evolution of the international environmental cooperation and the adoption of numerous multilateral agreements were closely linked to the progress in environmental science in its entirety, the "scientization" as it was called by *Brauch* and *Sprong* (2011), and to the changes on the global political scene in the second half of the 20th century (*Clark et al.*, 2001; *Faragó*, 2006).

Precedents. The policy-setting cases for acidification and ozone depletion served in some degree as precedents during the early period of the elaboration of the international mechanisms for tackling global climate change. This effect was profoundly justified because of some similarities in the socio-economic drivers, the applicability of the general principles of international environmental cooperation, the most typical response options (abatement/mitigation policies), and the specific situations of the various country groups. But, it turned out rather soon, there were considerably distinct aspects of the climate change policymaking that could not be overcome at such a pace, as it occurred for the two other environmental issues. These aspects stem from the complexity of the climate system *per se*, and also from the multiplicity, particular technology aspects, and the inertia of those economic sectors, which contribute to the escalation of this global problem. Therefore, the two above-mentioned precedential policy processes could have productive effects (directly or indirectly) only for a while on development of the international climate policy architecture. In course of time, this diversion became even more apparent as the science-policy gap was rapidly widening in terms of the improved scientific knowledge and the increasingly inadequate level of the overall climate policy responses.

The beginning. The human-induced climate change hazard was hypothesized and the acidifying air pollution problem was already noticed well before the middle of the previous century. Notably, the possibility of global warming caused by fossil fuel combustion was raised at the end of the 19th century (by *Arrhenius* in 1896 and by *Chamberlain* in 1899). Based on a limited set of surface temperature data series and information on "artificial production of carbon dioxide" from fossil fuel combustion available that time, *Callendar* (1938) asserted that global warming had begun and provided a draft assessment for its rate. In terms of the acidifying air pollutants, the harmful effects of emissions from a Canadian metal smelter on the neighboring areas of the USA can be mentioned as an early case of such a transboundary pollution. These effects were observed from the 1920s and resulted in an international conflict between the two countries. The conflict was settled by an arbitration procedure without any deep theoretical analysis of the pollution propagation, and the decision simply referred to the "injury by fumes in or to the territory of another state (..), when the case is of serious consequence and the injury is established by clear and convincing evidence" (*UN*, 2006). As a matter of fact, these environmental hazards together with the ozone layer problem became prevalent several decades later, when rapidly increasing attention was paid to them by the scientific community, their genuine mechanisms could be discovered, and the first concrete recommendations were formulated for their mitigation. That is why we focus on the parallelism and certain similarities of these scientific and policy-making processes from the mid-20th century.

Drivers. Before turning to the above-mentioned phases of detection and management of these atmospheric problems, some of those common *socio-economic drivers* are highlighted, because of which these hazards started to manifest themselves at a quick pace in the post-WW2 era, and in turn, the late 1960s and early 1970s marked the beginning of more focused scientific research nearly simultaneously in these environmental issues and the subsequent initial international political reactions. The post-war economic recovery followed by an economic boom in the OECD (formerly OEEC) countries, the rapid reconstruction and development in Eastern Europe from the 1950s, and the socio-economic changes in many developing countries went together with growing demand for natural resources and increased pollution in very diverse forms. These environmental pressures were significantly enhanced by the global population explosion and changing consumption patterns. The growth in the key economic sectors (energy, transport, agriculture, such industrial activities as metallurgy, chemical industry, etc.) was inadvertently leading to the intensification of large-scale atmospheric and other environmental problems (water pollution, loss of biological diversity, deforestation, chemical hazards, waste streams). Moreover, there are rather evident reasons that explain why these three atmospheric hazards were drawing increased attention with almost the same time lag, namely, the time period needed by these accumulating environmental pressures for exceeding some critical thresholds. Of course, other factors were also essential in this regard, like the fast development of environmental monitoring technics, systems and networks, methodologies, numerical models, and the international scientific cooperation.

2. Simultaneous knowledge development on emerging atmospheric hazards and the initial policy reactions

"The combustion of coal, oil, and gas (..) results in the discharge into the air of sulphur dioxide, carbon dioxide, carbon monoxide, oxides of nitrogen (..) Little is known, e.g., of what happens to our most common pollutant, SO_2, once it has been discharged into the atmosphere." (*PSAC*, 1965)

"It is recommended that in establishing standards for pollutants of international significance, Governments take into account the relevant standards proposed by competent international organizations (..) in planning and carrying out control programmes for pollutants distributed beyond the national jurisdiction." (*UNCHE*, 1972)

The massive atmospheric emission of disparate pollutants from human activities since the mid-20th century have triggered the increased interest of the research community to see whether these environmental pressures would lead to extensive adverse effects. Besides revitalizing some earlier conceptions or developing new ones in this regard, it was clear that first of all, sound environmental observations were necessary for reliable scientific investigations and conclusions. The International Geophysical Year (IGY) in 1957–58 offered a good opportunity to launch regular and internationally standardized environmental measurements. The data series from these measurements, the assessments of sources and volumes of airborne emissions, and the clarification of the relevant biogeochemical cycles greatly contributed to knowledge development concerning climate change, acidification, and ozone layer depletion by the late 1970s (i.e., during the above mentioned "inception phase"). As a consequence, these and some other emerging environmental hazards were acknowledged by policymakers, and the initial coordinated responses were agreed upon at their international meetings in 1972 (Stockholm) and 1975 (Helsinki). In this context, the atmosphere plays a particularly important role: "air pollutants move quickly and cover greater distances than do pollutants in watercourses or the marine environment. The atmosphere is in fact the planet's largest single shared resource" (*Kiss* and *Shelton*, 2007).

2.1. Systematic observations and initial findings

Observing atmospheric CO_2 changes. The hypothesis on the possibility of human-induced climate change could be better tested from the mid-20th century, when the after-war economy boost and industrial development resulted *inter alia* in rapidly growing fossil fuel based energy production. *Revelle* and *Suess* (1957) described it as a dangerous process and insisted on having more precise measurements and assessments: "Present data on the total amount of CO_2 in the atmosphere, on the rates and mechanisms of CO_2 exchange between the sea and the air (..) are insufficient to give an accurate base line for measurement of future changes in atmospheric CO_2. An opportunity exists during the International Geophysical Year to obtain much of the necessary information." As a follow-up, the rate of increase of the anthropogenic CO_2 emissions and atmospheric concentrations was re-assessed in 1958 (*Callendar*, 1958; *Bolin* and *Eriksson*, 1958), and accurate measurements of the atmospheric CO_2 started at the Mauna Loa Observatory in the same year. It was confirmed soon that this value had annually a "small but persistent increase" (*Keeling*, 1960). Based on that discovery, the USA President's Scientific Advisory Committee formulated its opinion that the changing chemical composition of the atmosphere *may* lead to a significant change of the climate already by the end of that century (*PSAC*, 1965).

Concerns about the SO_2 releases. The same period of time marked the increased attention to man-made atmospheric discharges of various pollutants, their transport and deposition, with a particular focus on the sulfur cycle (*Eriksson*, 1963). Similarly to the case of the carbon-dioxide, it became evident that for the sake of more accurate assessments, first of all systematic monitoring was necessary. The European Air Chemistry Network (EACN) was established in the middle of 1950s and substantially extended during the IGY. This issue was also raised on the other side of the Atlantic (*PSAC*, 1965): "The combustion of coal, oil, and gas in our homes, vehicles, and factories results in the discharge into the air of sulphur dioxide, carbon dioxide, carbon monoxide, oxides of nitrogen, and partially burned hydrocarbons. (..) Many of these pollutants released unintentionally or as a by-product are long-lasting, come from a multitude of sources, and are subject to transportation over great distances in air, water, or living organisms. All three characteristics make them very difficult to control. (..) The problem of air pollution calls for much research."

Systematic observations of O_3. It is noteworthy that the Global Ozone Observing System also started its operation in 1957 in the framework of the IGY (*WMO*, 2014). Initially it was based on an existing international monitoring network; afterwards, it was gradually extended, internationally standardized, and two decades later complemented with satellite measurements. Initially, the measurements were made from the ground, however, their series did not show any considerable trends by the 1970s.

2.2. Evidence-based identification of cause-effect relations

CO_2 emissions. The growing observational network, the Global Atmospheric Research Programme (GARP) from 1967, and the first simple global climate models (developed by *Manabe* and *Wetherald* in 1967, by *Budyko* in 1969, and by *Sellers* also in 1969) provided more information on the global climate system. It made possible better (conditional) assessments of the potential consequences of the steadily increasing CO_2 releases from fossil fuel combustion together with other greenhouse gas emissions. These developments were reflected in the scientific communication already in the early 1970s. According to *Keeling* (1970), the increasing human population in the 21th century "along with their other troubles, may also face the threat of climatic change brought about by an uncontrolled increase in atmospheric CO_2 from fossil fuels." *Bolin* and *Bischof* (1970) have derived estimates of the atmospheric CO_2 for the forthcoming decades by accepting certain assumptions, for instance on further rates of global fossil fuel combustion. It is remarkable that their estimate was 371–378 ppm for the year 2000, which proved to be very close to the factual value of 370 ppm obtained at Mauna Loa Observatory as the annual average for 2000 with its peak monthly value of 372 ppm in May that year.

SO_2 emissions. Those years became also memorable for understanding the transboundary "sulfur problem". The evidence-based hypothesis on the long-range transmission of airborne acidifying pollutants was raised by *Odén* (1968) by studying the series of precipitation chemistry measurements from the EACN. Systematic analyses by a couple of North-European researchers (supported by the Scandinavian Council for Applied Research) offered more arguments on this matter and resulted in setting up the international Cooperative Technical Programme to Measure the Long Range Transport of Air Pollutants by the OECD in April 1972 (*OECD*, 1977). These efforts were assisted by the establishment of the Background Air Pollution Monitoring System (BAPMoN) in 1970 and by a multi-annual programme on the Biogeochemical Cycles under the aegis of the Scientific Committee on Problems of the Environment (SCOPE) of the ICSU (*Svensson* and *Soderlund*, 1976). The tentative observational data and analytic studies confirmed the assumption on the long-range transport of those pollutants. Similarly to the CO_2 releases, the increasing fossil fuel combustion was primarily "blamed" for these emissions and their harmful

effects on ecosystems. Based on these studies, the Swedish experts decided to present this issue as a case study to the UN Conference on Human Environment to be held in June 1972 (*Bolin et al.,* 1971, 1972). Because of substantial scientific uncertainties and other reasons, representatives of a few key Western European emitters strongly denied the idea of the long-range atmospheric transmission of these pollutants (i.e., the possibility that pollutants from their sources can reach Scandinavian regions).

CFC emissions. The potentially harmful human effects on the stratospheric ozone layer have also piqued the interest of the research community just in the same time period. This quasi-coincidence was obviously triggered by the socio-economic drivers mentioned above (economic growth, technological progress, new production and consumption patterns, etc.). The recognition of the possibility of endangering the ozone layer did not stem from actual observations, but from theoretical studies. In the early 1970s, two specific human activities were identified as those, which can directly interfere with natural factors in controlling the ozone content in the lower stratosphere. *Crutzen* (1970) revealed that the nitrogen oxides emitted from the surface may influence the ozone photochemistry in the stratosphere, but the sources of these nitrous oxides remained unclear, that is, where those originate from (in respective volumes) and how they reach high-level altitudes. In retrospect, it seems so evident that the stratospheric supersonic transport aircrafts (SST) were named as important anthropogenic causes of this problem, since they directly released nitrogen oxides up there (*Johnston*, 1971). One year later it turned out that the NASA's space shuttle operations using solid rocket boosters of the Space Transportation Systems (STS) caused high amount of hydrogen chloride emissions in the stratosphere that might also contribute to the ozone destruction (*Stolarski* and *Cicerone*, 1974). Assumptions on the SST and STS as the main dangers for the ozone layer did not prove valid (the overall amounts of these emissions could not explain an extensive ozone depletion); nevertheless, those ideas were catalyzing very intense scientific research in this area. The attention was turned to the halocarbons when their very stable chemical property, persistence, and accumulation in the atmosphere was discovered (*Lovelock et al.*, 1973). The invention of chloroflourocarbons resulted in a breakthrough, *inter alia*, in the refrigerator industry and a boost of the production of these halocarbons from the 1950s. It was a crucial milestone in the scientific recognition, when *Molina* and *Rowland* (1974) demonstrated that these synthetic chemical compounds (notably, $CFCl_3$ and CF_2CL_2, i.e., CFC-11 and CFC-12) are responsible for the increasing volumes of chlorine in the stratosphere and in turn, for the ozone depletion. They also had a clear argument for the still missing detection of the "thinning" of the ozone layer by these halocarbons: it could not be "immediately felt after their introduction at ground level because of the delay required for upward diffusion up to and above 25 km."

2.3. *First international policy reactions*

Other preconditions. Therefore, the period of the late 1960s and early 1970s was crucial in the identification of the human causes for all the three large-scale atmospheric hazards, as it was indicated above together with demonstrating some common factors behind these processes and the parallelism of these discoveries. In spite of the considerable scientific uncertainties, the first general policy responses were already agreed upon internationally during those years. Besides the strengthened environmental observing systems and the increased concerns of the scientific community over the rapidly growing environmental pressures from different human activities, there was another important precondition for that progress, notably, the favourable geopolitical situation or more specifically, the global political atmosphere of the *détente* (*Clark et al.*, 2001; *Faragó*, 2006). This condition was essential in general for the initiation of international deliberations on the increasing environmental risks and eventually, for achieving consensus on the basic principles of cooperation and the initial concerted actions. The general tone was set by a UN resolution (*UNGA*, 1968), according to which: the General Assembly decided to convene the United Nations Conference on the Human Environment (UNCHE) in 1972, in particular because of "the continuing and accelerating impairment of the quality of the human environment caused by such factors as air and water pollution (..), which are accentuated by rapidly increasing population and accelerating urbanization". Among the various intensifying environmental problems (including those associated with the extraction of natural resources, chemical pollution, etc.), special attention was paid to the atmosphere-related ones, since primarily these could induce dangerous large-scale transboundary or even global ecological and socio-economic impacts.

UNCHE outcomes. Because of conflicting political and economic interests of various country groups (in Europe and also between the developed and developing countries) and the still rather limited scientific knowledge on the environmental issues concerned, the preparation of the UNCHE and its outcome documents was exceptionally complicated (*Engfeldt*, 2009). Eventually, that event could be considered as the first historical milestone in global environmental cooperation. The most important provisions of the adopted documents in relation to the subject of this study clearly demonstrate that the initial international political reflections were quite similar and rather cautious in terms of the anthropogenic factors of these large-scale atmospheric hazards (*UNCHE*, 1972). First of all, it was agreed that the relevant *monitoring systems* should be further developed, notably by setting up a global network of stations "for monitoring properties and constituents of the atmosphere on a regional basis and especially changes in the distribution and concentration of contaminants" (recommendation 79/b), and more specifically, by properly monitoring the environmental effects of energy use and production, including "the environmental levels resulting from emission of carbon dioxide, sulphur dioxide, oxidants, nitrogen oxides (NO_x), heat and particulates, as well as those from releases of oil and radioactivity" (r. 57/a). (The "oxidants" in this listing, supposedly was an implicit compromise wording already referring to ozone.) Reference was also made to the importance of the internationally coordinated *research programmes* to learn more on the causes and the possible impacts of air pollution and climate change (r. 57/b, r. 79/d) and to understand better "the causes of climatic changes whether these causes are natural or the result of man's activities" (r. 79/d). Beyond that, the very general principles and objectives were also agreed on the *mitigation policies*, which aim "to minimize the release to the environment of toxic or dangerous substances" (r. 71), to plan and carry out "control programmes for pollutants distributed beyond the national jurisdiction" (r. 72), and to bear "the responsibility to ensure that activities within their jurisdiction or control do not cause damage to the environment of other States or of areas beyond the limits of national jurisdiction" (principle 21). The adoption of the recommendations and principles by the conference can be considered as the beginning of the modern era of international environmental cooperation marked by strengthened science-policy links and numerous multilateral agreements: "The Stockholm Conference had immense value in drawing attention to the problem of environmental deterioration and methods to prevent or remedy it. The Conference was global both in its planetary conception of the environment, and in its view of institutional structures and world policies." (*Kiss* and *Sheltin*, 2007)

Sceptics. The histories of the three atmospheric topics considered here had also something else in common in those years, namely, the appearance of *counter-positions and sceptical views* by rejecting with counter-arguments or by simply denying the possibility of significant human influence on the natural processes in question. In general, scepticism in natural science is an important methodological approach; however, in these cases besides questioning the validity of the attribution of these hazards at least partially to some human activities and referring to differing scientific arguments, the denial of the hypotheses was sometimes seemingly backed by particular economic interests. For the acidification and ozone depletion problems, such a reminder might be pertinent in view of the recurrent debates on degrees of certainty and confidence in the context of anthropogenic climate change and the justification of the precautionary approach in policymaking. When in the early 1970s the hypothesis on the transboundary air pollution causing acidification in the North European countries was reaffirmed by Scandinavian experts, the possibility of such long-range transport was refused by many West European representatives, as recollected by *Seip* (2001): "British and Norwegian authorities came in conflict on the acid rain issue particularly since Great Britain was the largest contributor of acidifying deposition in Norway". Even after that the above-referred OECD project resulted in convincing observational information on this issue and the need for international regulation was raised in 1978, the initiative to draw up a convention on the reduction of sulphur dioxide emissions was "battered by delegations of the EEC countries, especially by France, the United Kingdom and the Federal Republic of Germany. In the course of the discussion, the United Kingdom's delegation expressed unequivocal doubt about the validity of the hypothesis of the transboundary character of acid rain" (*UNECE*, 2004b). Similarly, in the early 1970s, there were strong opponents of the SST and STS theories either by raising clear-cut and correct scientific thoughts (e.g., about negligible amounts of NOx emissions by SST and STS) or clearly representing some economic interests (in connection to the supersonic transport airplanes by the "Brussels Group" as documented by *Engfeldt*, 2009 and *Hamer*, 2002). After 1974, the scientifically much more established discovery of the ozone-depleting potential of CFCs was heavily challenged by the concerned industry groups: "both manufacturers and users of CFCs opposed any effort to regulate CFCs in aerosol spray cans. They questioned the validity of the theory, pointing out the uncertainties and noting the lack of supporting evidence" (*Morrisette*, 1989). Concerning the global climate change hazard, in the 1960s and early 1970s, both the theories on forthcoming global cooling (the beginning of a new glacial period) and on human induced global warming were promoted and communicated in parallel. This course has changed considerably when the scientific assumptions, evidences, and results were critically assessed in 1979 by the (first) World Climate Conference and by the Ad Hoc Study Group on Carbon Dioxide and Climate in the USA. The declaration of the Conference (*WMO*, 1979) and the report of the Group (*Charney et al.*, 1979) already focused on the global warming scenarios caused by increasing atmospheric CO_2 amounts from fossil fuel combustion, deforestation, and land use change. The "sceptical era" was generally overcome by about the late 1980s for the acidification and ozone depletion problems, but it has been prolonged for the climate change hazard for some understandable reasons.

The Helsinki process. The focus on the environmental problems was strengthened in the broad context of international cooperation and security. Formally, the Helsinki process leading to the 1975 Conference on Security and Co-Operation in Europe (CSCE) was a pan-European initiative yet of global significance. The negotiations have culminated in the adoption of the Final Act in 1975, which incorporated a chapter dedicated to the enhancement of environmental cooperation. This chapter of the document was not only reconfirming the most essential provisions of the UNCHE (e.g., the responsibility for transboundary and global environmental degradation, importance of preventive measures for the avoidance of environmental damages, development of environmental monitoring networks), but it stated more concretely the necessary steps regarding the acidification and the climate change problems. Obviously, the more definite formulation was made possible by the specific regional dimension of the CSCE (devoted to the East-West relations and the pan-European cooperation). In terms of these two atmospheric issues, there were already affirmative references to the *transboundary pollution* and to the *anthropogenic factors* (as compared to the "cautious" recommendations by the UNCHE). Accordingly, the participating States agreed (i) to develop an international programme for the monitoring and evaluation of the long-range transport of air pollutants, starting with sulphur dioxide and with possible extension to other pollutants; for the "desulphurization of fossil fuels and exhaust gases, pollution control of heavy metals, particles, aerosols, nitrogen oxides, in particular those emitted by transport, power stations, and other industrial plants; systems and methods of observation and control of air pollution and its effects, including long-range transport of air pollutants" and also (ii) to study the changes in climate "under the impact of both natural factors and human activities" (*CSCE*, 1975). The ozone layer issue also became a delicate topic during the preparations for the CSCE, as the discovery of the ozone-destroying effect of the CFCs was published in June 1974 (*Molina* and *Rowland*, 1974), and already in December that year, the U.S. House of Representatives held a hearing on this matter. Presumably, the U.S. representatives raised this theme during the international expert meeting in Oslo in December 1974 (*US-DoS*, 1974), where the proposals for the environmental chapter were discussed for the CSCE.

Consequently, in the late 1960s and early 1970s besides some other environmental problems, not only the scientific awareness and communication were significantly strengthening more or less simultaneously for the three rapidly emerging atmospheric hazards, but already these issues were addressed internationally by the policymakers. These *initial policy recommendations* agreed upon at the high-level meetings in 1972 and 1975 concentrated on the development of the environmental monitoring systems and the promotion of the international research cooperation in these areas in order to better understand the processes, their natural and anthropogenic drivers, the potential adverse impacts. Moreover, the general need for controlling the emissions of the relevant pollutants was also indicated but without any concreteness and targets. Already a few years later, the specific policy-planning started and some very concrete first measures were taken: a World Plan of Action on the Ozone Layer was adopted in 1977 by the UNEP; between 1977 and 1979 the non-essential use of CFCs were banned in the USA, Canada, Norway, and Sweden; the negotiations on controlling transboundary air pollution began at the end of 1978 under the UNECE auspices; and some policy-related aspects were already raised in connection with different climate change scenarios at a conference held in 1978 at IIASA.

3. Setting up the international response policy regimes

(On the policy regime of the 1979 Convention on Long-Range Transboundary Air Pollution:) "As a precedent, the regime has contributed to the adoption of global treaties and rules on air pollution." (*Byrne*, 2015)

"The Montreal Protocol (..) offers the precedent of international negotiation and agreement on global environmental problems." (*Morrisette*, 1989)

From the late 1970s, the research activities were intensified, the cause-effect relations were much better identified, the basic international mechanisms and response policies were formulated and gradually advanced for all the three large-scale atmospheric issues. The international policy framework established for the acidification and ozone layer problems served to some extent as precedents for the climate change negotiations. In the following, several key precedential components of both the pan-European acid rain policy regime and the global policy architecture for the ozone layer problem are highlighted; then the analogous features and building blocks of the international climate change policy settings are presented in order to demonstrate (*mutatis mutandis*) the "re-use" of the previously agreed and proved procedures.

3.1. Precedent-setting regional agreements to combat transboundary acidifying pollution

Reaffirming the acidification hazard. The long-range transport of the acidifying pollutants was profoundly ascertained in the late 1970s as much more observational data and improved numeric models became available. In this regard, the European Monitoring and Evaluation Programme (EMEP) played an important role owing to the systematic collection and provision of standardized atmospheric chemistry data from 1977 onward. The "acid rain" problem started to receive higher political attention internationally when the report of the above mentioned OECD programme was published in 1977 with the following conclusions (*OECD*, 1977): "Man-made emissions of sulphur dioxide in Europe are derived mainly from combustion of sulphur-containing coal and fuel oil. (..) The programme has confirmed that sulphur compounds do travel long distances (..) in the atmosphere and has shown that the air quality in any one European country is measurably affected by emissions from other European countries." This was an important catalyst to the international policy negotiations, but the real push for general acceptance of the need for urgent abatement measures was that when the long-range atmospheric transport of pollutants and the acid rains generated by them were made responsible for the extensive forest degradation in Germany (*Hinrichsen*, 1983). *Ulrich* (1983) categorically stated that the "emissions of strong acid formers like SO_2 and NO_x leads to the poisoning of the ecosphere (..) The only environmental factor for forest which has been changed is the 'chemical climate' by air pollution. There is therefore no doubt that this change is the driving force for a development in the ecosphere which is characterized not only by tree and forest die-back, but also by the acidification of waters and by disappearance of species at an increasing rate. The data about load, carrying capacity and visible damage are more than enough to claim a rapid and considerable reduction of air pollution to avoid a possible ecological catastrophe". It was followed by a significant expansion of the atmospheric chemistry observational network, refined assessments of sulphur emissions from different sources, and further development of the transport models, which altogether produced much clearer information on the widespread scale of this pollution problem, and on its anthropogenic factors (*Mylona*, 1993). The stages of science development and its influence on strengthening the acid rain policy regime are presented in detail by *Levy* (1995), *Menz* and *Seip* (2004), and also in the analytic review of the 25 years of the Convention on Long-range Transboundary Air Pollution (*UNECE*, 2004b). These studies demonstrated that the international policy-making from the 1980s closely followed and adequately reflected the advancement of "acidification science" with the adoption of increasingly ambitious targets and emissions reduction commitments for all relevant pollutants in order to minimize their harmful effects.

The acid rain policy regime. The Helsinki conference (1975) and the conclusion of the OECD programme on the Long Range Transport of Air Pollutants (*OECD*, 1977) were followed by launching in 1978 the negotiations on a pan-European agreement on transboundary pollution. Both the basic scientific and political prerequisites existed for that motion. As regards the latter, the visit of G. H. Brundtland, the Norwegian prime-minister to Moscow in 1978 and the bilateral consent on the importance of this matter proved to be one of the most significant political factors for the start of the multilateral negotiations. Eventually, the Convention on Long-Range Transboundary Air Pollution (CLRTAP) was adopted in Geneva in November 1979 and afterwards, in the succeeding two decades, it was complemented with a series of protocols on monitoring, on abatement of sulfur and nitrogen emissions, and on reduction of the adverse impacts. The *international acid rain policy regime* comprises of the provisions of this set of legal instruments, the agreed targets and policies together with the means of implementation introduced by a series of the Parties' decisions. We restrict our focus to the acidifying air pollutants (AAPs), however, from the early 1990s, this pan-European cooperation was broadened to cope more generally with transboundary air pollution, including abatement policies for VOCs, heavy metals, and POPs, and taking into account the harmful "multi-effects" of all these pollutants.

The framework agreement. The 1979 convention was a *framework type legal instrument*, as it was only demonstrating the general political consensus on the environmental risk caused by air-borne pollutants, however, without determining any particular obligations for the Parties on controlling the emissions of the AAPs. One reason for that was the still considerable level of uncertainties, so that implicitly, a precautionary approach was adopted by "recognizing the existence of *possible* adverse effects, in the short and long term, of air pollution including transboundary air pollution" (*UNECE*, 1979). Thanks to rapid verification of the transboundary movement of these pollutants and their adverse impacts, the precautionary approach was soon replaced by very concrete preventive measures in the first sulphur protocol in 1985, as the Parties already expressed their concern "that the present emissions of air pollutants *are causing* widespread damage" (*UNECE*, 2004a). Afterwards, more stringent legally binding emission reduction obligations were included in a series of subsequent protocols. It has meant a *stepwise or gradual strengthening* of the targets and obligations, which ultimately resulted in the very effective management of this environmental problem.

Quantified emissions control commitments were formulated by means of defining the reference levels (base years) and the limitation or reduction targets (*UNECE*, 2004a): in 1985 the 30% emission reduction for sulphur by 1993 compared to its 1980 level; in 1988 the stabilization of the NOx emissions or transboundary fluxes generally by 1994 at the level of 1987; more ambitious reduction levels in the second sulphur protocol in 1994. Eventually, the 1999 Gothenburg protocol took into account the combined adverse effects and set even more stringent reduction targets for all relevant pollutants: 65% for SO_2, 44% for NOx, 17% for NH_3 by 2010 below their 1990 emission levels. (This protocol was further amended later.)

Some differentiation was demanded by the countries as the required level of emissions reduction was gradually raised, so that the countries' different situations could be acknowledged in relation to: the responsibility for and contribution to this common environmental problem; the adverse effects; the abatement costs; and/or their capabilities to control these emissions. Such a differentiation of the commitments was introduced on a *country-by-country basis* when more ambitious reduction targets for sulphur were agreed in 1994, and also when the comprehensive "multi-pollutant and multi-effect" protocol was adopted in 1999 (*UNECE*, 2004a). According to this last protocol, country-specific reduction commitments were set for sulphur, nitrogen oxides, and ammonia (and also for VOCs).

Joint implementation was permitted by the 1994 protocol, according to which two or more Parties could jointly fulfil their emissions reduction commitments (if it seemed to lead to cost savings). As a matter of fact, the use of this option would actually mean *emission trading* between the Parties in such a way that the "host Party" undertake additional reductions to be accounted for the "donor Party", which pays for those "transferred" emission units, but not directly for any project resulting in those extra emission reductions. In reality, this instrument was never used, as the Parties could not agree on the specific conditions and rules of its application.

The active science-policy interaction was essential for the development of proper policies and mechanisms in this international cooperation. A close relation was established between the convention-related organs (primarily, the main governing organization, i.e., the Executive Body) and those international institutions (the Steering Body of the EMEP, Meteorological Synthetizing Centres), which regularly delivered information to the negotiators on the new observational and research results. Moreover, the Parties set up their own permanent working groups with the mandate to evaluate the scientific and technological developments, and if necessary, to recommend additional measures (Working Groups on Strategies, on Effects and on Abatement Techniques).

Enforcement. At last, we refer to the *compliance mechanism* that included procedures and institutional arrangements (Implementation Committee), which were adopted within the 1994 and 1999 protocols and aimed at reviewing the fulfilment of commitments and supporting the Parties to comply with them. It was a soft enforcement instrument, as the emphasis was on providing assistance to the Parties concerned, and actually, no sanctions could be proposed at all against a Party, which was found in non-compliance even with the emissions control obligations under the CLRTAP and its protocols.

3.2. The ozone layer policy regime as a global precedent for the climate policy mechanisms

Ozone science development. Contrary to the acidification problem, the scientific recognition of the ozone layer depletion hazard did not start with the actual observation of this dangerous phenomenon, but with the scientific cogitation in early 1970s about those substances, their anthropogenic sources and chemical reactions which could influence the stratospheric ozone. The potential risk of modification of the ozone layer by human activities was reconfirmed by reports (published by WMO, UNEP, U.S. NAS), which summarized the growing body of scientific results on this matter, and starting from 1977, these triggered the decisions to ban or at least to reduce the "non-essential use" of the CFCs in some countries. The UNEP undertook the international coordination from 1977 based on the "World Plan of Action for the Ozone Layer", and in 1981, the decision was made to begin drafting a global convention to protect the ozone layer (*Morrisette*, 1989). Understandably, concrete commitments could be adopted only after 1984, when the stratospheric ozone hole above the Antarctica was discovered and the assumptions on the role of CFCs in the ozone destruction were confirmed (*Farman et al.*, 1985). The thorough analysis of various ozone depleting substances (ODS), their chemical mechanisms, varying status of the ozone layer, and the adverse impacts of its depletion, as well as, the technological search for the "ozone friendly" chemical compounds were leading to gradual strengthening of international policy responses. Below, we turn only to some of those key elements of this international policy regime, which directly or indirectly served as precedents for the climate policy negotiations and their outcomes. A few of these elements somehow replicate those instruments at global level which were developed for the pan-European acid rain policy regime, whilst others were specifically introduced, for instance, to facilitate effective participation of the developing countries in the common endeavour to cope with this global hazard.

The gradual approach to the ozone layer depletion problem was similar to that for the acidification, namely this global issue was also addressed by the international community in a stepwise manner starting with a *framework type convention* (*UNEP*, 1985), which was followed by a protocol (*UNEP*, 1987) and a series a subsequent amendments and adjustments. Extension of the list of the controlled substances and setting new reduction targets occurred due to advancement in ozone science and technology (development of the substituting chemical compounds). The 1985 Convention emphasized only the importance of the *precautionary measures* and accordingly did not include any concrete immediate quantified objectives, but contained only a future oriented provision: "The Parties shall take appropriate measures (..) to protect human health and the environment against adverse effects *resulting or likely to result* from human activities which *modify or are likely to modify* the ozone layer" and named those hazardous substances which at that stage were "thought to have the potential to modify the chemical and physical properties of the ozone layer". As the discovery of the ozone hole was communicated shortly after concluding the convention, the negotiations were speeded up, and the 1987 Montreal Protocol (MP) already determined quantified reduction targets for the production of some ODS. The subsequent amendments and adjustments (*UNEP*, 2012) substantially extended the list of controlled substances and set more stringent reduction obligations for the Parties.

The basic commitments were formulated as required *quantified reduction rates* to be reached by some deadlines compared to a reference level (1986). In the 1987 Montreal Protocol, the longest term target was defined for 1999 and it aimed at a 50% reduction for the most "prominent" substances (five types of CFCs) by that year and beyond. For other substances (halons), a *stabilization obligation* was accepted, namely, the requirement that their national production volume should not exceed the reference level. In response to the increasing awareness of the ozone layer thinning danger and the ozone depleting potential of those substances, already in 1990, the deadlines for the 50% reduction target were moved backward to 1995, and it was agreed to fully phase-out the use of these synthetic chemical compounds from 2000. The further amendments and adjustments by 1999 did not only extend the lists of the substances, tightened the deadlines, and increased the reduction rates (ultimately referring to a consumption and production level that "does not exceed zero"), but also for many ODS even banned import from and export to the countries which were not Parties to the MP.

Some differentiation in terms of the controlling commitments were agreed already in 1987 in favour of the developing countries with relatively low level per capita ODS consumption. With this provision, the apparently less responsibility for the ozone depletion hazard and also the developmental needs of these countries were recognized. This group of countries became entitled for a ten years delay for the compliance with some of the Protocol's key obligations. The subsequent amendments and adjustments regularly turned back to and refined the terms of this differentiation.

Trading with production quotas and joint implementation as optional complementary instruments were defined by the 1987 Montreal Protocol. Under specific circumstances, the former one was an option for any two Parties according to which those could trade in a portion of production of some ODS, as long as the aggregated level of their productions would not exceed the sum of production limits set out for those Parties (*UNEP*, 2012). This opportunity was used by Australia and New Zealand in 1997. The joint implementation or *joint fulfilment* mechanism in principle could be applied by a group of countries, such as the members of the European Community.

Science-policy relations were of high significance for this matter, as well, especially for evaluation of the effectiveness of the agreed commitments and for provision of advices about additional, more ambitious targets, based on the advanced knowledge on the ozone depleting mechanisms and abatement options. For this purpose, expert panels were established with the mandate to provide scientific and technological assessments and proposals (Panels for Ozone Scientific Assessment, Environmental Effects Assessment, Technology and Economic Assessment).

Enforcement. A comprehensive procedure was put in operation for the evaluation of the occasional *non-compliance* of the Parties regarding the implementation of their commitments under the MP. The elaboration of this mechanism began in 1990, it was adopted in 1992, and substantially widened in 1998 (*UNEP*, 2012). It included detailed proceedings and an institutional component (Implementation Committee). Basically, recommendations were made for the Parties which were found in non-compliance with the control or the reporting obligations, moreover, financial means could be offered as assistance to achieve compliance. Beyond that, in principle, more serious measures could also be taken, such as the suspension of the rights of a Party to trade with production quotas, however, the use of the sanctions was generally avoided (*Sarma*, 2005).

A financial instrument was initiated in 1989 by the Parties to the Montreal Protocol "to recognize the urgent need to establish international financial and other mechanisms to enable developing countries to meet the requirements of the present and a future strengthened Protocol, thereby addressing the ozone depletion and related problems" (*UNEP*, 2012). Its operation started on an interim basis in 1990, but already two years later it was made final. This Multilateral Fund received financial contributions from the "non-developing countries", that is from the developed countries and the "countries with economies in transition" (EiTs) with a clear understanding that without such an instrument and technological support, the majority of the developing countries (DCs) would not be able to reduce and gradually phase out the ODS. In 1990, the financial assistance for capacity building was considered by the DCs as a condition for implementation of the control measures by them. The agreement on financial contributions involved that the Central and Eastern European countries (that is the EiTs) also became donors, whilst they started to face serious problems to fulfil their own obligations under the MP. Ultimately, it was the Global Environment Facility (GEF) that offered some financial assistance to these countries for meeting the ODS controlling targets.

A specific condition for entry into force (EiF) of the Protocol is also noteworthy, and essentially it was replicated for the international climate change policy regime with more or less similar justification. In general, it is customary to set a reasonable threshold number of acceding countries that should be reached for a multilateral agreement for its coming into force. (In this respect, "becoming a Party" in broad sense requires the deposition of the instrument of ratification, acceptance, approval, or accession.) In the case of the MP, one more essential condition was added, according to which it would enter into force provided that at least eleven such instruments had been deposited by countries "representing at least two thirds of 1986 estimated global consumption of the controlled substances". Determining such a bottom line for the aggregated reduction volume of the ODS consumption by those countries guaranteed the effectiveness of the implementation of this agreement. It was evident that the objectives of the MP could not be reached without the active participation of the "big consumers" of the ODS. Those years, the USA and the European Community together were responsible for more than half of the global consumption, while the large group of the developing countries only for about one seventh of that total amount (*UNEP*, 2005).

3.3. Replication of some precedential features in the international climate policy setup

Policy-relevant climate science: the outset. A new period started in the scientific understanding of and the elevated concern over the climate change hazard from the late 1970s. What was known and also the remaining knowledge gap concerning the cycles of the greenhouse gases (GHGs) and the effects of their increasing atmospheric concentrations were summarized *inter alia* in the *Charney* report (1979) and at international level, by the (first) World Climate Conference (*WMO*, 1979). According to our timeline terminology, the Conference's declaration properly reflected the end of the "inception phase" and the outset of the next phase for ascertaining the validity of the earlier assumptions on this complex issue: "Carbon dioxide plays a fundamental role in determining the temperature of the earth's atmosphere, and it appears plausible that an increased amount of carbon dioxide in the atmosphere can contribute to a gradual warming of the lower atmosphere, especially at high latitudes (..) but the details of the changes are still poorly understood". During the following decade, the expanding observational systems, the improved global climate models, as well as the synthetization of the multidisciplinary research results in the framework of the World Climate Programme and the programmes of many international organizations (ICSU, UNEP, WMO, IIASA, etc.) substantially contributed to the fast science development on climate variability and change (*Faragó*, 1981, 1991). In the second half of the 1980s, a series of international meetings were devoted not only to the discussion of the new scientific achievements, but also to the possible actions to mitigate this hazard. Experts reviewed the state-of-the-art of climate change science at the meetings held in 1985 and 1987 (Villach, Bellagio), which were followed by international conferences between 1988 and 1990 (Toronto, The Hague, Nordwijk), where already scientists and policymakers exchanged views on the probable adverse consequences and the policy options (*Bodansky*, 2001).

Climate change policy regime. The year of 1988 can be seen as the actual beginning of construction of the international climate change policy regime with several exceptionally important developments: the first proposal for a concrete GHG-emissions control target was formulated at the Toronto meeting, the IPCC[2] was established as the main channel of scientific information to the policymaking community, and the UN resolution was adopted on the "Protection of global climate for present and future generations of mankind" (*UNGA*, 1988). The findings of the first IPCC report in 1990 were essential motivations for the outcomes of the 2nd World Climate Conference and also for a further UN resolution at the end of that year, which were leading to the international negotiations from 1991 and ultimately, to adoption of the global agreement on climate change in 1992. The foundations of the policy regime defined by this UN Framework Convention on Climate Change (*UNFCCC*, 1992) were later on considerably complemented by the Kyoto Protocol (KP) in 1997 and by a series of decisions enframed in the Marrakesh Accords (MA) passed in 2001 by the Conference of the Parties (COP). The Convention was enacted in 1994, the Protocol's entry into force occurred ten years later, after which the terms of a

[2] Intergovernmental Panel on Climate Change

new round of negotiations were discussed in 2005 (Montreal) and agreed in 2007 (Bali Action Plan) on the continuation of the KP for the post-2012 period and the elaboration of a new global agreement. Eventually, (i) the KP was "prolonged" in 2012 by its Doha Amendment (DA) with new emission reduction commitments for the industrialized countries (ICs) for the 2013–2020 period, and (ii) a new universal legal instrument was adopted at the end of 2015. The latter one is the Paris Agreement (PA), which is also under the UNFCCC likewise the Kyoto Protocol and its Doha Amendment, but the PA is elaborated as a complex set of mechanisms and procedures for the post-2020 period with various general obligations *for all Parties*. (As a matter of fact, the PA established and defined only the "skeleton" of those mechanisms and procedures so that the concrete rules of their operation ought to be defined in the forthcoming years. Unfortunately, it is also valid for the Parties' concrete commitments: in particular, the PA does not include any concrete global and country level emissions control targets with the respective deadlines, and such nationally determined targets will be regularly determined, updated/upgraded, and communicated later.) Henceforth, we devote our attention to some of the *substantial components of the international climate policy architecture*[3]*, which had their precedents in acid rain and ozone layer policy regimes* (*Table 1*). Some of these elements appeared in other contemporary multilateral legal instruments, however, the influence of the policy mechanisms of the two other large-scale atmosphere-related environmental processes was especially prominent for the climate change issue. As the protocols on sulphur and nitrogen emissions were finalized in 1985 and 1988, respectively, and the Montreal Protocol on ozone layer protection was concluded in 1987, the fresh experiences on compromise-settings within those negotiating processes had also their reflections on the climate negotiations launched at the beginning of 1991.

[3] The present discussion of the international climate policy regime takes into account some key components of the Framework Convention, the Kyoto Protocol, the Marrakesh Accords, the Doha Amendment, some decisions by the Parties, and the Paris Agreement.

Table 1. Evolvement of the international policy regimes since the late 1970s and some of their analogous features (introduced by the acid rain and/or ozone layer regimes and replicated in the climate change policy settings)

	Acid rain policy regime	Ozone layer policy regime	Climate change policy regime
	1978- negotiations ***1979: "framework" Convention***	1977: World Plan of Action on the Ozone Layer (UNEP)	1979: World Climate Conference
1980-	***1985: Helsinki Protocol (sulphur)*** ***1988: Sofia Protocol (nitrogen)***	1981- negotiations ***1985: "framework" Convention*** ***1987:Montreal Protocol*** *(MP)*	1988: Toronto Conference 1989: Hague and Nordwijk Conferences
1990-	1994: Oslo Protocol (sulphur) 1999: Gothenburg Protocol (GP) (multi-pollutants)	1990-1999: Amendments and Adjustments of the MP	1990: 2nd World Climate Conf. 1991- negotiations ***1992: Framework Convention*** *(UNFCCC)* ***1997: Kyoto Protocol*** *(KP)* (completed with the 2001 Marrakesh Accords)
2000-	2012: Amendment and Adjustment of the GP	2007: Further adjustment of the MP	2005/2007/2011- new rounds of negotiations (Montreal, Bali, Durban) 2012: Amendment of the KP (Doha) ***2015: Paris Agreement*** *(PA)*

Feature and building block	Acid rain policy regime	Ozone layer policy regime	Climate change policy regime
Stepwise approach: gradual strengthening of the mitigation obligations	"framework" convention followed by protocols and a series of decisions	"framework" convention; its concretizing protocol followed by amendments, adjustments	framework convention; protocol (and decisions) and its amendment; a new, framework type "global" agreement (2015)
Mitigation obligations: quantified targets	quantified emissions control targets (AAPs)	quantified production control targets (ODS)	KP: quantified emissions control targets (GHGs); PA: nationally determined targets/efforts
Differentiation: differentiated obligations (for response policies and measures)	country-by-country targets (1994 Protocol)	MP: longer term compliance period for the developing countries	KP: concrete mitigation targets for ICs PA: targets to be communicated later; general reference to actions, enhanced efforts by DCs
Flexibility instruments: for cooperative fulfilment	joint implementation (1994 Protocol, but w/o rules)	joint fulfilment; trading with volumes of ODS-production	KP: joint implementation; trading with emission allowances; PA: cooperative mechanism/approach
Science-policy interface: institutional arrangements	expert level working group on effects, EMEP Steering Body	expert panels on strategies, effects, etc.	expert level body on scientific advice and close link with IPCC
Financial mechanism: for assisting developing countries		Multilateral Fund (1990-) (GEF to assist EiTs 1992-)	GEF climate portfolio (1996-); Green Climate Fund (2010-)
Compliance mechanism: for the facilitation and enforcement of implementation	facilitative mechanism (1994-)	facilitative mechanism, incl. potential sanctions (1992-)	KP: compliance mechanism, incl. potential sanctions (2001-) PA: facilitative mechanism
Conditions for entry into force: aggregated indicator		MP: threshold for aggregated production by the ICs	threshold for aggregated emissions (KP:) by the ICs, (PA:) by all Parties

Phased approach. Similarly to the acid rain and ozone layer policy regimes and for analogous reasons, the climate negotiations resulted in *gradually strengthened outcomes* by starting with a framework convention in 1992 and continuing with some more ambitious commitments and actions from 1997 on. In this case, such a stepwise approach was justified not only by slowly dissipating scientific uncertainties (e.g., on the forcing factors or the possible future behaviour of the system), but also by the prolonged discussions on the differentiated responsibilities for this global hazard and the considerable inertia of the key GHG emitting economic sectors. The responsibility was and remained a critical question, since it stemmed from the huge differences in the historical and gradually varying GHG emissions and in the consequent shares of the countries in the increase and excess of the atmospheric concentrations of these gases. Despite the framework character of the 1992 convention (according to its title and general substance), yet it contained an important commitment on emissions control by the industrialized countries, *viz.* the stabilization of their emissions by 2000 compared to the 1990 reference level (as a default baseline, while EiTs were entitled to have some flexibility in this regard). It was followed by the 1997 Kyoto Protocol already with a moderate emissions reduction commitment by almost the same country group, and by the 2012 Doha Amendment of the KP with even more stringent emission reduction obligations, but for a considerably smaller group of the industrialized countries. The particular *quantified emission limitation and reduction objectives* (QELRO) and commitments (QELRC) were defined in the 1997 KP and later in its 2012 amendment on a country-by-country basis similarly to the 1994 (second) sulphur protocol. Contrary to that approach, the 2015 Paris Agreement did not include any quantified mitigation target, but (i) it only concretized the ultimate objective of the Convention by referring to 2 °C and 1.5 °C as the critical limit values for the global average surface temperature increase above pre-industrial levels; and (ii) for the temperature goal, it included a rather general roadmap for the overall emissions control, i.e., to *reach global peaking of GHG emissions as soon as possible and to undertake rapid reductions thereafter*, so as to achieve a balance between anthropogenic emissions by sources and removals by sinks of GHGs in the second half of this century (in other words, to reach decarbonisation or zero net GHG emissions). As their contributions to the global response to climate change, the progressive quantified emissions control targets by the PA's Parties will be nationally determined and communicated later.

Differentiation. The concept of the common but differentiated responsibilities (CBDR) was unanimously accepted as the guiding principle for this policy regime. In particular, it meant the acknowledgment of the differences in the above-mentioned historical GHG emissions. Its consequence was the strong *differentiation of the obligations between the developed and developing countries*. In this regard, the countries' respective capabilities and national circumstances were also considered as important factors. This approach was clearly reflected in the emissions controlling provisions of the KP and DA, which set legally binding quantified *commitments* for the industrialized countries[4] (ICs) and referred to the mitigation *actions* of the developing countries (DCs) in line with the key preambular paragraph of the Convention: "Noting that (..) per capita emissions in developing countries are still relatively low and that the share of global emissions originating in developing countries will grow to meet their social and development needs". Moreover, the developed countries were also expected to undertake the provision of financial and technological assistance to the DCs in order to build and enhance their capacities for the assessment of emissions, development of climate response policies, and preparation for the adverse climatic impacts. The Paris Agreement repeated such a distinction, namely, by referring to emission reduction *targets* of the ICs and mitigation *efforts* of the DCs to be nationally determined, however, already encouraging the DCs to set also emissions control targets at a later stage. Some differentiation was also provided for other components of this policy regime (e.g., for the national communications on emissions and measures).

An international emission trading system was established by the KP in 1997. It was initiated by the USA by referring to its efficient internal (federal) SO_2 allowance trading scheme. Moreover, the *joint implementation* instrument was introduced as another flexibility mechanism, by means of which one industrialized country could transfer emission reduction units (quotas) originating from a project to another such country that partly or fully financed the project. In international terms, the KP's trading system was somewhat similar to the bilateral trading option for CFC production quotas under the 1987 MP, however, there was a very limited practical utilization of the latter one. A joint implementation option was agreed for the sulphur emissions by the 1994 protocol to the CLRTAP, but as it was indicated above, that was never used by any Parties in lack of the agreed rules for its application. Nevertheless, these two international precedents and operation of the above mentioned federal scheme in the USA provided useful background for the elaboration of the terms for those two supplementary mechanisms of the climate change policy regime. (The Clean Development Mechanism of the KP realized a very much different, innovative approach.) Because of significant differences in experiences and positions on such flexibility instruments, only the general provisions for the *market-based and non-market cooperative mechanisms* were included in the Paris Agreement, which applicability depends on when and how their terms and concrete procedures will be determined.

Science-policy relations. The state-of-art scientific knowledge closely motivated the rapid progress in the acid rain and ozone layer policy regimes, and some dedicated institutional arrangements were made in both cases to

[4] We use the term of "industrialized countries" (ICs) for the group of the developed countries and the countries with the economies in transition, which are listed in the Annex I of the UNFCCC and referred to also in the Annex B of the KP.

systematically channel the new observational and research information to the negotiators (through working groups and expert panels). These experiences have contributed to setting up the relevant institutional mechanisms for an interactive science-policy dialogue to assist the climate negotiations. For this purpose, the role and functions of a permanent advisory body were already defined by the 1992 Convention[5], and a close working contact was maintained with the IPCC. The periodically published assessment reports of the IPCC had significant influence on the multilateral negotiations and their outcomes: e.g., the conclusions of the 1990 first report on the Convention (1992), the outcomes of the second report in 1995 on the Kyoto Protocol (1997), and the policy relevant scientific assessments of the fifth report (2013/2014) on the elaboration and adoption of the Paris Agreement (2015).

<u>*Enforcement*</u>. A comprehensive mechanism was elaborated for the evaluation of occasional *non-compliance* of a Party with its commitments under the KP, which rules were adopted only in 2001 (as part of the Marrakesh Accords). The lessons from such instruments established earlier were taken into account, as well as, the very complex nature of reporting on the GHG emissions, various climate policies, and measures by the Parties, and as a consequence, the elaborateness of the KP's mechanism went well beyond that of the compliance systems for the acid rain and the ozone layer policy regimes: "The Kyoto Protocol has thus given rise to a non-compliance procedure, which is among the most elaborate and innovative of its kind, while the Compliance Committee (..) is one of the most powerful and independent committees of its kind established by an environmental convention" (*Maljean-Dubois*, 2010). For the sake of enforcement, one possible *sanction for non-compliance* could lead to the temporal suspension of the eligibility of a Party for using the KP's flexibility mechanisms. This option reminds a similar opportunity within the ozone layer policy regime, however, with more serious implications in the case of the KP. Recently, a more cautious formula was included in the Paris Agreement obviously because of the universal nature of certain obligations: a mechanism for the *facilitation of implementation* of and *promotion of compliance* with the provisions of the PA and the relevant committee with *only facilitative and non-punitive functions* (which concrete terms of reference should be determined later).

<u>*Financial assistance*</u> for the developing countries was considered as a crucial prerequisite for their participation in the common global climate protecting endeavour, so that the financial mechanism was established and outlined already in the framework convention, which operation was undertaken by the Global Environment Facility (GEF). Primarily, it aimed to assist the developing countries and, to a less extent, the countries with economies in

[5] "A subsidiary body for scientific and technological advice is hereby established to provide the Conference of the Parties (..) with timely information and advice on scientific and technological matters relating to the Convention." (UNFCCC, Art. 9.1) The author of this paper was elected as the first chairman of that body (SBSTA), and in that capacity (*ex officio*), he was also the member of the Bureau of the COP.

transition. In a sense it was comparable to the Multilateral Fund for the Montreal Protocol together with the support from the GEF to the EiTs. Moreover, such a similarity became even more apparent when the COP of the climate convention established its "own" Green Climate Fund in 2010 to channel financial resources to DCs to support their mitigation and adaptation related actions.

A specific condition for entry into force (EiF) has guaranteed that the KP could have its legal power only if the key "players" become Parties to it. This idea was similar to the special EiF criteria of the Montreal Protocol. Besides the requirement of having already at least 55 ratifyers, there was an additional condition, namely, this group of the Parties had to incorporate industrialized countries (ICs listed in Annex I of the Convention), which accounted in total for at least 55 percent of the total CO_2 emissions for 1990 of all the ICs. This very high threshold can be better understood by taking into account that in 1990 the Russian Federation and the USA together were responsible for more than half of that total. (Of course, this situation has profoundly changed when the USA pulled out of the Protocol.) The Paris Protocol formally repeats the similar 55–55 condition for its entry into force, however, because of its global nature, not exclusively the ratifying industrialized countries' emissions will be added up to meet the 55 percent emission threshold, but the annual emissions of all the ratifyers (those from the group of the developing countries, as well).

In sum, important precedential features of the acid rain and the ozone layer policy regimes had their positive effects on the construction of the climate change policy architecture, however, as it will be demonstrated below, after a while, the evolvement and effectiveness of the climate change policy mechanisms considerably diverged from those for the two other atmospheric issues.

4. Increasing science-policy gap in addressing the global climate change hazard

"The production and consumption of the majority of harmful ozone-depleting chemicals has been successfully phased out, in both developed and developing countries." (*UNEP*, 2012)

"Noting with grave concern the significant gap between the aggregate effect of Parties' mitigation pledges (..) and aggregate emission pathways consistent with having a likely chance of holding the increase in global average temperature below 2 °C or 1.5 °C above pre-industrial levels." (*COP Decision 2/CP.18*, 2012)

Effectiveness of acid rain and ozone layer policy regimes. When the 1997 Kyoto Protocol entered into force in early 2005, it was the general expectation that the international treatment of the climate change hazard will somehow follow the examples of the relatively rapid and effective development of the international policy mechanisms for tackling the "acid rain" (more generally, the long-range air pollution) and the ozone layer depletion problems. Due to the increasingly stringent measures, the emissions and transboundary transmissions of the AAPs have drastically dropped in the pan-European region. In the same way, thanks to gradually enhanced provisions of the MP, the production, consumption, and atmospheric release of an ever expanding group of ODS was taken under control, eventually many of these substances were phased-out and substituted by "ozone-friendly" ones for various applications. In these cases, the rapidly enriching knowledge base has had its decisive effect on policymaking besides many other supportive factors.

The climate change science-policy paradox. Contrary to the above cases, a growing gap could be observed primarily between the actual levels of the globally aggregated GHG emission reductions and the level of reductions that was from time to time recommended by the large group of scientists backing the work of the IPCC, the UNEP, and various international academic organizations. Since 1990, the IPCC has regularly published science-based assessments, *inter alia*, on those levels of global emission reductions, which would make possible, with certain degrees of confidence, the avoidance of dangerous human interference with the climate system. These were accompanied by evaluation of the mitigation potential of the economic sectors and by recommendations for specific mitigation and adaptation policies ("climate-friendly" measures in various sectors, sustainable forest management, opportunities for increased climate resilience, etc.). In addition to that, the UNEP issues Emissions Gap Reports (EGR) since 2010, and the scope of its reports is the comparison of the theoretical emissions reduction pathways for remaining below the presumably still safe global temperature increase limits with the actual, agreed, or pledged global emission reductions. In this section of the paper, the increasing deviations of the international policy responses from these science-based advices and the key factors of these deviations will be discussed. We consider the evolution of the science-policy interplay in terms of the influence of growing scientific awareness about the global climate change hazard on the international climate policy cooperation for the last four decades. This process was more or less analogous to those for the acidification and ozone depletion hazards for about two decades, however, for various reasons, there is a widening science-policy gap concerning especially the abatement or mitigation targets since the turn of the century in case of the climate change problem (*Table 2*). This is a *climate change science-policy paradox*, i.e., the contradiction between the increasing knowledge level on an environmental problem and the aggregated effect of the actions to cope with that problem. There are other forms of paradoxes embedded in the climate policies as contradictory feedbacks (*Fölster* and *Nyström*, 2010; *Jordan et al.*, 2012).

Table 2. Timeline of climate change science-policy relations
(S: short-term emissions control, L: longer-term emissions control; /1990 or /2000 is the reference year; "emissions" refer to GHG-emissions; * is for the "2°C limit" after 2007)

	Emissions control targets: science-based recommendations*	**Emissions control targets: policy approach or commitment**
1985-	1985 Villach; 1987 Villach, Bellagio S) stabilization of ICs emissions L) stabilization of the atmospheric concentrations	1988 Toronto; 1989 The Hague, Nordwijk, UNEP S) 20% reduction or stabilization of the ICs emissions by 2005 L) stabilization of the atmospheric concentrations
1990-	1990-1992 IPCC AR1 (1990 WG-III, 1992 Supplement) S) stabilization of ICs emissions L) stabilization of the atmospheric concentrations	1992 UNFCCC S) stabilization of ICs emissions by 2000 (/1990) L) stabilization of the atmospheric concentrations 1994 The Convention enters into force (EiF)
1995-	1995 IPCC AR2 S) reduction of ICs emissions L) stabilization of global CO_2-emissions within several decades followed by substantial reductions (/1990) 2001 IPCC AR3 S) reduction of the ICs emissions beyond KP levels L) stabilization of global emissions within few decades	1997 Kyoto Protocol (KP) S) 5% reduction of the ICs emissions by 2012 (/1990) L) reference to the ultimate objective of the Convention (stabilization of the atmospheric GHG concentrations) 2001 Marrakech Accords completing the rules for the KP 2004 Protocol's special EiF criteria are fulfilled (EiF: Febr. 2005)
2005-	2007 IPCC AR4 S) stabilization of global emissions within 10–15 years; 25–40% reduction of ICs emissions by about 2020 (/1990) L) global emission reductions: at least 50% by 2050; 80–95% reduction of the ICs emissions by 2050 (/1990) 2010 UNEP-EGR S) increase of global emissions: less than 17% by 2020 (/1990)	2005 Mandate for dialogue on long-term actions (Montreal) 2007 Mandate for negotiations on future actions (Bali) 2009 Copenhagen Accord (CA), a general reference to IPCC AR4; S) peaking of global and nat'l emissions "as soon as possible" according to CA: "Cancun pledges" by countries in 2010 2010 UNEP-EGR S) global effect of "pledges": 30–40% increase by 2020 (/1990) 2012 Doha Amendment to the KP S) 18% reduction of the ICs emissions by 2020 (w/o 5 ICs) (/1990)
2013-	2013-2014 IPCC AR5 S) emission peak years for all regions in 2010-2020; ca. 30% reduction of ICs CO_2-emissions by 2030 (/2010) L) 40-70% global emission reductions by 2050 (/2010) 2014, 2015 UNEP-EGR (scenarios from IPCC AR5 database) S) increase of global emissions: less than 14% by 2030 (/1990)	2015 INDCs by Oct 2015 (UNFCCC, 2015[1], UNEP-EGR, 2015[2]): S) global effect of INDCs[1]: 37–52% increase by 2030 (/1990) S) global effect of INDCs[2]: 40–54% increase by 2030 (/1990) 2015 Paris Agreement S) global peaking "as soon as possible" L) zero net emissions in the 2nd half of this century

4.1. The scientifically recommended and the actually accepted levels of mitigation responses

Initiatives for the climate change policy regime. The scientific community started to urge the policy measures on the climate problem from the mid-1980s. The conclusions of the 1985 Villach conference included the following recommended actions based on the assessment of the climate change hazard (*Villach*, 1985): "Governments (..) should take into account the results of this assessment in their policies on social and economic development, environmental programmes, and control of emissions of radiatively active gases. (..) Major uncertainties remain in predictions of changes (..) Nevertheless, the understanding of the greenhouse question is sufficiently developed that scientists and policy-makers should begin an active collaboration to explore the effectiveness of alternative policies and adjustments." As a follow-up, two expert-level meetings already focused on concretizing the policy areas which, according to the joint meeting report, should cover both the limitation and adaptation strategies. The priority actions for the former one included the re-examination of long-term energy strategies, reduction of deforestation, and increase of forest area, moreover, the limitation of the growth of non-CO_2 GHGs in the atmosphere. The report also suggested the examination "of the need for an agreement on a law of the atmosphere as a global commons or the need to *move towards a convention* along the lines of that developed for ozone" (*WMO-UNEP*, 1988). These science-based suggestions strongly motivated the outcomes of those conferences, which took place in 1988 and 1989 with the participation of many government representatives, as well. Their policy-oriented declarations included already some quantified proposals for emissions control and some other actions (afforestation, controlling other GHG emissions, international financial means, etc.). In this regard, the key points by the Toronto conference (1988) were as follows: *stabilization* of the atmospheric concentrations of CO_2, for which emission reductions of more than 50% would be necessary for long-term, and as an initial global goal, the reduction of emissions by approximately 20% of 1988 levels by the year 2005 should be achieved. The high-level meetings held in The Hague and Nordwijk in 1989 emphasized the need of *urgent stabilization of the emissions by the industrialized countries* (ICs) as a first step. The UNEP Governing Council reiterated a similar requirement for all the emissions of carbon dioxide and other greenhouse gases at its meeting in 1989 (Nairobi). As we see, these *international policy reactions were in line with the science-based recommendations at least with those that concerned the most immediate actions* (emission stabilization, launching negotiations).

Stages of mitigation policy development. From the early 1990s, the negotiations generally resulted in the shorter term mitigation obligations for subsequent decadal periods. The 1992 convention comprised of emission stabilization objectives for the ICs at the 1990 level by 2000. The 2007 Kyoto

Protocol set reduction obligations for them with the targets expressed as the annual averages for the 2008–2012 period. The Doha Amendment in 2012 defined new emission reduction commitments for a "shrunken" group of ICs by 2020. The negotiations on a new global instrument started about a decade ago and its preparations became more concentrated after 2012 with the intention to reach a deal on more ambitious actions for the post 2020 period. After 2009, many countries communicated their pledges and intentions with more or less concrete national targets for 2030 or some other target date. Eventually, that new agreement was concluded at the end of 2015, however without any concrete emission reduction "roadmap". The negotiations during all these stages could rely on inputs from the research community. The series of assessment reports of the IPCC from 1990 and the Emission Gap Reports (EGR) by the UNEP from 2010 presented scenarios with global emissions estimates, aggregated emissions of the industrialized countries, and relevant emission pathways, adherence to which could guarantee with some chance to stay below the 2 °C global warming limit. In order to demonstrate the changing science-policy gap, we now compare the science-based global emission recommendations with the global targets from the above-mentioned legal instruments or with aggregated effects of the countries' "pledges" provided at the later stages of this negotiating process.

The Convention. The IPCC published its first report in 1990 and issued supplemental assessments in early 1992. These reports included scenarios for GHG emissions control, and specifically, the IPCC's third working group (on the response strategies) provided initial evaluations on the feasibility of meeting the different quantitative targets. Besides a general reference to the urgency of the *stabilization of these emissions*, the 1990 and 1992 reports made clear that "in the near term, no significant progress in limiting global emissions will occur without actions by the industrialized countries. Some countries have already decided to stabilize or reduce their emissions". The rationality for a phased approach was also pointed out (*IPCC*, 1990–1992): "The IPCC recommends a programme for the development and implementation of global, comprehensive and phased action for the resolution of the global warming problem under a flexible and progressive approach." The existing uncertainties and the need for further in-depth studies warranted the carefulness of such formulations, i.e., the inadequacy of information available at that stage to make sound and detailed policy analyses. These complex IPCC messages had their equally cautious imprints on the ministerial declaration of the Second World Climate Conference (November 1990, Geneva) and also on the outcomes of the international negotiations, which culminated in adoption of the UN Framework Convention on Climate Change (UNFCCC). The convention included (i) short term obligations, such as the *emission stabilization commitment for the industrialized countries* (listed in the Annex I) by 2000 at the default 1990 reference level (base year) and a general provision for all Parties (i.e., also for the developing countries) to elaborate their national climate change programmes; and (ii) the long-term ultimate objective of the *stabilization of atmospheric GHG concentrations* at a level that would prevent dangerous anthropogenic interference with the climate system (*UNFCCC*, 1992). Obviously, both the scientific and policymaking communities wished to have some more time for getting more information on the climate change process, its expected impacts, and on the technical and economic feasibility of stronger policies. The Convention entered into force in 1994, and some years later it had a universal membership. Afterwards, the implementation and adequacy of this agreement was regularly discussed during the annual sessions of the Conference of the Parties (COP).

The Protocol. The next comprehensive assessment of the IPCC was completed in 1995 (*IPCC*, 1995). The refined scenarios for CO_2 *concentration stabilization* were linked to the relevant *emission pathways,* and it was made clear that even if global CO_2 emissions were maintained at then levels, they would lead to a nearly constant rate of increase in atmospheric concentrations for very long time. It was deduced that only the urgent halting of the emission growth followed by a systematic decrease of these emissions could lead to presumably still safe stabilization levels of the atmospheric GHG concentrations. More concretely, for instance, it was indicated that the 450 ppmv CO_2 stabilization scenario could be achieved only if global anthropogenic CO_2 emissions returned to the 1990 levels within approximately 40 years from that time, and dropped substantially below those levels subsequently. It was also clear from these scenarios and the related assessments that in order to achieve that global emission peaking, the industrialized countries had to commit themselves to considerable emission reductions (by taking into account their higher historical emissions, i.e., the CBDR principle). The new round of negotiations started in 1995 (based on the so-called "Berlin Mandate") and eventually those were leading to the preparation of the Kyoto Protocol (KP) and its adoption in 1997. The Protocol set an average 5% reduction obligation for the group of the industrialized countries (Annex I Parties) compared to the 1990 level of their emissions, to be achieved in the period of 2008–2012. *Although it was much lower than the GHG reduction levels stemming from the scientific evaluations, nevertheless, it was considered as a moderate but important short-term first stage in a stepwise approach.* In a sense, it still followed to some extent the initial phases of the acid rain and the ozone layer policy regimes. The detailed rules for some of the critical components of the KP were approved in 2001 (Marrakech Accords), and at last the KP came into force in early 2005 (already w/o the USA but thanks to the ratification by the Russian Federation in 2004, which was a decisive act in view of the specific EiF condition).

Coming to a standstill. In the meantime, the IPCC's third report was issued in 2001 and had some catalytic role on deliberations on the future climate policy cooperation that began in 2005 (after the KP entered into force). Based on that report, it was evident that for stabilizing the atmospheric CO_2 concentrations e.g., at 450 ppmv level, the *global emissions should reach a ceiling within a few decades* and already on short term, it "may require emission reductions during the period 2008 to 2012 in Annex I countries that are significantly stronger than the Kyoto Protocol commitments" (*IPCC*, 2001). Contrary to the essence of these conclusions, in 2005 (Montreal) the Parties could hardly reach consensus even on the formats and general objectives of dealing with the post-2012 period. It can be considered as the beginning of a rapidly widening gap between the global climate change science and the international policy responses. At least, the dispute on formalities of the future negotiations and their general directions could be resolved in 2007, and the clear-cut messages of the fourth IPCC report had some influence in that regard (*IPCC*, 2007). The report, especially, its part contributed by the third working group of the IPCC, clearly stated that: (i) keeping the 2° C objective within reach requires stabilization of the atmospheric concentration of GHGs in line with the lowest stabilization level assessed, i.e., 450 ppmv CO_2eq; (ii) this will assume that the *global GHG emissions peak within the next 10 to 15 years*, and then those are substantially *reduced at least by 50% below 1990 levels by 2050*; and (iii) the groups of the industrialized (ICs) and the developing countries (DCs) contribute to those short and long-term CO_2eq reduction goals in line with their different shares in the overall emissions. These pertinent short and long-term reduction targets *in 2020 and 2050 for the ICs are 25-40% and 80-95%*, respectively, while for the DCs their contributions were suggested as follows: substantial deviation of the emissions from baseline by 2020 in some developing regions and substantial deviation from baseline in all developing regions by 2050. These science-based assessments were indirectly cited in the 2007 negotiating mandate (Bali), however, after two years of intense deliberations instead of agreeing on new targets and commitments, the only concrete product of the Copenhagen summit (2009) was that the delegates took note of an accord that included indications for: *deep cuts in global emissions*; *peaking of global and national emissions as soon as possible*; *quantified economy wide emissions targets by the industrialized countries by 2020*. While these general provisions were not complemented with any concrete goals, all Parties were invited to submit their "pledges": quantified economy wide emissions targets for 2020 by the Annex I Parties and further mitigation actions by the non-Annex I Parties. These submissions were reviewed at next COP session (Cancun), and the total effect of these "Cancun pledges" was also compared with the emission pathways consistent with a "likely" chance of meeting the 2° C threshold (*UNEP*, 2010). The results of this gap analysis demonstrated the need to *limit the growth of overall emissions by 2020 to a maximum of 17% in contrast to the 30-40% range of the global emission increase* that was deduced from those pledges and the four policy scenarios (a combination of the unconditional and conditional pledges with "lenient" or strict rules of compliance).

"Prolonging" the Kyoto Protocol as a transient solution. We now turn our attention to the legally binding deal, which was arranged in 2011 and finalized in 2012 as an amendment to the KP by extending it to a second commitment period. This Doha Amendment (DA) included quantified emission limitation or reduction commitments (QELRC) by a group of the industrialized countries with the target year of 2020. The aggregated unconditional commitments equalled to 18% emission reduction, however, already five industrialized countries did not take part in this deal, namely: Canada, Japan, New Zealand, Russia, and the USA. Many participants of the deal indicated also a conditional higher emission reduction target (e.g., the EU-28 a 30% reduction besides the unconditional 20% target). If one were combining the emissions control "low pledges" of those five countries (e.g. 4% below the 1990 level by the USA) with the unconditional commitments by the ICs inscribed in the DA, then such a virtual aggregated target would result in a less than ten percent reduction by 2020 below the 1990 level by all the ICs (listed in the convention). Whatever would be the exact estimate for this whole group, *the aggregated target for 2020 could mean a significant decline from the science-based emission reduction range for the ICs that was derived in the 2007 IPCC report*. Moreover, the DA covered only about 15% of the global GHG emissions (*Sterk*, 2012), since it did not address the goals of the above mentioned five ICs, neither the actions by the DCs by 2020. Therefore, it remained unclear, how the overwhelming majority of the countries plan their concrete measurable, reportable, and verifiable mitigation and other climate related policies and measures. Nevertheless, the Doha Amendment is an essential achievement: without its adoption, apparently, no progress could be achieved at all in the parallel negotiations of a new global instrument.

New policy-relevant scientific assessments. The year of 2013 brought about a new stage both in the communication of new scientific results and the international climate policy cooperation. The first part of the fifth report of the IPCC was published in 2013 and it was followed by other volumes of the report in 2014. The statements on the human interference with the global climate system, on the scenarios of its future state, and on the expected impacts reflected a much higher level of confidence. Comprehensive information was also provided on the possible mitigation and adaptation strategies. Regarding the future emission pathways, besides the general indications of the need for substantial emissions reductions over the next few decades and for near zero net anthropogenic emissions by the end of the century, more concrete GHG emission reduction assessments were given for 2050 and some estimates only for the CO_2 emissions for 2030. The apparently most essential statement on the mid-century global emissions was as follows: "Emissions scenarios leading to GHG concentrations in 2100 of about 450 ppm CO_2eq or lower are likely to maintain warming below 2° C over the 21st century relative to pre-industrial levels. These scenarios are characterized by 40% to 70% global anthropogenic GHG emissions reductions by 2050 compared to 2010." For the same warming threshold (actually, for the relevant range of long-term CO_2eq concentration scenarios, i.e., for 430–530 ppm CO_2eq), regional emissions peak years were derived by means of different models, and CO_2 emission reductions in 2030 over the 2010 levels were also presented in the report (*IPCC*, 2013–2014). According to these calculations, *the peak years for all the regions were set between 2010 and 2020 in order to be in line with the above-mentioned scenarios; therefore, the global emissions ought not to grow after the end of the present decade*. But what might be much more informative for the negotiators, those were the assessments of the transient mitigation efforts by the regions (which lead to those 430–530 ppm CO_2eq scenarios in 2100): "The contribution of different regions to mitigation is directly related to the formulation of international climate policies. In idealized implementation scenarios, which assume a uniform global carbon price, the extent of mitigation in each region depends most heavily on relative baseline emissions, regional mitigation potentials, and terms of trade effects. (..) In general, emissions peak in the OECD-1990 sooner than in other countries with higher baseline growth. Similarly, emissions are reduced in the OECD-1990 countries by 2030 relative to today, but they may increase in other regions, particularly the fast-growing Asian and MAF regions." The concrete quantitative estimates (for the 430–530 ppm CO_2eq scenarios) suggest *the average 32% regional CO_2 emission reductions in 2030 below the 2010 emission levels for the group of the ICs* (the OECD members in 1990 and the EiTs), 35% reduction in average for the Latin-American region, and show a range of emissions control rates around zero (i.e., stabilization) for the Asian region and the MAF (Middle East and Africa). The above assessments offered important orientation values for the ongoing negotiations. The overall scale of these most recent emission-related figures for the 2° C criterion seems to be even more demanding than the ones from the previous assessments, in particular for the industrialized countries as a whole. By using the same scenarios from the IPCC database, the UNEP report (*UNEP*, 2014) offered even more relevant information for the gap assessments, namely the *global GHG emission levels in 2030* "for a likely chance of staying within the 2 °C limit" following a least-cost pathway from 2020 which are: 42 $GtCO_2eq$ (range: 31–44), or *+14% relative to 1990 emissions and –14% relative to 2010 emissions*. The use of 1990 default reference year and emissions level is essential not only for comparability purposes (with former assessments and commitments), but also for realizing the very significant actual changes, which clearly demonstrate the inadequacy of the existing policy responses since the early 1990s. Before turning to the most recent "offers", let us compare these theoretically critical thresholds with the actual data: *global emissions have grown since 1990 by more than 45%* and were approximately 54 $GtCO_2eq$ in 2012 (*UNEP*, 2014).

International climate policy cooperation beyond 2020. Now the basic question is that, how and to what extent these new science-based assessments were taken into account in the course of preparation and finalization of the new agreement adopted in 2015 for the post-2020 period. The too general, unquantified emissions control "roadmap" and the requirements of the Paris Agreement for all the Parties to communicate later their concrete emission-related contributions were already mentioned above and obviously, these provisions are not applicable at these stage for any science-policy gap assessment. The "recommended" global emissions reduction pathways presented by the IPCC or the UNEP would be valuable for top-down distribution approaches (based on the common but differentiated responsibilities), but as a matter of fact, the negotiations were again centered around a bottom-up process (likewise the KP and the DA). As a matter of fact, the majority of the countries (or country groups in the case of the EU) individually formulated and communicated their possible emissions control targets beyond 2020 in the framework of the "intended nationally determined contributions" (INDC). Obviously, the consideration of the aggregated global levels of these (unconditional and conditional) quantified national targets for 2030 or 2050 is especially important in light of the "reasons for concern" depicted by the IPCC in its latest report. The synthesis of these intended contributions submitted by October 2015 represented three quarters of Parties to the Convention and 86 percent of global emissions in 2010, and the aggregate effect for 2030 would be 56.7 (53.1 to 58.6) $GtCO_2eq$ in 2030 (*UNFCCC*, 2015). In relative terms, these estimates would mean 11–22% increase of the aggregated emissions in 2030 in relation to the 2010 level, or *37–52% increase in relation to the global emission level in 1990.* A rather similar assessment is derived in the Emission Gap Report (*UNEP*, 2015), namely, 54 $GtCO_2eq$ (range: 52–57) for 2030, which corresponds to *46% (range 40–54) relative increase compared to the 1990 level.* These clearly indicate a huge deviation from those targets which were considered necessary theoretically, and it means a further significant increase in the science-policy gap in tackling this hazardous global environmental process.

4.2. Some basic factors behind the difficulties with the climate change policy regime

There are several factors which may explain the complications with the international climate change policy-making. Their nature and significance can be better understood in a comparison with the acidification and ozone depletion cases. Four distinctive problematic areas are mentioned below; however, there are obviously other more or less critical ones, which should be taken into consideration to make the international policy regime more responsive to the climate change challenge.

<u>*The operation of the global climate system*</u> governed by internal and external, natural and anthropogenic factors seems to be much more complex than the mechanisms of the acidification and ozone layer depletion processes. As a consequence, the detection of the present climate change signal and its

attribution to different drivers (forcing factors) is rather problematic because of the relatively low *climate change signal-to-noise ratio* (where the "noise" is the climatic variability in this context) and because of the diverse interactions and characteristic timescales of natural and human-induced contributions to the GHG cycles and to the impacts of the changing climatic conditions. The problem of signal-to-noise ratio also appears in the climate modelling (*IPCC*, 2001); moreover, it necessitates careful approach to climate impact assessments and adaptation strategies as the impacts of the short-term and long-term processes overlap (*Czelnai*, 1980). The complexity of the system, in particular, the problems related to the detection of the global climate change signal are clearly manifested in a more prolonged and slower decrease of the *scientific uncertainty level* concerning the anthropogenic influences on the climate system and in turn, a longer time length between the improved degree of scientific knowledge and the agreements on the related international policy frameworks. That timespan was about one decade in case of the acidification and ozone depletion problems, but it took several decades for the climate change issue (with regard to the time periods between the confirmation of the adequate attribution hypotheses and the adoption of the first multilateral legal instruments).

The substantial historical differences in responsibilities of various countries and country groups for the emerging climate change hazard have been a crucial factor together with their *differing vulnerabilities, capabilities, socio-economic problems, and interests*, in influencing the international negotiations. The recognition of the mutual interdependence was the most important motivation ("push factor") to seek common ways and means for the solution of the three environmental problems discussed in this paper, but the above mentioned differences mattered much more seriously to the global climate policy-making case compared to the other two atmospheric problems.

All key economic sectors somehow have their part in the climate change problem as GHG emitters and/or bearers of the impacts: energy sector, transport, various industrial activities (e.g., metallurgy, cement production), agriculture, forestry, healthcare, water management, nature conservation, etc. This means that for all these sectors and socio-economic activities efficient mitigation and/or adaptation policies should be developed at all levels. Therefore, it necessitates *economy-wide* national measures, while many of these policy areas have essential international dimensions in our globalized world. Sectoral policy-making is especially challenging for those areas that are characterized by substantial *inertia*, which is typical of fossil fuel based energy and transport systems (also because of the so-called "lock-in" effects); to some extent, such inertia characterizes certain agricultural and industrial activities, as well. This situation was somewhat simpler for the other two environmental problems, especially in case of the ozone layer policy regime.

Technologies. At last, availability and effectiveness of the *abatement and control technologies* should be noted. For the acidification problem, relatively cost-effective emission source-oriented and end-of-pipe "technological fixes" could be shortly developed, such as the desulfurization of coal, crude oil or natural gas before their further utilization, the flue gas desulfurization technologies (which provide gypsum, a widely used material), or more generally, the industrial scrubbers for the AAPs, moreover, the catalytic converters for vehicles to reduce nitrogen emissions. The phase-out of the ODS and their replacement with "ozone-friendly" substitutes have become appropriate to cope with the ozone layer depletion hazard, which were accompanied by the disposal of the ODS from their surplus stocks or those recollected from various appliances. With the GHGs, in general, the situation is much more difficult, since there are no such relatively simple, cost-effective, widely applicable technological solutions. Some of the remarkable barriers to the existing carbon neutralizing technologies (including the so-called "negative emissions technologies", i.e., different land use, forestry related sequestration methods, or the rather controversial carbon capture and storage options) are referred to by *UNEP* (2014). Therefore, the gradual but comprehensive and environmentally sound *decarbonisation of the entire economic systems* based on sustainable production and consumption patterns, and parallel preparations for the already seemingly unavoidable changes can only be considered as the adequate strategy for tackling this global environmental problem.

5. Conclusions

The knowledge development and the initial steps in the international policy regime building in relation to the global climate change problem have been analyzed, as these proceeded parallel to the somewhat analogous processes for acidification and ozone layer depletion by the late 1970s. This synergy during the "inception phase" had some role not only in facilitating the enhancement of the global environmental observing systems and the international scientific cooperation, but also indirectly in conducting the relevant detection and attribution studies. With the rapid research progress on acidification and ozone layer depletion, the corresponding multilateral policy mechanisms were not only established and gradually strengthened within a relatively short time period, but some of their important features and building blocks served also as precedents or prototypes for the climate change policy architecture. But the climate change issue proved to be a much more complex problem, so the proper international policy responses could not be formulated so smoothly as it occurred for the other two large-scale atmospheric issues and their anthropogenic drivers. This kind of increasing asymmetry was also evaluated in this paper throughout the "international policy setup phase" by about the turn of the

20th century and the subsequent "divergent phase" for these environmental problems.

Some of the important factors behind this lagging of the climate change response policies were also mentioned, and none of them can be easily overcome. Yet, all those should be tackled adequately. The reason for this is clearly stated by the recent IPCC report (*IPCC*, 2013–2014): "Without additional mitigation efforts beyond those in place today, and even with adaptation, warming by the end of the 21st century will lead to high to very high risk of severe, widespread, and irreversible impacts globally (high confidence)." The directions of the further scientific research tasks are outlined by the IPCC and the World Climate Programme (i.e., its research component, WCRP); furthermore, an integrated concept is foreseen by the "Future Earth" programme, which is the ICSU initiative devoted to all key environment-related processes, their interactions, and possible future effects, including those associated with the climate change process. Concerning the science-based complex climate policy-making challenges, references were already made to the need of an economy-wide approach; however, it should be re-emphasized that the climate policy-making problem is not a self-contained one, but inherently linked to a large range of other challenges (e.g., addressing the unsustainable resource use and land management, increasing waste streams, loss of biodiversity). Anyway, in light of the already solid scientific achievements and the possibility of the abrupt and irreversible changes, accurate policy responses are necessary amid remaining uncertainties, as it was so formulated by Stephen H. Schneider, to whom the Synthesis Report of the latest IPCC assessment report was dedicated (*IPCC*, 2013–2014): "Policymakers struggle with the need to make decisions that have far-reaching and often irreversible effects on both environment and society with sparse and imprecise information. (..) Strictly speaking, a surprise is an unanticipated outcome; by definition it is an unexpected event. Potential climate change and, more broadly, global environmental change are replete with this kind of surprise because of the enormous complexities of the processes and relationships involved (such as coupled ocean, atmosphere, and terrestrial systems) and our insufficient understanding of them. (..) as the rate of change of CO_2 concentrations is one imaginable condition for surprise, the system would be less rapidly forced if decision makers chose to slow down the rate at which human activities modify the atmosphere. This would lower the likelihood of surprises." (*Schneider* and *Kuntz-Duriseti*, 2002). These ideas are even more valid in view of the latest observations and assessments. In principle, such an approach was reflected in the recently adopted new global deal, the Paris Agreement that stressed the need for an effective and progressive response to the urgent threat of climate change by reaching global peaking of greenhouse gas emissions as soon as possible and undertaking rapid reductions thereafter in accordance with best available science. But the setting of the relevant and concrete policy targets was postponed and consequently, as it was demonstrated in this paper, there is still a rapidly increasing science-policy gap in tackling this hazardous global problem.

References

Bodansky, D., 2001: The History of the Global Climate Change Regime. In (eds.: *Luterbacher, U.* and. *Sprinz, D.F*) International Relations and Global Climate Change. 23–40.

Bolin, B. and *Eriksson, E.*, 1958: Changes in the Carbon Dioxide Content of the Atmosphere and Sea due to Fossil Fuel Combustion. In (ed.: *Bolin, B.*) The Atmosphere and the Sea in Motion: Scientific Contributions to the Rossby Memorial Volume Rockefeller Inst. Press, New York, 130–142.

Bolin, B. and *Bischof, W.*, 1970: Variations of the carbon dioxide content of the atmosphere in the northern hemisphere. *Tellus 22*, 431–442.

Bolin, B., Odén, S., Tamm, C.O., Granat, L. and *Rodhe, H.*, 1971; 1972: Air pollution across national boundaries: the impact on the environment of sulfur in air and precipitation: Sweden's case study for the United Nations Conference on the Human Environment, 1972. The Swedish Preparatory Committee for the UN Conference on the Human Environment, Stockholm (1971) and Norstedt, Stockholm (1972).

Brauch, H.G. and *Sprong, U.O.*, 2011: Coping with Global Environmental Change in the Antropocene. In (eds. Brauch *H. G.* et al.) Coping with Global Environmental Change Spinger, 31–60.

Byrne, A., 2015: The 1979 Convention on Long-Range Transboundary Air Pollution: Assessing its Effectiveness as a Multilateral Environmental Regime after 35 Years. Transnational Environmental Law, March 2015, 1–31.

Callendar, G.S., 1938: The artificial production of carbon dioxide and its influence on temperature *Q. J. Roy. Meteor. Soc. 64*, 223–240.

Callendar, G.S., 1958: On the amount of carbon dioxide in the atmosphere. *Tellus 10*, 243–248.

Charney, J.G., Arakawa, A., Bolin, B., Dickinson, R.E., Goody, R.M., Leith, C.E., Stommel, H.E. and *Wunsch, C.I.*, 1979: Carbon Dioxide and Climate: A Scientific Assessment. Report of an Ad Hoc Study Group on Carbon Dioxide and Climate. Woods Hole, MA (July 23–27, 1979), National Academy of Sciences, Washington D.C.

Clark, W., Jäger, J., Cavender-Bares, J. and *Dickson, N.M.*, 2001: Acid Rain, Ozone Depletion, and Climate change: An Historical Overview. In (ed.: *Clark, W.C.*): Learning to Manage Global Environmental Risks. Vol. 1. M.I.T., 21–56.

Crutzen, P.J., 1970: Influence of Nitrogen Oxides on Atmospheric Ozone Content," *Q. J. Roy. Meteor. Soc.96*, 320–325.

CSCE, 1975: Final Act. Conference on Security and Co-Operation in Europe, Helsinki.

Czelnai R., 1980: Climate and Society: the Great Plain of the Danube Basin. In (eds.: *Ausubel, J.H., Biswas, A.K.*): Climatic Constraints and Human Activities. Pergamon Press, Oxford, 149–180.

Engfeldt, L-G., 2009: From Stockholm to Johannesburg and beyond. Ministry of Foreign Affairs, Sweden.

Eriksson, E., 1963: The yearly circulation of sulfur in nature, *J. Geophys. Res. 68*, 4001–4008.

Faragó T., 1981: The present role and tasks of the climate research. *Időjárás 85*, 162–172.

Faragó T., Führer E., Garbai L., Iványi Zs., Járó Z., Jászay T., Márkus L., Mika J., Molnár Á., Nováky B., Práger T., Szalai S., Szász G., Szentimrey T., Tóth L.F., 1991: Climate variability and change: Changes in composition of the atmosphere and in the climatic characteristics, detection, modelling, scenarios and impacts of the regional changes. (eds.: *Faragó T., Iványi Zs., Szalai S.*) Hungarian Ministry for Environment, Budapest.

Faragó T., 2006: The history, negotiations and general features of the agreements. In (ed.: *Faragó T.*) Multilateral environmental agreements and their implementation in Hungary. Ministry of Environment and Water, Budapest, 3–8.

Farman, J.C., Gardiner, B.G., and *Shanklin, J.D.*, 1985: Large losses of total ozone in Antarctica reveal seasonal ClOx/NOx interaction. *Nature 315*, 207–210.

Fölster, S. and *Nyström, J.*, 2010: Climate policy to defeat the green paradox. *Ambio 39*, 223–235.

Gupta, J., 1997: The History of Global Climate Governance. Cambridge University Press.

Hamer, M., 2002: Plot to undermine global pollution controls revealed. *New Scientist*, 2 Jan 2002

Hinrichsen, D., 1983: New acid rain data disclosed at Stockholm conference. *Unasylva* (International Journal of Forestry and Forest Industries), *35*.

IPCC, 1990–1992: Climate change: the First Assessment Report and the 1992 Supplement. IPCC, Geneva.

IPCC, 1995: Climate change: the Second Assessment Report. IPCC, Geneva.

IPCC, 2001: Climate change: the Third Assessment Report. IPCC, Geneva.

IPCC, 2007: Climate change: the Forth Assessment Report. IPCC, Geneva.

IPCC, 2013-2014: Climate change: the Fifth Assessment Report. IPCC, Geneva.

Johnston, H., 1971: Reduction of stratospheric ozone by nitrogen oxide catalysts from supersonic transport exhaust. *Science 173*, 517–522.

Jordan, A., Asselt, H., Berkhout, F. and *Huitema, D.*, 2012: Understanding the Paradoxes of Multilevel Governing: Climate Change Policy in the European Union. *Glob. Environ. Politics 12*, 43–66.
Keeling, C.D., 1960: The Concentration and Isotopic Abundances of Carbon Dioxide in the Atmosphere, *Tellus 12*, 200–203.
Keeling, C.D., 1970. Is Carbon Dioxide from Fossil Fuel Changing Man's Environment? *Proc. American Philosophical Society 114,* 1, 10-17.
Kiss, A. and *Shelton, D.*, 2007: Guide to International Environmental Law. Martinus Nijhoff Publ. Leiden and Boston
Levy, M.A., 1995: International Co -operation to Combat Acid Rain. In (eds.: *Bergesen, H.O.*, et al.,) Green Globe Yearbook of International Co-operation on Environment and Development, 1995, Oxford University Press, 59–68.
Lovelock, J.E., Maggs, R.J. and *Wade, R.J.*, 1973: Halogenated Hydrocarbons in and over the Atlantic. *Nature 241*, 194-196.
Maljean-Dubois, S., 2010: An Outlook for the Non-Compliance Mechanism of the Kyoto Protocol on Climate Change. Amsterdam Law Forum, [S.l.], Vol. 2, No. 2, 77-80.
Mészáros E., 1981: Atmospheric Chemistry - Fundamental Aspects. Elsevier (Amsterdam) and Akadémiai Kiadó (Budapest).
Menz, F.C. and *Seip, H.M.*, 2004: Acid rain in Europe and the United States: an update. *Environ.Sci. Policy 7*, 253–265.
Molina, M.J. and *Rowland, F.S.*, 1974: Stratospheric sink for chlorofluoromethanes: chlorine atom-catalysed destruction of ozone. *Nature 249*, 810–812.
Morrisette, P.M., 1989. The evolution of policy responses to stratospheric ozone depletion. *Nat. Resour. J. 29*, 793–820.
Mylona, S., 1993: Trends of Sulphur Dioxide Emissions, Air Concentrations and Depositions of Sulphur in Europe since 1880. NILU, Oslo, Technical Report No. 116.
Odén, S., 1968: The Acidification of Air and Precipitation and its Consequences in the Natural Environment. *Ecol. Comm. Bull. 1*, Swedish National Science Research Council.
OECD, 1977: The OECD Programme on Long Range Transport of Air Pollutants. Measurements and Findings. Organisation for Economic Co-operation and Development, Paris.
PSAC, 1965: Restoring the Quality of Our Environment, Report of the Environmental Pollution Panel, President's Science Advisory Committee, The White House, Washington D.C.
Revelle, R. and *Suess, H.E.*, 1957: Carbon Dioxide Exchange between Atmosphere and Ocean and the Question of an Increase of Atmospheric CO_2 during the Past Decades. *Tellus 9*, 18–27.
Róna Zs., 1909: Éghajlat, II. K. M. Természettudományi Társulat, Budapest, 526–527.
Sarma, M.: 2005: Compliance with the Montreal Protocol. Proc. 7th International Conference on Environmental Compliance and Enforcement. (Marrakech, 9–15 April 2005) Vol. 1.
Seip, H.M., 2001: Acid rain and climate change – Do these environmental problems have anything in common? *Cicerone 6*, 1–7.
Schneider, S.H. and *Kuntz-Duriseti, K.*, 2002: Uncertainty and Climate Change Policy. In (eds.: *Schneider, S.H., et al.*) Climate Change Policy: A Survey Island Press, 53–87.
Sterk, W., Arens, Ch., Kreibich, N., Mersmann, F. and *Wehnert, T.*, 2012: Sands Are Running Out for Climate Protection. The Doha Climate Conference Once Again Saves the UN Climate Process While Real Climate Action Is Shelved for Later. Wuppertal Inst. (accessed 2015-04-22).
Stolarski, R.S. and *Cicerone, R.J.*, 1974: Stratospheric chlorine: a possible sink of ozone. *Canadian J. Chemistry 52*, 1610–1615.
Svensson, B.H. and *Soderlund, R.* (eds.), 1976: Nitrogen, Phosphorus and Sulphur - Global Cycles. Report 7, Ecol. Bull., SCOPE, Stockholm.
Ulrich, B., 1983: Effects of acid deposition. In: Acid Deposition. Proc. of the CEC Workshop (Berlin, 9 Sept 1982), Reidel, 31–41, 43.
UN, 2006: Reports of International Arbitral Awards, Trail Smelter Case. UN, Vol. III, 1905–1982.
UNCHE, 1972: Declaration and Action Plan. UN Conference on the Human Environment, Stockholm.
UNECE, 1979: Convention on Long-Range Transboundary Air Pollution.
UNECE, 2004a: Handbook for the 1979 Convention on Long-Range Transboundary Air Pollution and its Protocols, Geneva, ECE/EB.AIR/85, UNECE, Geneva.
UNECE, 2004b: Clearing the Air – 25 years of the Convention on Long-range Transboundary Air Pollution, Geneva, ECE/EB.AIR/84, UNECE, Geneva.
UNEP, 1985: The Vienna Convention for the Protection of the Ozone Layer.
UNEP, 1987: Montreal Protocol on Substances that Deplete the Ozone Layer.
UNEP, 2005: Production and Consumption of Ozone Depleting Substances under the Montreal Protocol 1986-2004. Ozone Secretariat, UNEP, Nairobi.

UNEP, 2010: The Emissions Gap Report: Are the Copenhagen Accord pledges sufficient to limit global warming to 2° C or 1.5° C? A preliminary assessment, UNEP, Nairobi.
UNEP, 2012: Handbook for the Montreal Protocol on Substances that Deplete the Ozone Layer. UNEP, Nairobi.
UNEP, 2014: The emissions gap report, 2014. UNEP, Nairobi.
UNEP, 2015: The emissions gap report, 2015. UNEP, Nairobi.
UNFCCC, 1992: United Nations Framework Convention on Climate Change.
UNFCCC, 2015: Synthesis report on the aggregate effect of the intended nationally determined contributions. FCCC/CP/2015/7, 30 October 2015.
UNGA, 1968: Problems of the human environment. Resolution 2398 (XXIII), UN, New York.
UNGA, 1988: Protection of global climate for present and future generations of mankind. Resolution A/RES/43/53, UN, N.Y.
US-DoS, 1974: Oslo Air Pollution Conference Outlines European Monitoring Program. https://www.wikileaks.org/plusd/cables/1974OSLO05376_b.html (accessed 2015-04-22).
Villach, 1985: Statement by the UNEP/WMO/ICSU International Conference on The assessment of the role of carbon dioxide and of other greenhouse gases in climate variations and associated impacts (Villach, 9-15 October 1985).
WMO, 1979: WMO proceedings of the World Climate Conference (Geneva, 12-23 February 1979). WMO No. 537, Geneva.
WMO-UNEP, 1988: Developing Policies for Responding to Climate Change. WCIP-1, WMO, Geneva.
WMO, 2014: The Global Atmosphere Watch Programme. 25 years of global coordinated atmospheric composition observations and analyses. WMO No. 1143, Geneva.

IDŐJÁRÁS

Quarterly Journal of the Hungarian Meteorological Service
Vol. 120, No. 1, January – March, 2016, pp. 41–51

Analyses of temperature extremes in the Carpathian Region in the period 1961–2010

Mónika Lakatos [*1], **Zita Bihari** [1], **Tamás Szentimrey** [1], **Jonathan Spinoni** [2], and **Sándor Szalai** [3]

[1]*Hungarian Meteorological Service,*
Kitaibel P. u. 1, H-1024 Budapest, Hungary

[2] *Joint Research Centre*
TP 268 - Via E. Fermi, 2749 - 21027 Ispra (VA), Italy

[3] *Szent István University,*
Páter Károly utca 1, H-2100 Gödöllő,Hungary

**Corresponding authors E-mail: lakatos.m@met.hu*

(Manuscript received in final form October 7, 2015)

Abstract—The harmonized data derived in CARPATCLIM project has enabled the presentation of the most comprehensive picture of trends of extreme temperatures in the Carpathian Region. A set of climate change indicators derived from daily temperature data, focusing on extreme events, was computed and analyzed in this study. Annual extreme indices for the period 1961–2010 were examined. Trends in the gridded fields were calculated, mapped, and tested for statistical significance. Results showed significant changes mainly in temperature extremes associated with warming. A large part of the region showed a significant decrease in the annual occurrence of cold nights and an increase in the annual occurrence of warm nights. The growing season starts earlier in more than third part of the region. The trend and proportion of the area that sign significant change of warm extremes strengthen the obvious warming in the Carpathian Region.

Key-words: CARPATCLIM, Carpathian Region, climate indices, temperature extremes

1. Introduction

The impacts of climate change on society come forward mainly through extreme weather and climate events, such as heat waves, droughts, heavy rainfall, and storms. The climate change evokes increasing frequency of climate extremes

(*Easterling et al.*, 2000; *Moberg et al*, 2006; *Alexander et al.*, 2006; *Seneviratne et al.*, 2012; *Donat et al*, 2013, *IPCC*, 2014).

Climate change is expected to result in significant changes in the Carpathian Region to affect ecosystems and human activities (*UNEP,* 2007). To describe the changes of extremes, a sort of climate indices is used in general as prevailing indicators of changes in extremes. The European Climate Assessment and Dataset (ECA&D) (*Klein Tank* and *Konnen*, 2003) contains climate indices from countries across Europe located in the Carpathian Region amongst them.

The purpose of the current study is to analyze the trends of temperature extremes in the Carpathian Region by means of a high-quality and high-resolution ($0.1^{\circ} \times 0.1^{\circ}$) daily gridded dataset constructed in the framework of the CARPATCLIM Project (www.carpatclim-eu.org). A set of indices follows the definitions recommended by the WMO CCl/CLIVAR Expert Team on Climate Change Detection and Indices (ETCCDI) was computed and analyzed in this paper. The CARPATCLIM dataset currently represents the most comprehensive, homogenized, and harmonized gridded dataset of daily in-situ data available for the Carpathian Region. It has been used to climate variability and trend studies (*Spinoni et al.,* 2015a) and drought investigations (*Spinoni et al.,* 2013) for instance. The Carpathian Region are subjected to climate change and also to weather-related extremes such extreme temperatures and heavy rainfall based on CARPATCLIM dataset (*Lakatos et al.,* 2013, *Spinoni et al.,* 2015b).

In the next sections, we describe the dataset and the method to derive grids of the different extremes indices and the analysis of this dataset over the Carpathian Region. After the introduction, the data and the definition of climate indicators are set up. Then, after the description of the trend estimation and the results showed on graphs and maps, a brief summary concludes the paper.

2. Data

Studying the spatio-temporal changes of climate extremes can be implemented through the analysis of observations reliable both in time and space. In this paper we used the CARPATCLIM (Climate of Carpathian Region & Digital Atlas of the Region) dataset for calculation of trends of several climate indicators to detect changes in temperature extremes in the Carpathian Region. As result of a Hungarian initiative on creation high quality dataset over the Carpathian Basin, the European Commission financed the CARPATCLIM project to supply the data demand of Joint Research Center (JRC) Desert Action activity (*JRC*, 2010). The consortium led by the Hungarian Meteorological Service together with 10 partner organizations from 9 countries in the Carpathian Region with the JRC created a multi-variable, gridded daily dataset.

The outcome of the CARPATCLIM project are 0.1°(~10 km×10 km) resolution homogenized, gridded daily time series of various meteorological parameters from January 1, 1961 to December 31, 2010. The target area is partly includes the territory of the Czech Republic, Slovakia, Poland, Ukraine, Romania, Serbia, Croatia, Austria, and Hungary (*Fig. 1*).

The method and software used for data quality control, homogenization, data completion, and data harmonization was the Multiple Analysis of Series for Homogenization software (MASH version 3.03; *Szentimrey* 1999, 2008, 2011). Interpolation of the homogenized time series were carried out by applying the MISH (Meteorological Interpolation Based on Surface Homogenized Data Basis version 1.03; *Szentimrey* and *Bihari*, 2007) method. The complete procedure is described in details in the project deliverables which can be found on the website of the project: www.carpatclim-eu.org/pages/deliverables/ and *Spinoni et al.* (2015a).

The final outcome of the CARPATCLIM are quality controlled, homogenized, in-situ daily time series and gridded fields along with metadata catalogue containing the documentation of the datasets. The daily grids with the metadata are freely accessible for scientific purposes on the website of the project: www.carpatclim-eu.org.

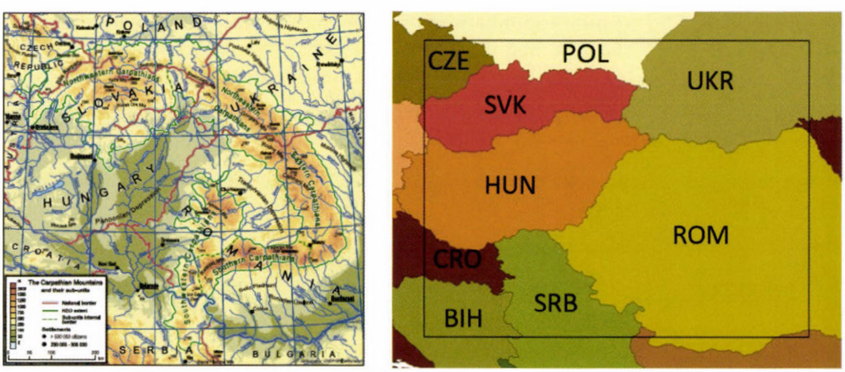

Fig. 1. The target area of the CARPATCLIM between latitudes 50°N and 44°N, and longitudes 17°E and 27°E approximately (left), and the political boundaries (right). (HUN: Hungary, SVK: Slovakia, CRO: Croatia, SRB: Serbia, ROM: Romania, UKR: Ukraine, BIH: Bosnia Hercegovina is not included in the project)

The preliminary analysis of the changes indicates that the temperature trend is variable in space in the Carpathian Region (*Spinoni et al.*, 2015a; *Lakatos et al.*, 2013). To do a further investigation into the spatio-temporal temperature trends in the Carpathian Region, we analyzed the trends of extreme temperature related indicators. Results are presentedin the next section.

3. Climate indices

The climate change indices (climate indicators) shown in this paper (*Table 1*) were calculated from the homogenized, gridded daily observations of maximum, minimum and daily average temperatures at each grid point of the region in question. We note that the daily average temperatures were derived as arithmetic means of homogenized daily maximum and minimum temperatures according to the CARPATCLIM consortium member's agreement (*CARPATCLIM Deliverable 3.7,* 2013). Percentile required for some of the temperature indices (*Table 1.*) were calculated for the climatological standard period 1961–1990.

Table 1. List of extreme temperature indices calculated and analyzed. Indices in bold represents those that are publically available in the CARPATCLIM dataset

Indicator name	Indicator definitions	Units
Cool nights TN10p	Cool nights when daily min temperature<10th percentile	days
Cool days TX10p	Cool days when daily max temperature<10th percentile %	days
Warm nights TN90p	Warm nights when daily min temperature>90th percentile %	days
Warm days TX90p	Warm days when daily max temperature>90th percentile %	days
Growing season length (5degree) GS5L*	**Annual count between first span of at least 6 days with TG>5 °C and first span after July 1 of 6 days with TG<5 °C (where TG is daily mean temperature)**	days
Growing season start (5degree) GS5Start	Daynumber at the end of the first span of at least 6 days with TG>5 °C (where TG is daily mean temperature)	daynumber
Growing season end (5degree) GS5End	Daynumber for the end of the last span of at least 6 days with TG>5 °C (where TG is daily mean temperature)	daynumber
Ice days ID	Annual count when daily maximum temperature<0°C	days
Severe cold days ECD	**Annual count when daily minimum temperature <–10 °C**	**days**
Frost days FD	**Annual count when daily minimum temperature <0 °C**	**days**
Summer days SU	**Annual count when daily max temperature >25 °C**	**days**
Hot days HD	**Hot days Annual count when daily max temperature >30 °C**	**days**
Extremely hot days EHD	**Annual count when daily max temperature >35 °C**	**days**
Warm spell duration WSDI	Annual count when at least six consecutive days of max temperature >90th percentile	days
Cold spell duration CSDI	Annual count when at least six consecutive days of min temperature <10th percentile	days

*Indices bolded are available on monthly and yearly scale in CARPATCLIM, except growing season length as it is available yearly

4. Trend estimation and results

The focus of this paper is to assess detailed regional changes of extreme temperatures in the Carpathian Region. The spatial high resolution of the gridded data can clearly highlight the regional trends. Linear trend was fitted to the indices series at each grid point, as it is widely used measure for presenting the changes. Although it is not certainly the best fit to the indices series, the results are comparable to other studies focusing on areas surrounding the Carpathian Region. Decadal changes of indices are shown on maps represent the 50 years period. The test of significance is based on student test (*Szentimrey*, 1989). Dots on maps indicates grid points where trends are significant at 5% significance level.

In this section the trend analysis for annual temperature indices are presented. The trends with their significance are featured on maps in some cases and in tables in other cases for space constraints, because all the indices were analyzed (*Table 1*). The time series plot of the indices supplemented occasionally by the 21-point smoothing functions (*Davis*, 1973) enables to demonstrate the decadal variations of the observed temperature extremes since the 1960's.

5. Annual indices

The temperature-related indices show significant warming trends widely in the Carpathian Region. Warming trends are generally stronger for indices derived from daily minimum temperature than for those derived from daily maximum temperature. This finding is in agreement with global studies, e.g., *Alexander et al.,* 2006 and *Donat et al.,* 2013.

For example, the frequency of cool nights (TN10p) (*Fig. 2a*) based on daily minimum temperatures is shown to have significantly decreased more than three-quarter to the region during the past 50 years from 1961 to 2010. The greatest magnitudes of the trends up to 8 days per decade are found over the bordering region of Ukraine and Romania, Poland, and fewer regions in Serbia. Regionally averaged the frequency of cool nights in the Carpathian Region has decreased by about a third (17 days) between the 1960s and the first decade of the 21st century (the average annual frequency during the 1961–1990 base period is by definition 53.3 days).

Correspondingly, the frequency of warm nights (TN90p) (*Fig. 2b*) in all grid points increased significantly. Regionally averaged, the frequency of warm nights has increased by about one and a half month (44 days) during the examined period (the average annual frequency during the base period is by definition 54.4 days). The strongest change occurred in the annual occurrence of warm nights (TN90p) among the temperature indices. The largest increasing is detected in wide regions in the territory of Serbia.

Examining daytime temperature extremes, the changes in cool days (TX10p) (*Fig. 2c*) and warm days (TX90p) (*Fig. 2d*) resulted in smaller variations compared to the cool and warm nights frequency changes. The trends of cool days are significant in the half of the Carpathian Region. The decrease is the highest between 4 and 5.3 days per decade, respectively, in the mid-Transdanubian regions and in the northern edge Hungary. Negative but non-significant change appears in the regions of the Pannonian Plain, the mountainous region in Romania, and the Romanian Plain. The warming trend results in more frequent warm days everywhere in the area. The warm days increasingly grow from northeast to southwest, by 40 days on average in the Carpathian Region.

Changes in percentile based indices seem to have occurred around the mid-1980s (*Fig. 3*). It denotes one decade lag to the mid-1970s, when the mean global temperature rise is reported (*Folland et al*, 2001).

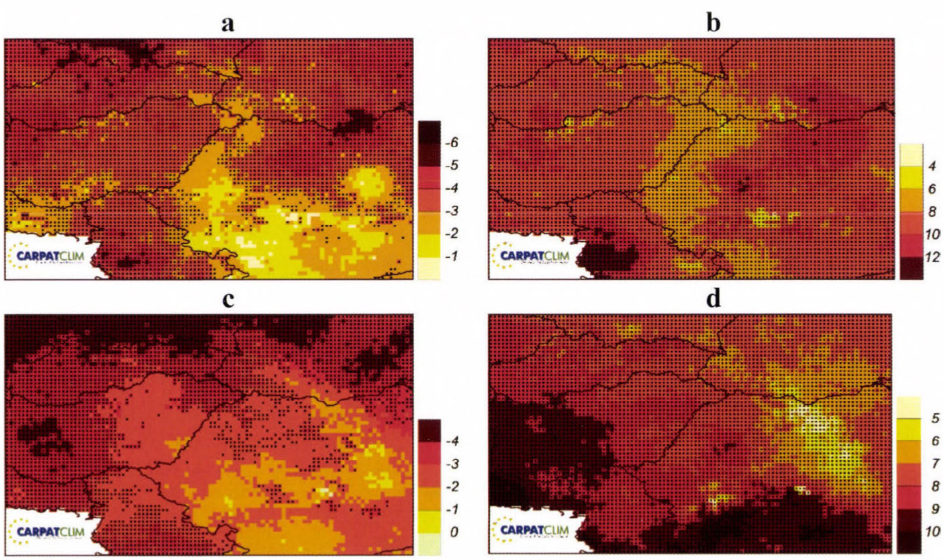

Fig. 2. Trends (in annual days per decade shown on maps) for annual series of percentile temperature indices for 1961–2010. (a) cool nights (TN10p), (b) warm nights (TN90p), (c) cool days (TX10p), (d) warm days (TX90p). Dots indicates regions where trends are significant at the 5% level.

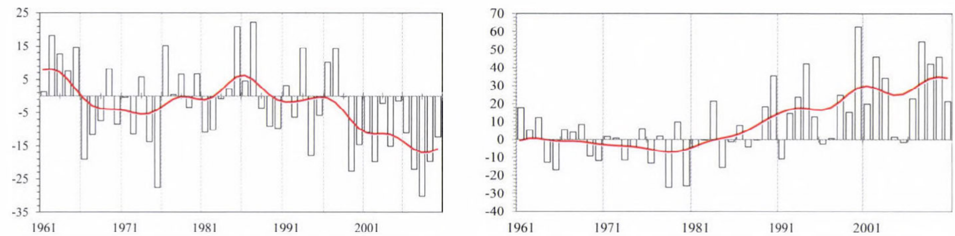

Fig. 3. The time series (columns) show the regional average annual values (in days per year) for cool nights (TN10p) (left) and warm days (TX90p) (right) as anomalies relative to the 1961–1990 mean values. The red line shows the 21-point Gaussian filtered data.

The effects of climate change clearly appear in agriculture and forestry in the region (*UNEP*, 2007). Production of these sectors is strongly influenced by the length of the growing season of the different species. Start date, end date, and the length of the vegetation period of the cold-tolerant (5 degree) species are investigated in this paper. *Fig. 4* shows that the growing season starts earlier, except for some sparsely located regions in higher elevation with statistically non-significant trend. Regions out of the Carpathians in Ukraine and Romania indicate either more than one month shift ahead. In the Transdanubian region in Hungary, in territory of Croatia and Serbia, the rowing season starts earlier, by 3 weeks in general.

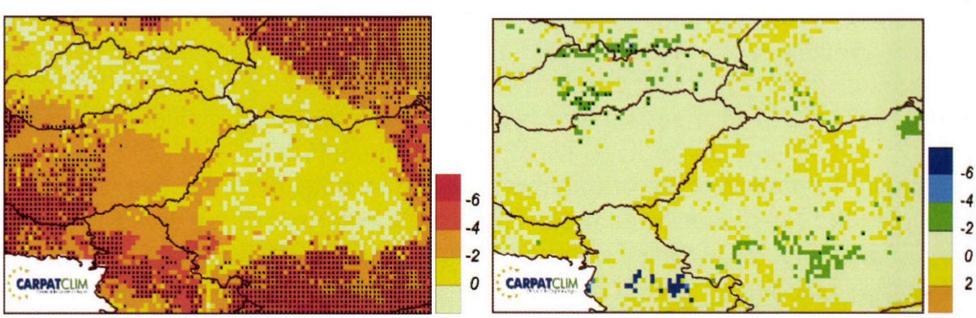

Fig. 4. Trends (in annual days per decade shown on maps) for annual series of growing season (5degree) start (GS5Start) (left) and growing season (5degree) end (GS5End) (right) for 1961–2010. Dots indicates regions where trends are significant at the 5% level.

The time series of the regionally averaged annual anomalies of growing season (5degree) start (GS5Start) show strong year by year variability (*Fig. 5*) of the starting date of the vegetation period. After tending towards to the earlier date to nighties, a slight increasing appear in the course. The years in the last decade of the 20th century put in the highest positive and negative anomalies.

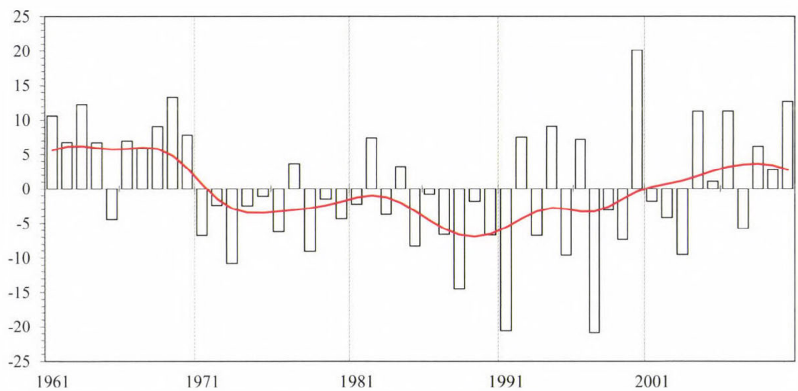

Fig 5. The time series (columns) show the regional average annual values (in days per year) for growing season (5degree) start (GS5Start) as anomalies relative to the 1961–1990 mean values. The red line shows the 21-point Gaussian filtered data.

The end of the 5°C vegetation period is not affected clearly by the warming tendency in the Carpathian Region (*Table 2*). The advanced start indicates longer growing season in the same but narrowed region as the GS5 significantly decreased (*Table 2*).

From the trend maps shown above, it can be seen that a wider area shows significant change in indices derived from minima than maxima. *Table 2* contains the areal average of the trend and the proportion of the area where the changes are significant by indices. The significantly increasing in warm nights and warm days show unanimously warming trend in the region. Significantly fewer cool days cases appear in more than a half part of the area, and less than a third part of the area non-significant change in cool nights cases. The growing season starts earlier in more than a third part of the region. The trend and proportion of the area that sign significant change of warm extremes strengthen the obvious warming in the Carpathian Region.

Table 2. Trends (in annual days per decade) for each index along with the percentage of grid points show either significant increase or decrease at the 5% level during the 1961–2010 period in the Carpathian Region

Indicator name	**Trend**	**Significant increase [%]**	**Significant decrease [%]**
Cool nights TN10p	–3.4	0	77.1
Cool days TX10p	–3.0	0	57.3
Warm nights TN90p	9.0	100	0
Warm days TX90p	8.1	100	0
Growing season length (5degree) GS5L	1.8	10.3	0
Growing season start (5degree) GS5Start	–2.5	0	30.3
Growing season end (5degree) GS5End	–0.7	0	0.7
Ice days ID	–1.8	0	16.7
Severe cold days ECD	–1.4	0	22.0
Frost days FD	–2.5	0	38.7
Summer days SU	3.7	97.9	0
Hot days HD	2.5	89.6	0
Extremely hot days EHD	1.4	40.0	0
Warm spell duration WSDI	4.1	96.1	0
Cold spell duration CSDI	–3.6	0	9.9

6. Conclusion

The focus of this paper was to assess detailed regional changes of extreme temperatures in the Carpathian Region. The CARPATCLIM dataset currently represents the most harmonized and comprehensive gridded dataset of several climate variables based on in situ observations in the Carpathian Region. A 15 pieces set of indices follows the definitions recommended by the WMO CCl/CLIVAR Expert Team on Climate Change Detection and Indices (ETCCDI) was computed and analyzed in this paper. Decadal changes and significance of indices are shown on maps represent the 50 years period, from 1961 to 2010.

According to our analyses, changes in cool nights and warm days have occurred around the mid-1980s according to the time series of areal averages of the indices. The significant increase in warm nights and warm days show unanimously warming trend in the region. Significantly fewer cool days cases appear in more than a half part of the area, and less than a third part of the area shows non-significant change in cool nights cases. The growing season starts earlier in more than third part of the region. In general, trends are stronger for indices derived from daily minimum temperature than for those derived from daily maximum temperature. The trends of the annual extreme temperature indices strengthened that the warming signal is obvious over the Carpathian Region. This type of study dealing with the investigation of climate extremes, observed trends, changes in frequency and intensity could contribute to the establishment of the adaptation strategies in the region. The seasonal changes of the temperature extremes and precipitations are also affect the natural ecosystems, agriculture, and the human health in the region. Our futher analyses will focus on those aspects.

References

Alexander, L.V., Zhang, X., Peterson, T.C.,. Caesar, J., Gleason, B., Klein Tank, A.M.G., Haylock, M., Collins, D., Trewin, B., Rahimzadeh, F., Tagipour, A., Rupa Kumar, K., Revadekar, J., Griffiths, G., Vincent, L., Stephenson, D.B., Burn, J., Aguilar, E., Brunet, M., Taylor, M., New, M., Zhai, P., Rusticucci, M., and *Vazquez-Aguirre, J.L.,*2006: Global observed changes in daily climate extremes of temperature and precipitation. *J. Geophys. Res. 111*, D05109.

CARPATCLIM Deliverable 3.7, 2013: http://www.carpatclim-eu.org/docs/deliverables/D3_7.pdf

Davis, J.C., 1973. Statistics and Data Analysis in Geology. Wiley International Edition, John Wiley & Sons, Inc., New York, 550 pp.

Donat, M.G., Alexander, L.V., Yang, H., Durre, I., Vose, R., Dunn, R.J.H., Willett, K.M., Aguilar, E., Brunet, M., Caesar, J., Hewitson, B., Jack, C., Klein Tank, A.M.G., Kruger, A.C., Marengo, J., Peterson, T.C., Renom, M., Oria Rojas, C., Rusticucci, M., Salinger, J., Elrayah, A.S., Sekele, S.S., Srivastava, A.K., Trewin, B., Villarroel, C., Vincent, L.A., Zhai, P., Zhang, X. and *Kitching, S.,*2013: Updated analysis of temperature and precipitation extreme indices since the beginning of the twentieth century: The HadEX2 dataset. *J. Geophys. Res. 118*, 2098–2118.

Easterling, D.R., Meehl, G.A., Parmesan, C., Changnon, S..A, Karl, T.R., and *Mearns, L.O.*, 2000: Climate extremes: observations, modeling and impacts. *Science 289*, 2068–2074.

Folland, C.K., et al., 2001: Observed variability and change. In (Eds.: *Houghton, J.T. et al.*) Climate Change 2001: The Scientific Basis. Contribution of Working Group I to the Third Assessment Report of the Intergovernmental Panel on Climate Change. Cambridge University Press, Cambridge, United Kingdom and New York, NY, USA.

IPCC, 2014: Climate Change 2014: Synthesis Report. Contribution of Working Groups I, II and III to the Fifth Assessment Report of the Intergovernmental Panel on Climate Change [Core Writing Team, *Pachauri, R.K.* and *Meyer, L.A.* (eds.)]. IPCC, Geneva, Switzerland.

JRC, 2010: Climate of the Carpathian Region. Technical Specifications (Contract Notice OJEU 2010/S 110-166082 dated 9 June 2010).

Klein Tank, A.M.G. and *Konnen, G.P.*, 2003. Trends in indices of daily temperature and precipitation extremes in Europe, 1946-99. *J. Climate. 16*, 3665–3680.

Lakatos, M., Szentimrey, T., Bihari, Z., and *Szalai, S.,* 2013: Creation of a homogenized climate database for the Carpathian region by applying the MASH procedure and the preliminary analysis of the data. *Időjárás 117*, 143–158.

Moberg, A., Jones, P.D., Lister, D., Walther, A., Brunet, M., Jacobeit, J., Alexander, L.V., Della-Marta, P.M., Luterbacher, J., Yiou, P., Chen, D., Klein Tank, A.M.G., Saladie, O., Sigro J., Aguilar, E., Alexandersson, H., Almarza, C., Auer, I., Barriendos, M., Begert, M., Bergström, H., Böhm, R., Butler, C.J., Caesar, J., Drebs, A., Founda, D., Gerstengarbe, F.-W., Micela, G., Maugeri, M., Österle, H., Pandzic, K., Petrakis, M., Srnec, L., Tolasz, R., Tuomenvirta, H., Werner, P.C., Linderholm, H., Philipp, A., Wanner, H., and *Xoplaki, E.,* 2006: Indices for daily temperature and precipitation extremes in Europe analyzed for the period 1901–2000. *J. Geophys. Res. 111,* D22106.

Seneviratne, S.I., Nicholls, N., Easterling, D., Goodess, C.M., Kanae, S., Kossin, J., Luo, Y., Marengo, J., McInnes, K., Rahimi, M., Reichstein, M., Sorteberg, A., Vera, C., Zhang, X., 2012: Changes in climate extremes and their impacts on the natural physical environment. In (eds.: *Field, C.B., Barros, V., Stocker, T.F., Qin, D., Dokken, D.J., Ebi, K.L., Ma strandrea, M.D., Mach, K.J., Plattner, G- K., Allen, S.K., Tignor, M.*, and *Midgley, P.M.*) Managing the Risks of Extreme Events and Disasters to Advance Climate Change Adaptation. Cambridge University Press, Cambridge, 109–230.

Spinoni, J., Antofie, T., Barbosa, P., Bihari, Z., Lakatos, M., Szalai, S., Szentimrey, T., and *Vogt, J.V.*, 2013: An overview of drought events in the Carpathian Region in 1961–2010. *Adv. Sci. Res. 10*, 21–32.

Spinoni, J., Szalai, S., Szentimrey, T., Lakatos, M., Bihari, Z., Nagy, A., Németh, Á., Kovács, T., Mihic, D., Dacic, M., Petrovic, P., Kržic, A., Hiebl, J., Auer, I., Milkovic, J.,Štepánek, P., Zahradnícek, P., Kilar, P., Limanowka, D., Pyrc, R., Cheval, S., Birsan, M.V., Dumitrescu, A., Deak, G., Matei, M., Antolovic, I., Nejedlik, P., ŠtastnÃ¡, P., Kajaba,P., Bochnícek, O., Galo, D., Mikulová, K., Nabyvanets, Y., Skrynyk, O., Krakovska, S.,Gnatiuk, N., Tolasz, R., Antofie, T. and *Vogt, J.*, 2015a: Climate of the Carpathian Region in the period 1961–2010: climatologies and trends of 10 variables. Int. J. Climatol. 35, 1322-1341.

Spinoni, J., Lakatos, M., Szentimrey, T., Bihari, Z., Szalai, S., Vogt, J. and *Antofie, T.*, 2015b: Heat and cold waves trends in the Carpathian Region from 1961 to 2010. *Int. J. Climatol. 35*, 4197–4209.

Szentimrey, T., 1989: A lineáris analitikus trendvizsgálat néhány elvi-módszertani kérdése. *Időjárás 93*, 151–156. (in Hungarian)

Szentimrey, T., 1999: Multiple Analysis of Series for Homogenization (MASH). Proceedings of the Second Seminar for Homogenization of Surface Climatological Data, Budapest, Hungary; WMO, WCDMP-No. 41, 27–46.

Szentimrey, T. and *Bihari, Z.*, 2007: Mathematical background of the spatial interpolation methods and the software MISH (Meteorological Interpolation based on Surface Homogenized Data Basis). Proceedings from the Conference on Spatial Interpolation in Climatology and Meteorology, Budapest, Hungary, 2004, COST Action 719, COST Office, 17–27.

Szentimrey, T., 2008: Development of MASH homogenization procedure for daily data. Proceedings of the Fifth Seminar for Homogenization and Quality Control in Climatological Databases, Budapest, 2006; WCDMP-No. 71, WMO/TD-NO. 1493, 2008, 123–130.

Szentimrey, T., 2011: Manual of homogenization software MASHv3.03. Hungarian Meteorological Service.

UNEP, 2007: Carpathians Environment Outlook. Geneva. http://www.grid.unep.ch.

IDŐJÁRÁS

Quarterly Journal of the Hungarian Meteorological Service
Vol. 120, No. 1, January – March, 2016, pp. 53–71

Analysis of climate change influences on the wind characteristics in Hungary

Csilla Péliné Németh[1*], **Judit Bartholy**[2], **Rita Pongrácz**[2], and **Kornélia Radics**[3]

[1]*Geoinformation Service of the Hungarian Defence Forces*
Szilágyi Erzsébet fasor 7–9., H-1024 Budapest, Hungary

[2]*Department of Meteorology, Eötvös Loránd University*
Pázmány Péter sétány 1/A, H-1117 Budapest, Hungary

[3]*Hungarian Meteorological Service*
Kitaibel Pál u. 1, H-1024 Budapest, Hungary

**Corresponding author E-mail: pelinenemeth.csilla@mhtehi.gov.hu*

(Manuscript received in final form July 3, 2015)

Abstract—Due to intense human presence and various anthropogenic activities, global climate change has been detected. Increasing temperature values and an overall warming are projected, which will certainly affect the global circulation patterns and regional climatic conditions throughout Europe. As an indirect consequence, global warming may also alter the wind conditions in the Carpathian Basin. In order to provide reliable projections for the future, the first task is to analyze wind climatology of the recent past using various tools from mathematical statistics.

In this paper, detailed analysis of observed wind fields, trends of different percentiles, return values, wind related climate indices, and their spatial distributions are discussed over Hungary using the homogenized Hungarian synoptic data sets and the homogenized and gridded CARPATCLIM database. Wind related climate indices are defined to evaluate the frequency occurrence and the trend of moderate and strong wind days at the stations in the last few decades. The annual daily maxima of wind speed and wind gust are determined on the basis of available time series fitted to the generalized extreme value distribution at every station and grid cell. 50-year and 100-year return values are estimated from these fitted distributions.

In addition, simulated wind climate variability is evaluated for the future periods of 2021–2050 and 2071–2100 relative to the 1961–1990 reference period. Since projected wind speed is highly overestimated by the simulation of the regional climate model RegCM for the reference period (1961–1990), a bias correction is necessary to apply to the raw simulated wind data using CARPATCLIM as a reference database. The bias correction method is based on fitting the empirical cumulative density functions of simulated daily time series to the observations for each gridcell using monthly multiplicative correction factors.

Key-words: Hungarian wind climate, extremes, homogeneity, CARPATCLIM, RegCM climate model

1. Introduction

Based on the observations, global climate change has reduced the Pole to Equator temperature gradient, which certainly affects the large scale circulation as well as regional climatic conditions. Besides the changes of mean climatic values, the entire distribution is changing, thus influencing intensity and frequency of climate extremes (*AghaKouchak et al.*, 2012). Various physical processes in the atmosphere lead to extreme values of meteorological elements. Weather and climate extremes (e.g., heat waves, extreme cold/hot conditions, too little/excessive precipitation, extreme winds) may especially affect exposed and vulnerable human and natural systems, therefore, development of appropriate action plans need detailed information on the past and future changes of extremes. It is essential to understand how and why climate extremes have changed recently, and how they will likely to change in the future.

Mid-latitude wind climate can be mainly determined by considering cyclogenesis processes and track analysis of high and low pressure systems over the continent. The surface winds are often depending on local conditions such as topography, geographical location, distance from large water bodies, and differential surface heating (*Oliver*, 2005). Examples of specific local wind include land/sea breeze, mountain/valley breeze, foehn winds formed by pressure or temperature gradient force. Moreover, local wind and instability can also be originated from (dust) storms.

Regional and local wind climate have direct effects on human activity, for instance, on aviation, urban planning (via impact on building design and air pollution), industry, energy sector, military operations, etc. Therefore, researchers, engineers, architects, designers need information about local wind climate as fine as possible. In most of the cases, their tasks and duties are strongly connected to appropriate analysis of meteorological and climatic problems, or they need to apply results of the analysis of regional or local wind fields to more specific, further impact studies. Moreover, many practical and theoretical problems in meteorology and climatology require accurate measurements of wind speed, direction, and gust. In order to ensure high quality of meteorological measurement systems, standards of measurements have been set by the World Meteorological Organization (WMO). Wind speeds are measured as 10-minute averages, wind gusts are the maximum speeds recorded within the 10-minute averages' period (*WMO*, 2008). The standard exposure height is 10 meter.

Direct wind climatological analysis of changes is hampered by the lack of several-decades-long, good quality, and homogeneous surface wind observations. Homogeneity of climate data is especially important when analyzing extremes, especially, at fine spatial scale. A climatological time series can be considered homogeneous if its variability is solely caused by changes in weather and climatic conditions (*Aguilar et al.*, 2005). However, wind as a meteorological element is especially sensitive to uncertainties caused by relatively small changes related to the measuring process, in the vicinity of the measuring equipment. For example, installation of a small building or changes in vegetation cover near the measuring equipment, or changes in instrumentation and measuring methods can produce bias in wind measurements (*Wan et al.*, 2010). When such a change occurs, it can result a discontinuity in the time series or a false trend (*Menne* and *Williams Jr.*, 2009). Therefore, quality control and homogenizing of available daily wind speed and wind gust data sets (1975–2012) were completed (*Péliné et al.*, 2014) in order to assess Hungarian wind climate trends, variability, frequency, and intensity of extreme wind events as reliable as possible. For this purpose, the MASH (Multiple Analysis of Series for Homogenization) procedure developed at the Hungarian Meteorological Service (*Szentimrey,* 1999) was applied to homogenize 19 Hungarian stations' daily wind speed and wind gust data sets.

The word "extreme" refers to many different issues in the climate research literature, so there is no unique, precise climatological definition of an extreme (*Stephenson*, 2008). For instance, extreme may be associated to a climate variable or an impact of specific climatic conditions. In the case of a climate variable (e.g., temperature, precipitation, wind speed, etc.), extremes can be well defined as a rarely occurring value, i.e., with small probability, in the tail of the probability density function ($f(x)$) of the given climate variable. In the case of an impact, an extreme can be less well defined, since quantity of impacts cannot be described in a unique way. It is important to mention that on one hand, rare events (e.g., tornado) may not necessarily cause damage, and their impact does not always lead to a disaster; on the other hand, non-extreme events (e.g., strong wind or regularly occurring storm) may cause devastating effects and severe damages in the environment. In this paper, we are focusing on the analysis of climate variables themselves.

Based on the Special Report on Managing the Risks of Extreme Events and Disasters to Advance Climate Change Adaptation (SREX) published by the International Panel on Climate Change (*IPCC*, 2012), extreme weather or climate events are the occurrence of a value of a weather or climate variable above (or below) a threshold value near the upper (or lower) ends of the range of observed values of the variable. For simplicity, both extreme weather events and extreme climate events are often referred to collectively as 'climate extremes' (*Seneviratne et al.*, 2012). They can be defined quantitatively in two ways: (1) related to their probability of occurrence, e.g., percentiles and return frequencies, (2) related to a specific (possibly impact-related) threshold.

Although the wind speed value itself is rarely used to define extreme events (e.g., mesoscale convective complex, cyclone, thunderstorm, squall lines, etc.) (*Peterson et al.*, 2008), wind speed thresholds may be used to characterize the severity of the phenomenon (e.g., the Saffir-Simpson scale for tropical cyclones). Changes in wind extremes may be resulted from changes in the intensity or location of their associated phenomena (e.g., change in local convective activity) or from other changes in the climate system such as the movement of large-scale circulation patterns (*IPCC*, 2012). Wind extremes may be described by a range of daily/monthly/yearly quantities such as high percentiles, maxima, or wind-related climate indices after checking data series for homogeneity.

Our main aim is to analyze the wind climate in Hungary, specifically, to estimate temporal and spatial distributions of mean and extreme wind speed. For this purpose, different percentile values and their trends are calculated, moreover, return values and wind-related climate indices are determined using observed (station and gridded) and projected (from climate model simulation) data sets.

2. Applied data and methodology

2.1. Applied statistical distributions

For the sake of practical simplicity and to reduce complex characteristics of time series during the analysis, data distributions are often estimated by mathematical functions that depend on a few parameters only, so the analysis task is simplified to estimation of these parameters.

The special cases of the three-parameter generalized extreme value (GEV) or Fisher-Tippet distribution (*Palutikof et al.*, 1999) is widely used in meteorology, which includes Gumbel (type 1), Frechet (type 2), and Weibull (type 3) distributions. Distribution of averaged wind speed (with averaging period of 10 min) may be estimated by the two-parameter Weibull distribution, whereas distribution of maximum wind speed during a given period can be described by Gumbel distribution (*Wilks*, 2006).

The Weibull distribution is governed by two parameters, i.e., a scale factor (λ [m/s], being proportional to the mean wind speed), and a form factor or shape parameter (k [dimensionless], describing the shape of the distribution).

The Weibull distribution function $F(u)$ can be written as follows:

$$F(u) = 1 - \exp\left(1 - \left(\frac{u}{\lambda}\right)^k\right), \tag{1}$$

where u is the wind speed with an averaging period of 10 min, λ is the scale factor, and k is the shape parameter.

From this, the Weibull probability density function $f(u)$ can be expressed as follows:

$$f(u) = k \cdot \left(\frac{u^{k-1}}{\lambda^k}\right) \cdot \exp\left(-\left(\frac{u}{\lambda}\right)^k\right). \tag{2}$$

Average wind speed $[\bar{u}]$ of the whole analyzed period can be described by the Weibull parameters using Gamma function (Γ) as follows:

$$[\bar{u}] = \lambda \cdot \Gamma\left(1 + \frac{1}{k}\right), \tag{3}$$

$$\Gamma(x) = \int_0^\infty e^{-u} u^{x-1}\, du. \tag{4}$$

For k=1 and 2, the Weibull distribution is identical to the exponential and Rayleigh distribution, respectively. For k=3.4, the Weibull distribution is similar to the Gaussian distribution (*Wilks*, 2006; *Emeis*, 2013).

Wind speed extremes can be characterized with estimation of high percentiles, wind speed related climate indices, and return values using different specific periods. The return value is a threshold value, which can be defined by a fitted model (*von Storch* and *Zwiers*, 1999). The value of the analyzed variable may occur or be exceeded once on average during the specific return period.

The probability of occurrence of extreme values can be described by a Gumbel distribution (*Gumbel*, 1958). Probability density function $f(x)$ and cumulative frequency distribution function $F(x)$ are expressed in Eqs. (5) and (6), respectively:

$$f(x) = e^{-x} e^{-e^{-x}}, \tag{5}$$

$$F(x) = e^{-e^{-x}}. \tag{6}$$

For estimation of return values, the inverse of Eq.(6) should be calculated (*Emeis*, 2013), which is the following percentile function $G(p)$:

$$G(p) = -\ln\left(-\ln(p)\right). \tag{7}$$

In practice, independent maxima of the time series (for example, yearly maxima of wind speed or wind gust) are sorted in ascending order, then, these sorted values are plotted against $G(p)$. Data, which follow a Gumbel distribution form a straight line, in conformity with its definition. Estimations of return values for specific return periods (e.g., 50 years or 100 years) are quite straightforward by using this graph. The extreme value expected to occur once in 50 years or 100 years can be calculated from the equation of the fitted extrapolated straight line ($u_{max} = a \cdot (-\ln(-\ln(p))) + b$). For example, if the return period $T = 100$ years then the probability of occurrence $p = \frac{1}{T} = 0.01$ in any particular year within this entire period, thus, $G(p = 0.99) = 4.6$, and the return value (u_{max}) can be calculated from the equation of the fitted linear line.

The probability for the 100-year return value to appear in a chosen 100-year period is $P = 1 - 0.99^{100} = 0.634$.

2.2. *Wind indices*

In order to analyze the extreme wind characteristics, climate indices can be used. Similarly to the widely used temperature and precipitation related climate indices (e.g., *Bartholy* and *Pongrácz*, 2007), wind related climate indices are defined in this study. They consider daily average wind speed as well as daily maximum wind gust values. Three types of indices are used here: (i) the number of days above or below a certain threshold value, (ii) the number of periods of consecutive days above or below these thresholds, and (iii) the maximum length of these periods. The applied time frame includes yearly, seasonal, and monthly basis. *Table 1* summarizes the indices evaluated in this paper.

Table 1. List of used wind related climate indices, their definitions and units.

No.	Index	Definition	Unit
1–3	wavgGTXX	Yearly/seasonal/monthly number of days with average wind speed exceeding XX m/s; v_{avg} > XX m/s, where XX = 15, 10, 8	days
4–6	wavgLTXX	Yearly/seasonal/monthly number of days with average wind speed below XX m/s; v_{avg} < XX m/s, where XX = 1, 3, 5	days
7–9	CwXXD	Yearly/seasonal/monthly number of periods of consecutive days with daily average wind speed exceeding XX m/s, where XX = 15, 10, 8	–
10–12	CwXXD	Yearly/seasonal/monthly number of periods of consecutive days with daily average wind speed below XX m/s, where XX = 1, 3, 5	–
13–15	CwXXDmax	Yearly/seasonal/monthly number of maximum consecutive days with daily average wind speed exceeding XX m/s, where XX = 15, 10, 8	days
16–18	CwXXDmax	Yearly/seasonal/monthly number of maximum consecutive days with daily average wind speed below XX m/s, where XX = 1, 3, 5	days
19–23	CgXXD	Yearly/seasonal/monthly number of periods of consecutive days with daily maximum wind gust exceeding XX m/s, where XX = 15, 20, 25, 30, 35	–
24–29	GustGTXX	Yearly/seasonal/monthly number of days with daily maximum wind gust exceeding XX m/s; v_{gust} > XX m/s, where XX = 15, 20, 25, 30, 35	days

2.3. *Bias corrected outputs of RegCM regional climate model*

In order to estimate the future changes in wind related climate extremes, regional climate model outputs serve as the basis. For this purpose, simulation of the RegCM regional climate model (*Torma et al.*, 2008, 2011) is used in this paper. For the reference period (1961–1990), model outputs overestimate the average wind speed for the Carpathian Basin. The overestimation of the yearly average wind speed is about 2 m/s, and the seasonal overestimation is the highest in winter (2.6 m/s in the gridcell centering 47.5°N and 19°E, which represent the Budapest agglomeration area). Therefore, simulated wind data should be bias-corrected for assessing extreme wind conditions as realistic as possible.

The probability density function (PDF) or the cumulative density function (CDF) describe completely the statistical properties of a dataset. If two data sets results in the same PDF or CDF then they can be considered statistically identical. The applied correction method is based on the study of *Pongrácz et al.* (2014), which uses the differences of the monthly empirical CDFs of RegCM model outputs and CARPATCLIM gridded data sets for the reference period. First, multiplicative correction factors $f_{multiplicative}$ are calculated on a monthly basis for the past (i.e., 1961–1990):

$$f_{multiplicative} = \frac{F_{obs}^{-1}(y)}{F_{model}^{-1}(y)} = \frac{x_{obs}}{x_{model}}, \tag{8}$$

where the probability-quantile of observations is x_{obs} and the probability-quantile of raw simulated data is x_{model}. Thus, the raw model data with CDF value p is corrected, and it becomes equal to CDF value of the observations. Then, these calculated factors are applied to the future periods (2021–2050, 2071–2100).

3. Results

Homogenized wind speed (1975–2012) and wind gust (1975–2013) measurements, as well as homogenized and gridded data sets of the CARPATCLIM (1961–2010) database are analyzed in order to assess Hungarian wind climate trends, variability, frequency, and intensity of extreme wind events. Average yearly wind speed is modified significantly by a homogenization procedure (*Péliné et al.*, 2014). Consequently, the fitted linear trends of average and different percentile values also changed at many stations compared to those before the homogenization. These differences emphasize that inhomogeneities in climatological time series may lead to false values and misinterpretations of detected changes.

The generalized extreme value distribution is fitted to the annual maxima of wind speed at every station and all the CARPATCLIM grid points, which were used to estimate 50-year and 100-year return values. *Fig. 1* summarizes these return values for 19 Hungarian synoptic stations based on the data sets during 1975–2012. The smallest and the largest return values are about 10 m/s and 25 m/s at Paks and Siófok, respectively.

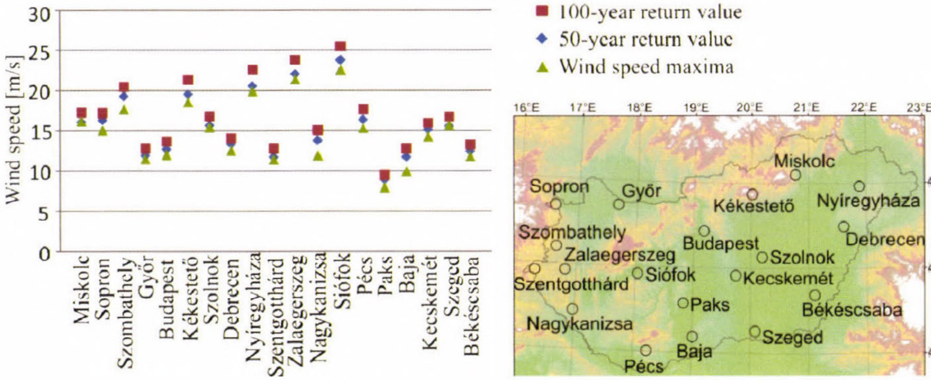

Fig. 1. Wind speed maxima and different return values [m/s] at the analyzed 19 stations calculated from 38-year time series (1975–2012).

In order to evaluate the spatial distributions of return values, gridded datasets can be used more efficiently. For this purpose, the quality-checked, homogenized, and interpolated gridded CARPATCLIM data series covering Hungary are used. *Fig. 2* shows both the 50-year and 100-year return values for the country, which result slight differences from the values calculated on the basis of station measurements. This is partially due to the fact, that daily wind speed of station data is calculated from at least eight measured data for a particular day, whereas CARPATCLIM daily 10-meter wind speed data sets have been created using three wind speed data (07, 14, and 21 UTC) from each day due to data availability for the whole period. (In the 1960's, data were recorded more rarely, in the 1960's than in the last few decades, so the night-time was less represented than nowadays).

Climate model experiments driven by gridded reanalysis fields (which are generated from measured and observed data) are essential, and provide important knowledge for modern climate research. However, the question arises how the different reanalysis data sets are reliable for estimation of wind climate parameters and validation of climate models. Global reanalysis data sets, i.e., ERA Interim, are used in our study, which is provided by the European Centre for Medium-Range Weather Forecasts (ECMWF) for researchers and climate modelers. ERA Interim is remarkably improved compared to the earlier ERA-40 reanalysis data sets (1957–2002) due to applied data assimilation methods and inclusion of more types of observations, e.g., satellite measurements (*Berrisford et al.*, 2009). In our study, datasets of wind components with fine resolution (0.50°) for the Carpathian Basin (45°–49.5°N and 15°–24°E) are analyzed for 1979–2012.

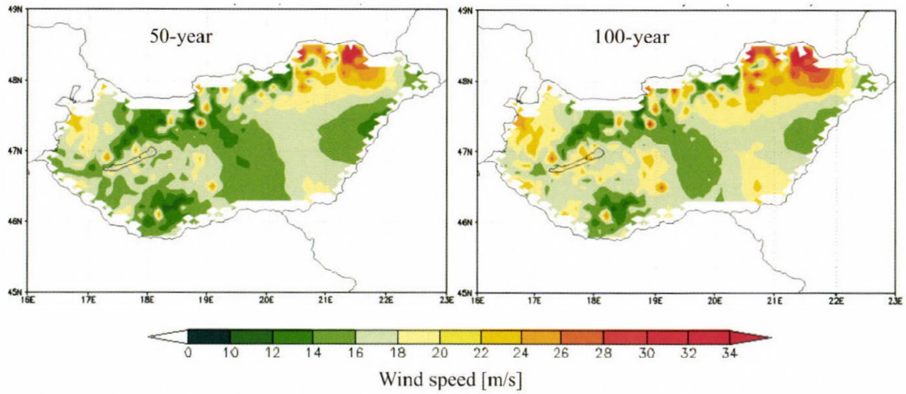

Fig. 2. 50-year and 100-year return values [m/s] calculated from CARPATCLIM data series (1961–2010).

Homogeneity of 10-meter daily average wind speed of 190 grid points of ERA Interim data sets is checked with MASH 3.03 software (*Szentimrey*, 2011) for the Carpathian Basin between 1979 and 2012. Results of homogenization proved that these gridded data series are homogeneous. Values of the applied test statistics for the characterization of inhomogeneity of time series were almost unchanged before and after homogenization and remained under the critical value (20.57; significance level: 0.05) at 72% of grid points. Values of yearly relative estimated inhomogeneity and yearly relative modification of time series differed from zero at 15% of all the grid points.

Weibull distributions are fitted in order to compare extremes of reanalysis and measured data series. Shape parameter (k) of the Weibull distribution describes frequencies of larger wind speeds. The larger the value of k, the smaller the variability of wind speed. Increasing scale parameter (λ) when constant shape parameter is assumed occurs as an elongation of the probability density function (pdf) along the abscissa with decrease and right-shift of the maxima of pdf (*Wilks*, 2006). Variability of scale parameter is smaller in ERA Interim grid points (3.06–3.83) compared to the synoptic stations (2.13–4.51). Values of the Weibull shape parameters of the reanalysis grid points are between 2.10 and 2.65, which are clearly larger than that is found in case of the stations data (1.38–2.16). This overestimation of the Weibull shape parameters reduces the variability of wind climatic conditions and the probability of extreme wind speed (*Rodrigo et al.*, 2013).

The main disadvantage of homogeneous gridded reanalysis data series is that spatial difference cannot be reproduced by reanalysis data unlike in case of station measurements. Monthly scale parameters of both station and gridded data averages are close in spring and summer, when regional differences are relatively small. The monthly average shape parameters are almost equal in June, however, in all the other months, overestimations are found at ERA Interim grid points compared to the station data.

Shape parameters are shown in *Fig. 3* as a function of scale parameter of the fitted Weibull distributions. Smaller shape parameter can occur in winter due to higher cyclone activity. Larger scale parameter was found in spring, when both the value and variability of monthly average wind speed are the largest. Average station shape parameters are generally overestimated by the average gridpoint shape parameters, similar conclusion is valid for the scale parameter. The only exception occurs in spring, when average station scale parameters are underestimated by the average gridpoint scale parameters. Because the scale parameter depends on wind speed, that is why the wind speed is overestimated, except in spring. The smallest differences (biases) of calculated parameters are observed in June and July.

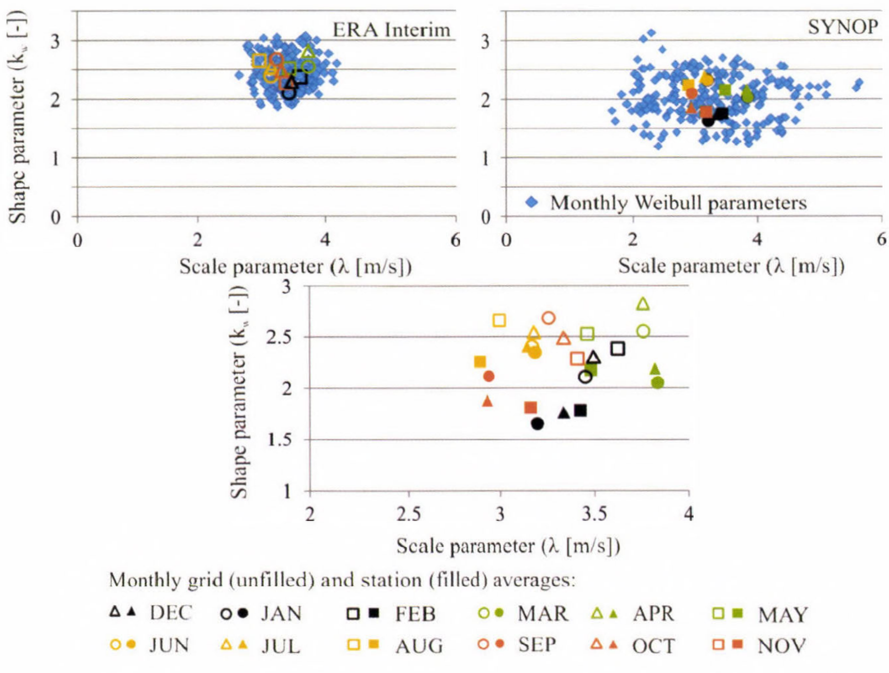

Fig. 3. Parameters of the Weibull distribution fitted to daily wind speed data series of grid points (upper left) and stations (upper right) in every month (blue) and in different seasons (winter – black, spring – green, summer – yellow, autumn – brown). Monthly grid (empty symbols) and station (filled symbols) averages are plotted in the lower diagram.

From the results discussed above, it can be concluded that significant differences exist between the statistical distributions of ERA Interim and synoptic station data, therefore, the further analysis of frequency occurrence, trend of moderate and strong wind days, and wind related indices are all based on more reliable measured data sets for Hungary.

Analysis of the indices listed in *Table 1* can answer whether the frequencies of windy, gusty days and calm periods have increased or decreased in the recent past. This is especially important from urban aspects, since air pollution in cities is a major environmental issue leading to many potential health problems.

Yearly number of days with average daily wind speed below 1 m/s, 3 m/s, and 5 m/s has increased during the analyzed period at most of the stations. Changes are statistically significant (on 0.05 confidence level) in all stations in case of 5 m/s (wavgLT5), and most of the stations in case of smaller thresholds (wavgLT1, wavgLT3). Yearly number of days with average wind speed exceeding 8 m/s has significantly decreased at every station, however, declining of the yearly number of stormy days (wind speed exceeding 15 m/s) is significant at four stations only (Szombathely, Szolnok, Zalaegerszeg, and Siófok).

Yearly number of periods of consecutive days (lasting 1–10 days) with daily average wind speed below 1 m/s (Cw1D) is shown in Fig. 4. These wind related climate indices decreased in Siófok for periods with different lengths, the longest recorded period lasted 10 days, which occurred in 1982. Increasing trends are found in Győr, which is in good agreement with the results of our previous analysis (*Péliné et al.*, 2014) concluding that the average wind speed declined at this station.

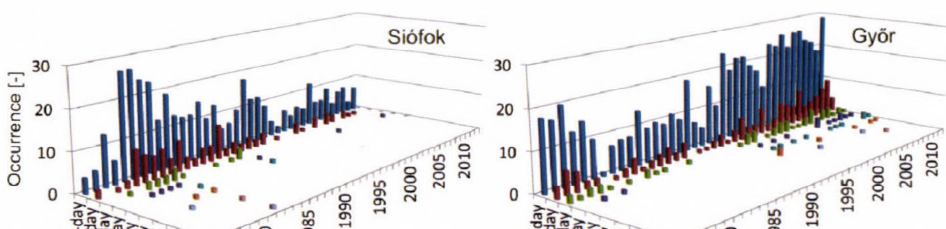

Fig. 4. Yearly Cw1D wind speed indices in Siófok and Győr calculated from homogenized data series.
Trend coefficients of the significant (confidence level: 0.05) changes are the following:
Siófok : 1-day: -0.31, 2-day: -0.12, 3-day: -0.04
Győr : 1-day: +0.41, 2-day: +0.12

Yearly numbers of maximum consecutive days below or above a certain daily average wind speed (below 1 m/s and 3 m/s, or above 8 m/s) are summed for all stations and for all years. Temporal changes of these cumulative indices are plotted in *Fig. 5*. Summed yearly numbers of maximum consecutive days below 3 m/s (above 8 m/s) wind speed, Cw3Dmax (Cw8Dmax) have increased (decreased) significantly, unlike Cw1Dmax, where the detected change is not significant.

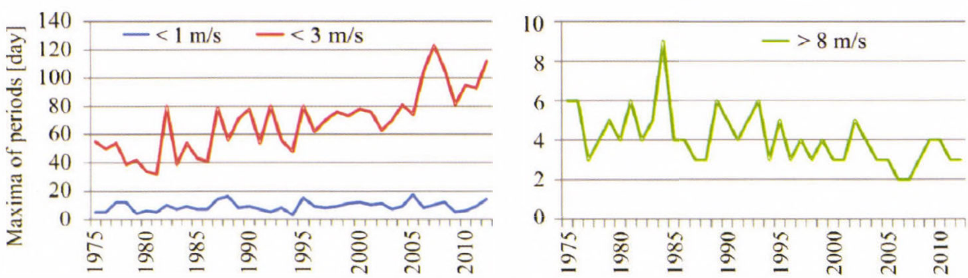

Fig. 5. Temporal changes of yearly Cw1Dmax, Cw3Dmax, and Cw8Dmax wind speed indices summed for all stations and calculated from homogenized data series.

Yearly and monthly number of days with daily maximum wind gust exceeding 15, 20, 25, 30, 35 m/s are calculated for every station from homogenized wind gust time series covering the time period 1975–2013. The temporal changes are estimated by fitting linear trends, for which the calculated trend coefficients are summarized in *Fig. 6*. Yearly trend coefficients of GustGT15 and GustGT20 indices are all negative in all stations, the decreasing trends are statistically significant (at 0.05 level). Due to the more rare occurrences of higher wind gusts, the trend coefficients tend not to be significant in case of GustGT25, GustGT30, and GustGT35. For instance, in case of the highest analyzed wind gust threshold (GustGT35), significant changes are found only at two stations (Miskolc and Zalaegerszeg).

In most of the months (from June to January, and also in April), decreasing trends can be detected at all the stations, similarly to the annual trends. Besides the general decreasing monthly trend coefficients, increasing monthly trends are also found at some stations in March. The lower graph of *Fig. 6* summarizes the linear trend coefficients for March. Overall, significant changes (with confidence level of 0.05) are found only at a few stations (Miskolc, Szentgothárd, Szolnok, Nyíregyháza, and Szombathely in case of different indices). Monthly trends are mostly small and not significant in February and May. However, all these results should be evaluated as a complex issue in the context of other wind-related climate indices. For instance, although the values of the rarely occurring GustGT25 index show increasing trend in March in Szombathely, most of the other wind-related indices (e.g., wavgGT8, wavgGT10, and wavgGT15) calculated from the daily average wind speed at this station have decreased significantly.

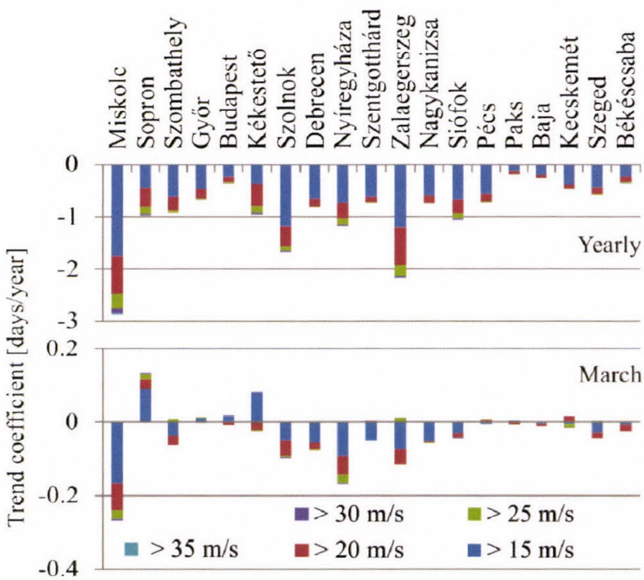

Fig. 6. Fitted linear trend coefficients of yearly (upper graph) and monthly (March, lower graph) number of days with daily maximum wind gust exceeding 15 m/s, 20 m/s, 25 m/s, 30 m/s, and 35 m/s wind gust at the analyzed stations calculated from homogenized data series (1975–2013).

Significant changes (confidence level: 0.05) are found in March as follows:

decreasing trend:	GustGT15: Miskolc, Szentgotthárd
	GustGT20: Miskolc, Szolnok
	GustGT25: Miskolc, Nyíregyháza
increasing trend:	GustGT25: Szombathely

In addition to the analysis of the recent past wind fields, the projected changes in the future are also important for possible impact analysis. For this purpose, simulated wind data are evaluated for the future periods of 2021–2050 and 2071–2100 relative to the 1961–1990 reference period.

First, validation of simulated data is illustrated for a selected gridpoint, located at 47.5°N and 19.0°E, which represents Budapest. Similarly to the other gridpoints within Hungary, the monthly mean wind speed calculated from CARPATCLIM data is overestimated substantially by the RegCM simulation in the 1961-1990 reference period (*Fig. 7*). The maximum and minimum bias of the monthly mean wind speed at this selected location is 2.7 m/s in January, and 0.8 m/s in June, respectively. The range of monthly wind speed biases changes with percentiles, in some months it reaches 4 m/s (*Fig. 8*). Percentile differences are the smallest in May and June, when small averaged differences (biases) of the calculated Weibull parameters have also been found between ERA Interim and observed data.

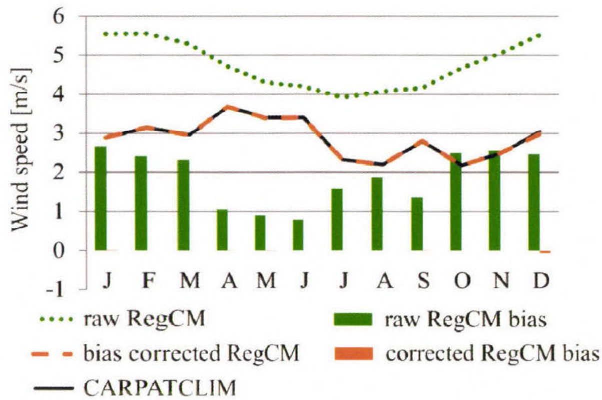

Fig. 7. Comparison of RegCM simulation and CARPATCLIM data: annual distribution of monthly mean wind speed (lines) and monthly mean wind speed bias (columns), for the gridpoint 47.5°N and 19.0°E, for the period 1961–1990.

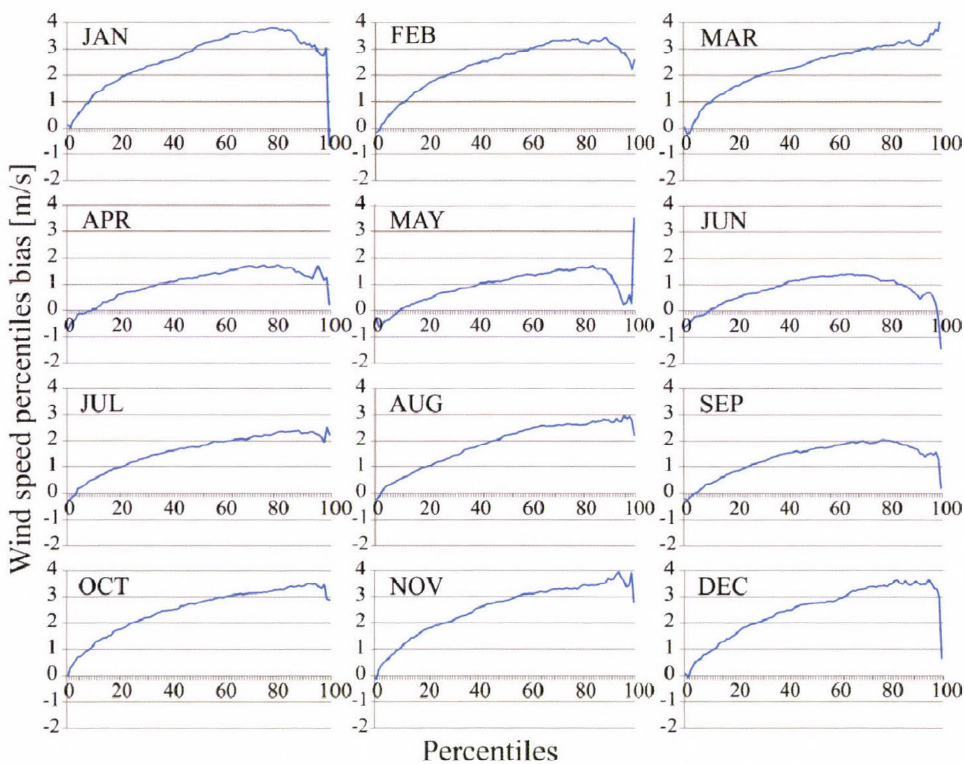

Fig. 8. Wind speed monthly percentiles biases calculated from differences of raw RegCM outputs (i.e., before completing any bias-correction) and CARPATCLIM for the gridpoint 47.5°N and 19.0°E covering the period 1961–1990.

Since projected wind speed is highly overestimated by the simulation of the regional climate model RegCM in the reference period (1961–1990), a bias correction is certainly necessary to apply to the raw simulated wind data using CARPATCLIM as a reference database. The bias correction method is based on fitting the empirical cumulative density functions of simulated daily time series to the observations for each gridcell using monthly multiplicative correction factors.

Fig. 9 compares the distributions of RegCM model outputs (raw and bias-corrected simulated wind data) to the CARPATCLIM wind data for the gridpoint 47.5°N and 19.0°E (representing Budapest) over the period 1961–1990. The charts clearly demonstrate that the differences between the two wind fields' distributions can be eliminated using the bias correction technique. (Similar good agreements are reached for each gridpoint.)

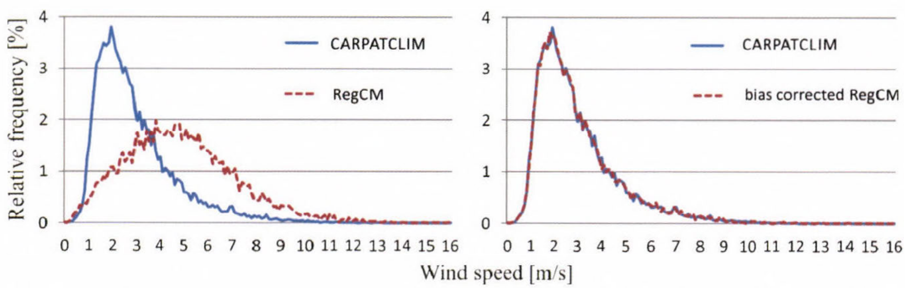

Fig. 9. Effect of bias correction of the simulated wind data. Comparison of relative frequencies of wind fields of CARPATCLIM to RegCM experiment for the period 1961–1990, for the gridpoint 47.5°N and 19°E, for raw simulated data (left) and bias-corrected data (right).

After determining the multiplicative correction factors on a monthly basis that correct the simulated wind speed of RegCM experiments, spatial distributions of the differences between the bias-corrected RegCM outputs and the CARPATCLIM wind speed data are calculated and mapped for different percentile values (0.50, 0.90, and 0.99) for the reference period 1961–1990, and for the projected periods (2021–2050 and 2071–2100). In case of the median and the upper decile (i.e., 0.50 and 0.90 percentiles, respectively), the difference in the reference period is less than 0.1 m/s in every gridcell for the whole year except in December, when the bias is between 0.1 m/s and 0.2 m/s. In the tail of the distribution larger differences can be found, for example, in case of the 0.99 percentile, the difference is reaching 1 m/s in some gridpoints (the monthly average difference value for all the percentiles is –0.04 m/s in the selected gridpoint in December).

For the evaluation of the projected climate change, bias-corrected RegCM outputs are used. Projected mean and extreme changes of wind conditions are analyzed. Differences between the future and past bias-corrected RegCM wind speed fields are mapped (*Fig. 10*) for different percentile values (0.90 and 0.99) for both analyzed future periods.

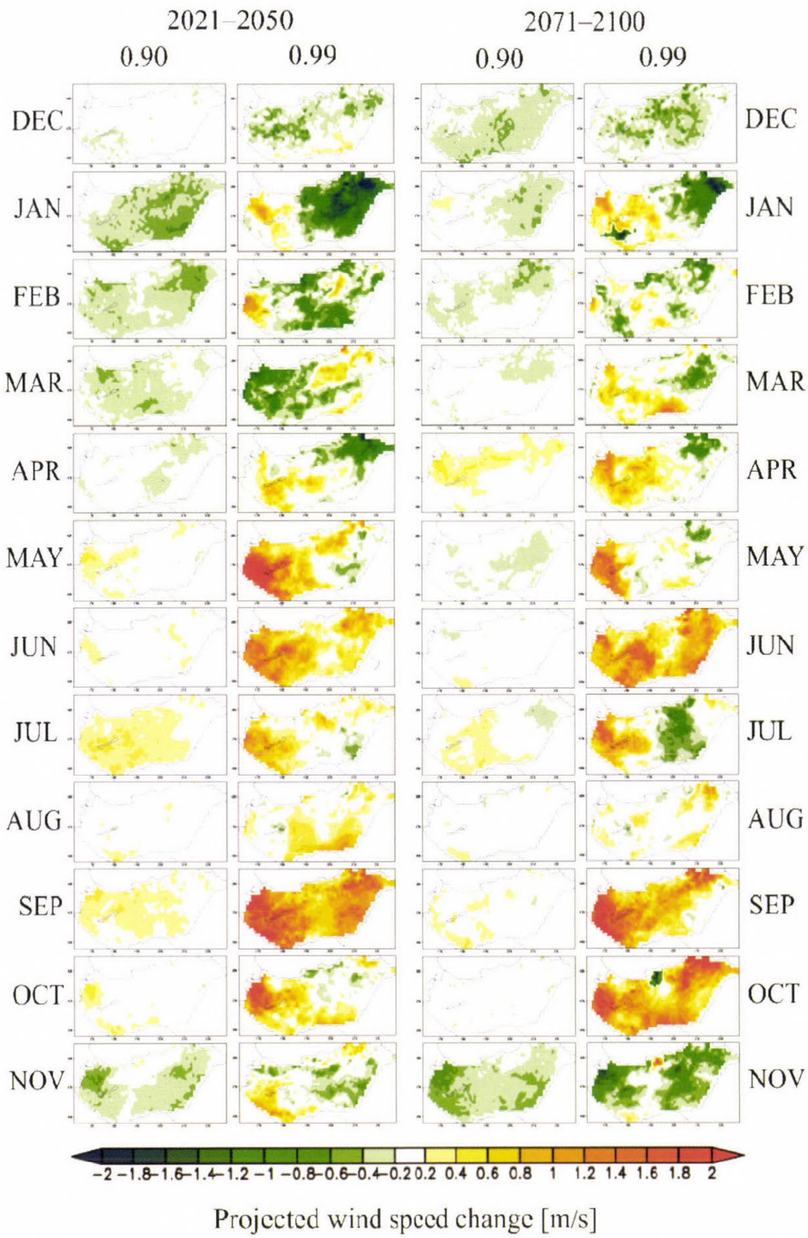

Fig. 10. Spatial distributions of the projected monthly mean changes of the 0.90 and 0.99 percentile values calculated from the bias-corrected RegCM wind speed data for the future periods (2021–2050 and 2071–2100).

Projected monthly changes in the 0.90 percentile are relatively small (the maximum is 0.6 m/s) for both periods, whereas changes in the 0.99 percentile values are projected to exceed 2 m/s in several regions in the country. Differences of the medians do not exceed 0.4 m/s.

4. Summary and conclusions

Our analysis of homogenized observed station and gridded wind data show overall decrease in the annual mean wind speed, which is consistent with the reduced Pole to Equator meridional temperature gradient in a warmer globe. Similar decreasing trend is also concluded by *Spinoni et al.* (2014) using CARPATCLIM data sets wind speed decrease in every season in Hungary.

Our results can be summarized as follows.

(1) Comparison of the raw and homogenized wind speed (1975–2012) and wind gust (1975–2013) measurements leads to different results, which highlight that inhomogeneities may mislead our conclusions.

(2) Wind climate extremes can be described by a range of daily/monthly/yearly quantities such as high percentiles, maxima, return values, and wind indices. For instance, overestimation of the Weibull shape parameters in ERA Interim reanalysis data (1979–2012) compared to synoptic stations reduces the variability of wind conditions and the probability of extreme wind speed. That is why the use of homogenous, quality-controlled, and reliable (measured) data series are essential when completing a reliable wind climatological analysis with special focus on extremes.

(3) GEV distributions are fitted to the annual daily maxima of wind speed at all the measuring stations and all the grid points of CARPATCLIM (1961–2010) database, which are used to estimate 50-year and 100-year return values. The return values are generally in the interval between 14 m/s and 20 m/s in most of Hungary, however, they exceed 26 m/s in the northeastern region of the country (in Nyíregyháza among the stations). The differences can partially be explained by the different calculation method of daily wind speed.

(4) Regarding the wind speed indices, yearly occurrence of days with small average wind speed has become more frequent, and the yearly number of days with average wind speed exceeding the larger thresholds has decreased. These negative trends are generally significant. Yearly number of periods of consecutive days with daily average wind speed below 3 m/s has also decreased significantly. Wind gust related indices has also decreased in general.

(5) Since simulated wind speed time series (using RegCM) highly overestimate the measurements in the reference period (1961–1990), and thus, do not reproduce the distribution of the CARPATCLIM daily wind speed values, a bias correction is applied to the simulated wind data using CARPATCLIM as a reference. Differences of the percentile values (between

raw simulated data of RegCM and the CARPATCLIM wind) are the smallest during months May and June. Similarly, the smallest biases of ERA Interim data compared to the station measurements are found in June and July. These results indicate that the larger bias values may be associated with winds resulted by winter storms.

(6) The application of bias correction substantially reduced the average monthly bias (practically to zero). The differences of the percentiles in the reference period are generally small, except in the tail of the distribution, where it can reach 1 m/s in some gridpoints in case of the 0.99 percentile value.

(7) Projected monthly changes in the median and the 0.90 percentile are relatively small (below 0.4 m/s and 0.6 m/s, respectively) for both future periods (2021–2050 and 2071–2100), however, estimated monthly changes of the 0.99 percentile may reach 2 m/s.

Acknowledgements—We are grateful to the Hungarian Meteorological Service and the Geoinformation Service of the Hungarian Defence Forces for the wind data of the Hungarian synoptic meteorological stations and CARPATCLIM data sets. This work was partially supported by the AGRÁRKLIMA2 project (VKSZ_12-1-2013-0034). Research leading to this paper has been supported by the Hungarian National Science Research Foundation under grant K-78125, and K109109.

References

AghaKouchak, A., Eesterling, D., Hsu, K., Schubert, S., Sorooshian, S., (ed.), 2012: Extremes in a changing climate. Water Science and Technology Library 65, Springer.

Aguilar, E., Peterson, T.C., Ramírez Obando, P., Frutos, R., Retana, J.A., Solera, M., Soley, J., González García, I., R.M. Araujo, R.M., Rosa Santos, A., Valle, V.E., Brunet, M., Aguilar, L., Álvarez, L., Bautista, M., Castañón, C., Herrara, L., Ruano, E., Sinay, J.J., Sánchez, E., Hernández Oviedo, G.I., Obed, F.,J.E. Salgado, J.E., Vázquez, J.L., Baca, M., Gutiérrez, M., Centella, C., Espinosa, J., Martinez, D., Olmedo, B., Ojeda Espinoza, C.E., Núñez, R., Haylock, M., Benavides, H., and *Mayorga, R.,* 2005: Changes in precipitation and temperature extremes in Central America and northern South America, 1961–2003. *J. Geophys. Res. – Atmospheres 110*, D23107.

Bartholy J. and *Pongrácz R.*, 2007: Regional analysis of extreme temperature and precipitation indices for the Carpathian Basin from 1946 to 2001. *Glob. Planet. Change,* 57, 83–95.

Berrisford, P., Dee, D.P., Fielding, K., Fuentes, M., Kallberg, P., Kobayashi, S., and *Uppala, S.M.,* 2009: The ERA-Interim Archive. *ERA Report Series No. 1. ECMWF:* Reading, UK.

Emeis, S., 2013: Wind energy meteorology. Atmospheric physics for wind power generation. Green Energy and Technology, Springer.

Gumbel, E.J., 1958: Statistics of extremes. Columbia University Press, New York and London.

IPCC, 2012: Managing the Risks of Extreme Events and Disasters to Advance Climate Change Adaptation. A Special Report of Working Groups I and II of the Intergovernmental Panel on Climate Change *[Field, C.B., V. Barros, T.F. Stocker, D. Qin, D.J. Dokken, K.L. Ebi, M.D. Mastrandrea, K.J. Mach, G.-K. Plattner, S.K. Allen, M. Tignor, P.M. Midgley (ed.)].* Cambridge University Press, Cambridge, UK, and New York, NY, USA.

Menne, M.J., and *C.N. Williams Jr.,* 2009: Homogenization of temperature series via pairwise comparisons. *J. Climate 22*, 1700–1717.

Oliver, J.E. (ed.), 2005: Encyclopedia of world climatology. Encyclopedia of Earth Science Series. Springer.

Palutikof, J.P., Brabson, B.B., Lister, G.H., and *Adcock, S.T.,* 1999: A review of methods to calculate extreme wind speeds. *Meteorol. Appl. 6*, 119–132.

Péliné, N.Cs., Bartholy, J., and *Pongrácz, R., 2014:* Homogenization of Hungarian daily wind speed data series, *Időjárás,* 118 (2), 119-132.

Peterson, T.C., Anderson, D., Cohen, S.J., Cortez, M., Murname, R., Parmesan, C., Phillips, D., Pulwarty, R., and *Stone, J.,* 2008: Why weather and climate extremes matter. In (ed.: *Karl, T.R.,*) Weather and climate extremes in a changing climate. Regions of focus: North America, Hawaii, Caribbean, U.S. Pacific Islands. US Climate Change Science Program and the Subcommittee on Global Change Research, Washington, DC, 11–33.

Pongrácz R., Bartholy J., and *Kis A.,* 2014: Estimation of future precipitation conditions for Hungary with special focus on dry periods. *Időjárás 118*, 305–321.

Rodrigo, J.S., Buchlin, J., van Beeck, J., Lenaerts, J.T.M., and *van den Brooke, M.R.,* 2013: Evaluation of the Antarctic surface wind climate from ERA reanalyses and RACMO2/ANT simulations based on automatic weather stations. *Climate Dynam. 40*, 353–376.

Seneviratne, S.I., Nicholls, N., Eastering, D., Goodness, C.M., Kanae, S., Kossin, J., Luo, Y., Marengo, J., McInnes, K., Rahimi, M., Reichstein, M., Sorteberg, A., Vera, C., and *Zhang, X.,* 2012: Changes in climate extremes and their impacts on the natural physical environment. In (eds.: *Field, C.B., Barros, V., Stocker, T.F., Qin D, Dokken, D.J., Ebi, K.L., Mastrandrea, M.D., Mach, K.J., Plattner, G-K., Allen, S.K., Tignor, M., Midgley, P.M.*) Managing the risk of extreme events and disasters to advance climate change adaption, A Special Report of Working Groups I and II of the Intergovernmental Panel of Climate Change (IPCC). Cambridge University Press, Cambidge/New York, 109–230.

von Storch, H. and *Zwiers, F.W., 1999:* Statistical analysis in Climate Research. Cambridge University Press.

Szentimrey T., 1999: Multiple Analysis of Series for Homogenization (MASH). Proceedings of the Second Seminar for Homogenization of Surface Climatological Data, Budapest, Hungary; WMO, *WCDMP-No. 41*, 27–46.

Szentimrey, T., 2011: Manual of homogenization software MASHv3.03. Hungarian Meteorological Service, Budapest.

Spinoni, J., Szalai, S., Szentimrey, T., Lakatos, M., Bihari, Z., Nagy, A., Németh, Á., Kovács, T., Mihic, D., Dacic, M., Petrovic, P., Kržič, A., Hiebl, J., Auer, I., Milkovic, J., Štepánek, P., Zahradnícek, P., Kilar, P., Limanowka, D., Pyrc, R., Cheval, S., Birsan, M., Dumitrescu, A., Deak, Gy., Matei, M., Antolovic, I., Nejedlík, P., Štastný, P., Kajaba, P., Bochnícek, O., Galo, D., Mikulová, K., Nabyvanets, Y., Skrynyk, O., Krakovska, S., Gnatiuk, N., Tolasz, R., Antofie, T., and *Vogt, J.,* 2014: Climate of the Carpathian Region in the period 1961–2010: climatologies and trends of 10 variables. *Int. J. Climatol. 35*, 1322–1341.

Stephenson, D., 2008: Definition, diagnosis, and origin of extreme weather and climate events. In (eds. *Diaz, H.F.* and *Murnane, R.J.*) Climate extremes and society. Cambridge University Press, Cambridge.

Torma Cs., Bartholy J., Pongracz R., Barcza Z., Coppola E., and *Giorgi F.,* 2008: Adaptation and validation of the RegCM3 climate model for the Carpathian Basin. *Időjárás 112*, 233–247.

Torma, Cs., Coppola, E., Giorgi, F., Bartholy, J., and *Pongrácz, R.,* 2011: Validation of a high resolution version of the regional climate model RegCM3 over the Carpathian Basin. *J. Hydrometeorol, 12*, 84–100.

Wan, H., Wang, X.L., and *Swail, V.R.,* 2010: Homogenization and trend analysis of Canadian near-surface wind speeds. *J. Climate 23*, 1209–1225.

Wilks, D. S., 2006: Statistical methods in the atmospheric sciences. International Geophysics Series, 91, Department of Earth and Atmospheric Sciences, Cornell University, Elsevier.

WMO, 2008: Guide to Meteorological Instruments and Methods of Observation. WMO-No. 8, 7th edition.

IDŐJÁRÁS

Quarterly Journal of the Hungarian Meteorological Service
Vol. 120, No. 1, January – March, 2016, pp. 73–84

Impact of climaticfactors on yield quantity and quality of grain crops

Márton Jolánkai, **Ákos Tarnawa**, **Csaba Horváth**, **Ferenc H. Nyárai**, and **Katalin Kassai***

SIU Crop production Institute, Páter Károly utca 1, 2100 Gödöllő, Hungary

**Corresponding author: Kassai.Katalin@mkk.szie.hu*

(Manuscript received in final form June 28, 2015)

Abstract—Weather impacts may have direct or indirect influence on the performance of agricultural production and food industry. The present problems are various, however, they can be sorted into two major groups: (1) factors that can be related to climate change processes like water scarcity, drought, meteorological extremities (temperature anomalies – frost, heat days, duration of unfavorable periods; precipitation – heavy rains, hail storms, land slide; air – storms, high wind, alterations of radiation and its postulates, (2) economic, social, and policy problems, that may have negative impact on the adaptability to meteorological factors in general and climate change processes in particular regarding food and agricultural production.

Changes in temperature may be of less importance concerning agriculture. Apart from a wide range of physiological problems, warming may have beneficial impacts as well; 1 °C rise in mean temperature may induce some 7 to 9 days of increment of the vegetation period, which could give a chance to use a +100 FAO group in maize production. On the other hand, warming of the summer period can be considered unfavorable. That may result in deterioration of sexual reproduction of most annual plants.

Changes in precipitation have more severe and determining consequences for crop production. Limited availability to water in the vegetation period may cause various direct deteriorating effects in cropping. Also, mild and dryer winter periods can be harmful contributing to epidemics and gradations of pests and diseases. Weed cenoses are also affected by climate change processes.

Economic vulnerability of agriculture in general and that of crop production in particular can be detected in most fields of the food chain. It is hard to estimate losses, but trends and the magnitude of these can be assessed. Grain crops represent a major source of arable output in Hungary. Half of the arable land is used for wheat and maize cropping. The grain yield of these two crops range from 9 to 15 million tons annually due to weather influences of the very crop year. The gap between them represents some 270 billion HUF on today's prices.

Key-words: climatic factors, crop production, yield quantity, yield stability

1. Introduction

Since the beginning of the human civilization, when man first tried to cultivate plants and recognized that crop plants do not give the same yield in each year, moreover, sometimes the differences could be very high, there is a profound interest to seek and learn possible reasons of that. According to the level of certain historical ages, this variance was explained by some supernatural forces. In accordance with the progress of society, more and more rational explanations were found up to now. On the basis of rationality, only scientifically approved causes could be accepted (*Jolánkai* and *Birkás*, 2007; *Jolánkai et al.*, 2008). In this way, crop science and practice become reasonable gradually. There are numerous factors that are having effect on yield (*Tarnawa* and *Klupács*, 2006), and among them there are some that could be influenced by the farmer and also a few others that could not be. The first group is the set of elements of agronomic management, the second group is the set of factors of environment (*Várallyay et al.*, 1985). In the set of environmental factors, there are some with more or less impact on yield (*Klupács et al.*, 2010), but according to former observations, weather plays a significant role (*Szöllősi et al.*, 2004). Even because crop production is not an indoor practice but mostly outdoor; the weather and climate may have high impact on that (*Láng et al.*, 2007). Weather impacts and climate change processes may have direct or indirect influence on the performance of agricultural production and food industry (*Veisz et al.* 1996; *Anda,* 2005; *Bozó et al.* 2010). Climate change impacts on crop production are due to weather anomalies and uncertain processes (*Varga-Haszonits,* 2003).

As the yields still show lower or higher fluctuation from the long term averages or trends, it should be more than useful to explore how they depend on each element of climate (*Pepó*, 2010). Certain crop species respond to climatic impact in different ways. The performance of maize crop is highly influenced by radiation and temperature (*Anda* and *Lőke,* 2004). The grain yield of maize is rather influenced by precipitation (*Anda et al.* 2002; *Lente* and *Pepó* 2009). Grain yield of wheat may vary in accordance with the weather conditions of the crop year. Yield stability depends on the optimum distribution of precipitation during the vegetative phenophases. Grain yield of wheat may vary in accordance with the weather conditions of the given crop year (*Bocz et al.,* 1983; *Pepó et al.*, 1986; *Pepó,* 2010; *Pepó* and *Győri,* 2005).

Changes in temperature may be of less importance concerning agriculture. Apart from a wide range of physiological problems, warming may have beneficial impacts as well; 1 °C rise in mean temperature may induce some 7 to 9 days of increment of the vegetation period, which could give a chance to use a +100 FAO group in maize production. On the other hand, warming of the summer period can be considered unfavorable (*Ladányi et al.,* 2001; *ADAM,* 2008). That may result in deterioration of sexual reproduction of most annual plants. Climatic conditions may have an impact on the performance of crop production. Apart from the growth and development of the crop plant, water availability within the crop site may be responsible for various phytosanitary problems, such as weed infestation, disease infections, and gradations of insect pests (*Nagy* and *Ján,* 2006, *Ács et al.,* 2008; *Várallyay,* 2008; *Pásztorová et al.*, 2011).

Recently, one of the most severe harm induced by insects may be related to the spread of western corn rootworm *Diabrotica virgifera virgifera* Le Conte (*Kiss* and *Edwards,* 2003). Spread of this insect species has been recorded since 1992 in Central Europe due to an anthropogenic failure. The pest has been imported from overseas during the Yugoslav war with a humanitarian aid transport to Europe. This insect has conquered gradually the whole territory of the Carpathian Basin in recent years. The gradation of Diabrotica in Hungary has started in 1996 and has been completed by 2002 (*Zsellér Hatala* and *Széll,* 2001; *Vidal et al.,* 2005; *Jolánkai et al.,* 2006).

Availability of water is a major stressor in relation with yield quality and quantity performance of winter wheat. Cereals represent a most plausible source of human alimentation in the world. Wheat provides a basic staple for mankind. This crop is one of the most important cereals in Hungary with a high economic value. Utility, market, and alimentation value of the crop is highly affected by climatic conditions and within that annual weather performances, as well as soil moisture conditions (*Ács et al.*; 2008; *Koltai et al.*, 2008; *Skalová et al.*, 2008; *Várallyay*, 2008). The aim of wheat production is twofold; to provide quantity and quality. Milling and baking quality of wheat is mainly determined by the genetic basis, however, it can be influenced by management techniques (*Pollhamerné,* 1981; *Nagy and Ján.*, 2006, *Varga et al.*, 2007; *Vida et al.,* 2005). In our previous studies, we have reported results regarding the role of water availability impacts on the quantity and quality of grain crops (*Gyuricza et al.,* 2012; *Horváth et al.* 2014; *Jolánkai et al.,* 2014). Since main quality indicators – protein, farinographic value, gluten content for wheat, as well as protein, starch, and fibre for maize – have a rather diverse manifestation, extensive studies were performed to gain more information concerning the behavior of them.

The present paper is intended to provide some information on the performance of wheat and maize, the major grain crop species produced in Hungary. The work of the research team was based on two sources, once on the results of long term small plot field experiments, while on the other hand, on the use of national databases of meteorology and agriculture.

2. *Materials and methods*

The materials and methods of the present study cover a rather broad field, since there are three slices of the research work done by the Szent István University, Crop Production Institute, Hungary (hereinafter SIU). Most of the results are based on experimental research, however, some evaluations were implemented by using national public data, or observation results published.

In long term field trials, a wide range of winter wheat *Triticum aestivum* L. varieties and maize *Zea mays* L hybrids were tested. The small plot trials were dirun at the Nagygombos experimental field. The soil type of the experimental field is chernozem (calciustoll). Annual precipitation of the experimental site belongs to the 550–600 mm belt of the northern edges of the Great Plain in a 40 years average, 1961–2000, while the average depth of groundwater varies between 2 and 3 metres.

Experiments have been conducted in split-plot design with four replications. The size of each plot was 10 m^2. Plots were sown and harvested by plot machines (standard Wintersteiger cereal and maize specific experimental plot machinery series). Various identical agronomic treatments were applied to plots. Plant protection and plant nutrition applications were done in single and combined treatments. All plots were sown with identical series of wheat varieties and maize hybrids for studying their performance in relation with agronomic impacts. Regarding water availability impacts, experimental mean values of respective treatments and homogenized bulk yield samples were used only. Precipitation records have been evaluated in relation with yield quantity and quality. Wheat grain quality parameters like protein, farinographic value, and wet gluten content were processed, as well as maize quality parameters; protein, starch, and fibre content. Quality characteristics were determined at the Research Laboratory of the SIU Crop Production Institute, according to Hungarian standards (*MSZ,* 1998). Grain yield samples and quality figures were correlated with precipitation parameters. Analyses were done by statistical programmes with respect to the methodology of phenotypic crop adaptation (*Eberhart* and *Russell* 1966; *Finlay* and *Wilkinson* 1963; *Hohls,* 1995).

The gradation of the western corn rootworm was analyzed from a point of view of crop production. The beetle has conquered within almost ten years the whole territory of the Carpathian Basin. The spread of Diabrotica in Hungary has started in 1996 and has been completed by 2002. Climatic factors of the gradation were evaluated. The meteorological database of the research referring to precipitation as well as temperature data was provided by the Hungarian Meteorological Service (OMSZ). Yearly and monthly data of precipitation and temperature of the respective years have been used during the evaluation. The spreading of the insect was recorded by digital mapping with the use of planimeter. Distances have been determined by GPS coordinates of the locations. Gradation reports and data of the spreading were obtained from the Ministry of Agriculture of Hungary as well as that of the phytosanitary authorities (NÉBIH). In the study, there were no entomological evaluations. All information regarding entomological aspects were adopted from specific reports on Diabrotica (*Kiss* and *Edwards,* 2003; *Zsellér Hatala* and *Széll,* 2001). Statistical evaluations, crop ecological model adaptations, and correlation calculations were done by regular methods (*Sváb,* 1981; *Finlay* and *Wilkinson,* 1963).

The present paper produces three slices of the results of the ongoing research in relation with weather impacts on grain production. Such an assessment has a diverse nature. Once, it is beneficial regarding the abundance and the duration of baseline data. On the other hand, it is restricted to the available structure, moreover, it is bound mainly to annual figures giving less chance for deep layer evaluations. However, the study could provide some novel specific information on crop performance.

3. Results and discussion

3.1. Yield stability

Hungarian agriculture is run mainly by rainfed technologies regarding field crops, since less than 7 percent of the arable land is equipped for irrigation. Changes in precipitation have more severe and determining consequences for crop production. Limited availability to water in the vegetation period may cause various direct deteriorating effects in cropping. Economic vulnerability of agriculture in general and that of crop production in particular can be detected in most fields of the food chain. It is hard to estimate losses, but trends and the magnitude of these can be assessed. Grain crops are a major source of field crop output. Half of the arable land is used for wheat and maize cropping. The grain yield of these two crops range from 9 to 15 million tons annually due to weather influences of the very crop year as it is indicated in *Figs. 1* and *2*. The gap between the total yield of the two crops represents some 230 billion HUF on today's prices (an estimated value of 386.6 billion HUF for the minimum and 616.2 billion HUF for the maximum within the time range).

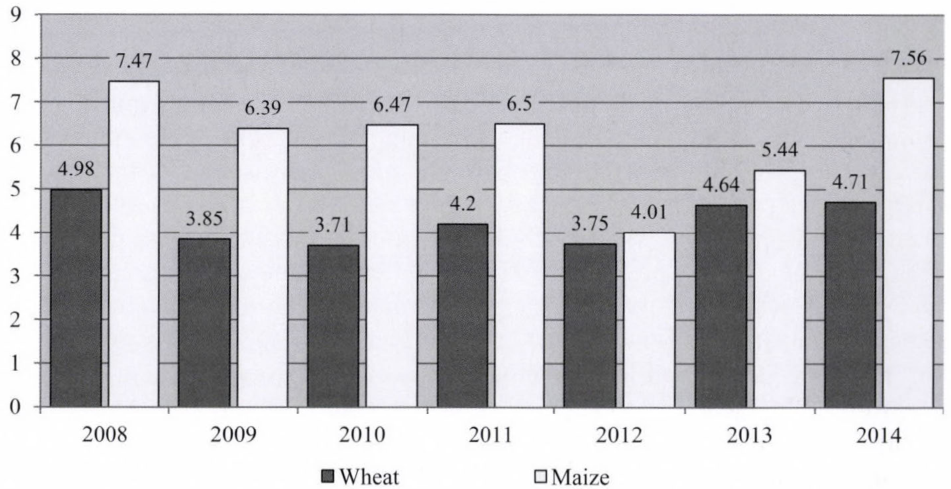

Fig. 1. Wheat and maize yield averages in Hungary, t/ha. (Source: KSH, 2008–2014)

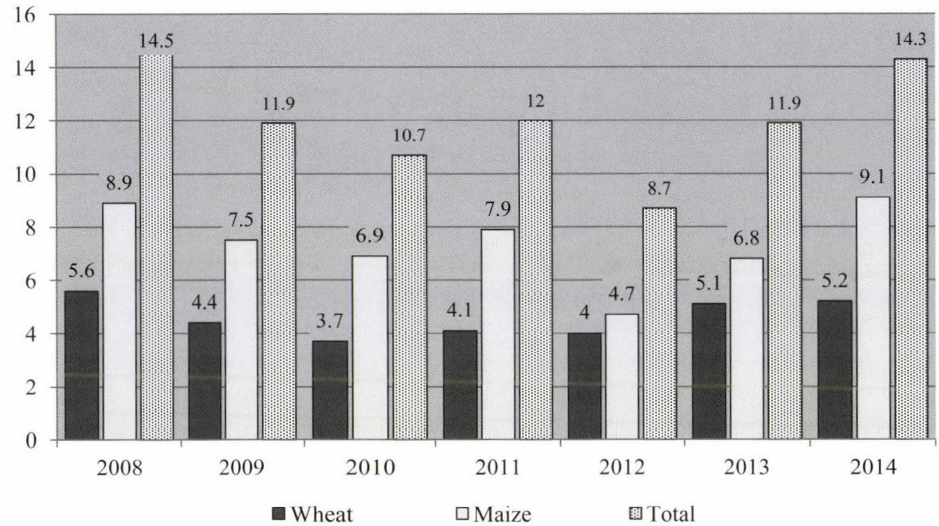

Fig. 2. Wheat and maize yields in Hungary, million t. (Source: KSH, 2008–2014)

3.2. Insect pest gradation

Availability to water during the vegetation period may cause various direct deteriorating effects in cropping. Also, mild and dryer winter periods can be harmful contributing to epidemics and gradations of pests and diseases. Weed cenoses may also be affected by climate change processes.

The basic hypothesis of the work was related to the performance of maize crop of the respective periods. Since all live populations in general and the reproductive activities of them in particular depend on the food availability, an assessment was implemented to find correlating factors. *Fig. 3* presents data on the annual spread of the insect pest with the maximum distance of migration of the respective crop year and the maize kernel yield. It has been observed that the magnitude of gradation was usually bigger in crop years with high grain yield. This phenomenon may be explained by the better habitat conditions of the actual crop year provided by the good plant performance. The trend of gradation has similarities with that of the maize kernel yield of the respective years, however, various other factors had to be evaluated as well. For example, there were crop years with 2 t yield differences when the gradation maximum distance was identical.

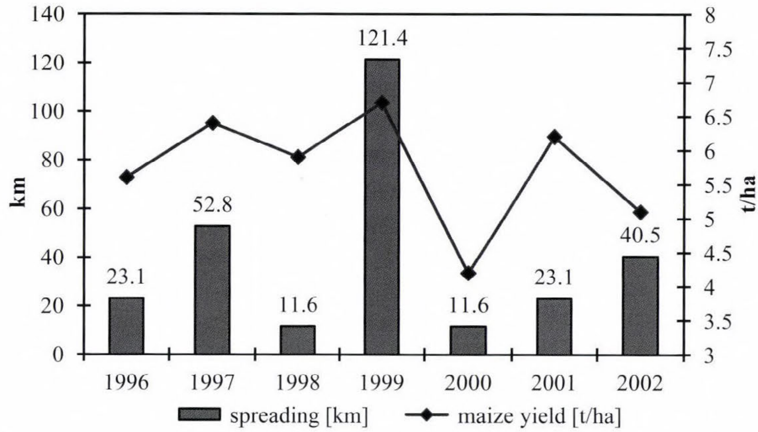

Fig. 3. The annual spread of *Diabrotica virgifera virgifera* and maize yields of respective years, 1996–2002.

In accordance with European entomological reports, the spreading of the insect has been performed by a pattern of concentric circles. The speed of gradation, the size and shape of the annually conquered area was different in each crop year observed. The correlation between maize yields and the magnitude of gradations indicated further studies in the field of meteorological data. In the study, precipitation of various periods within the crop year were evaluated in accordance with the life cycle information of the insect. Annual mean precipitation, the precipitation of the first six months of the year, and that of June month were checked. Temperature means of the respective periods were evaluated also. *Table 1* provides information on the correlation between the gradation and these meteorological data.

Table 1. Correlation between *Diabrotica* gradation and meteorological factors (1996–2002)

	r	*P*
Maize yield	0,683	0,95
Annual mean precipitation	0,248	ns
First 6 months' precipitation	0,236	ns
June precipitation	0,881	0,99
Annual mean temperature	–0,538	ns
First 6 months' temperarture	–0,604	ns
First 3 months' temperature	–0,196	ns

The research results of this study suggest that the amount of precipitation and temperature data had an indirect effect on the spread of the insect. Significant correlations were found in the case of annual harvested maize yields as well as the amount of precipitation of June month with the magnitude of the gradation of *Diabrotica virgifera virgifera* Le Conte. Since the study was based on crop production and geographic methodology using open access databases and observation results concerning gradation, further entomological studies are needed to clear the background of the results obtained.

3.3. Yield and quality of grain crops

Annual amounts of precipitation and winter wheat yields have been examined in a 15-year time range, while the same for maize has been investigated in a 9-year period at the Nagygombos experimental field of the SIU, Gödöllő. *Figs. 4* and *5* illustrate annual changes of yield and some quality parameters in accordance with the precipitation mean values. Yields and main quality characteristics were correlated with water availability.

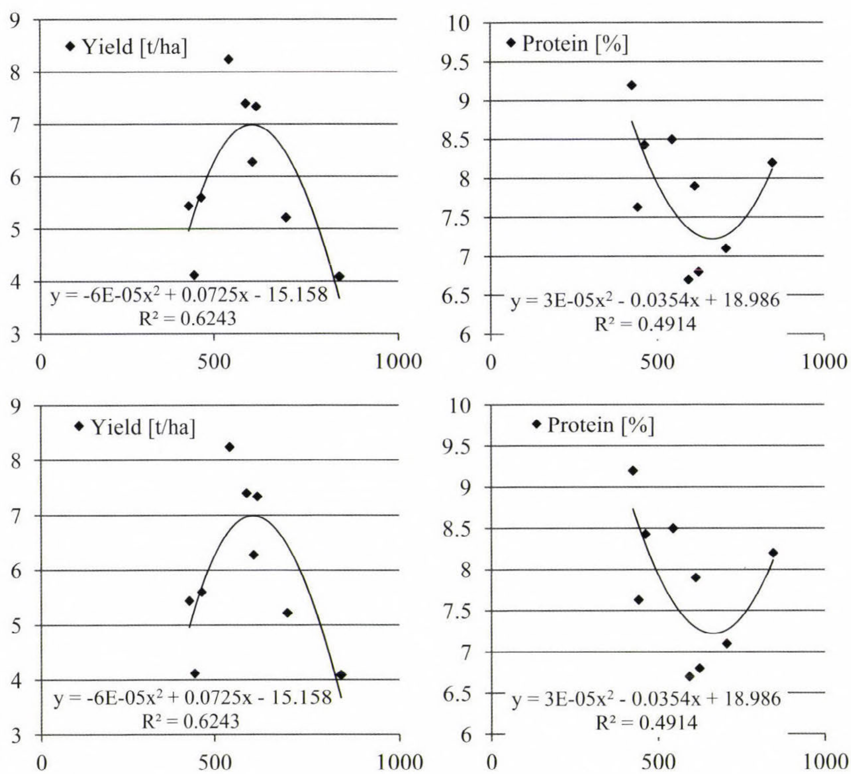

Fig. 4. The performance of grain yield, protein, starch, and fibre values of maize crop, Nagygombos, 2002–2010.

Yield quantity of maize crop proved to be highly variable. Years with low as well as too high precipitation had yield deteriorating effects. The highest yields were obtained in crop years of 600–700 mm. Protein values were smaller in rainy years. Starch values did not prove to have any correlations with precipitation. Fibre content values in certain crop years were randomly changing, however, no systematic trends could be observed.

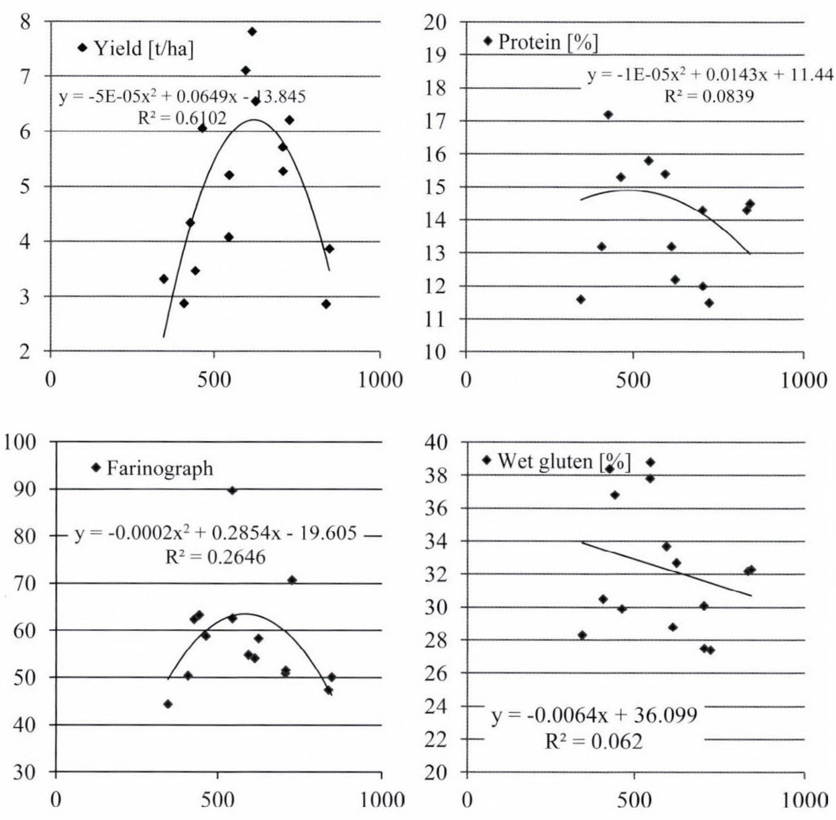

Fig. 5. The performance of grain yield, protein, farinographic value, and wet gluten % of wheat crop, Nagygombos, 1996–2010.

Yield figures were in accordance with annual precipitation patterns with an exception of some years when the distribution was irregular, e.g., in 1999 year, when 837 mm rainfall, one of the highest in the period examined was recorded, however, a severe drought spring was followed by an extreme moist summer obstructing the yield formation ripening, and harvest. Also, the year 2010 with the ever highest annual precipitation, 847 mm measured at the experimental site resulted in poor yield performance for both wheat and maize crops due long periods of water logging. Apart from these two years, the annual precipitation was in accordance with the water consumption of the respective crop species and their C3 and C4 physiological patterns.

Quality manifestation of winter wheat yields have been impacted by annual precipitation in general in accordance with previous reports (*Klupács et al.* 2010; *Pepó,* 2010). *Fig. 5* provides data regarding the changes in yield quality characteristics. Yield figures were in accordance with annual amounts of precipitation with two exceptions regarding the 1999 and 2010 crop years. Wet gluten, protein, and farinographic values had no significant relations with annual precipitation.

4. Conclusions

Weather impacts may have direct or indirect influence on the performance of agricultural production and food industry. Water availability can be considered as a basic factor related to yield quality and quantity performance of grain crops.

Yield stability of grain crops may be highly variable according to weather impacts. Yield losses may influence the whole of agricultural production. Grain crops are a major source of the output of field crops. Half of the arable land is used for wheat and maize cropping. The grain yield of these two crops range from 9 to 15 million tons annually due to weather influences of the very crop year. The gap between them represents some 270 billion HUF on today's prices.

The present study also summarizes results of an observation regarding the influences of climatic factors on the spread of an insect pest *Diabrotica virgifera virgifera* Le Conte. The research results suggest that the amount of precipitation and temperature data had an indirect effect on the spread of the insect. Significant correlations were found in the case of annual harvested maize yields as well as the amount of precipitation of June month with the magnitude of the gradation. Further entomological studies are needed to clear the background of the results obtained.

In an agronomic long-term trial, the impact of water availability on wheat and maize crop has been evaluated. Various crop years have had different impacts on crop yield quantity. Yield figures were not in significant correlation with annual precipitation in general. However, with an exception of two years of extremely high precipitation yield figures, they were in accordance with that. Moisture availability had diverse influence on quality manifestation. High precipitation has often resulted in poorer quality. Maize yields have been performing in a broader range than that of wheat. Maize quality parameters proved to be more stable than yield figures except for fibre content values.

Acknowledgements: Authors are indebted regarding support received from TÁMOP and VKSZ 12-1-2013-0034 – Agrárklíma 2 fund of the Government of Hungary.

References

Ács F., Horváth Á., and *Breuer H.* 2008: A talaj szerepe az időjárás alakulásában. *Agrokémia és Talajtan 57*, 225–238. (in Hungarian)

ADAM, 2008*:* ADAM Project Final Report. www.adamproject.eu

Anda, A., 2005: A klímaváltozás hazai mezőgazdasági következményei. *KLÍMA-21 Füzetek 41.* 18–29. (in Hungarian)

Anda, A., Lőke, Zs., and *Kirkovits, M.,* 2002: Kukorica néhány vízháztartási jellemzőjének szimulációja. *J. Centr. Eur. Agric. 3.* 95–103.

Anda, A. and *Lőke, Zs*., 2004: A sugárzás- és a hőháztartási mérleg komponenseinek alakulása eltérő sűrűségű kukorica hibridekben. *Növénytermelés 35*, 389–398. (in Hungarian)

Bocz. E. and *Pepó. P.,* 1983: A víz- és tápanyag szerepe a minőségben: Őszi búza. *Magyar Mezőgazdaság. 38*, 41. (in Hungarian)

Bozó, L., Horváth, L., Láng, I., and *Vári, A.* /Eds./, 2010: Környezeti Jövőkép – Környezet- és Klímabiztonság. Magyar Tudományos Akadémia, Budapest. (in Hungarian)

Eberhart. S.A. and *Russell W.A.*, 1966: Stability parameters for comparing varieties. *Crop Science. 6,* 36–40.

Finlay, K.W. and *Wilkinson, G.N.*, 1963: The analysis of adaptation in a plant breeding program. *Australian J. Agric. Res. 14*,. – 742–754.

Gyuricza, Cs., Balla, I., Tarnawa, Á., Nyárai, H.F., Kassai, K., Szentpétery, Zs., and Jolánkai M., 2012: Impact of precipitation on yield quantity and quality of wheat and maize crops. *Időjárás 116*, 211–220.

Hall, J., Held, H., Dawson, R., Kriegler, E., and *Schellnhuber, H.J.*, 2009: Imprecise probability assessment of tipping points in the climate system. *PNAS 106*, 5041–5047.

Hohls, T., 1995: Analysis of genotype environment interactions. *South African J. Science. 91*, 121–124.

Horváth, Cs., Kis, J., Tarnawa, Á., Kassai, K., Nyárai, H.F., and *Jolánkai, M.*, 2014: The effect of nitrogen fertilization and crop year precipitation on the protein and wet gluten content of wheat (*Triticum aestivum* L.) grain. *Agrokémia és Talajtan 63,* 159–164.

Jolánkai, M. and *Birkás M.* 2007: Global climate change impacts on crop production in Hungary. *Agriculturae Conspectus Scientificus 72*, 17–20.

Jolánkai, M., Nyárai, H.F., Tarnawa, Á., Klupács, H., and *Farkas I.*, 2008: Plant and soil interrelations. *Cereal Res. Commun. 36,* Suppl. 7–10

Jolánkai, M., Szentpétery, Zs., and *Tarnawa, Á.*, 2006: Klimatikus tényezők hatása a *Diabrotica virgifera virgifera* Le Conte terjedésére. XVI. Keszthelyi Növényvédelmi Fórum, VE Georgikon, Keszthely, 37–40.

Jolánkai M., Tarnawa Á., and *Horváth, Cs.*, 2014: A klímaváltozás hatása a gabonanövények minőségére, élelmiszerbiztonságára. In: Klímaváltozás és következményei: a globális folyamatoktól a lokális hatásokig. 40. Meteorológiai Tudományos Napok. OMSZ. Budapest (abstract) 11.

Kiss, J. and *Edwards C.R.* 2003: Spread of western corn rootworm. gau.hu/nvtt/home.htm

Klupács, H., Tarnawa, Á., Balla, I., and *Jolánkai, M.*, 2010: Impact of water availability on winter wheat (Triticum aestivum L.) yield characteristics. *Agrokémia és Talajtan 59*,151–156.

Koltai, G., Milics, G., Neményi, M., Nagy, V., and *Rajkai, K.*, 2008: Plant water supply of layered alluvial soils under different weather conditions. *Cereal Res. Commun. 36, Suppl.* 167–171.

Ladányi, M., Horváth, L., Gaál, M., and *Hufnagel L.*, 2001: An agro-ecological simulation model system. *Appl. Ecol. Environ. Res. 1,* 47–74.

Láng, I., Csete, L., and *Jolánkai, M.* /Eds./, 2007: A globális klímaváltozás: hazai hatások és válaszok. A VAHAVA Jelentés. Szaktudás Kiadó Ház, Budapest.(In Hungarian)

Lente, Á. and *Pepó, P.*, 2009: Az évjárat és néhány agrotechnikai tényező hatása a kukorica termésére csernozjom talajon. *Növénytermelés 58 (3)*, 39-51.

MSZ, 1998: MSZ 6383:1998, 824/2000/EK Grain quality standards, Hungary.

Nagy, V. and *Ján, H.*, 2006: Method to estimate the critical soil water content of limited availability for plants. *Biologia 61. Suppl. 19.* 289–293.

Pásztorová, M., Skalová, J., and *Vitková, J.*, 2011: Analisys of impact of management on groundwater level of abrod wetland. *Növénytermelés 60, Suppl.* 361–364.
Pepó, P., 2010: Adaptive capacity of wheat (Triticum aestivum L.) and maize (Zea mays L.) crop models to ecological conditions. *Növénytermelés. 59. Suppl.* 325–328.
Pepó, P. and *Győri, Z.*, 2005: A study of the yield stability of winter wheat varieties. *Cereal Res. Commun. 33*, 769–77.
Pepó, P., Győri, Z., and *Pepó, P.*, 1986: Agrotechnikai tényezők és az évjárat hatása az őszi búzafajták szemtermésének kémiai összetételére. *Növénytermelés. 35.* 17–24.
Pollhamer, E., 1981: A búza és a liszt minősége. Mezőgazdasági Kiadó, Budapest. (In Hungarian)
Skalová, J. and *Jaros, B.*, 2008: Soil water regime assessment in Morava basin. *Cereal Res. Commun. 36. Suppl.*, 243–246.
Sváb, J., 1981: Biometriai módszerek a kutatásban. Mezőgazdasági Kiadó, Budapest. (In Hungarian)
Szöllősi, G., Ujj, A., Szentpétery, Zs., and *Jolánkai, M.*, 2004: A szántóföldi növénytermesztés néhány agroökológiai aspektusa. *AGRO-21 Füzetek 37*, 77–88.
Tarnawa, Á. and *Klupács, H.*, 2006: Element and energy transport model for an agricultural site. *Cereal Res. Commun. 34*, 85–89.
Várallay, Gy., Szűcs, L., Zilahy, P., Rajkai, K., and *Murányi, A.*, 1985: Soil factors determining the agroecological potential of Hungary. *Agrokémia és Talajtan. 34, Suppl.* 90–94.
Várallyay, G., 2008: Extreme soil moisture regime as limiting factor of the plants' water uptake. *Cereal Res. Commun. 36, Suppl.* 3–6.
Varga, B., Svečnjak, Z., Jurković, Z., and *Pospišil, M.*, 2007: Quality responses of winter wheat cultivars to nitrogen and fungicide applications in Croatia. *Acta Agronomica Hungarica 55.*, 37–48.
Varga-Haszonits, Z., 2003: Az éghajlatváltozás mezőgazdasági hatásának elemzése, éghajlati szcenáriók. *AGRO-21 Füzetek 31*, 9–28.
Veisz, O., Harnos, N., Szunics, L., and *Tischner, T.*, 1996: Owerwintering of winter cereals in Hungary in the case of global warming. *Euphytica 92*, 249–253.
Vidal, S., Kuhlmann, U., and *Edwards, C.R.*, /Eds/ 2005: Monitoring of western corn rootworm (*Diabrotica virgifera virgifera* LeConte) in Europe 1992-2003. cabi.org/cabebooks/ ebook/20053000958. 29–39.
Zsellér Hatala, I. and *Széll, E.*, 2001: Results of biological observations of western corn rootworm in 2000 in Hungary. IWGO 7th Meeting of Diabrotica Subgroup. Stuttgart, Germany (abstract) 16.

IDŐJÁRÁS

Quarterly Journal of the Hungarian Meteorological Service
Vol. 120, No. 1, January – March, 2016, pp. 85–101

Some physiological responses of agricultural crops to global warming

Angéla Anda* and **Gábor Soós**

University of Pannonia Georgikon Faculty,
P.O. Box 71, Keszthely, Hungary H-8361

**Corresponding authors E-mail: anda-a@georgikon.hu; anda@keszthelynet.hu*

(Manuscript received in final form March 13, 2015)

Abstract—Food production is largely affected by weather variables; the year-to-year yield variations are due to changes in air temperatures, precipitation, and other meteorological elements. The crop-weather relationship is interaction, therefore, the agriculture is also responsible for greenhouse gas emissions (land clearing, fossil fuel use, rice cultivation, livestock production, N fertilization). The advantage of agricultural models is that they could simulate the above relations quantitatively. However, there are a variety of dynamic models dealing with crop-environment interactions in different levels from local to global one. The start of the studies used to be the cognition of crop growth and development by description of governing physiological and physical processes. The economic models close the range of investigations through impact estimation of climate change on the whole agricultural sector.

The first part of this study is devoted to some selected basic crop-environment relations from the literature. The second half of the work is dealing with on-site case study for maize, whereby different scenarios were established to project the crop response (stomatal resistance, photosynthesis) to various aspects of global climate change. The results of the crop microclimate simulation model were treated with restraint, because the majority of weather influences might have additive or synergistic impacts causing more severe damages than simulation models ever estimate. A simple example may be a stressed crop that become more sensitive to damaging pests and diseases excluding fully from most of the dynamic models. Despite known weaknesses of crop-environment models, the end-users (farmers, politicians) can respond more specifically to climate change besides such widely applied interventions as using warmth- or drought tolerant species, altering dates of planting and harvesting, irrigation, modification of cultivation systems, etc.

Key-words: climate change, agriculture, physiological processes, simulation model, maize

1. Introduction –brief selection from the related literature

Increasing demand for food is caused by the world's population growth and higher per capita income of well-developed countries. In addition to the amount of food, its distribution between different regions is also uneven; abundance and shortage of food are present at the same time. The most important task of the agriculture is to meet the higher demands, and to overcome the increasing risks with better management regarding agricultural food production. After FAO 2009's origin report, the number of people suffering from hunger is over a billion. Not encouraging for the future, that we have to nourish nine billion people by 2050 (*Godfray et al.,* 2010). The reasons of hunger are manifold from low agricultural productivity, lack of knowledge about cultivation facilities, poorness, overpopulation, poverty, etc. Luckily, majority of the above mentioned difficulties are not characteristic for Hungary, although there is also a contingency to improve the Hungarian agricultural production. The Carpathian Basin occupying a transition region of the precipitation pattern in Europe is probably one of the most sensitive places regarding impacts of global warming (*Torma et al.* 2010, *Giorgi* and *Coppola,* 2007). Whilst the climatic projections for different regions of Hungary may vary temporally (they are getting better and better), the sensitivity remains the same, which is caused by the special pool-type geographical position of the country.

Not to mention of all social causes of uneven food distribution, only one of the possible reasons will be discussed, namely the weather. The most vulnerable farmers are the rainfed crop growers due to extremely high rainfall variability (within a season and between seasons), and the intentions that force them to avoid risks, the meteorological hazards. The global climate change concerns both sides. *Easterling et al.* (2007) found that even a 2 °C warming in global air temperatures by 2100 (IPCC low emissions; SRES: B1) may destabilize the current farming systems reconfiguring the contemporary food distribution. The size of land for cultivation is strictly limited. One of the most important tasks in mitigating the negative impacts of global warming may be to produce more production from less land (*Vermeulen et al.*, 2012).

Consequences of global climate modification include warming, variation in precipitation events, and shifting of seasonal (phenological) cycles. Among these three terms, the precipitation projections are the most uncertain. Phenology (length and timing of the various phenological stages) comprises periodic life cycle of crops largely depending on weather conditions. The phenological phases are governed by the interaction of genetic characteristics and weather conditions (in temperate climate mostly temperatures and day length), that are modified by land cultivation to gain the highest yield (*van Bussel et al.*, 2011, *Kirby et al.*, 1987). In phenological observations, the impact of temperature has of primary importance. Air temperature directly determines the ratio of the biochemical processes (enzyme activity, cell die). Temperature has no less significant impact on the sequence of development stages. Phenological shifts modify the distribution of the species ranges, e.g., migrations toward higher elevation and latitude (*Vitassea et al.* 2011, *Bertin*, 2008). The extension of the photosynthetically active period may effect crop growth positively on the mid- and high latitudes (*Menzel* and *Fabian,* 1999) due to enhancing the carbon-uptake period, which stems from earlier leaf emergence and later leaf senescence. At the same place, shorter season for field crops could have rather negative impacts through blocking the formation of the yield components (*Chmielewski et al.*, 2004). Surprisingly, in Germany, despite of warming of the last two decades, no strong effect on fruit (apple) yield formation was observed so far (*Chmielewski et al.*, 2004). However, a question may arise: till what time?

During the past few decades, most of the studies were focusing on the changes of the natural vegetation only, and limited number of papers were dealing with the trends of agricultural crops (*Schelling,* 2000), despite their significance in reducing negative influences of climate change. Direction and magnitudes of observed phenology trends showed a different picture over Europe between the time period of 1986 and 2006 using satellite images (*Ivits et al.*, 2012). The authors reported that until north-eastern Europe deployed a trend to an earlier and longer vegetation period, in central Europe the length of the season exhibited rather stable indicating a shift towards an earlier start of the entire growing season. At the same time, the Mediterranean areas displayed a phenological shift towards later dates with both earlier and shorter growing seasons, depending on the actual place of observation. On the basis of a twenty six years analysis *Brown et al.* (2012) found, that one third of the cereal's growing area has experienced changes in the length of the growing seasons on global level; on most areas the length of the growing seasons was with 2.3 days/year longer on average, since 1981. The above authors reported both negative and positive trends in the start of the vegetation period depending on the country and region studied. Considerable variability among crop species and observation ways has to take into account to get well-appreciated future phenological estimations. In the past three decades, variation in weather (temperature, precipitation, solar radiation) jointly increased the wheat yield in northern China by 0.9–12.9%, however, they reduced wheat yield in southern China by 1.2–10.2%, with a large spatial difference (*Tao et al.*, 2014). The above authors reported that the wheat growth period before anthesis and the whole growing season were shortened, however, the length of reproductive growth period was significantly prolonged. In Europe, Hungary included, an earlier beginning of the growing season and a longer growing period may be waited. In Hungary, *Gaál* (2008) reported 12-17 days longer vegetative period for 2050, favorable for the warm season plants. Non-standard results were also born in the literature such as from *Brown et al.* (2012). The authors concluded that due to variations in weather effects on crop production, in the northern hemisphere the humidity based, while in the southern hemisphere, the accumulated growing degree days concept fitted better, when phenological models were applied. This concern likely may be expanded on larger scale only. It is well known by many investigators that significant differences are expected on country level.

Perennial crops as fruit trees and grapes are the most vulnerable classes considering the negative effects of global warming. For European temperate tree species, an average increase of the growing period of 11 days has been reported from the 1960s to the end of the 20th century by *Menzel* and *Fabian* (1999). *Richardson et al.* (2013) chronicled phenological advances of approximately 3–8 days for each 1 °C growth in air temperature for the same group of trees. *Taylor et al.* (2008) assumed that one of the reasons of the extended vegetation period may be the elevated CO_2 that delayed the autumn coloration and senescence in trees. The warming trend in our present climate is expected to continue, so in case of grapes, the ripening period will be characterized by higher temperatures worsening the berry quality (*Fila et al.*, 2014). This means that the Italian traditional grape growing areas will be in serious risk. *Jones* (2012) in Quebec suggested to explore new cultivation areas, previously cool regions, where the climate change towards for more favorable environmental conditions for grapes. The current Hungarian grape growing regions may shift into another maturity group due to more rapid phenological development (*Ladányi,* 2008).

At the very beginning of climate change impact studies, the most controversial part was the possible effect of elevated CO_2 on crop physiological processes. Studies in phenological shifts are important, because physiological processes related to the carbon cycle, plant-water relation, or nutrient uptake are directly mediated by phenology (*Noormets et al.*, 2009). *Richardson et al.* (2013) reported spring onset of photosynthesis by about 3 days at +1°C anomaly in spring air temperature that grew the photosynthetic activity and respiration by 35±5 and 20±3 $gCm^{-2}/°C^{1}$, respectively in a deciduous forest. Finally, the photosynthetic gains were positive, +9±2 $gCm^{-2}/°C^{1}$ on the study site. It is important to mention that in dry conditions, the influence of precipitation may exceed the effect of higher temperature on the intensity of carbon-assimilation. *Ma et al.* (2007) gave a good example for a grassland at California, in which 1 mm increment in springtime precipitation gave 2 gCm^{-2} growth in daily productivity of the ecosystem.

Doubling of the current ambient CO_2 raised the growth with 10–20 and 40–45% in C_4 and C_3 crops, respectively (*Ghannoum et al.*, 2000). Increasing atmospheric CO_2 concentration has long been known to stimulate C_3 photosynthesis better than photosynthesis of C_4 crops. The C_4 crop's photosynthesis regarded an improved version of the C_3 pathway that raises the level of the photosynthetic efficiency in addition to lower evapotranspiration rate. The advantage of C_4 crops is the lower photorespiration in comparison to C_3 ones. The C_3 crops will benefit net photosynthetic rate, stomatal resistance, and transpiration water loss. The photosynthetic way of C_4 crops was implemented due to the less favorable environmental conditions of their native places (dry and hot environments). The C_4 crops have higher production rates than that of the C_3 ones because of the gains in the used water and CO_2 values. On ecosystem level, the type of the photosynthetic pathway impacts the carbon fixation, on the one hand influencing the size of food resources for animal feeding purposes, and on the other hand effecting the amount of CO_2 released back to the atmosphere.

One of the possible impacts of increasing CO_2 levels may be the increase in stomatal resistance, causing less transpiration intensity (*Ainsworth et al.*, 2002), lowering the latent heat loss that increases canopy surface temperatures (*Bernacchi et al.*, 2007). This process will likely increase in heat and drought stress, declining the crop productivity (*Cias et al.*, 2005). *Leaky et al.* (2009) noted that in addition to higher photosynthetic activity of C_4 crops at elevated CO_2 level, the concomitant reduced water use and lower stress levels could play a more important role than the increased photosynthesis.

Although the crop response patterns could not be generalized (*Richardson et al.,* 2013), each one-day increase in the length of the growing season rose the yearly evapotranspiration water loss by 1.6 mm on a Mediterranean grassland (*Ryu et al.*, 2010). Contrary to the results of *Rye et al.* (2010), *Richardson et al.* (2013) found weak correlation between length of the growing season and yearly evapotranspiration total in both deciduous (9 species) and evergreen (12 species) forests (*Richardson et al.*, 2010).

However, it is obvious that phenology effects canopy microclimate, less information is available about the multitude ways in which phenology influenced canopy feedbacks to regional-scale weather patterns (*Penuelas et al.*, 2009). More observations are necessary to get reliable results for levels excessing microclimate.

The water budget–crop canopy relationship is a less known process in spite of its everyday practical use in irrigation, in which water inputs such as precipitation and irrigation, and outputs as evapotranspiration and outflows have to be considered. Precise estimation of water balance terms is almost impossible, because they use a lot of variables and parameters that are inferring and roughly measured from the sides of soil (water storage, infiltration rate, hydraulic conductivity, etc.), plant (phenology, root depth, volume, hydraulic properties, hydraulic conductivity, different types of leaf resistances, crop level characteristics, etc.), agronomic practices (cultivation, canopy level characteristics, etc.), actual weather conditions impacting the crops (interception), and climate change (changing meteorological elements excluding precipitation and temperatures) (*Savé et al.*, 2012, *IPCC* 2007). A model prediction for maize in Portugal showed an increase in actual evapotranspiration of maize in spring, when soil water content was still enough to cover the increased water demand of crop. Oppositely to observations for spring, in summer, a decline in maize evapotranspiration was observed due to soil moisture reduction, in total providing an increase in irrigation necessity of the studied area (*Savé et al.*, 2012). The general tendency of climate modification suggests that in temperate climate, a moderate increment in the irrigation necessity can be waited until 2050, while by the end of the 21th century, an extension of the irrigation period should be waited, irrespective to investigated crop species. The higher water use of vegetation may interact with the environment providing a feedback that currently seems to be difficult to quantify accurately. Due to the complexity of maize physiological responses to variation in environmental conditions, and to early initiation of the season, the shortening of 33% in the growing period (10 days) may be waited using B1 SRES scenario (*Warrington et al.*, 1999). This number was registered much higher in apple trees up to 20–25 days by the above authors for the Mediterranean area. Summing the earlier comments, we assume increasing irrigation water amounts during this century ranging from 40 to 250% depending on the crop species and growing area of the agricultural crops (*Savé et al.*, 2012).

2. Simulation of maize photosynthesis and stomatal resistance: an on-site case study

2.1. The purpose of the on-site simulation

The likely effect of increased evapotranspiration and modification in plant growth as a result of global warming are less known, however large amount of investigations was devoted to this topic (*Graaff et al.*, 2006). Due to the foregoing special behaviour of C_4 crops, it seems to be evident, that their response to elevated CO_2 received less attention than the more sensitive C_3 crops. In this study use of maize was motivated because C_4 stomata are as responsive, and in some cases more so, than C_3 stomata (*Anda* and *Dióssy,* 2010, *Triggs et al.*, 2004). We aimed to project the impacts of climate change on some maize microclimate and crop properties applying the Crop Microclimate Simulation Model (CMSM) of *Goudriaan* (1977) driven by scenario output from regional climate model. Drivers of climate change (meteorological elements and crops) interact with each other under field conditions. As the systematic synthesis regarding the impact of different meteorological and crop feature combinations is not very common, we wanted to investigate the variations in microclimatic elements and maize physiological properties resulted from climate modification side by side. Though conclusion of *Ehleringer* and *Thure* (2002) seems notable as they assume that at rising CO_2 levels the ambient gas concentration will once again cross a threshold value, where C_4 plants loose their competitive advantage over C_3 plants from the standpoint of reduced photorespiration and enhanced light-use efficiency. Maybe results of this case study should contribute to preparations in mitigating negative impacts of future climate modifications.

In order to develop proper long-term adaptation and mitigation strategies, detailed observations about on-site weather-crop responses concerning influence of climate modification are also necessary. In this study the modelling tool was applied to estimate the possible impacts of climate change on physiological characteristics of maize grown at Keszthely (Hungary). To achieve this goal, thirty-year crop and climate observations served as an archive of inputs for the CMSM model (*Goudriaan,* 1977). The principle of analogy was applied when choosing the proper crop and weather inputs for a specified scenario.

2.2. The modelling outline of crop features and inputs

Oppositely to other simulated microclimate and crop characteristics, the CMSM calculates the net photosynthesis (F) empirically on canopy level (*Goudriaan,* 1977; *Goudriaan* and *van Laar,* 1994):

$$F = (F_m - F_d)[1/\exp(R_v \varepsilon / F_m)] + F_d, \tag{1}$$

where F_m is the top of assimilation, F_d is the dark respiration, R_v is the absorbed short wave radiation (per LAI), ε is the slope of the curve of F-R_v at low light intensities, or light use efficiency ($17.2 \cdot 10^{-9}$ kgJ^{-1} for maize). The size of respiration was assumed to be –0.1 of the F_m (*Goudriaan,* 1989).

The Eq. (1) was the basis in simulation of leaf stomatal resistance (r_{leaf}) as follows:

$$F = \frac{1.83 \cdot 10^{-6}(C_e - C_r)}{1.66 r_{leaf} + 1.32 r_{b,h}}, \tag{2}$$

$$r_{leaf} = \frac{1.83 \cdot 10^{-6}(C_e - C_r)}{1.66F} - 0.795 \quad [\mathrm{sm^{-1}}], \tag{3}$$

where $r_{b,h}$ is the boundary layer resistance, 1.66 is the ratio between diffusivities for CO_2 and water vapor, $1.83 \cdot 10^{-6}$ converts CO_2 concentration into $kgCO_2\ m^{-2}$ at 20°C, C_e is the external CO_2 concentration, C_r is assumed regulatory CO_2 concentration, 1.32 is coming from conversion of r_{bh} for CO_2.

The sensible heat flux (Q_{Hi}) in the i layer is as follows:

$$Q_{Hi} = \rho c_p \frac{(T_{ci} - T_{ai})}{r_{aHi}}, \tag{4}$$

where T_{ai} is air temperature in the i layer [K], T_{ci} is canopy temperature in the i layer [K], r_{aHi} is aerodynamic resistance for sensible heat transfer in the i layer [sm^{-1}], ρ is air density [kgm^{-3}], c_p is specific heat of air [Jkg^{-1}/K^{1}].

The latent heat flux (λE_i) in the i layer is:

$$\lambda E_i = \rho c_p \{e_s(T_{ci}) - e_s\} / [\gamma(r_{awi} + r_{ci})] \tag{5}$$

where $e_s\ (T_{ci}) - e_i$ is difference between saturation vapour concentration at plant temperature and actual vapor concentration [m^3m^{-3}], r_{awi} is aerodynamic resistance for water vapour transfer in the i layer [sm^{-1}], r_{ci} is crop resistance in the i layer [sm^{-1}], γ is psychrometric constant [0.5 $gm^{-3}K^{-1}$].

More details about model structure, functioning and on-site validation of simulated variables were published earlier by *Anda* and *Dióssy* (2010), *Anda* and *Kocsis* (2008) and *Dióssy* and *Anda* (2009).

A short growing season maize acted as test crop in the model. The inputs were site and plant specific parameters and variables (geographical position of the study place, plant height, maize leaf density in three different crop layers), soil properties (actual soil moisture, physical soil characteristics) and locally collected meteorological data (on hourly basis). The meteorological elements were observed at Agrometeorological Research Station of Keszthely by using standard QLC-50 type automatic climate station. In the reference scenario (1961-90) monthly average soil moisture of -7 bar water potential was applied as an average soil moisture in July (*Table 1*). The crop characteristics such as plant height, LAI and leaf density were measured at the station between 1981 and 2010. In selection of crop characteristics for different scenarios, analogy was looking from the on-site historical measurements during the past three decades. The reference run and the present (past decade: 2004–2013) had 340 and 380 ppm (*Haszpra et al.*, 2012) atmospheric CO_2 concentrations in July, respectively. In addition five scenarios were created, in which the projections had doubled CO_2 level (760 ppm) that corresponded with the RCP6 scenario (*Moss et al.*, 2010). As the highest value, a medium range forecast for atmospheric CO_2 composition by the RCP6 scenario was applied with smooth transition towards concentration stabilization level after 2100 achieved by linear adjustment of emissions around 2100 (*vanVuuren et al.*, 2014). The RCP6, among other Representative Concentration Pathways, was adopted by the IPCC fifth Assessment Report (AR5) in 2014 (IPCC, 2014). Number 6 (Wm^{-2}) means the range of radiative forcing for 2100, relative to pre-industrial values. Associated temperature rise projection is 3.2 degrees. The intercellular CO_2 level was kept in one third of the open air one (*Anda* and *Kocsis,* 2008).

Model runs were exemplified for an "average" day in July (warmest and driest months at Keszthely).

From the model outputs, crop properties were presented for the middle (cob) layer of fully grown maize. The layer of cob formation is assumed to be the most intensive regarding the crop physiological processes.

Table 1. Summary of the used scenarios

Scenario	Air temp.	Soil moisture	CO_2 conc. Ambient air	LAI	Abbrev.
	Means for month July				
Reference	**20.3 °C**	**–7 bar**	**340 ppm**	**2.8**	**Ref***
Actual	20.8 °C	–7.7 bar	380 ppm	2.8	Act
2 × CO_2	20.3 °C	–7 bar	760 ppm	2.8	2 × CO_2
Scenario 1.	+2 °C*	–25%*	760 ppm	2.5	Scen1
Scenario 2.	+4 °C*	–40%*	760 ppm	1.5	Scen2
Scenario 3.	+6 °C*	–55%*	760 ppm	1.5	Scen3

Assuming normal distribution of both samples, paired *t*-test was used to evaluate differences between model runs performed by SPSS 17.0 Program Package. In accordance to the null hypothesis, if the mean value of differences is equal to 0, then the two samples are statistically the same. The significance level was fixed at 5%.

2.3. Discussion of the simulation results

Presently, new scenarios are applied describing the recent and future atmospheric composition including CO_2 level. These new scenarios allow a smooth transition to the future projections harmonizing with historical data (*Moss et al.*, 2008). In the projected global average air temperatures, four multi-gas emission scenarios were adapted from literature and updated for release as Representative Concentration Pathways (RCPs), with the range from 1.5 to 4.5 °C for the lowest RCP3-PD and for the highest RCP8.5 scenarios, respectively (*Moss et al.*, 2010). The range of radiative forcing are 3 and 8.5 Wm^{-2} in the scenarios RCP3-PD and RCP8.5, respectively. The assumption complemented and actualized the previous scenario-based estimations of atmospheric composition known as SRES scenarios (SRES: Special Report on Emissions Scenarios, *Nakicenovic et al.*, 2000). Scenarios in this study was about in the middle of RCP ones.

The opening of the pores that can be expressed by the stomatal resistance values has of primary importance in crop photosythetic activity due to regulation of admitted CO_2 and released water vapor. The balance between these two decisive factors may be the promise of high crop productions.

The CMSM assumes the closed pores as 2000 sm^{-1} that happens when the wilting point (–14 bar soil water potential) or sunset is reached. The midday minimum r_s of 379 sm^{-1} was calculated by the model for cob level that is about three times higher than that of the on-site measured absolute minimum r_s value for July.

In our model estimation, the lowest daily mean r_s of 577 sm^{-1} was observed in the Ref scenario (*Fig. 1*). In each scenario the daily mean r_s values significantly increased compared to the index of the period of 1961–90. A moderate but highly significant increment of 13.7% (P<=0.001) in daily average r_s of present days was simulated, probably due to warmer July temperatures (+0.5°C) and reduced monthly rainfall sums (–22%) during the past decade. Result of this simulation was in accordance to findings of *Erdélyi* (2008), who observed shortened phenological phases in maize due to temperature rises in Hungary. The only doubled CO_2 had the highest impact on maize r_s; the growth of 59.1% was highly significant (P<=0.001) with respect to Ref. The elevated CO_2 level itself narrowed the pore openings more than a half that reduced the daily mean water loss about 0.5 mm on an average day in July. On a monthly basis it is equivalent to 15 mm water decline for the whole month. This reduction in transpired water amount may be the on-site positive impact of global warming. Regarding the three scenarios with gradually intensified warming and drying, the daily average r_s increases were 54.2% (P<=0.001), 41.6% (P<=0.014) and 45.4% (P<=0.006) in Scen1, 2 and 3, respectively comparing to the r_s values of the reference period. There is an apparent contradiction between the increases of r_s in Scen1 being higher than in Scen2 and 3, but only until biological variables are taken into account by involving the size of LAI. The possible reason might had been the way of crop – and weather – input selection, the used analogies from the past. On the basis of local measurements, drastic LAI decline from LAI=2.5 to LAI=1.5 was performed in the last two scenarios (Scen1, 2), where the lower transpiring surface size and r_s might regulate the rate of transpiration together. Results of this study suggested that simulation of Scen1 kept the r_s values close to the resistance curve of only raised CO_2 scenario, implying that the negative consequences resulted from variable modifications included to Scen1 avoided strong variation in the r_s.

Tendency in daily change of r_s values was similar in model runs with the particularity that the simulated r_s values were similar to each other at high solar radiation, just about solar noon. In the case of high solar angles, the stomatal resistance values of the different scenarios were closer to each other and to the Ref run as well.

Besides daily mean r_s values, the opening time of the pores was also shifted in some of the model scenarios. Earlier on-site studies showed that the opening of pores in July used to be at 6 a.m. under clear-sky weather conditions (*Anda* and *Lőke,* 2003, *Anda et al.*, 1997). In reality, the stomatal resistance measurements of the early morning hours may be hampered by cloudiness or dewfall. The 6 a.m. pore opening was simulated only in the first three scenarios (Ref, Act, Scen1); opening time of all the other scenarios were shifted to 7 a.m. The stomatal closure time of the last three scenarios was delayed one hour either; it was 8 p.m. instead of 7 p.m. Duration of "active" pores remained the same in each scenario.

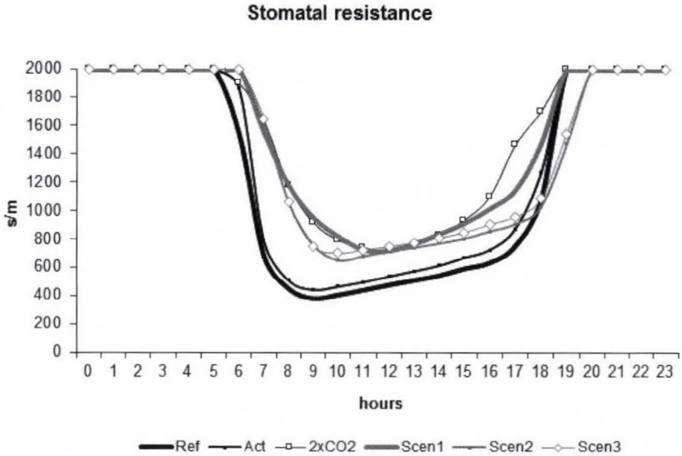

Fig. 1. Diurnal variation of simulated stomatal resistance ($r_s sm^{-1}$) in maize for Keszthely, during an average sample day in July. Results are presented for the cob level. Inputs of different scenarios and their abbreviation are in the text. Closure of stomata was assumed as 2000 sm^{-1}.

The CO_2 is one of the basic materials in photosynthesis; the higher the CO_2 concentration is, the more intense the biological process will be. The favorable effect of increased CO_2 level is widely applied long ago as CO_2-fertilization under closed growing conditions (greenhouses). The gain in carbon assimilation depends on the other physiological process, on the rate of respiration as well. At nighttime, there was no difference in respiration intensity of used scenarios (*Fig. 2*); see negative data of the *Fig. 1* by night.

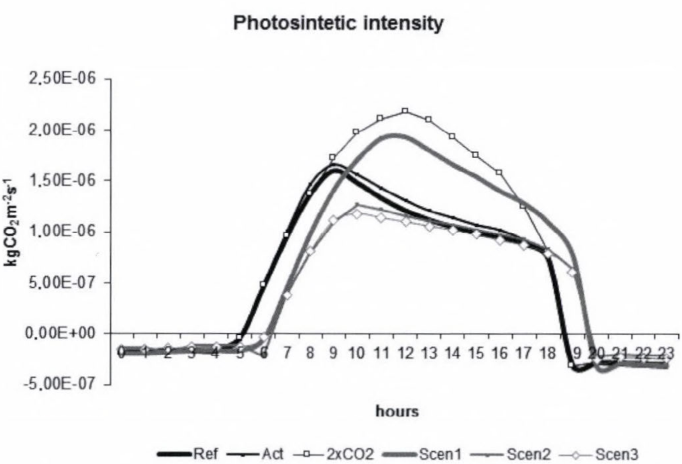

Fig. 2. Daily change in maize photosynthetic intensity ($kgCO_2m^{-2}/s^1$) during daytime hours and respiration rate ($kgCO_2m^{-2}/s^1$) by night in different scenarios for Keszthely.

Ref run was the lowest photosynthetic activity treatment in this study. Higher photosynthetic rates were simulated in all other scenarios in spite of increased r_s values, likely due to elevated CO_2 concentrations. During the past decade, the Ref photosynthesis value increased to 6.2% ($P<=0.001$) indicating an on-site positive direction of present climate modifications. Summary of the statistical analysis of different scenarios was placed in *Table 2*. Supposing otherwise unchanged weather, the Scen with doubled CO_2 level produced the highest increase of 36.1% ($P<=0.003$) in daily mean photosynthetic rate. This favorable influence could not be entirely realized with significant weather changes. As it was presented earlier in data for r_s, temperature increase of +2 °C increased with 22.7% ($P<=0.065$) rather than decreased the intensity of photosynthesis. A moderate decline was present in Scen1 with respect to doubled CO_2 scenario. We assume that this temperature rise of 2 °C together with moderate soil moisture decline does not provide a strong threat for growing maize at the surroundings of Keszthely. Photosynthesis dropped only in cases with warming exceeding +4°C and stronger soil moisture cuts. In spite of doubled CO_2, like a tendency, the daily mean photosynthesis rates were reduced by 14.1% ($P<=0.493$) and 18.6% ($P<=0.273$) in the Scen2 and 3, respectively. In these two latter scenarios, not only the expected warming but strong reduction in precipitation was also taken into account.

The energy retained by plant stands is distributed among the energy-users. The largest of all the users is the energy spent for evapotranspiration (about 70%) as latent heat flux that protects the crops from overheating. About one-third part of net radiation dissipates from the canopy as sensible heat, forming the microclimate of crops. Only a few percent of energy is utilized in the process of photosynthesis. There was a real surprise, that significant changes in both energy fluxes were only observed at doubled external CO_2 concentrations (*Figs. 3* and *4*). Elevated carbon-dioxide closing stomata gap decreased the transpiration of maize. Decline of 15.6% ($P<=0.001$) in the latent heat flux of Scen $2xCO_2$ was simulated when comparing to Ref run. The other scenarios of latent heat fluxes did not differ statistically either from each other or Ref (see also *Table 2*). The opposite modification occurred for sensible heat fluxes. Elevated CO_2 ($2xCO_2$) increased the sensible heat flux with 21.9% ($P<=0.001$) in comparison to Ref. Similarly to latent heat fluxes, in addition to Scen of $2xCO_2$, there was no significant modification in the sensible heat fluxes in any scenarios when compared to Ref one.

Table 2. Paired Samples Test of the outputs of the scenarios (Significant results are in bold)

	Paired Differences					t	df	Sig. (2-tailed)
				95% Confidence Int. of the Differences				
	Mean	Std. Dev.	SE	Lower	Upper			
Stomatal resistance								
Ref - Act	–55.542	75.277	15.366	–87.328	–23.755	–3.615	23	**.001***
Ref – 2×CO_2	–257.042	289.505	59.095	–379.289	–134.794	–4.350	23	**.000***
Ref - Scen1	–233.458	258.245	52.714	–342.506	–124.411	–4.429	23	**.000***
Ref - Scen2	–148.208	273.335	55.794	–263.628	–32.789	–2.656	23	**.014***
Ref - Scen3	–169.500	274.221	55.975	–285.293	–53.707	–3.028	23	**.006***
Photosynthetic intensity								
Ref - Act	–3.67E-8	4.3E–8	8.77E-9	–5.48E-8	–1.85E-8	–4.179	23	**.000***
Ref – 2×CO_2	–2.51E-7	3.67E–7	7.49E–8	–4.06E-7	–9.65E-8	–3.357	23	**.003***
Ref - Scen1	–1.61E-7	4.07E-7	8.31E-8	–3.33E-7	1.09E–8	–1.938	23	.065
Ref - Scen2	4.53E-8	3.19E-7	6.51E-8	–8.93E-8	1.8E-7	.697	23	.493
Ref - Scen3	6.85E-8	2.99E-7	6.1E-8	–5.78E-8	1.95E-7	1.122	23	.273
Sensible heat flux								
Ref - Act	–1.202E0	5.334E0	1.088E0	–3.454E0	1.050E0	–1.104	23	.281
Ref - 2×CO_2	–1.116E1	1.347E1	2.750E0	–1.685E1	–5.477E0	–4.060	23	**.000***
Ref - Scen1	–5.53E0	2.37E1	4.84E0	–1.56E1	4.49E0	–1.142	23	.265
Ref - Scen2	–1.36E0	2.15E1	4.39E0	–1.04E1	7.71E0	–.311	23	.759
Ref - Scen3	1.42E0	2.14E1	4.38E0	–7.63E0	1.05E1	.325	23	.748
Latent heat flux								
Ref – Act	–4.208E-1	4.336E0	8.851E-1	–2.251E0	1.410E0	–.475	23	.639
Ref - 2×CO_2	1.370E1	1.516E1	3.0964E0	7.298E0	2.011E1	4.426	23	**.000***
Ref - Scen1	6.272E0	3.311E1	6.760E0	–7.713E0	2.025E1	.928	23	.363
Ref - Scen2	1.580E0	3.703E1	7.560E0	–1.405E1	1.722E1	.209	23	.836
Ref - Scen3	–3.529E-1	3.793E1	7.743E0	–1.637E1	1.566E1	–.046	23	.964

* Significant difference

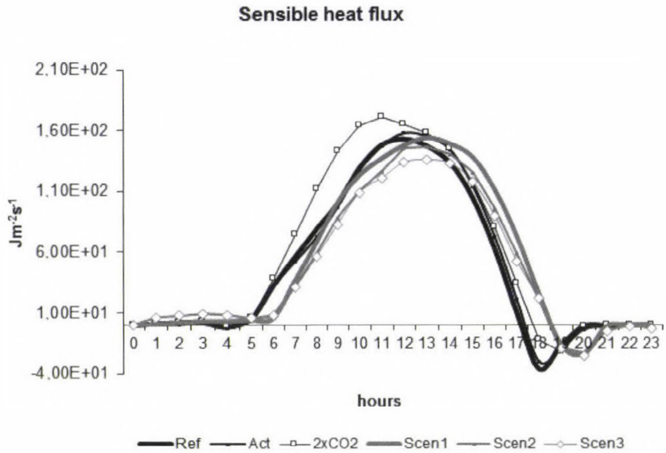

Fig. 3. Daily change in maize sensible heat flux (Jm^{-2}/s^{1}) in different scenarios for Keszthely.

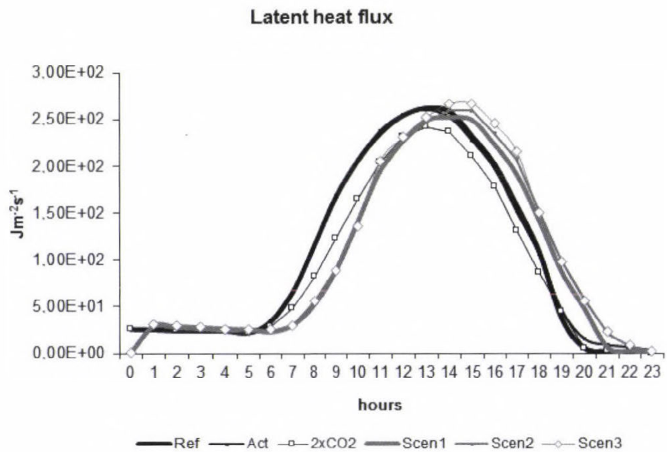

Fig. 4. Diurnal variation of latent heat flux (Jm^{-2}/s^{1}) in maize for Keszthely, during an average sample day in July.

3. Conclusion

In accordance to projected future weather scenarios, our region is expected to have more frequent and longer drought periods than at present. On the basis of scenarios, an increased importance of irrigation is expected when mitigating the on-site negative impacts of future climate change.

References

Ainsworth, E.A., Davey, P.A., Bernacchi, C.J., Dermody, O.C., Heaton, E.A., Moore, D.J., Morgan, P.B., Naidu, S.L., Ra, H.S.Y., and *Zhu, X.G.*, 2002: A metaanalysis of elevated [CO_2] effects on soybean (*Glycine max)* physiology, growth and yield. *Global Change Biol. 8*, 695–709.

Anda, A. and *Dióssy, L.*, 2010: Simulation in maize-water relations: a case study for continental climate (Hungary). *Ecohydrology 3*, 487–496.

Anda, A. and *Kocsis, T.*, 2008: Impacts of atmospheric CO_2 enrichment on some elements of microclimate and physiology of locally grown maize. *Appl. Ecol. Env. Res. 6*, 85–94.

Anda, A. and *Lőke,* Zs., 2003*:* Simulation of factors influencing maize transpiration: stomatal resistance, crop temperature and intensity of photosynthesis. *Növénytermelés 52,* 351–363. (In Hungarian)

Anda, A., Páll, J., and *Lőke,* Zs., 1997*:* Measurement of mean stomatal resistance in maize. *Időjárás 101,* 275–288.

Bernacchi, C.J., Kimball, B.A., Quarles, D.R., Long, S.P., and *Ort, D.R.,* 2007: Decreases in stomatal conductance of soybean under open air elevation of CO_2 are closely coupled with decreases in ecosystem evapotranspiration, *Plant Physiol. 143,*134–144.

Bertin, R.I., 2008: Plant phenology and distribution in relation to recent climate change. *J. Torrey Bot. Soc. 135*, 126–146.

Brown, M.E., de Beurs, K.M., and *Marshall, M.*, 2012: Global phenological response to climate change in crop areas using satellite remote sensing of vegetation, humidity and temperature over 26 years. *Remote Sens. Environ. 126,* 174–183.

vanBussel, L.G.J., Ewerta, F., and *Leffelaar, P.A.*, 2011: Effects of data aggregation on simulations of crop phenology. *Agric. Ecosyst. Environ. 142*, 75–84.

Chmielewski, F.M., Müller, A., and *Bruns*, E., 2004: Climate changes and trends in phenology of fruit trees and field crops in Germany, 1961–2000. *Agric. Forest Meteorol. 121*, 69–78.

Ciais, P.H., Reichstein, M., Viovy, N., Granier, A., Ogee, J., and *Allard, V.*, 2005: Europe-wide reduction in primary productivity caused by the heat and drought in 2003. *Nature 437*, 529–533.

Dióssy, L. and *Anda, A.*, 2009: Consequences of climate change on some maize characteristics in Hungary. *Időjárás 113,* 145–156.

Easterling, W.E., Aggarwal, P.K., Batima, P., Brander, K.M., Erda, L., Howden, S.M., Kirilenko, A., Morton, J., Soussana, J.F., Schmidhuber, J., and *Tubiello, F.N.,* 2007: Food, fibre and forest products. In (Eds. *Parry, M.L., Canziani, O.F., Palutikof, J.P., van der Linden, P.J., Hanson, C.E.*) Climate Change 2007: Impacts, Adaptation and Vulnerability. Contribution of Working Group II to the Fourth Assessment Report of the Intergovernmental Panel on Climate Change. Cambridge University Press, Cambridge, UK, 273–313.

Ehleringer, J.R. and *Thure, E.C.*, 2002: C_3 and C_4 Photosynthesis. In: The Earth system: biological and ecological dimensions of global environmental change. In (Eds. *Mooney, H.A., Canadell, J.G.*)Encyclopedia of Global Environmental Change II., John Wiley & Sons, Ltd, Chichester.

Erdélyi, É., 2008: The potential impacts of climate change on main field crops and their yield, case studies. *Klíma-21 Füzetek 55*, 53–79. (English Special Edition).

FAO, 2009: The State of Food Security in the World. Food and Agriculture Organization of the United Nations, Rome.

Fila, G., Gardiman, M., Belvini, P., Meggio, and *F., Pitacco, A.*, 2014: A comparison of different modelling solutions for studying grapevine phenology under present and future climate scenarios. *Agric. Forest Meteorol. 195–196*, 192–205.

Gaál, M., 2008: Expected changes in climatic conditions of main crops. *Klíma-21 Füzetek, 55*, 28–35. (English Special Edition).

Gioirgi, F. and *Coppola, E.*, 2007: European climate-change oscillation (ECO). *Geophys. Res. Lett. 34*, L21703.

Ghannoum, O., von Caemmerer, S., Ziska, L.H., and *Conroy, J.P.*, 2000: The growth response of C4 plants to rising atmospheric CO_2 partial pressure: a reassessment. *Plant Cell Environ. 23*, 931–942.

Godfray, H.C.J., Beddington, J.R., Crute, I.R., Haddad, L., Lawrence, D., Muir, J.F., Pretty, J., Robinson, S., Thomas, S.M., and *Toulmin, C.*, 2010: Food security: the challenge of feeding 9 billion people. *Science 327*, 812–818.

Goudriaan, J., 1977: Crop Micrometeorology: A Simulation Study. Simulation Monographs. Pudoc, Wageningen.

Goudriaan, J., 1989: Simulation of micrometeorology of crops, some methods and their problems, and a few results. *Agric. Forest Meteor. 47*, 239–258.

Goudriaan, J., and *van Laar, H.H.*, 1994: *Modelling Potential Crop Growth Processes*. Kluwer Academic Publishers, Dordrecht-Boston-London. pp 238.

Graaff, M.A.D., Groenigen, K.J.V., Six, J., Hungate, B., and *Kessel, C.V.*, 2006: Interactions between plant growth and soil nutrient cycling under elevated CO_2: a metaanalysis. *Glob. Change Biol.*, *12*, 15–20.

Haszpra, L., Ramonet, M., Schmidt, M., Barcza, Z., Patkai, Z., Tarczay, K., Yver, C., Tarniewicz, J., and *Ciais, P.*, 2012: Variation of CO_2 mole fraction in the lower free troposphere, in the boundary layer and at the surface. *Atmos. Chem. Phys. 12. 18*, 8865–8875.

IPCC, 2007. In: Core Writing Team, *Pachauri*, R.K., *Reisinger*, A. (Eds.), *Climate Change2007: Synthesis Report*. Contribution of Working Groups I, II and III to the Fourth Assessment Report of the Intergovernmental Panel on Climate Change. IPCC Secretariat, Geneva.

IPCC, 2014: Climate Change 2014: Synthesis Report. Contribution of Working Groups I, II and III to the Fifth Assessment Report of the Intergovernmental Panel on Climate Change [Core Writing Team, *Pachauri, R.K.* and *Meyer, L.A.* (eds.)]. IPCC, Geneva, Switzerland.

Ivits, E., Cherlet, M., Tóth, G., Sommer, S., Mehl, W., Vogt, J., and *Micale, F.*, 2012: Combining satellite derived phenology with climate data for climate change impact assessment. *Glob. Planetary Change 88–89*, 85–97.

Jones, *N.K.*, 2012: The influence of recent climate change on wine regions in Quebec, Canada. *J. Wine Res. 23*, 103–113.

Kirby, E.J.M., Porter, J.R., Day, W., Adam, J.S., Appleyard, M., Ayling, S., Baker, C.K., Belford, R.K., Biscoe, P.V., Chapman, A., Fuller, M.P., Hampson, J., Hay, R.K.M., Matthews, S., Thompson, W.J., Weir, A.H., Willington, V.B.A., and *Wood, D.W.*, 1987: An analysis of primordium initiation in Avalon winter wheat crops with different sowing dates and at nine sites in England and Scotland. *J Agr. Sci.109*, 123–134.

Ladányi, M., 2008: Viticulture challenges under changing climate in Hungary. *Klíma-21 Füzetek 55*, 36–52. (English Special Edition).

Leakey, *A.D.B., Ainsworth, E.A., Bernacchi, C.J., Rogers, A., Long, S.P.,* and *Ort, D.R.*, 2009: Elevated CO_2 effects on plant carbon, nitrogen and water relations: six important lessons from FACE. *J. Experim. Bot. 60*, 2859–2876.

Lara, M.V. and *Andreo, C.S.*, 2011: C_4 Plants Adaptation to High Levels of CO_2 and to Drought Environments. In: (Ed.: *Arun Shanker*) Abiotic Stress in Plants - Mechanisms and Adaptations. In Tech Europe, Rijeka, Croatia.

Ma, S., Baldocchi, D.D., Xu, L., and *Hehn, T.*, 2007: Inter-annual variability in carbon dioxide exchange of an oak/grass savanna and open grassland in California. *Agric. Forest Meteorol. 147*, 157–171.

Menzel, *A.* and *Fabian*, *P.*, 1999: Growing season extended in Europe. *Nature 397*, 659-662.

Moss, R.H., Edmonds, J.A., Hibbard, K.A., Manning, M.R., Rose, S.K., vanVuuren, D.P., Carter, T.R., Emori, S., Kainuma, M., Kram, T., Meehl, G.A., Mitchell, J.F.B., Nakicenovic, N., Riahi, K., Smith, S.J., Stouffer, R.J., Thomson, A.M., Weyant, J.P., and *Wilbanks, T.J.*, 2010: The next generation of scenarios for climate change research and assessment. *Nature 463*, 747–756.

Moss, R., Babiker M., Brinkman S., Calvo E., Carter T.R., Edmonds J., Elgizouli I., Emori S., Erda L., Hibbard, R. Jones, M. Kainuma, J. Kelleher, J.-F. Lamarque, M.R. Manning, B. Matthews, J. Meehl, L. Meyer K., Mitchell J.F.B., Nakicenovic N., O'Neill B., Pichs R., Riahi K., Rose S.K., Runci P., Stouffer R.J., vanVuuren D.P., Weyant J.P., Wilbanks T.J., van Ypersele J.P., and *Zurek M.*, 2008: Towards New Scenarios for Analysis of Emissions, Climate Change, Impacts, and Response Strategies: IPCC Expert Meeting Report, 19–21 September 2007. Noordwijkerhout. The Netherlands.

Nakicenovic, N. and *Swart, E.*, (Eds.), 2000: *IPCC* Special Report on Emissions Scenarios. Cambridge, United Kingdom, Cambridge University Press.

Noormets, A., (Ed.), 2009. Phenology of Ecosystem Processes. Springer, New York, 275 pp.

Penuelas, J., *Rutishauser, T.*, and *Filella, I.*, 2009: Phenology feedbacks on climate change. *Science 324*, 887–888.

Richardson, A.D., Keenan, T.F., Migliavacca, M., Ryu, Y., Sonnentag, O., and *Toomey, M.*, 2013: Climate change, phenology, and phenological control of vegetation feedbacks to the climate system. Review. *Agric. Forest Meteorol. 169*, 156–173.

Richardson, A.D., Black, T.A., Ciais, P., Delbart, N., Friedl, M.A., Gobron, N., Hollinger, D.Y., Kutsch, W.L., Longdoz, B., Luyssaert, S., Migliavacca, M., Montagnani, L., Munger, J.W., Moors, E., Piao, S., Rebmann, C., Reichstein, M., Saigusa, N., Tomelleri, E., Vargas, R., and *Varlagin, A.*, 2010: Influence of spring and autumn phonological transitions on forest ecosystem productivity. *Philosoph. Trans. R. Soc. B-Biol. Sci. 365*, 3227–3246.

Ryu, Y., Baldocchi, D.D., Verfaillie, J., Ma, S., Falk, M., Ruiz-Mercado, I., Hehn, T., and *Sonnentag, O.*, 2010: Testing the performance of a novel spectral reflectance sensor, built with light emitting diodes (LEDs), to monitor ecosystem metabolism, structure and function. *Agric. Forest Meteorol. 150*, 1597–1606.

Savé, R., de Herralde, F., Arand, X., Plab, E., Pascual, D., Funes, I., and *Biel, C.*, 2012: Potential changes in irrigation requirements and phenology of maize, apple trees and alfalfa under global change conditions in Fluvià watershed during XXIst century: Results from a modeling approximation to watershed-level water balance. *Agric. Water Management 114*, 78–87.

Schelling, K., 2000: Aufbau eines operationellen ferner Kuhdungs und GIS-gestützten Systems zur Zustandsbeschreibung, Ertrags und Qualitätsabschätzung von Braugerstenbeständen. PhD Thesis. Rheinische Friedrich-Wilhelms-Univ., Bonn.

Taylor, G., Tallis, M.J., Giardina, C.P., Percy, K.E., Miglietta, F., Gupta, P.S., Gioli, B., Calfapietra, C., Gielen, B., Kubiske, M.E., Scarascia-Mugnozza, G.E., Kets, K., Long, S.P., and *Karnosky, D.F.*, 2008: Future atmospheric CO_2 leads to delayed autumnal senescence. *Global Change Biol. 14*, 264–275.

Tao, F., Zhang, Z., Xiao, D., Zhang, S., Rötterd, R.P., Shia, W., Liu, Y., Wang, M., Liu, F., and *Zhang, E.*, 2014: Responses of wheat growth and yield to climate change in different climate zones of China, 1981–2009. *Agric. Forest Meteorol. 189–190*, 91–104.

Torma, Cs., Coppola, E., Giorgi, F., Bartholy, J., and *Pongrácz, R.*, 2010: Validation of a High-Resolution Version of the Regional Climate Model RegCM3 over the Carpathian Basin. *J Hydromet. 12*, 84–100.

Triggs J.M., Kimball B.A., Pinter P.J. Jr, Wall G.W., Conley M.M., Brooks T.J., LaMorte R.L., Adam, N.R., Ottman, M.J., Matthias, A.D., Leavitt, S.W., and *Cerveny, R.S.*, 2004: Free-air carbon dioxide enrichment (FACE) effects on energy balance and evapotranspiration of sorghum. *Agric. Forest Meteorol.124*, 63–79.

Vermeulen, S.J., Aggarwal, P.K., Ainslie, A., Angelone, C., Campbell, B.M., Challinor, A.J., Hansen, J.W., Ingram, J.S.I., Jarvis, A., Kristjanson, P., Lau, C., Nelson, G.C., Thornton, P.K., and *Wollenberg, E.*, 2012: Options for support to agriculture and food security under climate change. A review. *Environ. Sci. & Policy 15*, 136–144.

Vitassea, Y., Francois, C., Delpierre, N., Dufrêne, E., Kremer, A., Chuine, I., and *Delzon, S.*, 2011: Assessing the effects of climate change on the phenology of European temperate trees. *Agric. Forest Meteor. 151*, 969–980.

vanVuuren, D.P., Kriegler, E., Neill, B.C.O., Keywan Riahi, K.L.E, Carter, T.R., Edmonds, J., Hallegatte, S., Kram, T., Mathur, R., and *Winkler, H.*, 2014: A new scenario framework for Climate Change Research: scenario matrix architecture. *Climate Change 122*, 373–386.

Warrington, I., Fulton, T., Halligan, E., and *De Silva, H.*, 1999: Apple fruit growth and maturity are affected by early season temperatures. *J. Amer.Soc. Horticultural Sci. 124*, 468–477.

IDŐJÁRÁS
Quarterly Journal of the Hungarian Meteorological Service
Vol. 120, No. 1, January – March, 2016, pp. 103–125

Climate change effects on structural reliability in the Carpathian Region

Árpád Rózsás*[1], Nauzika Kovács[1], Vigh László Gergely[1], and Miroslav Sýkora[2]

[1]*Department of Structural Engineering, Budapest University of Technology and Economics, Műegyetem rkp. 3-9., Kmf. 85, H-1111 Budapest, Hungary*

[2]*Klokner Institute, Czech Technical University in Prague, Solinova 7, 16608 Prague, Czech Republic*

**Corresponding author E-mail: rozsas.arpad@epito.bme.hu,*

(Manuscript received in final form September 23, 2015)

Abstract—Climate change affects not only the natural but also the built environment. The latter comprises large part of societal wealth, and it is a crucial component of developed economies. The focus of this paper is the quantitative assessment of the reliability of load bearing structures in changing climate. Despite its significance, relatively few quantitative studies are available on this topic, and particularly the Carpathian Region has been analyzed insufficiently. Therefore, the aim of this paper is (*i*) to present two quantitative studies on structures and climate change for the Carpathian Region, and (*ii*) to give an overview about approaches in civil engineering in relation to climate sciences, thus to trigger and facilitate future cooperation. The first part of the study is about the carbonation-induced corrosion of reinforced concrete structures analyzed considering six climate change scenarios. The results show that the depassivation probability can double from the beginning to the end of the 21st century. For structures executed in 2000, the effects will be subtle within the first half of the century, whilst the considerable changes are expected in the other 50 years. The second part of the study is about ground snow load and its effect on structural failure probability. It focuses on probabilistic models and statistical uncertainties, and draws attention to the significance of uncertainties arising from the insufficient number of observations. These uncertainties are typically neglected in current civil engineering practice, and they are especially important for climate change, for which the historical observations are not representative of the future environment. Bayesian statistical approach is used to handle these uncertainties. The analyses show that statistical uncertainties can have several order of magnitude effect on failure probability, thus their neglect is not justified. Additionally, long-term trends in historical snow observations are analyzed using stationary and non-stationary generalized extreme value distributions. Statistically significant decreasing trends ($p < 10\%$) are found for numerous locations, but they are practically significant only for a few in respect of structural reliability. The results of both studies indicate that climate change can have significant practical consequences on structures and should be considered by civil engineering profession. Revision of design standards and further research in cooperation with meteorologist seem to be needed to explore and reduce the impacts of climate change on load bearing structures in the Carpathian Region.

Key-words: climate change, civil engineering, reliability, probabilistic analysis, Bayesian statistics, snow action, non-stationary models, concrete carbonation, durability, Carpathian Region

1. Introduction

The basic objective of civil engineering is to design, build, and operate facilities which serve societal needs. This is to be accomplished among various uncertainties, e.g., uncertain material properties, uncertain future usage, very rare natural or manmade hazards. The designers must then ensure that the frequency of failures does not exceed a level acceptable by society. A major source of uncertainty is associated with actions such as wind, snow, earthquakes, traffic which should be reliably predicted and anticipated during the design process. Currently applied models for representation of these actions are prevalently based on historical experience and on the assumption of stationarity. However, observations of the past decades and sophisticated climate models imply that relying solely on past experience may be misleading. It is expected that climate change will (and very likely already did) considerably alter environmental conditions and extremes (*IPCC,* 2012; *Milly et al.*, 2008; *Retief et al.*, 2014). Thus, there is an urgent need to revise current design provisions and to incorporate the predicted effects of climate change.

Since engineering works are crucial components of industrialized societies and intended to be used by many generations – their service life is often over 100 years –, it is imperative to consider the expected effects of climate change. It is substantially cheaper to reduce the impacts of climate change today by designing resilient structures rather than to cope with more severe impacts by rehabilitations of existing structures in future. It is estimated that in 2010, climate change had already contributed to economic losses about 1% of global GPD; a considerably increase is expected in the future (*DARA*, 2012).

The potential adverse effects of climate change on structures are recognized and investigated for several regions and countries, e.g., Ireland (*CIACC*, 2009), Canada (*ACC*, 2008), and the United Kingdom (*IECCA*, 2011). These studies mainly focus on identifying and enumerating the effects and possible issues. Only relatively few quantitative numerical studies are available. Numerical researches are conducted in Australia within the framework of a national flagship program (*Nguyen et al.*, 2010; *Stewart* and *Wang*, 2011; *Wang et al.*, 2010).

To the authors' knowledge, few studies have been focused on construction works in the Carpathian Region and most of them intended to draw attention to the issue of climate change without any quantitative analysis (*Lenkei*, 2007; *Timár*, 2010; *VAHAVA*, 2010) or focusing on building physics and energetics (*Medgyasszay et al.*, 2007). A study by *Horváth* and *Pálvölgyi* (2011) is quantitative but not focused on structural or reliability aspects. That is why the authors conduct quantitative analysis of climate change on load bearing structures to provide first insights and to support decision making. The aims of this paper are:

- to present two quantitative studies dealing with typically neglected though important aspects in civil engineering;
- to give a broader view about relation of civil engineering with meteorology, thus to facilitate cooperation between experts, and to bridge the gap between engineering and climate sciences;
- to draw attention of civil engineers to challenges related to climate change.

The contribution summarizes the main findings of the previous conference contributions by the authors (*Rózsás* and *Kovács*, 2013a; *Rózsás et al.*, 2015; *Rózsás* and *Vigh*, 2014), and extends them by providing a broader perspective. The first study is dealing with carbonation induced corrosion of concrete structures considering six climate change scenarios. The second study is focused on modeling of extreme snow events, long-term trends in meteorological observations, and their effect on failure probability with special focus on statistical uncertainties. Both topics seem to be underestimated and often neglected in the present practice.

2. Climate change and civil engineering

2.1. Impacts of climate change on civil engineering structures

There is a virtually unanimous consensus among climate scientist that climate change is an ongoing process, largely caused by human activity, and urgent, large-scale measures are needed to avoid dangerous, irreversible, practically uncontrollable consequences (*Anderegg et al.*, 2010; *IPCC*, 2014; *Leshner et al.*, 2009; *UNFCCC*, 2010).

Climate change response strategies can be divided broadly into two categories: mitigation and adaptation (*IPCC*, 2001). These two strategies are often interrelated, i.e., by enhanced corrosion protection of bridges, future durability issues are moderated (adaptation) along with decreasing the green-house gas emissions by reducing traffic congestion and detours due to reduced maintenance (mitigation). Given the predicted severe consequences of climate change (*Warren*, 2011), surprisingly few studies are focused on large scale mitigation only. A notable exception is the research group of Mark Jacobson, which demonstrated that transition to renewables in the US of the all-purpose energy system (for electricity, transportation, heating/cooling, and industry) is economically and technologically feasible by 2050 (*Jacobson et al.*, 2015).

Table 1 summarizes some effects of climate change which bear relevance to construction works.

Corrosion related issues deserve special attention, since durability requirements and regulations are typically underdeveloped in standards. Furthermore, the corrosion related effects and costs are enormous but they are typically considerably underestimated, partially as they are not accompanied by singular catastrophic events. The most costly natural disaster in history, the 2011 Tōhoku earthquake and tsunami with $235 billion damage as high estimate (*WB*, 2011), is only one-fourth of the annual corrosion related losses in the US (over $1 trillion). The latter number is estimated using the 2013 level GDP of the US and approximating the sum of direct and indirect corrosion costs to be 6% of the GDP (*Koch et al.*, 2001).

The aging and deteriorating bridges are common and urgent issue worldwide. As an example, in Hungary 60% of the bridge population is over 50 years old (*KKK*, 2012), and 25% of highway bridges are rated with local or global deficiencies (rating 4 or 5 on a 5 scale measure with 5 as the worst) (*Tóth*, 2012); similar figures apply for the Czech Republic. Moreover, the infrastructure comprises a great amount of national wealth in every country, e.g., in the UK at least 50% (*Long*, 2007). In Hungary, the transportation infrastructure is about one-fifth of the total national wealth, and it generates 5–6% of the GDP. 2–3% of GDP is annually devoted to its development (*KKK*, 2008).

2.2. Design standards – Eurocodes

Standards and design provisions are the main instruments of everyday engineering practice, aiming to design and construct reliable structures. Practicing engineers have typically insufficient knowledge or lack of time to conduct advanced analyses beyond provisions in standards; therefore, it is largely the responsibility of the research community to address challenges and needs of society. The importance of this task is well illustrated by that the built environment comprises about 80% of the national wealth of developed nations (*Sarja*, 2005).

Table 1. Selected projected impacts of climate change with relevance on load bearing structures.

Description	Climate	Struct. eng.
For the Central European region, the mean recurrence time of the current (1981–2000) 20 years return period daily precipitation maxima is expected to reduce to 16–10 years for 2046–65 period, and to 16–7 years for 2081–2100 period. The ranges are covering 50% of the considered climate models and corresponding to B1, A1B, and A2 scenarios (*IPCC*, 2012).	Precipitation	Floods, slope stability, landslides, scours
For the Central European region, the mean recurrence time of the current (1981–2000) 20 years return period daily temperature maxima is expected to reduce to 10–2 years for 2046–65 period, and to 6–1 years for 2081–2100 period. The ranges are covering 50% of the considered climate models and corresponding to B1, A1B, and A2 scenarios (*IPCC*, 2012).	Temperature	Expansion joint, rail track buckling, increased stresses
Using the 1951–80 period as reference, the monthly temperature during northern hemisphere summers are expected to increase significantly. The percentage of global land area with over 3 and 5 sigma reference thresholds are predicted to increase from less than 1% to 19% and from less than 1% to 2–3%, respectively, by 2100 for RCP2.6 scenario. The percentage of the global land areas in the same order for RCP8.5 scenario are 87% and 58% (*Dim* and *Alexander*, 2013). The former scenario or concentration pathway (RCP2.6) is very likely already unattainable, and the latter (RCP.8.5) represents the most severe, business-as-usual case with increasing greenhouse gas emission to the end of the 21st century.		
The probability of mega-heatwaves, such as the 2003 and 2010 summer extremes in Europe, are predicted (A1B scenario) to increase 5 to 10 times within the next 40 years (*Barriopedro et al.*, 2011).		
For some regions in Australia (Cairns, Townsville, Rockhampton, and Brisbane), climate change induced mean wind damage losses can increase by \$2.8, \$7.1 and \$15 billion by 2030, 2050, and 2100, respectively. For new constructions, the increase of the wind pressure design value is a cost-effective adaptation measure (*Stewart* and *Wang*, 2011).	Wind	Roofs, claddings
For reinforced concrete structures, *Stewart et al.* (2011) found that in Australia the carbonation-induced corrosion damage risk can increase by 40–460% at the end of the 21st century, compared to year 2000 as reference. The same study demonstrated that chloride ion induced damage risk can increase by 6–15%.	Combined*	Corrosion
Nguyen et al. (2013) studied the atmospheric corrosion of metal fasteners in timber construction for Australia under the A1FI scenario (most severe among considered scenarios) using the most severe global circulation models, and found 40% and 20% increase in corrosion rate for Brisbane and Melbourne, respectively, by 2100 comparing with 1990 as reference.		

*The combination of multiple meteorological changes can be important for corrosion, where typically the interplay of multiple factors is crucial, e.g., wet-dry surface alteration and temperature change.

To illustrate where and how climate change and climate research are connected to standards, the conceptual framework of standardization and its relation to engineering practice is depicted in *Fig. 1*. The process starts with gathering theoretical and empirical information to identify the physical and probabilistic models required to represent the behavior of various structures and their loads. These coupled physical-probabilistic models are applicable to structural design. However, they are excessively complex for everyday use. Therefore, the probabilistic models are replaced with approximate deterministic methods, where sufficient reliability is achieved by application of safety factors. These factors are calibrated to more advanced probabilistic models to ensure the target reliability, which should represent an optimum value for the whole society considering human, environmental, and economic aspects (*Steenbergen et al.*, 2015). This procedure is conceptual since the subject is overly complex and uncertain, thus these calculations cannot be precisely completed. The acceptable level of failure probability is typically expressed in terms of target reliability, which is based on expert judgement, comparative analysis of human risk acceptance and perception, and limited quantitative analysis. In Europe, for a typical building, the annual target failure probability of 10^{-6} is selected for structural failure. It should be noted that this is a nominal value for decision making, and does not correspond to actual failure rates that are typically governed by uncertainties not covered in standards such as human errors and negligence. These account for about 80% of the observed failures (*Melchers*, 2002; *Melchers et al.*, 1983).

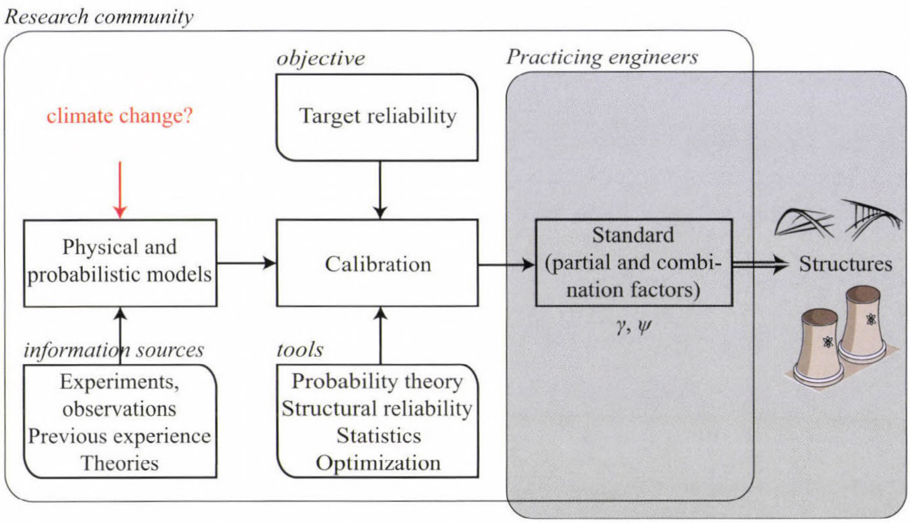

Fig. 1. Conceptual framework of standard calibration and its connection to engineering practice.

Hereafter, we focus mainly on the common European standard for basis of design – EN 1990 (hereafter 'Eurocode' for brevity). It is based on the limit state concept, i.e., the boundary between meeting (safe) and failing to fulfill a demand (failure) is sharp, characterized by a sudden change in performance. This is illustrated in *Fig. 2* along with the requirements and limit states of the Eurocode. The three principal requirements that a structure should fulfill are:

- structural resistance (avoid partial or full collapse);
- serviceability (not to impede usage, operation);
- durability (limit deterioration).

These are treated in the framework of ultimate (ULS) and serviceability limit states (SLS). The basic approach to verification of the limit states in the Eurocode is the partial factor method.

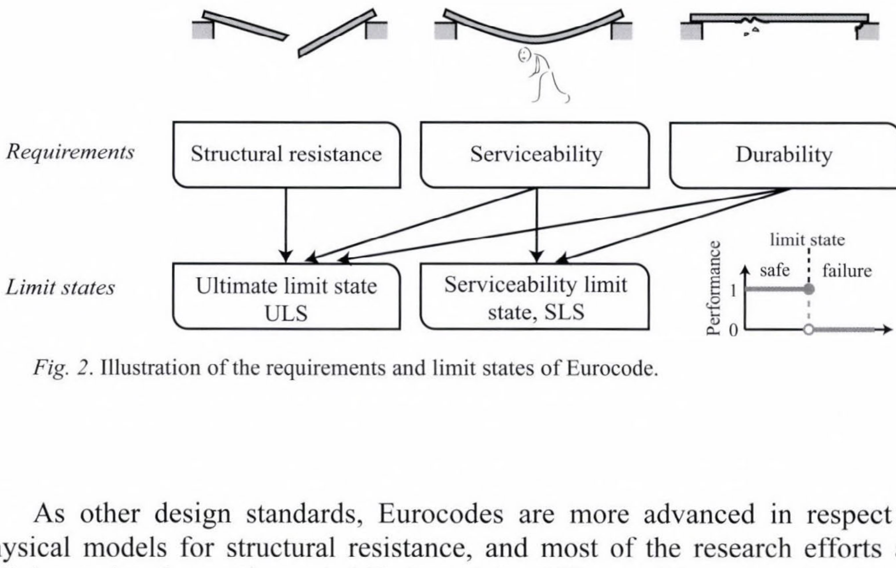

Fig. 2. Illustration of the requirements and limit states of Eurocode.

As other design standards, Eurocodes are more advanced in respect of physical models for structural resistance, and most of the research efforts are still devoted to these. The probabilistic and durability models are less developed; however, this biased focus is not justified. The disproportional development of physical and probabilistic models renders the advances in the former less effective (*McRobie*, 2004), e.g., the impact of 10% improvement in a resistance model of steel members is overweighed by the uncertainties in the probabilistic load models. Regarding durability, the economic cost of corrosion is enormous, typically much larger than those associated with structural failures, e.g., in the US the total cost of weather-related disasters for 22 years ($380 billion) is comparable to the annual direct cost of metallic corrosion ($276 billion, 3% of the US, GDP). Moreover, the indirect costs, associated with the loss of productivity, are estimated to be equal of direct costs (*Koch et al.*, 2001). In respect of climate change, these findings suggest that probabilistic analysis and durability issues are of utmost importance.

2.3. Methodology

Analysis and plan of responses to climate change are inherently probabilistic and interdisciplinary issues. This probabilistic nature is in-line with engineering work, which has to cope with numerous uncertainties by means of the probability theory, statistics, and structural reliability. In reliability analyses, the failure probability of structures and structural elements is estimated using the limit state concept. A limit state function ($g(\mathbf{X})$) is typically formulated as the difference of capacity and demand:

$$g(\mathbf{X}) = capacity - demand\,, \tag{1}$$

thus $g(\mathbf{X}) < 0$ describes exceedance of the limit state (*Fig. 3*). All relevant basic variables ($\mathbf{X}$) are represented as random variables with their probability density functions. The failure (violation of limit state) probability then can be calculated as the integral of the joint density function $f_{\mathbf{X}}(\mathbf{x})$ of basic variables over the $g(\mathbf{X}) < 0$, failure region:

$$P_{\mathrm{f}} = P\left(g(\mathbf{X}) < 0\right) = \int\limits_{g(\mathbf{X})<0} f_{\mathbf{X}}(\mathbf{x}) \cdot d\mathbf{x}\,. \tag{2}$$

The above – typically high-dimensional – integral is usually approximated by numerical techniques especially tailored for the particular features of structural reliability problems (*Lemaire et al.*, 2010; *Melchers*, 2002). The design point (*Fig. 3)*, associated with the highest density value on the failure surface ($g(\mathbf{X}) = 0$) is an important element of reliability analysis, that provides information about the importance of random variables and failure probability. Although in this paper the comparisons and conclusions are solely based on the failure probabilities, structural reliability analyses are often extended to risk-based decision making problems considering economic and environmental consequences, and human safety as well (*Köhler*, 2011).

Both in civil engineering and climate sciences, coupled physical-probabilistic models are used to represent complex systems and to propagate uncertainties. In climate sciences, estimates of the first two moments (mean, standard deviation) of random variables are typically sufficient, in civil engineering, full specification and propagation of random variables are necessary to calculate low failure probabilities.

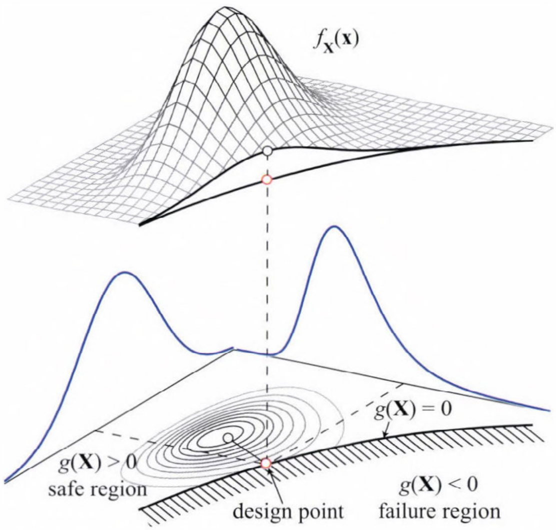

Fig. 3. Illustration of the limit state function, design point, and the safe and failure performance regions.

3. Probabilistic analysis of reinforced concrete structures exposed to carbonation

3.1. Carbonation of reinforced concrete structures

Concrete is the most widely used manufactured material worldwide as its constituents are widely available, it can be casted into almost any shape, and it has favorable physical properties to work together with steel reinforcement. A particularly important property is that concrete provides an alkaline environment, which prevents the atmospheric corrosion (oxidation) of the embedded steel elements, i.e., ensures the passivation of steel. Carbonation of concrete is a chemical process which leads to lower pH value and corollary to the depassivation of steel. Since the oxidation product (rust) has smaller density than the steel, the process leads to cracking and spalling of concrete (*Fig. 4* - the numbers of states are related to those in *Fig. 5*), and ultimately can induce serviceability and structural resistance problems.

3.2. Probabilistic analysis

Carbonation is the most common corrosion cause of reinforced concrete that affects almost every structure. It is mainly driven by the CO_2 concentration of the surrounding air which diffuses into the concrete and reacts with it (*Fig. 4*); thus, the expected increase of CO_2 in the future might considerably accelerate the process. To investigate this, time-variant probabilistic analysis (*Melchers*,

2002) is performed considering six climate change scenarios. For simplicity, only the depassivation period is taken into account, which is typically longer than the propagation period (*Fig. 5*), and it is expected to give good indication of the possible changes regarding the entire corrosion process.

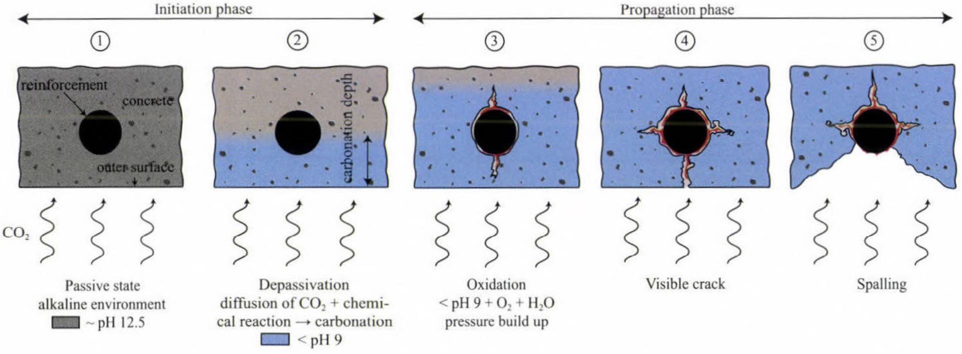

Fig. 4. Carbonation process of reinforced concrete, illustration of initiation and propagation phases.

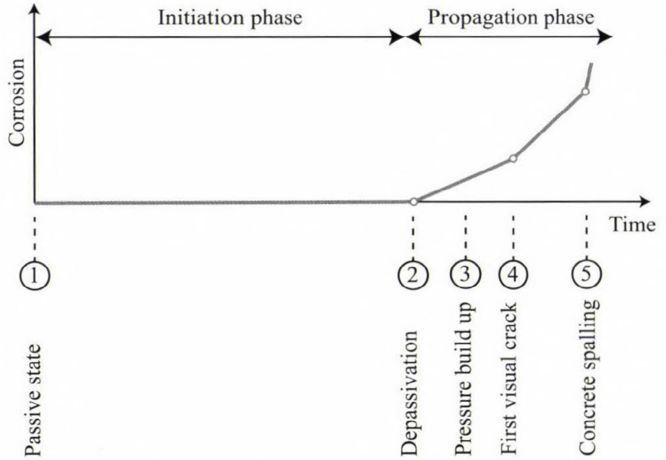

Fig. 5. Evolution of carbonation-induced corrosion in time.

The corrosion model and probabilistic description of basic variables provided by *fib* - the International Federation for Concrete Structures is adopted (*CEB/fib*, 2006). The corrosion model based on Fick's law of diffusion was extended by the authors to the case of time-varying CO_2 concentration (*Rózsás* and *Kovács*, 2013b). Six SRES climate change scenarios are considered: three scenarios within the rapid economic growth family A1: the A1FI (fossil intensive), A1T (predominantly non-fossil), and A1B (balanced) scenarios, and additionally the A2 (regionally oriented economic), B1 (global environmental sustainability), and B2 (local environmental sustainability) scenarios (*IPCC*, 2007) with probabilistic representation of CO_2 level, number of rainy days, and relative humidity. Additionally, a reference scenario corresponding to a constant CO_2 level for the year 2000 is considered as representing the provisions solely based on past experience.

Reliability analyses are completed for a hypothetical structure built in 2000, assuming 100 years design working life. The structure is thus expected to operate without major structural maintenance within this period. The minimal durability provisions of EN 1992-1-1 for design of concrete structures and the superseded Hungarian national standard (*ÚT*, 2002) are analyzed. The latter is motivated by the fact that significant portion of the Hungarian bridge inventory is constructed according to the pre-Eurocode national standards. It is anticipated that the neighboring countries in Central Europe had similar provisions, thus the results are indicative for their conditions as well.

The depassivation probabilities for each decade in the 2000–2100 period are calculated using crude Monte Carlo simulation. Various exposure classes (XC2, XC3, XC4) and cement types (CEM I 42.5 R, CEM I 42.5 R+FA) are considered to cover a large range of reinforced concrete structures. The exposure classes correspond to different environmental conditions differentiated by the duration and frequency of wet and dry phases (*CEN*, 2000, 2004). For example, XC2 class belongs to wet, rarely dry environment which is typical for industrial floors and building foundations, and XC4 represents cyclic wet and dry environment which is applicable for bridge piers, piles, and bridge superstructures.

4. Results

The time-course of the depassivation probabilities are illustrated in *Fig. 6*, the blue lines are representing the six climate change scenarios, while the yellow stands for the reference model.

The SRES scenarios are unanimously predicting increase in the depassivation probability compared with the reference model. The difference between the climate change scenarios and reference model becomes more substantial with increasing time. With the exception of EC-XC4, the durability provisions yield to greater depassivation probability than the selected 10% target (*CEB/fib*, 2006). The deficiency in the ÚT provisions is particularly apparent for CEM I 42.5 R cement, for which the target probability is reached within 30–40 years, even with the reference model, and the depassivation probability at 2100 is about 0.4 (*Fig. 6*). This means that for 4 out of 10 such structures, the depassivation of the reinforcement can be expected. The expected changes in carbonation depth (*Fig. 4*) and depassivation probability for the 2000–2100 reference period are summarized in *Table 2.* The numbers show that although the smallest relative changes are expected for the ÚT provisions, in absolute terms they are performing the worst (*Fig. 6*). Additionally, albeit the EC-XC4 provision has the largest relative increase (>100%), it still complies with the 10% limit value.

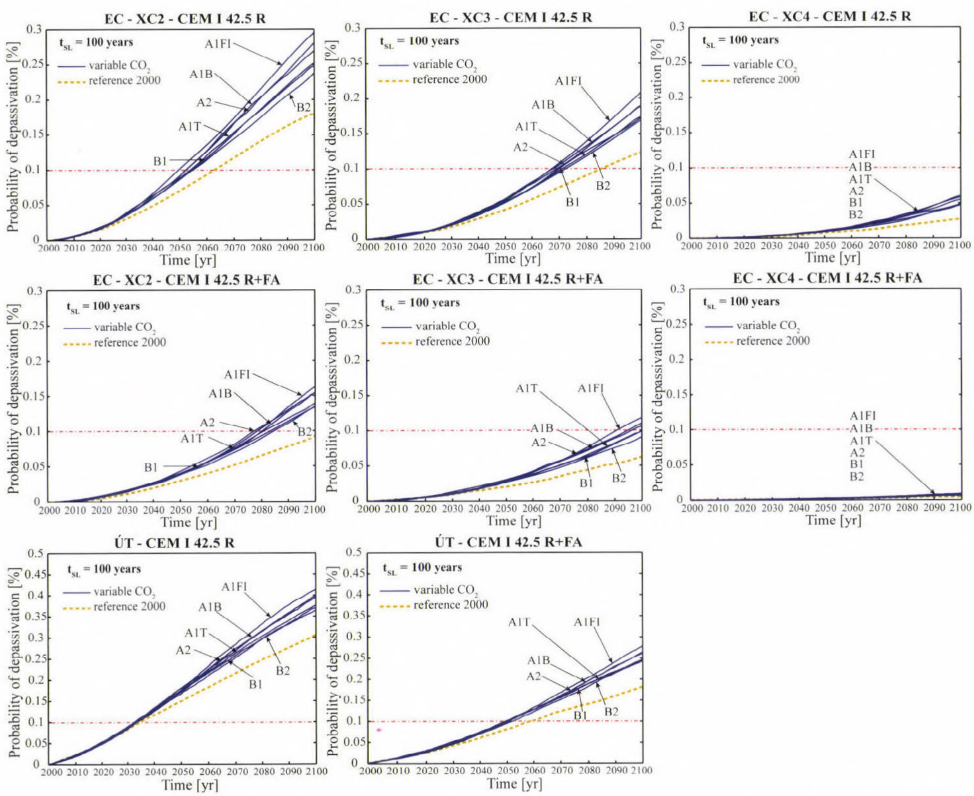

Fig. 6. Probability of depassivation corresponding to a hypothetical structure built in 2000 with 100 years design working life (t_{SL}), and using the provisions of Eurocodes (EC) and the superseded Hungarian national standard (ÚT) for multiple exposure classes (XC2-4), cement types (CEM I 42.5 R, CEM I 42.5 R+FA), and climate change scenarios (A1FI, A1T, A1B, A2, B1, B2). The selected target probability is 10% (*Rózsás* and *Kovács*, 2013a).

Table 2. Increase in carbonation depth (x_c) and depassivation probability (P_f) compared to the reference model, the intervals cover the considered six climate change scenarios (*Rózsás* and *Kovács*, 2013a).

		CEM I 42.5 R		CEM I 42.5 R+FA	
Standard	**Exposure class**	Δx_c [%]	ΔP_f [%]	Δx_c [%]	ΔP_f [%]
Eurocode	XC2	11 – 20	33 – 61	13 – 21	55 – 90
	XC3	12 – 21	44 – 73	12 – 20	50 – 82
	XC4	12 – 20	70 – 115	10 – 19	65 – 100
ÚT	–	11 – 20	21 – 36	13 – 21	33 – 55

The following conclusions are drawn from the probabilistic analysis:

- It is expected that the increased CO_2 concentration will lead to practically significant increase of depassivation probability compared with the reference model based on concentration corresponding to year 2000. The probability can increase by 115% until the end of the 21st century (*Table 2*).
- Most of the analyzed EC and ÚT durability provisions do not meet the considered 10% target probability, not even for the reference scenario (no climate change). By 2100, the EC and ÚT regulations can yield to 2.5 and 4.0 times greater depassivation probability, respectively, than the target, considering the most commonly used CEM I 42.5 R cement type (*Fig. 6*).
- For structures built in 2000, the effect of climate change is expected to be subtle till the middle of the 21st century, the practically significant effects are predicted for the second half of the century.

The findings indicate that the revision of the current durability provisions would be timely. To select appropriate adaptation measures, the analysis should be extended with the propagation phase of the corrosion and with economic cost analysis. These findings are deemed indicative, even if the presented analysis is intentionally simplified. For large structures, spatial variability in material and geometry characteristics needs to be taken into account, and the optimum target reliability may be different from the level indicated by the *fib* bulletin (*Holický*, 2011; *Sýkora* and *Holický*, 2013).

5. Snow extremes and structural failure probability

5.1. The effect of statistical uncertainties

In contrast with the serviceability and durability requirements, the target failure probability for ultimate limit states – associated with partial or full collapse of structures or structural members – is several orders of magnitude smaller. It is typically determined by distribution fractiles to which no observations are available (
Fig. 8). For example, for meteorological extremes, commonly 50–100 years of observations are available, but failure probabilities of about 10^{-4} in 50 years should be calculated and justified. Therefore, it is of crucial importance to account for statistical uncertainties which arise from the scarcity of available information. It is alarming that the current practice in civil engineering commonly neglects these uncertainties and uses 'best' point estimates such as maximum likelihood estimates, thus leads to deceptive confidence.

Coles et al. (2003) report the 'embarrassingly frequent' occurrence of events believed to be quasi-impossible, and partially attribute this to the neglect of statistical uncertainties in probabilistic models. Statistical uncertainty is composed of parameter estimation uncertainty and model selection uncertainty. The former is the uncertainty in the identification of the parameters of a particular probabilistic model, while the latter is the uncertainty in the identification of the generating model type. Both of these uncertainties are illustrated in *Fig. 7*, parameter estimation uncertainty by confidence bands, and the model selection uncertainty by considering multiple models. *Fig. 7* shows the annual ground snow maxima for two representative locations of the Carpathian Region: Budapest represents low-land areas with Fréchet-like distribution (skewness$<$1.14), and the Slovakian Tatra Mountains represents mountainous areas with Weibull-like distribution (skewness$<$1.14). The data are obtained from the CARPATCLIM project as snow water equivalents in daily temporal resolution covering the 1961–2010 period (*Szalai et al.*, 2013).

The interval coloring in *Fig. 7* and
Fig. 8 is 'ink-preserving', i.e., the same 'amount of ink' is used for every vertical section, hence creating a linear transition from the narrowest (dark blue) to the widest interval (white). In a particular 2×2 figure, equal ranges have the same color on each subplot, thus the models are directly comparable based on coloring as well. *Fig. 7* shows that moving away from the observations, the confidence bands are substantially widening. The difference between the models is remarkable, especially the narrow confidence band of the Gumbel distribution, which often does not encompass the largest observations.

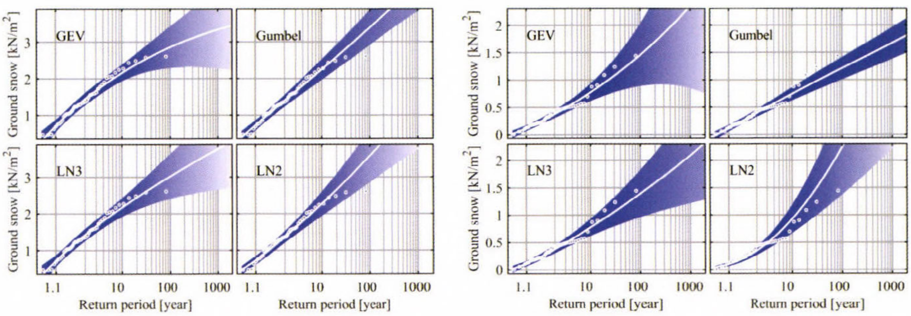

Fig. 7. Illustration of statistical uncertainty for annual maxima of ground snow load in Gumbel space, maximum likelihood fit with 90% confidence band (delta method). Slovakian Tatra Mountains (left), Budapest (right). GEV – generalized extreme value distribution, LN3 – three-parameter lognormal distribution, LN2 – two-parameter lognormal distribution.

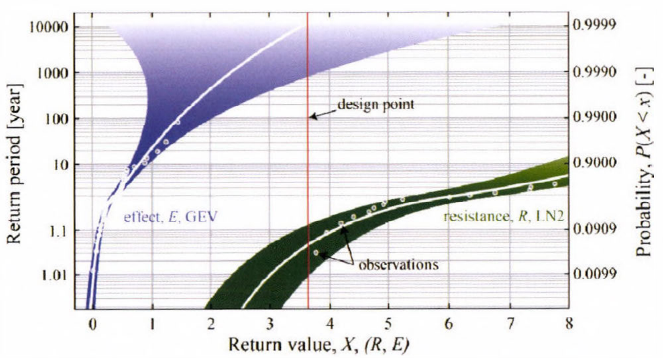

$$g = R - E$$

$$R \sim \text{GEV}; \quad E \sim \text{LN2}$$

	mean	CoV	n_{obs}
R	6.4	0.3	20
E	0.4	0.7	49

$$P_f = 1.8 \times 10^{-5}$$

Fig. 8. Illustration of parameter estimation uncertainty and its relation to design point for a simplified reliability problem, maximum likelihood fit with 90% confidence band (delta method). E is inferred from the annual ground snow maxima of Budapest, also used in *Fig. 7*.

5.2. Reliability analyses

Failure probability is determined by the very uncertain tail of distributions. *Fig. 8* shows cumulative distribution functions of resistance and effect random variables for a simple limit state function. The probabilistic models of the random variables are inferred from a limited number of observations, and the parameters are selected to represent a lightweight steel structure subjected to snow load. The parameter estimation uncertainty is substantial as the confidence bands at the design point (red line) show. This small example well illustrates that using only the point estimates (white lines) conveys false confidence in the models.

The confidence interval around the maximum likelihood point estimate (ML) illustrates the extent of parameter estimation uncertainty. However, this frequentist approach does not allow incorporating parameter estimation uncertainty directly into failure probability. This can be accomplished within the Bayesian paradigm, which bases the inference on the relative evidence of the parameter values given a dataset (*Spiegelhalter* and *Rice*, 2009). Additionally, it treats the distribution parameters as random variables, thereby enabling to integrate them into the failure probability. Herein Bayesian posterior predictive distribution (BPP) is chosen to take into account parameter estimation uncertainty (*Aitchison* and *Dunsmore*, 1980). For comparison, Bayesian posterior mean (BP) as Bayesian point estimate is also considered, this represents a model without parameter estimation uncertainty. For all Bayesian calculations, vague priors are used.

To compare these approaches and to further illustrate the effect of statistical uncertainties, a steel frame is analyzed in the following section (*Rózsás* and *Vigh*, 2014). Reliability of such lightweight structures is often dominated by snow load. The simple 2D steel frame, illustrated in *Fig. 9*, with a span of 12 m and bay width of 5 m is subjected to self-weight, permanent load, wind load, and snow load. The hypothetical structure is located in Budapest, the annual snow maxima presented in the right side of *Fig. 7* are used to infer the distribution parameters.

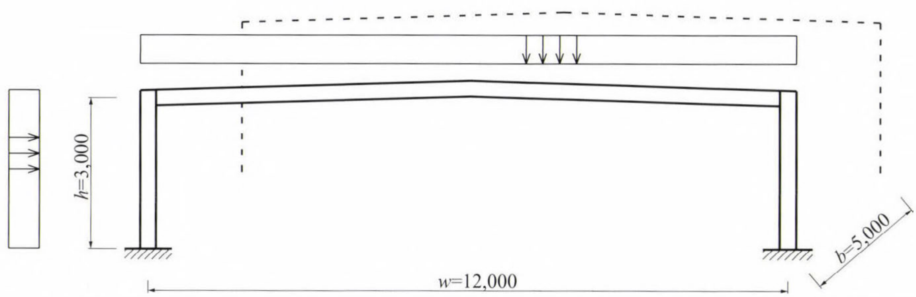

Fig. 9. Steel frame exposed to permanent, snow, and wind load (*Rózsás* and *Vigh*, 2014).

The structure (cross-section dimensions) is designed in accordance with Eurocode 3 (*CEN*, 2005) with full (100%) utilization. Parametric study is completed, in which:

- the ratio of the snow load to the whole load effect, χ, is varied and the structure is accordingly redesigned for each case;
- two distribution types and
- three distribution parameter estimation techniques are tested for annual maxima of the ground snow load.

6. Results

Left part of *Fig. 10* compares the annual failure probabilities calculated by different parameter estimation techniques, using Gumbel distribution. It appears that BP and ML may underestimate the statistical uncertainties and the failure probability of the structure. It is clear that this effect becomes more significant with an increasing snow load ratio.

For different distribution types and parameter estimations, right part of *Fig. 10* shows the failure probability in function of the snow load ratio. It is confirmed that the probability of failure may considerably increase if the snow load follows GEV distribution. It is also shown that GEV is more sensitive for the incorporation of parameter estimation uncertainty.

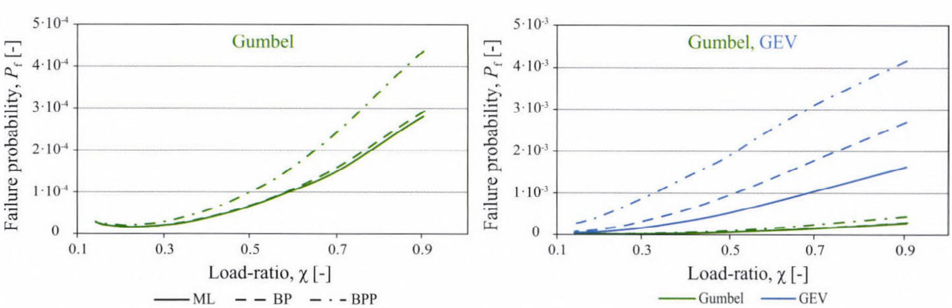

Fig. 10. Effect of distribution parameter estimation techniques on annual failure probability (P_f) in respect of load ratio (χ).
ML: Maximum likelihood, BP: Bayesian posterior; BPP: Bayesian predictive posterior.

Fig. 10 confirms that:

- The parameter estimation uncertainty in snow model has a significant effect on the reliability, in case of Gumbel and GEV distributions the incorporation of this uncertainty yields to about 1.4 and 5 to 6 times greater failure probability, respectively.
- The GEV-ML model leads to about 7 times greater failure probability than the Gumbel-ML model which is adopted in the Eurocode.

The consideration of these uncertainties can be especially important for safety critical facilities such as nuclear power plants.

6.1. Non-stationary extremes - long-term trends in time

The analyses in the preceding sections are based on stationary probabilistic models; however, some studies concerning snow precipitation found decreasing trend in Europe. *Birsan* and *Dumitrescu* (2014) have analyzed historical observations from Romania and detected decrease in snowfall days (82% of stations) with substantial decrease in snow depth (18% of stations) and snow coverage (29% of stations). *Marty* and *Blanchet* (2012) have found statistically significant (p<5%) decreasing long-term trends in annual maxima snow depth for the Swiss Alps.

Time trends in annual maxima of ground snow load and their effect on structural reliability have been insufficiently studied for the Carpathian Region so far. Therefore, the long-term trends in annual snow maxima are analyzed for the entire region using the data from CARPATCLIM database (*Szalai et al.*, 2013).

Initially, a straight line is fitted to the annual maxima in least square sense. The slope parameter (m) with a representative location is illustrated in *Fig. 11*. Decreasing trend in annual snow maxima is found for 97% of the studied region.

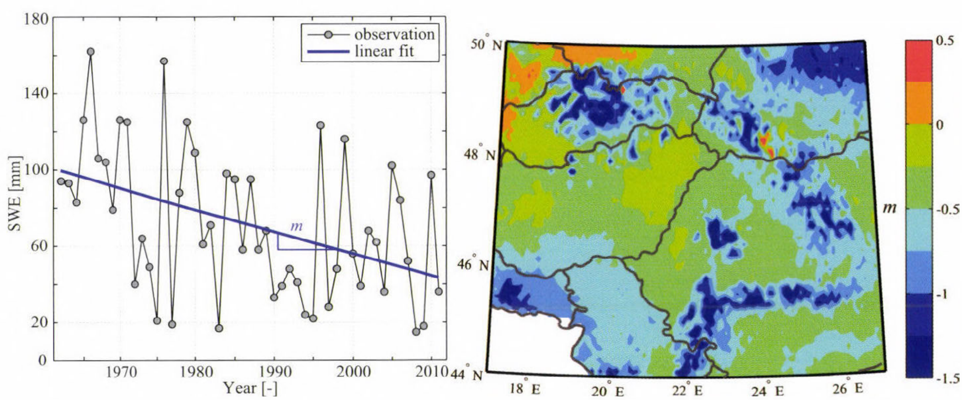

Fig. 11. A representative location with decreasing trend (left), and map of the linear trend line's slope parameter m in mm/year (right) (*Rózsás et al.*, 2015).

Then, stationary and various non-stationary univariate generalized extreme value distributions are fitted to each grid points. Maximum likelihood method is used for parameter identification, and likelihood ratio and Akaike information criterion based comparison are applied to detect statistically significant trends. The Akaike weight (*Burnham* and *Anderson*, 2002) based comparison of stationary and non-stationary (linear trend in location parameter) models are presented in *Fig. 12.* The likelihood ratio and Akaike weight based comparisons identified numerous locations with statistically significant ($p<10\%$) trends. However, further reliability analyses revealed that these trends are often not practically significant in respect of structural reliability. This is mainly attributed to the considerable uncertainty of the probabilistic snow model in the range of the design point. For locations where practically significant trend is identified the change is favorable, i.e., the increase of reliability can be expected.

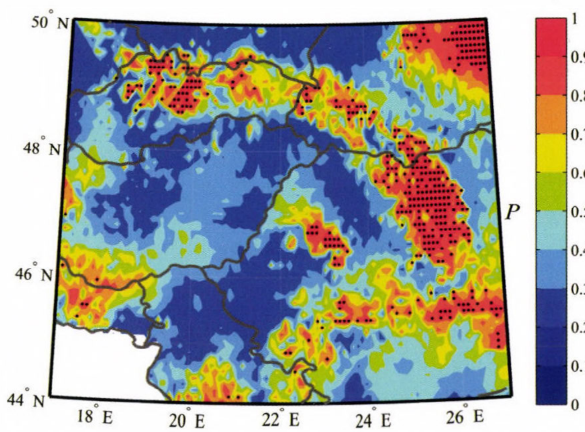

Fig. 12. Akaike weight based comparison of stationary and non-stationary (linear trend in location parameter) generalized extreme value distributions. $P>90\%$ locations are marked with black dots. P expresses the probability that the non-stationary model fits better the data than the stationary in Kullback-Leibler divergence sense (*Rózsás et al.*, 2015).

Similar calculations are completed for the Carpathian Region considering climate projection until the end of the 21st century. The preliminary results indicate decreasing trend in ground snow load and negligible effect on strucural reliability for some selected locations (*Kámán*, 2014). However, it requires further research to decide whether the results of global circulation models can reasonably predict such extremes which needed in structural reliability analyses.

7. Summary and concluding remarks

In this paper, we argued that civil engineering structures comprise great value and are crucial components of industrialized societies, thus the investigation of climate change impacts is necessary. An overview about civil engineering and its relation to climate change and climate sciences is given to facilitate future cooperation. Two numerical studies for the Carpathian Region suggest:

Concrete carbonation

- It is expected that the increased CO_2 concentration will lead to practically significant increase of depassivation probability compared with the reference model, with year 2000 level concentration. The probability can increase by 115% until the end of the 21st century.
- For structures built in 2000, the effect of climate change is expected to be subtle till the middle of the 21st century, the practically significant effects are predicted for the second half of the century.
- Uncertainty in projected environmental parameters affects significantly structural reliability estimates and improved quantification of this uncertainty by climate scientists and statisticians is needed.

Snow load

- Statistical uncertainties in probabilistic models of annual maxima of ground snow load can have significant effect and may considerably increase (with order of magnitude) the failure probability. Their neglect can lead to practically significant underestimation of failure probability.
- Analyzing historical observations, statistically significant decreasing trend ($p<0.1$, $P>0.9$) is found in annual maxima of ground snow load for numerous locations; however, practical significance is found only for a few, and the changes are favorable from reliability point of view.
- As the aforementioned conclusions can be generalized for other climatic actions, in particular for wind speeds, essential contribution of meteorologists and statisticians to civil engineering includes improved projections for trends and extremes in local weather events, and specification of uncertainties for large, 500-1000 years return period events.

Based on these findings, revision of design standards and further joint research of meteorologists and civil engineers are recommended to explore and reduce the impacts of climate change on load bearing structures. Steps are to be made as soon as possible due to the inertial effect of today decisions on climate system (*WBGU*, 2009).

Acknowledgements: The personal communications and help from the Hungarian Meteorological Service's researchers in respect of meteorological data and climate change models are greatly acknowledged, especially those of Gabriella Szépszó. This work was partly supported by the

International Visegrad Fund Intra-Visegrad Scholarship (contract no. 51401089), by the János Bolyai Research Scholarship of the Hungarian Academy of Sciences, and by the Czech Science Foundation (project no. P105/12/G059). The meteorological data were made available by the CARPATCLIM Database © European Commission - JRC, 2013. The calculations were completed using Matlab (*MATLAB*, 2014), R (*R Core Team*, 2014), and FERUM (*Der Kiureghian et al.*, 2006), the work and commitment of the developers of these applications are highly appreciated. All the related codes/scripts, processed data, and results are available from the corresponding author.

References

ACC, 2008: Adapting to Climate Change, Canada's First National Engineering Vulnerability Assessment of Public Infrastructure. Canadian Council of Professional Engineers.

Aitchison, J. and *Dunsmore, I.R.*, 1980: Statistical Prediction Analysis. New York, USA: Cambridge University Press.

Anderegg, W.R.L., Prall, J.W., Harold, J., and *Schneider, S.H.*, 2010: Expert credibility in climate change. *Proc. National Academy Sciences, 107*, 12107–12109.

Barriopedro, D., Fischer, E.M., Luterbacher, J., Trigo, R.M., and *García-Herrera, R.*, 2011: The Hot Summer of 2010: Redrawing the Temperature Record Map of Europe. *Science, 332*, 220–224.

Birsan, M.-V. and *Dumitrescu, A.*, 2014: Snow variability in Romania in connection to large-scale atmospheric circulation. *Int.J.Climatology, 34*, 134–144.

Burnham, K.P. and *Anderson, D.R.*, 2002: Model Selection and Multimodel Inference. A Practical Information-Theoretic Approach (2nd ed.). New York: Springer-Verlag.

CEB/fib., 2006: Model Code for Service Life Design. *Bulletin 34.* Lausanne, Switzerland: International Federation forStructural Concrete.

CEN, 2000: Concrete - Part 1: Specification, performance, production and conformity, in EN 206-1. Brussels, Belgium: EuropeanCommittee for Standardization.

CEN, 2004: Eurocode 2: Design of concrete structures. Part 1-1: General rules and rules for buildings. Brussels, Belgium.

CEN, 2005: Eurocode 3: Design of steel structures - Part 1-1: General rules and rules for buildings.

CIACC, 2009: Ireland at Risk - No.2: Critical Infrastructure, Adaptation for Climate Change. The Irish Academy of Sciences. Dublin, Ireland.

Coles, S., Pericchi, L.R., and *Sisson, S.*, 2003: A fully probabilistic approach to extreme rainfall modeling. *J. Hydrology 273,* 35–50.

DARA, 2012: A Guide to the Cold Calculus of a Hot Planet: DARA andthe Climate Vulnerable Forum Climate Vulnerability Monitor.

Der Kiureghian, A., Haukaas, T., and *Fujimura, K.*, 2006: Structural reliability software at the University of California, Berkeley. *Structural Safety, 28*, 44–67.

Dim, C. and Alexander, R., 2013: Historic and future increase in the global land area affected by monthly heat extremes. *Environmental Research Letters, 8*(3), 034018.

Holický, M., 2011: Forensic engineering of structures with durability problems. *Proceedings of the Institution of Civil Engineers-Structures and Buildings, 164*(1), 19-25. doi: DOI: 10.1680/stbu.9.00021.

Horváth, S. and *Pálvölgyi, T.*, 2011: Buildings and climate change: impacts on roofs and vulnerability to wind storms. *Építőanyag, 63*, 62–66. (In Hungarian).*IECCA*, 2011: Infrastructure, engineering and climate change adaptation: ensuring services in an uncertain future. London, UK.

IPCC, 2001: Climate Change 2001: Impacts, Adaptation, and Vulnerability. Contribution of Working Group II to the Third Assessment Report of the Intergovernmental Panel on Climate Change. Cambridge, UK.

IPCC, 2007: Synthesis Report. Contribution of Working Groups I, II and III to the Fourth Assessment Report of the Intergovernmental Panel on Climate Change. Geneva, Switzerland. https://www.ipcc.ch/pdf/assessment-report/ar4/syr/ar4_syr_frontmatter.pdf.

IPCC, 2012: Managing the Risks of Extreme Events and Disasters to Advance Climate Change Adaptation. Cambridge, UK, and New York, NY, USA.

IPCC, 2014: Climate Change 2014: Synthesis Report. . IPCC. Geneva, Switzerland.

Jacobson, M.Z., Delucchi, M.A., Bazouin, G., Bauer, Z.A.F., Heavey, C.C., Fisher, E., Morris, S.B., Piekutowski, D.J.Y., Vencill, T.A., and *Yeskoo, T.W.*, 2015: 100% clean and renewable wind, water, and sunlight (WWS) all-sector energy roadmaps for the 50 United States. *Energy Environ. Sci.* 8, 2093–2117.

Kámán, Cs., 2014: Structural Reliability of Steel Frames. With emphasis on snow loads considering historical data and future projections. Master of science thesis, Budapest University of Technology and Economics, Budapest, Hungary.

KKK, 2008: A közlekedés helyzete Magyarországon 2007. Budapest: Közlekedésfejlesztési Koordinációs Központ. (In Hungarian).

KKK, 2012: Híd Önálló Osztály. Híd Adattábla. Retrieved 04 April, 2012, from 3k.gov.hu/pages/ index.jsp?p=2&id=1829 (In Hungarian).

Koch, G.H., Brongers, M.P.H., Thompson, N.G., Virmani, Y.P., and *Payer, J.H.*, 2001: Corrosion Costs and Preventive Strategies in the United States. National Technical Information Service. (FHWA-RD-01-156). Springfield.

Köhler, J., 2011: Risk and Safety in Engineering. Web lectures. Zurich, Switzerland.

Lemaire, M., Chateauneuf, A., and *Mitteau, J.-C.*, 2010: Structural Reliability: Wiley.

Lenkei, P., 2007: Climate change and structural engineering. *Periodica Polytechnica, 51*, 47–50.

Leshner, A.I., Lane, T., Grove, T.L., Berenbaum, M.R., Seitter, K., Alley, M., Ho, T.-h.D., Morton, S.C., Johnson, L., Holsinger, K.E., Quesenberry, K., Power, M., Brown, W.Y., Kloeppel, B.D., Arnold, D.N., Huelsenbeck, J., Bertsch, P., and *Anthes, R.A.* 2009: Letter sent to the U.S. Senate by 18 leading American scientific organizations: American Association for the Advancement of Science. April 9, 2015. aaas.org/sites/default/files/migrate/uploads/1021climate_letter1.pdf.

Long, E.A., 2007: Sustainable bridges through innovative advances. Paper presented at the Joint ICE and TRF Fellows Lecture.

Marty, C. and *Blanchet, J.*, 2012: Long-term changes in annual maximum snow depth and snowfall in Switzerland based on extreme value statistics. *Climatic Change, 111*, 705–721.

MATLAB, 2014. The Language of Technical Computing (Version R2014a (8.3.0.532)). Natick, Massachusetts: MathWorks Inc. Retrieved from http://www.mathworks.com/products/matlab/.

McRobie, A., 2004: The Bayesian View of Extreme Events. Paper presented at the Henderson Colloquium, Magdalene College, Cambridge.

Medgyasszay, P., Horváth, S., Beliczay, E., Licskó, B., Meydl, S., and *Varga, I.L.*, 2007: A Nemzeti Éghajlatváltozás háttéranyagaként az éghajlatváltozás csökkentése és az alkalmazkodás lehetőségei az épített környezet alakításával. (In Hungarian).

Melchers, R.E., 2002: Structural Reliability Analysis and Prediction (2nd ed.). Chichester, UK: John Wiley and Sons Ltd.

Melchers, R.E., Baker, M.J., and *Moses, F.*, 1983: Evaluation of experience. *IABSE reports, 47*, 21–38.

Milly, P.C.D., Betancourt, J., Falkenmark, M., Hirsch, R.M., Kundzewicz, Z.W., Lettenmaier, D.P., and *Stouffer, R.J.*, 2008: Stationarity Is Dead: Whither Water Management? *Science, 319*, 573–574.

Nguyen, M.N., Wang, X., and Chen, D., 2010: An Investigation of Extreme Heatwave Events and Their Effects on Building & Infrastructure. CSIRO.

Nguyen, M.N., Wang, X., and *Leicester, R.H.*, 2013: An assessment of climate change effects on atmospheric corrosion rates of steel structures. *Corrosion Engin. Sci. Technol. 48*, 359–369.

R Core Team, 2014: R: A language and environment for statistical computing. Vienna, Austria: R Foundation for Statistical Computing.

Retief, J.V., Diamantidis, D., Barnardo-Viljoen, C., and *van der Klashorst, E.*, 2014: Extreme actions and climate change: experience gained in South Africa and Germany. *Civil Engin. Environ. Syst., 31*, 179–188.

Rózsás, Á. and *Kovács, N.*, 2013a: Carbonation of Concrete Infrastructure in Hungary in the Light of Climate Change. Paper presented at the Second Conference of Junior Researchers in Civil Engineering, Budapest.

Rózsás, Á. and *Kovács, N.*, 2013b: Probabilistic Assessment of the Effect of Climate Change on the Carbonation of Concrete Structures in the Carphatian Basin. Paper presented at the Creative Construction Conference, Budapest, Hungary. July 6–9, 2013.

Rózsás, Á., Sýkora, M., and *Vigh, L.G.*, 2015: Long-term Trends in Annual Ground Snow Maxima for the Carpathian Region. Paper presented at the Engineering Mechanics 2015, Svratka, Czech Republic. May 11–15, 2015.

Rózsás, Á. and *Vigh, L.G.*, 2014: On the Reliability of Steel Frames Exposed to Snow Load. Considering the Effect of Epistemic Uncertainty. Paper presented at the 7th European Conference on Steel and Composite Structures, Naples, Italy.

Sarja, A., 2005: Integrated Life Cycle Design of Structures: e-Library: Taylor & Francis.

Spiegelhalter, D. and *Rice, K.*, 2009: Bayesian statistics *Scholarpedia, 4,* 5230.

Steenbergen, R.D.J.M., Sykora, M., Diamantidis, D., Holicky, M., and *Vrouwenvelder, A.C.W.M.*, 2015: Target reliability levels for assessment of existing structures based on economic optimisation and human safety criteria. *Struct. Concrete*, doi: 10.1002/suco.201500022.

Stewart, M.G. and *Wang, X.*, 2011: Risk Assessment of Climate Adaptation Strategies for Extreme Wind Events in Queensland. CSIRO. Canberra, Australia.

Stewart, M.G., Wang, X., and *Nguyen, M.N.*, 2011: Climate change impact and risks of concrete infrastructure deterioration. *Engin. Struct. 33*, 1326–1337.

Sýkora, M. and *Holický, M.*, 2013: Durability Assessment of Large Surface. Paper presented at the Safety, Reliability, Risk and Life-Cycle Performance of Structures and Infrastructures - Proceedings of the 11th International Conference on Structural Safety and Reliability ICOSSAR 2013, New York, USA.

Szalai, S., Auer, I., Hiebl, J., Milkovich, J., Radim, T., Stepanek, P., Zahradnicek, P., Bihari, Z., Lakatos, M., Szentimrey, T., Limanowka, D., Kilar, P., Cheval, S., Deak, G., Mihic, D., Antolovic, I., Mihajlovic, V., Nejedlik, P., Stastny, P., Mikulova, K., Nabyvanets, I., Skyryk, O., Krakovskaya, S., Vogt, J., Antofie, T., and *Spinoni, J.*, 2013: Climate of the Greater Carpathian Region. www.carpatclim-eu.org.

Timár, A., 2010: Impacts of climate change on the Hungarian road infrastructure. *Pollack Periodica, 5*, 37–52.

Tóth, E., 2012: Országos közúti hídjaink megóvása, hídgazdálkodása, aktuális feladatai. *Journal of the Hungarian Steel Structure Association, 9*, 28–31. (In Hungarian).

UNFCCC, 2010: Report of the Conference of the Parties on its fifteenth session, held in Copenhagen from 7 to 19 December 2009. Addendum. Part Two: Action taken by the Conference of the Parties at its fifteenth session. United Nations. (FCCC/CP/2009/11/Add.1). Copenhagen.

ÚT, 2002: Design of Concrete, Reinforced Concrete and Prestressed Concrete Road Bridges. in Code of Roadbridges 4, in Hungarian: Magyar Útügyi Társaság. (In Hungarian).

VAHAVA, 2010: Climate Change and Hungary: Mitigating the Hazard and Preparing for the Impacts. The "VAHAVA" Report. Budapest.

Wang, X., Nguyen, M., Stewart, M.G., Syme, M., and *Leitch, A.*, 2010: Analysis of Climate Change Impacts on the Deterioration of Concrete Infrastructure. CSIRO. Canberra.

Warren, R., 2011: The role of interactions in a world implementing adaptation and mitigation solutions to climate change (Vol. 369).

WB, 2011: The recent earthquake and tsunami in Japan: implications for East Asia. *World Bank. East Asia and Pacific Economic Update, 1.*

WBGU, 2009: Solving the climate dilemma: The budget approach. Special Report. German Advisory Council on Global Change. Berlin, Germany.

INSTRUCTIONS TO AUTHORS OF *IDŐJÁRÁS*

The purpose of the journal is to publish papers in any field of meteorology and atmosphere related scientific areas. These may be

- research papers on new results of scientific investigations,
- critical review articles summarizing the current state of art of a certain topic,
- short contributions dealing with a particular question.

Some issues contain "News" and "Book review", therefore, such contributions are also welcome. The papers must be in American English and should be checked by a native speaker if necessary.

Authors are requested to send their manuscripts to

Editor-in Chief of IDŐJÁRÁS
P.O. Box 38, H-1525 Budapest, Hungary
E-mail: journal.idojaras@met.hu

including all illustrations. MS Word format is preferred in electronic submission. Papers will then be reviewed normally by two independent referees, who remain unidentified for the author(s). The Editor-in-Chief will inform the author(s) whether or not the paper is acceptable for publication, and what modifications, if any, are necessary.

Please, follow the order given below when typing manuscripts.

Title page: should consist of the title, the name(s) of the author(s), their affiliation(s) including full postal and e-mail address(es). In case of more than one author, the corresponding author must be identified.

Abstract: should contain the purpose, the applied data and methods as well as the basic conclusion(s) of the paper.

Key-words: must be included (from 5 to 10) to help to classify the topic.

Text: has to be typed in single spacing on an A4 size paper using 14 pt Times New Roman font if possible. Use of S.I. units are expected, and the use of negative exponent is preferred to fractional sign. Mathematical formulae are expected to be as simple as possible and numbered in parentheses at the right margin.

All publications cited in the text should be presented in the *list of references*, arranged in alphabetical order. For an article: name(s) of author(s) in Italics, year, title of article, name of journal, volume, number (the latter two in Italics) and pages. E.g., *Nathan, K.K.,* 1986: A note on the relationship between photosynthetically active radiation and cloud amount. *Időjárás 90,* 10-13. For a book: name(s) of author(s), year, title of the book (all in Italics except the year), publisher and place of publication. E.g., *Junge, C.E.,* 1963: *Air Chemistry and Radioactivity.* Academic Press, New York and London. Reference in the text should contain the name(s) of the author(s) in Italics and year of publication. E.g., in the case of one author: *Miller* (1989); in the case of two authors: *Gamov* and *Cleveland* (1973); and if there are more than two authors: *Smith et al.* (1990). If the name of the author cannot be fitted into the text: *(Miller,* 1989); etc. When referring papers published in the same year by the same author, letters a, b, c, etc. should follow the year of publication.

Tables should be marked by Arabic numbers and printed in separate sheets with their numbers and legends given below them. Avoid too lengthy or complicated tables, or tables duplicating results given in other form in the manuscript (e.g., graphs).

Figures should also be marked with Arabic numbers and printed in black and white or color (under special arrangement) in separate sheets with their numbers and captions given below them. JPG, TIF, GIF, BMP or PNG formats should be used for electronic artwork submission.

More information for authors is available: journal.idojaras@met.hu

Published by the Hungarian Meteorological Service

Budapest, Hungary

INDEX 26 361

HU ISSN 0324-6329

IDŐJÁRÁS

QUARTERLY JOURNAL OF THE HUNGARIAN METEOROLOGICAL SERVICE

CONTENTS

VOL. 120 * NO. 2 * APRIL – JUNE 2016

IDŐJÁRÁS

Quarterly Journal of the Hungarian Meteorological Service

Editorial Office: Kitaibel P.u. 1, H-1024 Budapest, Hungary
P.O. Box 38, H-1525 Budapest, Hungary
E-mail: journal.idojaras@met.hu
Fax: (36-1) 346-4669

Indexed and abstracted in Science Citation Index Expanded™ and Journal Citation Reports/Science Edition
Covered in the abstract and citation database SCOPUS®

Subscription by mail:
IDŐJÁRÁS, P.O. Box 38, H-1525 Budapest, Hungary
E-mail: journal.idojaras@met.hu

IDŐJÁRÁS

Quarterly Journal of the Hungarian Meteorological Service
Vol. 120, No. 2, April – June, 2016, pp. 127–161

Effect of weather conditions on annual and intra-annual basal area increments of a beech stand in the Sopron Mountains in Hungary

Ernő Führer[1], **Márton Edelényi**[2], **László Horváth**[3*], **Anikó Jagodics**[1], **László Jereb**[2], **Zoltán Kern**[4], **Andrea Móring**[5], **Ildikó Szabados**[6], and **Zoltán Pödör**[2]

[1]*National Agricultural Research and Innovation Centre, Forest Research Institute, Paprét 17, 9400 Sopron, Hungary*

[2]*Institute of Informatics and Economics, Simonyi Károly Faculty of Engineering, Wood Sciences and Applied Arts, University of West Hungary, Bajcsy-Zsilinszky utca 9, 9400 Sopron, Hungary*

[3]*MTA-SZIE Plant Ecology Research Group, Szent István University, Páter Károly utca 1, Gödöllő, 2100, Hungary*
and
Hungarian Meteorological Service, Gilice tér 39, 1181 Budapest, Hungary

[4]*Institute for Geological and Geochemical Research, Research Centre for Astronomy and Earth Sciences, MTA, Budaörsi út 45, 1112 Budapest, Hungary*

[5]*Centre for Ecology and Hydrology, Penicuik, EH16 0QB, United Kingdom, and University of Edinburgh, Edinburgh, EH9 3JN, United Kingdom*
and
Hungarian Meteorological Service, Kitaibel Pál utca 1, 1024 Budapest, Hungary

[6]*Ministry of Agriculture Kossuth tér 11, 1055 Budapest, Hungary*

[*]*Corresponding author Email: horvath.laszlo.dr@gmail.com*

(Manuscript received in final form February 29, 2016)

Abstract—We studied the effect of meteorological parameters such as average monthly temperature and sum of precipitation on basal area increment (BAI) of a beech stand in the Sopron Mountains in subalpine climate in Hungary between 1985 and 2007. The applied multivariate regression analysis takes into account the influence of the weather conditions on increments also in the previous two years. Results indicated that precipitation generally stimulated the BAI in the studied stand, while above average temperature during the growing season depressed it. One of the dominant periods for growing of basal area is the autumn of the penultimate year when precipitation and temperature has positive and negative effect on increment, respectively. In the main growing period (spring-early summer) the previous year's precipitation has positive, while autumn temperature has negative effect. Current spring to early summer precipitation enhances the beech growth, and in contrary, the mean temperature in June-July has negative effect on the BAI. There is a breakpoint in the trend of meteorological variables at about 1999. A significant decrease was observed in the growth of beech in the summer months in the period of 2000–2007 compared to growth between 1985 and 1999 probably caused by the changed meteorological conditions. The maximum growth shifted from June to May, and the relative share of spring months in the BAI has increased since 2000. Drastic loss in increments can be observed in July and August, which was partly compensated in autumn. The long-term trend of annual BAI is continuously decreasing; comparing the two periods, the average yearly increments decreased from 21 cm^2 to 12 cm^2. According to forecasted climate change, not only further loss in growth but also drastic decay in vitality and tolerance can be expected for beech at this site over the 21st century.

Key-words: beech, growth, basal area increment, climate change, production

1. Introduction

At the beginning of the 1990's, several studies reported a more intensive growth of forests over Central Europe in the last third of the 20th century than before (*Pretzsch*, 1992; *Bräker*, 1996; *Spiecker et al.*, 1996; *Zingg*, 1996; *Kahle et al.*, 2008). Studying the reasons, it was found that the change in growth was related partly to the longer vegetation period (*Hasenauer et al.*, 1999), and partly to earlier blooming and leaf unfolding (*Menzel* and *Fabian*, 1999). Changes in the climatic conditions significantly enhanced the intensity of photosynthetic activity and respiration, resulting in change of growth (*Kozlowski et al.*, 1991; *Larcher*, 2001; *Somogyi*, 2008). However, the results are frequently contradictory when studying the relation of changing climate and tree growth in larger geographical scale. One of the reasons is that in the comparisons of different observations and measurements, the favorable or unfavorable climate conditions of the investigated areas were disregarded (*Mátyás et al.*, 2010). When water supply is not limited, the rising temperature can lead to substantial, even 50% increase in growth for beech in contrast to arid regions.

Numerous reports have been published concerning tree growth, especially for organic matter production of beech. These studies mainly focused on the causal relationships as consequences of changed climatic conditions. For example, *Dittmar et al.* (2003) studied the effect of climate on the growth of beech stands in European mountainous (>800 m) and hilly (<700 m) regions. They found that temperature and precipitation in the summer of the given year have an inverse effect on annual growth. While in higher regions there is positive relation with increasing temperature, higher precipitation reduces the yearly growth. For lower regions these relations are just the opposite.

Cool and wet autumn at the year before was found to enhance the radial growth of beech for a Romanian stand (*Kern* and *Popa*, 2007). On the other hand, the late summer high temperature has negative influence on the growth.

Ježík et al. (2011) studied the influence of climate on the yearly production in the whole growing season, on the basis of biweekly dendrometer observation in Slovakia. They showed a positive effect of precipitation at the beginning of growing season, and this influence tends to be reverse with time during summer period with parallel growing importance of precipitation, especially at the end of summer and beginning of autumn.

Another Slovakian study reported positive effect of precipitation on beech growth in August in the previous year and in June-July in the same year; while temperature of the previous summer reduced the growth (*Petráš* and *Mecko*, 2011). Other investigations in Germany (*Scharnweber et al.*, 2011; *van der Maaten*, 2012) and France (*Michelot et al.*, 2012) pointed out positive effect of precipitation in the given year and negative influence of temperature.

In Slovenia (*Čufar et al.*, 2008), it was found that the May and July precipitation enhances the production significantly; similarly to the precipitation in August of the previous year. Other dominant climate parameters are the temperature minima in March and the maxima in August.

In this study we analyzed the weekly observations of basal area increment (BAI) in a beech stand for 22 years (1985–2007) in relation to the main meteorological parameters determining the growth, i.e., monthly mean air temperature and sum of precipitation. The length of data series allows a reliable correlation analysis between the increments and meteorological factors as well as to fit a model to the growth by multivariate linear regression analysis. A relatively rich literature can be found dealing with annual growth rates based primarily on tree-ring derived parameters, however, the strength of this study is the length of the intra-annual time series offering a unique opportunity to analyze the intra-annual growth trends of European beech on a 22-year timescale. The results will support evaluation of future growth expectations; namely, which climate components and in which periods have the greatest effect on the basal area increment of trees. The aim of this study is to evaluate this effect.

2. Methods and materials

2.1. Characterization of the site of investigation

During the selection of the test stand, it was a primary criterion that the tree species, i.e., the beech (*Fagus sylvatica* L.) should be important in the given landscape from both an ecological as well as forest economical point of view. The Sopron Mountains lie at the border of Austria and Hungary (*Fig. 1*), where beech is indigenous (*Magri*, 2008; *Führer et al.*, 2010). The forest type is *Oxalis acetosella* with a single crown-storied, completely closed beech forest. Its age at the beginning of the observations was 85 years based on the data of National Forestry Database in 1985. In the early 2008 the forest was harvested. Due to the forest restoration technology used between the World Wars, which succeeded in 5–15 years, there can be a difference of about 10 years among certain trees. The stand was on a slight, south-east facing slope at approximately 400 meters above the mean sea level. Coordinates are: 47° 39'20"N and 16° 28'58" E, the bedrock is gneiss, and the soil is a type of Luvisols according to the WRB 2014 classification system (*IUSS*, 2014). The climate is sub-alpine.

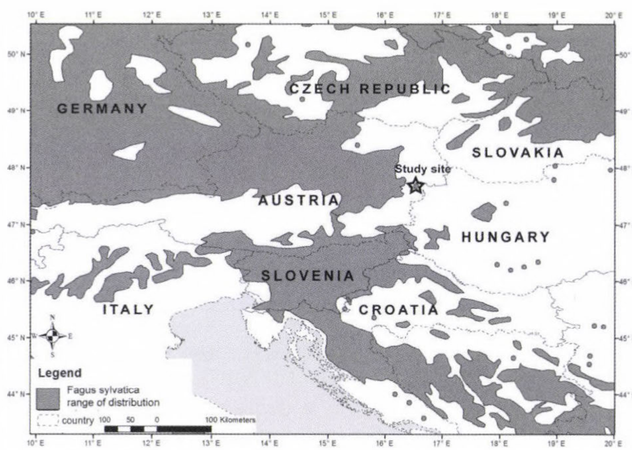

Fig. 1. Location of the study site and the distribution of beech (*Fagus sylvatica*). Distribution boundaries are retrieved from the *EUFORGEN* (2009) database.

The studied plot was a 50×50 m parcel, representing average stand in its characteristics. The height and diameter at breast height (DBH) of every tree were surveyed regularly. The stand was well growing; stem number was 362 pcs ha^{-1}, stand volume is 732 m^3 ha^{-1}, average DBH and height were 37 cm and 32 m, respectively.

Based on the survey – trunk by trunk –, we determined the social position (dominant, co-dominant, suppressed) of trees and the structure of the stand. Using the results of this analysis, we selected seven beech trees (*Table 1*) with average parameters, representative for the whole stand. Suppressed trees were not considered in the selection since their growth is heavily affected by their social status beside weather.

Table 1. Initial data of trunks equipped by dendrometers at the start of measurement; *d*=diameter at breast height (DBH); *BA* = basal area; *h* = tree height

Number of trunks	***d* (cm)**	***BA* (cm^2)**	***h* (m)**
11	37.5	1103	32.0
14	38.2	1147	32.0
15	37.7	1117	33.0
16	33.2	864	31.5
19	41.7	1368	33.8
20	37.7	1117	32.2
21	37.8	1125	31.0
mean	**37.7**	**1120**	**32.2**

2.2. Dendrometer measurements

We installed Liming-dendrometers (*Liming*, 1957) on selected trees for weekly observations, and the change of perimeter over 22 years (1985–2007, without the year of 1998) was recorded. Following forestry practice, the bronze dendrometer-bands were installed permanently at breast-height. It should be emphasized that the circumferential change represents the total change in circumference outside the bark and not necessarily the actual wood increment. The largest source of noise could be the thermal expansion of the stem. Linear thermal expansion coefficient of bronze is 17–18 μm m^{-1} °C^{-1} (*Hidnert* and *Krider*, 1947). Respecting that the monthly mean air temperature is similar at the start and at the end of yearly observations (March: 3.0±2.32 °C and November: 2.8±2.02 °C), differences in thermal expansion in March and November are practically negligible. For vegetation period, however, we estimated the anomaly caused by thermal expansion by comparing the circumferential increment of trees with thermal expansion. The calculated error was below 1 percent.

In spite of weekly observations, first of all we aimed to get information of monthly, seasonal, and yearly increments. Beside monthly growth increments of different stages of growing periods (initial: April, main: May-August, and final:

September-October), monthly meteorological parameters were also analyzed. The separation of the different growth stages (*Table 2*) enables the examination of change in these growth stages in relation to climate conditions over the long (more than two decades) observation period. To assess the effect of climate variability, investigation of yearly distribution of growth intensity is indispensable. Many papers have been published studying increments on a shorter (daily) time-scale (e.g., *Deslauriers et al.*, 2003; 2007a; 2007b). In these studies, with the applied measurement methodology, short-term growth of trees was separated from swelling and shrinkage caused by temperature and humidity. These observations are suitable to find deeper eco-physiological relationships. However, our observations, due to the potential, future application of the results in forestry practice, aimed the exploration of organic matter production of longer periods (within a year) as a function of weather parameters.

Table 2. Mean meteorological data (*p*: precipitation, *t*: temperature) in the reference (1961–1984) and observation (1985–2007) periods in different time intervals. The significance level in temperature differences was calculated by t-test.

Growing periods	Months												Measurement intervals 1961–1984		1985–2007		1961–2007		t-test for *t*
	1	2	3	4	5	6	7	8	9	10	11	12	*p* (mm)	*t* (°C)	*p* (mm)	*t* (°C)	*p* (mm)	*t* (°C)	significance level
Year	■	■	■	■	■	■	■	■	■	■	■	■	757	7.5	764	8.2	761	7.9	0.0013**
Dormant	■	■	■								■	■	211	–0.3	230	0.2	221	0.0	0.2023
Growing				■	■	■	■	■	■	■			546	13.1	533	13.9	540	13.5	0.0001**
Initial				■									62	7.6	54	8.3	58	8.0	0.0663*
Main					■	■	■	■					355	15.7	342	16.8	349	16.2	0.0001**
Intensive						■							100	15.5	89	16.1	95	15.8	0.9950
Critical							■						93	17.5	79	18.8	86	18.2	0.0200**
Final									■	■			129	10.7	137	11.0	133	10.9	0.3798

* indicates significance levels, below 0.1,
** indicates significance levels, below 0.05

2.3. Characterization of climate

For characterization of the climate of the test site – generally and for the examined period –, we used gridded climate data interpolated from homogenized monthly precipitation and temperature series derived from the network of the Hungarian Meteorological Service (*Szentimrey et al.*, 2010; *Lakatos et al.*, 2013). By homogenization the effect of any disturbance affecting the measurements over the studied period is removed, keeping the signal of the climate change. Beside the climate characterizations, we attempted to find relationship between increments and monthly precipitation and temperature variations in the different years.

2.4. Evaluation methods

The basal area implement (BAI) is steadily increasing or asymptotically stabilizing for mature trees (*Bouriaud* and *Popa*, 2009; *Fekedulegn et al.*, 2003; *Muzika et al.*, 2004; *Piovesan et al.*, 2008). Since studied trees were obviously mature specimens (older than 85 years), from the beginning to the termination of observations the prevailing negative BAI trend (see Results) cannot reflect a biological trend; therefore, the otherwise mandatory detrending step was neglected and the raw BAI series were used.

According to a survey of European literature, both simple monthly mean weather data (*Dittmar et al.*, 2003; *Szabados*, 2006; *Kern* and *Popa*, 2007; *Maxime* and *Hendrik*, 2011; *Scharnweber et al.*, 2011) and data for longer periods (*Pichler* and *Oberhuber*, 2007; *Novák et al.*, 2010) were used in studying the relationship between weather conditions and growth of trees. The delayed effect of changing weather conditions are taken into account applying pre-defined periods within a year (*Briffa et al.*, 2002; *Büntgen et al.*, 2006; *Gutiérrez et al.*, 2011). Weather conditions of these periods can be represented by the combination (sums or averages) of parameters for different months. For this purpose, beside the analysis of monthly increments, we used the CReMIT method (Cyclic Reverse Moving Intervals Technique, *Pödör et al.*, 2014). A brief description is provided in the Appendix.

The basal area increment and organic matter production of trees are closely related to the transpiration (water flux) and photosynthetic activity. These physiological processes relate to leaves so the quantity and quality of foliage fundamentally affect the growth of trees. For deciduous species, the area and quality of leaves, reproduced year-by-year, depend on the quality and quantity of shoots. Many studies take into account the effect of meteorological parameters of the previous year (*Dittmar et al.*, 2003; *Di Filippo et al.*, 2007; *Kern* and *Popa*, 2007; *Maxime* and *Hendrik*, 2011; *Scharnweber et al.*, 2011; *Michelot et al.*, 2012; *Tegel et al.*, 2014). According to *Gruber* (2004), the number of shoots is determined by the circumstances of initiation of bud growth (primordia): i) this process is determined two years before the appearance of leaves on shoot; ii) the differentiation of primordia into short or long shoots happens a year before the formation of foliage. The more buds are developing long shoots the higher is the probability of higher leaf number; iii) the morphological quality of leaves (surface area and thickness) are determined in the given year, especially in April and May.

We were looking for relationships between climatological statistics and the increments of trees by linear regression analysis, and checked the significance of the found relationships by t-test.

2.5. Multivariate regression models

Based on the above calculations, we constructed multivariate linear regression models for all possible, at least two-component subgroups of independent variables. Using the significant ($p<0.1$) components, we generated all of the mathematically possible multivariate climate index (CI) models for temperature and precipitation and for the two components together on monthly and periodic level, and for the combination of these terms. Then, from the derived regression equations we selected the relevant and statistically significant ones ($p<0.05$). Beyond the ecophysiological considerations we selected them according to the value of the corrected coefficient of determination (R2adj). R2adj, in contrast with the simple coefficient of determination, takes into account the number of parameters as well as observations used in the model; hence, it is more suitable for comparison of multivariate models. In this way, taking into account the relevant and the most significant parameters, we derived the climate indices that have relatively the strongest influence on the increment over the 22 years.

2.6. Breakpoint analysis

A long data series usually includes significant breakpoints. This is true for not only our increment data series but also for our homogenized climate dataset, which – as we mentioned above – is still affected by climate change. During analyses we have to try to separate the data – though by controlled way – into sub-intervals as objectively and uniformly as possible by a principle equally applicable for all of variables. However, changes occur in longer time-interval we can still mark out breakpoints that relatively sharply separate the data series into fragments. There are different methods in the literature to mark breakpoints to detect shift in data series, e.g., by comparison of partial means by Students' t-test, by minimizing the standard deviation, by cumulative sum of anomalies, by Pettitts' non-parametric approach (*Pettitt*, 1979), and by analyzing the signal to noise ratio (*Sneyers*, 1992; *Mares* and *Mares*, 1994).

In our work, we applied the first approximation based on the theory that the difference in averages of sub-intervals separated by breakpoints are significantly higher than that of sub-intervals separated randomly. We tried to divide our meteorological time series into only two parts. To compare means we applied the t-test. This method supposes the normal distribution of meteorological datasets, which was verified by the Shapiro-Wilk test.

3. Results

3.1. Climate description of the test site

Between 1961 and 2007, the average yearly precipitation amount was 761 mm. The share of this was 540 mm in the growing period (April-October), while the rest (only 221 mm) was measured in the dormant period (November-March) (*Table 2*). This means that, beside the water stored in the soil in the dormant period, the water supply was enough in the physiologically active growing season for organic matter production. Regarding the share of precipitation in the different growing periods, the ratios were 11% in the initial growing period (58 mm), 65% in the main growing period (349 mm), and 24% (133 mm) in the final growing period. In the most intensive growing period in June, the average precipitation of 47 years was 95 mm month^{-1} (18%).

The annual mean air temperature at the test site was 7.9 °C. Average temperatures of growing and dormant periods were 13.5 and 0.0 °C, respectively. The average temperature in the different phases of growing season were: 8.0 °C in the initial, 16.2 °C in the main, and 10.9 °C in the final periods.

Due to their high temperature, July and sometimes August are the most critical months; in these months the mean monthly temperature exceeds the 18 °C, and the daily maxima are frequently between 30 and 35 °C. These high extremes substantially depress the photosynthetic activity. Weather conditions changed comparing the measurement period (1985–2007) to the previous years (1961–1984), especially in temperature, where an evident increase can be observed between the two periods (*Table 2*). The performed t-test shows that – excluding the dormant and final periods – there are statistically significant differences between the two examined periods at the $p<0.1$ significance level. The mean air temperature of the main growing season was higher by 1.1 °C in the measurement period. The difference is even higher in the critical month (July) when it is 1.3 °C, accompanied by a reduced amount (14% less) of precipitation. This means that the probability of drought was higher in the measurement period than before.

The mean growing season air temperature shows an evident (significant) change, especially for the period of BAI measurements (*Fig. 2*). Regarding the extremes, there were five years (1962, 1965, 1978, 1980, 1984) with lower than 15 °C mean temperature for the main growing phase during the reference period (1961–1984), while in the observation period there was not any years with the same mean temperature below 15 °C. Furthermore, in the main growing period of reference years (1961–84), year with average temperature higher than 17 °C occurred once (1983), whilst it was observed seven times in the following 23 years (1992, 1994, 2000–2003, and 2007). We can also see that the highest monthly mean temperature in the main growing season was 17.4 °C (1983) in the reference period, in contrast with 19.4 °C (2003) in the observation period.

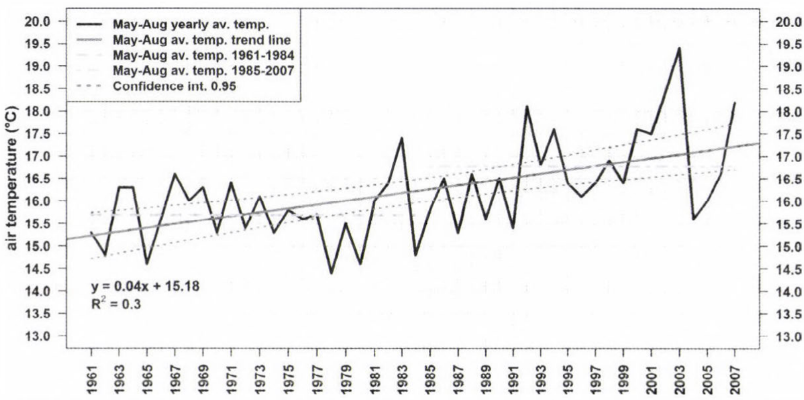

Fig. 2. Trend of average air temperature in the main growing season at the test site in the reference years (1961–1984) and in the observation period (1985–2007) (n=47, p<0.001).

The changes are represented also by the climate classification of the years according to forestry climate categories. Based on the forestry aridity index (FAI) developed for Hungary (*Führer et al.*, 2011), there were 18 years (75%) with beech climate category between 1961 and 1984, while in the observation period there was only 11 years (48%) (*Table 3*). Hence, drier and warmer years than beech climate, i.e., hornbeam-oak, sessile oak-Turkey oak, and forest-steppe climate were more frequent in the observation period (52%) than before (25%). It means that the climate did not evidently belong to beech category during the observation period. Respecting the whole 47 years we can conclude, that in most part of the period, the site can be characterized as beech climate zone (in 62% of years), whilst other years (38%) were characterized by warmer-drier weather conditions as *Table 3* shows.

Table 3: Share of years in different forestry climate categories according to Forestry Aridity Index by *Führer et al.* (2011)

Periods	Forestry climate categories			
	Beech	Hornbeam-oak	Sessile oak-Turkey oak	Forest-steppe
Reference years 1961–1984	18 (75%)	2 (8.3%)	2 (8.3%)	2 (8.3%)
Observation period 1985–2007	11 (48%)	9 (39%)	2 (8.7%)	1 (4.3%)
Total 1961–2007	29 (62%)	11 (23%)	4 (8.5%)	3 (6.4%)

There were substantial variations in the precipitation and temperature conditions among different months also in the observed period. On the basis of the above mentioned t-test and breakpoint analysis, we were looking for years in the period of 1985–2007, where precipitation and temperature averages before and after the given year were significantly different concerning simple monthly and special periodic data (*Table 4*). We supposed, that when significant change is observed in the given year or one year before/after in monthly or periodic climatic variables determining the growth, a parallel change is expected in the basal area growth as well in the same period. In the vegetation period (April-October), significant change of temperature and precipitation were observed between 1990 and 2000 over the 22-year-long period of investigations. While in the months determining the growth, the precipitation amount was decreasing, upward shifts were observed for the temperature after the breakpoint. For example, the mean temperature in June was higher by 1.86 °C after 1992 and the average yearly precipitation amount were lower by 41 mm after 1998 than before.

Table 4. Breakpoint analysis of monthly precipitation and temperature data

Months	**Precipitation (mm)**				**Temperature (°C)**			
	Year	**Before**	**After**	**Difference**	**Year**	**Before**	**After**	**Difference**
4	2000	58.46	43.86	–14.60	1998**	7.82	9.08	1.26
5	2000**	101.09	66.42	–34.67	1993	12.84	14.07	1.23
6	1998**	112.88	71.43	–41.45	1992**	14.85	16.71	1.86
7	1996*	67.11	97.98	30.87	2001*	18.51	19.62	1.11
8	1990**	113.6	85.82	–27.78	1990*	17.53	18.82	1.29
9	1995	68.19	92.97	24.78	1995	13.95	13.05	–0.90
10	1990**	28.32	60.64	32.32	1998	7.99	9.01	1.02
9–10	1990**	91.72	148.06	56.34	1990	11.31	10.83	–0.48
5–8	2000	384.28	311.50	–72.78	1992**	15.99	17.14	1.15
4–10	2000*	574.45	498.87	–75.58	1998**	13.56	14.37	0.81

significance levels: *indicates $p<0.1$; **indicates $p<0.05$

3.2. Interannual, seasonal, and monthly variation of increments

The annual average increment calculated from weekly observations was 17.9 cm^2, with a minimum of 5.52 and a maximum of 31.3 cm^2 in the whole observation period. The growth begins in the first half of April and ends by the middle of October. Data in *Table 5* shows that 88% of organic matter is produced in the main growing season, while its fractions are only 5.3% and 6.2% for the initial and final periods, respectively. These results are in accordance with previous results from Hungary (*Somogyi*, 2008; *Mátyás et al.*, 2010). Increments of different trees differ not only in yearly growth but also in the share in growth of the different growing periods. For example, the tree with poor growth (No. 14) showed that the less increment is produced in the main growth period the larger is the production in the initial and final period compared to an "average" tree.

Table 5. Absolute (BAI) and relative (RBAI) increments of beech trees in different growing periods in average and in cases of trees with the largest (No. 15) and the smallest (No. 14) growth

Growing periods	Average tree		Tree No. 15		Tree No. 14	
	BAI (cm^2)	RBAI (%)	BAI (cm^2)	RBAI (%)	BAI (cm^2)	RBAI (%)
Initial	0.94	5.3	1.74	5.5	0.56	10.2
Main	15.9	88.5	27.8	88.8	4.33	78.4
Final	1.11	6.2	1.81	5.7	0.63	11.4
Total	17.9	100	31.3	100	5.52	100

BAI records showed quite strong coherence among the measured trees for all seasons and the full period as well. The temporarily stable and good coherence is substantiated by the high mean within-tree correlation coefficients (at least $r=0.37$ in all cases at $p=0.05$ or lower significance level), which validates that a common signal is captured by the averaged BAI record (*Fig. 3*). The annual BAI shows a significant decreasing trend during the investigated period. According to the findings of *Fekete* (1958) and *Mendlik* (1967), beech stands between the ages of 80–120 years grow slowly but significantly in basal area. A negative trend in BAI of mature trees is a strong indication of a stress induced decline in tree growth (*Pedersen*, 1998; *Jump et al.*, 2006; *Peñuelas et al.*, 2008; *Piovesan et al.*, 2008). The trend can be correlated with the evident temperature increase in the given period (*Fig. 2*).

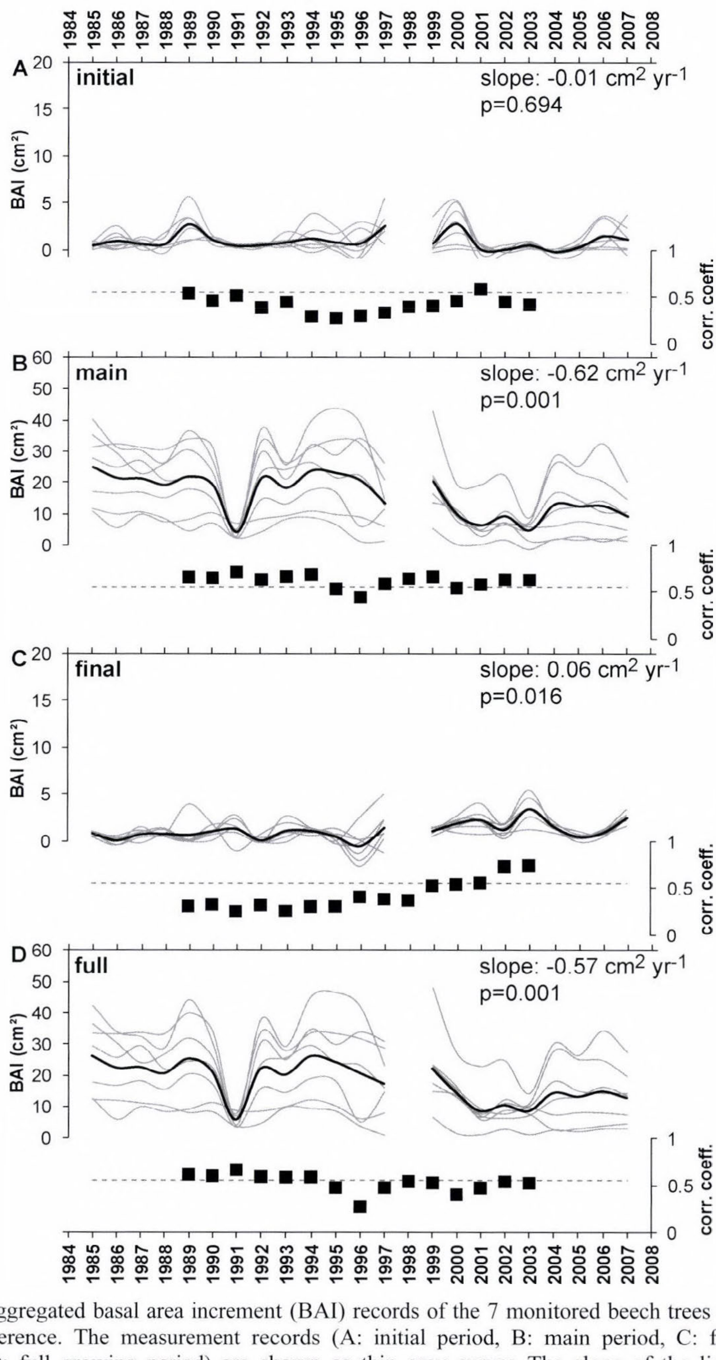

Fig. 3. Aggregated basal area increment (BAI) records of the 7 monitored beech trees and their coherence. The measurement records (A: initial period, B: main period, C: final period, D: full growing period) are shown as thin grey curves. The slope of the linear regression and the corresponding p-value are displayed at the top right corner. The average coefficients of between-tree moving window correlation calculated in 9-year windows are shown below the curves (black square). Dashed horizontal lines show the p=0.1 level.

The year of 1991 was extraordinary, because the mean growth was only 5.77 cm^2 that is only one third of the multi-year average (*Table 6*). In this year, the share of growth in the initial and final periods was higher than the average: 8% (0.44 cm^2) and almost 23% (1.31 cm^2), respectively, while in the main period it was only 70% (4.02 cm^2).

Table 6. Absolute (BAI) and relative (RBAI) yearly increments in different growing periods in average and in a wet-cool (1991) and a dry-warm (2003) year

Growing periods	1985–2007		1991		2003	
	BAI (cm^2)	RBAI (%)	BAI (cm^2)	RBAI (%)	BAI (cm^2)	RBAI (%)
Initial	0.94	5.3	0.44	7.6	0.52	6.0
Main	15.9	88.5	4.02	69.7	6.09	70.8
Final	1.11	6.2	1.31	22.7	1.99	23.2
Total	17.9	100	5.77	100	8.60	100

Fig. 3 shows that in the years 1991 and 2001–2003, the yearly increment values were well below the average. The reason for rather low growth in 1991, beside biological reasons, can be the extreme weather in that year. The yearly precipitation was 849 mm, 12% higher than the multi-year average. However, the distribution of precipitation among the growing phases was unfavorable. The precipitation amount in the winter half-year (November 1990–April 1991), which is an essential water supply for the growth in April, was 190 mm, 32% less than the 47 year average (279 mm). It suggests that recharge of the shallow groundwater reservoir of soil in the dormant and the initial periods were only partial.

In the following two months (May–June), when growth is generally the highest, the precipitation was 329 mm, 84% higher than the multi-year average (178 mm). In the same time, the mean monthly air temperature in these months was 14.4 °C lower by 2.2 °C than the average. Consequently, because of suppressed transpiration induced by the higher humidity and the lower temperature, the intensity of photosynthesis reduced as well, resulting in lower assimilation. This deficit in growth was not recovered in later phases not even with the 330 mm precipitation in the rest of the growing cycle. The growth in the final growing period is 23%, which ratio is systematically higher than that of the 22-year average (6.7%).

The year of 2003 was extreme as well. The yearly precipitation was only 558 mm, 27% less as usual. While precipitation in the dormant and initial periods (216 mm) was similar to the long-term mean (221 mm), in May and June, in the intensive period was only 108 mm, 39% less than the average

(178 mm). At the same time, the average monthly temperature in these months was 18 °C in contrast to the average, 14.5 °C. The means of daily maxima were 21 and 25 °C in May and June, respectively, so drought and heat stress were accompanied, suppressing the organic matter production. The BAI in this year was 8.6 cm^2, shared by 6% in the initial period, and 71% in the main growing period (*Table 6*). It seems that trees tried to partly compensate the loss of production by the largest growth detected for the final period (1.99 cm^2) in this year (*Fig. 3c*).

From the analysis of different years it seems, that the yearly BAI showed a great variability not only year-by-year but also in share among the different growing periods (*Fig. 4*). Generally, when the increment is less in the main period, the ratio is higher in the final stage. This kind of relationship cannot be found in growth between the initial and the main period. The highest growth in the initial period (2.84 cm^2, and 20%) was observed for the year of 2000. This phenomenon can be attributed to the favoring weather conditions, i.e., in the dormant and initial periods the precipitation was 340 mm in total, 21% higher than the 47-year average. The water supply from soil was enough to start the physiological processes, and at the same time the mean monthly temperature was higher by 1.1 and 3.4 °C than the averages (2.9 and 7.9 °C) in March and April, respectively, both favoring the early and intensive growing.

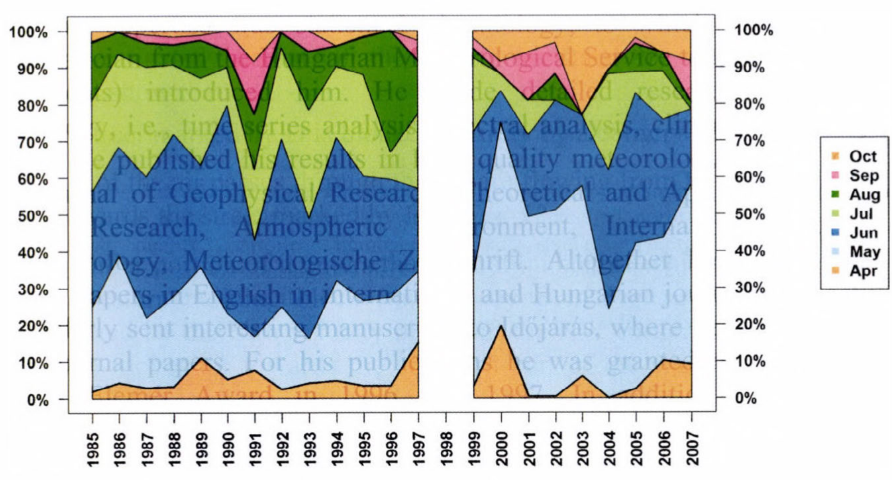

Fig. 4. Share of relative monthly increments of different years.

The length of the initial period was relatively short in agreement with observations in the last two decades: the transition period between winter and summer passes quickly. On the other hand, the main growing period became warmer and warmer, and in July and August, the photosynthesis frequently halted almost completely because of the high daily temperature and low humidity (*Lin et al.* 2012). Later, when hot days were over, it starts again, especially from the beginning of fall to the middle of it. Measurements confirm that ratio of organic matter produced in the final growing cycle is higher and higher, and the magnitude is in a close relationship with growing conditions prevailed in the previous periods; i.e., when organic matter production is low in the main period it is higher than the average in the final cycle. While BAI in the initial period does not show any significant variation during the 22 years, growth significantly decreased in the main and increased in the final periods (*Fig. 5*).

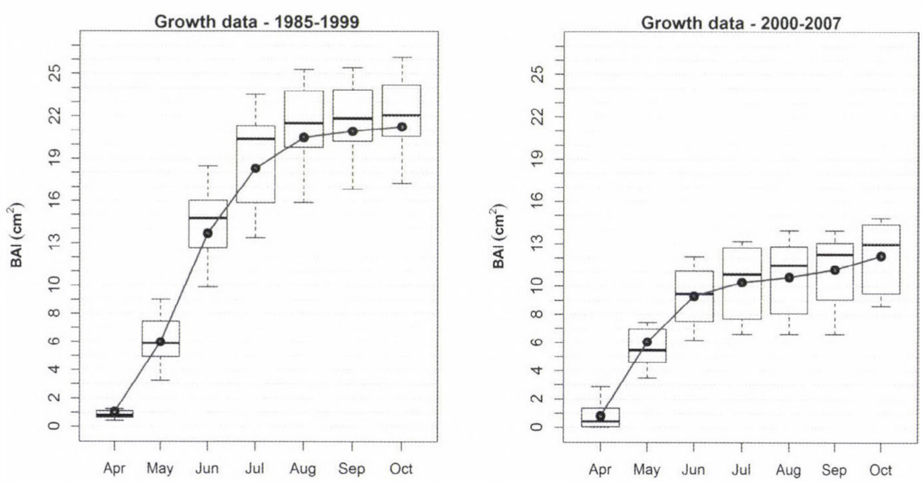

Fig. 5. Cumulative average monthly increments in the periods of 1985–1999 and 2000–2007.
circle: arithmetic mean,
horizontal black line: median,
bottom and top of boxes: lower (Q1) and upper (Q3) quartiles,
error bars: minima and maxima when they are within the 1.5 times of interquartile range (IQR); otherwise the 1.5 times of IQR from Q3 and Q1.

Analyzing the monthly increments separately, we can observe the highest average growth in June (6.08 cm^2), followed by May (5.05 cm^2), July (3.31 cm^2), and August (1.52 cm^2) during the examined 22 years. On the basis of breakpoint analysis with exception of May, September, and October, significant changes are detected between 1999 and 2001 in each month in the main growing period (May-August), and in the whole vegetation period (April-October) (*Table 7*). The breakpoint analysis clearly shows significantly higher mean increments in years before breakpoint in summer, while the trend is just opposite for autumn. For this reason, we analyzed separately the increments of the 1985–1999 and 2000–2007 time intervals. The mean monthly increments differed significantly in the two periods (*Fig. 6*), not only in absolute value but also in the share of the month in the total yearly growth. In years before breakpoint (1985–1999), the highest average increment was detected in June (7.69 cm^2), followed by increments, in order: May: 4.94 cm^2, July: 4.64 cm^2, August: 2.19 cm^2, April: 1.04 cm^2, September: 0.45 cm^2, and October: 0.30 cm^2. In contrast, after the breakpoint (2000–2007), the highest mean BAI appeared earlier, in May: 5.23 cm^2. It means a 6% increase compared to the monthly averages in earlier years. However, it was followed by a dramatic decrease in June, July, and August: 3.26; 0.99; and 0.37 cm^2 (–57; –79; –83% changes), respectively, that was only partly compensated by the slight growth enhancement detected in September (0.52 cm^2) and October (0.98 cm^2). Data clearly showed a drastic decrease in average yearly increments (from 21.19 cm^2 to 12.15 cm^2) in the second period. While the trend of growing does not differed substantially in April-May (*Fig. 3a*), the cumulative increments decreased by 32; 44; 48 % in June, July, and August of the second time interval, respectively (*Fig. 5*). The cumulative deficit in increments till August (48%) compared to the first period is partly compensated (down to 43%) by the relatively higher increments in September and October.

Table 7. Break-point analysis of increments

Month	Brake-point (year)	Increment (cm^2)		
		Before	After	Difference
4	2001*	1.16	0.51	–0.65
5	1990	5.92	4.79	–1.13
6	2000**	7.69	3.26	–4.43
7	2000**	4.64	0.99	–3.65
8	1999**	2.31	0.39	–1.92
9	1990	0.28	0.53	0.25
10	1994**	0.24	0.79	0.55
9, 10	1990*	0.62	1.17	0.56
5, 8	2000**	19.45	9.85	–9.60
4, 10	2000**	21.42	12.15	–9.27

significance levels: *indicates $p<0.1$; **indicates $p<0.05$

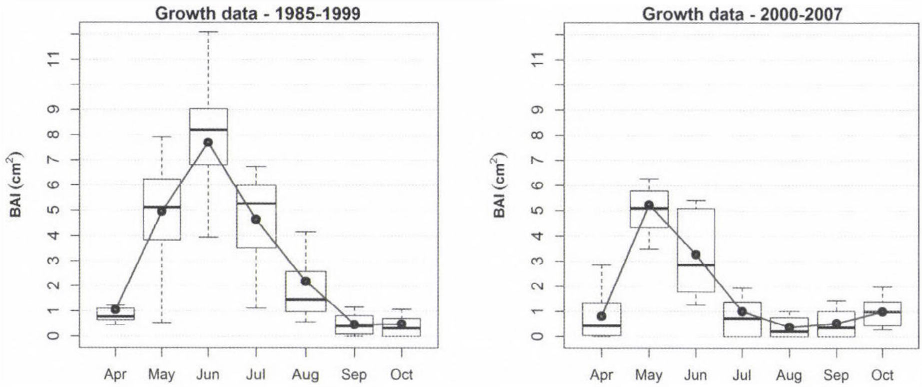

Fig. 6. Absolute average monthly increments in the periods of 1985-1999 and 2000-2007. Legends: refer to *Fig. 5.*

3.3. Relationship between increments and meteorological parameters

For evaluation we applied the linear correlation analysis based partly on monthly and partly on periodic (mean temperature and precipitation sum of a few neighboring months) components (CReMIT). Significant relations between them are compiled in *Table 8*. From correlation coefficients (r), the direction and the rate of the effect can be studied.

Table 8. Significant correlations between BAI and monthly (M) or periodic (P) meteorological variables

M	t_{-2} (Oct)	t_{-1} (Jun)	t_{-1} (Nov)	t (Jun)	p_{-2} (Jun)	p_{-2} (Nov)	p_{-1} (May)	p (Apr)	p (Jun)
r	–0.41*	–0.42*	–0.53**	–0.53**	0.50**	0.49**	0.44**	0.45**	0.46**

P	t_{-2} (Oct-Nov)	t_{-1} (Apr-Jun)	t_{-1} (Oct-Nov)	t (Jun-Jul)	p_{-2} (Jul-Sep)	p_{-2} (Oct-Nov)	p_{-1} (May-Jun)	p (Feb-Apr)	p (Apr-Jun)
r	–0.44**	–0.45**	–0.66**	–0.43**	–0.47**	0.47**	0.44**	0.47**	0.42*

r=correlation coefficient; t=temperature; p=precipitation; significance levels: *=$p<0.1$; **= $p<0.05$
lower indices –1 and –2 refer to the year before and two years before, respectively

It depends on many factors which month or time period has significant effect on the growth of European beech. *Jump et al.* (2010) and *Mátyás* (2010) found increasing climatic effect at the trailing edges compared to other sites. *Maxime* and *Hendrik* (2011) pointed out the importance of elevation above sea level in the investigation of climate and production relationship. *Dittmar et al.* (2003) showed that relations clearly depend on the elevation. These facts support the possible effects of site-specific features in relationships in many cases.

For monthly components (m), there are significant inverse relationships at 90% probability level between BAI and temperature in October two years before ($t_{-2(Oct)}$) and in June one year before ($t_{-1(Jun)}$), as well as at 95% level for temperature in November one year before ($t_{-1(Nov)}$) and in June in the same year ($t_{(Jun)}$). The negative sign indicates that the temperature conditions in the examined stand are out of optimum range for the beech species (*Čufar et al.*, 2008; *Petras* and *Mecko*, 2011; *Scharnweber et al.*, 2011; *Michelot et al.*, 2012). For monthly precipitation correlations are positive at 95% probability level in all cases (two years before in June: $p_{-2(Jun)}$ and November: $p_{-2(Nov)}$, one year before in May: $p_{-1(May)}$, and in the same year in April: $p_{(Apr)}$ and June: $p_{(Jun)}$), i.e., the higher precipitation favors growth (*Lebourgeois et al.*, 2005; *Werf et al.*, 2007; *Čufar et al.*, 2008; *Prislan et al.*, 2013). Significantly affecting components can be observed in the main periods of important physiological processes (budding, defoliation in previous year, organic matter production).

We handled maximum three consecutive months as a period. Over these periods we calculated average temperatures and precipitation sums. It can be noted that the months that are dominant in correlation for monthly components are also dominant in the periodic components.

The results of the multivariable linear regression analysis are displayed in *Table 9*, where beside the corrected coefficient of determination (R^2_{adj}), the simple coefficient of determination (R^2) are also indicated. The R^2_{adj} considers the number of independent variables in the models.

Based on the climate indices, CI_{tm} and $CI_{pm,}$, calculated from only monthly data, it can be concluded that monthly precipitation ($R^2_{adj} = 0.65$) has higher influence on growth than monthly temperature ($R^2_{adj} = 0.44$). This supports the finding of *Gutiérrez et al.* (2011), i.e., temperature affects the organic material production in shorter (days, weeks) periods than that of precipitation. The same findings were published firstly by *Ellenberg* (1988) and justified later also by others (*Geßler et al.*, 2007; *Werf et al.*, 2007). The relation is more significant, $R^2_{adj}=0.71$, in the case of joint climate index (CI_{tpm}), regarding monthly temperature and precipitation data.

Table 9. The selected climate index models (CI)

Model	R^2_{adj}	R^2
$CI_{tm} = -1.44 \times t_{-1(Nov)} - 1.79 \times t_{(Jun)} + 49.82$	0.44	0.49
$CI_{pm} = 0.10 \times p_{-2(Nov)} + 0.06 \times p_{-1(May)} + 0.07 \times p_{(Apr)} + 0.03 \times p_{(Jun)} - 1.04$	0.65	0.70
$CI_{tpm} = 0.09 \times p_{-2(Nov)} + 0.06 \times p_{-1(May)} - 0.87 \times t_{-1(Nov)} + 0.04 \times p_{(Apr)} - 0.9 \times t_{(Jun)} + 22.25$	0.71	0.77
$CI_{ts} = -2.01 \times t_{-2(Oct-Nov)} - 1.28 \times t_{-1(Apr-Jun)} - 2.80 \times t_{-1(Oct-Nov)} - 0.04 \times t_{(Jun-Jul)} + 61.18$	0.55	0.62
$CI_{ps} = 0.06 \times p_{-2(Oct-Nov)} + 0.04 \times p_{-1(May-Jun)} + 0.02 \times p_{(Apr-Jun)} - 1.39$	0.45	0.54
$CI_{tps} = -0.03 \times p_{-2(Jul-Sep)} - 2.13 \times t_{-2(Oct-Nov)} - 2.88 \times t_{-1(Oct-Nov)} + 0.04 \times p_{(Feb-Apr)} - 0.02 \times p_{(Apr-Jun)} - 0.42 \times t_{(Jun-Jul)} + 57.83$	0.65	0.73
$CI_{tpms} = 0.96 \times t_{-2(Oct)} + 0.1 \times p_{-2(Nov)} - 1.34 \times t_{-1(Apr-Jun)} + 0.03 \times t_{-1(May-Jun)} - 1.31 \times t_{-1(Oct-Nov)} + 0.06 \times p_{(Apr)} - 0.01 \times p_{(Jun)} - 0.98 \times t_{(Jun)} + 37.84$	0.71	0.81

t=temperature, p=precipitation, m=monthly, s=seasonal
lower indices –1 and –2 refer to the year before and two years before, respectively

The coefficient of determination calculated for the periodical additive temperature climate index (CI_{ts}) is $R^2_{adj} = 0.55$, a little higher than that for monthly components. In contrast, the same coefficient for precipitation (CI_{ps}) is lower than for the monthly components, $R^2_{adj} = 0.45$. That is, for periodic climate indices the temperature has higher influence than precipitation. When considering the additive effect of periodic temperature and precipitation parameters (CI_{tps}), we can conclude that the relation is less significant than for monthly components ($R^2_{adj} = 0.65$).

Corrected coefficient of determination of model calculated both with monthly and periodic components (CI_{tpms}) gives a strong relationship with $R^2_{adj} = 0.71$. Temporal variations of observed and modeled basal area increment are presented in *Fig. 7* for models of CI_{tpm}, CI_{tps}, and CI_{tpms}. Except of a few years (e.g., 1991), it is evident that observed values fits well within the upper and lower confidence limits of the models.

We have analyzed the relationship between monthly increments and meteorological variables. As we pointed out in the breakpoint analysis, year-by-year changes in meteorological conditions may be reflected in changes of increments. From results in *Table 7* it can be seen, that, e.g., substantial decrease occurred in June in increments from 2000. Two years before this decrease, a significant precipitation decrease started in June (*Table 4*, *Fig. 8*) accompanied by a delayed increase in growth in the following years. Mean temperature in June still increased well before this decrease (since 1992), probably also affecting the increments in June of later years. Therefore, we examined by linear regression analysis the relationship between increments and meteorological variables (precipitation, temperature) in each month of the vegetation period. *Table 10* shows significant relationships in increments as the function of mean temperature and precipitation in May and June. In May, July, and August, the joint effect of temperature in the given month and a month before in the increments is more significant than that of the given month. The sign of correlation coefficient shows a positive effect of temperature in the monthly growth in spring (April, May), while later, rising temperature does not favor the increments.

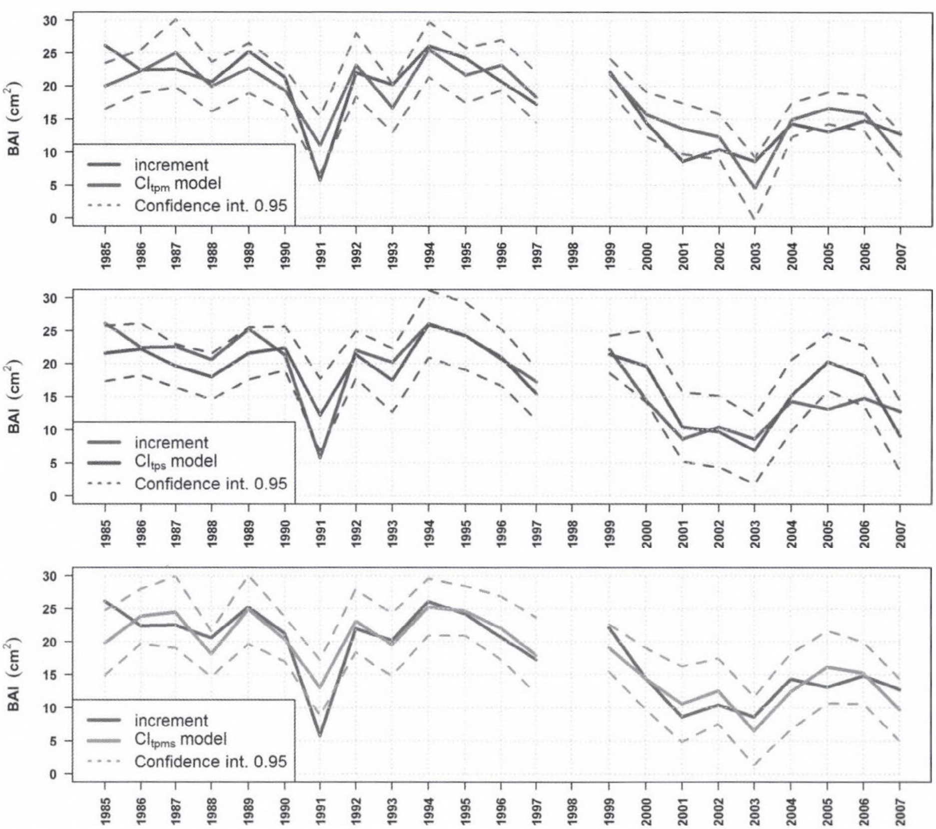

Fig. 7. Variation of the measured and modeled basal area increment (BAI) for models of CI_{tpm}, CI_{tps}, and CI_{tpms} (n=22, p<0.001).

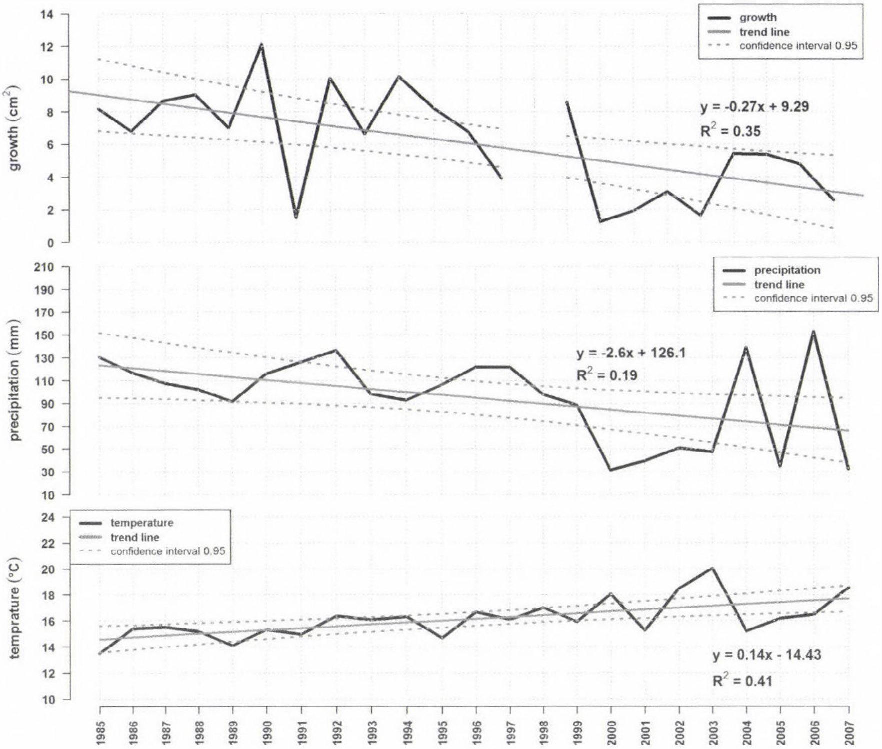

Fig. 8. Trend of increments (n=22, p<0.01), mean temperature, and precipitation in June (n=23, p<0.001).

Table 10. Correlation coefficients (r) of regression between monthly increments and meteorological variables

Meteorological parameters	**Months** 4	5	6	7	8	9	10
Precipitation in the given month	0.301	–0.371*	0.507**	–0.245	0.264	0.415*	–0.049
Precipitation in the given and preceding months	0.266	–0.125	0.250	0.236	0.288	0.167	–0.161
Mean temperature in the given month	0.196	0.392*	–0.506**	–0.051	–0.321	–0.273	–0.048
Mean temperature in the given and preceding months	0.315	0.653**	–0.412*	–0.488**	–0.489**	–0.157	–0.030

significance levels: *indicates p<0.1; **indicates p<0.05

4. Discussion

The largest growths were detected in May and June in the studied beech stand over the studied 22 years. Average BAI observed were 5.02 and 6.08 cm^2 (28 and 34%) in May and June, respectively (alltogether 62% of yearly growth). While in May trend could not be observed for growth ($y = -0.0018 \times x + 5.0698$, R2=4x 10–5), there was a negative significant trend in June (*Fig. 8*; $y = -0.27 \times x + 9.29$, R2=0.35). As a consequence, while in the first 11 years of observation the mean BAI in June was almost the double of that of May (8.03 vs. 4.84 cm2), in the second 11-year period growth in May exceeded the production of June (5.20 vs. 4.12 cm^2). This phenomenon was related to the positive trend of average temperature and the negative trend of increments in June over the years (*Fig. 8*) (there is no significant trend for precipitation in June). In contrast, in May there is a positive relationship between the BAI and the mean temperature (*Fig. 9*). This shows that the intensive growing period started earlier in the 2000s, which projects an increase of sub-Mediterranean climate influence at the observation site, obviously modifying the spread of beech. Our results underline the determining effect of May and June in organic matter production of beech in agreement with other studies from Europe (*Dittmar et al.*, 2003; *Lebourgeois et al.*, 2005; *Di Filippo et al.*, 2007; *Garamszegi* and *Kern*, 2014).

It is worth also mentioning, that the total BAI loss and the increased BAI in the final period is accompanied with opponent changes in growth signal coherence. Mean within-trees correlation slightly decreased for the total and significantly increased for the final period following the detected breakpoint.

As it can be seen from the calculated regressions (*Table 8*) as well as from the climate indices (*Table 9*), increments of trees are influenced by the climate of different months or periods not only in the given year but also in the previous two years. Analyzing the data, the following general tendencies can be seen. Taking into account the sign and magnitude of coefficients in the tables, the precipitation has positive effect on growth while the influence of temperature is the opposite.

Precipitation in autumn (October, November) two years before a given year has generally positive effect on girth growth. In the previous year, positive influence of precipitation can be observed in spring in the most intensive growing periods (May, June). In the given year, the precipitation – in spite of a few exceptions – has dominantly positive effect in the period of February-July, especially in the initial growing period (April) and at the beginning of the main growing period (May, June) when majority of increment is realized. Negative influence of air temperature is realized in autumn (October-November) one or two years before the given year but the effect of temperature can also be observed in spring-summer one year before, and it is evident in the given year in early summer, mostly in June.

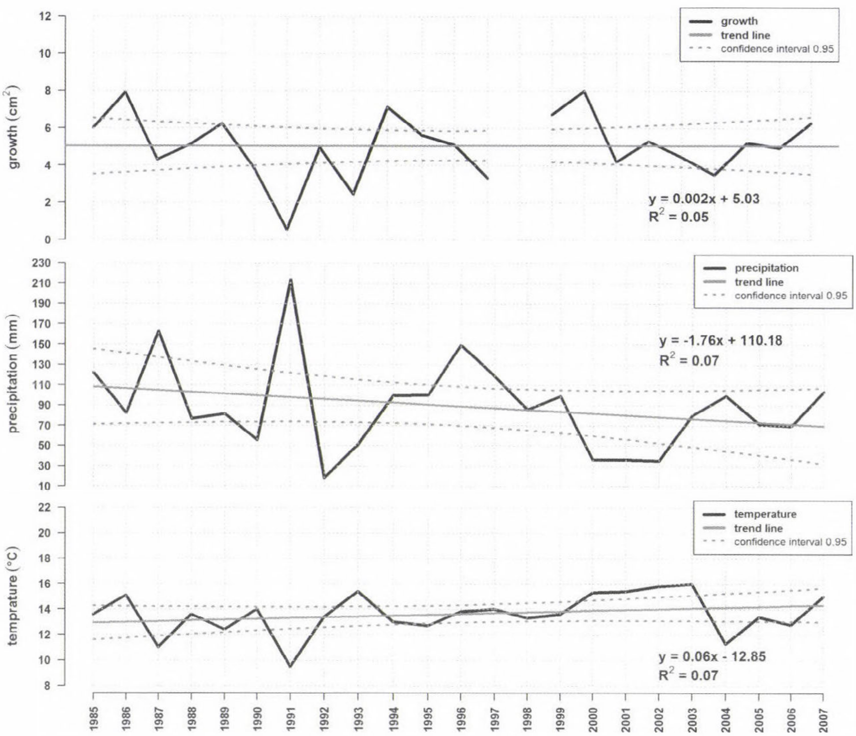

Fig. 9. Trend of increments (n=22, p<0.01), mean temperature, and precipitation (n=23, p<0.001) in May.

The examined stand according to the forestry aridity index (*Führer et al.*, 2011) definitely belonged to the beech climate zone. However, since the end of the 1980s, a drastic change was observed. The sum of precipitation decreased by 10%, nearly by 3%, and by 14% in the initial, main, and final growing stages, respectively, during the 1991–2007 period compared to the 1961–1990 reference period (*Table 11*). These changes are already higher than the forecasted data for 2035–2065 calculated by the REMO model (*Gálos et al.*, 2007). At the same time, temperature showed a steady increasing trend in almost each different growing (sub)period within the year. The change in the initial period is 0.7 °C, while in the main growing period it is as high as 1.2 °C. If the tendencies of precipitation and temperature keep on following the climate change scenario of the REMO model, living conditions of beech in the surroundings of the monitored stand will change to such an extent that can lead to not just increment decrease (*Piovesan et al.*, 2008), but also potential extinction.

Table 11. Climate parameters in the reference period (1961–1990), in the period of investigation (1991–2007), and forecasted by REMO model (*Gálos et al.*, 2007) (2035–2065) in absolute and relative values

Growing Period (Months 1–12)	Time intervals (years)									
	1961–1990		1991–2007				2035–2065			
	p (mm)	*t* (°C)	*p* (mm)	d*p* (%)	*t* (°C)	d*t* (°C)	*p* (mm)	d*p* (%)	*t* (°C)	d*t* (°C)
Year (1–12)	753	7.6	774	2.8	8.4	0.8	775	2.9	9.5	1.9
Dormant (11–3)	216	–0.2	228	5.5	0.4	0.6	238	10.2	1.7	1.9
Growing (4–10)	536	13.2	547	2.1	14.1	0.9	537	0.2	15.1	1.9
Initial (4)	60	7.7	54	–10.0	8.4	0.7	63	5.0	9.0	1.3
Main (5–8)	352	15.8	343	–2.6	17.0	1.2	332	–5.7	17.7	1.9
Final (9–10)	124	10.8	150	21.0	11.0	0.1	142	14.5	13.2	2.4
Intensive (6)	100	15.3	86	–14.0	16.5	1.2	91	–9.0	17.4	2.1

The coinciding breakpoint detected in the series of climate and BAI suggests that the significant change in climate parameters affected the production as well. Both the strength and the sign of the relationship between the climate and the growth data changed, as it is illustrated by the correlation coefficients between the BAI and the FAI (*Führer et al.*, 2011) or EQ (*Ellenberg*, 1988) drought indices (*Table 12*) separately in the two periods until and after 1999. While climate was favoring for growth of beech (1985–1999) represented clearly by beech climate (FAI=4.01), only the monthly precipitation sum in FAI from May to August had significant influence on the yearly production. The increase of summer precipitation negatively affected the yearly growth in this period. After the climate became dryer and warmer from 2000, the mean FAI has changed to the border of beech/hornbeam-oak climate (FAI=4.82), and this enhanced climate stress has stronger effects on the yearly growth. These results support the observations of *Mátyás* (2010) and *Garamszegi* and *Kern* (2014) who pointed out the increasing climate sensitivity of beech towards the border of beech/hornbeam-oak climate. This manifests not only in the decline or the fall of trees but also in the decrease of growth accompanied with unfavorable economic impact, i.e., the decreasing profitability of forest management (*Führer et al.*, 2013).

An earlier basal area increment survey performed near the town of Gödöllő, Hungary, between 1974 and 1983 (*Járó* and *Tátraaljai*, 1985) for different species (ten deciduous and seven pine stands) showed that the growth generally started before the middle of April for all species of deciduous trees and ended before the end of August. Growth in September was observed in the case of only a few species, such as black locust, hornbeam, and 'I-214' poplar, and it lasted only for a few days. For pines, the growth started two weeks earlier and ended generally in the first third of October. Thus, the average length of the growing period for deciduous species was 139 and for pines it was 190 days.

Table 12. Correlation coefficients between average yearly BAI and drought indices (FAI, EQ); their precipitation (P_{FAI}, P_{EQ}) and temperature (T_{FAI}, T_{EQ}) components in periods of 1985–1999 and 2000–2007

Periods	P_{FAI}	P_{EQ}	T_{FAI}	T_{EQ}	**FAI**	**EQ**
1985–1999	–0.50*	–0.23	0.10	0.15	0.29	0.27
2000–2007	0.48	0.40	–0.75**	–0.37	–0.69*	–0.55

significance levels: * indicates $p<0.1$; **indicates $p<0.05$

According to our phenological observations parallel with BAI measurements in the Sopron Mountains, the beech came into leaf from the middle of April and ended at the end of the same month. The period of autumn discoloration of leaves ranged between the beginning and the end of October, while defoliation occurred till the middle of November. It means, that the average length of time period for photosynthetic, i.e., growing processes was 173 days.

Since the start of the initial growing period was the same in the Gödöllő region for 1974–83 as at the Sopron Mountains for 1985–2007, and the lengths were equally two weeks for both regions, the reason for the difference between the two growing periods is the different length of the main growing periods. In the Gödöllő region, the 103-day-long main growing period lasted till the middle of July, when 93.3% of organic material was produced. In the case of beech stand in the Sopron region the same portion of organic matter (93.3%) was produced, but it occurred till the end of August over a 140-day-long main growing period. The final period was of the same length at both areas, finished at the end of August and in the first third in October at Gödöllő and Sopron regions, respectively. The reason for the different length or timing of the main and final cycles, beside the differences in species, is the difference in climate conditions. Namely, whilst the average yearly precipitation in the Gödöllő region was 544 mm and the yearly average temperature was 9.5 °C, these values were much higher for precipitation (764 mm) and lower for temperature (8.2 °C) for the Sopron area in the measurement periods, i.e., the Gödöllő area is drier and warmer compared to the Sopron Mountain region.

Similar results to the Sopron region was reported for an old-growth beech near Solling, Germany (*Schulze*, 1970; *Schulze et al.*, 1977), where the number of days with positive carbon dioxide balance during a year reached 176, which implies that the growing period might be shorter. Partition of cambium can also be observed for beech at the later stage of growing period; that is, the initial rapid growth of beech may even stop at the end of July and in August, starting again in September, lasting to early October (*Schmitt et al.*, 2000; *Werf et al.*, 2007). This phenomenon was also observed near Sopron in 2003, when, as the consequence of extremely dry summer, the growth was suppressed in July and August and started again in September lasting till the middle of October when an additional 20% of yearly growth was produced.

Although, it can be generally stated that annual increment is largely determined by weather conditions in the given year and also in the previous two years, months with the strongest impact are probably determined not only by climate parameters, but also the genetic properties of trees beside the seasonality in temperature and precipitation characteristics. While in the neighboring Slovenia precipitation in May-June of the given year has the most important effect on increments of trees (*Čufar et al.*, 2008), and in the Mediterranean region (Albania, Macedonia) the June-September temperature has a negative effect on growth (*Tegel et al.*, 2014), in the Sopron Mountains, where both the yearly precipitation amount and the temperature is lower, the dominant parameter for growth is the precipitation in April and June. In addition, while in Germany the temperature in July in the given year and a year before are dominant for growth (*Gruber*, 2002), in the Sopron region the June temperature in the given year and a year before are determinant.

This overview suggests that further research efforts on beech physiology is needed to give successful explanation on which climatic conditions (monthly or periodic) are the primary drivers of organic matter production through biochemical processes. For this reason, calculation of universal climate index for general use is still not possible, but it can be done in a similar way for stands in different climate and genetic conditions.

As we have already seen above, there were substantial variations in precipitation and temperature conditions among different months during the observed period. On the basis of linear regression analysis, the growth in May and June significantly depends on the average temperature and precipitation. The sign of correlation coefficient shows a positive relation between growth and temperature in spring, but in the following months the relation is negative (*Table 10*). The effect of precipitation is just the opposite; in springtime the precipitation shows negative correlation with growth, while in the following periods the relation is positive.

The breakpoint analysis in the period of 1985–2007 indicates significant shifts in the monthly precipitation and temperature between 1990 and 2000 (*Table 4*). After the breakpoints we found positive and negative shifts for temperature and precipitation, respectively. We suppose that the observed decrease of increments (*Table 7*) is due to the change in meteorological conditions, and taking into account the predicted climate change scenarios these phenomena will proceed in the future. The change in meteorological conditions are reflected not only in the decrease of yearly increment but also in decreasing share of summer, increasing relative share of spring, and importance of autumn months' conditions in the yearly growth. In addition, growth in May became dominant after the breakpoint instead of June, and the share of July and August drastically decreased in that period (*Fig. 4*). E.g., the increments in July were zero in three years (2002, 2003, and 2007) and were, similarly, zero in four years in August (2000, 2001, 2003, and 2004). This phenomenon is in connection not only with the meteorological conditions of July/August in the given year but also with the climate in preceding months or periods even two year before.

The determining effect of May and June in organic matter production of beech were reported previously as well (*Dittmar et al.*, 2003; *Lebourgeois et al.*, 2005; *Di Filippo et al.*, 2007). According to earlier observations (*Járó* and *Tátraaljai*, 1985), in Hungarian conditions the maximum growth can be observed in June for almost all of tree species. *Knott* (2004) examined a beech stand in an average year of 2001 (elevation: 470 m, DBH: 38 cm, yearly mean air temperature: 7.9 °C, precipitation: 761 mm year^{-1}). The increments for trees have the maximum in summer (increments in July, June, Aug, May are: 30.3%, 27.4%, 21.6%, and 16.0%, respectively). Precipitation in July and August was above the average. This could be the reason of the relatively higher increments in the summer months compared to our test site. This statement is, however, no longer valid for our beech stand, where the maxima of growth shifted to May. It may be an indirect indication of the climate change (*Werf et al.*, 2007; *Ježík et al.*, 2011; *Čufar et al.*, 2012).

Signs of change in relative share of different months and the increasing share of spring in increments were reported earlier similarly to our findings. *Ježík* et al. (2011) investigated beech trees in 2003–2008 with similar climate conditions (elevation: 470 m, DBH: 32–36 cm, yearly mean air temperature: 7.9 °C, precipitation: 715 mm year^{-1}). They found that at the start of the vegetation season, increments positively correlated with temperature. In summer it was hampered by long-term heat waves and the positive influence of precipitation became more pronounced. In view of the predicted climate change, they expected a shift in the culmination of beech seasonal diameter increase towards May caused by warmer springs and a higher frequency of summer droughts and heat waves.

Werf et al. (2007) also pointed out the effect of drought in the year of 2003 to the increment. They measured the increments of beech when summer temperature was 2.1 °C higher and precipitation was 59% lower than the 100-year average (9.5 °C, 760 mm). In summer drought the growth ceased, but it recovered after the drought as it was observed in our test stand after a significant change in summer temperature and precipitation since 2000. The decrease in increment is evident in the dry season, since soil drought stimulates increased stomatal resistance with parallel decrease of photosynthetic activity for European beech (*Priwitzer et al.*, 2014).

5. Conclusions

There were characteristic breakpoints both in meteorological parameters and in beech increments in the Sopron Mountains between 1999 and 2000. The negative shift in precipitation and positive shift in temperature caused a dramatic decrease in growth in summer. There was a shift in maximum monthly increments from June to May, indicating the effect of the climate change on seasonal growth of beech. Significant, dramatic decrease in growth can be observed in July and August that was not observed before. Due to the warmer spring and the arid summer months, the relative share of spring and importance of autumn months increased and expectedly will be increasing in the future. The phenomena of low or zero growth in July and August, observed often after 2000, probably will be more frequent in the future, taking into account the predicted climate change scenarios. The long-term trend of yearly basal area increment is continuously decreasing; the average yearly increments halved between 1985 and 2007.

According to multivariable regression analysis on independent variables derived by CReMIT, the yearly basal area increment is affected not only by meteorological parameters but also the climate of the previous two years. Precipitation generally favors organic matter production in contrast with temperature. Interestingly, one of the dominant periods for basal area increment is the autumn two years before a given year (October-November), when precipitation has positive influence and temperature has negative effect on the increment, i.e., the wet and cool autumn in that year favors organic matter production. Regarding the preceding year, precipitation in the main growing period (spring-early summer) has positive while temperature in autumn has negative effect. Finally, in the current year, precipitation in spring-early summer (especially in April-June) helps the growth of trees, and in contrary, the temperature in that period has negative effect on the increment. There is a negative relationship between the observed basal area increment and the mean temperature in June (July).

The share of basal area increment in the main growing cycle is continuously decreasing which is partly compensated by a parallel increase of it in the final growing period as the climate at the studied region, in the Sopron region, Hungary has become warmer. This phenomenon underlines the general observations made in Hungary. The warming climate has negative effect on the production of trees. According to forecasted climate change, when temperature in early summer in Hungary will be higher and higher, not only the loss in growth but also the drastic decay in vitality and tolerance of trees can be expected.

It seems that the rate of increments is controlled by weather parameters in earlier phenological phases in previous years as well as through the effect of different physiological processes described above (defoliation, bud structure production, cupules production, etc.), at least for the examined stand. The direct generalization of the observations is hardly possible regarding the high differences in species composition, genetics, climate, pedology, hydrology, etc., among the different regions, as we saw in the discussion through examples for other sites for Hungary as well as for Slovenia and Germany. However, the tools and methods applied in this paper are suitable to study other areas to determine which periods and which weather components have the greatest influence on the yearly increments of trees.

Acknowledgements—This work was supported by the Hungarian Scientific Research Fund (OTKA CK 80305/80335]; by the NAIK KFI (RD011-12) and the "Scientific analysis of Earth-system data and its communication for the society with tolls of recent informatics" (TAMOP-4.2.2.C–11/1/KONV-2012-0015) projects sponsored by the EU and the European Social Fund. Thanks to the "Lendület" program of the Hungarian Academy of Sciences (LP2012-27/2012). Authors thank *dr. Andreas Rigling* for the useful advices to improve the manuscript. Thanks to *Margit Horoszné Gulyás* for the basemap of *Fig. 1*.

Appendix

Brief description of CReMIT

Let be given a time series and its natural period denoted by P. The elements of this time series are stored in vector ts. Let the first element of ts, ts_1 be the chronologically latest element, and natural numbers will be assigned to the data accordingly:

$$ts = \begin{pmatrix} ts_1 \\ ts_2 \\ \vdots \\ ts_m \end{pmatrix}.$$

Let be denoted by SP ($1 \leq SP \leq P$) the starting point of the currently applied investigation, this is the SPth element of the vector ts. Special windows are applied on the vector ts, the time shifting (i) and width (j) values of a window are defined based on this index. The minimal value of time shifting can be 0 (i=0), and the minimal window width can be 1 (j=0). Based on the periodicity P of the basic time series, the above defined window will be periodically repeated with the maximum cycle number (MCN). The value of MCN depending on the defined parameters (SP, i, j) can be created:

$$MCN = \left[\frac{n-(SP+i+j)}{P}\right]+1,$$

where square brackets is for the integer part function.

The starting and end point indices of the windows created with the actual SP, i, and j values can be defined as $[SP + i + l \times P; SP + i + j + l \times P]$, where $0 \leq l \leq MCN$. Two temporal vectors are defined for the storage of the index values determining the limits of the windows using these parameters. Let us denote by:

$$index_{begin} = \begin{pmatrix} SP + i + 0 * P \\ SP + i + 1 * P \\ \vdots \\ SP + i + (MCN - 1) * P \end{pmatrix},$$

$$index_{end} = \begin{pmatrix} SP + i + j + 0 * P \\ SP + i + j + 1 * P \\ \vdots \\ SP + i + j + (MCN - 1) * P \end{pmatrix}.$$

By using the above defined index vectors, a pre-defined transformation function TR can be applied on the elements of the individual windows.

$$tr\_x_{SP,i,j} = \begin{pmatrix} TR(index_{begin}[1]; index_{end}[1]) \\ TR(index_{begin}[2]; index_{end}[2]) \\ \cdots \\ TR(index_{begin}[MCN]; index_{end}[MCN]) \end{pmatrix}$$

Based on the starting point ($1 \leq SP \leq P$), the maximum time shifting value I ($0 \leq i \leq I$), and the maximum window width J ($0 \leq j \leq J$) pre-defined on the basis of the task, all the potential $tr\_x_{SP,i,j}$ transformed vectors can be generated on a systematic way. The above mentioned MCN value defines the number of windows for the current parameters (SP, i, j) and the dimension of the transformed vector.

The different phases of the CReMIT are: i) data preparation, ii) creation of the secondary dataset, and iii) analyses of the whole datasets. Considering technical points of view, creation of secondary dataset can be determined by the maximum seasonal shift and length of the investigated period. Hence, by using an appropriate aggregation function (TR) (e.g., mean, sum, minimum, maximum) new, complex data sets can be derived consistently from the original data. The CReMIT has been applied for weather parameters in this work. The relevant time intervals to the growth data of the given year were selected using a maximum three years of shift compared to the data of increment, with a maximum of 12 month of an interval length. In this manner, beside the meteorological data for the given year, we involved the mean temperature and precipitation sum data also for the previous two years with a length of 1–12 months (secondary dataset).

References

Bouriaud, O. and *Popa, I.*, 2009: Comparative dendroclimatic study of *Scots pine*, *Norway spruce*, and *Silver fir* in the Vrancea Range, Eastern Carpathian Mountains. *Trees 23*, 95–106.

Bräker, O.U., 1996: Growth trends of Swiss forests, tree-ring data Case study Toppwald, In (Eds.: *Spiecker, H., Mielikäinen, K., Köhl, M., Skovsgaard, J.P.*) Growth trends in European forests. Springer, Berlin, Heidelberg pp. 199–217.

Briffa, K.R., Osborn, J.T., Schweingruber, H.F., Jones, D.P., Shiyatov, G.S., and *Vaganov, A.E.*, 2002: Tree-ring width and density data around the Northern Hemisphere, Part 1, local and regional climate signals. *Holocene 12*, 737–757.

Büntgen, U., Frank, C.D., Schmidhalter, M., Neuwirth, B., Seifert, M., and *Esper, J.*, 2006: Growth/climate response shift in a long subalpine spruce chronology. *Trees 20*, 99–110.

Čufar, K., Prislan, P., de Luis, M., and *Gričar, J.*, 2008: Tree-ring variation, wood formation and phenology of beech (*Fagus sylvatica*) from a representative site in Slovenia, SE Central Europe. *Trees 22*, 749–758.

Čufar, K., de Luis, M., Saz, M.A., Črepinšek, Z., and *Kajfež-Bogataj, K.*, 2012: Temporal shifts in leaf phenology of beech (*Fagus sylvatica*) depend on elevation. *Trees 26*, 1091–1100.

Deslauriers, A., Morin, H., Urbinati, C., and *Carrer, M.*, 2003: Daily weather response of balsam fir (*Abies balsamea* (L.) Mill.) stem radius increment from dendrometer analysis in the boreal forests of Québec (Canada). *Trees 17*, 477–484.

Deslauriers, A., Rossi, S., and *Anfodillo, T.*, 2007a: Dendrometer and intra-annual tree growth: What kind of information can be inferred? *Dendrochronologia 25*, 113–124.

Deslauriers, A., Anfodillo, T., Rossi, S., and *Carraro, V.*, 2007b: Using simple causal modeling to understand how water and temperature affect daily stem radial variation in trees. *Tree Physiol. 27*, 1125–1136.

Di Filippo, A., Biondi, F., Čufar, K., De Luis, M., Grabner M., Maugeri M., Presutti Saba E., Schirone, B., and *Piovesan, G.*, 2007: Bioclimatology of beech (*Fagus sylvatica* L.) in the Eastern Alps: spatial and altitudinal climatic signals identified through a tree-ring network. *J. Biogeo. 34*, 1873–1892.

Dittmar, C., Zech W., and *Elling, W.*, 2003: Growth variations of common beech (*Fagus sylvatica* L.) under different climatic and environmental conditions in Europe – a dendroecological study. *Forest Ecol. Manag. 173*, 63–78.

Ellenberg, H., 1988: Vegetation ecology of Central Europe. 4th ed. Cambridge University Press. Cambridge.

EUFORGEN, 2009: Distribution map of Beech (*Fagus sylvatica*) EUFORGEN 2009, www.euforgen.org. (last accessed: 15 Jan 2015).

Fekedulegn, D., Hicks, R.R., and *Colbert, J.J.*, 2003: Influence of topographic aspect, precipitation and drought on radial growth of four major tree species in an Appalachian watershed. *Forest Ecol. Manag. 177*, 409–425.

Fekete, Z., 1958: Fatermési és faállományszerkezeti vizsgálatok hazai bükkösökben. Mezőgazdasági Kiadó, Budapest, pp. 108.

Führer, E., Mátyás, C., Csóka, G., Lakatos, F., Bordács, S., Nagy, L., and *Rasztovits, E.*, 2010: Current status of European beech (*Fagus sylvatica* L.) genetic resources in Hungary. *Communicationes Instituti Forestalis Bohemicae 25*, 152–163.

Führer, E., Horváth, L., Jagodics, A., Machon, A., and *Szabados, I.*, 2011: Application of a new aridity index in Hungarian forestry practice. *Időjárás 115*, 103–118.

Führer, E., Jagodics, A., Juhász, I., Marosi, G., and *Horváth, L.*, 2013: Ecological and economical impacts of climate change on Hungarian forestry practice. *Időjárás 117*, 159–174.

Gálos, B., Lorenz, P., and *Jacob, D.*, 2007: Will dry events occur more often in Hungary in the future? *Envir. Res. Lett. 2*, 034006.

Garamszegi, B. and *Kern, Z.*, 2014: Climate influence on radial growth of *Fagus sylvatica* growing near the edge of its distribution in Bükk Mts., Hungary. *Dendrobiol. 72*, 93–102.

Geßler, A., Keitel, C., Kreuzwieser, J., Matyssek, R., Seiler, W., and *Rennenberg, H.*, 2007: Potential risks for European beech (*Fagus sylvatica* L.) in a changing climate. *Trees 21*, 1–11.

Gruber, F., 2002: Wachstum von Altbuchen (*Fagus sylvatica* L.) auf einem Kalkstandort (Göttinger/Södderich) in Abhängigkeit von der Witterung III Bohrkenanalysen. *Allgemeine Forst- und Jagdzeitung 173*, 117–122.

Gruber, F., 2004: Die Steuerung des sogenannten „Blattverlust" der Buche (*Fagus sylvatica* L.) durch die Witterung. *Allgemeine Forst- und Jagdzeitung 175*, 83–94.

Gutiérrez, E., Campelo, F., Camarero, J.J., Ribas, M., Muntán, E., Nabais, C., and *Freitas H.*, 2011: Climate controls act at different scales on the seasonal pattern of *Quercus ilex* L. stem radial increments in NE Spain. *Trees 25*, 637–646.

Hasenauer, H., Nemani, R.R., Schadauer, K., and *Running, S.W.*, 1999: Forest growth response to changing climate between 1961 and 1990 in Austria. *Forest Ecol. Manage. 122*, 209–219.

Hidnert, P. and *Krider, H.S.*, 1947: *Thermal expansion of some copper alloys*. U. S. Department of Commerce National Bureau of Standards Research Paper RP1838; J. Res. National Bureau of Standards 39, 419-424.

IUSS, 2014: IUSS Working Group WRB, World Reference Base for Soil Resources 2014. International soil classification system for naming soils and creating legends for soil maps. World Soil Resources Reports No. 106, FAO, Rome.

Járó, Z. and *Tátraaljai, E.*, 1985: A fák éves növekedése. *Erd. Kut. 76–77*, 221–234.

Ježík, M., Blaženec, M., Střelcová, K., and *Ditmarová, Ľ.*, 2011: The impact of the 2003–2008 weather variability on intra-annual stem diameter changes of beech trees at a submontane site in central Slovakia. *Dendrochronologia 29*, 227–235.

Jump A.S., Hunt J., and *Peñuelas J.*, 2006: Rapid climate change-related growth decline at the southern range edge of *Fagus sylvatica*. *Global Change Biol. 12*, 2163–2174.

Jump, A.S., Cavin, L., and *Hunter, P.D.*, 2010: Monitoring and managing responses to climate change at the retreating range edge of forest trees. *J. Environ. Monit. 12*, 1791–1798.

Kahle, H.P., Karjalainen, T., Schuck, A., Ågren, G.I., Kellomäki, S., Mellert, K., Prietzel, J., Rehfuess, K.E., and *Spiecker, H.* (Eds.), 2008: Causes and consequences of forest growth trends in Europe – Results of the Recognition Project. EFI Research Report 21. Brill Academic Publisher, Leiden, Boston, Köln, 262 pp.

Kern, Z. and *Popa, I.*, 2007: Climate-growth relationship of tree species from a mixed stand of Apuseni Mts, Romania. *Dendrochronologia 24*, 109–115.

Knott, R., 2004: Seasonal dynamics of the diameter increment of fir (*Abies alba* Mill.) and beech (*Fagus sylvatica* L.) in a mixed stand. *J. Forest Sci. 50*, 149–160.

Kozlowski, T.T., Kramer, P.J., and *Pallardy, S.G.*, 1991: The physiological ecology of woody plants. Academic Press, San Diego, London.

Lakatos, M., Szentimrey, T., Bihari, Z., and *Szalai, S.*, 2013: Creation of a homogenized climate database for the Carpathian region by applying the MASH procedure and the preliminary analysis of the data. *Időjárás 117*, 143–158.

Larcher, W., 2001: Ökophysiologie der Pflanzen. 6. Aufl. Ulmer, Stuttgart.

Lebourgeois, F., Bréda, N., Ulrich, E., and *Granier, A.*, 2005: Climate – tree-growth relationships of European beech (*Fagus sylvatica* L.) in the French permanent plot network (RENECOFOR). *Trees 19*, 385–401.

Liming, F.G., 1957: Homemade dendrometers. *Forestry 55*, 575–577.

Lin, Y.S., Medlyn, B.E., and *Ellsworth, D.S.*, 2012: Temperature responses of leaf net photosynthesis: the role of component processes. *Tree Physiol. 32*, 219-231.

Maaten, van der, E., 2012: Climate sensitivity of radial growth in European beech (*Fagus sylvatica* L.) at different aspects in southwestern Germany. *Trees 26*, 777–788.

Magri, D., 2008: Patterns of post-glacial spread and the extent of glacial refugia of European beech (*Fagus sylvatica*). *J. Biogeogr. 35*, 450-463.

Mares, C. and *Mares, I.*, 1994: *Climate change-points in the precipitation time series from Romania.* In: Atmospheric Physics and Dynamics in the Analysis and Prognosis of Precipitation Fields (Proceedings of the meeting). Rome, 176–180.

Mátyás, C., 2010: Forecasts needed for retreating forests (Opinion). *Nature 464*, 1271.

Mátyás, C., Nagy, L. and *Ujvári-Jármay, É.*, 2010: Genetically set response of trees to climatic change, with special regard to the xeric (retreating) limits. *Forstarchiv 81*, 130–141.

Maxime, C. and *Hendrik, D.*, 2011: Effects of climate on diameter growth of co-occurring *Fagus sylvatica* and *Abies alba* along an altitudinal gradient. *Trees 25*, 265–276.
Mendlik, G., 1967: A zalai bükkösök fatermési vizsgálata. *Az Erdő 16*, 76–82.
Menzel, L. and *Fabian, P.*, 1999: Growing season extended in Europe. *Nature 397*, 659.
Michelot, A., Bréda, N., Damesin, C., and *Dufrêne, E.*, 2012: Differing growth responses to climatic variations and soil water deficits of *Fagus sylvatica*, *Quercus petraea* and *Pinus sylvestris* in a temperate forest. *Forest Ecol. Manag. 265*, 161–171.
Muzika, R.M., Guyette, R.P., Zielonka, T., and *Liebhold, A.M.*, 2004: The influence of O_3, NO_2 and SO_2 on growth of *Picea abies* and *Fagus sylvatica* in the Carpathian Mountains. *Envir. Poll. 130*, 65–71.
Novák, J., Slodičák, M., Kacálek, D., and *Dušek, D.*, 2010: The effect of different stand density on diameter growth response in Scots pine stands in relation to climate situations. *J. Forest Sci. 56*, 461–473.
Pedersen B.S., 1998: The role of stress in the mortality of Midwestern oaks as indicated by growth prior to death. *Ecology 79*, 79–93.
Peñuelas, J., Hunt, J.M., Ogaya R., and *Jump, A.S.*, 2008: Twentieth century changes of tree-ring $\delta^{13}C$ at the southern range-edge of *Fagus sylvatica*: increasing water-use efficiency does not avoid the growth decline induced by warming at low altitudes. *Global Change Biol. 14*, 1076–1088.
Petráš, R. and *Mecko, J.*, 2011: Effect of climatic factors on the dynamics of radial increments of *Norway spruce*, *European beech* and *sessile oak*. *J. Forest Sci. 57*, 293–302.
Pettitt A.N., 1979: A non-parametric approach to the change-point problem. *Appl. Statist. 28*, 126-135.
Pichler, P. and *Oberhuber, W.*, 2007: Radial growth response of coniferous forest trees in an inner Alpine environment to heat-wave in 2003. *Forest Ecol. Manag. 242*, 688–699.
Piovesan, G. Biondi, F., Filippo, A.D., Alessandrini, A., and *Magueri M.*, 2008: Drought-driven growth reduction in old beech (*Fagus sylvatica* L.) forests of the central Apennines, Italy. *Global Change Biol.14*, 1265–1281.
Pödör, Z., Edelényi, M., and *Jereb, L.*, 2014: Systematic Analysis of Time Series – CReMIT. *Infocommunicat. J. 6*, 16-22.
Pretzsch, H., 1992: Zunehmende Unstimmigkeit zwischen erwartetem und wirklichem Wachstum unserer Waldbestande. *Forstwiss. Cent. Bl. 111*, 336–382.
Prislan, P., Gričar, J., de Luis, M., Smith, K.T, and *Čufar, K.*, 2013: Phenological variation in xylem and phloem formation in *Fagus sylvatica* from two contrasting sites. *Agr. Forest Meteorol. 180*, 142–151.
Priwitzer, T., Kurjak, D., Kmeť, J., Sitková, Z., and *Leštianska, A.*, 2014: Photosynthetic response of European beech to atmospheric and soil drought. *Lesn. Cas. For. J. 60*, 31–37.
Scharnweber, T., Manthey, M., Criegee, C., Bauwe, A., Schroder, C, and *Wilmking, M.*, 2011: Drought matters – Declining precipitation influences growth of *Fagus sylvatica* L., *Quercus robur* L. in north-eastern Germany. *Forest Ecol. Manag. 262*, 947–961.
Schmitt, U., Möller, R., and *Eckstein, D.*, 2000: Seasonal wood formation dynamics of beech (*Fagus sylvatica* L.) and black locust (*Robinia pseudoacacia* L.) as determined by the "pinning" technique. *Angewandte Botanik 74*, 10–16.
Schulze, E.D., 1970: Der CO_2-Gaswechsel der Buche (*Fagus silvatica* L.) in Abhängigkeit von den Klimafaktoren im Freiland. *Flora 159*, 177–232. (In German)
Schulze, E.D., Fuchs, M.I, and *Fuchs, M.*, 1977: Spatial distribution of photosynthetic capacity and performance in a mountain spruce forest of Northern Germany I Biomass distribution and daily CO_2 uptake in different crown layers. *Oecologia (Berl.) 29*, 43–61.
Sneyers, R., 1992: On the use of statistical analysis for the objective determination of climate change. *Meteorol. Z. 1*, 247–256.
Somogyi, Z., 2008: Recent trends of tree growth in relation to climate change in Hungary. *Acta. Silv. Lign. Hung. 4*, 17–27.
Spiecker, H., Mielkainen, K., Köhl, M., and *Skovsgaard, J.P.* (Eds). 1996: Growth Trends in European Forests: Studies from 12 Countries. European Forest Institute Research Report Nr. 5. Springer-Verlag, Berlin, 372 pp.
Szabados, I., 2006: The effect of the precipitation on the tree ring width. *Carpath. J. Earth. Env. 1*, 39–44.

Szentimrey, T., Bihari, Z., and *Lakatos, M.,* 2010: Quality control procedures in MISH-MASH systems. European Conference on Applied Climatology (ECAC), 13–17 September 2010, Zürich, Switzerland.
Tegel, W., Seim, A., Hakelberg, D., Hoffmann, S., Panev, M., Westphal, T., and *Büntgen, U.,* 2014: A recent growth increase of European beech (*Fagus sylvatica* L.) at its Mediterranean distribution limit contradicts drought stress. *Eu. J. Forest Res. 133,* 61–71.
Werf, van der, G.W, Sass-Klaassen, U.G.W, and *Mohren, G.M.J.,* 2007: The impact of the 2003 summer drought on the intra-annual growth pattern of beech (*Fagus sylvatica* L.) and oak (*Quercus robur* L.) on a dry site in The Netherlands. *Dendrochronologia 25,* 103–112.
Zingg, A., 1996: Diameter and basal area increment in permanent growth and yield plots in Switzerland. In (Eds.: *Spiecker, H., Mielikäinen, K., Köhl, M., Skovsgaard, J.P.*). Growth trends in European forests. Springer, Berlin, Heidelberg, 239–265.

IDŐJÁRÁS
Quarterly Journal of the Hungarian Meteorological Service
Vol. 120, No. 2, April – June, 2016, pp. 163–181

A closure study on aerosol extinction in urban air in Hungary

Ágnes Molnár [1*], **Dénes Párkányi** [2], **Kornélia Imre** [1], **Vera Gácser** [3], and **Edit Czágler** [4]

[1]*MTA-PE Air Chemistry Research Group, Veszprém, P.O.Box 158, H-8201 Hungary*
[2]*Centre for Energy Research, Hungarian Academy of Sciences, Budapest 114, P.O. Box 49, H-1525 Hungary*
[3]*University of Pannonia, Veszprém, P.O.Box 158, H-8201 Hungary*
[4]*Hungarian Meteorological Service, Budapest P.O. Box 39, H-1186 Hungary*

[*]*Corresponding author E-mail: amolnar@almos.uni-pannon.hu*

(Manuscript received in final form November 13, 2015)

Abstract—In this study, we present our results from an investigation into the use of visibility data as a viable tool for the survey of long-term variations in air quality. We found that visibility data in general can be used to estimate atmospheric aerosol extinction coefficients, and that PM_{10} can be successfully estimated from aerosol chemical composition. Our results indicate that PM_{10} concentrations provide a good basis for the reconstruction of aerosol extinction coefficients. It was also shown that both derived (from visibility) and reconstructed aerosol extinction coefficients were in good accordance with each other, mainly in the case of dry aerosols. Ambient values can be determined if an adequate hygroscopic growth rate for aerosol extinction is considered. We also found that a rather precise estimation of extinction coefficient can be reached if a modified version of the widely used IMPROVE formula is applied.

Key-words: visibility, reconstruction of extinction coefficient, PM_{10}, aerosol composition

1. Introduction

Visibility (VIS) is a good, simple indicator of air quality. It is well known that VIS is inversely related to atmospheric extinction. Light extinction is controlled by the scattering and absorption of air molecules and aerosol particles and is proportional to the number concentration of molecules and particles. The number of air molecules is a function of temperature and pressure; however, its variation does not result in a significant change in VIS. Drastic decreases or increases in visibility can be attributed to variations in aerosol concentration and changes in the physical and chemical properties of the particles.

According to the Koschmieder theory (*Koschmieder*, 1924), visibility is determined by

$$VIS = \frac{\ln 0.02}{\sigma_{ext}} = \frac{3.912}{\sigma_{ext}}. \tag{1}$$

In the formula, the constant of 3.912 represents the 2% contrast threshold of daylight visual detection of objects against the sky horizon, and σ_{ext} is the total extinction of solar radiation at 550 nm wavelength.

The scattering and absorption efficiencies of particles are functions of aerosol chemical composition and particle size. Sulfates, nitrates, and organics generally contribute to scattering, while elemental and organic carbon compounds are mainly responsible for absorption (e.g., *Malm et al.,* 1994; *Tao et al.,* 2012). Particles participate most in light extinction when their size is in the optically active size range (0.1–1.0 μm). On the other hand, the water vapor content of air (specifically relative humidity) has a significant influence on ambient light extinction as a consequence of water soluble and hygroscopic compounds in the aerosol. According to previous studies, hygroscopic growth can cause the scattering coefficient of dry particles to be doubled or greater as a result of increases in relative humidity (e.g., *Horvath,* 1992; *Seinfeld* and *Pandis,* 1998). Consequently, variations in aerosol concentration (through their size and chemical composition) control changes in dry extinction/visibility; however, in ambient air, water content can also play a major role in light attenuation and visibility impairment (e.g., *Jung et al.,* 2009; *Cheng et al.*, 2011).

High concentrations of air pollutants are a prevalent cause of air quality impairment in both cities and remote areas. Visibility can vary within a wide range, from a few meters to a few hundred kilometers (*Horvath,* 1995; *Singh* and *Dey*, 2012), and can easily become a critically important parameter in the everyday functioning of cities, because low visibility can obstruct surface and aerial traffic, and thereby, unfavorably impact businesses, public safety, and even tourism.

Despite the significant influence of water vapor, visibility (extinction) data provide an efficient and inexpensive tool for the study of long-term variations in air quality and may be utilized as a proxy for the concentration of aerosols and trace gases (*Singh* and *Dey*, 2012). For several decades, an empirical formula for calculating the light extinction coefficient as a function of chemical species in the $PM_{2.5}$ particulate matter has been used by the Interagency Monitoring of Protected Visual Environments (IMPROVE) network (*Hand et al.*, 2011; *Malm et al*, 2013). The IMPROVE program is a cooperative measurement effort among the U.S. Environmental Protection Agency (EPA), federal land management agencies, and state agencies (*Hand et al.*, 2011). The IMPROVE network has collected air quality data since 1988. The main goals of this program are to monitor real-time visibility and aerosol conditions in 156 mandatory Class I areas throughout the United States to identify aerosol species and their emission sources that are responsible for anthropogenic visibility impairment and to study and document long-term trends in air quality and visibility.

The empirical formula used by the IMPROVE network is based on the relationship between light extinction and aerosol chemical composition. The light extinction coefficients of an external mixture of aerosols can be estimated by assuming a linear combination of mass concentrations (M_j) and the corresponding extinction efficiencies (α_j) of different aerosol species (*Hand et al.*, 2011):

$$\sigma_{ext} = \sum \alpha_j \cdot M_j. \tag{2}$$

To account for the hygroscopic effect, extinction efficiencies are multiplied by a humidification factor that is computed by assuming a size distribution and a composition-dependent hygroscopic growth factor. The IMPROVE formula (see later Eq. (7)) is used to reconstruct σ_{ext} (corresponding to 550 nm wavelength) based on measurements of aerosol composition (ammonium sulfate, ammonium nitrate, particulate organic matter, light absorbing carbon, soil, and coarse mass) and a Rayleigh scattering term (*Hand* and *Malm*, 2007). The units of aerosol extinction coefficient and Rayleigh scattering are Mm^{-1}, mass concentrations are given in $\mu g\ m^{-3}$, and mass extinction (scattering and absorption) efficiencies have units of $m^2\ g^{-1}$.

The empirical IMPROVE formula has been applied extensively for different environments, from regional background to urban areas. An important issue is whether this algorithm, which is designed for background air, can be applied in cities. *Cabada et al.* (2004) found that by applying this formula during the Pittsburgh Air Quality Study, the scattering coefficient could be reproduced based on bulk $PM_{2.5}$ composition with relative success. Furthermore, in a number of studies, the extinction coefficient or visibility of megacities in China was reconstructed based on this formula. *Cao et al.* (2012) found that in

Xi'an, China, the model underestimated the measured extinction coefficient and that ammonium sulfate was the largest contributor. *Cheng et al.* (2011) in Jinan, *Pan et al.,* (2009) at a rural site near Beijing and *Tao et al.* (2012) in the Guangzhou urban area all concluded that the IMPROVE formula can provide realistic estimates of the real atmospheric extinction in cases where the relative humidity (RH) was less than 70% (*Tao et al.,* 2012). Under high RH, due to the hygroscopicity of the particles, the absorbed water plays a much greater role in limiting visibility. The study by *Singh* and *Day* (2012), conducted in the megacity of Delhi, India, resulted in similar conclusions. They found that below 80% RH, aerosols contribute ~90% to the observed visibility degradation, but that above 80% RH, the aerosol relative contribution decreases rapidly due to the strong impact of hygroscopicity. Visibility is most sensitive to water-soluble particles and soot in all seasons.

In this work, we studied and discussed the following issues:

a. How the extinction coefficient derived from visibility data can be estimated using the PM_{10} mass and chemical composition;

b. How PM_{10} can be reconstructed from the chemical composition of PM_{10};

c. How PM_{10} can be modelled from visibility observations. This information can result in a retrospective estimation of PM_{10} for periods when PM_{10} data are not available;

d. How the derived extinction coefficient (from VIS) corresponds to the reconstructed data;

e. Similar to other studies, we applied the IMPROVE formula in Budapest. We aimed to clarify how it can be applied in a Central European city and how the parameters in the formula should be changed to better reproduce the measured extinction coefficient;

f. How the hygroscopic effect should be considered to obtain a viable ambient extinction coefficient.

2. Experimental

2.1. Sampling

In this study, data from two sampling campaigns representing winter (February 2 – March 2, 2009) and summer (July 20 – August 20, 2009), aerosols are presented. In both cases, the sampling was conducted at the Marczell György Observatory of the Hungarian Meteorological Service. This site is located in the south-eastern part of Budapest, Hungary. Here, at a standard synoptic weather station, meteorological parameters, including visibility, temperature, and dew point temperature, are measured on an hourly basis. Visibility is also determined by visual observation. In the observatory, there is also an urban background air pollution monitoring site operated by the Hungarian Air Quality Network (www.levegominoseg.hu), which provides PM_{10} mass concentration. PM_{10} is monitored using the β-gauge method (*Chueinta* and *Hopke*, 2001).

In addition to these routine measurements, aerosol samples were collected daily to determine their chemical composition. A two-stage multi-jet impactor was applied at a sampling rate of 20 Lmin^{-1}. The PM_1 fraction was collected on quartz filters, and $PM_{1\text{-}10}$ was sampled on Al-foils. From these samples, the inorganic ion (sulfate, nitrate, chloride, ammonium, sodium, potassium, and magnesium) and total carbon contents were measured. Inorganic ion content was determined by ion chromatography (Dionex, 2120) with a detection limit below 10 ppb. The total carbon concentrations of the aerosol samples were measured using an Astro Model 2100 TOC analyzer. This method is based on NDIR absorption. The detection limit of these measurements was 2 μg C.

In the winter campaign, the scattering coefficient of aerosol at 550 nm was also monitored using an M903 integrating nephelometer calibrated with carbon dioxide. These data were used to reconstruct the scattering coefficient (see in Section 3.3). Unfortunately, in the summer campaign, this measurement was not available due to instrument failure. In both campaigns, the daily average absorption coefficients of the aerosol samples were determined indirectly. We supposed that the majority of absorbing components (soot) can be found in the PM_1 aerosol. Using the PM_1 quartz filters, the absorbance of the samples was determined (Eq. (3)). The light transmittance of blank and exposed filters was measured by PSAP (particle soot absorption photometer) at 550 nm. Their ratio gave transmittance (T), and absorbance (A) was derived by

$$A = \log\left(\frac{1}{T}\right). \tag{3}$$

Considering the air volume (V) and surface (S) of the filter, the average absorption coefficient was estimated:

$$\sigma_a = \frac{A \times S}{V}. \tag{4}$$

This method was checked with parallel measurements. During the summer campaign, a PSAP was operated to directly monitor the absorption coefficient. Using the same PSAP, the absorption coefficient was measured both directly and indirectly. From the direct measurements, the daily average absorption coefficients are calculated and compared to the absorption coefficients resulted from the indirect method. The results of this comparison are shown in *Fig. 1*. One can conclude that the absorption coefficients determined in both ways are linearly related, as the average difference between them was 2.16 ± 2.39 Mm^{-1}. This means that the absorption coefficient was slightly overestimated (less than 10%) when it was calculated using the transmittance of the aerosol filter.

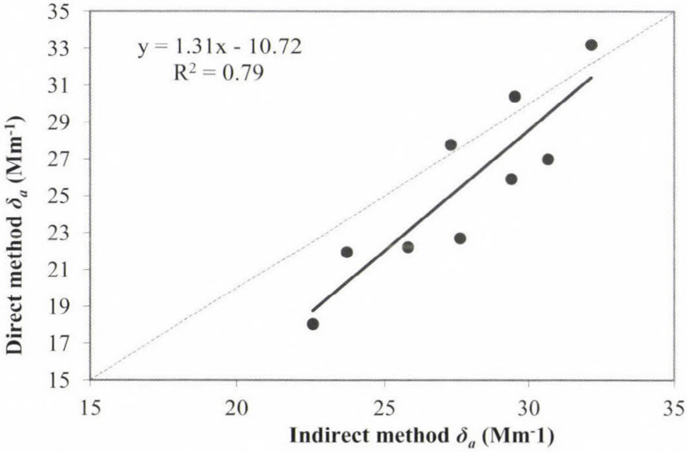

Fig. 1. Comparison of directly and indirectly measured absorption coefficients.

Finally, the organic and elemental (light absorbing) carbon contents of the samples were differentiated. We assumed that the total carbon content of the aerosol would be composed of organic and elemental fractions and that the inorganic carbon would be negligible (see in detail in Section 3.1). The elemental fraction was estimated from the absorption coefficient, considering a mass absorption coefficient of 10 m^2g^{-1}. Additionally, organic carbon was calculated as the difference between the total carbon (TC) and elemental carbon concentrations.

2.2. Extinction coefficient and the effect of hygroscopicity

Visibility (VIS) is generally determined by the light extinction of aerosol particles and air molecules. The extinction coefficient (σ_{ext}) can be estimated by means of Koschmieder theory (see Eq. (1)) which refers to 550 nm wavelength.

As previously mentioned, due to the hygroscopicity of the particles, relative humidity also plays an important role in determining visibility. The hygroscopic effect was excluded from the data sets by using the γ-approach as described by, e.g., *Zhou et al.* (2001):

$$\sigma_e = 10^c \times \left(1 - \frac{RH(\%)}{100}\right)^{-\gamma}, \tag{5}$$

$$f(RH) = \sigma_{RH}/\sigma_{40\%}. \tag{6}$$

We found that hygroscopic growth of the extinction coefficient (Eq. (6)) derived from VIS data was substantially different in winter and summer, as shown in *Table 1*. In winter, the aerosol was found to be much more hygroscopic than in summer, and the increase in the particle growth rate with rising RH was considerably greater than that in summer (e.g., at 80% RH, the growth rate was twice as much in winter than summer). As a result, considering the same PM_{10} concentrations, this difference yields a doubled extinction coefficient in winter compared with the summer values.

Table 1. Hygroscopic growth rate of extinction coefficients as a function of relative humidity

Relative humidity (%)	**Winter**	**Summer**	**Winter/Summer**
40	1.0	1.0	1.0
50	1.2	1.1	1.1
60	1.6	1.2	1.2
70	2.2	1.4	1.5
80	3.4	1.7	2.0
90	7.3	2.3	3.1

3. Results and discussion

3.1. Chemical composition and reconstruction of PM_{10}

The PM_{10} mass concentration was more variable during the winter campaign. In winter and summer, the average PM_{10} concentrations were 32 μgm^{-3} and 23 μgm^{-3}, respectively, with maximum concentrations of 107 μgm^{-3} and 54 μgm^{-3}. These average concentrations do not differ significantly from those obtained in three Austrian cities (*Gomišček et al.,* 2004), and Bologna, Italy (*Matta et al.,* 2003). In Vienna, Linz, Graz, and Bologna, the winter and summer PM_{10} concentrations varied in the ranges of 27–39 μgm^{-3} and 17–26 μgm^{-3}, respectively (*Gomišček et al.,* 2004; *Matta et al.,* 2003). In Lens, France (*Waked et al.,* 2014), the overall PM_{10} concentrations were lower, and in winter and summer, the values were 20 μgm^{-3} and 14 μgm^{-3}, respectively. Chemical analysis showed that in Budapest, carbonaceous compounds dominated the PM_{10} compositions, and the mass fractions of organic compounds in winter and summer were 35% and 27%, respectively. In Bologna and Lens, the mass fraction of organic carbon in PM_{10} was rather similar to that of Budapest (Bologna: winter 35% and summer 37% (*Matta et al.,* 2003); Lens: winter 34% and summer 27% (*Waked et al.,* 2014)). In contrast, in Budapest, elemental carbon represented 13% and 14% of PM_{10}, which was generally higher than the EC/BC data published for the other urban background sites around Europe. In

Barcelona, London North Kensington, Lugano (*Reche et al.,* 2011), Bologna (*Matta et al.,* 2003), and Lens (*Waked et al.,* 2014), the mass fractions of EC/BC in PM_{10} were in the range of 4%–10%.

In Budapest, the inorganic compounds were 16% (winter) and 18% (summer) of the total PM_{10} mass. These results are in accordance with earlier results obtained for PM_{10} in Budapest (*Maenhaut et al.,* 2005), but they are significantly lower than those found in other cities. It was found that in winter and summer in Bologna, inorganic species were 53% and 41% of PM_{10} (*Matta et al.,* 2003), while in Lens their contributions were 52% and 42% (*Waked et al.,* 2014).

During both campaigns in Budapest, all components analyzed from the filters were found dominantly in PM_1 as shown in *Table 2*. Among inorganic ions, nitrate was dominant in winter, whereas in summer, sulfate was found in highest concentrations, which is similar to results obtained in other cities. In Bologna, nitrate concentrations were almost 3 times higher than those of sulfate (*Matta et al.,* 2003), whereas in Lens, nitrate was twice as high as sulfate (*Waked et al.,* 2014). The lower nitrate concentrations in summer are the result of the temperature dependency of ammonium nitrate volatility, which was also indicated by lower nitrate fractions among the fine mode compared with the values obtained in winter. Yearly increases in sulfate concentrations during summer months are already known (e.g., *Hidy et al.,* 1978). Higher photochemical activities in summer result in higher rates of SO_2 conversion, which yield summertime maximums in sulfate concentrations. *Table 2* shows that the contributions of fine sulfate, ammonium, and total carbon to PM_{10} were significantly higher during summer than in winter. In contrast, the other components were less accumulated in PM_1 in summer than winter. Specifically, the fraction of fine nitrate concentration decreased from 80% (winter) to 70% (summer).

Table 2. PM_{10} aerosol composition and PM_1 mass fractions (%). The standard deviation is given in parentheses.

	Winter		**Summer**	
	Concentration (μgm^{-3})	**Fraction in PM_1 (%)**	**Concentration (μgm^{-3})**	**Fraction in PM_1 (%)**
chloride	2.4 (4.4)	85 (15)	1.1 (1.2)	77 (17)
nitrate	7.1 (3.6)	80 (12)	2.2 (0.9)	70 (8)
sulfate	4.2 (2.8)	80 (12)	6.2 (2.7)	93 (4)
sodium	2.0 (0.9)	95 (7)	1.4 (1.3)	65 (30)
ammonium	1.6 (1.6)	82 (17)	0.9 (0.5)	94 (13)
potassium	0.6 (0.3)	96 (5)	0.7 (0.5)	77 (18)
magnesium	0.1 (0.1)	85 (14)	0.2 (0.1)	71 (10)
calcium	1.3 (0.6)	81 (14)	1.7 (0.9)	69 (13)
total carbon	12.5 (6.6)	81 (4)	6.5 (1.2)	88 (7)

The total carbon concentration was twice as much in winter than in summer, and in both seasons more than 80% of the total carbon (TC) concentration was found in PM_1 (see *Table 1*). It is supposed that fine TC is composed primarily of organic and elemental carbon, and that the contribution of inorganic carbon (carbonate) can thus be neglected (e.g., *Karanasiou et al.,* 2011). Carbonate may be present in the coarse fraction; however, its presence has not been ubiquitously confirmed. According to a European survey (*Sillanpää et al.,* 2005), among six cities (Duisburg, Prague, Amsterdam, Helsinki, Barcelona, and Athens), carbonate was detected in the coarse mode in only the two Mediterranean cities. It should be mentioned that in Barcelona and Athens, the coarse fraction of the aerosol was greater than fine, whereas in Duisburg, Prague, and Amsterdam, similarly to Budapest, the fine mode dominated. Other results obtained for Chinese cities also showed the inorganic carbon (carbonate) content of the aerosol to be rather low (*Wang et al.,* 2010). Considering these results, we neglected the contribution of inorganic carbon in both the fine and coarse size ranges. Upon further evaluation, we supposed that the total carbon of PM_{10} was composed of organic and elemental (light absorbing) carbon and that this latter could be exclusively found in the fine fraction (PM_1).

The aerosol chemical composition was reconstructed on the basis of PM_{10}, and the inorganic and carbonaceous compounds were all considered. The chemical mass closure of the inorganic constituents was based on stoichiometry. In addition, based on the recommendations of *Stelson* and *Seinfeld* (1981), other alkaline (potassium) and alkaline earth metallic (calcium and magnesium) ions were included in the reconstruction of the PM_{10} mass. Excess nitrate was assumed to be organic nitrate (e.g., *Fry et al.,* 2014), and the organic and elemental carbon mass concentrations were estimated using conversion factors of 1.4 and 1, respectively. The average chemical composition of the reconstructed aerosol is shown in *Fig. 2*. It should be mentioned that in summer, the inorganic fraction of the aerosol was composed mainly of sulfate containing compounds. In contrast, during the winter season, nitrate compounds dominated the inorganic aerosol fraction, and sulfates (generally in the form of ammonium sulfate) gave a smaller contribution.

Finally, the reconstructed and the directly measured PM_{10} (by the β-gauge monitor described in Section 2.1) mass concentrations were compared. *Fig. 3* shows that these mass concentrations agreed relatively well in both sampling campaigns. In winter, PM_{10} is overestimated by 3.2 μgm^{-3}, whereas in summer, the directly measured PM_{10} is slightly lower than the reconstructed value.

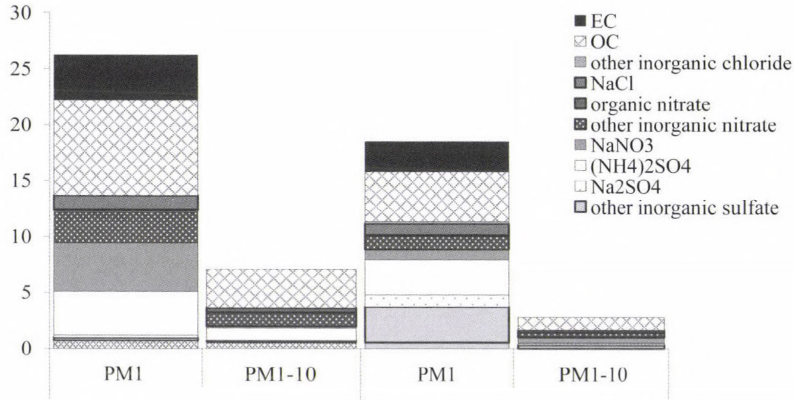

Fig. 2. Chemical mass closure of PM_1 and $PM_{1\text{-}10}$ in Budapest.

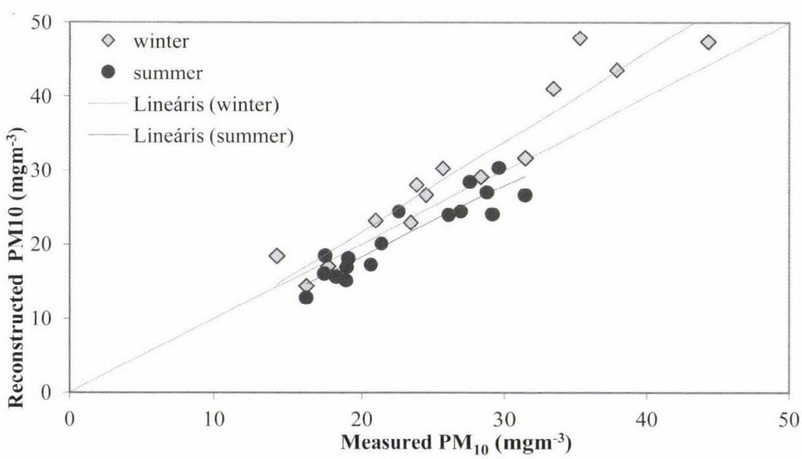

Fig. 3. Reconstructed vs. measured PM_{10} concentration.

3.2. *Visibility and extinction coefficient (VIS, $\sigma_{e,VIS}$)*

Temporal variations in PM_{10}, visibility, and RH are presented in *Figs. 4a* (winter) and *4b* (summer). The relationship among the parameters is clear. Low visibility coincides with high PM_{10} concentrations and/or high RH; conversely, high visibility occurs when PM_{10} and RH are low. As an example, in *Fig. 4a*, one can follow the development of a winter air pollution episode beginning on February 18 and finishing on February 25. Parallel to a general increase in PM_{10} (occasionally exceeding 100 μgm^{-3}), visibility decreased (average VIS = 7 km), which was disrupted by a change in RH. In summer, aerosol aging processes also influence variations in visibility. *Bäumer et al.* (2008) demonstrated that when the prevailing air mass undergoes an aging process, and as a result, a significant decrease in VIS is observed, an increase in PM_{10} can be detected.

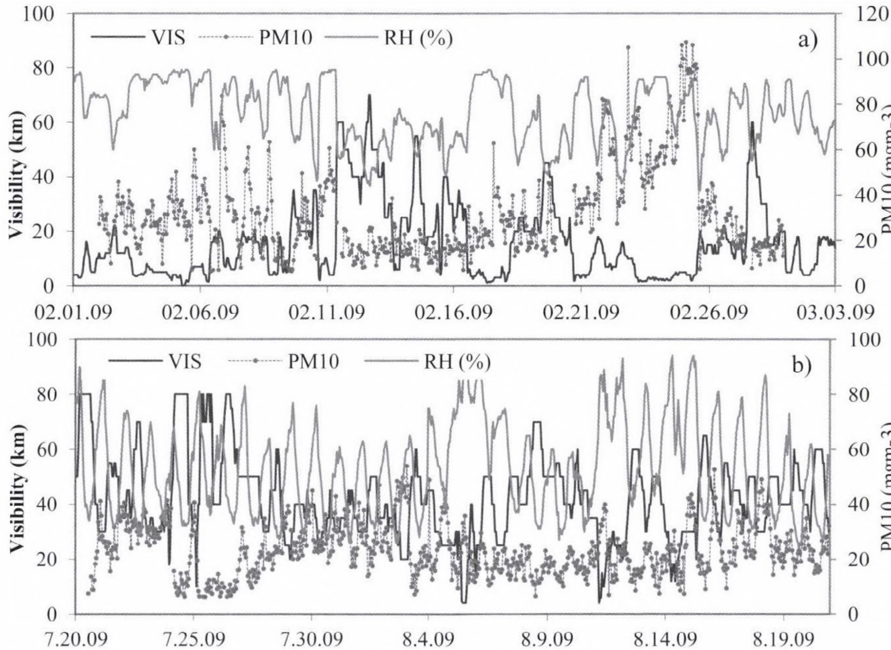

Fig. 4. Temporal variation in VIS, PM_{10} and RH during winter (a) and summer (b) campaigns.

In *Figs. 5a* and *5b*, temporal variations in the ambient and dry extinction coefficients are presented. The ambient extinction coefficients were derived from VIS (Eq. (1)), whereas the dry extinction data referring to 40% RH was obtained by means of the γ-approach (see Eqs. (5) and (6) in Section 2.2). In winter and summer, the average ambient extinction coefficients were 550 Mm^{-1} and 103 Mm^{-1}, and the dry average values were 126 Mm^{-1} and 87 Mm^{-1}, respectively. The difference between the ambient and dry extinction coefficients is attributed to the hygroscopic behavior of the aerosol. The effect of hygroscopicity on the aerosol extinction was particularly important in winter (see *Fig. 5a* and *Table 1*). The significant variation in hygroscopic growth rate is assumed to be the result of seasonal changes in PM_{10} chemical composition.

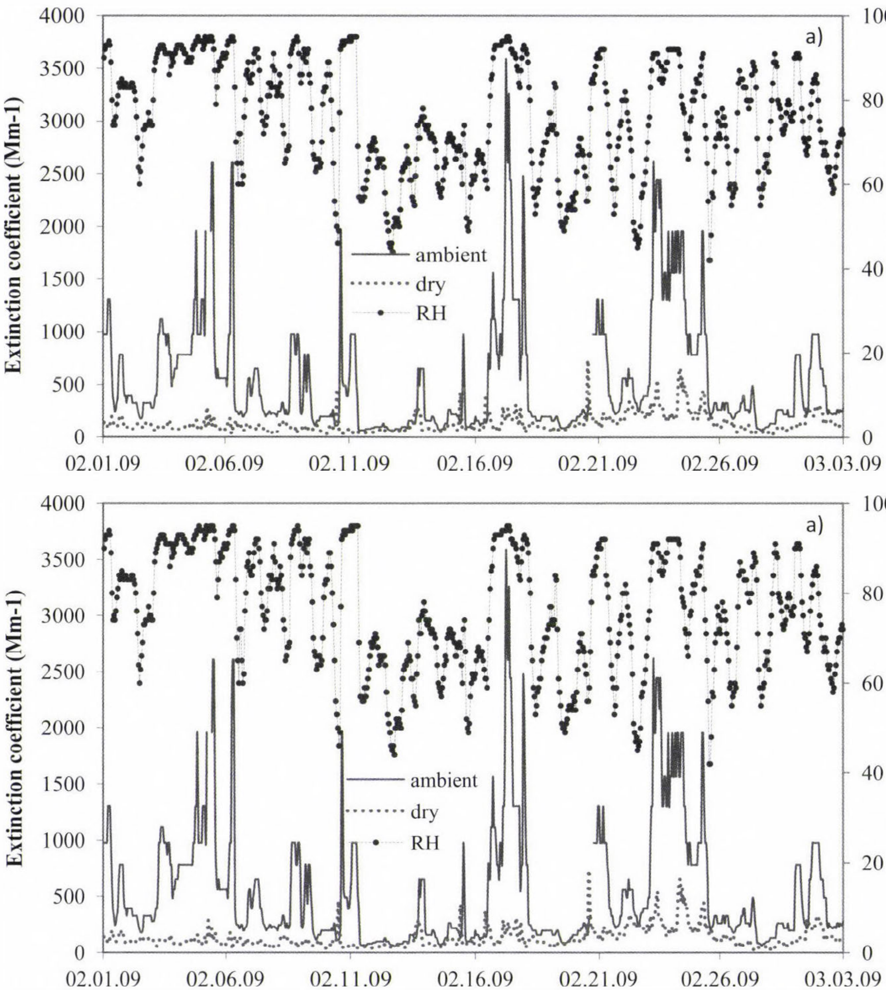

Fig. 5. Temporal variation in the ambient and dry extinction coefficients during winter (a) and summer (b) campaigns in 2009.

The relationship between PM_{10} and dry extinction coefficient is presented in *Fig. 6*. In both seasons, dry extinction coefficient varied similarly as a function of PM_{10}. Based on a linear regression analysis of the combined data sets, the dry mass extinction efficiency was 2.2 m^2g^{-1}, with a correlation coefficient of 0.52. This value is in accordance with the mass extinction efficiencies found in typical continental air. According to *Nemuc et al.* (2013), the mass extinction efficiencies of PM_{10} are typically in the range of 2.2 and 2.7 m^2g^{-1}, which was further confirmed by the value of 2.6 m^2g^{-1} that was obtained at the Hyytiälä Forestry Field Station in central Finland (*Virkkula et al.,* 2011).

Moreover, in urban air, the mass extinction coefficients of PM_{10} do not differ significantly from those obtained for background air. For reference, *Kim* (2015) and *Jung et al.* (2009) reported mass extinction efficiencies of 2.7 m^2g^{-1} and 2.5 m^2g^{-1} for Seoul, Korea, and Beijing, China, respectively.

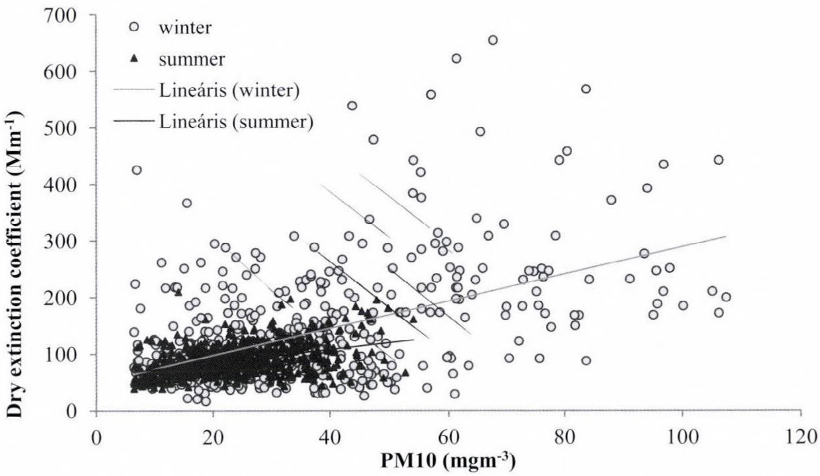

Fig. 6. PM_{10} vs. dry extinction coefficient during the winter and summer campaigns. The relationship between the parameters is statistically significant (at p=99.9%).

3.3. Reconstruction of extinction coefficient

The reconstruction of extinction coefficients is based on the well-known relationship between light extinction and aerosol composition. Sulfate, nitrate, and organic constituents have greater importance in scattering, whereas elemental carbon is more responsible for light absorption. Based on the concentration of different compounds and their mass extinction efficiencies, the extinction coefficient can be estimated (see Eq. (2)) (*Ouimette* and *Flagan*, 1982; *Mészáros*, 1999, *Seinfeld* and *Pandis*, 1998). This method has been well applied for a long time by the IMPROVE program (*DeBell et al.,* 2006) using the following equation:

$$\sigma_e \approx 3 \times f \times \left[(NH_4)_2SO_4\right] + 3 \times f \times \left[NaNO_3\right] + 4 \times \left[OC\right] + 10 \times \left[EC\right] + 1 \times \left[groundbased\right] + 0.6 \times \left[coarse\right] + 10 \times (Rayleigh). \quad (7)$$

To reconstruct the ambient extinction coefficient, the dry extinction coefficient was first estimated. In the estimation, we used aerosol chemical composition and optical data, which were independently monitored from visibility. In winter, aerosol scattering and absorption coefficients were measured along with visibility by integrating a nephelometer and PSAP (see details in Section 2.1). The dry aerosol scattering coefficient was measured by the nephelometer and calculated using the gamma approach (Eq. (5)) that is used when estimating visibility. To estimate dry aerosol scattering, the main aerosol components including ammonium sulfate, ammonium, sodium, and other nitrates as well as organic compounds were taken into account. Multiple regression analysis was applied to determine mass scattering efficiencies. In addition to scattering, aerosol absorption was considered, and EC was calculated from the absorption coefficients of the aerosol daily samples (see details in Section 2.1.). Finally, Rayleigh scattering, which is a function of air temperature and pressure, was determined. We found that the reconstructed dry extinction coefficient can be calculated with the following equation:

$$\sigma_{dry} \approx 2.3 \times \left[(NH_4)_2SO_4\right] + 1.7 \times \left[NaNO_3 + KNO_3 + Ca(NO_3)_2 + Mg(NO_3)_2\right] + 1.5 \times \left[OC\right] + 10 \times \left[EC\right] + 12\left(Rayleigh\right). \quad (8)$$

When comparing the mass scattering/absorption efficiencies used in the IMPROVE network to our results, some similarities and differences were noticed. Our equation refers to PM_{10}, whereas in the IMPROVE network, $PM_{2.5}$ and coarse particles are considered separately. The mass scattering efficiencies of ammonium sulfate and nitrate salts were rather similar ($\approx$ 2 m^2g^{-1}) to those identified by the IMPROVE network (3 m^2g^{-1}), although our obtained value was 30% smaller. In contrast to the inorganic species, the difference in mass scattering efficiencies for the organics is quite high (this study: 1.5 m^2g^{-1}; IMPROVE: 4 m^2g^{-1}). One possible explanation for the smaller values could be the difference between PM_{10} and $PM_{2.5}$, not differentiated in this study.

In addition, for the sake of simplicity, we modeled the dry extinction coefficient on the basis of only sulfate and nitrate ion as well as, organic and elemental carbon concentrations. In this case, the reconstruction equation was

$$\sigma_{dry,anions} = 4.3 \times \left[SO_4^{2-}\right] + 1.3 \times \left[NO_3^-\right] + 1.5 \times \left[OC\right] + 10 \times \left[EC\right] + 12\left(Rayleigh\right). \quad (9)$$

Comparing our models (Eqs. (8) and (9)) to the IMPROVE model (Eq. (7)), we concluded that all three models gave similar results for the reconstruction of the dry extinction coefficient. In *Table 3* the relationships between reconstructed and "observed" (calculated from visibility) extinction coefficients are shown. These relationships are characterized by linear regression equations and correlation coefficients. On the basis of these parameters, one can conclude that dry extinction data can be almost equally reconstructed by all three models. In other words the IMPROVE model – which is constructed for background aerosol – also provides sufficiently good estimation of dry extinction coefficient even in urban air, in Budapest. This is in agreement with other studies which indicated similar conclusions in megacities of Beijing and Delhi: in relatively dry atmosphere, this model provided realistic estimation of the ambient extinction coefficient (*Tao et al.*, 2012; *Sing* and *Day*, 2012). It has to note, that our models (mainly Eq. (9)) require less input data than the IMPROVE model; and for this reason they can be more easily applied for the available data sets.

Table 3. Relationship between reconstructed (three models) and "observed" extinction coefficients

	Linear regression equation	Correlation coefficient
Dry aerosol		
Eq. (8)	y = 0.65x+10.4	0.577
Eq. (9)	y = 0.64x+20.5	0.619
IMPROVE	y = 0.76x+11.0	0.562
Ambient aerosol		
Eq. (8)	y = 0.96x-27.9	0.926
Eq. (9)	y = 0.97x-16.7	0.935
IMPROVE	y = 0.24x+53.7	0.779

Note: x and y are the extinction coefficient from VIS and the reconstructed (by models) extinction coefficients, respectively.

To reconstruct the ambient extinction coefficient, the hygroscopic growth of the extinction coefficient obtained from visibility data was calculated as:

$$\sigma_{ambient} = f \cdot \sigma_{dry}. \tag{10}$$

Then, the inorganic (sulfate and nitrate salts (Eq.8) or ions (Eq.9)) and organic (OC) parts in our models were multiplied by these growth factors (*f*). The adequacy of the models for the reconstruction of ambient extinction coefficients is shown in *Table 3*. In each season, the adequate hygroscopic growth rates were considered. We can conclude that both approaches are suitable for the reconstruction of the extinction coefficient; however, they slightly underestimate the ambient extinction coefficient when compared to visibility data.

Figs. 7a and *7b* show the agreement of ambient extinction in more detail. We can conclude that the temporal variation in the ambient extinction coefficient is well represented by both models, but the actual extent of σ is generally underestimated by the model equations.

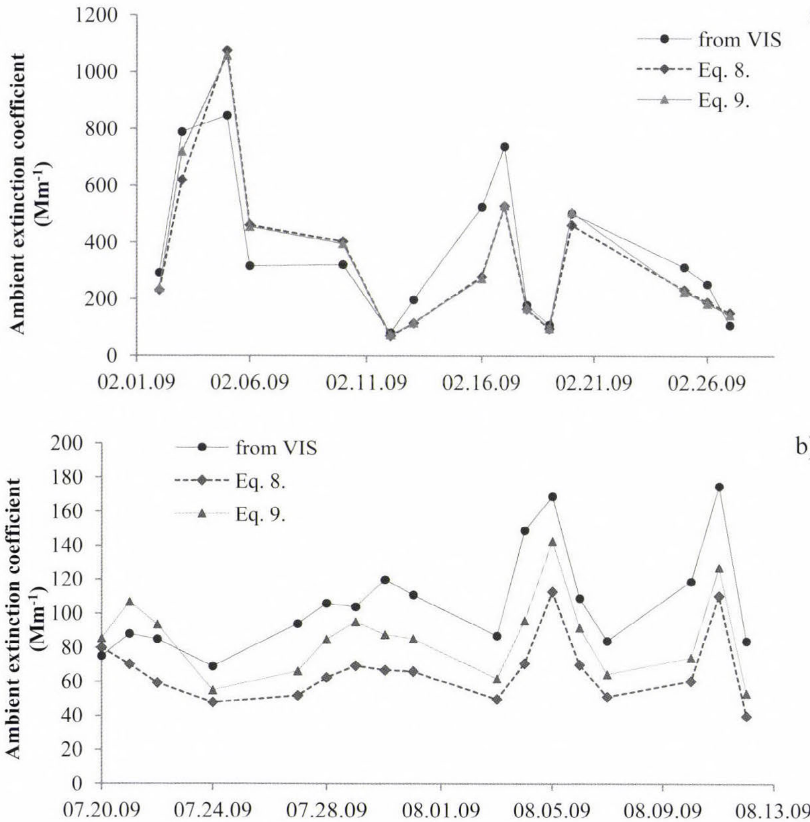

Fig. 7. Temporal variation in the ambient extinction coefficients.

Finally, we compared the three model results obtained for ambient air. We found that the results substantially differ if IMPROVE or our models are applied (see *Table 3*). The main reason for the discrepancy between modeled dry and ambient extinction coefficients can arise from the different consideration of aerosol hygroscopicity. In the case of IMPROVE, model hygroscopic growth is supposed only for ammonium sulfate and sodium nitrate content, while in our models the hygroscopicity of organic species is also involved. It supported by the well-known fact that an important part of organic compounds is hydrophilic, even water soluble. As a result, our models provide more realistic estimation of the ambient extinction coefficient compared to the IMPROVE model. This draws the attention to the significance of aerosol hygrosopicity, concerning both the inorganic and organic contents of the particles. The application of proper hygroscopic growth rate (which is a function of the chemical composition; and has significant seasonality) plays very important role in the reconstruction of ambient extinction coefficient.

4. Conclusions

Based on our results, we can conclude that visibility (extinction) data provide an efficient and inexpensive tool for the survey of long-term variations in air quality and may be utilized as a proxy for PM_{10} concentration. We have found that visibility data can generally be used to estimate atmospheric aerosol extinction coefficients, even in a retrospective manner. The closure experiment has shown that PM_{10} can be successfully estimated by chemical composition and that the PM_{10} concentration can be estimated from visibility/extinction coefficient data (using the Koschmieder theory). Our results indicate that the PM_{10} concentration (measured or modeled from the chemical composition) provides a good basis for the reconstruction of aerosol extinction coefficients. It is also shown that the derived (from VIS) and reconstructed (from PM_{10} or the aerosol chemical composition) aerosol extinction coefficients are in good accordance with each other, mainly in the case of dry aerosols. Ambient values can be estimated if the adequate hygroscopic growth rate for the aerosol extinction is considered. We have also found that a rather precise estimation of extinction coefficient can be reached if a modified version of the widely used IMPROVE formula is applied.

Acknowledgements: Authors are grateful for the support of Hungarian Scientific Research Fund (OTKA), project number K 113059.

References

Bäumer, D., Vogel, B., Versick, S., Rinke, R., Möhler, O., and *Schnaiter, M.,* 2008: Relationship of visibility, aerosol optical thickness and aerosol size distribution in an ageing air mass over South-West Germany. *Atmos. Environ. 42*, 989–998.

Cabada, J.C., Khlystov, A., Wittig, A.E., Pilinis, C. and *Pandis, S.N.,* 2004: Light scattering by fine particles during the Pittsburgh Air Quality Study: Measurements and modeling. *J. Geophys. Res. 109*, D16S03.

Cao, J.-J. Wang, Q.-Y, Chow, J.C., Watson, J.G., Tie, X.-X., Shen, Z.-X., Wang, P., and *An, Z.-S.,* 2012: Impacts of aerosol compositions on visibility impairment in Xi'an, China. *Atmos. Environ. 59*, 559–566.

Cheng, S.-H., Yang, L.-X., Zhou, X.-H., Xue, L.-K., Gao, X.-M., Zhou, Y. and Wang, W.-X., 2011: Size-fractionated water-soluble ions, situ pH and water content in aerosol on hazy days and the influences on visibility impairment in Jinan, China. *Atmos. Environ. 45,* 4631–4640

Chueinta, W. and *Hopke, P. K.,* 2001: Beta gauge for aerosol mass measurement. *Aerosol Sci. Technol. 35*, 840–843.

DeBell, L.J., Gebhart, K.A., Hand, J.L., Malm, W.C., Pitchford, M.L., Schichtel, B.A, and *White, W.H.,* 2006: IMPROVE (Interagency Monitoring of Protected Visual Environments): Spatial and Seasonal Patterns and Temporal Variability of Haze and its Constituents in the United States. Report IV CIRA Report ISSN: 0737-5352-74, Colorado State Univ., Fort Collins.

Fry, J.L., Draper, D.C., Barsanti, K.C., Smith, J.N., Ortega, J., Winkler, P.M., Lawler, M.J., Brown, S.S., Edwards, P.M., Cohen, R.C., and *Lee, L.,* 2014: Secondary organic aerosol formation and organic nitrate yield from NO_3 oxidation of biogenic hydrocarbons. *Environ. Sci. Technol. 48*, 11944–11953.

Gomišček, B., Hauck, H., Stopper, S., and *Preining, O.,* 2004: Spatial and temporal variations of PM1, PM2.5, PM10 and particle number concentration during the AUPHEP—project. *Atmos. Environ. 38,* 3917–3934

Hand, J. L., Malm, W. C., 2007: Review of aerosol mass scattering efficiencies from groundbased measurements since 1990, *J. Geophys. Res.-Atmospheres, 112,* (D18).

Hand, J.L., Copeland, S.A., Day, D.E., Dillner, A. M., Indresand, H., Malm, W.C., McDade, C.E., Moore, C.T.Jr., Pitchford, M., L., Schichtel, B.A., and *Watson, J.G.,* 2011: Spatial and Seasonal Patterns and Temporal Variability of Haze and its Constituents in the United States. Report V: June 2011. IMPROVE report, Cooperative Institute for Research in the Atmosphere, Colorado State University, Fort Collins, USA.

Hidy, G.M., Mueller, P.K., and *Tong, E.Y.,* 1978: Spatial and temporal distributions of airbone sulfate in parts of the United States, *Atmos. Environ. 12,* 735.

Horvath, H., 1992: Effect on visibility, weather and climate. In (Eds. *Radojevicc M.* and *Harrison R.M.*) Atmospheric Acidity: Sources, Consequences and abatement Elsevier Applied Science, London, 435-466.

Horvath, H., 1995: Estimation of the average visibility in central Europe, *Atmos. Environ., 29,* 241–246.

Jung, J., Lee, H., Kim, Y.J., Liu, X., Zhang, Y., Hu, M. and *Sugimoto, N.,* 2009: Optical Properties of Atmospheric Aerosols Obtained by in Situ and Remote Measurements during 2006 Campaign of Air Quality Research in Beijing (CAREBeijing-2006). *J. Geophys. Res. 114.*

Karanasiou, A., Diapouli, E., Cavalli, F., Eleftheriadis, K., Viana, M., Alastuey, A., Querol, X., Reche, C., 2011: On the quantification of atmospheric carbonate carbon by thermal/optical analysis protocols. *Atmos. Meas. Tech., 4,* 2409–2419.

Kim, K.W., 2015: Optical Properties of Size-Resolved Aerosol Chemistry and Visibility Variation Observed in the Urban Site of Seoul, Korea. *Aerosol Air Qual. Res. 15,* 271–283.

Koschmieder, H., 1924: Theorie der horizontalen sichtweite, Beitr. *Phys. frei. Atmos., 12,* 171–181.

Maenhaut, W., Raes, N., Chi, X., Cafmeyer, J., Wang, W., and *Salma, I., 2005:* Chemical composition and mass closure for fine and coarse aerosols at a kerbside in Budapest, Hungary, in spring 2002, *X Ray Spectrom., 34,* 290–296.

*Malm, W.C., Sisler, J. F., Huffman, D., Eldred, R. A.,*and *Cahill, T. A.,* 1994: Spatial and seasonal trends in particle concentration and optical extinction in the United States, *J Geophys Res. 99,* 1347–1370.

Malm, W.C., Schichtel, B.A., Barna, M.G., Gebhart, K.A., Rodriguez, M.A., Collett Jr., J.L., Carrico, C.M., Benedict, K.B., Prenni, A.J., and *Kreidenweis, S.M.,* 2013: Aerosol species concentrations and source apportionment of ammonia at Rocky Mountain National Park, *J. Air Waste Mgmt. Assn. 63,* 1245-1263.

Matta, E., Facchini, M.C., Decesari, S., Mircea, M., Cavalli, F., Fuzzi, S., Putaud, J.-P. and *Dell'Acqua, A.,* 2003: Mass closure on the chemical species in size-segregated atmospheric aerosol collected in an urban area of the Po Valley, Italy. *Atmos. Chem. Phys., 3,* 623–637.

Mészáros, E., 1999: Fundamentals of Atmospheric Aerosol Chemistry. Akadémiai Kiadó, Budapest.

Nemuc, A., Vasilescu, J., Talianu, C., Belegante, L., and *Nicolae, D.,* 2013: Assessment of aerosol's mass concentrations from measured linear particle depolarization ratio (vertically resolved) and simulations. *Atmos. Meas. Tech., 6,* 3243–3255.

Ouimette, J.R., and *Flagan R.C.,* 1982: The extinction coefficient of multicomponent aerosols. *Atmos. Environ. 16,* 2405–2419.

Pan, X.L., Yan, P., Tang, J., Ma, J.Z., Wang, Z.F., Gbaguidi, A., and *Sun, Y.L.,* 2009: Observational study of influence of aerosol hygroscopic growth on scattering coefficient over rural area near Beijing mega-city. *Atmos. Chem. Phys. 9,* 7519–7530.

Reche, C., Querol, X., Alastuey, A., Viana, M., Pey, J., Moreno, T., Rodríguez, S., Gonzalez, Y., Fernández-Camacho, R., de la Rosa, J., Dall'Osto, M., Prevôt, A.S.H., Hueglin, C., Harrison, R.M., and *Quincey, P.,* 2011: New considerations for PM, Black Carbon and particle number concentration for air quality monitoring across different European cities, *Atmos. Chem. Phys., 11,* 6207– 6227.

Seinfeld, J.H. and *Pandis, S.N.,* 1998: Atmospheric Chemistry and Physics. John Wiley & Sons.

Sillanpää, M., Frey, A., Hillamo, R., Pennanen, A.S. and *Salonen, R.O.*, 2005: Organic, elemental and inorganic carbon in particulate matter of six urban environments in Europe. *Atmos. Chem. Phys., 5,* 2869–2879.

Singh, A. and Dey, S., 2012: Influence of aerosol composition on visibility in megacity Delhi. *Atmos. Environ. 62,* 367–373.

Stelson, A.W. and *Seinfeld, J.H.*, 1981: Chemical mass accounting of urban aerosol. *Environ. Sci. Technol. 15,* 671–679.

Tao, J., Cao, J.-J., Zhang, R.-J, Zhu, L. H., Zhang T., Shi S., and *Chan, C.-Y.*, 2012: Reconstructed light extinction coefficients using chemical compositions of PM2.5 in winter in urban Guangzhou, China. *Adv. Atmos. Sci., 29,* 359–368.

Zhou, J., Swietlicki, E. and Berg, O.H., 2001: Hygroscopic properties of aerosol particles over the central Arctic Ocean during summer. J Geophys Res. 32, 32111-32123.

Virkkula, A., Backman, J., Aalto, P.P., Hulkkonen, M., Riuttanen, L., Nieminen, T., dal Maso, M., Sogacheva, L., de Leeuw, G., and Kulmala, M., 2011: Seasonal Cycle, Size Dependencies, and Source Analyses of Aerosol Optical Properties at the SMEAR II Measurement Station in Hyytiälä, Finland. *Atmos. Chem. Phys. 11,* 4445–4468.

Waked, A., Favez, O., Alleman, L. Y., Piot, C., Petit, J.-E., Delaunay, T., Verlinden, E., Golly, B., Besombes, J.-L., Jaffrezo, J.-L., and *Leoz-Garziandia, E.*, 2014: Source apportionment of PM_{10} in a north-western Europe regional urban background site (Lens, France) using positive matrix factorization and including primary biogenic emissions, *Atmos. Chem. Phys., 14,* 3325-3346.

Wang, G., Xie, M., Hu, S., Gao, S., Tachibana, E., and *Kawamura, K.*, 2010: Dicarboxylic acids, metals and isotopic compositions of C and N in atmospheric aerosols from inland China: implications for dust and coal burning emission and secondary aerosol formation, *Atmos. Chem. Phys.,* 10, 6087–6096.

IDŐJÁRÁS

Quarterly Journal of the Hungarian Meteorological Service
Vol. 120, No. 2, April – June, 2016, pp. 183–198

Analysis of annual and seasonal temperature trends using the Mann-Kendall test in Vojvodina, Serbia

Milivoj B. Gavrilov[1*], **Ivana Tošić**[2], **Slobodan B. Marković**[1], **Miroslava Unkašević**[2], and **Predrag Petrović**[3]

[1]*University of Novi Sad, Faculty of Sciences, Chair of Physical Geography, Trg Dositeja Obradovića 3, 21000 Novi Sad, Serbia*

[2]*University of Belgrade, Faculty of Physics, Institute of Meteorology, Dobračina 16, 11000 Belgrade, Serbia*

[3]*Republic Hydrometeorological Service of Serbia, Kneza Višeslava 66, 11000 Belgrade, Serbia*

[*]*Corresponding author E-mail*: gavrilov.milivoj@gmail.com

(Manuscript received in final form March 9, 2015)

Abstract—The annual and seasonal trends of mean, maximum, and minimum temperatures were analyzed on the territory of Vojvodina, north Serbia. We used observed, quality controlled, homogenized, and spatially averaged data from 9 meteorological stations during two periods: 1949–2013 and 1979–2013. Positive trends were found in 29 out of the 30 analyzed time series using a linear tendency (trend) equation, while negative trends were found in only 1 case. After the application of the classical Mann-Kendall (MK) test, statistically significant positive trends were confirmed in 15 series, while in remaining cases, statistically significant trends were not confirmed. After applying the modified MK test, positive trends were found in 26 series, and 4 cases were with no trend. We find that significant positive trends are dominated during the year, spring and summer; and they are most numerous in the time series of monthly mean temperatures. In accordance with the behavior of analyzed trends, the increase of temperatures is dominant in Vojvodina.

Key-words: annual and seasonal temperature trends, Mann-Kendall test, Vojvodina

1. Introduction

According to the *IPCC* (2007) report, the average global surface temperature of the world has increased by 0.74 °C in the past 100 years. This increase in the global temperature is not homogeneously distributed over the Earth's surface. It varies among regions and locations. The seasonal and annual Central European series of the mean temperature exhibited an increasing trend during the period 1951–1990 in most regions (*Brázdil et al.*, 1996). Using data recorded daily from 168 stations across Europe, *Klein Tank et al.* (2002) showed that trends in mean temperature have increased during the period from 1946 to 1999.

Analysis of the surface air temperature observed at stations located in all regions of the Mediterranean basin indicated a cooling during the period 1955–1975, and a strong warming during the 1980s and the first half of the 1990s (*Piervitali et al.*, 1997). Warming trends in the Mediterranean region (*Böhm et al.*, 2001; *Alcamo et al.*, 2007) occurred largely during the summer season, thereby intensifying summertime drought and irrigation problems. *Brunetti et al.* (2004) noted that the temperature trend in Italy was positive for each season in the south, and for autumn and winter in the north. *Feidas et al.* (2004) examined trends of annual and seasonal surface air temperature time series for 20 stations in Greece for the period 1955–2001. They found that Greece, in general, exhibits a cooling trend in winter, whereas in summer it exhibits an overall warming trend. The significant increase in average temperature over the Iberian Peninsula in recent decades was found by *Brunet et al.* (2007).

In Serbia, the mean summer temperature increased in Belgrade after 1975 (*Unkašević et al.*, 2005). Using the extreme temperatures at 15 meteorological stations during the period 1949–2009, an analysis of the extreme temperature indices suggested that the Serbian climate has become warmer over the last 61 years (*Unkašević* and *Tošić*, 2013). In addition to these results, the climate in Serbia was studied in other recent papers (*Đorđević*, 2008; *Unkašević* and *Tošić*, 2009a; *Gavrilov et al.*, 2010; *Pavlović Berdon*, 2012). Also, the weather and climate of Vojvodina were investigated in several papers (*Gavrilov et al.*, 2011; *Hrnjak et al.*, 2014; *Tošić et al.*, 2014; *Gavrilov et al.*, 2015).

In this study, we focus on analyzing the recent trends in the annual and seasonal temperatures over Vojvodina, Serbia. We find that the period from 1949 to 2013 contains more than two 30-year climatic cycles and, therefore, the results could be a good indicator for recent climate interpretations. Our paper is organized as following: Section 2 presents a description of the research region and data; methodology is described in detail in Section 3; the obtained results are presented in Section 4; and discussion and conclusions are given in Sections 5 and 6.

2. Data

2.1. Region

Vojvodina is a region in northern Serbia, located in the southeastern part of the Carpathian (Pannonian) Basin, encompassing the confluence area of the Danube, Sava, and Tisa rivers (*Fig. 1*). More than 60 % of this lowland area is covered by loess and loess-like sediments (*Marković et al.*, 2008). The most distinctive landforms of the Vojvodina region are two mountains: Fruška Gora Mountain, which is situated between the Danube and Sava rivers, and Vršac Mountain, which is located in the southeastern part of the region. In addition to these physical features of the region, there are sandy and lower areas-alluvial plains.

The climate of Vojvodina is moderate continental with cold winters and hot and humid summers, and with a large range of extreme temperatures featuring inconsistent amounts of rainfall over the course of months. The average annual air temperature was 11.1 °C and annual amount of precipitation (*Tošić et al.*, 2014) was 606 mm between 1949 and 2006.

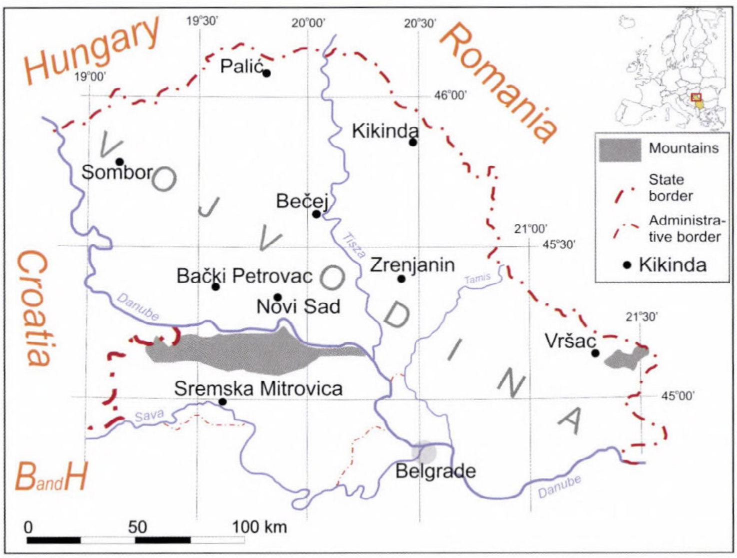

Fig. 1. The region of Vojvodina and position of meteorological stations.

2.2. *Data used*

In this work, an analysis of surface air temperature trends in Vojvodina from 9 meteorological stations was performed. The locations of stations are presented in *Fig. 1* and their geographical coordinates and altitudes are given in *Table 1* in accordance with the *Republic Hydrometeorological Service of Serbia* (2014). All stations have relatively similar altitudes, varying between 75 m and 102 m. Only stations that have almost continuous raw data sets of temperatures for the period between 1949 and 2013 were selected. The selected period is the longest of all observation periods in Vojvodina with standardized measurements and controlled data (*WMO*, 2012) on a large number of meteorological stations. Thus, it can be considered that these selected data and period are the most representative for the region of Vojvodina.

Table 1. List of meteorological stations, their geographical parameters and missing data for the period 1949–2013

Meteorological stations	**Geographical parameters**			**Missing data (%)**		
	Latitude (°)	**Longitude (°)**	**Altitude (m)**	T	T_x	T_n
Bački Petrovac	45.37	19.57	85	0.05	0.05	0.05
Bečej	45.63	20.03	75	0.54	1.57	1.54
Kikinda	45.85	20.47	81	0.0	0.0	0.0
Novi Sad	45.33	19.85	86	0.0	0.0	0.0
Palić	46.10	19.77	102	0.76	0.38	0.38
Sombor	45.77	19.15	87	1.54	1.54	1.54
Sremska Mitrovica	45.00	19.55	82	0.0	0.0	0.0
Vršac	45.15	21.32	83	0.0	0.0	0.0
Zrenjanin	45.37	20.42	80	0.0	0.0	0.0

Three used raw data sets of surface air temperatures are: monthly mean temperatures, T, monthly maximum temperatures, T_x, and monthly minimum temperatures, T_n. Monthly mean temperatures are obtained as the average of the daily mean temperatures, while monthly maximum/minimum temperatures are the maximum/minimum values of daily temperatures in corresponding month. As shown in *Table 1*, raw data were complete at five stations, while at four stations missing data were varied from 0.05 % to 1.57 %. We used the method/software MASH (*Szentimrey*, 1999) for data homogenization and filling in the missing raw data in accordance with the *CarpatClim project* (2014).

Of these three homogenized data sets, new data sets were created: average of stations over the territory of Vojvodina annual and seasonal mean, maximum, and minimum temperatures, T, T_x, T_n, respectively. The standard seasons definitions are used: winter (DJF), spring (MAM), summer (JJA), and autumn

(SON) during two periods: 1949–2013 ($P1$), and 1979–2013 ($P2$). We expect from the data processing in the first period to give the state of surface air temperature trends for longest continuous observation period (65 years) in Vojvodina. We also expect the second period to show the temperature trends during the last 35 years (5 years more than one 30-year climate standard), when global warming became the most intense (*Hardy*, 2006).

In the continuation of this research, the data base was formed by year (Y), four seasons (DJF, MAM, JJA, and SON), three types of temperatures (T, T_x, and T_n), and two periods ($P1$ and $P2$). The total number of series was 30 that were used for the trend calculation. Each of these 30 cases is marked with the acronym consisting of the abbreviation for the year/seasons, period, and type of temperature (*Table 2*).

Table 2. List of 30 time series to calculate surface air temperature trends in Vojvodina

	Year	**Winter**	**Spring**	**Summer**	**Autumn**
T	Y-T-$P1$	DJF-T-$P1$	MAM-T-$P1$	JJA-T-$P1$	SON-T-$P1$
	Y-T-$P2$	DJF-T-$P2$	MAM-T-$P2$	JJA-T-$P2$	SON-T-$P2$
T_x	Y-T_x-$P1$	DJF-T_x-$P1$	MAM-T_x-$P1$	JJA-T_x-$P1$	SON-T_x-$P1$
	Y-T_x-$P2$	DJF-T_x-$P2$	MAM-T_x-$P2$	JJA-T_x-$P2$	SON-T_x-$P2$
T_n	Y-T_n-$P1$	DJF-T_n-$P1$	MAM-T_n-$P1$	JJA-T_n-$P1$	SON-T_n-$P1$
	Y-T_n-$P2$	DJF-T_n-$P2$	MAM-T_n-$P2$	JJA-T_n-$P2$	SON-T_n-$P2$

3. Methodology

Three statistical approaches were used to analyze the temperature trends in 30 time series. First, the tendency (linear trend) equation (e.g., *Draper* and *Smith*, 1966) was calculated for each time series. Second, in all cases, the trend magnitude was calculated from the trend equation. Finally, in the third approach, all trends were assessed using the Mann-Kendall (MK) test, completely independent of the first approach (*Mann*, 1945; *Kendall*, 1975; *Gilbert*, 1987).

3.1. The trend equation

The first statistical approach was to calculate the trend equation of temperature using linear regression (e.g., *Draper and Smith*, 1966), as

$$y = ax + b, \tag{1}$$

where y is the temperature in °C, a is the slope, x is the time in years, and b is the temperature at the beginning of the period.

This approach has been long utilized in this type of research (e.g., *Wibig* and *Glowicki*, 2002; *Feidas et al.*, 2004), because it gives results which are simple to interpret; both graphically and analytically on the basis of the shape and parameters of the trend equation. For instance, the sign of the temperature trend depends on the value of the slope. In this kind of interpretation when the slope is greater than zero, less than zero, or equal to zero, the sign of the *trend is positive* (increase), *negative* (decrease), or *there is no trend* (no change), respectively.

3.2. The trend magnitude

In the second statistical approach, the trend magnitude was defined, as the difference in temperature between the beginning and the end of the period, which was obtained from the linear trend equation (*Gavrilov et al.*, 2015), or which is calculated as follows,

$$\Delta y = y(P_b) - y(P_e), \tag{2}$$

where Δy is the trend magnitude in °C. Values $y(P_b)$ and $y(P_e)$ represent temperatures from the trend equation in the beginning, P_b, and at the end period, P_e. Recall that two periods $P1$ and $P2$ have two beginning: $P_b = 1949, 1979$; and common end: $P_e = 2013$, with the exception of winter, where the periods were shorter for one year at the beginning and the end.

For a better understanding of the trend magnitude, we note the following. First, when Δy is greater than zero, less than zero, or equal to zero, the sign of the trend is *negative* (decrease), *positive* (increase), or *no trend* (no change), respectively. Second, when Δy is less than or equal to the standard error of the temperature measurement, certainly *there is no trend.*

The trend equation, trend magnitude, linear trend line, and annual course of temperature were computed and plotted for each time series using MATLAB scripts.

3.3. The Mann-Kendall test

In the third statistical approach, the MK test was applied to assess the significance of temperature trends. This test is widely used in the analysis of the climatological time series, for example: temperature and precipitation in earlier researches (e.g., *Gan*, 1995), as well as in recent researches (e.g., *Mavromatis* and *Stathis*, 2011; *Karmeshu*, 2012); extreme temperatures (e.g., *Serra et al.*, 2001; *Wibig* and *Glowicki*, 2002); hail (e.g., *Gavrilov et al.*, 2010, 2013); aridity (e.g., *Hrnjak, et al.*, 2014); evapotranspiration (e.g., *Tabari et al.*, 2011); and atmospheric deposition (e.g., *Drapela* and *Drapelova,* 2011); then in the hydrological time series (e.g., *Yue* and *Wang*, 2004); and other geophysical time series, such as: freeze and thaw soil (e.g., *Sinha* and *Cherkauer*, 2008); because the MK test is simple and robust, it can cope with missing values and values below the detection limit.

According to the MK test, two hypotheses were tested: the null hypothesis, H0, that *there is no trend* in the time series; and the alternative hypothesis, Ha, that *there is a significant trend* in the series, for a given α significance level (e.g., *Onoz* and *Bayazit*, 2003). Probability, p, in percent was calculated (e.g., *Karmeshu*, 2012; *Gavrilov et al.*, 2017) to determine the level of confidence in the hypothesis. If the computed value p is lower than the chosen significance level α (e.g., α=5 %), the H0 (*there is no trend*) should be rejected, and the Ha (*there is a significant trend*) should be accepted. In case p is greater than the significance level α, the H0 (*there is no trend*) cannot be rejected. We used XLSTAT software (http://www.xlstat.com/en/) for calculating the probability, p, and hypothesis testing.

It is considered that accepting the Ha indicates that a trend is statistically significant. On the other hand, acceptance of the H0 implies that there is no trend (no change), while often in practice, the trend equation and the trend magnitude indicates that there is a trend. Therefore, to reduce the doubt in analyzing the temperature trends with two independent statistical approaches, trend equation and applying the previous or classical interpretation of the MK test, the modified interpretation of the MK test (*Gavrilov, et al.*, 2015; *Gavrilov, et al.*, 2017) will be used. The difference between these two MK tests is in the number of levels of confidence. The classic MK test has only two levels of confidence: (i) *there is a significant positive/negative trend* and (ii) *there is no trend.* The modified MK test declares four levels of confidence, when p is:

(1) less or equal than 5 %, *there is a significant positive/negative trend*;

(2) greater than 5 %, and less or equal than 30 %, *there is a moderately positive/negative trend*;

(3) greater than 30 %, and less or equal than 50 %, *there is a slightly positive/negative trend*; and

(4) greater than 50 %, *there is no trend.*

As it can be seen, in cases (1) and (4) both interpretations of the MK tests have the same meaning. Differences occur in cases (2) and (3), where the classical MK test claims *there is no trend*, and the modified MK test allows trend with reduced levels of confidence. It is clear that modified interpretation is more subtle, and it enables obtaining diverse assessments.

4. Results

4.1. Parameters of trend

Figs. 2–4 show annual and seasonal mean, maximum, and minimum temperatures during the period 1949–2013 with two trend equations (Eq. (1): above (1949–2013) and below (1979–2013); and two trend lines: for longer and shorter period, respectively. The trend magnitude, Δy, and the probability of the confidence, p, for each time series over the territory of Vojvodina are shown in *Table 3*, respectively.

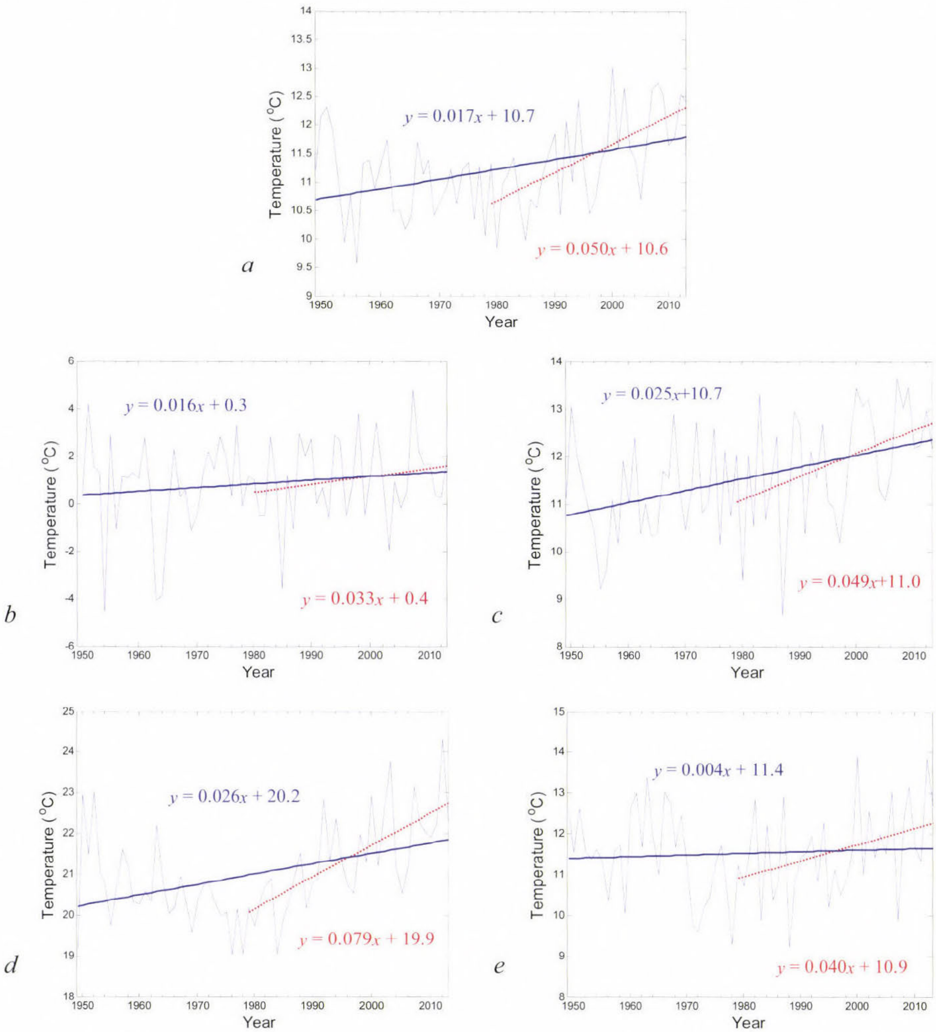

Fig. 2. Average annual and seasonal temperatures, trend equations, and trend lines for couples of time series: Y-*T*-*P*1 and Y-*T*-*P*2; DJF-*T*-*P*1 and DJF-*T*-*P*2; MAM-*T*-*P*1 and MAM-*T*-*P*2; JJA-*T*-*P*1 and JJA-*T*-*P*2; and SON-*T*-*P*1 and SON-*T*-*P*2 on panels a-e, respectively.

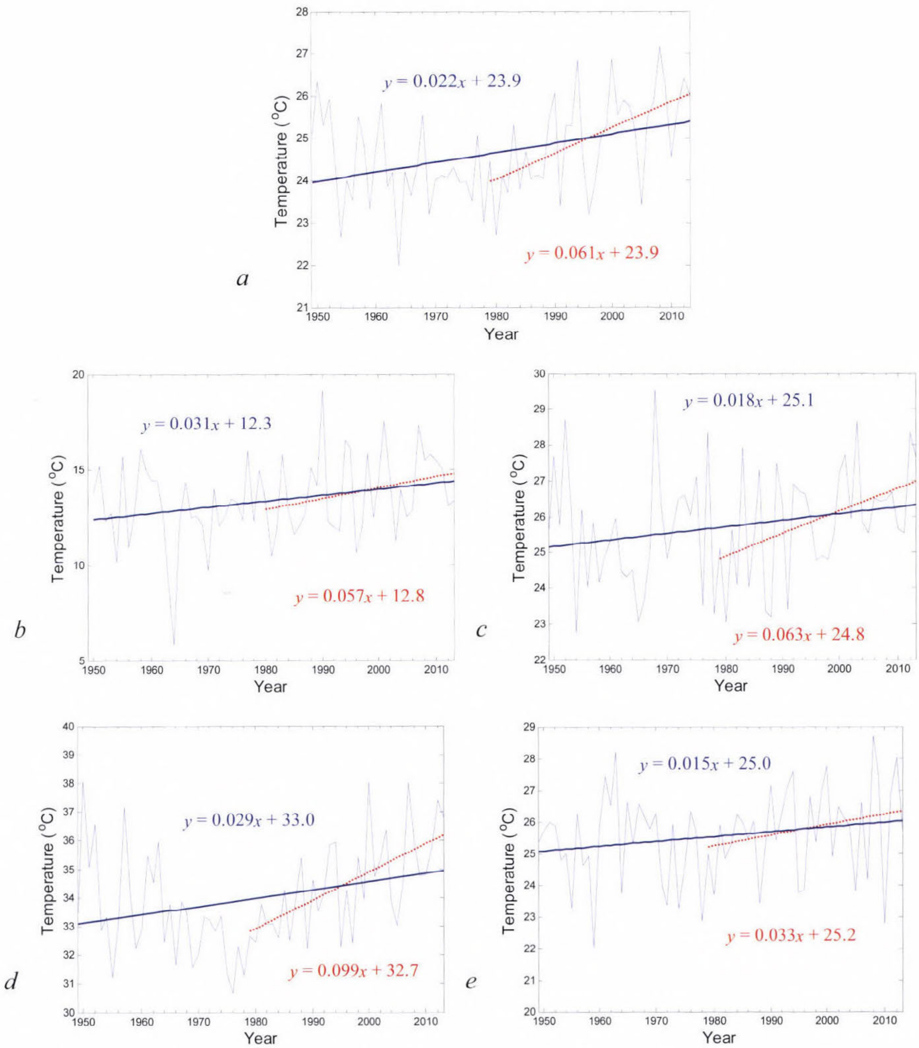

Fig. 3. As in *Fig. 2* but for T_x.

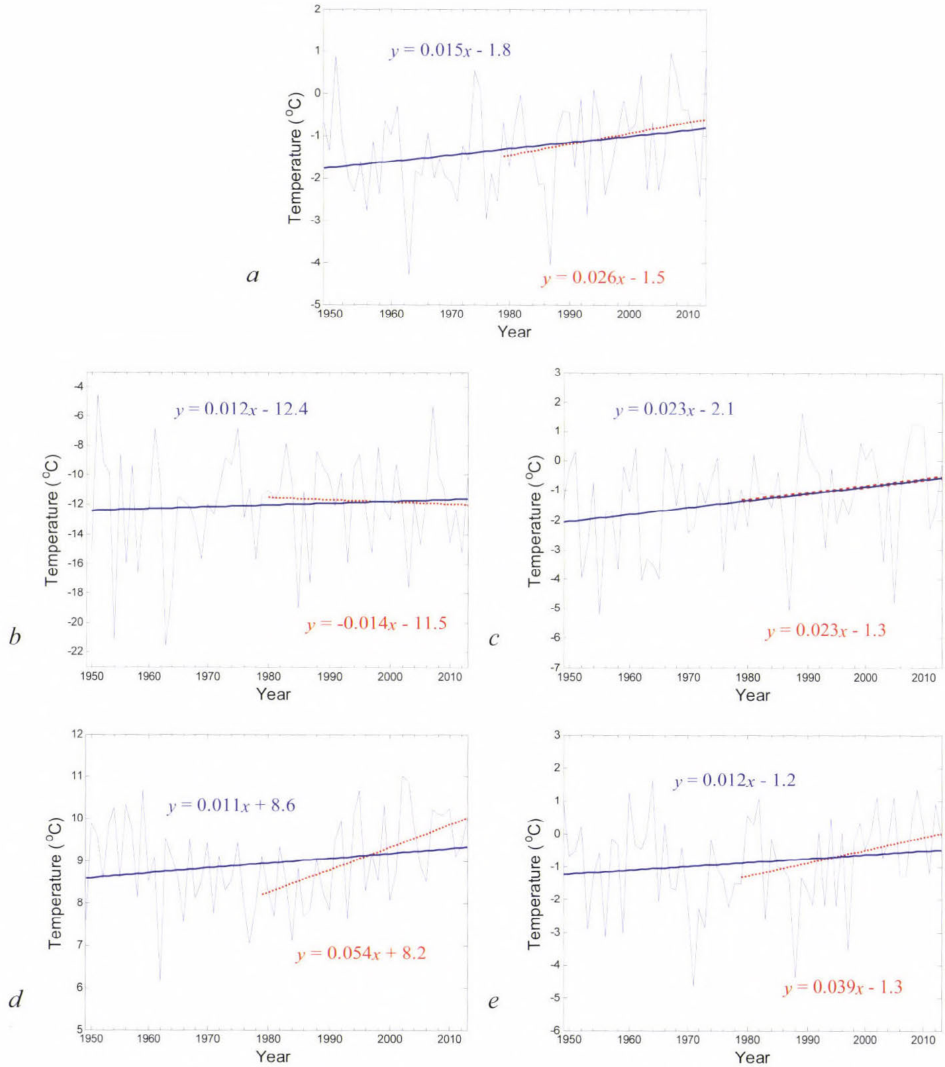

Fig. 4. As in *Fig. 2* but for T_n.

Table 3. The trend magnitude, Δy, and the probability of the confidences, p, for all time series

	T				T_x				T_n			
	$P1$		$P2$		$P1$		$P2$		$P1$		$P2$	
	Δy (°C)	p (%)	Δy (°C)	p (%)	Δy (°C)	p (%)	Δy (°C)	p (%)	Δy (°C)	p (%)	Δy (°C)	p (%)
Y	−1.1	0.13	−1.7	<0.01	−1.6	0.47	−2.1	0.04	−1.0	4.45	−0.9	24.65
DJF	−1.0	53.15	−1.1	36.11	−2.0	12.61	−1.9	11.00	−0.8	75.00	0.5	55.63
MAM	−1.6	0.07	−1.7	1.63	−1.2	5.86	−2.1	3.02	−1.5	3.24	−0.8	33.71
JJA	−1.6	0.10	−2.7	<0.01	−1.8	0.69	−3.4	0.01	−0.7	18.34	−1.8	0.27
SON	−0.2	60.64	−3.1	2.07	−1.0	8.84	−1.1	7.83	−0.7	12.92	−1.3	13.59

4.2. Evaluation of trends

In strictly formal terms, some trends can be observed in all cases (see *Figs. 2–4*). However, all trends do not have the same sign, magnitude, and probability. To obtain a final evaluation of the temperature trends in Vojvodina, all numerical parameters, the visual representation of trends and, most importantly, the results of both MK tests, were used.

Figs. 2–4 and *Table 3* show that the trend for 29 time series is *positive*, and it is *negative* only for the case DJF-T_n-$P2$. MK testing proves whether these statements are true.

As the computed probability values p for $P1$ cases: Y-T, MAM-T, JJA-T, Y-T_x, JJA-T_x, Y-T_n, and MAM-T_n; and for $P2$ cases: Y-T, MAM-T, JJA-T, SON-T, Y-T_x, MAM-T_x, JJA-T_x, and JJA-T_n, are lower than the significance level, α, the H0 should be rejected, and the Ha should be accepted for all of these cases. The risks to reject the H0 are lower than 4.45 %. The statement that *there is a significant trend* is correct in these cases with a probability greater than 95.55 % in both MK tests.

As values p for $P1$ seasons: DJF-T, SON-T, DJF-T_x, MAM-T_x, SON-T_x, DJF-T_n, JJA-T_n, and SON-T_n, and for $P2$ time series: DJF-T, DJF-T_x, SON-T_x, Y-T_n, DJF-T_n, MAM-T_n, and SON-T_n are greater than α, the H0 cannot be rejected. The risks to reject the H0 while it is true are between 5.86 % and 75.00 %. In accordance with the classical MK tests, all cases are declared as *there is no trend*; while the modified MK test declared the first, second, sixth, and thirteenth cases as *there is no trend*, the ninth and fourteenth cases as *there is a slightly positive trend*, and the remaining cases as *there is a moderately positive trend.*

In addition, *Figs. 2–4* show that in P2 the trend lines have greater slope in all time series for T and T_x, and in case T_n in 3 out of 5 time series. Only for the case DJF-T_n-$P1$ slope is greater than DJF-T_n-$P2$, while for the time series MAM-T_n-$P1$ and MAM-T_n-$P2$ slopes (a=0.023) are equal.

The main results of our analysis of temperature trends in Vojvodina are summarized in *Table 4*. The results are classified according to all time series, temperatures (T, T_x, T_n), and methods (the trend equation, the classical and the modified MK tests).

Table 4. The main results of the analysis of temperature trends in Vojvodina

Time series	The trend equation	The classical MK test	The modified MK test
$\boldsymbol{T}$			
Y-T-$P1$	*positive trend*	*positive significant trend*	*positive significant trend*
Y-T-$P2$	*positive trend*	*positive significant trend*	*positive significant trend*
DJF-T-$P1$	*positive trend*	*no trend*	*no trend*
DJF-T-$P2$	*positive trend*	*no trend*	*positive slightly trend*
MAM-T-$P1$	*positive trend*	*positive significant trend*	*positive significant trend*
MAM-T-$P2$	*positive trend*	*positive significant trend*	*positive significant trend*
JJA-T-$P1$	*positive trend*	*positive significant trend*	*positive significant trend*
JJA-T-$P2$	*positive trend*	*positive significant trend*	*positive significant trend*
SON-T-$P1$	*positive trend*	*no trend*	*no trend*
SON-T-$P2$	*positive trend*	*positive significant trend*	*positive significant trend*
$\boldsymbol{T_x}$			
Y-T_x-$P1$	*positive trend*	*positive significant trend*	*positive significant trend*
Y-T_x-$P2$	*positive trend*	*positive significant trend*	*positive significant trend*
DJF-T_x-$P1$	*positive trend*	*no trend*	*positive moderate trend*
DJF-T_x-$P2$	*positive trend*	*no trend*	*positive moderate trend*
MAM-T_x-$P1$	*positive trend*	*no trend*	*positive moderate trend*
MAM-T_x-$P2$	*positive trend*	*positive significant trend*	*positive significant trend*
JJA-T_x-$P1$	*positive trend*	*positive significant trend*	*positive significant trend*
JJA-T_x-$P2$	*positive trend*	*positive significant trend*	*positive significant trend*
SON-T_x-$P1$	*positive trend*	*no trend*	*positive moderate trend*
SON-T_x-$P2$	*positive trend*	*no trend*	*positive moderate trend*
$\boldsymbol{T_n}$			
Y-T_n-$P1$	*positive trend*	*positive significant trend*	*positive significant trend*
Y-T_n-$P2$	*positive trend*	*no trend*	*positive moderate trend*
DJF-T_n-$P1$	*positive trend*	*no trend*	*no trend*
DJF-T_n-$P2$	*negative trend*	*no trend*	*no trend*
MAM-T_n-$P1$	*positive trend*	*positive significant trend*	*positive significant trend*
MAM-T_n-$P2$	*positive trend*	*no trend*	*positive slight trend*
JJA-T_n-$P1$	*positive trend*	*no trend*	*positive moderate trend*
JJA-T_n-$P2$	*positive trend*	*positive significant trend*	*positive significant trend*
SON-T_n-$P1$	*positive trend*	*no trend*	*positive moderate trend*
SON-T_n-$P2$	*positive trend*	*no trend*	*positive moderate trend*

5. Discussion

It is difficult to find identical results in neighboring areas, but there are similarities. For example, greater increase of the absolute maximum temperature (0.16 °C/year) than the absolute minimum temperature (0.12 °C/year) obtained *Unkašević et al.* (2005) for Belgrade during the period 1975–2003. Similarly to our results, *Brázdil et al.* (1996) concluded that in ten countries in Central and Southeast Europe between 1951 and 1990, there had been an increase in both annual maximum and minimum temperatures. *Brunetti et al.* (2004) found that trends in the annual temperature series ranged from 0.4 °C/(100 years) for the north to 0.7 °C/(100 years) for the south of Italy. These conclusions are in agreement with the *IPCC* report (2007), in which the increase in the global temperature is not homogeneously distributed on the Earth surface.

In *Fig. 2a* we show three characteristic time intervals in the behavior of the annual mean temperature. The higher temperatures are at the beginning and the end of the $P1$ period, and the lower temperatures are in the middle of the period from 1970s until the mid 1980s. Our results are in accordance with the results of *Unkašević* and *Tošić* (2009b). Analyzing the temperature data from 1949 to 2007, they found that the slow decrease of summer temperatures until 1975 was followed by a temperature increase that lasted until 2007 in Belgrade (Serbia). Obtained temperature changes in Vojvodina are very similar to the behavior of global temperature during the same period (*Hardy*, 2006), where the increase of the temperature was started in the mid-1980s. It seems that there is a coincidence of regional temperature changes in Vojvodina and global temperature change.

6. Conclusions

An analysis of annual and seasonal trends of mean, maximum, and minimum surface air temperatures in Vojvodina for two periods: 1949–2013 and 1979–2013 was performed. Temperature trends in 30 time series were analyzed using (i) the trend equation, (ii) the trend magnitude calculated from the trend equation, and (iii) the MK test in the classical and modified declaration. The main conclusion can be summarized as follows:

(a) In accordance with the trend equations, positive trends were found in 29 out of 30 time series, and negative trend was found in only one case.

(b) Using the classical MK test, significant positive trends were found in 15 series; 8 in the shorter period, and 7 in the longer period; and no trend was found in 15 cases. The significant positive trends are dominated during the year, spring, and summer, where it was found in 14 out of 18 cases. From the three types of temperatures, T, T_x, and T_n, significant positive trends were found 7, 5, and 3 times, respectively.

(c) Based on the modified MK test, positive (significant, moderate, and slight) trends were confirmed in 26 (15, 9, and 2, respectively) series.

(d) The increase of the temperature was found in 29 time series in a wide range of values from 0.2 °C to 2.0 °C for the longer period and from 0.8 °C to 3.4 °C for the shorter period. The decrease of the temperature was found only for the minimum temperatures during the winter for the shorter period. The increase of temperatures was higher for the shorter period, than for the longer period.

As shown, the positive temperature trends and the increase of temperatures are dominant in Vojvodina. This behavior of the temperature resembles the warming in the Northern Hemisphere (e.g., *CRU*, 2003).

Acknowledgements: This study was supported by the Serbian Ministry of Science, Education and Technological Development, under Grants No. 176013 and 176020. The authors are grateful to Mr. Momčilo Gavrilov, who carefully read the manuscript. The authors sincerely appreciate the efforts of anonymous reviewer in improving this manuscript.

References

Alcamo, J., Moreno, J.M., Nováky, B., Bindi, M., Corobov, R., Devoy, R.J.N., Giannakopoulos, C., Martin, E., Olesen, J.E. and *Shvidenko, A.*, 2007: Europe. In (Eds.: *Parry, M.L., Canziani, O.F., Palutikof, J.P., van der Linden, P.J., Hanson, C.E.*), Climate Change 2007: Impacts, Adaptation and Vulnerability. Contribution of Working Group II to the Fourth Assessment Report of the Intergovernmental Panel on Climate Change. Cambridge University Press, Cambridge, UK, 541–580.

Böhm, R., Auer, I., Brunetti, M., Maugeri, M., Nanni, T. and *Schöner, W.*, 2001: Regional temperature variability in the European Alps: 1760-1998 from homogenized instrumental time series. *Int. J. Climatol. 21*, 1779–1801.

Brázdil, R., Budíková, M., Auer, I., Böhm, R., Cegnar, T., Faško, P., Lapin, M., Gajić-Čapka, M., Zaninović, K., Koleva, E., Niedźwiedź, T., Ustrnul, Z., Szalai, S. and *Weber, R.O.*, 1996: Trends of maximum and minimum daily temperatures in central and southeastern Europe. *Int. J. Climatol. 16*, 765–782.

Brunet, M., Jones, P.D., Sigro, J., Saladie, O., Aguilar, E., Moberg, A., Della-Marta, P.M., Lister, D., Walther, A. and *López, D.*, 2007: Temporal and spatial temperature variability and change over Spain during 1850-2005. *J. Geophys. Res.*: *Atmosph. 112*, 1984–2012.

Brunetti, M., Buffoni, L., Mangianti, F., Maugeri, M. and *Nanni, T.*, 2004: Temperature, precipitation and extreme events during the last century in Italy. *Glob. Planet. Change 40*, 141–149.

CarpatClim (Climate of the Carpathian Region) project, 2014: http://www.carpatclim-eu.org/pages/deliverables/ (accessed 29 December 2014).

CRU (Climate Research Unit), 2003: Global average temperature change 1856–2003. http://www.cru.uea.ac.uk/cru/data/temperature/ (accessed 21 July 2014).

Feidas, H., Makrogiannis, T. and *Bora-Senta, E.*, 2004: Trend analysis of air temperature time series in Greece and their relationship with circulation using surface and satellite data: 1955-2001. *Theor. Appl. Climatol. 79*, 185–208.

Drapela, K. and *Drapelova, I.*, 2011: Application of Mann-Kendall test and the Sen's slope estimates for trend detection in deposition data from Bílý Kříž (Beskydy Mts., the Czech Republic) 1997–2010. *Beskydy 4*, 133–146.

Draper, N.R. and *Smith, H.*, 1966: Applied Regression Analysis. Wiley, New York.

Đorđević, S.V., 2008: Temperature and precipitation trends in Belgrade and indicators of changing extremes for Serbia. *Geographica Pannonica 12*, 62–68.
Gan, T.Y., 1995: Trends in air temperature and precipitation for Canada and north-eastern USA. *Int. J. Climatol. 15*, 1115–1134.
Gavrilov, M.B., Lazić, L., Pešić, A., Milutinović, M., Marković, D., Stanković, A. and *Gavrilov, M.M.*, 2010: Influence of Hail Suppression on the Hail Trend in Serbia. *Phys. Geography 31*, 441–454.
Gavrilov, M.B., Lazić, L., Milutinović, A., and *Gavrilov, M.M.*, 2011: Influence of Hail Suppression on the Hail Trend in Vojvodina, Serbia. *Geographica Pannonica 15*, 36–41.
Gavrilov, M.B., Marković, S.B., Zorn, M., Komac, B., Lukić, T., Milošević, M. and *Janićević, S.*, 2013: Is hail suppression useful in Serbia? - General review and new results. *Acta Geographica Slovenica 53*, 165–179.
Gavrilov, M.B., Marković, S.B., Jarad, A. and *Korać, V.M.*, 2015: The analysis temperature trends in Vojvodina (Serbia) from 1949 to 2006. *THERMAL SCIENCE 19*, 339–350.
Gavrilov, M.B., Marković, S.B., Janc, N., Nikolić, M., Valjarević, A., *Zorn, M., Komac, B., Punišić,* M. and *Bačević*, N., 2017: The assessment of average annual temperature trends using the Mann-Kendall test in the territory of Kosovo. *Acta Geographica Slovenica* (in press).
Gilbert, R.O., 1987: Statistical Methods for Environmental Pollution Monitoring. Wiley, New York.
Hardy, J.T., 2006: Climate Change - Causes, Effects and Solutions. Wiley. Chichester.
Hrnjak, I., Lukić, T., Gavrilov, M.B., Marković, S.B., Unkašević, M. and *Tošić*, I., 2014: Aridity in Vojvodina, Serbia. *Theor. Appl. Climatol. 115*, 323–332.
IPCC, 2007: *Climate Change*. The physical science basis. In (Eds.: *Solomon, S., Qin, D., Manning, M., Chen, Z., Marquis, M., Averyt, K.B., Tignor, M., Miller, H.L.*), Contribution of Working Group I to the Fourth Assessment Report of the Intergovernmental Panel on Climate Change. Cambridge University Press, Cambridge and New York.
Karmeshu, N., 2012: Trend Detection in Annual Temperature & Precipitation using the Mann Kendall Test - A Case Study to Assess Climate Change on Select States in the Northeastern United States. Master's thesis, University of Pennsylvania.
Kendall, M.G., 1975: Rank correlation methods. Charles Griffin, London.
Klein Tank, A.M.G., Wijngaard, J.B., Können, G.P., Böhm, R., Demarée, G., Gocheva, A., Mileta, M., Pashiardis, S., Hejkrlik, L., Kern-Hansen, C., Heino, R., Bessemoulin, P., Müller-Westermeier, G., Tzanakou, M., Szalai, S., Pálsdóttir, T., Fitzgerald, D., Rubin, S., Capaldo, M., Maugeri, M., Leitass, A., Bukantis, A., Aberfeld, R., Van Engelen, A.F.V., Forland, E., Mietus, M., Coelho, F., Mares, C., Razuvaev, V., Nieplova, E., Cegnar, T., Antonio López, J., Dahlström, B., Moberg, A., Kirchhofer, W., Ceylan, A., Pachaliuk, O., Alexander, L.V. and *Petrovic, P.*, 2002: Daily dataset of 20th-century surface air temperature and precipitation series for the European Climate Assessment. *Int. J. Climatol. 22*, 1441–1453.
Mann, H.B., 1945: Nonparametric tests against trend. *Econometrica 13*, 245–259.
Marković, S.B., Bokhorst, M., Vandenberghe, J., Oches, E.A., Zöller, L., McCoy, W.D., Gaudenyi, T., Jovanović, M., Hambach, U. and *Machalett, B.*, 2008: Late Pleistocene loess-paleosol sequences in the Vojvodina region, North Serbia. *J. Quaternary Sci. 23*, 73–84.
Mavromatis, T. and *Stathis, D.*, 2011: Response of the Water Balance in Greece to Temperature and Precipitation Trends. *Theor. Appl. Climatol. 104*, 13–24.
Onoz, B. and *Bayazit, M.*, 2003: The Power of Statistical Tests for Trend Detection. *Turkish J. Engineer. Environ. Sci. 27*, 247–251.
Pavlović Berdon, N., 2012: The Impact of Arctic and North Atlantic Oscillation on Temperature and Precipitation Anomalies in Serbia. *Geographica Pannonica 16*, 44–55.
Piervitali, E., Colasino, M. and *Conte, M.*, 1997: Signals of climatic change in the Central-Western Mediterranean basin. *Theor. Appl. Climatol. 58,* 211–219.
Republic Hydrometeorological Service of Serbia (*RHSS*), 2014: Website of the RHSS, http://www.hidmet.gov.rs/ (accessed 21 July 2014).
Serra, C., Burgueño, A. and *Lana, X.*, 2001: Analysis of maximum and minimum daily temperatures recorded at Fabra Observatory (Barcelona, NE Spain) in the period 1917–1998. *Int. J. Climatol. 21*, 617–636.
Sinha, T. and *Cherkauer, K.A.*, 2008: Time Series Analysis of Soil Freeze and Thaw Processes in Indiana. *J. Hydrometeorol. 9*, 936–950.

Szentimrey, T., 1999: Multiple Analysis of Series for Homogenization (MASH). Proceedings of the Second Seminar for Homogenization of Surface Climatological Data, Budapest, Hungary; WMO, WCDMP-No. 41, 27–46.

Tabari, H., *Marofi, S.*, *Aeini, A.*, *Talaee, P.H.* and *Mohammadi, K.*, 2011: Trend Analysis of Reference Evapotranspiration in the Western half of Iran. *Agricult. Forest Meteorol. 151*, 128–136.

Tošić, I., *Hrnjak, I.*, *Gavrilov, M.B.*, *Unkašević, M.*, *Marković, S.B.* and *Lukić, T.*, 2014: Annual and seasonal variability of precipitation in Vojvodina, Serbia. *Theor. Appl. Climatol. 117*, 331–341.

Unkašević, M., *Vujović, D.* and *Tošić, I.*, 2005: Trends in extreme summer temperatures at Belgrade. *Theor. Appl. Climatol. 82*, 99–205.

Unkašević, M. and *Tošić, I.*, 2009a: Changes in the extreme daily winter and summer temperatures at Belgrade. *Theor. Appl. Climatol. 89*, 239–244.

Unkašević, M. and *Tošić, I.*, 2009b: An analysis of heat waves in Serbia. *Glob. Planetary Change 65*, 17–26.

Unkašević, M. and *Tošić, I.*, 2013: Trends in temperature indices over Serbia: relationships to large-scale circulation patterns. *Int. J. Climatol. 33*, 3152–3161.

Wibig, J. and *Glowicki, B.*, 2002: Trends of minimum and maximum temperature in Poland. *Climate Res. 20*, 123–133.

WMO (*World Meteorological Organization*), 2012: Technical Regulations, Volume I: General Meteorological Standards and Recommended Practices. Documents No. 2. Geneva, World Meteorological Organization, Switzerland.

Yue, S. and *Wang, C.*, 2004: The Mann-Kendall Test Modified by Effective Sample Size to Detect Trend in Serially Correlated Hydrological Series. *Water Resour. Manage. 18*, 201–218.

IDŐJÁRÁS

Quarterly Journal of the Hungarian Meteorological Service
Vol. 120, No. 2, April – June, 2016, pp. 199–229

Wind tunnel and computational fluid dynamics study of wind conditions in an urban square

Márton Balczó* and **András Tomor**

Theodore von Kármán Wind Tunnel Laboratory
Department of Fluid Mechanics, Faculty of Mechanical Engineering,
Budapest University of Technology and Economics
Bertalan L. u. 4-6, H-1111 Budapest, Hungary

Authors E-mail: balczo@ara.bme.hu; tomor@ara.bme.hu

**Corresponding author*

(Manuscript received in final form March 23, 2015)

Abstract—Recognizing the role of urban squares in city life, the paper focuses on wind conditions at squares, with the objective to understand the building-scale flow phenomena influencing the wind comfort of pedestrians and the dispersion of pollutants. Wind tunnel testing of a selected square has been carried out at two wind directions, as well as accompanying computational fluid dynamics (CFD) simulations were performed using the MISKAM microscale model. The high spatial resolution experimental and CFD data allowed the identification of flow structures, like separation bubbles, vortices, high-speed zones in and around the square. Based on the analysis of numerical and experimental data obtained, the MISKAM model is able to resolve the flow field in a complex urban setting with some limitations. In a second step, the model was then used to run further numerical simulations, to compare fully built-up areas to an area with a square, and to assess the influence of tree plantings on the square. Results regarding the latter indicate that below tree crown height, flow velocity and turbulent kinetic energy are both decreased by about one fourth due to the vegetation. It is also shown that the presence of the square increases wind speed in connecting streets and induces longitudinal flows even in streets perpendicular to the approaching wind direction. The time-resolved wind tunnel measurements also allowed presenting the local velocity statistics as wind roses. Using these, we identified locations with non-isotropic turbulence and alternating wind directions.

Key-words: urban square, flow field, velocity fluctuation, urban vegetation, wind tunnel

1. Introduction

Urban flow and dispersion has been the subject of hundreds of research papers in the past, though only review articles (*Britter* and *Hanna,* 2003; *Ahmad et al.,* 2005; *Belcher et al.,* 2013; *Blocken,* 2014) may be cited here. While there is a huge selection of studies on ventilation and pollutant dispersion in urban street canyons, street intersections and regular arrangements of building blocks, there are few detailed analyses of the flow and dispersion phenomena specifically at urban squares. A square is defined as an open, typically four-sided area surrounded by buildings, with length to width ratio not necessarily equaling one. Squares fulfil important functions in urban life: they facilitate playing and sporting grounds, dining opportunities, markets, and open-air events. The creation of squares from the demolition of defunct residential or industrial buildings is an option in urban redevelopment programs. The longer residence time of pedestrians on squares explains why wind conditions and pollutant dispersion are of interest.

Only a few papers dealt with air pollution and flow phenomena specifically in urban squares. *Gadilhe et al.,(*1993) studied a semi-circular square and found recirculation zones behind the upstream located buildings of the square. *Parra et al.* (2010) showed using CFD simulations that depending on wind direction, locally released pollutants can be trapped in the separation vortices behind those buildings, and concentration distribution on the square is quite inhomogeneous. Obstacle resolving test cases of whole districts like the 'Michel-Stadt' semi-idealized urban dataset of *Bastigkeit* (2011) also include squares, among other features of an urban geometry, so there is experimental and numerical data available (*Hertwig et al.,* 2012; *Rákai* and *Kristóf,* 2013). However, the specialities of the flow in the squares were not separately addressed in these studies. Also, measurement data with higher spatial resolution would allow a more detailed analysis of the flow in the squares.

In the present paper, a typical urban square, József Nádor Square (coordinates 47.498 N, 19.050 E) in downtown Budapest will be investigated. It measures approximately 150×60 m, and is surrounded from all sides by building blocks of 28 m average height. The connecting streets are relatively narrow; their width to height (*w/h*) ratio is about 0.5. The square has unfavorable ventilation. Moreover, on its northern side it is bordered by the extremely busy József Attila Street with approx. 2000 vehicles/hour in rush hours, emitting a considerable amount of pollutants.

The area is heavily polluted with concentration levels well above the limit, as it was proven in an earlier paper (*Balczó* and *Lajos,* 2012), in which we investigated the site by using CFD simulations of the surroundings. The annual averages of NO_x concentrations at ground level in the north of the square showed values about twice as high as the annual limit. Also, the data of the on-site air quality monitoring station was analyzed and compared to the CFD results. CFD predictions of annual NO_x averages deviated just 16% or less from the measured concentration values.

In the present study, wind tunnel measurements of a 1:350 scale model and computational fluid dynamics (CFD) simulations were carried out to understand the flow phenomena in the square and its surroundings. The flow field measurements were performed in a Göttingen-type wind tunnel by using laser-doppler velocimetry (LDV). In order to achieve proper flow field results, an urban-type atmospheric boundary layer was modeled in the wind tunnel and checked by vertical profile measurements.

The flow around exactly the same model geometry was simulated using the MISKAM flow and dispersion model, developed by *Eichhorn et al.*(1988). This CFD model solves the Reynolds-averaged Navier-Stokes (RANS) equations on a Cartesian non-equidistant grid and applies a modified K-ε closure adapted to urban flows. In the next step, the dispersion of pollutants can be calculated by solving the Reynolds-averaged advective diffusion equation. For detailed description of the current version 6, see *Eichhorn* (2011). The model underwent detailed evaluation in the past decade both according to the evaluation guideline VDI 3783/9 (*VDI,* 2005) performed by *Eichhorn* and *Kniffka* (2010) and it also took part in the model evaluation study of the European research Action COST 732 (*Schatzmann et al.,* 2010). Evaluation using the more complex MUST data set was published by *Balczó* and *Eichhorn* (2009) and *Goricsán et al.* (2011), testing with other data sets by *Olesen et al.* (2009).

The MISKAM model is able to run on standard personal computers, and its applicability to problems in urban environment has been shown in several publications (*Benson et al.,* 2007; *Balczó et al.,* 2009; *Donnelly et al.,* 2009; *Belalcazar et al.,* 2010; *Flassak et al.,* 2010; *Balczó et al.,* 2011). MISKAM was used as wind field and turbulence input for other dispersion models (*Leuzzi et al.,* 2010; *Letzel et al.,* 2012).

Due its simple setup and handling, the code is not only used by experts with deep knowledge of fluid dynamics, but also by many environmental agencies, authorities, and consulting engineers. While the application of high-end CFD models (e.g., LES) is not realistic in the regulatory / air quality assessment field at the present, MISKAM and other purpose-built RANS models form a significant step forward from earlier non-CFD (Gaussian, empirical, etc.) models applied in this area, when more accuracy in urban micro scale investigations is needed. Thus, the secondary objective of this work is to assess the capabilities of a CFD RANS model intended for regulatory use on complex real-world geometry.

2. Experimental setup

2.1. Wind tunnel and measurement setup

Experiments were carried out in the 3.8 m long and 2.6 m wide open test section of the large horizontal wind tunnel of the Budapest University of Technology and Economics. Model and boundary layer generation devices are mounted on a horizontal plate of 2.5 m width. *Fig. 1* shows the measurement layout. During the measurements, the fibre-optic laser doppler velocimetry (LDV) probe accessed the flow from below through a glass plate; therefore, the flow was not disturbed by the probe. A two-component LDV system was applied; hence, the horizontal velocity components u and v could be determined using the mentioned arrangement. The system consists of an air-cooled 300 mW Argon-Ion laser, generating a multiple frequency beam which goes through beam splitter and a Bragg cell to generate shifted and unshifted 488 and 514.5 nm (blue and green) beams. The four beams then pass through a fibre optic cable towards the LDV optics with 363 mm focal length and 61 mm clear aperture. Measurement volume has a diameter of 90 μm and 1.3 mm length. Laser light from the olive oil seeding particles passing the measurement volume is reflected back into the optics leading to photomultipliers and then digitized and analyzed by FSA3500 DSP-based signal processing unit. Burst frequencies are determined by autocorrelation. Burst velocities are weighted with gate time to get average velocities.

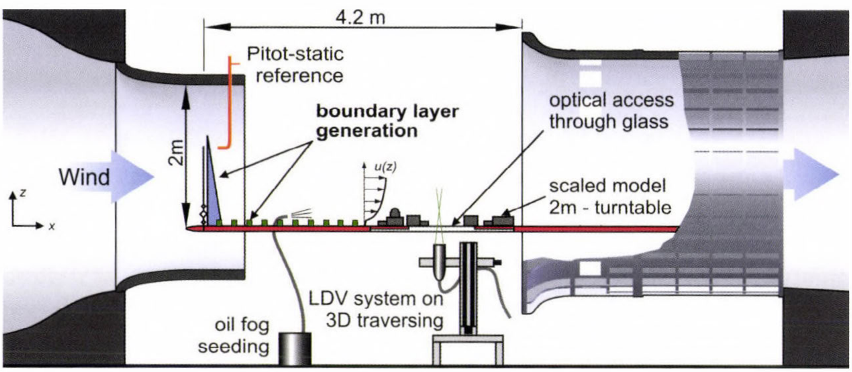

Fig. 1. The measurement layout including spikes, crossbars, and roughness elements in the preparatory section of the wind tunnel, the model arranged in the test section of the wind tunnel, and the LDV probe below the test section.

During the test campaign, different averaging times were used. At the incoming boundary layer measurement (Subsection 2.2), 200.000 velocity samples (bursts) were collected in up to 5 min, and during the flow field measurement of the square (Subsection 2.3), about 5000 samples were collected during the selected 50 s averaging time. The representativeness of measured velocity averages and standard deviations was checked during a few measurements of longer duration.

2.2. Atmospheric boundary layer generation

Following the well-established procedure of boundary layer generation in wind tunnels (see, e.g., *Gromke* and *Ruck,* 2005) and *Kozmar* (2011), an urban-type atmospheric boundary layer was generated in the wind tunnel modeling the natural ABL described in ESDU 72026 (*ESDU,* 1972), ESDU 85020 (*ESDU,* 2001), and VDI 3783/12 (*VDI,* 2004) by placing vortex generators, crossbars, and roughness elements into the preparatory section of the wind tunnel. The mentioned arrangement can be seen in *Fig. 1*. Vertical profiles of the developed boundary layer were measured using the LDV system at the centre of the turntable without the city model. Boundary layer parameters were determined from the mean velocities $\bar{u}(z)$ and $\bar{v}(z)$ in streamwise and lateral direction; as well as from their respective standard deviations $\sigma_u(z)$ and $\sigma_v(z)$. Turbulence intensity in the x- and y-direction (I_u and I_v) are defined as $\sigma_u(z) / \bar{u}(z)$ and $\sigma_v(z) / \bar{v}(z)$. Longitudinal integral length scale of turbulence using autocorrelation is given by:

$$L_{u,x} = \int_0^\infty R_{uu}(\Delta x) d\Delta x, \tag{1}$$

with R_{uu} – autocorrelation coefficient of the of the $u(z,t)$ – velocity time-series in x-direction.

Fig. 2 shows the profile of the dimensionless mean velocity into the main flow direction (a) and the turbulence intensity profiles I_u and I_v (b and c). Mean velocity $\bar{u}$ was approximated with the power law in the form

$$\frac{\bar{u}(z)}{u_{ref}} = \left(\frac{z - d_0}{z_{ref} - d_0} \right)^\alpha, \tag{2}$$

where α is the exponent, z is the height, z_{ref} is the reference height (height of the modeled boundary layer), u_{ref} is the mean velocity at the reference height and d_0 is the displacement height. In order to obtain dimensionless mean velocities, local velocities $u(z)$, were divided by the reference velocity u_{ref} = 4.60 m/s, which was measured at the reference height z_{ref} = 309.50 mm (108 m full scale).

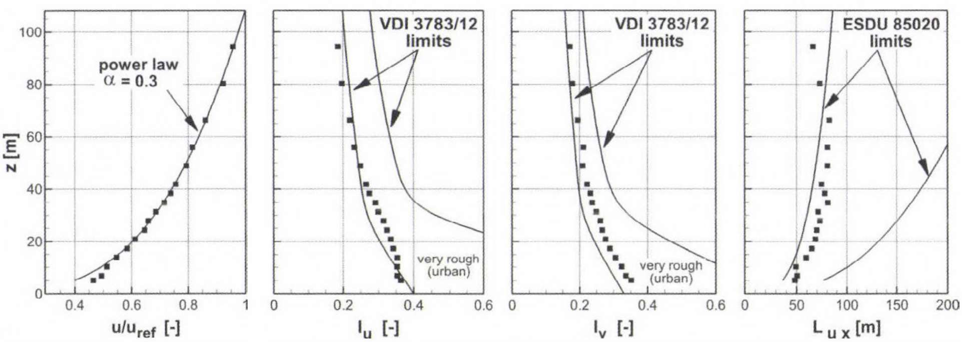

a **b** **c** **d**

Fig. 2. Approach flow variables as a function of full scale height: (a) dimensionless mean velocity u/u_{ref}; (b) streamwise turbulence intensity I_u compared with urban type ABL turbulence given in VDI 3783/12; (c) lateral turbulence intensity I_v; (d) streamwise integral length scale of turbulence $L_{u,x}$ compared with ESDU 85020 data.

Displacement height was considered to be zero at the boundary layer measurement without the city model. (In measurements with the model on the turntable, the first few rows of buildings will elevate the boundary layer to the displacement height of ~ 0.75 h, as it can be seen later in the profiles of *Figs. 7–9*.)

The above parameters of an urban-type atmospheric boundary layer are specified by several guidelines and standards. According to ESDU (1972), the power law exponent α = 0.3 can be accepted for the representation of the urban atmospheric boundary layer. Turbulence intensity I_u profile shows some differences compared with VDI (2004) data; however, below the full scale height of 60 m, the agreement between the standard and measured data is perfect.

The integral length scale profile $L_{u,x}$ is shown in *Fig. 2 (d)*. The $L_{u,x}$ values – scaled up using the scale factor 1:350 – were compared with ESDU (2001) data. The integral length scale profile $L_{u,x}$ agrees well with the suggestions of the standard except above 80 m full scale height.

Based on the profile measurements, the generated atmospheric boundary layer was considered to be an accurate model of the ABL approaching the investigated square.

2.3. *Model construction and the final measurement layout*

The 1:350 scale model of the quarter around József Nádor Square was modeled with buildings prepared using waterjet-cut plywood and hotwire-cut rigid foam, and the whole model was placed on a wooden circular plate with a diameter of 2 m. An 800 × 800 mm opening in the middle of the plate covered by a pane of glass provided optical access to the flow from beneath the model. Although roof shape has certain effects on the flow, these effects were neglected in order to simplify the CFD model and mesh generation. According to this, the buildings of the experimental model were also modeled as blocks with flat rooftops and classified heights in 1.5 m steps. József Nádor Square and the surrounding quarter can be seen in *Fig. 3*, the model is shown in *Fig. 4*, left.

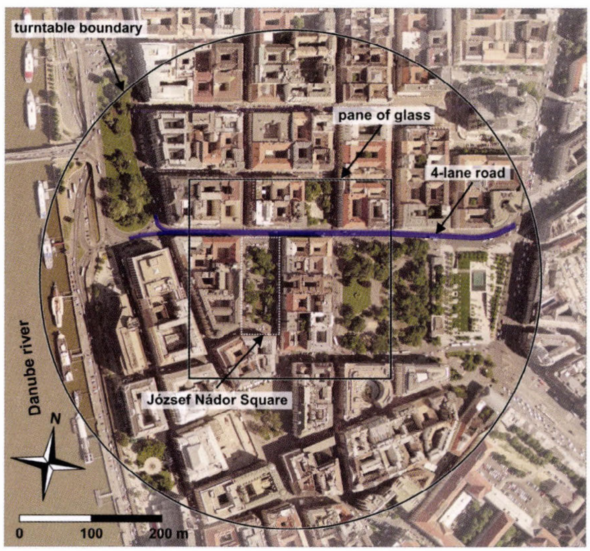

Fig. 3. Aerial photograph of József Nádor Square and the surrounding quarter; the edge of the wooden turntable and the pane of glass are also marked.

Flow velocities were measured along 23 vertical profiles and three horizontal planes (see later in *Fig. 5*). Local mean velocities, $\bar{u}$ and $\bar{v}$, were normalized to the reference velocity u_{ref} = 3.02 m/s, which was measured at the building mean height h = 80 mm during the boundary layer measurements; h is the mean building height in model scale. The mean building height in full scale is h = 28 m.

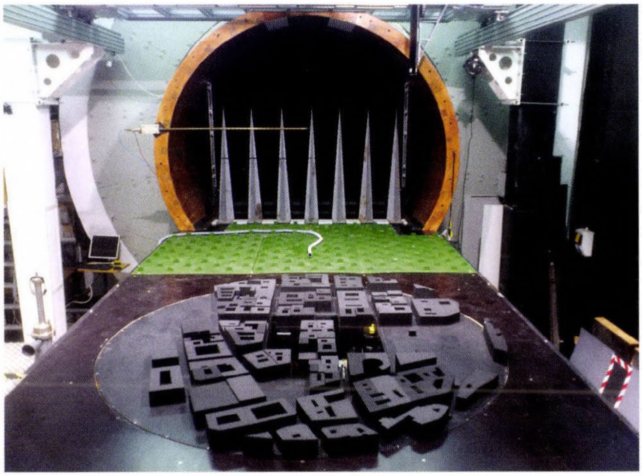

Fig. 4. The model in wind tunnel. Buildings are painted black to reduce laser reflections.

The parameters discussed herein can be calculated with the following formulas. Dimensionless mean velocity u_d and v_d in the x- and y-direction is calculated as $u_d = u/u_{ref}$ and $v_d = v/u_{ref}$, respectively. Dimensionless velocity fluctuations σ_{ud} and σ_{vd} are defined as $\sigma_{ud} = \sigma_u/u_{ref}$ and $\sigma_{vd} = \sigma_v/u_{ref}$ with velocity standard deviations σ_u and σ_v.
Dimensionless horizontal mean velocity magnitude v_{md} :

$$v_{md} = \sqrt{u_d^2 + v_d^2}\,. \tag{3}$$

Dimensionless turbulent kinetic energy K_d :

$$K_d = \frac{1}{2} \cdot \left(\sigma_{ud}^2 + \sigma_{vd}^2\right). \tag{4}$$

It must be noted that the calculated turbulent kinetic energy calculated from Eq. (4) differs from the real one, because the vertical velocity component w and its standard deviation σ_w could not be measured using the applied arrangement. Thus, K_d is the contribution of horizontal velocity components to turbulent kinetic energy.

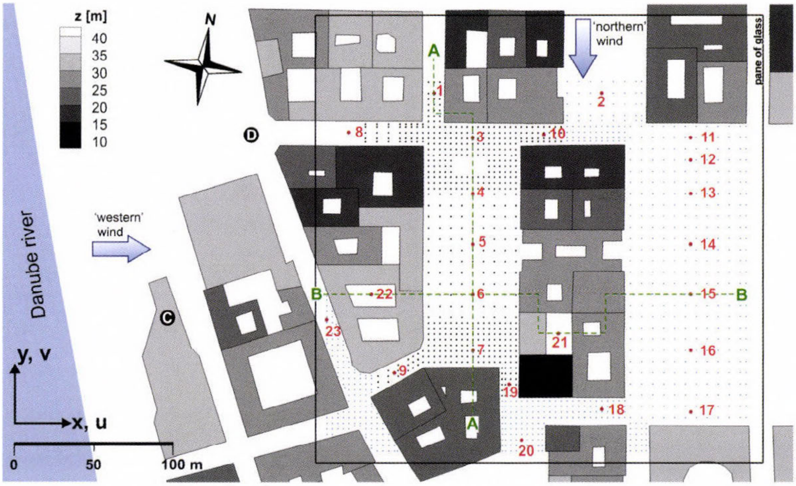

Fig. 5. Wind directions and measurement locations on the wind tunnel model. Buildings are colored by their full scale height. Red circles: vertical profile (VP) measurements; black dots: horizontal plane measurements at 0.25 *h*, 0.5 *h,* and *h* heights; blue dots: additional horizontal plane measurements at 0.5 *h* height.

2.4. Wind directions

During the flow field measurements in the model of József Nádor Square, two wind directions were investigated: approximately northern wind direction, 351.7 degree to north, and 261.7 degree to north, approximately western wind direction. The selected two wind directions mean that wind blows at 'northern' wind exactly along the long axis of the square, at which its length to height ratio *l/h* of the square is 5.3, and at 'western wind' exactly along the short axis of the square with *l/h* equaling 2.1. Wind statistics were available from three neighboring meteorological stations, which are in 2.5–10 km distance. Their averaged wind rose shows north and west-northwest as the prevailing wind directions, thus the selected wind directions are close to the prevailing ones.

3. Numerical setup

Setup of the CFD simulation carried out at 'northern' (351.7 deg) wind direction followed the best practice guideline given by *Franke et al.* (2007). The computational domain included the buildings modeled in the wind tunnel in full scale inside a 700 m diameter circle around József Nádor Square corresponding to the 2 m diameter turntable, with proper inlet, outlet, and side distances to the domain boundary. Domain size was thus 1000 × 1100 × 500 m. Grid resolution of the non-equidistant Cartesian grid applied by MISKAM varied from 4–6 m horizontally and 1 m vertically between buildings down to 1.5 m horizontally and 0.6 m vertically around József Nádor Square near the ground, up to a total of approximately 5 million grid cells.

Regarding grid independency of the computational mesh, earlier MISKAM simulations of a simplified symmetrical street canyon geometry by *Balczó et al.* (2009) showed that it can be reached at an average of 0.5 m cell size (with refinements of 0.1 m at building leading edges). However, this resolution could not be replicated in the current complex, large-domain case with hundreds of buildings due to memory limitations of the 32 bit code. The current resolution can be seen as typical for the MISKAM model when applied in environmental impact assessment studies by agencies on a daily basis.

The predefined boundary condition types of MISKAM (see *Eichhorn,* 2011) were used: buildings represented as block outs from the Cartesian grid, on the surfaces no-slip conditions applied using wall functions, the roughness length on the surfaces set to 0.01 m. At the inlet boundaries an equilibrium logarithmic profile was generated by MISKAM automatically with initial roughness length z_0 of 0.2 m. The reference velocity was set to 3.02 m/s at h=28 m, as measured in wind tunnel.

The comparison of the CFD approaching flow profile to the profile measured in the empty wind tunnel shows certain disagreement in terms of both mean velocity and turbulence (*Fig. 6*).Turbulence underestimation in boundary layer profiles over flat terrain is a common error of K-ε turbulence closures as shown, e.g., by *Olesen et al.* (2008). It is expected, however, that the first few rows of buildings will act as boundary condition generators, and the profiles will be assimilated to each other. This will be checked later comparing CFD and wind tunnel vertical velocity profiles at locations near the square.

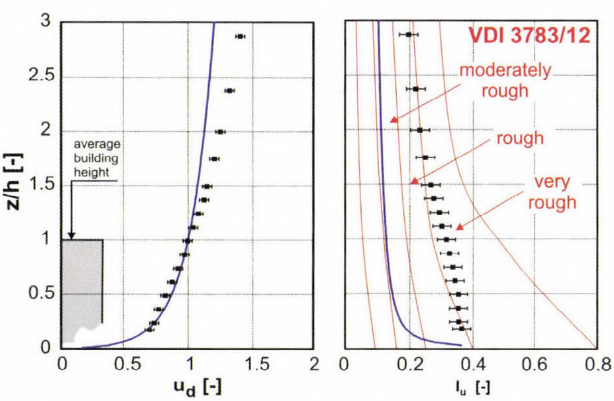

Fig. 6. Streamwise u_d dimensionless velocity and I_u turbulence intensity profiles. Simulation: continuous blue line, wind tunnel measurement: dots with error bars. *h*: average building height. Red lines: VDI 3783/12 limits.

4. Results and discussion

In the course of the analysis of results, first we will identify the major flow structures using vertical profile diagrams, and velocity and turbulence plots in horizontal planes in Sections 4.1 and 4.2. Although the vertical velocity component was not directly measured, some of the data allow us to draw conclusions about the vertical velocities and the three dimensional flow structures in Section 4.3. Section 4.4 shows time-resolved wind tunnel data in order to analyze unsteady phenomena in the square. In Section 4.5, the flow in the square is compared statistically with the flow in neighboring streets and to a case in which the square is replaced by a block of buildings. Additionally, we assess the influence of street vegetation in Section 4.6, and then discuss the performance of the CFD model in Section 4.7.

In the following comparison plots, turbulent kinetic energy K_d determined in simulations was always multiplied by 2/3, in order to approximate the contribution of horizontal velocity fluctuations to the turbulent kinetic energy, which was actually measured in the wind tunnel.

4.1. Analysis of vertical profiles

The 23 dimensionless vertical velocity profiles give a first insight into the flow field at the square. Our expectation is that the streamwise velocity component (v in case of northern wind direction) will follow the approaching wind profile (*Fig. 6*) above rooftop level, but around and below rooftop level it will deviate significantly.

Fig. 7 shows vertical profiles of mean velocity from both the wind tunnel and CFD simulation, streamlines from CFD and turbulent kinetic energy from the wind tunnel in the mid-plane of the square (cross section A-A in *Fig. 5*). The building located at the northern end of the square generates backflow (marked with A in *Fig. 7*). The presence of this recirculation zone is visible on profiles VP3 and VP4. The streamlines originating from one source point indicate that there is significant inflow from x direction (from the connecting street) into the core of the separation zone.

From the middle of the square (approximately 2.5 h distance, B in *Fig. 7*)), streamlines reach the bottom on the square and stagnation point develops in front of the downstream building block. Close to the ground (marked with C in *Fig. 7*), again backflow can be observed in the wind tunnel measurements, showing the presence of a *horseshoe vortex*, which is unfortunately not resolved by the CFD. Otherwise, CFD follows the measurements quite well, especially above rooftop level, proving the assumption made earlier, that the slight differences in incoming boundary conditions are assimilated, as the flow reaches the square. Near the ground, the streamwise flow velocities are overestimated by CFD.

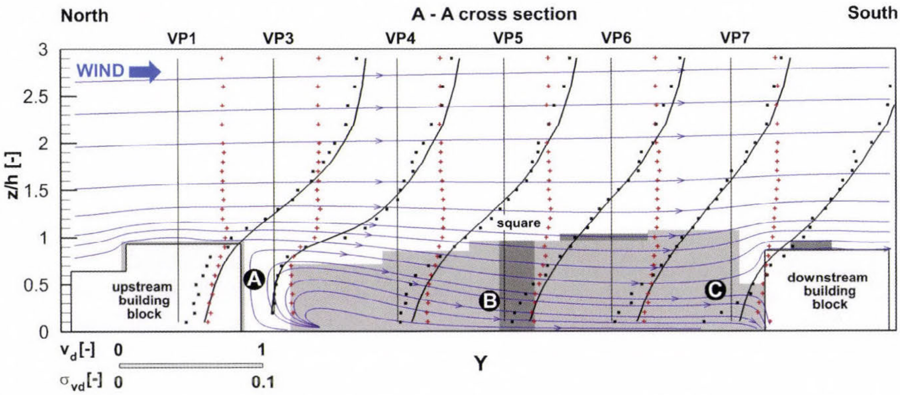

Fig. 7. Flow field at northern wind direction along the square (A –A cross section of *Fig. 5*). Black squares and continuous lines: normalized streamwise mean velocity component v_d from measurement and simulation, crosses: normalized velocity standard deviation σ_{vd} from wind tunnel measurement. Streamlines in blue are from the simulation. Note that VP1 lies in a connecting street, not on the square itself.

The flow field in a cross-section of the square at western wind is depicted in *Fig. 8* (cross section B - B of *Fig. 5*). In this direction, the square is only 2 h wide.

- Measurement shows strong backflow on the square up to rooftop level (VP6). Streamlines indicate a vortex with horizontal axis dominating the whole square. Similar backflow can be seen behind the downstream building block.

- Despite their small size, building inner yards have street-canyon-like horizontal vortices (VP22, VP21).

At both wind directions, turbulent kinetic energy K_d is almost constant above rooftop level (with an occasional, slight maximum at 1.2–1.7 h height), and decreases underneath rooftop level towards the ground by about one third. In building inner yards, its value goes down to less than one half.

For the generalized, quantitative description of the flow in urban squares, we compare the averaged vertical velocity profiles in the square (VP 3–7) at the two wind directions in *Fig. 9*. While above 1.5 h, all profiles run close together, there are differences below that level. Most remarkably, at western wind, speeds are higher than at northern wind. Nevertheless, in none of the cases it is higher than 0.5. Also, compared to the averaged profiles measured in the connecting streets (VP 1, 8, 9, 10, 18, 23), wind speed in the square is approximately the same.

CFD results, available at northern wind direction, overlap almost perfectly the wind tunnel measurement data.

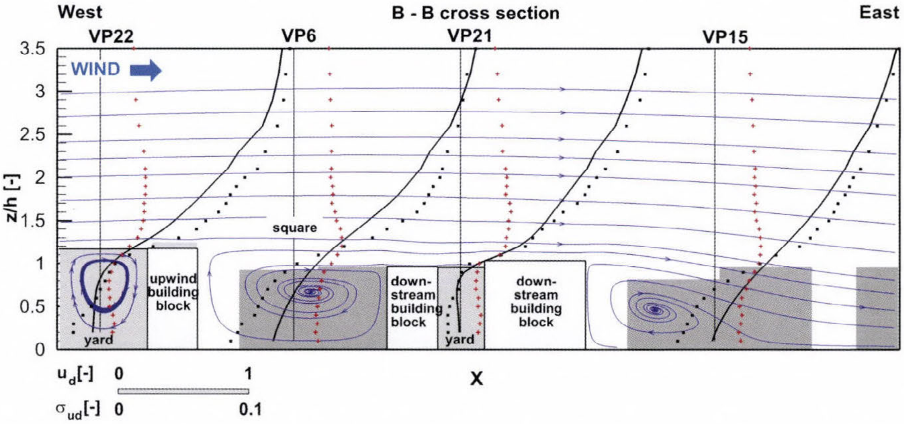

Fig. 8. Flow field at western wind direction along the square (B – B cross section of *Fig. 5*). Black squares: normalized streamwise mean velocity u_d from measurement, crosses: normalized velocity standard deviations σ_u from wind tunnel measurement. Streamlines are from simulation. Please note that profile VP21 is about 30 m off-plane towards south.

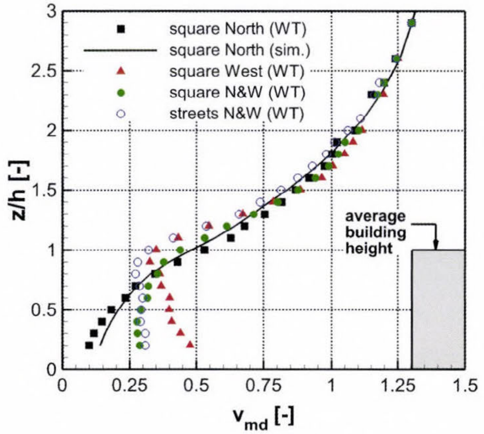

Fig. 9. Averaged vertical profiles of velocity magnitude v_{md} in the square (VP 3-7). Black: at northern, red: at western wind direction. For comparison, an overall average of vertical profiles in the connecting streets (VP 1, 8, 9, 10, 18, 23) is shown with blue.

4.2. Flow field in horizontal planes

Flow velocities were measured along three horizontal planes at 0.25 *h*, 0.5 *h,* and *h*, corresponding to 7, 14, and 28 m in full scale (20, 40, 80 mm in model scale).

Planes 1 and 3 included 568 measurement points; plane 2 consists of 1287 points (see *Fig. 5*). The positioning accuracy was less than 0.5 mm. The normalized horizontal velocity magnitude v_{md} at northern wind direction on the three horizontal planes can be seen in *Fig. 10*, with wind tunnel data in the left and CFD data in the right column. *Fig. 11* shows the normalized turbulent kinetic energy distributions in the same wind direction. *Fig. 12* shows the same variables but in western wind direction. Scalar variables are interpolated from the measurement points onto the planes using inverse-distance interpolation, and streamlines are integrated from the velocity vectors.

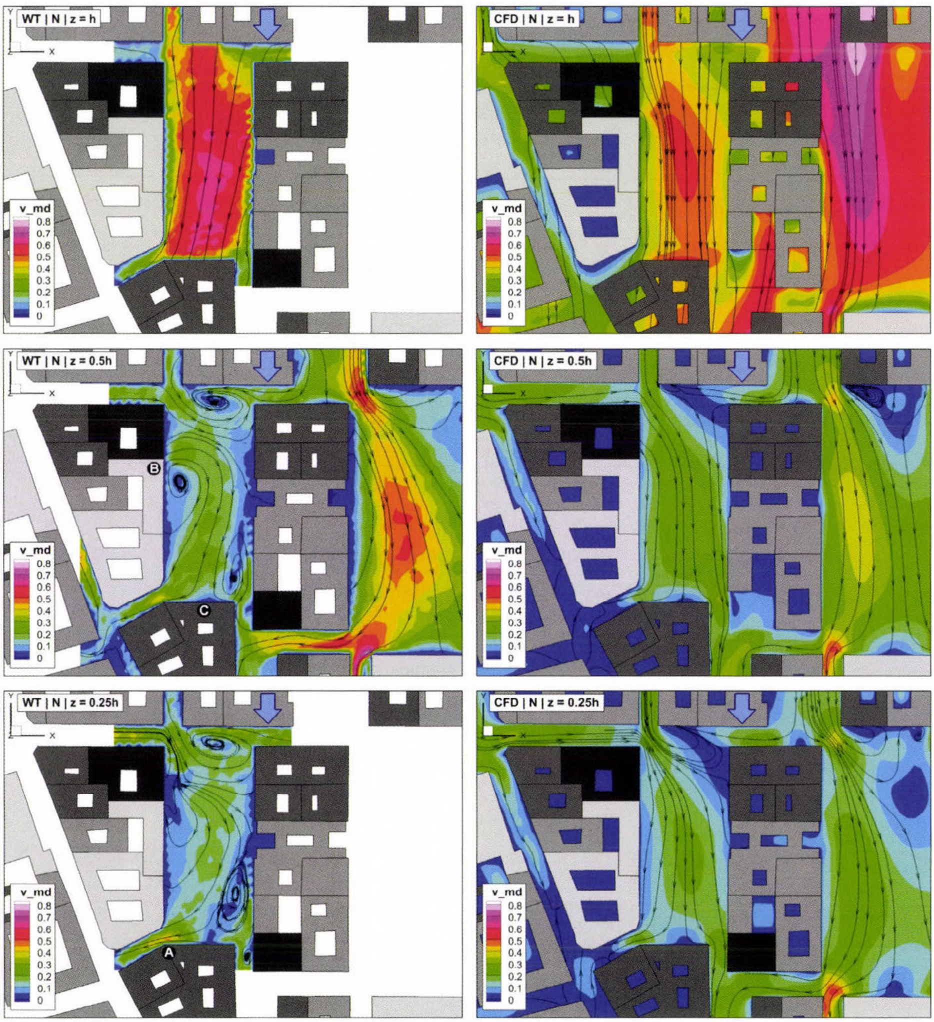

Fig. 10. Normalized horizontal velocity magnitude v_{md} distributions on three horizontal planes at northern wind direction. Left column: wind tunnel measurement; right column: CFD simulation.

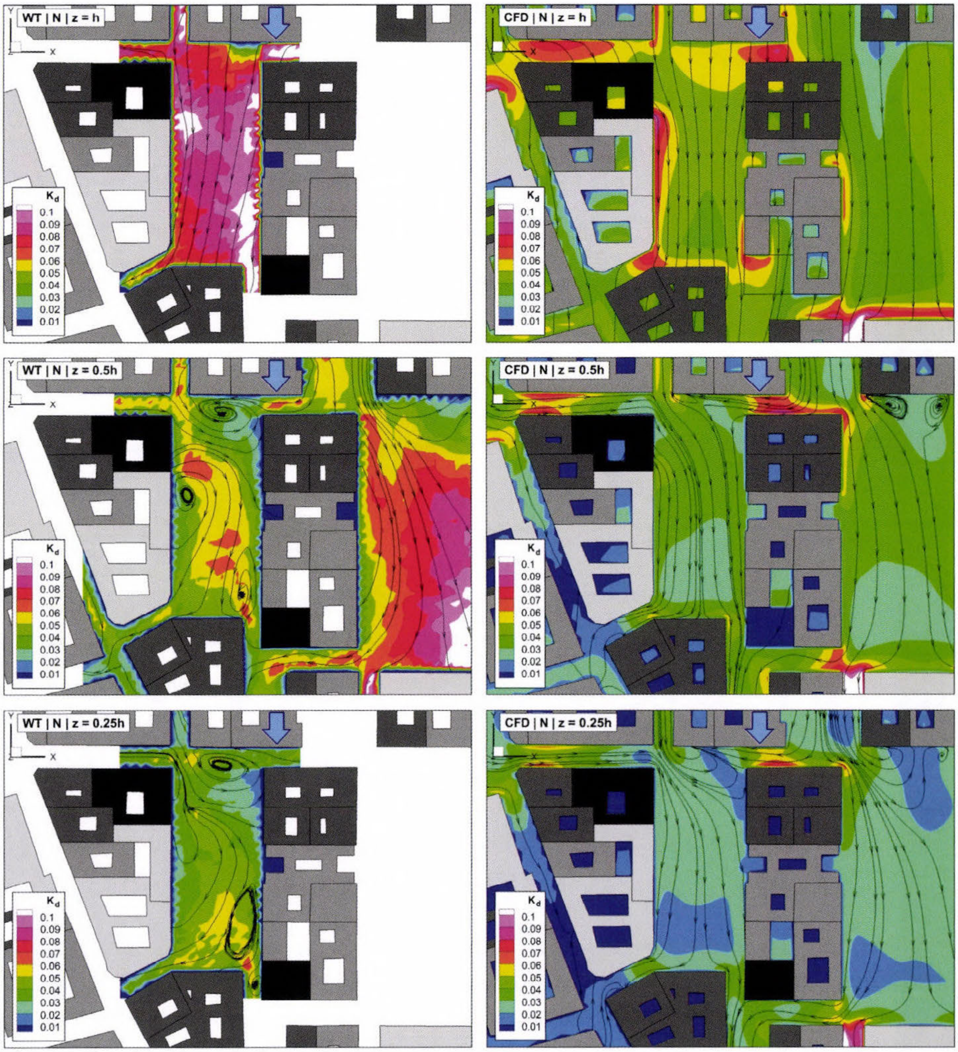

Fig. 11. Normalized turbulent kinetic energy K_d distributions on three horizontal planes at northern wind direction. Left column: wind tunnel measurement; right column: CFD simulation.

As regards the velocity fields in northern wind direction, the highest velocity values were measured at $z = h$. No backflow is observable at this height. At lower heights, mean velocity values are also lower, at 0.25 h less than 5–25% of the reference wind speed in the square itself. Top wind speed in the square is at the corner of the downstream (southern) building block, marked with A in *Fig. 10*. Outside the square, velocity magnitude of up to 0.8 can be seen at corners southward the open space in the eastern part of the measurement area.

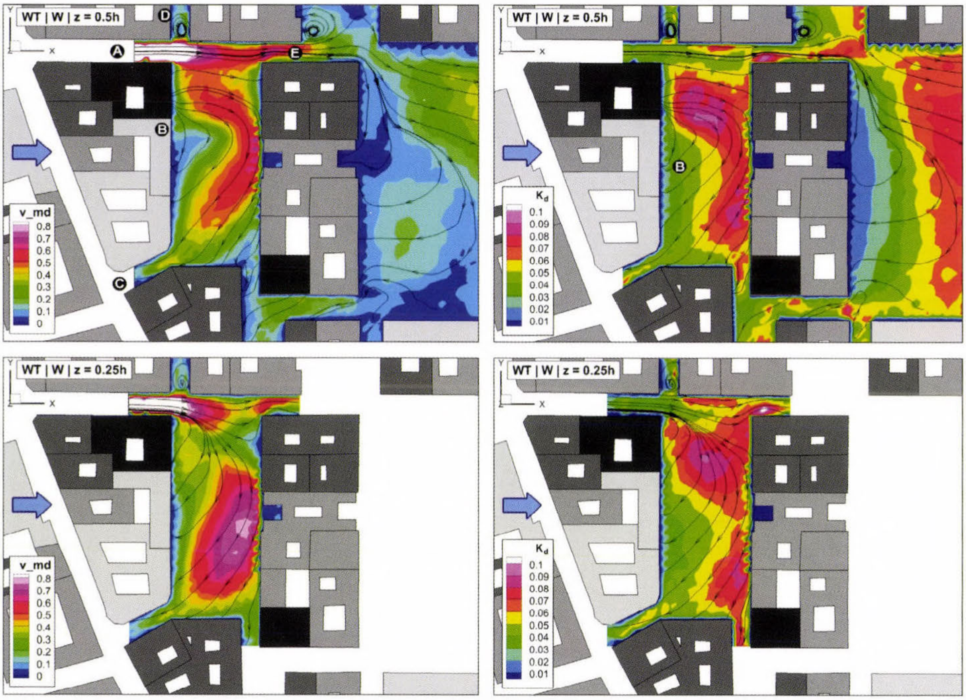

Fig. 12. Normalized horizontal velocity magnitude v_{md} (left column) and normalized turbulent kinetic energy K_d (right column) on two horizontal planes at western wind direction.

Analyzing the streamlines, it can be stated that the flow forms three major vortices in this wind direction. Their vertical extension does not reach the reference height h but is clearly present at $z = 0.25\ h$ and $z = 0.5\ h$. The northern vortex is in the separation zone of the northern block, and the middle one is obviously caused by the second, taller building of the western building block, marked with B in *Fig. 10*.

Air enters the square from the northern streets and leaves it by passing through the south-western connecting street. Interestingly, backflow is detected in the south-eastern connecting street, so the outflow is blocked here. A stagnation point can be found in the front of the southern building (marked with C in *Fig. 10*), where vertical profile VP7 suggests the presence of a horizontal vortex (B in *Fig. 7*). A significant proportion of the air, which arrives from northern connecting streets, is trapped in the first (north-eastern) vortex of the square.

CFD simulations only resolve the vortex in the north-eastern corner of the square, although in smaller size, and only visibly at 0.25 h height. While the other vortices are suppressed, which gives a velocity field much more in line with the incident wind direction, the magnitude of velocity is about the same as in the measurement.

The average level of turbulent kinetic energy K_d (*Fig. 11*) is the simulated about 2/3 of that measured in the wind tunnel. It increases with the height and has a maximum at the average building height h. Values of the turbulent kinetic energy are usually smaller in the vicinity of the walls. This agrees well with the expectations, because both the mean velocity and the standard deviation values are lower near the walls.

Due to the stagnation point anomaly (*Kato* and *Launder,* 1993), CFD results for K_d predict peaks near building leading edges, which are not present in the measurement.

In western wind direction, flow velocities were measured along two horizontal planes at 0.25 h and 0.5 h corresponding to 7 and 14 m in full scale (20 and 40 mm in model scale). Plane 1 covers just the square and connecting streets; plane 2 covers the whole area. The velocity and turbulent kinetic energy distributions on the two horizontal planes can be seen in *Fig. 12*.

In terms of the velocity fields on the horizontal planes, it can be stated that the measured velocity values at 0.5 h are not significantly larger than the values at 0.25 h. Moreover, in the middle and eastern part of the square velocity values at 0.25 h are larger than the values at 0.5 h. The highest velocities were measured in the connecting street at the NW corner of the square at both heights; mean velocity values approximate the reference wind speed in the western part of the investigated section of the street, indicated by A in *Fig. 12*. The streamlines show that:

- The street marked by D is blocked entirely by a corner vortex.
- Most of the air passes through the square flowing from the street marked by A towards the street marked by E in *Fig. 12*.
- A smaller portion of it enters the separation bubble which is formed behind the western building block (marked by B in *Fig. 12*). However, this is modified by the high velocity inflow at the NW corner to a helical vortex, which moves air towards the southern part of the square, and pushes air through the southern connecting streets even opposite to the incident wind direction. The high velocity inflow is caused by the direct, unobstructed inflow from the river Danube (mark D in *Fig. 5*).

Thus, despite the wind coming from the west, there is a significant north to south convection in the square. It is remarkable that the flow field is very similar to that in a street canyon at slanted wind direction (*Czáder et al.,* 2009) with a huge street canyon vortex superposed to a velocity component along the street canyon.

4.3. *Three-dimensionality of the flow*

Because of the vertical arrangement of the LDV probe under floor, we were not able to measure the vertical velocity component w directly. However, the measured mean horizontal flow field ($\underline{v}_{hor\,d}$) let us calculate the vertical velocity gradient based on the continuity equation:

$$-\frac{\partial w_d}{\partial z} = \left(\frac{\partial u_d}{\partial x} + \frac{\partial v_d}{\partial y}\right) = div\left(\underline{v}_{hor\,d}\right). \tag{5}$$

On the horizontal ground surface, obviously w must be 0. At a small height, slightly above the ground surface, vertical velocity, if there is any, must decrease towards the surface. Thus, we can distinguish three cases for the w velocity component in horizontal planes near the ground:

a. the flow is horizontal ($w = 0$), thus $\partial w / \partial z = 0$ and $\mathrm{div}(v_{\mathrm{hor\,d}}) = 0$,

b. vertical inflow occurs ($w < 0$), flow towards the ground must be decelerated ($\partial w / \partial z < 0$), thus the flow field in horizontal plane will diverge ($\mathrm{div}(v_{\mathrm{hor\,d}}) > 0$),

c. vertical outflow occurs ($w > 0$), flow accelerates upwards ($\partial w / \partial z > 0$), and the horizontal flow field will converge ($\mathrm{div}(v_{\mathrm{hor\,d}}) < 0$).

In conclusion, positive values of the horizontal divergence near the ground are related to updrafts, while negative values indicate downdrafts. The relationship is demonstrated at 0.25 h height in plot a and b of *Fig. 13* using CFD results at northern wind direction. Divergence calculated from wind tunnel data in northern and western wind direction is shown in plot c and d of *Fig. 13*. The results are obviously subject of considerable noise; however, the major spots of vertical air movements are clearly recognizable.

- In case of northern wind direction, *updrafts in the wake* of the northern (upstream) building block and at building walls of the north-eastern corner can be seen, as well as a downdraft in the northern centre of the square caused by the inflow at the northeast corner.
- In case of western wind direction, the magnitude of divergence is significantly larger and shows a *single, massive helical vortex* with horizontal axis dominating the square, causing updrafts on the western and downdrafts on the eastern side.
- Up- and downdrafts can be seen in many of the connecting streets in both wind directions. Considering the direction of streamlines in the streets, these indicate *weak helical vortices* (street canyon vortices with some advection along the street axis).

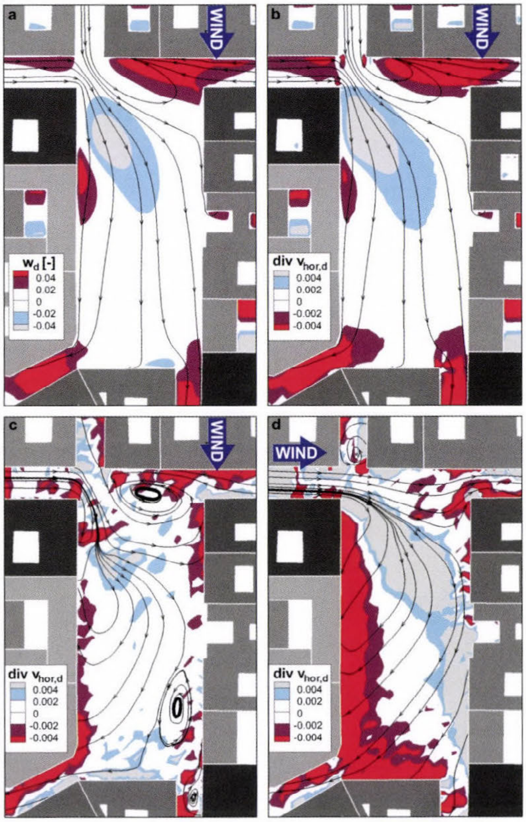

Fig. 13. Vertical air velocity and horizontal divergence in the square at 0.25 h height. Reddish colors: updraft, light colors: downdrafts. Values close to 0 are blanked. From left to right: (a) CFD simulation: normalized vertical velocity in northern wind direction; (b) CFD simulation: div($v_{hor\ d}$) in northern wind direction; (c) wind tunnel measurement: div($v_{hor\ d}$) in northern wind direction, (d) wind tunnel measurement: div($v_{hor\ d}$) in western wind direction.

4.4. Analysis wind speed and direction fluctuations

The time-resolved LDV data captured simultaneously for both horizontal wind directions contain information about turbulence anisotropy and spectral properties. Up to this point, from the turbulent quantities, only turbulent kinetic energy was analyzed.

For a more detailed analysis, simultaneous u and v time series were captured at a horizontal plane at 0.5 h height at several measurement locations, and the occurrence frequency of the instantaneous horizontal wind vector $\underline{v}_{i,d}$ at a certain location was visualized by wind roses (polar area diagrams). Thirty one selected wind roses are shown in *Fig. 14*, colored by the instantaneous velocity magnitude. Also, streamlines colored by the average horizontal velocity magnitude v_{md} are shown.

- Each illustrated wind rose is placed at the location of the given measurement point.
- The roses are divided into 10-degree spokes representing the probability of 10-degree wind direction sectors.
- Each spoke is subdivided into color-coded bands that show velocity ranges.

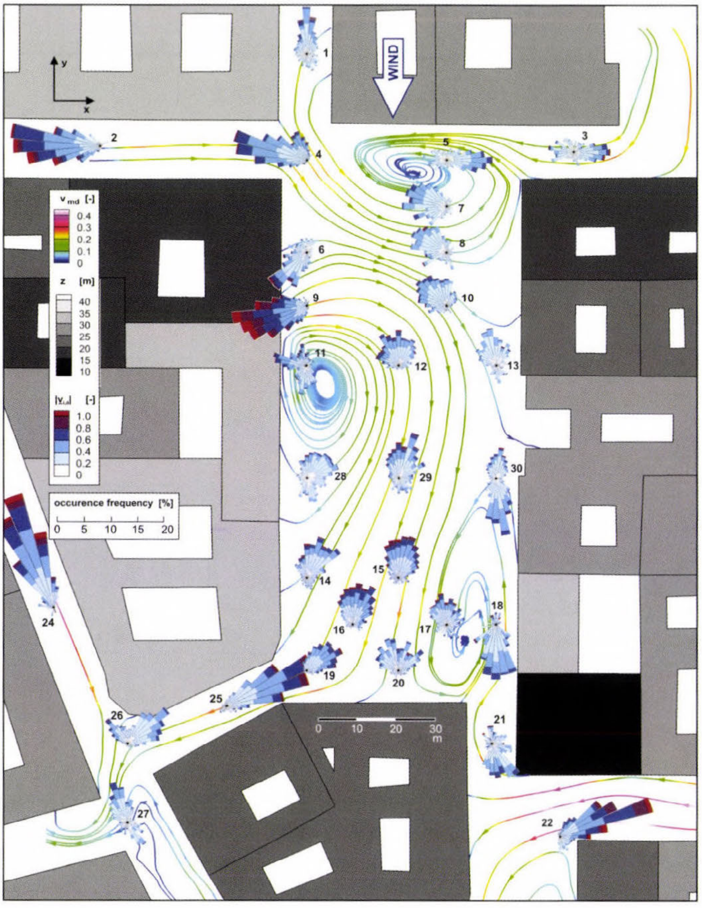

Fig. 14. Flow field and wind roses in the investigated area in northern wind direction at 0.5 *h* height. Streamlines are colored by normalized average velocity magnitude v_{md}, buildings by their full scale height, and wind roses by the magnitude of the instantaneous normalized wind vectors $\underline{v}_{i,d}$. Note that the two velocity scales are different. The wind roses show the occurrence frequency of 10-deg wind direction sectors.

It is important to point out that as opposed to the usual application of wind roses – representing annual wind statistics –, the current wind roses show the statistics of wind speed and direction at a single incident wind direction. The wind roses presented in *Fig. 14* can be organized into different groups based on their shape:

1. Wind roses with a single dominant wind direction and small deviations can be found in streets with one-directional flow (WR2, 24) channeled along the streets' main axis. Backflow (90–270 degree to the main wind direction) is negligible. While the average velocity magnitude is 0.3–0.4, wind velocities of larger than 1 (wind gusts) have also a significant probability.
2. Fan-tail shaped wind roses appear in several locations on the square, but not in the connecting streets (WR 7, 8, 10, 12, 14–16, 19, 20, 31). Obviously, far from walls which restrict perpendicular movements, velocities can fluctuate in all directions. Deviations of up to +/–90 degree from the main wind direction can occur; also, a low percentage of backflow can be seen.
3. Wind roses with more than one peak can be observed in streets (WR 3, 21, 26, 27). The double peaks mean that at a given wind direction, flow is coming once from one end of the street, once from the other end. WR 26, located in an intersection, shows peaks 90 degree to each other, which can be explained by the angle of the connecting streets.
4. Wind roses with more than one peak can be seen also near the core of vortices of the mean wind field (WR 5, 11, 21). This can be explained by the slight movement of the vortex core, meaning that the measurement location is once on one side, and once on the other side of the vortex core, thus flow direction is reversed.
5. Finally, points on the boundary of a vortex of the mean flow can have multiple peaks, again explained by the slight movement of the cores as in WR 30. Here, instantaneous velocity magnitude reaches 0.6, while average velocity is just 0.05.

Regarding the temporal sequence of velocity fluctuations, double peaks in the histogram of velocity time series recorded in location types 4 and 5 prove the periodic switching between wind directions. *Fig. 15* shows the continuous velocity histograms of the v_d stream-wise velocity component, as captured by the LDV system. The wind rose WR 15, classified as type 2 shows a more Gaussian-like distribution; in contrast to this, the type 5 wind rose WR 30 shows double peaks indicating periodic or mode-locking flow switching between a northern (positive v_d) and a southern (negative v_d) flow state. The consequences of such flow switching on pollutant dispersion are significant, see, e.g., the observations of *Klein et al.* (2011) made at smoke plume dispersion visualisations in urban environment.

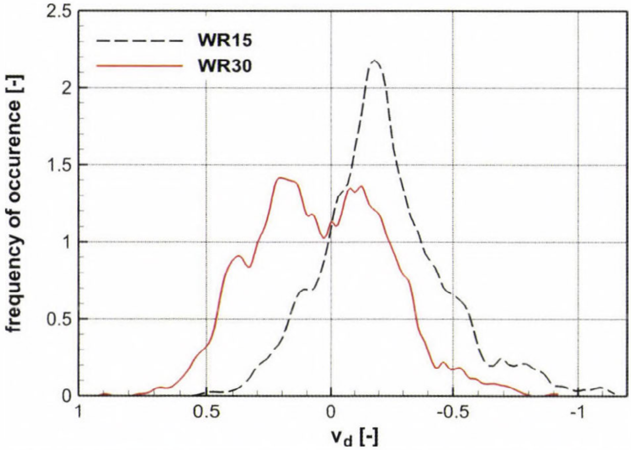

Fig. 15. Comparison of type 2 (WR 15) and type 5 (WR 30) wind velocity distributions (northern wind direction).

4.5. CFD results and their validation with the experimental data

The secondary objective of this paper is to show the applicability of a CFD RANS model, predominantly used in the regulatory and consulting field, in a complex urban environment. The model was able to resolve some, but not all of the flow structures dominating the square in question. The surface flow direction in the streets connected to the square is well predicted in four from five cases (see *Fig. 10*). Velocity magnitudes are qualitatively well predicted. More problems were experienced with turbulence: the prediction of K_d is often wrong, and does not give the model any information on the anisotropic and occasionally mode switching behavior of the flow discovered in Section 4.4, which has obvious consequences for dispersion phenomena, too.

In *Table 1,* hit rates of the CFD simulation are summarized. Hit rate q is defined as the percentage of those simulation data (prediction) which are inside an allowed range of the measurement (observation):

$$q = \frac{N}{n} = \frac{1}{n}\sum_{i=1}^{n} N_i \quad with \ N_i = \begin{cases} 1 \ for \ \left|\frac{P_i - O_i}{O_i}\right| \leq D \ or \ \left|P_i - O_i\right| \leq W \\ 0 \ else \end{cases}, \tag{7}$$

where P_i are the prediction (simulation) data, O_i are the observation (measurement) data, D is the allowed relative deviation, e.g. 25%, W – allowed absolute deviation or threshold, usually the measurement uncertainty of the observation.

Table 1. Hit rates calculated for the MISKAM simulations. Note that the velocity component parallel to the approach flow is v in northern wind and u in western wind direction

	Number of points	**Hit rate [%] for variable:**			
		u_d	v_d	v_{md}	K_d
Allowed relative dev. D [-]		0.25			
Allowed absolute dev. W [-]		0.026	0.026	0.03	0.006
Vertical profiles	601	36	76	74	9
Horizontal planes	1855	28	29	33	32

Hit rate calculations were performed for all vertical profiles and all horizontal planes separately, all together for 2456 measurement points, and for different variables. As it could be seen earlier in Section 4.1, vertical profiles of streamwise flow velocity above rooftop level agreed the best with the measurement (*Figs. 7* and *8*). Thus, their hit rates are accordingly high. Flow in horizontal planes is much more difficult to predict, and hit rates are generally lower on horizontal planes. Lateral flow velocity and turbulent kinetic energy were less well predicted than the streamwise velocity, and have consequently worse hit rates.

It must be noted that hit rates for calculations made by the same model, but for different test cases, might be significantly different: hit rate is also a measure for the difficulty of the test case, and not only for the performance of the model.

4.6. Comparison with fully built-up area

In the following, the CFD model is applied to answer questions regarding different urban planning scenarios. As mentioned already in the introduction, creating new urban squares by removal of defunct building blocks is often part of urban redevelopment programmes. The question is what the consequences of such a transformation on the ventilation of the whole area are. To create a reference case representing the situation before such a transformation, a numerical model was set up, in which the square was replaced by a building block consisting of four buildings of various height (23, 32, 26, and 29 m) as shown in *Fig. 16b*. CFD simulation results obtained with this geometry of a fully built-up area can then be compared with the ones with the existing square that represents the situation after the hypothetical redevelopment. Comparison is limited to the prevailing northern wind direction.

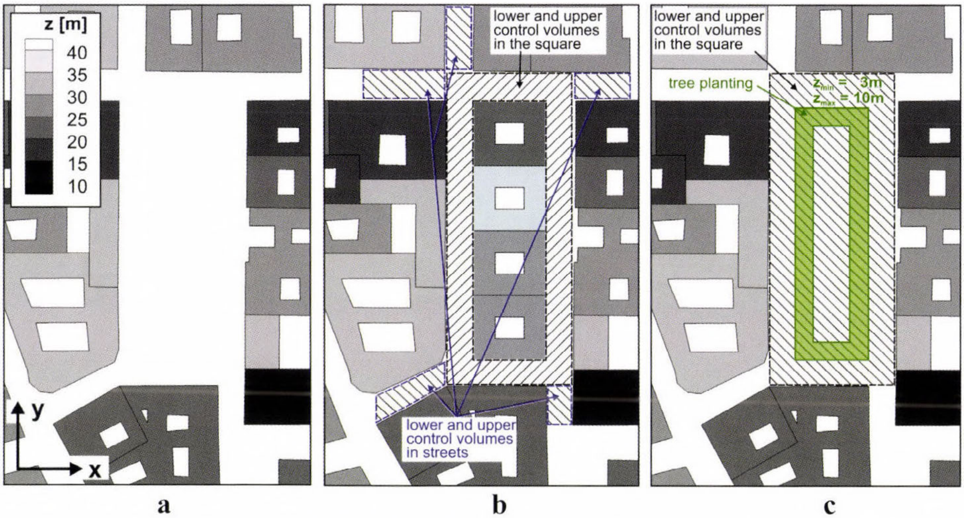

Fig. 16. (a) actual geometry of the square, (b) built-up area instead of the square representing a reference case *before* a hypothetical urban redevelopment programme; right: square with tree planting. Hatched areas with dashed borders show the control volumes used for averaging.

To perform a statistical analysis of the simulation results obtained, v_{md} and K_d are averaged for the control volume depicted in *Fig 16b* (hatched areas). The control volume consists of four parts: lower volumes from 0 to 0.5 h and upper volumes from 0.5 h to h height on the square itself and in the connecting streets, respectively.

In *Table 2,* the averaged variables are shown for the two cases and then the percent change Δv_{md} *[%]= [*v_{md} *(with square) -* v_{md} *(built-up area)] /* v_{md} *(built-up area)* is listed. Percent change of turbulent kinetic energy ΔK_d [%] is similarly defined.

The data in *Table 2* suggest that average wind speed on the square itself is overall increasing, but only by 2% when establishing a square compared with a fully built-in area. Such slight change consists of a significant increase of v_{md} above 0.5 h and a decrease of less extent below it. The average wind speed in the connecting streets increases dramatically upon removal of the central building block. At low level, below 0.5 h, the change is more than 50%. The comparison of turbulence from CFD results is in light of the discrepancies observed previously and is not fully to be trusted, nevertheless K_d in connecting streets is increasing, and on the square itself decreasing.

Table 2. Changes of average velocity magnitude and turbulent kinetic energy in the square and in connecting streets when comparing a built-up area and area with square. Δv_{md} [%]= [v_{md} (with square) – v_{md} (built-up area)] / v_{md} (built-up area), ΔK_d [%] similarly defined

	v_{md} built-up area	v_{md} area with square	Δv_{md} [%]	K_d built-up area	area with square	ΔK_d [%]
in the square						
below 0.5h	0.164	0.138	**–16%**	0.049	0.032	–35%
above 0.5h	0.251	0.285	**14%**	0.084	0.063	–25%
average from 0 to h	0.207	0.211	**2%**	0.066	0.047	–29%
in connecting streets						
below 0.5h	0.108	0.166	**54%**	0.036	0.047	30%
above 0.5h	0.145	0.184	**27%**	0.065	0.076	17%
average from 0 to h	0.126	0.175	**39%**	0.051	0.062	21%

4.7. *Influence of vegetation*

The increase of urban vegetation is seen undoubtedly as a positive measure to improve sustainability and human comfort in today's urban architecture. As in an urban square the flow is much less obstructed by buildings than in street canyons, thus we expect a remarkable influence of vegetation on flow velocities.

In the simplified model investigated in wind tunnel, the influence of vegetation has been neglected, although a proper method to model vegetation in wind tunnel tests has already been developed by *Gromke* (2011).

The CFD model MISKAM allows the modeling of vegetation using a porosity approach, as described by *Eichhorn* (2011) and validated by wind tunnel experiments by *Balczó et al.* (2009) and *Czáder et al.* (2009). The vegetation defined as a porous medium exerts an influence on the fluid flow by its viscous and form drag (*Gross,* 1993). The total drag force, e.g., in x coordinate direction, is described by the following formula:

$$F_{veg,x} = \rho\, c_{d0}\, b u |\underline{v}| \; , \tag{6}$$

where ρ is the fluid density [kg/m^3]; c_{d0} is the leaf drag coefficient [-]; b is the leaf area density (LAD), the projected leaf surface area per unit volume [m^2/m^3]. The obtained drag force is embedded in the RANS equation as a negative source. Furthermore, the effects of vegetation on the turbulence are also taken into account by extending the K-ε equations with new terms.

The tree planting's shape at the square (*Fig. 16*, right) is simplified: we study a homogeneous tree crown region of rectangular shape from 3 m to 10 m height and 8 m width. The centre of the region is empty, imitating a usual urban park with grass area in the middle. Leaf area density (LAD) throughout the crown region is assumed 1 m^2/m^3 based on the data of *Larcher* (2001), which is a typical value for urban tree plantings.

Table 3 summarizes the obtained results with tree planting and the comparison with the treeless case. Similarly to Section 4.6, v_{md} and K_d are averaged for two control volumes below and above 0.5 h. However, in this case the whole square is covered by the control volume (hatched area in *Fig. 16*, right). Decrease of velocity magnitude v_{md} by 21% below 0.5 h can be observed. Above 0.5 h the influence is negligible. The same can be said as regards turbulent kinetic energy, the value in the square is decreased by 27% below 0.5 h height. The change of K_d is also detectable above 0.5 h (–5%).

Table 3. Influence of tree plantings as determined by CFD simulations

	v_{md} **without trees**	v_{md} **with trees**	Δv_{md} [%]	K_d **without trees**	**with trees**	ΔK [%]
below 0.5 h	0.138	0.108	–21%	0.032	0.023	–27%
above 0.5 h	0.285	0.281	–1%	0.063	0.059	–5%
average from 0 to h	0.211	0.195	–8%	0.047	0.041	–13%

Looking at flow field plots of the CFD simulation with tree planting (not shown here), some further observations could be made: velocity decreases up to 30% inside the tree crowns. In some locations outside the crown region, the flow accelerated slightly, due to displacement effect of the trees. K_d is decreasing not only in the control volume, but also in the connecting streets, up to 30 m distance from the square. These preliminary findings fit well the observations made by *Gromke* and *Ruck* (2009) and *Balczó et al.* (2009) about the influence of vegetation in a street canyon, although a more detailed analysis might reveal further details.

5. Conclusions

The urban square investigated, although slightly simplified in geometry, can be seen as a test case of high complexity level, similarly to real urban areas. Despite this fact, the results allow more generalized conclusions to be made, which can be valid for squares of similar size:

- Average pedestrian level wind speed on the square, while significantly smaller than the above rooftop wind speed, is varying with wind direction strongly between normalized values of 0.1 and 0.5. Wind gusts can be higher than the average wind speed at rooftop level on a few locations.
- The exact location of high-speed spots in the square near the ground depends on wind direction, but is usually near building corners and at the mouth of connecting streets.
- The square influences flow in the connecting streets as well. Flow is induced in these by the developing flow structures in the square even in perpendicular or opposite direction to the approach wind. CFD results suggest that wind speed can increase up to 50% in the connecting street compared to a case in which no square is present.
- In both investigated wind directions, distinct and complex flow fields were observed, as a result of superposition of flow advection, corner vortices, separation bubbles, street canyon, and horseshoe vortices. These average flow fields are supposed to have major influence on wind comfort of pedestrians and the dispersion of pollutants, the latter of which is an objective of future studies on the square.
- For the study of flow unsteadiness, the representation of two-dimensional time-resolved data in the form of wind roses (polar area diagrams) placed over the average flow field proved to be a useful tool. Wind roses could be classified according to their shape to identify the spots, where turbulence is non-isotropic and/or flow direction is alternating.
- Tree plantings in the square are decreasing wind velocity and turbulence in the square affecting mainly the lower half of the square, where the tree crowns are located. However, turbulence changes have further reaching influence in the upper half of the square and in connecting streets, too.

We applied the MISKAM microscale flow model to the case geometry. The estimation of the measured flow field is reasonable, when average velocity magnitude comes into question. Despite the large difference in the incoming turbulence, K_d is only underpredicted by about one third on average.
However, there are certain non-negligible flaws of the simulation, like smaller or fully suppressed vortices in the mean flow field on the square. These errors can

be traced back to the commonly known turbulent kinetic energy overprediction of K-ε type closures in stagnation points.
The flow intermittency effects not resolved by MISKAM are originated from the steady RANS approach used by this class of models. As, e.g., *Letzel et al.* (2008), *Nakayama et al.* (2014) have shown, large eddy simulation (LES) applied in an urban environment can give superior results in this regard, although at the cost of much higher computational time and power requirements, which are mostly unavailable at the moment among the users of CFD models in the regulatory / urban planning field.

Recommendations for urban planning

The implications of our observations on urban planning are manifold. The flow structures in an urban square result from incoming and outgoing flow through the connecting streets. As observed, even a single gap in a building block or a lower building can modify the flow field significantly in the square. Thus, measures of local governments like permission to raise buildings to uniform height around the square will influence the flow field in the vicinity.

When establishing a new urban square in a fully built-up area, an overall increase of wind speed in neighboring streets can be expected, which will increase ventilation of the area. While this is an advantage, the high speed spots observed near the corners of connecting streets in the square might be less welcome and can cause human discomfort. However, as vegetation can decrease wind speeds locally, planting of trees on proper locations can help avoiding too high local wind speeds.

An urban (re)development project, such as establishing a new square, or the building or replacement of buildings in an urban neighborhood can be optimized using CFD tools like the MISKAM model used in this paper. One can find the optimal building configuration or the best tree planting patterns, hence the outcome of such a project can be improved in respect of quality of living.

Acknowledgements: The scientific work presented in this article was supported by the projects K108936 "Flow and dispersion phenomena in urban environment" of the Hungarian Scientific Research Fund and the New Széchenyi Plan project TÁMOP-4.2.1/B-09/1/KMR-2010-0002 "Development of quality-oriented and harmonized R+D+I strategy and functional model at BME".

LIST OF SYMBOLS

Name	unit	definition
b	m^2/m^3	leaf area density (LAD): projected leaf surface area per unit volume
c_{d0}	-	leaf drag coefficient
d_0	m	displacement height
$F_{veg,x}$	N/m^3	drag force from vegetation in x coordinate direction
h	m	average building height
I_u , I_v , I_w	-	turbulence intensity in x, y, and z direction
K	m^2/s^2	turbulent kinetic energy
K_d	-	dimensionless turbulent kinetic energy
$L_{u,x}$	m	integral length scale of turbulence in x direction
q	%	hit rate
u, v, w	m/s	velocity components in x, y, and z direction
$\bar{u}$, $\bar{v}$, $\bar{w}$	m/s	averaged velocity components in x, y, and z direction
u_{ref}	m/s	reference wind speed
u_d, v_d, w_d	-	dimensionless wind velocity x, y, and z direction
$\underline{v}$	m/s	flow velocity vector
$\underline{v}_{hor\ d}$	-	dimensionless velocity vector in horizontal (xy) plane
v_{md}	-	dimensionless velocity magnitude in horizontal direction
z_{ref}	m	reference height (height of the modelled boundary layer)
Δv_{md}	-	difference of dimensionless velocity magnitude between two cases
Δv_{md} [%]	-	percent difference of dimensionless velocity magnitude between two cases
ρ	kg/m^3	fluid density
σ_u, σ_v, σ_w	m/s	standard deviation of velocity in x, y, and z direction
σ_{ud}, σ_{vd}, σ_{wd}	-	dimensionless standard deviation of velocity in x, y, and z direction

References

Ahmad, K., Khare, M., and *Chaudhry, K.,* 2005: Wind tunnel simulation studies on dispersion at urban street canyons and intersections - a review. *J. Wind Engin. Indust. Aerodynam. 93*, 697–717.

Balczó, M., Balogh, M., Goricsán, I., Nagel, T., Suda, J. M., and *Lajos, T.,* 2011: Air quality around motorway tunnels in complex terrain – Computational Fluid Dynamics modeling and comparison to wind tunnel data. *Időjárás 115,* 179–204.

Balczó, M. and *Eichhorn, J.,* 2009: Refined MISKAM simulations of the Mock Urban Setting Test. Proceedings of the XXIII. MicroCAD International Scientific Conference, Miskolc, Hungary, 19–20 March 2009, 7–12.

Balczó, M., Gromke, C., and *Ruck, B.,* 2009: Numerical modeling of flow and pollutant dispersion in street canyons with tree planting. *Meteorol. Z.18,* 197–206.

Balczó, M. and *Lajos, T.,* 2012: Active reduction of air pollutant concentrations at an urban square. Proceedings of the 8th International Conference on Urban Climate (ICUC 8), Dublin, Ireland, August 6-10, 2012.

Bastigkeit, I., 2011: Erzeugung von Validierungsdaten für wirbelauflösende mikroskalige Strömungs- und Ausbreitungsmodelle. PhD thesis, University of Hamburg.

Belalcazar, L.C., Clappier, A., Blond, N., Flassak, T., and *Eichhorn, J.*, 2010: An evaluation to the estimation of road traffic emission factors from tracer studies. *Atmos. Environ. 44,* 3814–3822

Belcher, S.E., Coceal, O., Hunt, J.C.R., Carruthers, D.J., and *Robins, A.G.*, 2013: Atmospheric Dispersion Modelling Liaison Committee Report: ADMLC-R7 Annex B: A review of urban dispersion modelling

Benson, J., Ziehn, T., Dixon, N.S., and *Tomlin, A.S.*, 2007: Global sensitivity analysis of a 3D street canyon model - Part II: Application and physical insight using sensitivity analysis, *Atmos.Environ.42,* 1874–1891.

Blocken B. ,2014: 50 years of computational wind engineering: past, present and future. *Journal of Wind Engin. Indust. Aerodynam. 129,* 69–102.

Britter, R.E. and *Hanna, S.R.*, 2003: Flow and dispersion in urban areas. *Ann. Rev. Fluid Mechanics 35*, 469–496.

Czáder, K., Balczó, M., and *Eichhorn, J.*, 2009: Modelling of flow and dispersion in a street canyon with vegetation by means of numerical simulation. Proceedings of the XXIII. MicroCAD International Scientific Conference, Miskolc, Hungary, 19-20 March 2009, 47–52.

Donnelly, R.P., Lyons, T.J., and *Flassak, T.*, 2009: Evaluation of results of a numerical simulation of dispersion in an idealised urban area for emergency response modelling. *Atmos. Environ.43,* 4416–4423.

Eichhorn, J., 2011: MISKAM - Manual for version 6, Giese-Eichorn, Wackernheim, Germany

Eichhorn, J. and *Kniffka, A.*, 2010: The numerical flow model MISKAM: State of development and evaluation of the basic version. *Meteorol. Z. 19,* 81–90.

Eichhorn, J., Schrodin, R., and *Zdunkowski, W.*, 1988: Three-dimensional numerical simulations of the urban climate. *Beit. Physik Atmosphäre 61,* 187–203.

ESDU, 1972: Characteristics of wind speed in the lower layers of the atmosphere near the ground: strong winds (neutral atmosphere). Engineering Sciences Data Unit 72026

ESDU, 2001: Characteristics of atmospheric turbulence near the ground Part II: single point data for strong winds (neutral atmosphere). Engineering Sciences Data Unit 85020

Flassak, T., Janicke, U., and *Ketzel, M.*, 2010: Comparison of ground-level centreline concentrations calculated with the models OML, AERMOD/PRIME, MISKAM and AUSTAL2000 against the Thompson wind tunnel data set for simple stack-building configurations. 13th International Conference on Harmonisation within Atmospheric Dispersion Modelling for Regulatory Purposes, Paris, 1.-4. June 2010. Paper No. 163.

Franke, J., Hellsten, A., Schlünzen, H., and *Carissimo, B.*, 2007: Best practice guideline for the CFD simulation of flows in the urban environment. COST Office, Brussel

Gadilhe, A., Janvier, L., and *Barnaud, G.*, 1993: Numerical and experimental modelling of the three-dimensional turbulent wind flow through an urban square. *J. Wind Engin. Industrial Aerodynam. 46–47,* 755–763.

Goricsán, I., Balczó, M., Balogh, M., Czáder, K., Rákai, A., and *Tonkó, Cs.*, 2011: Simulation of flow in an idealised city using various CFD codes. *Int. J. Environ. Poll. 44,* 359–367.

Gromke, C. and *Ruck, B.*, 2005: Die Simulation atmosphärischer Grenzschichten in Windkanälen. Proc. 13. GALA Fachtagung: "Lasermethoden in der Strömungsmesstechnik", 6 – 8 September 2005, BTU Cottbus.

Gromke, C. and *Ruck, B.*, 2009: On the impact of trees on dispersion processes of traffic emissions in street canyons. *Bound-Lay. Meteorol. 131,* 19–34.

Gromke, C., 2011: A vegetation modeling concept for Building and Environmental Aerodynamics wind tunnel tests and its application in pollutant dispersion studies, *Environ. Pollut. 159*, 2094–2099.

Gross, G., 1993: Numerical Simulation of Canopy Flows. Springer Verlag.

Hertwig, D., Efthimiou, G.C., Bartzis, J.G., and *Leitl, B.*, 2012: CFD-RANS model validation of turbulent flow in a semi-idealized urban canopy. *J.Wind Engin. Indust. Aerodynam. 111,* 61–72.

Kato, M. and *Launder, B.*, 1993: The modelling of turbulent flow around stationary and vibrating square cylinders. Ninth Symposium on Turbulent Shear Flows, Kyoto, Japan, August 1993, 10.4.1–10.4.6.

Klein, P., Leitl, B., and *Schatzmann, M.*, 2011: Concentration fluctuations in a downtown urban area. Part II: analysis of Joint Urban 2003 wind-tunnel measurements. *Environ. Fluid Mech. 11,* 43–60.

Kozmar, H., 2011: Wind-tunnel simulations of the suburban ABL and comparison with international standards. *Wind Structures 14,* 15–34

Larcher, W., 2001: Ökophysiologie der Pflanzen. Stuttgart, Verlag Eugen Ulmer.

Letzel, M.O., Krane, M., and *Raasch, S.*, 2008: High resolution urban large-eddy simulation studies from street canyon to neighbourhood scale. *Atmos. Environ. 42,* 8770–8784.

Letzel, M.O., Flassak, T., and *Angel D.*, 2012: Verbesserung der AUSTAL2000-Ergebnisse durch Strömungs- und Turbulenzübernahme aus MISKAM. Gefahrstoffe Reinhaltung der Luft 72, Juli/August 2012, 329–333.

Leuzzi, G., Balczó, M., Amicarelli, A., Monti, P., Eichhorn, J., and *Thomson, D.J.*, 2010: Street canyon concentration estimation coupling the RANS model MISKAM and the micromixing Lagrangian model LAGFLUM. Proceedings of the 13th International Conference on Harmonization within Atmospheric Dispersion Modelling for Regulatory Purposes (HARMO13), Paris, France, June 1-4, 2010. 821–825.

Nakayama, H., Leitl, B., Harms, F., and *Nagai, H.*, 2014: Development of local-scale high-resolution atmospheric dispersion model using large-eddy simulation. Part 4: turbulent flows and plume dispersion in an actual urban area. *J. Nuclear Sci. Technol. 51,* 626–638

Olesen, H., Baklanov, A., Bartzis, J., Barmpas, F., Berkowicz, R., Brzozowski, R., Buccolieri, R., Carissimo, B., Costa, A., Di Sabatino, S., Efthimiou, G., Franke, J., Goricsán, I., Hellsten, A., Ketzel, M., Leitl, B., Nuterman, R., Polreich, E., and *Tavares, R.*, 2008: The MUST model evaluation exercise: Patterns in model performance. *Croatian Meteorolog. J. 43,* 403–408.

Olesen, H.R., Berkowicz, R.L, Ketzel, M., and *Løfstrøm, P.*, 2009: Validation of OML, AERMOD/PRIME and MISKAM using the Thompson wind tunnel data set for simple stack-building configurations. *Bound-Lay. Meteorol. 131,* 73–83.

Parra, M., Santiago, J., Martín, F., Martilli, A., and *Santamaría, J.*, 2010: A methodology to urban air quality assessment during large time periods of winter using computational fluid dynamic models. *Atmos. Environ. 44,* 2089–2097.

Rákai, A., and *Kristóf, G.*, 2013: Microscale Obstacle Resolving Air Quality model evaluation with the Michelstadt case. *The Scientific World Journal 2013,* Article ID 78174

Schatzmann, M., Olesen, H.R., and *Franke, J.*, 2010: COST 732 Model Evaluation Case Studies: Approach and Results. Brussels, COST Office.

VDI, 2004: VDI 3738 Part 12. Environmental meteorology - Physical modelling of flow and dispersion processes in the atmospheric boundary layer. Application of wind tunnels. VDI Commission for Air Quality Management, Düsseldorf.

VDI, 2005: *VDI 3783, Blatt 9: Environmental meteorology - Prognostic microscale windfield models - Evaluation for flow around buildings and obstacles.* VDI Commission for Air Quality Management, Düsseldorf.

IDŐJÁRÁS

Quarterly Journal of the Hungarian Meteorological Service
Vol. 120, No. 2, April – June, 2016, pp. 231–254

Implementation and validation of a bulk microphysical model of moisture transport in a pressure based CFD solver

Norbert Rácz* and **Gergely Kristóf**

Department of Fluid Mechanics,
Budapest University of Technology and Economics (BME),
Bertalan L. u. 4-6, H-1111 Budapest, Hungary
E-mails: racz@ara.bme.hu; kristof@ara.bme.hu

**Corresponding author*

(Manuscript received in final form Auguszt 6, 2015)

Abstract—We study wet cooling tower plume formation involving mesoscale meteorological effects (such as stratification or compressibility). This was achieved by incorporating transformations and volume source terms into a pressure based computational fluid dynamics (CFD) solver (ANSYS-FLUENT). Moisture dynamics is taken into account with a bulk microphysical model that was recently implemented into the solver.

This model has been validated against known numerical solutions of idealized two-dimensional dry and wet thermals. In particular, the overall thermal profile and the liquid water concentration field indicated good model performance. Model performance has also been compared with measurements for the formation of a large wet cooling tower plume. Simulations are encouraging with regard to the predictability of cumulus like plume structures with complex thermal stratification, the overall liquid water content along the plume axis, and also the turbulent fluctuations caused by the vertical movements in the plume.

The advantage of this approach is that a uniform physical description can be used for close- and far-field flow by using a single unstructured mesh with local refinements. This allows for investigating the finely structured microscale flow phenomena around complex orographic features in a single framework.

Key-words: humidity transport, wet adiabatic processes, phase change, rising thermal, wet cooling tower plume

1. Introduction

A clear trend can be seen in the development of mesoscale meteorological codes towards the usage of higher resolution numerical models incorporating multiple physical effects in order to better describe the atmosphere, give higher resolution models for urban environments, or give higher fidelity forecasting. This is well reflected in the "urbanization" of mesoscale meteorological models (*Yamada*, 2003; *Otte et al.*, 2004; *Ooka et al.*, 2010), where microscale physical effects are introduced.

Another approach for multi-scale modeling is when computational fluid dynamical (CFD) solvers are adapted to handle mesoscale effects. The purpose of this paper is to enhance the latter approach.

General purpose CFD solvers are already widely used in modeling the ventilation of urban areas (*Mochida et al.*, 1997; *Balczó et al.*, 2011; *Kristóf* and *Balogh*, 2010). These solvers are capable of handling complex topography, buildings and have a wide variety of turbulence and physical models, effective numerical techniques, and parallelization.

In order to handle mesoscale effects in a general purpose CFD solver, we have recently developed a method (*Kristóf et al.*, 2009). The atmospheric stratification, the Coriolis force, and baroclinicity are taken into account by using simple (scale and shift) transformations of state variables (pressure, density, temperature), vertical velocity, and altitude, and including additional source terms in the conservation equations. The model was successfully validated (*Kristóf et al.*, 2009). Further simulations by *Rácz et al.* (2013) were performed around more complex geometrical features, idealized barriers, and real terrain, demonstrating the capabilities of this CFD based approach.

The contribution of this paper is to extend our original 2009 model with a proper moisture (humidity transport and phase change) model. We validate this extended model with numerical solutions of idealized two-dimensional dry and wet thermals and experimental data for a full-scale three-dimensional wet cooling tower plume formation with different environmental stratifications.

Several researchers investigated the behavior of cooling tower plumes from different aspects in the past decades. Wet cooling towers are widely used in the power generation industry, since it is relative easy to build and cheap to operate especially in regions where limited water resources are available for cooling purposes (*Al-Waked* and *Behnia*, 2006).

Most of the earlier studies are from the early 1970s related to the design, construction, and operation of nuclear and coal fired power plants. The performance of cooling towers is an important topic as the energy demand is growing. Few percent increase in overall efficiency in power generation could lead to high amount of total energy savings. Therefore, number of researches investigated the effect of changes in environmental conditions to the tower performance. *Al-Waked* and *Behnia* (2006) and *Lohasz* and *Csaba* (2012) studied the effects of crosswind, *Kloppers* and *Kröger* (2005), *Overcamp* and *Hoult* (1971), *Barber et al.* (1974) studied temperature and humidity inversion and other parameters with CFD methods under different operating conditions. These effects are important since they could lower the efficiency of cooling towers (*Wei et al.*, 1995).

The visibility was not a great concern at that time, instead the plume rise of dry and wet plumes were investigated (*Hanna*, 1972; *Weil*, 1974). Wet cooling towers, however, do not have much control over the visible plume. (*Tyagi et al.*, 2012) The exhaust of the tower is generally saturated, and during certain weather conditions, it cannot be absorbed completely by the surrounding air. As a result, it will appear as fog and visible to human eye.

Another important aspect regarding wet cooling tower operation is the prevention of the growth of legionella bacteria in the cooling water. The various legionella species are the cause of Legionnaires' disease in humans, and the transmission is via the exposure to aerosols. The bacteria could live and travel hundreds of meters or even kilometers from the source (*Greig et al.*, 2004) .

Nowadays, environmental impacts are becoming more and more important concentrating not only on toxic materials but also on the visibility of water vapor plumes. The reduction of visibility conditions, the local reduction of solar radiation, and the interaction with low level clouds, in particular the fog, are in concern nowadays. The latest literature review about cooling towers shows different options for reducing and manipulating the visible plume using hybrid cooling towers, wet–dry cooling towers, dry cooling towers, and so on, depending on the need and demand. The formation of a visible water vapor plume is directly related to the water mass fraction, temperature, exhaust velocity of the tower, and also ambient meteorological conditions. In more recent studies, *Wang et al.* (2007), *Xu et al.* (2008) and *Wang et al.* (2009) investigated the control and abatement of plumes emitted by large commercial buildings by reheating the exhaust with heat pumps or solar collectors. *Sturman* and *Zawar-Reza* (2011) predicted the yearly visibility of a stack plume of a planned industrial site with an atmospheric mesoscale pollution model (TAPM) by providing boundary conditions from the meteorological code. *Presotto et al.* (2005) investigated the possibility of reducing the plume visibility by lowering the exit temperature of a petrochemical refinery.

There is usually no contaminant involved, but there is a risk of the plume's material returning to the ground level causing local fogging, ice formation, or entrainment of saturated air into other adjacent towers. *Mokhtarzadeh-Dehghan et al.* (2006) and *Spillane* and *Elsum* (1983) investigated the occurrence of rain and fog and the possibility of plum blow-out by strong winds. Their investigation showed that the fog can extend to the ground in cases, where the plume interacts with the wake of the tower and the ambient temperature is very low.

Number of researchers worked on the effect of drift deposition as it could be objectionable due to human health hazards. Their purpose was to investigate the effects of ambient conditions and absolute humidity, droplet output temperature, and the affected area (*Lucas et al.*, 2010). Drift of small water droplets from mechanical and natural draft cooling towers can contain salt particles, water treatment chemicals, and bacteria. *Meroney* (2006) recommends a CFD protocol to correct drift and deposition predictions provided by current analytic models to take into account building effects.

Wet cooling tower plumes can also play a role in the formation of different kinds of hydrometeors. *Campistron* (1987) and *Huff* (1972) studied snowfalls caused by cooling towers and they found that the rate of precipitation can even be enhanced by a factor of two.

The increasing computational power makes the CFD based approach more and more affordable. Several investigations showed that CFD models are valid in predicting the flow field, performance, or drift deposition predictions of micro scale flow around cooling towers (*Balczó et al.*, 2011; *Kristóf and Balogh*, 2010; *Meroney*, 2006). We have successfully extended the capabilities of CFD solvers (*Kristóf et al.*, 2009; *Rácz et al.*, 2013) in order to simulate atmospheric scale flows. In this paper, a further enhanced model version will be shown that is capable of predicting moist dynamics through the implementation of condensation and phase change models.

In the next chapter, an overview will be given about the existing tools for modeling plume dispersion and about their advantages and limitations, a short description of the mesoscale model extension that we have recently validated, and more details on the further developed model version that also takes into account moist dynamics. In the third and fourth chapters, the model validation will be shown against calculations with meteorological codes and field measurements followed by the conclusions.

2. Mathematical model

Theories for describing the heat, mass, and momentum transfer inside natural draft cooling towers have long been established by authors in the early 1900s. These works (*Lewis*, 1922; *Robinson*, 1923) include also heat transfer due to vaporization, and therefore, they are applicable to the prediction of wet tower performance. These analysis and simplifications are still in use today, and several numerical models have been developed based on this study in order to describe transfer processes inside cooling towers (*Al-Waked and Behnia*, 2006).

Wide range of model complexity can be found in the literature regarding the modeling of plume formation outside of the tower. These models include simpler algebraic models towards more complex integral models, atmospheric dispersion models, or CFD based approaches. Commonly used plume models are based on conservation equations describing the entrainment processes of ambient air along the plume axis.

Several authors (*Hanna*, 1976; *Hanna et al.*, 1982) studied the dynamics of plume motion and developed numerical models. *Slawson and Csanady* (1967), *Wigley and Slawson* (1971), and *Csanady* (1973) identified three phases, the initial, intermediate, and final phases of plume rise. They developed a rise model for jets that is also applicable to ambient conditions with stable stratification.

Widely used models, e.g., the analytical models of *Briggs* (1975, 1984) and *Weil* (1974) describe reasonably well the first phase of plume rise near the source, however, they are valid only for constant density gradient and wind speed (*Briggs*, 1984). With the detrainment concept of *Netterville* (1990), the transitional region and the leveling can also be described. *Davidson* (1989, 1994) developed a formulation that is able to predict both plume rise and dilution.

The entrainment is often modeled by using different empirical coefficients (*Schatzmann and Policastro*, 1984). One reason of difference between model results of different formulations is due to the differences in empirical coefficients applied to obtain the analytic solution.

Early models did not account for phase change of water during the plume development and neglect the effect of turbulence to the entrainment. *Gangoiti et al.* (1997) and *Janicke and Janicke* (2001) have developed Gaussian dispersion type models that included prediction of condensation and are also applicable to complex wind fields. Condensation and evaporation of droplets is important, since it changes buoyancy by introducing and removing latent heat during the rise and leveling. The lack of plume condensation causes the underestimation of plume rise in simpler models.

Another usual limitation is the improper handling of the complex atmospheric stratification and wind fields. Simplifications often assume winds depending only on the height above the ground, or constant wind speed and direction along the plume axis. In the case of complex input meteorological conditions data are often extrapolated from nearby meteorological stations to represent ambient conditions at the source. However, this causes accuracy problems (*Presotto et al.*, 2005). Simpler models could give good results in certain conditions when the lower few 100 meters of the atmosphere is linearly stratified. However, in the cases of high exhaust temperatures, the plume can penetrate deeply into the atmosphere crossing different layers with different lapse rates. This is typical for stack plumes of wet scrubbers with high exhaust temperatures.

The proper estimation of plume rise height is especially important when the deposition of plume particles or ground level concentration is to be calculated. *Policastro et al.* (1978) compared drift deposition models to experimental data and found that the existing models did not perform well.

The formulation of *Briggs* (1984) extended with empirical coefficients for plume trajectory are in use in environmental protection regulatory models (*Gangoiti et al.*, 1997). For short-range transport, the modifications to the EPA

Point, Area Line Source Algorithm (PAL2.1), the EPA Industrial Source 5 Complex Short Distance 3 (ISCST3) model, and the Argonne National Laboratory Seasonal/Annual Cooling Tower Impact (SACTI) model ((*Carhart and Policastro*, 1991; *Policastro et al.*, 1994) are used. Some of the limitations described above were addressed later in the development of ISC-PRIME and AERMOD-PRIME models in order to replace ISC3 series models ((*Schulman et al.*, 1997; *Petersen*, 2004)). The current trend in modeling for urban air pollution is focused on the improvement of advection in atmospheric dispersion models (atmospheric dispersion models TAPM, Ausplume, and CALPUFF (*Brown and Fletcher*, 2005)) and integrating them with local scale models (see, e.g., the EUROTRAC-2 subproject SATURN; (*Moussiopoulos*, 2010)). These models are currently accepted by regulatory authorities.

In the last decade, new generation of Gaussian dispersion models were introduced with a better description of real physical processes in the atmospheric boundary layer. Examples are the Danish OML model (*Olesen et al.*, 2007), or the British UK-ADMS model (*Carruthers* and *McHugh*, 2009). These often contain integrated systems for different purposes: street canyon models, Gaussian plume models, Eulerian grid models and dispersion model. These model families could give reasonable results in the far field, however, it could give under or overestimation by a factor of two when complex topography and buildings are considered and near filed concentration is a concern (*Mcalpine* and *Ruby*, 2004; *Olesen et al.*, 2007).

CFD based tools have also been used recently to assess plume visibility (*Brown* and *Fletcher*, 2005). Current CFD models however have limited capabilities. They were mostly used to investigate the wind field under steady state conditions, not representing the spatial and temporal variability of the meteorological fields especially around complex terrain (as recognized by *Brown and Fletcher* (2005). They often include assumptions for the vertical atmospheric profiles that do not reflect real conditions (as cautioned by *Presotto et al.* (2005)), and frequently exclude effects of surface vegetation and soil. These issues have been addressed by introducing the transformation method described in (*Kristóf et al.*, 2009; *Rácz et al.*, 2013) and (*Kristóf* and *Balogh*, 2010).

Using the commercial CFD tool ANSYS-FLUENT, continuity, momentum and energy equations are solved based on the finite volume method in an unsteady conservative form. Through user defined functions (UDF), the user can modify the governing equations of the CFD code by adding appropriate source/sink terms to the governing equations (Eqs. (1)–(6)). The current adaptation method can also be implemented in other CFD solvers having UDF capabilities such as ANSYS-CFX, StarCD, or the open source solver Openfoam.

$$\nabla \cdot \tilde{v} = 0\,, \tag{1}$$

$$\frac{\partial}{\partial t}(\rho_0 \tilde{\mathbf{v}}) + \nabla \cdot (\rho_0\, \tilde{\mathbf{v}} \otimes \tilde{\mathbf{v}}) = -\nabla \tilde{p} + \nabla \cdot \boldsymbol{\tau} + (\tilde{\rho} - \rho_0)\mathbf{g} + \mathbf{F} \quad , \tag{2}$$

$$\frac{\partial}{\partial t}\left(\rho_0 c_p \tilde{T}\right) + \nabla \cdot \left(\tilde{v}\, \rho_0\, c_p \tilde{T}\right) = \nabla \cdot \left(K_t \nabla \tilde{T}\right) + S_T \,, \tag{3}$$

$$\frac{\partial}{\partial t}(\rho_0\, k) + \nabla \cdot (\rho_0\, \tilde{v}\, k) = \nabla \cdot \left(\frac{\mu_t}{\sigma_k} \nabla k\right) + G_k + G_b - \rho_0\, \varepsilon + S_k \,, \tag{4}$$

$$\frac{\partial}{\partial t}(\rho_0\, \varepsilon) + \nabla \cdot (\rho_0\, \tilde{v}\, \varepsilon) = \nabla \cdot \left(\frac{\mu_t}{\sigma_\varepsilon} \nabla \varepsilon\right) + \rho_0\, C_1\, S\, \varepsilon - \rho_0\, C_{2\varepsilon} \frac{\varepsilon^2}{k + \sqrt{\nu\, \varepsilon}} + C_{1\varepsilon} \frac{\varepsilon}{k} C_{3\varepsilon} G_b + S_\varepsilon \,, \tag{5}$$

$$\tilde{\rho} = \rho_0 - \rho_0\, \beta\left(\tilde{T} - T_0\right). \tag{6}$$

In the equation system $\tilde{v}, \tilde{p}, \tilde{\rho}, \tilde{T}$ are the transformed field variables of velocity, pressure, density, and temperature. c_p and β are the specific heat capacity of dry air at constant pressure and the thermal expansion coefficient. From the velocity vector ($\tilde{v} = u\, i + v\, j + \tilde{w}\, k$) only the vertical component was affected by the transformation. τ contains the viscous and turbulent stresses, $g = -g\, k$ is the gravitational force per unit, mass and $g = 9.81\,[\mathrm{N\ kg^{-1}}]$. Turbulent transport is modeled by the realizable k–ε turbulence model with full buoyancy effects (Eqs. (4) – (5)) developed by *Shih et al.* (1994), where σ_k and σ_ε are the turbulent Prandtl numbers for k and ε, respectively. The turbulent viscosity μ_t and the turbulent heat conduction coefficient K_t are evaluated on the basis of turbulence kinetic energy (k) and dissipation rate (ε) fields. The constant values of $C_{1\varepsilon}$, $C_{2\varepsilon}$, the expressions of C_1 and $C_{3\varepsilon}$, the turbulence production and buoyancy terms G_k and G_b, and the modulus of mean rate-of-strain tensor (S) can be referred either from CFD literature (*Shih et al.*, 1994) or from software documentation (*ANSYS Inc.*, 2013). r_0 and T_0 are reference (sea level) values of density and temperature. Volume sources, responsible for the handling of mesoscale effects, S_T, S_k, and S_ε in Eqs. (3) – (5), as well as vector $F = S_u\, i + S_v\, j + S_w\, k$ in Eq. (2), are functions of local values of field variables. The components of the Coriolis force are included in **F** through S_u, S_v, *and* S_w.

The interested reader is referred to (*Kristóf et al.*, 2009) and (*Rácz et al.*, 2013) where a full description and validation cases of the transformation method can be found, therefore, further details regarding the basic equations are not given here.

Several authors treated moisture by means of various warm cloud microphysical models of different complexity. These approaches range from simple single-moment (*Kessler*, 1969) and two-moment (*Ziegler*, 1985; *Cohard* and *Pinty*, 2000; *Morrison et al.*, 2005) bulk parameterizations to more complex bin microphysics schemes (*Feingold et al.*, 1994; *Kogan*, 1991; *Ackerman et al.*, 2004). Typically in bulk microphysics, the liquid water is separated into two categories: non-precipitable cloud water and precipitable rain water (*Kessler*, 1969).

2.1. Transport equations

The extended commercial CFD solver we used is essentially closed source, but it is allowed to setup and use arbitrary number of passive scalar equations during the solution. Therefore, in order to describe the phase change, three additional scalar equations (Eqs. (7) – (9)) were considered for the number concentration of cloud condensation nuclei n_{CCN} (in order to track CCN depletion and entrainment effects, where subscript CCN refers to cloud condensation nuclei) and the number of condensed water droplets N_c together with total water content of air q_t. Rain water is currently neglected, since condensation will determine the growth of drops smaller than about 20 μm and no larger droplets are expected during the initial rise of a thermal or during the cooling tower plume rise.

$$\frac{\partial \rho n_{CCN}}{\partial t}+\frac{\partial}{\partial x_i}\left(\rho u_i n_{CCN}-\Gamma\frac{\partial n_{CCN}}{\partial x_i}\right)=\left(S_{n_{CCN}}\right)_{act}+\left(S_{n_{CCN}}\right)_{evap}+\left(S_{n_{CCN}}\right)_{sed}, \tag{7}$$

$$\frac{\partial \rho q_t}{\partial t}+\frac{\partial}{\partial x_i}\left(\rho u_i q_t-\Gamma\frac{\partial q_t}{\partial x_i}\right)=\left(S_{q_t}\right)_{act}+\left(S_{q_t}\right)_{cond/evap}+\left(S_{q_t}\right)_{sed}, \tag{8}$$

$$\frac{\partial \rho N_c}{\partial t}+\frac{\partial}{\partial x_i}\left(\rho u_i N_c-\Gamma\frac{\partial N_c}{\partial x_i}\right)=\left(S_{N_c}\right)_{act}+\left(S_{N_c}\right)_{cond/evap}+\left(S_{N_c}\right)_{sed}, \tag{9}$$

$$q_t=q_v+q_l\,, \tag{10}$$

where q_v and q_l are the specific humidity of water vapor and liquid water per unit mass. Γ is the diffusion coefficient of the given scalar.

In order to simulate mean sizes and concentrations of droplets in wet plumes, the scheme needs to represent processes that would affect the droplet spectra of the plume (right side of Eqs. (7) – (9)). These are the activation of droplets on condensation nuclei, condensation/evaporation of droplets, entrainment of ambient air (*Warner*, 1969; *Paluch* and *Knight*, 1984; *Brenguier* and *Grabowski*, 1993; *Su et al.*, 1998; *Lasher-trapp et al.*, 2005), and additional activation of droplets (*Warner*, 1969; *Pinsky* and *Khain*, 2002).

The relationship between droplet number (N_c) and liquid water content (q_l) is determined by using a log-normal droplet size distribution function (Eqs. (11) – (12)):

$$n_c(r)=\frac{N_c}{r\sigma_c\sqrt{2\pi}}\exp\left(-\frac{1}{2\sigma_c^2}\left(\ln\frac{r}{r_0}\right)^2\right), \tag{11}$$

$$\bar{r}_3 = r_0 \exp\left(\frac{3}{2}\sigma_c^2\right) \text{ and } \rho q_l = \frac{4}{3}\pi \bar{r}_3^{\,3} \rho_w N_c, \tag{12}$$

where r is the droplet radius, r_0 is the distribution median value, σ_c is the logarithmic standard deviation, $\bar{r}_3$ is the mean mass radius, and ρ_w is the density of water.

Atmospheric aerosols and cloud condensation nuclei play an important role in the condensation of droplets and evolution of clouds. In this study, the method described by *Cohard et al.* (1998) was chosen to describe the relationship between supersaturation and the nucleated number of droplets (N_{CCN}), as it is computationally more efficient, gives more robust estimates (*Grabowski*, 2006), and requires less programming efforts.

$$N_{CCN} = Cs^k F\left(\mu, \frac{k}{2}; \frac{k}{2}+1; -\beta s^2\right), \tag{13}$$

where C = 3270 cm^{-3} is a parameter of the nucleation process, s is the supersaturation, F is the hyper-geometric function and $\mu = 0.7$, $\beta = 136$, and $k = 1.56$ are parameters characterizing the aerosol distribution of a continental type of air mass. Eq. (13) is the extension of the simple and famous power law formula of *Twomey* (1959) but improved to give better results from weak to strong supersaturations.

Given the number of nucleated drops, the source term due to nucleation can be calculated assuming heterogeneous nucleation (*Pruppacher et al.*, 1998).

$$\left(S_{N_c}\right)_{act} = \frac{1}{\Delta t}\max\left(N_{CCN,\max} - N_c, 0\right), \tag{14}$$

where Δt is the numerical time step. It is assumed that condensation and evaporation proceed through changes of q_c without any effects on N_c (*Richard and Chaumerliac*, 1989) except during activation of CCN and total evaporation of smaller droplets.

2.2. Droplet growth by activation and diffusion

Once droplets are activated, the two primary components of their growth are the vapor diffusion and collision-coalescence. Since rain water is neglected, only growth by diffusion is considered. The critical radius of newly formed droplets can be calculated according to the Köhler theory (see, e.g., (*Pruppacher et al.*, 1998)).

$$\left(r_{crit}\right)_{act} = \frac{4}{3} M_w \sigma_w R \rho_w T(s/100), \tag{15}$$

where M_w and σ_w are the molecule mass and surface tension of the water substance, R and T are the universal gas constant and the physical temperature of ambient air.

The corresponding source term due to activation for the liquid water content is:

$$\left(S_{q_t}\right)_{act} = \frac{4\pi\rho_w}{3\rho} r_{crit}^3 \left(\frac{\partial N_c}{\partial t}\right)_{act}, \tag{16}$$

The condensation rate can be calculated based on (*Pruppacher et al.*, 1998):

$$\left(S_{q_t}\right)_{cond/evap} = \frac{4\pi r (s - A + B) f_v}{G(T,p)}, \tag{17}$$

where A, B, and f_v express curvature, solute, and ventilation effects and $G(T, p)$ is a term dependent on local thermodynamic variables.

$$A = \frac{2\sigma_w}{R_v T \rho_w r}, \quad B = \frac{\varepsilon \nu \Phi_s M_w m_a}{M_s (m - \rho_w m_a / \rho_s)}, \quad G(T,p) = \frac{L_v}{k_a T}\left(\frac{L_v}{R_v T} - 1\right) + \frac{R_v T}{p_{sat} D_v}, \tag{18}$$

where ε is the water-soluble fraction of the aerosol, the product $\upsilon\Phi_s$ is the van't Hoff factor, ρ_s and m_a are the aerosol density and mass, m is the droplet mass, M_w and M_s are the molecular mass of water and solute, L_v is the latent heat of evaporation, R_v is the specific gas constant of water vapor, k_a and D_v are the modified thermal conductivity and diffusivity of air and water vapor, p_{sat} is the saturated vapor pressure over flat water surface at environmental temperature.

2.3. Partial and total evaporation of droplets

Droplets evaporate once convected to unsaturated regions ($s < 0$). This process is described based on the work of *Chaumerliac et al.* (1987). Due to partial evaporation, drops with a size smaller than a certain threshold (r_{crit}) will be removed from the system, therefore resulting a decrease in N_c. The corresponding source term is:

$$\left(S_{N_c}\right)_{evap} = \frac{1}{\Delta t} \int_0^{r_{crit}} \frac{N_c}{r\sigma_c\sqrt{2\pi}} \exp\left(-\frac{1}{2\sigma_c^2}\left(\ln\frac{r}{r_0}\right)^2\right) dr, \tag{19}$$

where r_{crit} can be calculated as follows:

$$r_{crit} = \sqrt{(-2\ A3^{-1}\ s\ \Delta t)}, \tag{20}$$

$$A3 = \frac{\rho_w R_v T}{p_{sat} D_v} + \frac{L_v \rho_w}{k_a T}\left(\frac{L_v}{R_v T} - 1\right). \tag{21}$$

Total evaporation of droplets will occur when the calculated mass of evaporated drops is larger than the mass present in the given volume. In this case $Nc = 0$ and the local CCN number is regenerated. The sedimentation terms on the right side of Eqs. (7) – (9) can be used to describe the settling of droplets, however, the settling terms are not considered here, as they are expected to be small in certain plume dispersion cases (*Bouzereau et al.*, 2008).

The superstauration s is calculated based on the saturation pressure (Eq. (22)). It is calculated for flat water surfaces based on the formula of *Bolton* (1980). The expression is accurate to 0.3% for –35 °C < T < 35 °C temperature range.

$$p_{sat} = 6.112 \exp\left(\frac{17.67\,T}{243.5 + T}\right), \tag{22}$$

where T and p_{sat} are in °C and hPa.

The following expressions give the connection between water vapor mass fraction and vapor pressure:

$$p_v = \left(\frac{q_v}{0.622 + q_v}\right) p, \tag{23}$$

where p_v and p are the vapor partial pressure and the pressure of moist air.

Finally, the supersaturation is given by the following formula:

$$s = \frac{p_v}{p_{sat}} - 1, \tag{24}$$

In the following chapter, the transformation and the microphysics scheme will be validated against the simulation of an idealized two-dimensional rising thermal and three-dimensional full scale plume dispersion cases.

3. *Results*

3.1. *Numerical experiments with two-dimensional rising thermals*

It is common in the development of microphysical schemes, that researchers test their models' behavior with idealized two-dimensional simulations. A frequently used generic test case is a rising thermal simulation in a stably stratified environment. Two types are common in the literature, one where the development of the thermal is initiated by surface heating (see, e.g., (*Klaassen* and *Clark*, 1985)) and another type when an initial perturbation (potential temperature, vapor content, etc.) is placed in the domain at a certain height. The latter one, described by *Grabowski* and *Clark* (1991), will be used here as a test case for validation, as it allows shorter computation due to not simulating the initial development phase of the thermal.

3.1.1. *Rising thermal in a dry stable atmosphere*

In order to separate the moist dynamics from discretization effects, the rise of a dry thermal in a Bousinesq fluid was simulated first.

The model domain was 3.6 km wide in the horizontal and 2.4 km in the vertical direction with equidistant mesh resolution. Different grid sizes of 20, 10, 5, 2.5, and 1.25 m were tested in order to see mesh sensitivity of the solution. The lateral boundaries were defined as periodic boundary, the top and bottom boundaries as free slip adiabatic walls. The initial circular perturbation was placed at $x = 0$ km and $z = 0.8$ km with a radius of 500 m and 0.5 K higher initial temperature than the constant ambient temperature 287 K. Third order MUSCL schemes (monotone upstream-centered schemes for conservation laws, (*van Leer*, 1979)) were used when solving the momentum and energy equations, as they can effectively suppress the non-physical oscillations with the introduction of adaptive numerical dissipation into numerical solutions. All transformation source terms in Eqs. (2)–(5) were turned off in this case. The total flow time was 8 min with a time step of 1 s. Results were compared to standard nonoscillatory MPDATA simulations showed in Section 4 in *Margolin et al.* (1997).

At 20 m and lower resolutions, results were starting to degrade rapidly, the interfacial eddies were smeared out (not shown here). A converged solution could be obtained at higher resolutions, the 5, 2.5, and 1.25 m cases were virtually identical (see *Fig. 1*). During the solution, the viscosity was explicitly defined and was varied among the different cases. *Fig. 2* shows that the results are less sensitive to the changes of the predefined viscosity in the investigated range.

Overall, a good correspondence can be found regarding the gross features; the rise height and size of the final shape of the bubble agrees well. There are differences in the fine details, though, the size and position of interfacial eddies slightly differ from the MPDATA solutions.

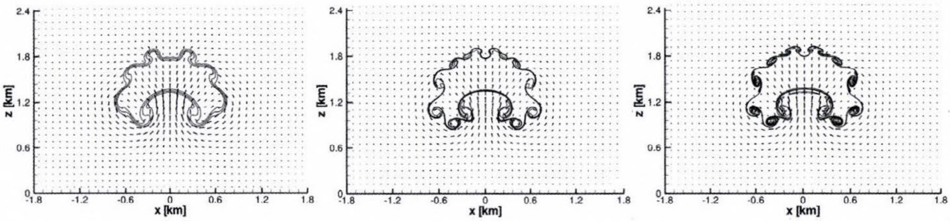

Fig. 1. Mesh sensitivity of the developed interfacial eddies. The equidistant mesh resolution is 20 m, 5 m, 1.25 m from left to right, and the viscosity is 0.5 $m^2 s^{-1}$ for all cases.

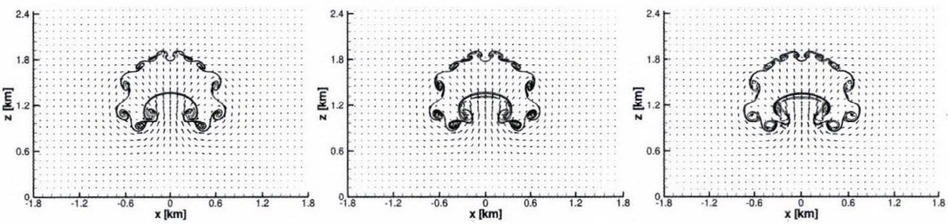

Fig. 2. Sensitivity of the developed interfacial eddies to the viscosity. The viscosity is 1, 0.5, 0.1 $m^2 s^{-1}$ from left to right, and the mesh resolution is 2.5 m for all cases.

3.1.2. Rising of a moist thermal

Model behavior changed significantly when moist dynamics were activated. The domain in this case was the same as above with an equidistant resolution in both spatial directions of 40, 20, 10, 5, 2.5 m. The initial perturbation of relative humidity (RH = 100 %) was placed at 0.8 km height with a diameter of 200 m that was smoothly relaxed to the environmental value within approximately 250 m radius. The environmental base state stability and the relative humidity were set to $d\ln\theta/dz = 1.3\ 10^{-5}\ m^{-1}$ and 20%, and the perturbation relaxation of RH was defined as:

$$RH = 20\% + 80\% \cos^2\left(\frac{\pi}{2}\frac{r-200}{100}\right), 200\text{m} < r < 300\text{m}. \tag{25}$$

The lateral, top, and bottom boundaries were defined as periodic and free slip adiabatic walls with a temperature of 289 K at the lower surface. The eddy viscosity of the air was explicitly defined and varied between 0.25 and 2 $m^2 s^{-1}$ among the simulation cases.

Third order MUSCL schemes, pressure staggering option (PRESTO) (*ANSYS Inc.*, 2013) were used when solving the momentum and energy equations, and for pressure interpolation. Results were compared to series of non-oscillatory MPDATA solutions presented in Section 3 in (*Grabowski* and *Clark*, 1991)

The general formation of the liquid water field of the thermal is illustrated in *Fig. 3*. During the initial 4 min of rise, a very good match can be found. This period was weakly affected by the mesh resolution or the predefined viscosity (not shown here). At higher resolutions (5 m and 2.5 m), the model predictions were fairly close to the semi-Lagrangian and Eulerian MPDATA solutions, the overall shape and rise height were similar, the interfacial eddies were well resolved. Differences can be found in the fine details, though, the exact position and shape of interfacial eddies are somewhat different but still close to the semi-Lagrangian model results that is superior in capturing the interface instability (see Section 4a of *Grabowski* and *Smolarkiewicz* (1996)). At low spatial resolutions, the CFD model still captured the overall shape, but the quality degraded quickly, no interfacial eddies could be found at 20 m resolution. However, the erosion of cloud water field was not as strong as the Eulerian MPDATA model showed at the same resolution.

Overall, the model output is in *Figs. 4* and *5* suggest that the results are converging to a common solution, and it is in a good agreement with the MPDATA results. Differences are possibly due to the different numerical schemes and the lack of precipitation scheme in the CFD model.

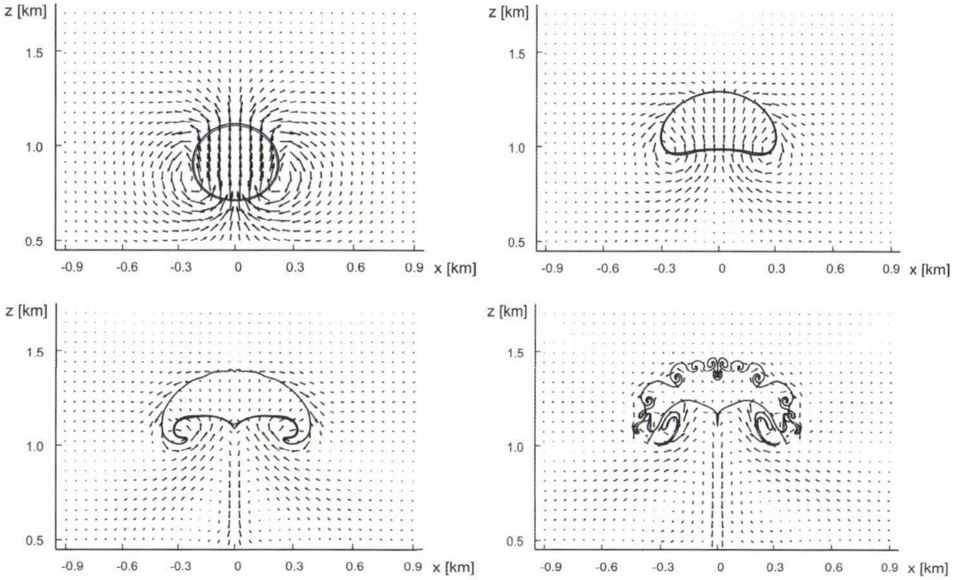

Fig. 3. Development of the initial water vapor perturbation. Isolines of q_l field at $t = 2$, 4, 6, and 8 min of the moist thermal rise. The viscosity and the mesh resolution are 0.5 $m^2 s^{-1}$ and 2.5 m in each panel. Contour intervals for q_l are 0.05, 0.1, 0.2, and 0.3 g kg^{-1}.

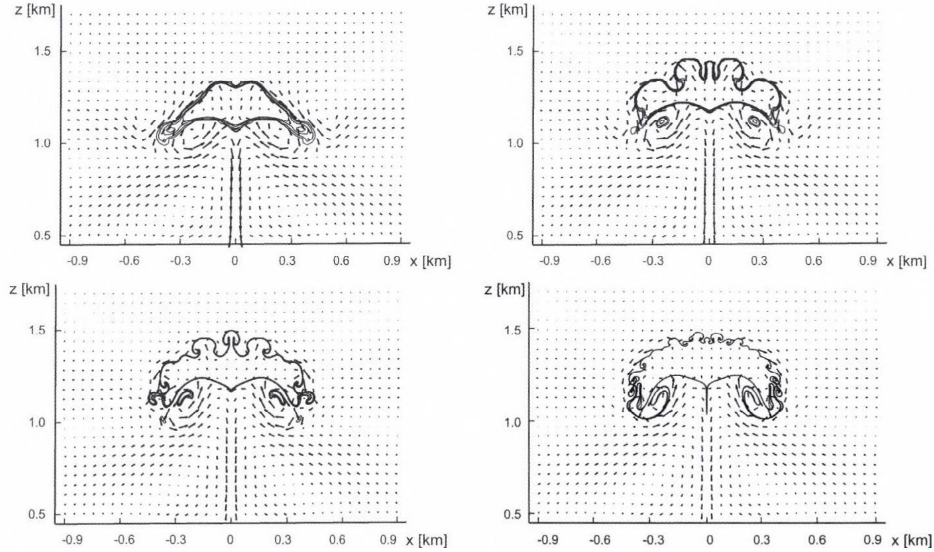

Fig. 4. Same as *Fig. 3.* but for different mesh resolutions. From left to right, the mesh sizes are 20, 10, 5, and 1.25 m. The viscosity is 0.5 m^2s^{-1}.

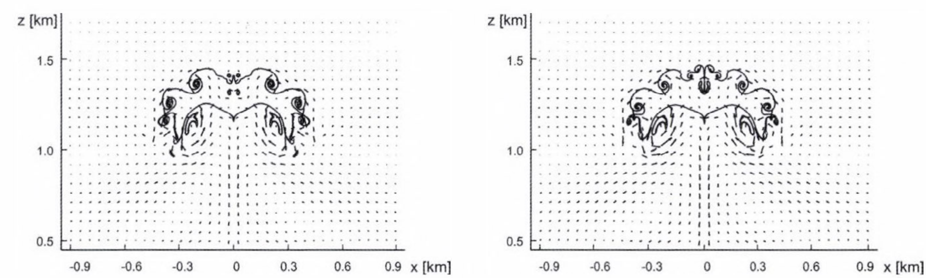

Fig. 5. Same as *Fig. 3* but for different viscosities. Mesh resolution is 2.5 m, viscosity is 0.1 and 0.25 $m^2 s^{-1}$ (from left to right).

3.2. Simulation of plume formation of a wet cooling tower, the Bugey 1980 field campaign

In this chapter, the CFD simulation results will be compared to full scale measurement data that was collected during a large measurement survey around wet cooling towers of a nuclear power plant around Bugey, France. Radiosoundings, droplet spectra, airborne measurements, measurements describing the ambient thermodynamic states as well as photographic records are available for comparision (*Bouzereau et al.*, 2008).

3.2.1. Initial and boundary conditions

During the campaign, very different plume shapes were observed from which two of the characteristic cases were selected for comparison. The first one (March 11, 1980) was characterized by high wind shear, conditionally unstable stratification, and an upper layer with high relative humidity. The second one (March 12, 1980) had lower ambient wind speed, more stable stratification and as a result, smaller horizontal plume extent characterized by sharp plume bent-over.

The domain in both cases covers a 10 km × 4 km area with a total height of 4 km. An equidistant grid was used during the simulations with a resolution of 40 m that was adaptively refined in two steps around the tower and the plume, resulting a minimum grid size of 10 m in critical areas. The interpolated initial and boundary profiles for the domain as well as the plume exit conditions, the vertical velocity, temperature, turbulence profiles, and the liquid water content were based on the radiosoundings and previous calculations of *Bouzereau et al.* (2008) (see *Fig. 6* for the atmospheric profiles and *Table 1* for tower exit conditions). Turbulent kinetic energy k and its dissipation ε at the tower exit were set to 1.7 $m^2 s^{-2}$ and 0.07 $m^2 s^{-3}$ in both cases. Droplet number concentration at the tower exit was deduced from measurements, i.e., $N_c = 10^4$ cm^{-3}. The nucleation parameterization was after *Cohard et al.* (1998) using parameters for a continental type of air mass, i.e., $C = 3270$ cm^{-3}, $k = 1.56$, $\mu = 0.70$, $\beta = 136$, and $\sigma_c = 0.28$. The time step was 1 s and the total integration time was 3600 s in both cases.

Table 1. Plume exit conditions for March 11 and 12, 1980. Exit conditions for the towers 4E–W and 5E–W are given separately. Subscript "env" refers to environmental values. The tower exit temperature ΔT is given compared to the environmental values. w and q_l are the vertical velocity component and the liquid water content, respectively, at the tower exit.

Tower exit conditions	q_l **[g kg^{-1}]**		ΔT **[°C]**		w **[ms^{-1}]**		T_{env} **[°C]**	p_{env} **[Pa]**
	4E-W	5E-W	4E-W	5E-W	4E-W	5E-W		
March 11	0.889	0.719	18.34	17.77	3.8	3.73	4.44	97771
March 12	0.8	0.8	18.2	17.7	3.8	3.7	3.31	97994

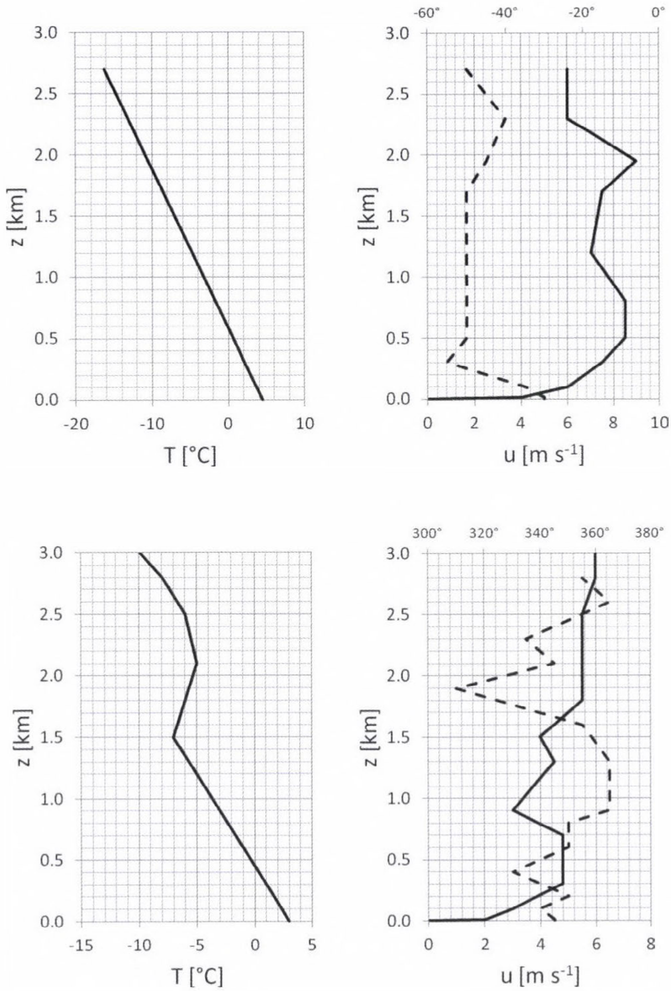

Fig. 6. Ambient initial and boundary conditions for the March 11, 1980 (top) and March 12, 1980 (bottom) cases. Left panel: ambient temperature. Rigth panel: wind speed (solid line) and wind direction (dashed line).

3.2.2. Simulation results of plume formation

Moist air is injected at the tower exit into the atmosphere characterized by strong shear with a high relative humidity upper layer, resulting in a periodic cumulus like plume formation farther downstream of the tower. This phenomena is well captured by the CFD code compared to visual observations and existing calculations (see Chapter 4 and Appendix A of *Bouzereau et al.* (2008)). The oscillation in the liquid water content (LWC) field observed as rising thermals in *Fig. 7.* shows a wave length of about the same as the model output of the MERCUR code presented in *Bouzereau et al.* (2008) and of the observations. The first thermal-like structure appears closer downstream of the tower in the CFD model, that could be explained by differences in the turbulence level, and by the effect of higher resolution mesh in critical areas.

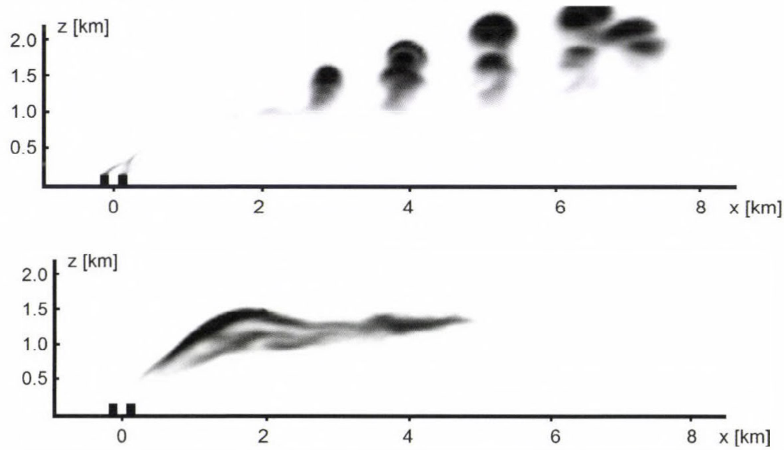

Fig. 7. Volume rendering of the LWC field of the simulated plumes, March 11, 1980 (top) and March 12, 1980 (bottom). The field is transparent below $q_l = 0.01$ g kg^{-1} and opaque when higher than 1.0 g kg^{-1} with 0.1 g kg^{-1} steps in the opacity.

A quantitative comparison is shown in *Fig. 8* where CFD model output is plotted against available aircraft data. In order to obtain valuable results on plume formation and dispersion, it is important to have good initial data on the vertical thermal structure as well as wind shear and humidity. The temperature field was well captured by the simulation, it follows the ambient temperature profile, and the aircraft data lies well between the simulated extremum. The maximum simulated values of LWC field were also compared to recorded data during the campaign. Although aircraft data for LWC was not available for comparison for the initial rise, in the layer between 900 m and 1800 m the simulation compares well, tendencies in liquid water field are well captured for the high wind case with a slight overestimation along the plume axis. During aircraft data sampling, data for instantaneous vertical velocity was also collected. This cannot be compared directly to simulation output, as vertical velocity from URANS simulations does not contain the fluctuation component of the wind speed. However, it is possible to deduce approximate values from the turbulence kinetic energy field. The survey shows significant fluctuations in the velocity field, which is also well reflected in the simulation results.

The simulated plume height could be extracted from *Fig. 8*, where the liquid water content is starting to drop significantly. The simulation showed slight overestimation for the high wind case, it gave values between 2000 m and 2500 m, while during the survey a height of ~1950 m and ~2250 m was observed.

In general, the model showed good overall performance with the CFD model improved with the bulk microphysical scheme. Further steps will include the implementation of sedimentation and precipitation schemes.

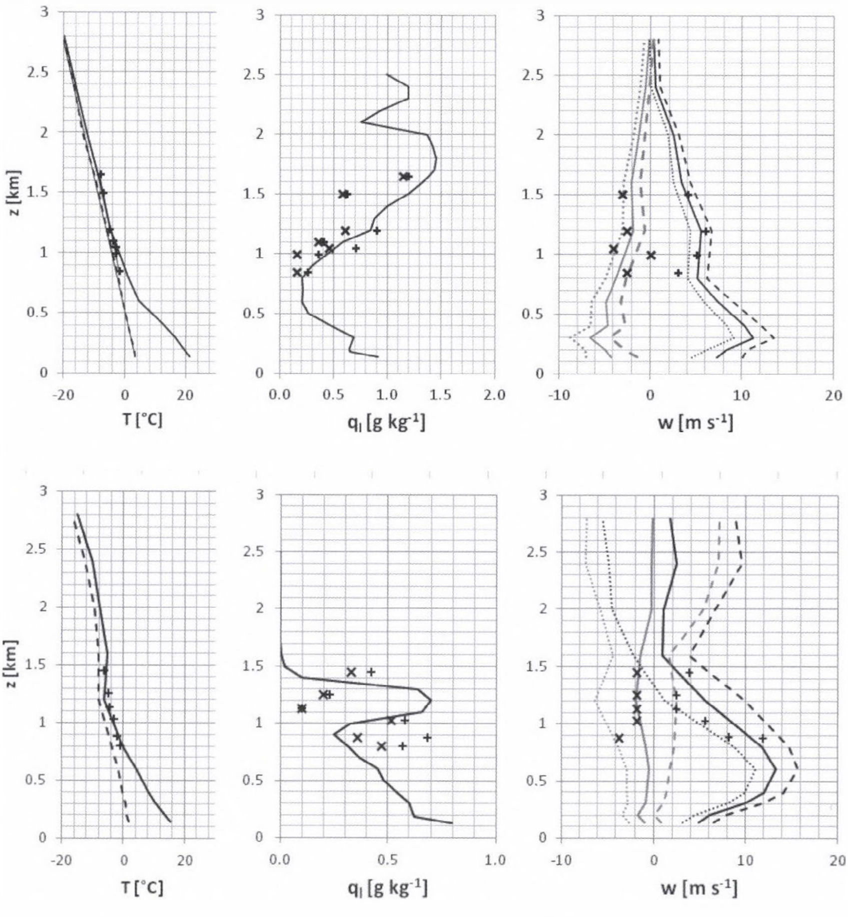

Fig. 8. Simulation results for March 11, (top panels) and March 12,1980 (bottom panels) compared to the aircraft measurements. On the left: maximum (solid line) and minimum (dashed line) of the simulated temperature. Symbols: measured temperature average through the plume. Center: predicted maximum of the LWC field (solid line) at each level. Symbols: 'x' and '+' represent the measured minimum and maximum of the LWC. Right panels: simulated vertical velocity *w* (solid lines: maximum in black, minimum in grey). Doted and dashed lines show the fluctuation components. Symbols: 'x' and '+' represent the minimum and maximum instantaneous vertical velocities observed at each flight level.

4. Summary and conclusions

A transformation method was developed in the past in order to extend the capabilities of commercial CFD solvers with mesoscale effects. Thermal stratification, adiabatic cooling caused by hydrostatic pressure driven expansion, compressibility, and Coriolis force were taken into account with the help of a transformation system and customized volume sources applied to the governing equations. In this paper further advances were shown. A bulk warm microphysical scheme was implemented in the solver in order to simulate humidity transport and phase change in atmospheric flows.

Model results were successfully validated with the rise of idealized two-dimensional dry and wet thermals. We have then applied the model to the simulation of wet plume formation originated from a cooling tower of a large nuclear power plant.

Results obtained from our simulations are encouraging with regard to the predictability of cumulus-like plume structures in the far field of the tower formed in complex wind field and thermal stratification, the overall liquid water content along the plume axis, and also the turbulent fluctuations caused by the vertical movements in the plume.

Using only one single unstructured grid and a uniform physical description for close- and far-field flow, one can take the advantage of the model adaption in the simulation of mesoscale atmospheric phenomena. In a single framework, one can investigate the finely structured microscale flow around complex geometrical features, such as flow around buildings with pollution dispersion or study the close- and far-field of wet cooling tower plumes and its effects to the environment.

Acknowledgments: The scientific work presented in this article was supported by the project K108936 "Flow and dispersion phenomena in urban environment" of the Hungarian Scientific Research Fund.

References

Ackerman, A. S., Kirkpatrick, M. P., Stevens, D. E., and *Toon, O. B.*, 2004: The impact of humidity above stratiform clouds on indirect aerosol climate forcing. *Nature 432*, 1014–1017.

Al-Waked, R., and Behnia, M., 2006: CFD simulation of wet cooling towers. *Appl. Therm. Eng. 26*, 382–395.

ANSYS Inc., 2013: FLUENT 13 documentation. In: Fluent User Services Center.

Balczó, M., Balogh, M., Goricsán, I., Nagel, T., Suda, J., and *Lajos, T.*, 2011: Air quality around motorway tunnels in complex terrain–Computational Fluid Dynamics modeling and comparison to wind tunnel data. *Időjárás 115*, 179–204.

Barber, F., Martin, A., Shepherd, J., and *Spurr, G.*, 1974: The persistence of plumes from natural draft cooling towers. *Atmos. Environ. 8*, 407–418.

Bolton, D., 1980: The computation of equivalent potential temperature. *Mon. Weather Rev. 108*, 1046–1053.

Bouzereau, E., Musson Genon, L., and *Carissimo, B.*, 2008: Application of a semi-spectral cloud water parameterization to cooling tower plumes simulations. *Atmos. Res. 90*, 78–90.

Brenguier, J.-L., and *Grabowski, W. W.*, 1993: Cumulus entrainment and cloud droplet spectra: A numerical model within a two-dimensional dynamical framework. *J. Atmos. Sci. 50*, 120–136.

Briggs, G. A., 1975: Plume rise predictions. *Lect. Air Pollut. Environ. Impact Anal. AS, 59-1 1.*

Briggs, G. A., 1984: Plume rise and buoyancy effects. *Atmos. Sci. Power Prod.* 327–366.

Brown, G. J., and Fletcher, D. F., 2005: CFD prediction of odour dispersion and plume visibility for alumina refinery calciner stacks. *Process Saf. Environ. Prot. 83*, 231–241.

Campistron, B., 1987: Interaction between a natural snowfall and a cooling tower plume: An experimental study with a millimetric Doppler radar. *Atmos. Environ. 21*, 1375–1383.

Carhart, R. A. and *Policastro, A. J.*, 1991: A second-generation model for cooling tower plume rise and dispersion—I. Single sources. *Atmos. Environ. Part A. Gen. Top. 25*, 1559–1576.

Carruthers, D. and *McHugh, C.*, 2009: Comparison of ADMS and AERMOD meteorological preprocessor and dispersion algorithms. Proc. Air Waste Manag. Assoc. Air Qual. Model. Next Gener. Model.

Chaumerliac, N., Richard, E., Pinty, J.-P., and *Nickerson, E. C.*, 1987: Sulfur scavenging in a mesoscale model with quasi-spectral microphysics: Two-dimensional results for continental and maritime clouds. *J. Geophys. Res. Atmos. 92*, 3114–3126.

Cohard, J., Pinty, J., and *Bedos, C.*, 1998: Extending Twomey's analytical estimate of nucleated cloud droplet concentrations from CCN spectra. *J. Atmos. Sci., 55,* 3348–3357.

Cohard, J.-M. and *Pinty, J.-P.*, 2000: A comprehensive two-moment warm microphysical bulk scheme. I: Description and tests. *Q. J. Roy. Meteorol. Soc. 126*, 1815–1842.

Csanady, G. T., 1973: Turbulent diffusion in the environment. D. Reidel Pub. Co.,.

Davidson, G. A., 1989: Simultaneous trajectory and dilution predictions from a simple integral plume model. *Atmos. Environ. 23*, 341–349.

Davidson, G. A., 1994: Dimensionless correlations for buoyant plume behaviour in cross-flows and scaling criteria for physical modeling of dispersion processes. *J. Wind Eng. Ind. Aerodyn. 51*, 135–155.

Feingold, G., Stevens, B., Cotton, W. R., and *Walko, R. L.*, 1994: An explicit cloud microphysics/LES model designed to simulate the Twomey effect. *Atmos. Res. 33*, 207–233.

Gangoiti, G., Sancho, J., Ibarra, G., Alonso, L., García, J. A., Navazo, M., Durana, N., and *Ilardia, J. L.*, 1997: Rise of moist plumes from tall stacks in turbulent and stratified atmospheres. *Atmos. Environ. 31*, 253–269.

Grabowski, W. W., 2006: Indirect impact of atmospheric aerosols in idealized simulations of convective – radiative quasie quilibrium. *J. Clim. 19*, 4664–4682.

Grabowski, W. W., and *Clark, T. L.*, 1991: Cloud–environment interface instability: Rising thermal calculations in two spatial dimensions. *J. Atmos. Sci. 48*, 527–546.

Grabowski, W. W., and *Smolarkiewicz, P. K.*, 1996: Two-time-level semi-Lagrangian modeling of precipitating clouds. *Mon. Weather Rev. 124*, 487–497.

Greig, J. E., Carnie, J. A., Tallis, G. F., Ryan, N. J., Tan, A. G., Gordon, I., Zwolak, B., Leydon, J. A., Guest, C. S., and *Hart, W. G.*, 2004: An outbreak of Legionnaires' disease at the Melbourne Aquarium, April 2000: Investigation and case-control studies. *Med. J. Aust. 180*, 566–572.

Hanna, S. R., 1972: Rise and condensation of large cooling tower plumes. *J. Appl. Meteorol. 11*, 793–799.

Hanna, S. R., 1976: Predicted and observed cooling tower plume rise and visible plume length at the John E. Amos power plant. *Atmos. Environ. 1967 10*, 1043–1052.

Hanna, S. R., Briggs, G. A., and Hosker, R. P. J., 1982: *Handbook on Atmospheric Diffusion*.

Huff, F. A., 1972: Potential augmentation of precipitation from coolingtower effluents. *Bull. Am. Meteorol. Soc. 53*, 639–644.

Janicke, U., and Janicke, L., 2001: A three-dimensional plume rise model for dry and wet plumes. *Atmos. Environ. 35*, 877–890.

Kessler, E., 1969: On the distribution and continuity of water substance in atmospheric circulations. *Meteor. Monogr., Amer. Meteor. Soc. No. 32*, 84.

Klaassen, G. P. and *Clark, T. L.*, 1985: Dynamics of the cloud-environment interface and entrainment in small cumuli: Two-dimensional simulations in the absence of ambient shear. *J. Atmos. Sci. 42*, 2621–2642.

Kloppers, J. C. and *Kröger, D. G.*, 2005: Influence of temperature inversions on wet-cooling tower performance. *Appl. Therm. Eng. 25*, 1325–1336.

Kogan, Y. L., 1991: The simulation of a convective cloud in a 3-D model with explicit microphysics. part I: Model description and sensitivity experiments. *J. Atmos. Sci. 48*, 1160–1189.

Kristóf, G. and *Balogh, M.*, 2010: Fine scale simulation of turbulent flows in urban canopy layers. *Időjárás 114*, 135–148.

Kristóf, G., Rácz, N., and *Balogh, M.*, 2009: Adaptation of pressure based CFD solvers for mesoscale atmospheric problems. *Bound.-Lay. Meteorol. 131*, 85–103.

Lasher-trapp, S. G., Cooper, W. A., and *Blyth, A. M.*, 2005: Broadening of droplet size distributions from entrainment and mixing in a cumulus cloud. *Q. J. Roy. Meteorol. Soc. 131*, 195–220.

Van Leer, B., 1979: Towards the ultimate conservative difference scheme. V. A second-order sequel to Godunov's method. *J. Comput. Phys. 32*, 101–136.

Lewis, W. K., 1922: The evaporation of liquid into gas. *Trans ASME 44*, 325–340.

Lohasz, M. M., and *Csaba, G.*, 2012: Investigation of exit loss of cooling towers at different wind speeds and Archimedes numbers. Proceeding of THMT-12. Proceedings of the Seventh International Symposium On Turbulence, Heat and Mass Transfer Palermo, Italy, 24-27 September, 2012, Connecticut, Begellhouse, 11.

Lucas, M., Martínez, P. J., Ruiz, J., Kaiser, A. S., and *Viedma, A.*, 2010: On the influence of psychrometric ambient conditions on cooling tower drift deposition. *Int. J. Heat Mass Transf. 53*, 594–604.

Margolin, L., Reisner, J. M., and *Smolarkiewicz, P. K.*, 1997: Application of the volume-of-fluid method to the advection–condensation problem. *Mon. Weather Rev. 125*, 2265–2273.

Mcalpine, J. D. and *Ruby, M.*, 2004: Using CFD to study air quality in urban microenvironments. Environmental Sciences and Environmental Computing. Vol. II, P. Zannetti, Ed., Vol. II of, The EnviroComp Institute, 1–31.

Meroney, R., 2006: CFD prediction of cooling tower drift. *J. Wind Eng. Ind. Aerodyn. 94*, 463–490.

Mochida, A., Murakami, S., Ojima, T., Kim, S. J., Ooka, R., and *Sugiyama, H.*, 1997: CFD analysis of mesoscale climate in the Greater Tokyo area. *J. Wind Eng. Ind. Aerodyn. 67-8*, 459–477.

Mokhtarzadeh-Dehghan, M. R., König, C. S., and *Robins, a. G.*, 2006: Numerical study of single and two interacting turbulent plumes in atmospheric cross flow. *Atmos. Environ. 40*, 3909–3923.

Morrison, H., Curry, J. A., and *Khvorostyanov, V. I.*, 2005: A new double-moment microphysics parameterization for application in cloud and climate models. Part I: description. *J. Atmos. Sci. 62*, 1665–1677.

Moussiopoulos, N., 2010: Air quality in cities: SATURN: EUROTRAC-2 Subproject final report. Springer, Berlin,.

Netterville, D. D. J., 1990: Plume rise, entrainment and dispersion in turbulent winds. *Atmos. Environ. Part A. Gen. Top. 24*, 1061–1081.

Olesen, H. R., Berkowicz, R., Ketzel, M., and *Løfstrøm, P.*, 2007: Validation of OML, AERMOD/PRIME and MISKAM using the Thompson wind tunnel data set for simple stack-building configurations. 6th International Conference on Urban Air Quality, Cyprus, March 27-29, 2007.

Ooka, R., Sato, T., Harayama, K., Murakami, S., and *Kawamoto, Y.*, 2010: Thermal energy balance analysis of the Tokyo metropolitan areausing a mesoscale meteorological model incorporating anurban canopy model. *Bound.-Lay. Meteorol. 138*, 77–97.

Otte, T. L., Lacser, A., Dupont, S., and *Ching, J. K. S.*, 2004: Implementation of an urban canopy parameterization in a mesoscale meteorological model. *J. Appl. Meteorol. 43*, 1648–1665.

Overcamp, T. J, and *Hoult, D. P.*, 1971: Precipitation in the wake of cooling towers. *Atmos. Environ. 5*, 751–765.

Paluch, I. R., and *Knight, C. A.*, 1984: Mixing and the evolution of cloud droplet size spectra in a vigorous continental cumulus. *J. Atmos. Sci. 41*, 1801–1815.

Petersen, R. L., 2004: ISC3 and PRIME versus wind tunnel observations for a power plant with hyperbolic cooling towers. 13th Conference on the Applications of Air Pollution Meteorology, Fifth Conference on Urban Environment, Vancouver, BC 23-26 August 2004.

Pinsky, M. B., and Khain, A. P., 2002: Effects of in-cloud nucleation and turbulence on droplet spectrum formation in cumulus clouds. *Q. J. Roy. Meteor. Soc. 128*, 501–533.

Policastro, A. J., Dunn, W. E., Breig, M., and *Ziebarth, J.*, 1978: Comparison of ten drift deposition models to field data acquired in the Chalk Point dry tracer experiment. Environmental Effects of Cooling Tower Plumes, Symposium on (Supplement),May 2-4, 1978, U. ofMaryland, 76–84.

Policastro, A. J., Dunn, W. E., and *Carhart, R. A.*, 1994: A model for seasonal and annual cooling tower impacts. *Atmos. Environ. 28*, 379–395.

Presotto, L., Bellasio, R., and *Bianconi, R.*, 2005: Assessment of the visibility impact of a plume emitted by a desulphuration plant. *Atmos. Environ. 39*, 719–737.

Pruppacher, H. R., Klett, J. D., and *Wang, P. K.*, 1998: Microphysics of Clouds and Precipitation. *Aerosol Sci. Technol. 28*, 381–382.

Rácz, N., Kristóf, G., and *Weidinger, T.*, 2013: Evaluation and validation of a CFD solver adapted to atmospheric flows: Simulation of topography-induced waves. *Időjárás 117*, 239–275.

Richard, E., and *Chaumerliac, N.*, 1989: Effects of different rain parameterizations on the simulation of mesoscale orographic precipitation. *J. Appl. Meteorol. 28*, 1197–1212.

Robinson, C. S., 1923: The design of cooling towers. *Mech Eng 15*, 99–102.

Schatzmann, M., and *Policastro, A. J.*, 1984: An advanced integral model for cooling tower plume dispersion. *Atmos. Environ. 18*, 663–674.

Schulman, L. L., Strimaitis, D. G., and *Scire, J. S.*, 1997: Addendum to ISC3 user's guide: the prime plume rise and building downwash model.

Shih, T. H., Liou, W. W., Shabbir, A., Yang, Z., and *Zhu, J.*, 1994: A new k-epsilon eddy viscosity model for high Reynolds number turbulent flows: Model development and validation. *Comput. Fluids 24*, 227–238.

Slawson, P. R. and *Csanady, G. T.*, 1967: On the mean path of buoyant, bent-over chimney plumes. *J. Fluid Mech. 28*, 311–322.

Spillane, K. T. and *Elsum, C. C.*, 1983: Prediction of cloud effects in chimney plumes. *Atmos. Environ. 17*, 983–990.

Sturman, A. and *Zawar-Reza, P.*, 2011: Predicting the frequency of occurrence of visible water vapour plumes at proposed industrial sites. *Atmos. Environ. 45*, 2103–2109.

Su, C.-W., Krueger, S. K., McMurtry, P. A., and *Austin, P. H.*, 1998: Linear eddy modeling of droplet spectral evolution during entrainment and mixing in cumulus clouds. *Atmos. Res. 47–48*, 41–58.

Twomey, S., 1959: The nuclei of natural cloud formation part II: The supersaturation in natural clouds and the variation of cloud droplet concentration. *Geofis. Pura e Appl. 43*, 243–249.

Tyagi, S. K., Pandey, a. K., Pant, P. C., and *Tyagi, V. V.*, 2012: Formation, potential and abatement of plume from wet cooling towers: A review. *Renew. Sustain. Energy Rev. 16*, 3409–3429.

Wang, J., Wang, S., Xu, X., and *Xiao, F.*, 2009: Evaluation of alternative arrangements of a heat pump system for plume abatement in a large-scale chiller plant in a subtropical region. *Energy Build. 41*, 596–606.

Wang, S. W., Tyagi, S. K., Sharma, A., and *Kaushik, S. C.*, 2007: Application of solar collectors to control the visible plume from wet cooling towers of a commercial building in Hong Kong: A case study. *Appl. Therm. Eng. 27*, 1394–1404.

Warner, J., 1969: The microstructure of cumulus cloud. Part I. general features of the droplet spectrum. *J. Atmos. Sci. 26*, 1049–1059.

Wei, Q. D., Zhang, B. Y., Liu, K. Q., Du, X. D., and *Meng, X. Z.*, 1995: A study of the unfavorable effects of wind on the cooling efficiency of dry cooling towers. *J. Wind Eng. Ind. Aerodyn. 54-55*, 633–643.

Weil, J. C., 1974: The Rise of moist, buoyant plumes. *J. Appl. Meteorol. 13*, 435–443.

Wigley, T. M. L., and *Slawson, P. R.*, 1971: On the condensation of buoyant, moist, bent-over plumes. *J. Appl. Meteorol. 10*, 253–259.

Xu, X., Wang, S., and *Ma, Z.*, 2008: Evaluation of plume potential and plume abatement of evaporative cooling towers in a subtropical region. *Appl. Therm. Eng. 28*, 1471–1484.

Yamada, T., 2003: Numerical simulation of airflows around buildings by using a mesoscale atmospheric model. Air & Waste Management Associations 96th Annual Conference and Exhibition, San Diego, California, June 23 - 25, 2003, San Diego, California.

Ziegler, C. L., 1985: Retrieval of thermal and microphysical variables in observed convective storms. Part 1: Model development and preliminary testing. *J. Atmos. Sci. 42*, 1487–1509.

IDŐJÁRÁS
Quarterly Journal of the Hungarian Meteorological Service
Vol. 120, No. 2, April – June, 2016, pp. 255–264

Correlation analysis of tilted and horizontal photovoltaic panel's electricity generation and horizontal global radiation

Miklós Horváth* and **Tamás Csoknyai**

Department of Building Services and Process Engineering,
Budapest University of Technology and Economics,
Műegyetem rkp. 3-9., 1111 Budapest, Hungary

**Corresponding author E-mail: horvath@epgep.bme.hu*

(Manuscript received in final form June 3, 2015)

Abstract—Present paper aims at analyzing the correlation between global radiation and electricity production of photovoltaic (PV) panels. In case of high correlation, the electricity production can be estimated by the measured or predicted global radiation. Such solution can be applied for forecast purposes if global radiation data are available. On the other hand, global radiation can be measured based on the performance of a small and cheap PV system, which can be a reasonable solution if global radiation data is not available and a high precision monitoring system is too expensive.

The study is based on on-site measurements for the period of four months. At the station, seven PV panels are installed with different orientation and tilt angle and their electricity production is registered. The solar radiation is measured with a pyranometer. In the first group, there are four PV panels. One is placed horizontally and the other three are placed with a tilt angle of 45°. In the second, three-panel group the panels are placed with 90° tilt angle. The station is located in Debrecen, Hungary and the paper focuses on the Hungarian climatic conditions.

The research proves that the correlation strongly depends on the orientation and the tilt angle of the panel, and for prediction and estimation purposes the 45° tilted, south oriented surface is the most recommended option.

Key-words: PV panels, electricity production, energy performance, monitoring, global radiation, on-site monitoring, daily courses of electricity production

1. Introduction

For PV system installations it is fundamental to estimate the energy output of the systems. In most cases PV panels are placed with optimized tilt angle and orientation. A four-step optimization is described by Mehleri et al. (*Mehleri et al.*, 2010). The first step of the optimization process is to select the best performing diffuse radiation model to calculate the radiation components. As a second step, the global radiation can be calculated from the previously calculated radiation components for any tilt angle and orientation. As a third step, linear regression and RBF (radial basis-function) are applied to identify the best fitting model for the measured global radiation data. Further on, this model was used for the calculations. As a fourth step, a nonlinear programming (NLP) problem is formulated taking into account constraints and limitations of the system.

In several cases, the PV panels cannot be optimally tilted and as a result are oriented simply according to the site conditions. Several papers were published on this issue. A case study on a Korean office building was made by Hwang et al. *(Hwang et al.*, 2012). In that paper different options were examined focusing on the energy output of the BIPV (building integrated PV) arrays. The aim of the study was to determine the maximal electricity production for different tilt angles and orientations along with the effect of the installation distance to module length ratio. The study found that "it is efficient to install BIPV systems at a horizontally inclined angle of 60° and a vertically inclined angle that is smaller than 15°".

A different research was conducted in Australia, where PV production was measured at different tilt angles and orientations (*Yan et al.*, 2013). The measured electricity output was compared to calculated data, and the results showed that the chosen model was acceptable, thus further calculations and optimization were made. Based on the measurements and calculations, the yearly system efficiency and energy output for different orientations and the optimal tilt angle and orientation were determined.

Further parametric analysis was carried out by Bhattacharya et al. in Rajasthan, India (*Bhattacharya et al.*, 2014). The aim of the research was to perform PV output modeling under the climatic conditions of India. The effect of orientation, tilt angle, temperature, and humidity on the PV system efficiency and energy output was examined. The meteorological parameters were collected from five different stations, and the effect of orientation and tilt angle was examined by applying model calculations. The conducted research included determination of optimal orientation and tilt angle.

Further research was conducted by *Ding et al.* for three different stations, from which two were located in the USA and the third one in Kenya, Africa (*Ding et al.*, 2015). In the paper, different PV types and ways of their installation were examined and their effect on the PV system output and efficiency was monitored. They proved that by using the optimal orientation and tilt angle, the output of the system can be increased by 30%. As a result of PV type investigations, it was clearly visible that not optimal placement of PV panels in some cases can lead to significant drop in the system efficiency. Consequently, for such panels, imperfect installation must be avoided.

Mulcué-Nieto and Mora-López examined the effect of orientation and tilt angle of PV panels at several stations in Columbia and Spain *(Mulcué-Nieto* and *Mora-López,* 2015). As a result of the research, it was concluded, that in case of nation-wide characterization it is necessary to divide the country into appropriate zones. In case of Columbia, the zone borders were defined by longitudes. In each zone, the incoming solar energy was calculated for big cities within the region. The results were taken as an average for the given area. The results also showed that the effect of orientation is smaller in countries which are exposed to higher diffuse radiation.

In case of nearly zero energy buildings (NZEB), it is important to utilize the renewable energies to a high extent. Sánchez and Izard performed a research aiming at the determination of energy yield of PV panels placed on the external walls of buildings (*Sánchez* and *Izard,* 2015). The measurement was performed on southwest facing façades. In addition, four other orientations were also modeled. It was concluded, that in the case of PV panels placed on the southwest side of the building, a more balanced and stable electricity output is produced, which better fits the electricity consumption.

The aim of this paper is to determine the electricity production of different PV panel installations under climatic conditions of Hungary. The output of PV panels is also compared to the global radiation measured on a horizontal surface. In the paper, the measurement station is described along with its limitations.

2. Measurement station

The measurement station is located in Debrecen, Hungary, in the 'Megújuló Energiapark' (4031 Debrecen, Kishegyesi út 187.). The solar radiation is measured with a KIPP & ZONEN CM-3 pyranometer, which is placed at 2 m above the ground (*Fig. 1*). The radiation measuring device is connected to a Campbell CR 1000 data logger. The sample rate of the device is 1 s, which is collected by the data logger. The data logger from the 1 s data calculates 10 min averages. The data logger is connected to a server through an Ethernet interface (NL120), and sends data every 10 minutes.

At the station the PV panels are installed in two groups (*Fig. 2*). The installed PV panels are Istar Solar® IS4000P, with 210 W peak power. The manufacturer's catalog claims a maximal efficiency of 15.4% for these panels. There are four PV panels in the first group. One is placed horizontally and the other three are placed with a tilt angle of 45°. The inclined PV panels are oriented to the east, south and west. In the second group, three panels are placed with 90° tilt angle facing towards east, south and west. The beginning of data logging was September 20, 2014. The electricity output of PV panels is measured and logged every 10 minutes.

In this paper, data from September 20, 2014 to January 18, 2015 were analyzed. The measured data were first processed in order to exclude errors, and then statistical analysis was performed for the filtered data.

Fig. 1. The KIPP & ZONEN CM-3 pyranometer at the station.

Fig. 2. The PV arrays at the station.

3. Measured data and statistical analysis

3.1. Correlation of PV electricity production and global radiation measured on a horizontal plane

The daily average of global radiation and PV output of the horizontal PV panel for the entire period of monitoring are shown in *Fig. 3*. From the figure it can be seen, that the electricity output is at least twice as high as the output in December and January.

Based on the measured output of the horizontal PV panel and the global radiation, the calculated average efficiency of the PV panel is 14%. The calculated daily maximum efficiency was 19%, whilst the lowest was nearly 0%. The actual maximal daily efficiency was higher than the PV panel's maximum efficiency of 15.4% given by the manufacturer. The reason for the higher efficiency is possibly a result of a shading obstruction on the global radiation measurement device. This resulted in a lower value of measured global radiation, while the unshaded PV panels production was not lower. The calculated correlation coefficient of the measured global radiation and PV output was 0.930.

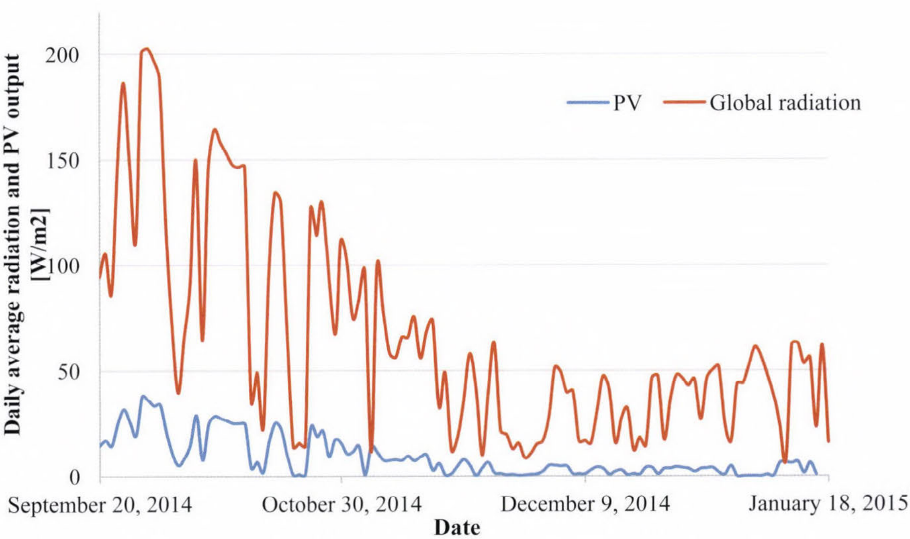

Fig. 3. Daily average of global radiation and PV output.

3.2. *Comparison of the outputs of tilted, oriented and horizontally installed PV panels*

The output of different PV panels are shown in *Table 1*. The table shows that with PV panels oriented to the south, more energy can be produced, than with a horizontally placed PV panel. The results also show that the biggest energy yield in the autumn-winter period is on a 90° tilted, south oriented panel, due to the low solar altitude. On the East oriented surface the incoming energy was nearly equal to the energy output of the horizontal panel. The east and west oriented, 45° tilted panels could produce acceptable amount of electricity, however, the 90° tilted panels oriented the same way have low energy output. Based on the values of correlation coefficients, it can be concluded that only the 45° tilted, south oriented PV panel has similar production profile to the horizontal one. The other panels show significant differences, thus they cannot be characterized by the horizontal panel.

Table 1. The produced electricity and calculated correlation coefficient for each PV panel in comparison with the horizontal panel's measurement data

	0°	S45°	S90°	E45°	E90°	W45°	W90°
Produced electricity [%]	100	119.6	136.1	101.3	47.9	72.9	39.6
Correlation [–]	1	0.930	0.818	0.853	0.556	0.758	0.300

For the measurement period, the daily average output profile was developed for every month for every panel. *Fig. 4* shows the daily average electricity output for the horizontally placed PV panel. The daily electricity production drops by 75% in the winter months compared to the daily data of September. This is due to the lower solar altitude and the higher fraction of diffuse radiation during winter.

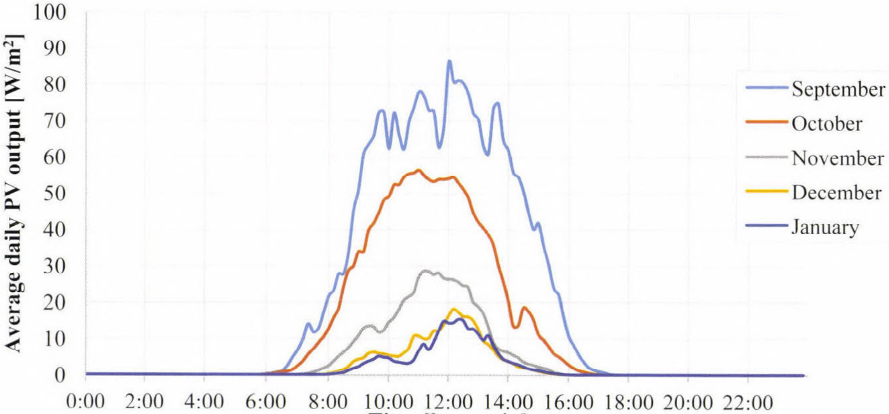

Fig. 4. Daily average electricity output of the horizontal PV panel.

The electricity output of the south oriented PV panels is shown in *Fig. 5* and *Fig. 6*. From the figures it can be seen that in case of south oriented panels, the daily electricity output is nearly symmetrical. In *Fig. 6* it is presented that in December and January in the morning and afternoon, small peaks occur at the low solar altitude. These small peaks can be results of a shading object, as in case of the 45° tilted surface, these peaks do not occur.

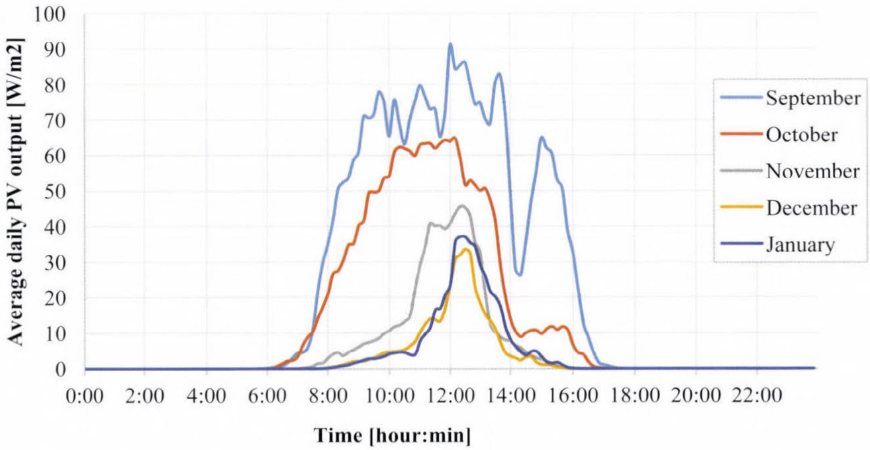

Fig. 5. Daily average electricity output of the 45° tilted, south oriented PV panel.

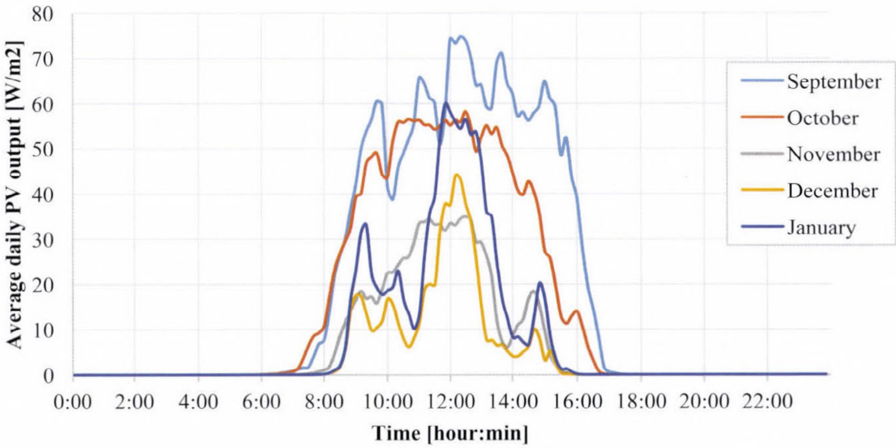

Fig. 6. Daily average electricity output of the 90° tilted, south oriented PV panel.

For east oriented PV panels, the daily electricity profiles are shown on *Fig. 7* and *Fig. 8*. On the 45° tilted panel, the highest energy output can be seen before 14:00, in case of the 90° tilted panel, the peak of the output can be found around 10:00. In case of the 45° tilted panel, a setback occurs in every month except October, this can be a result of shading objects. For the 90° tilted panel, the peak of electricity production is in the morning, when the panel is receiving direct sunlight, whilst in the afternoon the panel can not utilize the incoming diffuse radiation.

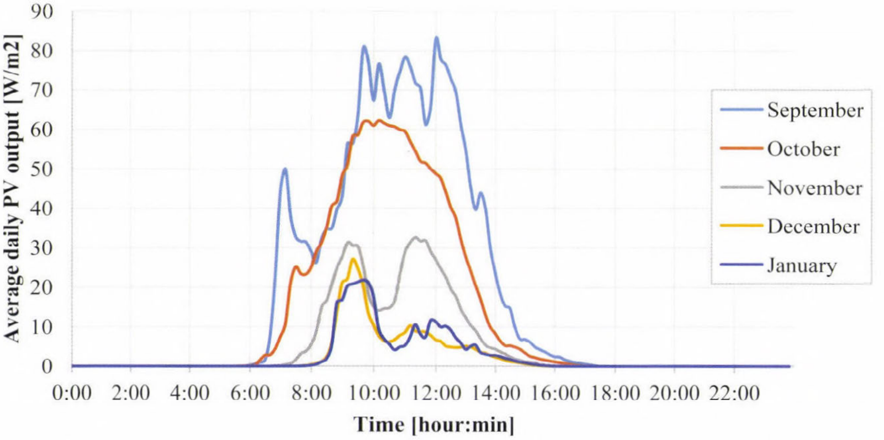

Fig. 7. Daily average electricity output of the 45° tilted, east oriented PV panel.

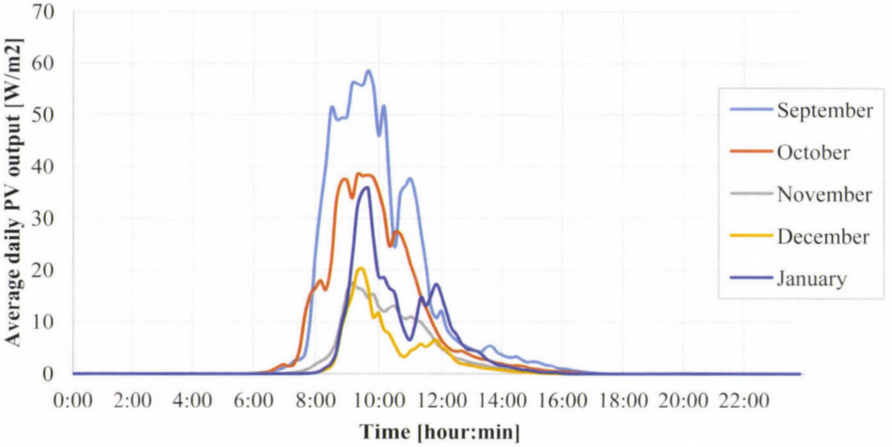

Fig. 8. Daily average electricity output of the 90° tilted, east oriented PV panel.

The average daily electricity output of west oriented surfaces are shown in *Fig. 8* and *Fig. 9*. For the west oriented surfaces nearly the same conclusions can be made as for the east oriented surfaces. The only significant difference is the time of the highest production, which, in case of west oriented surfaces, occurs in the afternoon. In *Fig. 8* it is visible, that after 12:00, the output of the panel experiences a setback which could be a result of a shading object. This problem in September is not occurring, possibly due to higher solar altitude. In *Fig. 9*, for the 90° tilted panel this setback is not visible, which also proofs the theory of the shading object.

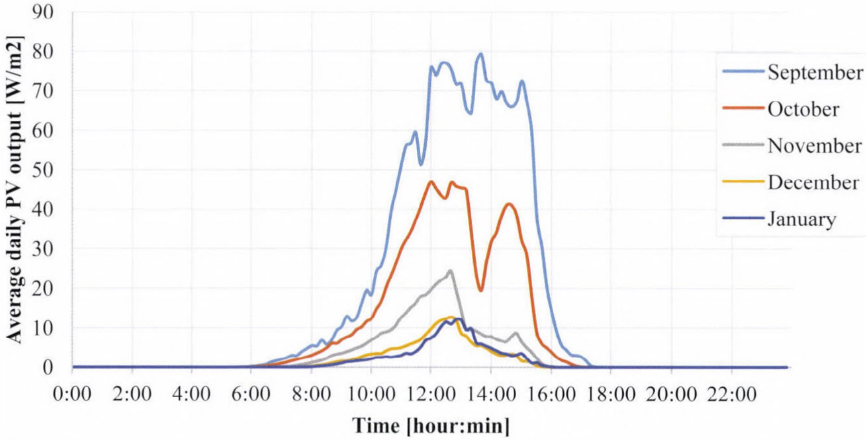

Fig. 8. Daily average electricity output of the 45° tilted, west oriented PV panel.

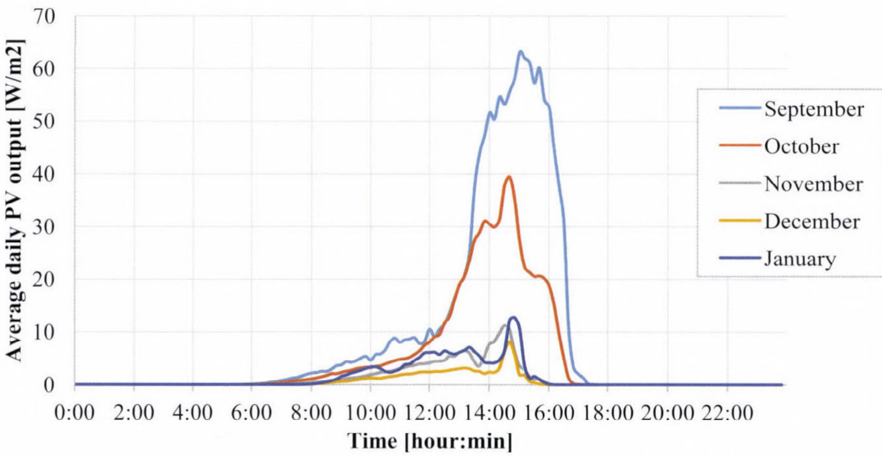

Fig. 9. Daily average electricity output of the 90° tilted, west oriented PV panel.

4. Summary

In this paper, a PV panel measurement station was described and the measured data from this station was statistically analyzed. The Hungarian station is unique due to the fact that at this station the outputs from differently oriented and tilted PV panels and global radiation are measured at the same time.

From the data measured it was concluded that, in case of the horizontally installed PV panel, the average efficiency is 14%. The correlation coefficient of the horizontal PV output and the measured global radiation is 0.930. This correlation coefficient proves linear correlation between the two datasets.

In the paper the measured PV outputs were compared. According to the measurement, in the autumn-winter period the highest energy yield is on the vertical, south oriented PV panel. Compared to the horizontal PV panel, only the south oriented panels have higher energy output in the measurement period.

Based on the values of correlation coefficients, it can be concluded that only the 45° tilted, south oriented PV panel has similar production profile to the horizontal one. The other panels show significant differences, thus they cannot be characterized by the horizontal panel.

References

Bhattacharya, P., Dey, S., and *Mustaphi, B.*, 2014: Some Analytical Studies on the Performance of Grid Connected Solar Photovoltaic System with Different Parameters. *Procedia Materials Science 6*, 1942–1950.

Ding, Y., Young, M., Zao, Y., Traverse, C., Benard, A., and *Lunt, R.R.*, 2015. Influence of photovoltaic angle-dependence on overall power output for fixed building integrated configurations. *Sol. Ener. Mat. Sol. C. 132*, 523–527.

Hwang, T., Kang, S. and *Kim, J.T.*, 2012. Optimization of the building integrated photovoltaic system in office buildings. Focus on the orientation, inclined angle and installed area. *Energ. Buildings 46*, 92–104.

Mehleri, E.D., Zervas, P.L., Sarimveis, H., Palyvos, J.A., and *Markatos, N.C.*, 2010. Determination of the optimal tilt angle and orientation for solar photovoltaic arrays. *Renew. Energ. 35*, 2468–2475.

Mulcué-Nieto, L.F. and *Mora-López, L.*, 2015. Methodology to establish the permitted maximum losses due to shading and orientation in photovoltaic applications in buildings. *Appl. Energ.* 137, 37–45.

Sánchez, E. and *Izard, J.*, 2015. Performance of photovoltaics in non-optimal orientations: An experimental study. *Energ. Buildings 87*, 211–219.

Yan, R., Saha, T.K., Meredith, P., and *Goodwin, S.*, 2013. Analysis of yearlong performance of differently tilted photovoltaic systems in Brisbane, Australia. *Energ. Convers. Manage. 74*, 102–108.

NEWS

IN MEMORIAM ISTVÁN MATYASOVSZKY (1960–2015)

István Matyasovszky died suddenly at his family's home in Érd at Christmas tim, on December 25, 2015. He was only 55. He is survived by his wife, Ildikó Simon; an adult daughter, Csilla, and younger twin daughters, Emma and Nelli who surely foresee difficult years without their father.
István Matyasovszky graduated as a meteorologist at the Eötvös Loránd University in 1984 with the second large group of students (altogether 15) having meteorology as a unique major subject. Most of his fellow graduated students are still working for the Hungarian Meteorological Service (e.g., Ákos Horváth, István Ihász, Márta Puskás, László Tölgyesi, and Szilvia Jenki). He started to work for the Department of Meteorology right after the graduation, and two years later he obtained the title of dr.univ. with a dissertation on the analysis of the statistical structure of the long temperature time series of Central England. He spent his entire academic career at the Eötvös Loránd University, first as a researcher, then, as assistant professor (from 1990), and finally as associate professor (since 1997). From 1991 to 1995 he spent 30 months at the University of Nebraska-Lincoln as visiting scientist, where he made joint research with Prof. István Bogárdi.
His main expertise was statistical climatology, to which Ottó Gulyás (a mathematician from the Hungarian Meteorological Service teaching generations of students) introduced him. He made detailed research on statistical climatology, i.e., time series analysis, spectral analysis, climate variability and change. He published his results in high quality meteorology-related journals, e.g., Journal of Geophysical Research, Theoretical and Applied Climatology, Climate Research, Atmospheric Environment, International Journal of Biometeorology, Meteorologische Zeitschrift. Altogether he had 51 and 30 research papers in English in international and Hungarian journals, respectively. He regularly sent interesting manuscripts to Időjárás, where he published a total of 19 journal papers. For his publications he was granted by the Szádecky-Kardoss Elemér Award in 1996 and 1997. In addition, the Hungarian Meteorological Society awarded him the Róna Zsigmond Award in 1992, and the Hungarian Academy of Science granted him the Bolyai János Fellowship during 1998-2001. He authored the book titled Statistical Climatology, which is a well-written basis for current students and anyone interested in the common scientific area of mathematics and climatology. For his great contribution to the national research and university teaching in meteorology, he received the Pro Meteorologia Award in 2005. His influence on meteorology-related research is very high, which is illustrated by the high number of independent citations (752 according to MTMT). In 2015, he obtained the DSc degree of the Hungarian

Academy of Science with his dissertation on new statistical methodologies applied to climatological studies.
He died unexpectedly, unpredictably – he was not ill. The recent years were probably the most happy and successful period both in his private life with having a supporting wife and two small children, and his academic career with completed DSc degree. He could have several decades ahead being spent in peace with his family, achieving more research goals with great success, and teaching several more generations of students to statistical climatology... We will surely miss István and will preserve his legacy at the Department of Meteorology at the Eötvös Loránd University.

Judit Bartholy

INSTRUCTIONS TO AUTHORS OF *IDŐJÁRÁS*

The purpose of the journal is to publish papers in any field of meteorology and atmosphere related scientific areas. These may be

- research papers on new results of scientific investigations,
- critical review articles summarizing the current state of art of a certain topic,
- short contributions dealing with a particular question.

Some issues contain "News" and "Book review", therefore, such contributions are also welcome. The papers must be in American English and should be checked by a native speaker if necessary.

Authors are requested to send their manuscripts to

Editor-in Chief of IDŐJÁRÁS
P.O. Box 38, H-1525 Budapest, Hungary
E-mail: journal.idojaras@met.hu

including all illustrations. MS Word format is preferred in electronic submission. Papers will then be reviewed normally by two independent referees, who remain unidentified for the author(s). The Editor-in-Chief will inform the author(s) whether or not the paper is acceptable for publication, and what modifications, if any, are necessary.

Please, follow the order given below when typing manuscripts.

Title page: should consist of the title, the name(s) of the author(s), their affiliation(s) including full postal and e-mail address(es). In case of more than one author, the corresponding author must be identified.

Abstract: should contain the purpose, the applied data and methods as well as the basic conclusion(s) of the paper.

Key-words: must be included (from 5 to 10) to help to classify the topic.

Text: has to be typed in single spacing on an A4 size paper using 14 pt Times New Roman font if possible. Use of S.I. units are expected, and the use of negative exponent is preferred to fractional sign. Mathematical formulae are expected to be as simple as possible and numbered in parentheses at the right margin.

All publications cited in the text should be presented in the *list of references*, arranged in alphabetical order. For an article: name(s) of author(s) in Italics, year, title of article, name of journal, volume, number (the latter two in Italics) and pages. E.g., *Nathan, K.K.,* 1986: A note on the relationship between photosynthetically active radiation and cloud amount. *Időjárás 90,* 10-13. For a book: name(s) of author(s), year, title of the book (all in Italics except the year), publisher and place of publication. E.g., *Junge, C.E.,* 1963: *Air Chemistry and Radioactivity.* Academic Press, New York and London. Reference in the text should contain the name(s) of the author(s) in Italics and year of publication. E.g., in the case of one author: *Miller* (1989); in the case of two authors: *Gamov* and *Cleveland* (1973); and if there are more than two authors: *Smith et al.* (1990). If the name of the author cannot be fitted into the text: (*Miller,* 1989); etc. When referring papers published in the same year by the same author, letters a, b, c, etc. should follow the year of publication.

Tables should be marked by Arabic numbers and printed in separate sheets with their numbers and legends given below them. Avoid too lengthy or complicated tables, or tables duplicating results given in other form in the manuscript (e.g., graphs).

Figures should also be marked with Arabic numbers and printed in black and white or color (under special arrangement) in separate sheets with their numbers and captions given below them. JPG, TIF, GIF, BMP or PNG formats should be used for electronic artwork submission.

More information for authors is available: journal.idojaras@met.hu

Published by the Hungarian Meteorological Service

Budapest, Hungary

INDEX 26 361

HU ISSN 0324-6329

IDŐJÁRÁS

QUARTERLY JOURNAL
OF THE HUNGARIAN METEOROLOGICAL SERVICE

CONTENTS

VOL. 120 * NO. 3 * JULY – SEPTEMBER 2016

IDŐJÁRÁS

Quarterly Journal of the Hungarian Meteorological Service

Editorial Office: Kitaibel P.u. 1, H-1024 Budapest, Hungary
P.O. Box 38, H-1525 Budapest, Hungary
E-mail: journal.idojaras@met.hu
Fax: (36-1) 346-4669

Indexed and abstracted in Science Citation Index Expanded™ and Journal Citation Reports/Science Edition
Covered in the abstract and citation database SCOPUS®

Subscription by mail:
IDŐJÁRÁS, P.O. Box 38, H-1525 Budapest, Hungary
E-mail: journal.idojaras@met.hu

IDŐJÁRÁS
Quarterly Journal of the Hungarian Meteorological Service
Vol. 120, No. 3, July – September, 2016, pp. 267–282

Overview of the tropospheric ozone problem: formation, measurements, trends, and impacts (Hungarian specialties)

Zita Ferenczi[1*] and **Kornélia Imre**[2]

[1]*Hungarian Meteorological Service, Gilice tér 39, H-1181 Budapest, Hungary*

[2]*MTA-PE Air Chemistry Research Group, Egyetem út 10, H-8200, Veszprém, Hungary*

[*]*Corresponding author E-mail: ferenczi.z@met.hu*

(Manuscript received in final form February 1, 2016)

Abstract—Ground-level or tropospheric ozone (O_3) is an oxidant air pollutant that has harmful effect on human health and vegetation, however, it is a short-lived greenhouse gas. Ozone is a secondary pollutant; which means that it is not directly emitted in the ambient air, but also produced from the photochemical oxidation of non-methane volatile organic compounds (NMVOCs), methane (CH_4), or carbon monoxide (CO) in the presence of nitrogen oxides (NO_x). It is destroyed both photochemically and through deposition to the surface. Summarizing the chemistry of ozone is complex and non-linear. Background concentrations of ground-level ozone in Europe do not show a significant downward trend, but in Hungary essential reduction (–0.28 $\mu g/m^3$) was observed at K-puszta station in the last decades. In the monthly distribution the amplitude decrease with increase in altitude, at K-puszta 45.1 $\mu g/m^3$, while at Nyírjes 36.6 $\mu g/m^3$ amplitudes were observed. Based on our data we found that the ozone gradient is about +1.4 $\mu g/m^3/m$. Breathing ozone can result in a number of negative health effects that are observed in relevant segments of the population. Ozone also is known as the air pollutant most damaging to agricultural crops and other plants. This article gives a general overview of the ozone problem focusing on the Hungarian specialties.

Key-words: air quality, ground level ozone measurements, AOT40, trends, vegetation

1. Introduction

In recent decades, ozone has been received increasing attention in the analysis of the regional and local air quality. In addition to being very important for sustaining life near the Earth's surface by absorbing hazardous UV radiation within the stratosphere, ozone is one of the most important greenhouse gases (*Paoletti* and *Cudlin,* 2012).

In the troposphere it is a strong oxidant air pollutant affecting human health and natural ecosystems, and reducing crop yields (*Wilkinson et al.,* 2012). Its concentration has doubled between the end of the 19th century and the 1980's. The annual average in the Northern Hemisphere has risen to 60–90 μg/m^3, and recently it increased with a further 10 μg/m^3 (*Wilson et al.,* 2012). In spite of the international agreements aimed to decrease the precursor gas emission, its concentration has been increasing (*Derwent et al.,* 2003, *Dentener et al.,* 2005). The reasons of the increase of ground level ozone concentration have not yet been understood well scientifically, but likely the sectors such as international shipping and air transport could be responsible for it, because the emissions of precursor gases from these activities are not regulated strictly enough (*Dentener et al.,* 2005). Since the sources of ozone are not confined to a smaller area but can be found worldwide, the problems related to ozone pollution has to be managed globally. Ground-level ozone episodes, when O_3 concentrations may reach at 400 μg/m^3 or more, occur in polluted regions under hot and sunny conditions. This has been ascribed to photochemical processes due to the occurrence on a large scale of favorable meteorological circumstances (*Guicherit* and *Van Dop,* 1977). The long-range transport of tropospheric ozone and its precursors have important impact on O_3 concentrations at regional and local scales. In the low to midlatitudes, O_3 transport from the polluted source regions like North/South America, Europe, and Asia generally accounts for more than 50% of ozone even in remote locations (*Sudo* and *Akimoto,* 2007).

The Council Directive on air pollution by ozone (92/72/EEC) defines several threshold levels, and it establishes a harmonized procedure for monitoring and exchanging data. It also arranges to provide the public with information when warning and information threshold levels are exceeded.

- Health protection threshold: days with an 8-hour average ozone concentration of more than 120 μg/m^3.
- Population information threshold: the hourly average ozone concentrations exceed 180 μg/m^3.
- Population warning threshold: the hourly average ozone concentrations exceed 360 μg/m^3.

Air pollution is a process that introduces diverse pollutants into the atmosphere that cause harm to humans, other living organisms, and the natural environment (*Brauer et al.,* 2012; *Kim et al.,* 2013). The effects of O_3 found that exposure to ambient O_3 levels is linked to such respiratory ailments as asthma, inflammation, and premature aging of the lung, and to such chronic respiratory illnesses as emphysema and chronic bronchitis (*Delfino et al.,* 1998). More than two million deaths are estimated to occur globally each year as a direct consequence of air pollution through damage to the lungs and the respiratory system (*Shah et al.,* 2013). Among these deaths, around 2.1 and 0.47 million are caused by fine particulate matter (PM) and ozone, respectively (*Chuang et al.,* 2011; *Shah et al.,* 2013).

Besides positive CO_2 and nitrogen fertilization, many studies have show that ozone and its precursors are efficiently transported in the regional scale and consequently ozone tends to present relatively high background levels in rural areas. Over 90% of vegetation damage may be result of tropospheric ozone alone (*Adams et al.,* 1986). Previously, it was thought that tropospheric ozone is an urban problem, elevated O_3 concentrations are now recognized as extending far beyond city limits. Elevated concentrations in rural regions significantly affect crop yields, forest productivity, and natural ecosystems. Evaluations of the national economic impact of ozone on crop yield have indicated values of the order of US$ 2-4 billion in the United States and of 4 billion EUR in Europe (*Murphy et al.,* 1999, *Holland et al.*, 2002).

Ozone in the ground level is also expected to contribute to the devastation of building and material. In developed countries, where the control of emissions of air pollutants are relatively efficient, and the emission projections for the precursor gases indicate continuous decrease (*Kelly et al.,* 2010), the O_3 concentration will likely decline in the next decades. Although the climate change will complicate the picture the rate of decline will be slowed down. Due to the climate change heat waves may occur more often and could cause extremely high ozone concentrations for a short time. This fact could also demonstrate that while O_3 as a greenhouse gas affects the climate, the climate change will result weather conditions which may lead to the elevation of O_3 concentration in the ground level. It also shows that the climate change is one of the most complex problems, and this also proves the importance the international cooperation to solve the issue of air quality. Currently, in Europe the revised Gothenburg protocol specifies emission reduction commitments for precursors. In case of Hungary the emission reduction of volatile organic compounds (VOCs) was committed by 30 percent as NO_x by 42 percent, both of them are precursor gases of ozone.

1.1. Ozone formation and air quality

Ozone is found in two different areas of the atmosphere – the stratosphere and the troposphere. In the stratosphere, ozone provides a protective shield by filtering out the dangerous ultraviolet radiation from the sun. Here the ozone molecules are formed by the photo-dissociation of molecular oxygen, and the atomic oxygen reacts with molecular oxygen to produce ozone.

Tropospheric ozone is not emitted directly in to the atmosphere, so it is described as a secondary air pollutant. It is an important atmospheric oxidant, smog component, and a short-lived greenhouse gas. In the troposphere, it is formed by photochemical reactions of nitrogen oxides with volatile organic compounds, methane, and/or carbon monoxide in the presence of sunlight. NO_x is primarily a product of fossil fuel combustion (63%), but secondarily it is a result of biomass burning (14%) (*IPCC,* 2001). Natural vegetation is a source of VOCs, which decompose into peroxy radicals, which react with NO to produce NO_2. In urban regions with high concentrations of NO_x, ozone production is generally VOC-limited, whereas in suburban or rural regions with low NO_x levels, ozone production is NO_x-limited. The different spatial distributions of NO_x and VOC production, as well as NO destruction of ozone, often result in the largest ozone concentrations downwind of urban centers, rather than in urban areas themselves (*Gregg et al.,* 2003). Transport of the chemical mixtures eventually results photodissociation and O_3 transformation at sites quite distant from original source of the precursor emissions. Increasing rate emissions of its precursors have caused ozone concentrations to experience a strong increase in highly populated continental regions during the last century (*Marenco et al.*, 1994). Tropospheric ozone concentrations can also be influenced by UV radiation. A rise in UV radiation intensity is expected to decrease tropospheric ozone in a clean environment, while increased UV in regions with precursors (NO_x, CO, CH_4) rich atmospheres will lead to increased tropospheric ozone concentrations. Mainly in summer months, when conditions of O_3 formation improve (high temperature, radiation, wind stagnation), O_3 levels typically rise even in remote background areas. Ozone is, therefore, no longer just an issue for air quality, but a complex environmental problem.

1.2. Ozone measurements and trends in Europe and Hungary

The analysis of European rural background ozone trends between 1996–2005 had carried out by *Wilson et al.* (2012). They processed data available from the EMEP and GAW monitoring stations and concluded that, on the European scale only slight increase in ozone levels (0.32–0.04 $\mu g/m^3$ per year) with a total range of 2.56 to 2.1 $\mu g/m^3$ per year can be determined. The greatest reduction is observed at K-puszta, Hungary (–4.11% per year). The first trend analysis using the tropospheric ozone measurements from K-puszta was published by *Haszpra et al.* (2003). In this paper, 0.64 $\mu g/m^3$ per year increasing ozone trend was determined for the time period of 1990–2002.

In Hungary, the Hungarian Meteorological Service is responsible for the rural ground-level ozone measurements. The institute maintains three background monitoring stations, where tropospheric ozone measurements are carried out beside the observation of other pollutants. Since the stations are located in different geographical environments from plains to mountains, this effect is reflected in the measured data. *Fig. 1* shows the positions of the monitoring stations in Hungary.

Farkasfa background air pollution monitoring station is located in the western part of Hungary (46°54'37" N, 16°18'34" E, 312 m asl), at the area of the Őrség National Park. The station is surrounded by forest and no essential local source can be found nearby. The tropospheric ozone measurements started at this station in 1996. For many reasons, the ozone measurements were interrupted between 2005–2006, but in May of 2006, the operation of the station restarted.

K-puszta is the regional background air pollution monitoring station located in the central part of Hungary, on the Hungarian Great Plain (46°58' N, 19°33' E, 125 m asl). The station is located in a big forest clearing. In the wider region, agricultural fields, forest patches, pastures, and open bushy regions can be found. The prevailing wind blows from the west-to-north sector. The nearest town (Kecskemét, approximately 112 thousand inhabitants) is about 15 km to the southwest. The tropospheric ozone measurements started at this station in 1990. K-puszta monitoring station belongs to the European air quality monitoring (e.g., EMEP) and the Global Atmosphere Watch (GAW) networks. The station was also involved in the Tropospheric Ozone Research, a Sub-Project of EUROTRAC project (*Haszpra et al.,* 1997).

Nyírjes background air pollution monitoring station is located in the Mátra Mountains, in the northeast part of Hungary (47°52' N, 19°57' E, 702 m asl). The tropospheric ozone measurements started at this station in 1996.

Fig. 1. Location of the ground-level background ozone monitoring stations in Hungary

2. Results

2.1. Annual trend in background stations

This part concerns the background stations for the annual trend analysis over the 1996–2014 period. Atmospheric lifetimes of ozone precursors are long enough to allow them to be transported on long distance, but the range of the impact depends on meteorological and geographical conditions. Although the stations are located in background areas, the local topography and surroundings are different. These circumstances undoubtedly may influence the ozone concentration. *Fig. 2* shows the calculated ozone trends for the Hungarian monitoring stations. We assumed that the trends are linear calculated by deseasonalizing the ozone time series. Mann-Kendall analysis of Sen-Theil slopes was used for the calculations.

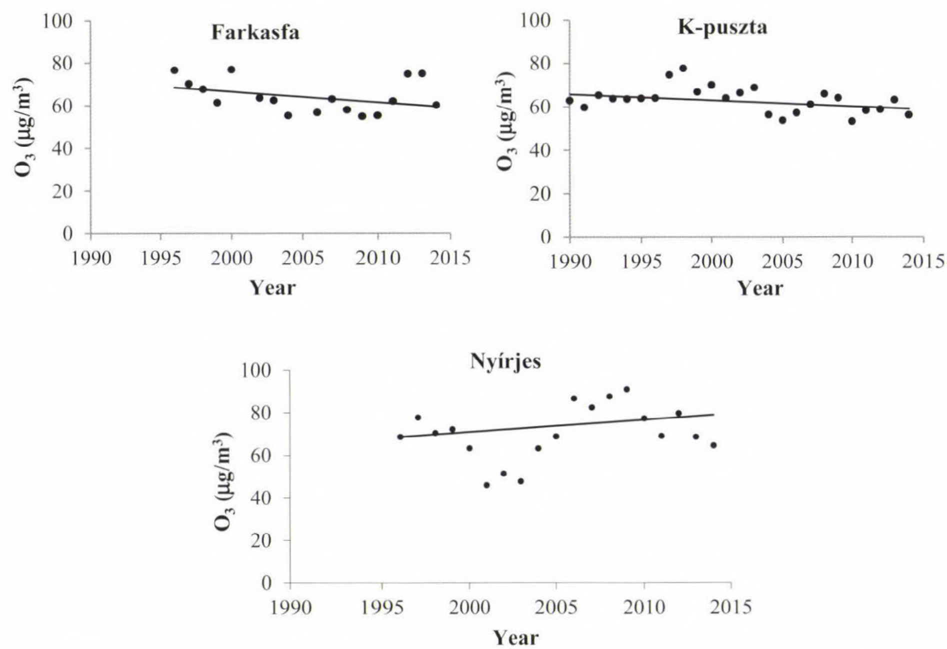

Fig. 2. Ozone trends detected at the Hungarian background air quality monitoring stations (dots = annual mean).

In case of Farkasfa and K-puszta stations, decreasing trends can be observed, while in case of Nyírjes station, the trend is increasing in average but there are intervals when the ozone concentration decreased for a few years (between 1997–2002 and 2009–2014). The trend determined for K-puszta using our 25 years data is –0.276 µg/m^3 per year, but the trend determined by *Wilson et al.* (2012) using only 10 years (between 1996–2005) shows more intensive decreasing (–1.826 μg/m^3 per year). Similar results were found by *Sicard et al.,* (2013) over the period 2000–2010, when annual mean concentrations decreased by 0.43% per year at rural sites. Explanation of the maximum values and evolution could be in the local and annual meteorological conditions. At K-puszta, the concentration values usually higher than at Farkasfa that can be explained on one hand by the different meteorological conditions (higher temperature) and higher altitude on the other hand by the ozone plumes coming from Budapest city (*Mészáros et al.,* 2009). The decreasing trends at Farkasfa and K-puszta can be attributed to the reduction in NO_x and VOC emission within Europe. Background concentrations of ozone in Europe are influenced significantly by emissions of precursor gases outside the continent (*Guerreiro et al.,* 2014). Changes of the annual mean of ozone concentrations could have been caused by the precursor gas emission, the effect of the long-range transport of ozone and pre-gases, and the meteorological situation (heat waves, rainfall). *Fig. 3* shows the abatement in NO_x and VOC levels in Hungary that could have caused the reductions in episodic peak ozone levels.

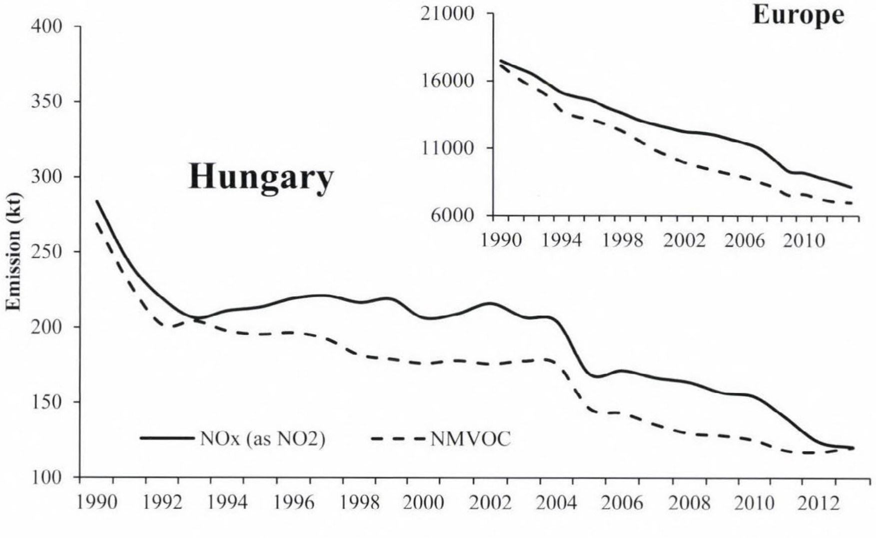

Fig. 3. Anthropogenic NO_x (as NO_2) and NMVOC emissions 1990-2013 for Hungary and Europe (Source: www.ceip.at).

According to *Sicard et al.* (2009), between 1995 and 2003, a rate of –0.48% per year for stations below 1000 m asl and +1.75% per year for stations above 1000 m asl were observed. They mentioned that the possible explanations could be the following:

1.) If ozone is produced in lower field from exhaust and industrial sources, it goes up with the favour of the temperature inversion phenomenon. At high altitude, ozone stagnates to form a reservoir layer.

2.) Altitude sites are not influenced by the ozone destruction by nitrogen oxides. Indeed, the NO concentration, emitted mainly by the road transport, are weak in the higher altitude. In addition, there are biogenic VOC emissions, emitted by the vegetation, which can increase the ozone production.

3.) Approximately 10% of tropospheric ozone is estimated to be of stratospheric origin.

It is also known that background ozone level increases with the height in the lower troposphere. Based on our data (average ozone concentration from 1996 to 2014), a change in the ozone vertical gradient is clearly visible (see *Fig. 4*). The ozone gradient is about +1.4 $\mu g/m^3/m$. This spatial distribution shows an interesting pattern, because the most urban-influenced site (K-puszta) has the lowest concentration, while either the distance or the elevation is not more efficient contribution to reach this high ozone concentration. However, this problem is quite complex, further investigation is needed to explain these findings.

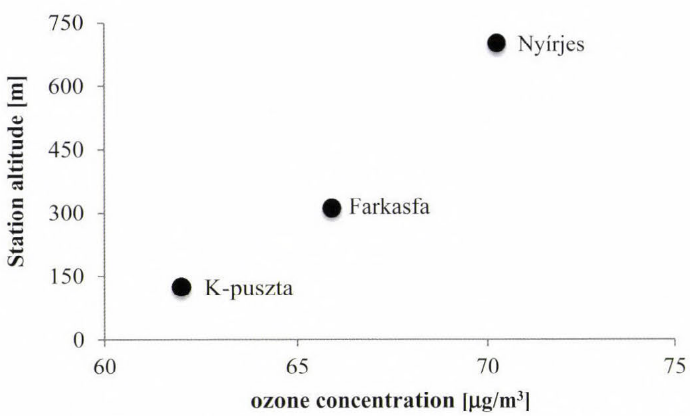

Fig. 4. The total average ozone concentration depending on the station altitude.

2.2. Seasonal trend analysis

The monthly means of ozone concentration were also determined for the three stations. *Fig. 5* presents the results of this investigation. The three diagrams reflect that the ozone has different yearly variation on the sites. The biggest amplitude can be observed at K-puszta (45.1 μg/m^3), while the lowest at Nyírjes (36.6 μg/m^3). This result is reflects the fact that Nyírjes is a mountain station where the amplitude of the monthly and daily ozone concentrations are much lower than at the plain stations (*Chevalier et al.,* 2007).

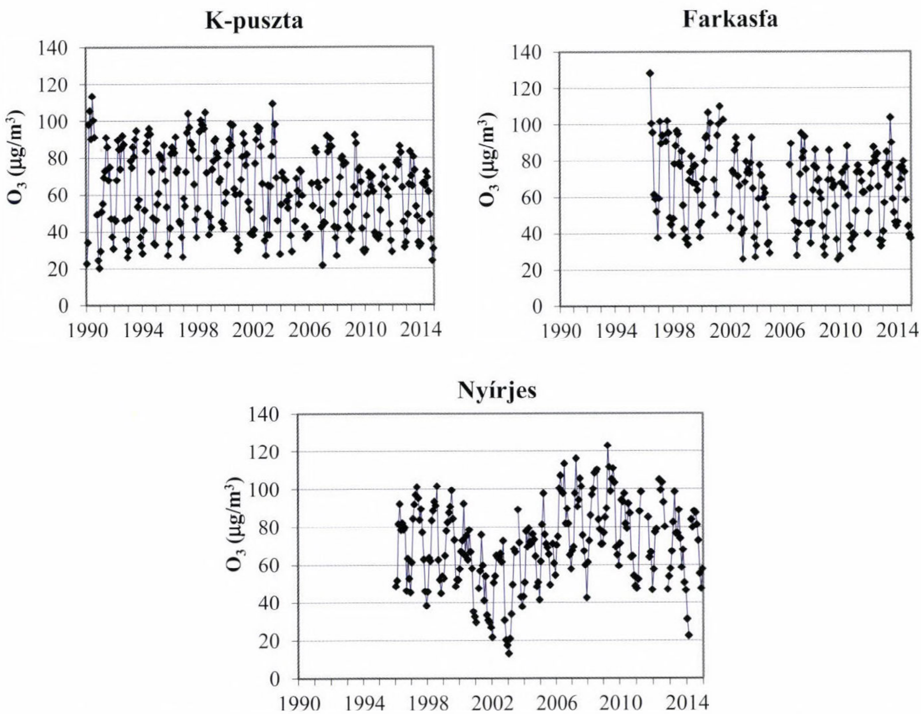

Fig. 5. Temporal variation of observed monthly mean ozone concentrations detected at the Hungarian background air quality monitoring stations (dots = monthly mean).

The trends for the 5th, 50th, and 95th percentiles of ozone concentrations show a decrease for Farkasfa and K-puszta while an increase for Nyírjes (*Fig. 6*). In case of Farkasfa and K-puszta, the 95th percentile decreasing trend is much larger and the 5th percentile decreasing trend is much lower than the median trend. It means that the decreasing trends of the yearly mean values are basically caused by the decreasing maximum concentration values, while the minimum values show a moderate rising.

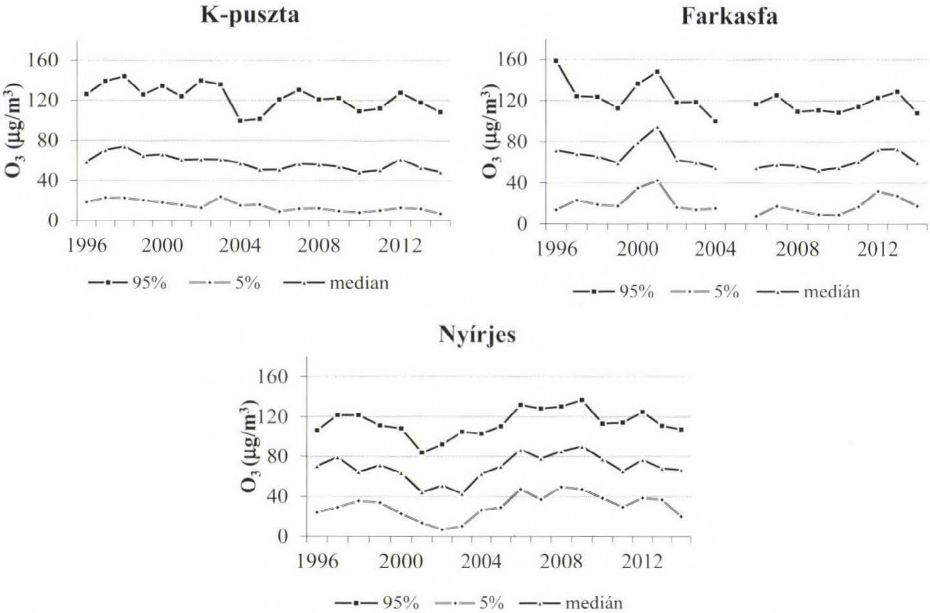

Fig. 6. Temporal variation of the annual 95th, 50th, and 5th percentiles of ozone concentrations detected at the Hungarian background air quality monitoring stations.

In case of Nyírjes, in all three percentiles (95th, 50th, 5th) a rising trend was found (see *Table 1*). The mean ozone concentration is known to strongly increase with altitude in the troposphere mainly in the first 1000 m. The comparison of the results of the three Hungarian stations also shows that the minimum ozone concentration is rising with the altitude. This can be explicable with that the ozone content is eroded near the surface by deposition and titration that dominate in the boundary layer at the yearly time-scale.

Table 1. Mean trends by stations for the 5th, 50th, and 95th percentiles of ozone concentrations

	Trend (μg/m³/yr)		
Station	**5th percentile**	**median**	**95th percentile**
K-puszta	–0.75	–0.97	–1.24
Farkasfa	–0.20	–0.58	–1.23
Nyírjes	+0.76	0.67	+0.67

Sicard et al. (2013) found that background ozone concentration decreased of –1.1% per year with annual averages and –0.9% per year with median values. They observed that the number of concentration values above 65 μg/m^3 increased significantly (1% per year), and the 25th percentiles decreased of –0.4% per year over the 2000–2008 period. Based on these and our results the background ozone level seems to increase. However the maximum ozone concentration shows decreasing trend, there are several days when the values reach a threshold. The exceedance days of air quality threshold values for ozone at the Hungarian background air quality monitoring stations decreased in the last 25 years in connection with the emission reduction of precursor gases. The number of days when the O_3 concentration exceeds the previously defined threshold values for ozone was also determined using the Hungarian monitoring data (*Fig. 7*). At our stations, the ground-level ozone has never exceeded the population warning threshold in the examined period, but the ozone concentrations were quite often above the other threshold values. The ozone concentration exceeded the health protection threshold more than 100 times per year only at K-puszta in the time period of 1997–2002. Since K-puszta is a background station, it might be better termed "urban-affected", because of advected urban plumes from Budapest that affect concentration characteristics. Because Nyírjes and Farkasfa are beyond the reach of urban plumes or other anthropogenic effects, they can show small seasonal variations in ozone concentration.

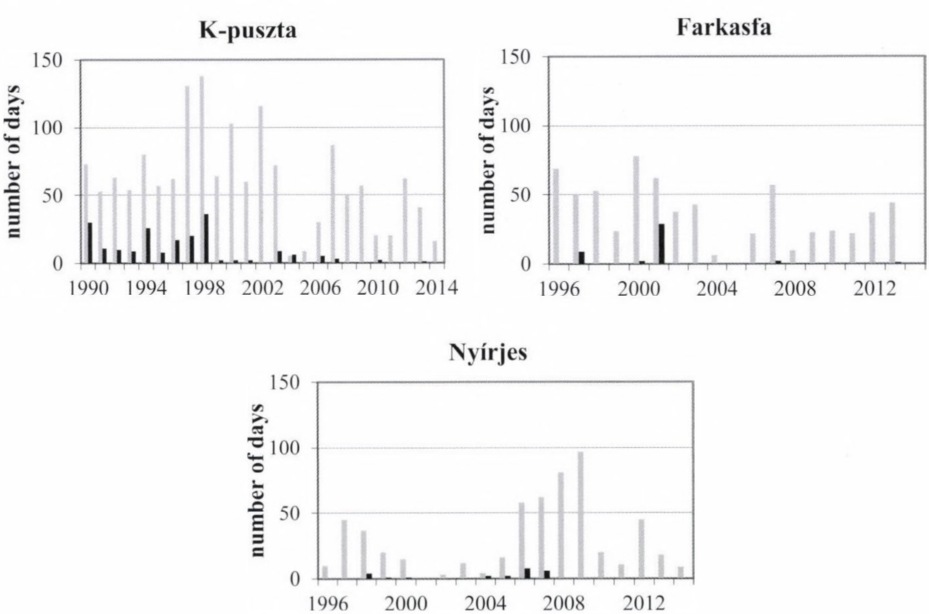

Fig. 7. Exceedance days of air quality threshold values for ozone at the Hungarian background air quality monitoring stations (gray = health protection threshold, black = population information threshold).

The frequency distribution of the hourly ozone concentrations was also calculated. For the comparability of the results, we used only the data from the time period 1996–2014 at all three stations. From many European country's data it can be concluded, that the proportion of ozone concentration range of 40–78 μg/m^3 has increased, while the proportion in the category, 80–118 μg/m^3 has not changed in the summer months. The main differences in terms of frequency distribution can be found in the winter season between the mountain and plain stations. *Fig. 8* shows the results of this examination. The data availability for the stations and for the time period of 1996–2014 was: Farkasfa 80%, K-puszta 90%, Nyírjes 86% (in case of K-puszta, the data availability was 87% for the time period of 1990–2014). The highest ground level ozone concentrations can be expected at Farkasfa in June and July, at K-puszta in June, July, and August, while at Nyírjes only in July.

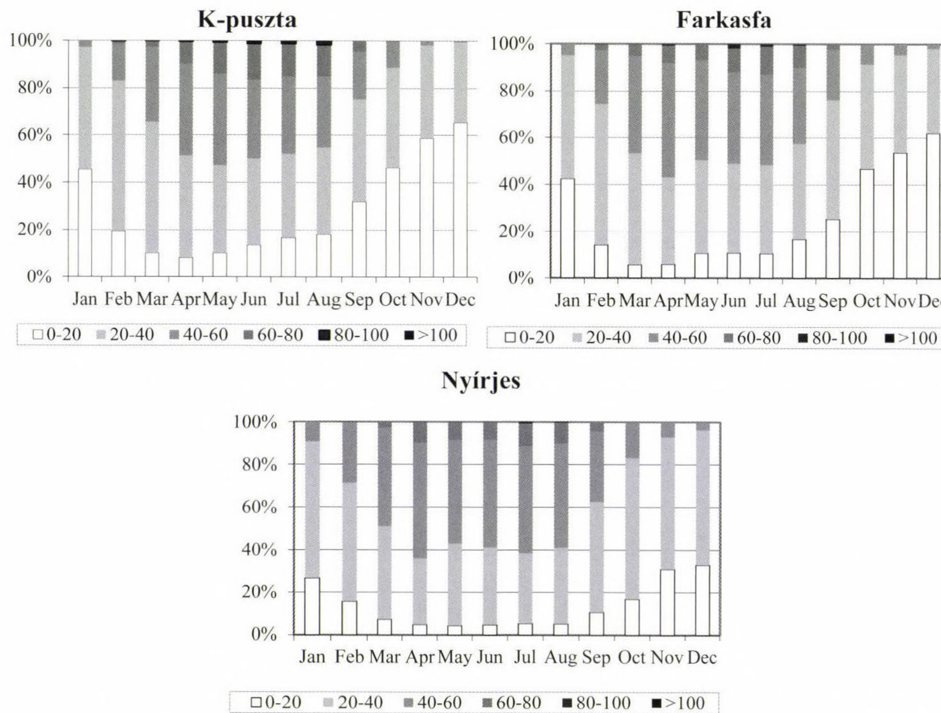

Fig. 8. Frequency distribution of ozone concentrations (hourly values) at the Hungarian background air quality monitoring stations.

2.3. *AOT trends*

Among the European standards, AOT40 index is generally used for the protection of the vegetation. AOT40 is defined as the sum of differences between the hourly mean concentration and the 80 μg/m³ threshold value for each hour when the concentration exceeds 80 μg/m³. Then these values are summarized each day from May 1 to July 31, for the time period of 8–20 hours. In this study we found significant differences among the stations (see *Fig. 9*).

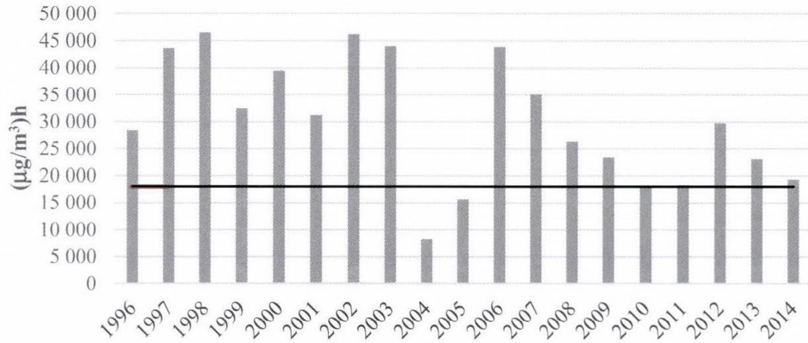

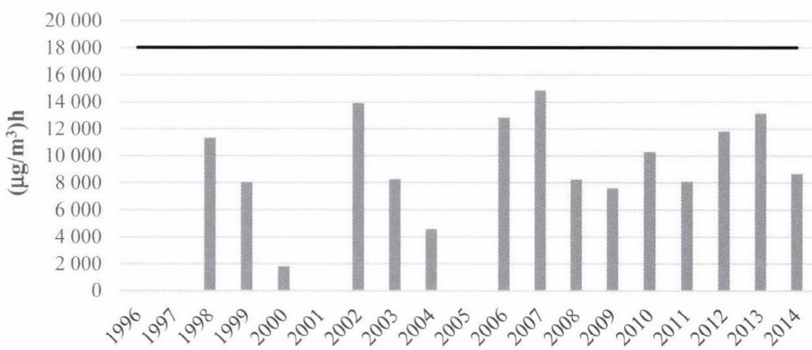

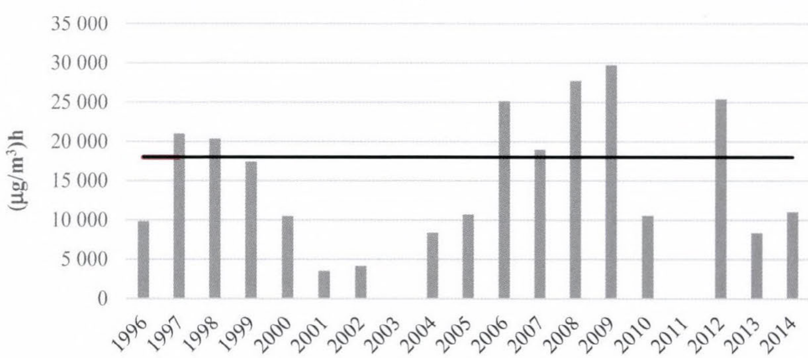

Fig. 9. AOT40 values (μg/m³)h at the Hungarian background air quality monitoring stations (horizontal black line = threshold value).

Despite the Hungarian declining ozone concentration trends (see *Fig. 2*), AOT40 did not show any trend. In case of K-puszta, the AOT40 exceed the limit value in most cases, while at Farkasfa the calculated AOT40 has never been exceeded the limit value, and at Nyírjes the AOT40 exceeded the limit value only in some cases. Nyírjes and Farkasfa stations are located in areas devoid of local pollution sources, which can be a possible reason for the AOT40 values. In contrast, K-puszta is located in the direction of Budapest's plume, and due to its geographic position, the annual average temperature is higher than in the other stations, which favors for the higher ozone concentration, consequently for higher value of AOT40.

Between 21% and 69% of agricultural crops in the EEA-32 (European Economic Area) were exposed to O_3 levels above the EU target value for protecting vegetation (18 000 ($\mu g/m^3$)h for AOT40) from 2002 to 2010, mostly in southern and central Europe (*EEA*, 2013). Reduction of yield with increasing ozone over a 80 $\mu g/m^3$ threshold, resulting in a 10% reduction in yield for ozone levels commonly found in southern Europe (*Fuhrer et al,* 1997). In Hungary, mainly the beans have shown ozone-injury symptoms.

3. Conclusion

In this paper, recent results on ozone levels and trends at background sites located in Hungary are discussed. Studies have shown that concentrations of ozone in the Hungarian background stations are influenced by emissions of precursor gases outside the continent. The Mann-Kendall test was used to detect the trend from background ozone concentrations. In case of Farkasfa and K-puszta stations, decreased trends (–0.498 $\mu g/m^3$ and –0.277 $\mu g/m^3$) can be observed, while in case of Nyírjes station, the trend is increasing (0.567 $\mu g/m^3$) in average, but there are intervals when the ozone concentration decreased for a few years. In the monthly distribution, the ozone concentrations show different variation. The amplitude decreased due to the increase in altitude, at K-puszta 45.1 $\mu g/m^3$, while at Nyírjes 36.6 $\mu g/m^3$ amplitudes were observed. Since K-puszta is a background station, it might be better termed "urban-affected", because of advected urban plumes from Budapest that affect concentration characteristics. Nyírjes and Farkasfa are beyond the reach of urban plumes or other anthropogenic effect, they can show small seasonal variations in ozone concentration. Based on our data, we found that the ozone gradient is about +1.4 $\mu g/m^3/m$. We observed that in case of Farkasfa and K-puszta, the 95th percentile decreasing trend is much larger and the 5th percentile decreasing trend is much lower than the median trend. It means that the decreasing trends of the yearly mean values are basically caused by the decreasing maximum concentration values. According to AOT40, we found big differences between the stations, however, the data did not show any trend. As Nyírjes and Farkasfa are located in areas devoid of local pollution sources, the values of AOT40 were low, in contrast to K-puszta, where the AOT40 were higher in every year, consequently.

Acknowledgements: Present article was published in the frame of the project TÁMOP-4.2.2.A-11/1/KONV-2012-0064: „Regional effects of weather extremes resulting from climate change and potential mitigation measures in the coming decades". The project is realized with the support of the European Union, with the co-funding of the European Social Fund.

References

Adams, R.M., Hamilton, S.A., and *McCarl, B.A.,* 1986: The benefits of pollution control: the case of ozone and U.S. Agriculture. *Am. J. Agric. Econ. 68*, 886–893.

Brauer, M., Amann, M., Burnett, R.T., Cohen, A., Dentener, F., Ezzati, M., Henderson, S.B., Krzyzannowski, M., Martin, R.V., Dingenen, R. Donkelaar, A., and *Thurston, G.D.,* 2012: Exposure assessment for estimation of the global burden of disease attributable to outdoor air pollution. *Environ. Sci. Technol. 46*, 652–660.

Chevalier, A., Gheusi, F., Delmas, R., Ordóñez, C., Sarrat, C., Zbinden, R., Thouret, V., Athier, G., and *Cousin, J.-M.,* 2007*:* Influence of altitude on ozone levels and variability in the lower troposphere: a ground-based study for western Europe over the period 2001–2004. *Atmos. Chem. Phys. Discuss 7*, 1327–1356.

Chuang, K.-J., Yan, Y.-H., Chiu, S.-Y., and *Cheng T.J.*, 2011: Long-term air pollution exposure and risk factors for cardiovascular diseases among the elderly in Taiwan. *Occup. Environ. Med., 68*, 64–68.

Dentener, F., Stevenson, D., Cofala, J., Mechler, R., Amann, M., Bergamaschi, P., Raes, F., and *Derwent, R.*, 2005: The impact of air pollutant and methane emission controls on tropospheric ozone and radiative forcing: CTM calculations for the period 1990–2030. *Atmos. Chem. Phys., 5*, 1731–1755.

Delfino, R.J., Murphy-Moulton, A.M., and *Becklake, M.R.,* 1998: Emergency room visits for respiratory illnesses among the elderly in Montreal: association with low level ozone exposure. *Environ. Res. 76*, 67–77.

Derwent, R.G., Jenkin, M.E., Saunders, S.M., Pilling, M.J., Simmonds, P.G., Passant, N.R., Dollardf, G.J., Dumitreanf.P., and *Kent, A.*, 2003: Photochemical ozone formation in north west Europe and its control. *Atmos. Environ 37*, 1983–1991.

EEA, 2013: Exposure of Ecosystems to Acidification, Eutrophication and Ozone (Indicator CSI 005) 2013: http://www.eea.europa.eu/data-and-maps/indicators/exposure-of-ecosystems-to-acidification-2/exposure-of-ecosystems-to-acidification-5.

Fuhrer, J., Skarby, L., and *Ashmore, M.R.,* 1997: Critical levels for ozone effects on vegetation in Europe. *Environ. Pollut. 97*, 91–106.

Gregg, J.W, Jones, C.G., and *Dawson, T.E.,* 2003: Urbanization effects on tree growth in the vicinity of NewYork City, *Nature 424*, 183–187.

Guerreiro, C.B.B., Foltescu, V., and *de Leeuw, F.,* 2014: Air quality status and trends in Europe. *Atmos. Environ. 98,* 376–384.

Guicherit, R. and *Van Dop, H.,* 1977: Photochemical production of ozone in Western Europe (1971–1975) and its relation to meteorology. *Atmos. Environ. 11*, 145–155.

Haszpra, L., Bozó, L., Ferenczi, Z., and *Sándor, V.,* 1997: Formation and transport of tropospheric ozone in Hungary. *Troposph. Ozone Res. 6*, 317–321.

Haszpra, L., Ferenczi, Z., Lagzi, I., and *Turányi, T.,* 2003: Formation of tropospheric ozone in Hungary. Tropospheric Ozone Research, Final Report of Subproject TOR-2, EUROTRAC-2, ISS, Munich, 87–89.

Holland, M., Mills, G., Hayes, F., Buse, A., Emberson, L., Cambridge, H., Cinderby, S., Terry, A., and *Ashmore, M.,* 2002: Economic Assessment of Crop Yield Losses from Ozone Exposure. Report to U.K. Department of Environment Food and Rural Affairs under Contract 1/3/170. Centre for Ecology and Hydrology, Bangor. Available at: http://www.airquality.co.uk/archive/reports/.

IPCC (Ed.), Climate Change 2001: The Scientific Basis, Cambridge University Press, New York.

Kelly, A., Lumbreras, J., Maas, R., Pignatelli, T., Ferreira, F., and *Engleryd, A.* 2010: Setting national emission ceilings for air pollutants: policy lessons from an ex-post evaluation of the Gothenburg Protocol. *Environ. Sci. Policy 13*, 28–41.

Kim, K.-H., Jahan, S.A. and *Kabir, E.*, 2013: A review on human health perspective of air pollution with respect to allergies and asthma. *Environ. Int. 59*, 41–52.

Marenco, A., Gouget, H., Nédélec, P., and *Pages, J.-P.:* 1994: Evidences of a long term increase in tropospheric ozone in Pic du Midi data series: consequences in the positive radiative forcing. *J. Geophys. Res. 99*, 16617–16632.

Mészáros, R., Szinyei, D., Vincze, C., Lagzi, I., Turanyi, T., Haszpra, L., and *Tomlin, A.S.,* 2009: Effect of the soil wetness state on the stomatal ozone fluxes over Hungary. *Int. J. Environ. Pollut. 36,* 180–194.

Murphy, J.J., Delucchi, M.A., McCubbin, D.R., and *Kim, H.J.,* 1999: The cost of crop damage caused by ozone air pollution from motor vehicles. *J. Environ. Manage. 55,* 273–289.

Paoletti, E. and *Cudlin, P.*, 2012: Ozone, climate change and forests. *Environ. Pollut. 169,* 249.

Sicard, P., Coddeville, P., and *Galloo, J.C.,* 2009: Near-surface ozone levels and trends at rural stations in France over the 1995–2003 period. *Environ. Monit. Assess. 156*, 141–157.

Sicard, P., De Marco, A., Troussier, F., Renou, C., Vas, N., Paoletti, E., 2013: Decrease in surface ozone concentrations at Mediterranean remote sites and increase in the cities. *Atmos. Environ. 79,* 705–715.

Shah, A.S.V., Langrish, J.P., Nair, H., McAllister, D.A., Hunter, A.L., Donaldson, K., Newby, D.E., and *Mills, N.L.,* 2013: Global association of air pollution and heart failure: a systematic review and meta-analysis. *The Lancet 382*, 1039–1048.

Sudo, K. and *Akimoto, H.,* 2007: Global source attribution of tropospheric ozone: Long-range transport from various source regions. *J. Geophys. Res. 112*, D12302.

Wilkinson, S., Mills, G., Illidge, R., and *Davies, W.J.,* 2012: How is ozone pollution reducing our food supply? *J. Experiment. Botany 63*, 527–536.

Wilson, R.C., Fleming, Z.L., Monks, P.S., Clain, G., Henne, S., Konovalov, I.B., Szopa, S., and *Menut, L.,* 2012: Have primary emission reduction measures reduced ozone across Europe? An analysis of European rural background ozone trends 1996–2005, *Atmos. Chem. Phys. 12*, 437–454.

IDŐJÁRÁS

Quarterly Journal of the Hungarian Meteorological Service
Vol. 120, No. 3, July – September, 2016, pp. 283–300

Intra-urban temperature observations in two Central European cities: a summer study

Enikő Lelovics[1], **János Unger**[*1], **Stevan Savić**[2], **Tamás Gál**[1], **Dragan Milošević**[2], **Ágnes Gulyás**[1], **Vladimir Marković**[3], **Daniela Arsenović**[3], and **Csilla V. Gál**[4]

[1] *Department of Climatology and Landscape Ecology, University of Szeged P.O. Box 653, 6701 Szeged, Hungary*

[2] *Climatology and Hydrology Research Centre, Faculty of Science, University of Novi Sad; Trg Dositeja Obradovića 3, 21000 Novi Sad, Serbia*

[3] *Center for Spatial Information of Vojvodina, Faculty of Science, University of Novi Sad, Trg Dositeja Obradovića 3, 21000 Novi Sad, Serbia*

[4] *College of Architecture, Illinois Institute of Technology, Chicago, Illinois 60616-3793, USA*

[*] *Corresponding author E-mail:* unger@geo.u-szeged.hu

(Manuscript received in final form October 8, 2015)

Abstract—This paper presents an urban climatological application of the urban monitoring systems – recently implemented in Szeged, Hungary and Novi Sad, Serbia – using the first set of data collected during the summer of 2014. In order to ensure a representative number and placement of stations, the selection of measurement sites was based on Local Climate Zone (LCZ) maps developed for both cities. Present paper concentrates only on the intra-urban temperature pattern characteristics expressed by the thermal reactions of the different LCZ classes in both cities. The daily temperature indices (e.g., summer days) have the highest values in the densely built up LCZs. The diurnal cycle of surplus temperatures by LCZ classes under anticyclonic weather conditions were found to be similar in the two cities with higher absolute values in the case of Novi Sad. During summer, the diurnal variation of conventional heat island intensity confirms the general knowledge that it remains positive with highest values at night, while negative values occur predominantly during the day.

Key-words: urban climate, Local Climate Zones, monitoring networks, intra-urban and inter-urban temperature comparison, summer, Szeged, Novi Sad

1. Introduction

It is well established that urbanization alters the radiative, thermal, moisture, and aerodynamic properties of the environment, which therefore modifies the water and energy balance of the overlaying atmosphere (*Chandler*, 1965; *Oke*, 1982). The importance of urban climate is highlighted by its effects on urban energy and water management (e.g., *Santamouris et al.*, 2001; *Kolokotroni et al.*, 2006; *Balling* and *Gober*, 2006) as well as on human health (e.g., *Tan et al.*, 2010; *Gabriel* and *Endlicher*, 2011). The urban heat island (UHI) effect – the temperature surplus of built-up areas – is one of the most studied characteristics of the city's modified thermal environment (*Oke*, 1987).

In Central Europe, climate change is expected to increase the frequency, duration, and intensity of heat waves (*IPCC*, 2012; *Pongrácz et al.*, 2013), along with thermal stresses experienced by people (*Tomlinson et al.*, 2011). With reduced nocturnal cooling, the climate of cities is expected to make these already adverse projections worse, as elevated heat loads are linked to higher morbidity and mortality rates (*Petralli et al.*, 2012). Thus, monitoring the spatial and temporal patterns of the elevated urban temperature is an important task that can help both in the mitigation of and in the adaptation to the altered circumstances of the future. Besides monitoring, modeling also plays an important role in this regard. However, modeling requires data obtained from measurements for input and validation.

Air temperature in the city varies according to the properties of the urban environment and the characteristics of the regional climate as modified by hills, water bodies, etc. (*Chandler*, 1965). Urban climatology has traditionally relied on a temperature difference between a pair of stations to describe the climate of cities in reference to its background climate: the 'urban' station is generally located in the inner city (e.g., an old meteorological station of the town), while the 'rural' one, placed outside the city, served as the reference. Through an extensive literature review, *Stewart* (2007) drew attention to the marked difference that exists between station pairs, and which makes inter-urban cross comparisons between different cities almost impossible. For example, in some cases the urban station is located at an airport next to the city, while in other cases it is placed in a paved parking lot or in an urban park. As a consequence, the local climatic differences that exist between measurement sites are the sum of the background climate and urban effects, and the two cannot be separated (*Lowry*, 1977).

In order to investigate the spatial pattern of the air temperature fields in cities, mobile measurements utilizing instrumented vehicles – such as *Bottyán* and *Unger* (2003) – are used. But, they are based on occasional measurements, therefore not suited to monitoring simultaneously both the spatial and temporal development of the urban heat island. However, they are applicable to be the basis of empirical models that are capable of estimating urban temperature patterns based on surface properties (e.g., *Balázs et al.*, 2009).

One way to automate urban measurements is through remote sensing, as done for example by *Bartholy et al.* (2009). However, this method has its limits as well: first, establishing the linkage between the surface temperatures detected by satellites and the actual temperatures within the urban canopy is not straightforward (*Weng*, 2009); second, data can only be obtained during clear-sky conditions.

Another way of measurement automation is offered by the use of automatic weather stations (AWSs). This is a more suitable approach to study the UHI's spatial and temporal resolution, and it can be refined by increasing the density of the stations as far as it is needed (limited by financial sources). They are also applicable for method development and public information as well. The need of operational urban meteorological networks is underpinned for example by *Grimmond et al.* (2010) and *Muller et al.* (2013a). Existing global AWSs networks are primarily utilized for operative tasks, such as to provide input to numerical weather forecast models or for the notification of the public. These networks are, however, not applicable for urban climate investigations. While urban AWS networks are most suited for such analyses, they are rather rare. Despite the fact that the rules for establishing urban weather stations are less strict (*Oke*, 2006) than those for ordinary meteorological stations (*WMO*, 2008), sensor deployment in urban areas presents other challenges (e.g., safety concerns regarding sensor placement, or the increased network density required for the characterization of small-scale phenomena). There are only a few local scale urban heat island monitoring networks in Europe (*Table 1*), whereas they are more prevalent in other parts of the world such as in Oklahoma, USA (*Basara et al.*, 2011), Tokyo, Japan (*Mikami et al.*, 2003), Taipei, Taiwan (*Chang et al.*, 2010), and Hong Kong, China (*Hung* and *Wo*, 2012).

According to the experiences of former networks, there are three critical issues to solve: (i) placing the instruments – which is necessarily a compromise between WMO standards, safety, and maintenance criteria and representativity; (ii) data storing and transferring; (iii) power supply. As in this case a relatively dense network is needed (several sensors), it is expected that the instruments should be small, low-cost, and have possibility to transfer data via wireless methods (e.g., *Petralli et al.*, 2011; *Chapman et al.*, 2014). In general, existing networks have two shortcomings from the viewpoint of urban climatology: the placement of measurement sites is either not representative of the built characteristics of the city (as e.g., in Berlin, where only LCZ classes with natural land cover and open built-up characteristics are investigated by *Fenner et al.* (2014)), or the description of the sites' environment does not use any standardized method. These issues are originated from different purposes of the networks (e.g., educational, meso-meteorological) and the lack of communication between research groups. Consequently, it is hard to compare their reported results.

Table 1. Local scale urban temperature monitoring systems in Europe with some characteristics

Country, city	Number of sensors	Area (km^2)	Operating	Aim, instruments, experiences
England, Birmingham	111		2013–	– denser network in the downtown area and sparser in the outskirts (*Young et al.*, 2012) – data are transmitted through WiFi – Vaisala WXT-520s, low-cost Aginova sensors (*HiTemp*, 2014; *Chapman et al.*, 2012)
England, London	91	1580	2009–	– educational aim, located at schools – data are transmitted through WiFi (*Davies et al.*, 2011)
Finland, Helsinki	100	150	2005–	– research in mesoscale meteorology –Vaisala WXT-510 – data are transmitted via the mobile phone network (*Dabberdt et al.*, 2005)
Germany, Berlin	10	890	2000–	– different types of sensors and radiation shields – five sites (classified as LCZ A, LCZ A, LCZ B, LCZ 5 and LCZ 6, respectively) – data are transmitted through Ethernet cable (*Muller et al.*, 2013a; *Fenner et al.*, 2014)
Italy, Florence	35		2004–	– located randomly in districts characterized by distinct spatial configurations – HOBO PRO Temp/Rh Data Loggers (, 2013)

Urbanized areas can be classified according to their ability to interact with near-surface atmosphere and establish their typical local-scale thermal environments. Classification can either be used for mapping and spatial analysis, or for the characterization of measurement sites based on their induced local climate. Over the past years, the increased need to use well-established and universally applicable system of categories for the description of measurement sites (e.g., *Muller et al.*, 2013b) stimulated efforts to develop an appropriate site classification system. One such approach is the frequently used Local Climate Zones (LCZ) system (*Stewart* and *Oke*, 2012). It is based on a worldwide survey of urban climate studies (*Stewart*, 2007, 2011) and is influenced by earlier concepts (*Auer*, 1978; *Ellefsen*, 1991; *Oke*, 2006). The LCZ system was developed to standardize measurement site description and, therefore, to facilitate intra-urban and inter-urban cross comparisons. The major advantages of LCZ system is that it is a global classification scheme, it contains limited number of classes, and the classes are separated by the main thermal characteristic of the urban surface. The LCZ system does not cover entirely the spatial heterogeneity of the thermal pattern because it is affected by far more and complex processes, but it describes the most important features, thus it can be a good basis for local and regional scale climate models in order to estimate the intra-urban temperature patterns.

The objective of this paper is twofold. First, it introduces the urban climate monitoring and visualization systems recently implemented in two Central European cities. Second, the paper presents the analysis on temperature and partly on humidity data in the first complete summer (2014) period: (1) the validation of the measurement equipment used in the networks; (2) intra-urban and inter-urban comparison of the sites' (representing different LCZs) thermal behavior; and (3) the evaluation of the systems' usefulness.

2. Study areas

Szeged (Hungary) and Novi Sad (Serbia) are located in the Pannonian Plain in Central Europe. They have similar geographical and climatic environments. According to the climate classification system developed by Köppen, both cities belong to the Cfb climate category – temperate warm climate with a rather uniform annual distribution of precipitation (*Kottek et al.*, 2006).

Szeged has 160,000 inhabitants and its terrain is almost completely flat with average height around 79 m a.s.l. While the administrative area of Szeged is 281 km^2, the urbanized area is only about 30 km^2. The avenue-boulevard structure of the city was built to follow the axis of the river Tisza. It is characterized by a densely built up city center, with blocks of flats in the northern part of the city, as well as family homes and warehouses at the outskirts.

Novi Sad consists of two parts. The larger part is located between 80 and 86 m a.s.l. on a plain, whereas the smaller, southern part is situated on the northern slopes of the Fruška Gora hills. With an area of 80 km^2, it is the second largest city of Serbia with a population of 340,000. The River Danube flows through the southern and south-eastern edges of the city. It has a densely built-up central area and an industrial zone at the northern part of the city (*Savić et al.*, 2013).

3. Monitoring networks and data

The development of the online urban climate monitoring systems in Szeged, Hungary and Novi Sad, Serbia is funded by the Hungary-Serbia IPA Cross-border Co-operation EU Programme (*URBAN-PATH*, 2015) (*Fig. 1*). The systems record directly measured temperature and relative humidity, along with a calculated human comfort index which is not applied in our study. The systems present the data by maps and graphs, which together with the archived materials are freely available on the project's website (www.urban-path.hu). The development of the monitoring systems is based on the LCZ mapping method (for the details see *Lelovics et al.*, 2014). According to *Unger et al.* (2014), there are 24 and 27 stations in the seven and eight LCZ classes occurring in and around Szeged and Novi Sad, respectively (*Fig. 1*).

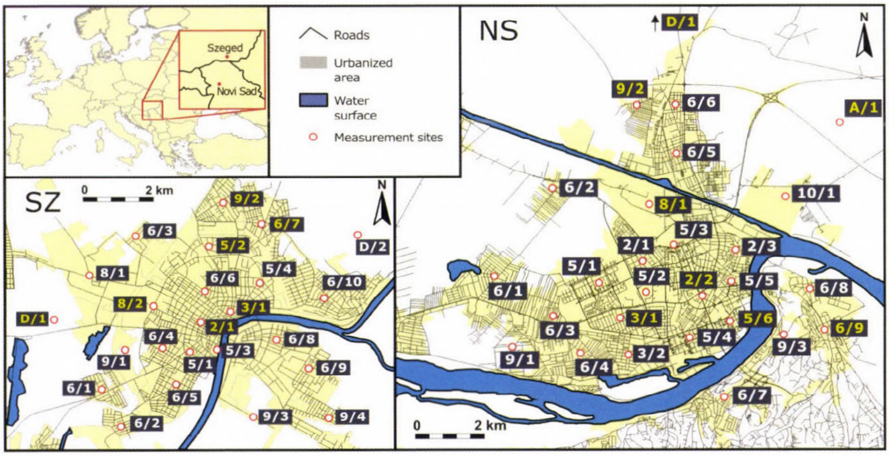

Fig. 1. Maps of the urban monitoring networks in Szeged (SZ), Hungary and Novi Sad (NS), Serbia. In the sites' identification number, the first digit refers to the LCZ class (*Stewart* and *Oke*, 2012) and the second one is an assigned number. Yellow identification numbers are the selected stations for the analysis presented in this paper. The details about the stations and their environs are listed in *Table 2*.

In the case of our networks, the response for the challenges mentioned in Section 1 is (i) to select sites with homogeneous neighborhood and mount them onto lamp posts; (ii) to store data on microSD card and transfer automatically through a 3G network; and (iii) to use batteries charged from the power supply of the city lights. Once the appropriate sites for the stations were selected, the instruments were mounted on lamp posts at 4 m above ground level for security reasons. For further technical details see *Unger et al.* (2015).

In this study, seven and eight measurement sites were selected for the analysis in Szeged and Novi Sad, respectively, representing the LCZ types occurring in the study areas. These sites are in the center of their LCZ areas, and also the surroundings are the most homogenous. The selected sites per LCZ classes and the typical values of surface parameters of their 250 m radius environment are listed in *Table 2*. The aerial photographs in *Fig. 2*. show a set of selected sites as examples with their surroundings.

Table 2. Typical surface properties of the 250 m radius environment around the selected sites. Abbrevations refer to surface properties: ISF – impervious surface factor, BSF – building surface factor, PSF – pervious surface factor, ALB – albedo, SVF – sky view factor, HRE – height of roughness elements. Upper lines refer to Szeged, bottom lines to Novi Sad

LCZ class (after 36)	Number of sites	HRE [m]	SVF	BSF	ISF	PSF	ALB	land use: 1: EEA Urban Atlas (*EEA*, 2010) for Szeged 2: Corine Land Cover (*Bossard et al.*, 2000) for Novi Sad
LCZ2:	1	13.5	0.6099	0.4316	0.4454	0.1229	0.1503	60% urban continuous, 20% industrial, 17% roads, 3% green[1]
compact midrise	3	16.2-20.8	0.4715–0.5892	0.2598–0.3752	0.5930–0.6293	0.0186–0.1472	0.1545–0.1677	100% urban discontinuous[2]
LCZ3:	1	9.5	0.6746	0.3681	0.4682	0.1637	0.1514	70% urban continuous, 13% roads, 12% industrial, 4% green[1]
compact lowrise	2	12	0.5860–0.6102	0.2168–0.2704	0.6435–0.6621	0.0861–0.1211	0.1676–0.1701	100% urban discontinuous[2]
LCZ5: open midrise	4	11.7–20.6	0.6909–0.8015	0.1183–0.3338	0.3718–0.5162	0.2526–0.5099	0.1441–0.1453	7–77% urban continuous, 0–43% urban dense, 0–31% urban medium, 4–41% industrial, 10–11% roads, 0–5% urban green, 0–35% water bodies[1]
	6	15.9–25.7	0.6407–0.8840	0.0852–0.3499	0.4553–0.6749	0.0763–0.3314	0.1631–0.1836	60–100% urban discontinuous, 0–40% roads[2]
LCZ6: open lowrise	10	3.1–5.5	0.8244–0.9562	0.1002–0.2475	0.2829–0.4925	0.2863–0.6101	0.1375–0.1780	0–87% urban continuous, 0–88% urban dense, 0–21% urban medium, 5–14% roads, 0–11% industrial, 0–11% agricultural, 0–7% urban green[1]
	9	12	0.6268–0.9967	0.1837–0.2136	0.6248–0.8632	0.0819–0.3752	0.1594–0.1827	80–100% urban discontinuous, 0–20% urban green, 0–20% roads[2]
LCZ8: large lowrise	2	4.9	0.9463	0.1545	0.5757	0.2697	0.1347–0.1508	59–81% industrial, 6–9% roads, 0–12% urban continuous, 0–10% water, 0–9% urban dense, 1–7% urban green[1]
	1	12	0.8355	0.3050	0.4676	0.2274	0.1701	100% industrial[2]
LCZ9: sparsely built	4	2.8	0.9965	0.0062–0.2100	0.0209–0.0500	0.7500–0.9729	0.1351–0.1655	0–64% urban medium, 0–67% agricultural, 0–48% urban green, 0–24% urban low density, 0–23% urban dense, 0–18% water bodies, 0–8% urban very low density, 0–9% roads[1]
	3	12	0.8233	0.0000–0.0950	0.2551–0.5551	0.3499–0.7922	0.1675–0.1855	20–90% agricultural, 10–80% urban discontinuous[2]
LCZ10:	0	–	–	–	–	–	–	100% industrial[2]
heavy industry	1	12	0.9617	0.0180	0.5683	0.4137	0.1787	
LCZA:	0	–	–	–	–	–	–	100% forest[2]
dense trees	1	0	1.0000	0.0000	0.2078	0.7922	0.1515	
LCZD: low	2	0	1.0000	0.0000	0.0000–0.1000	0.8000–1.0000	0.1447–0.1563	83–97% agricultural, 3–14% industrial[1]
plants	1	0	1.0000	0.0000	0.3119	0.6881	0.1240	100% agricultural[2]

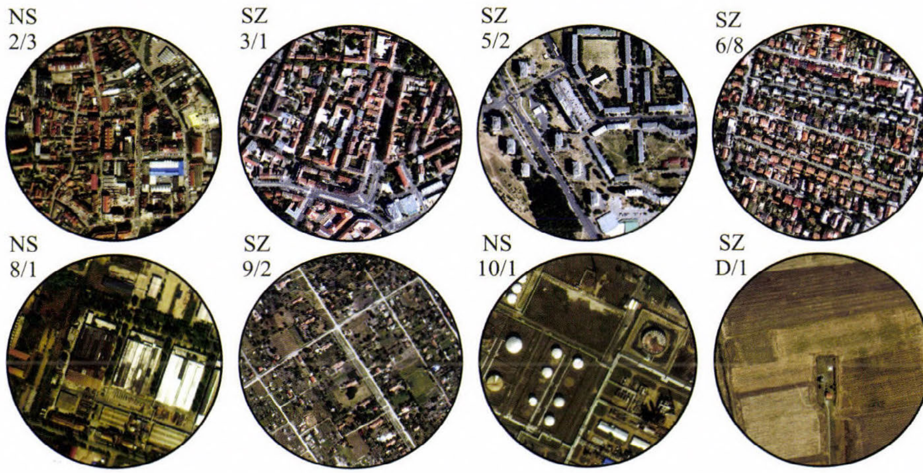

Fig. 2. Aerial photographs illustrating selected measurement sites with their 250 m radius environments (Szeged (SZ), Novi Sad (NS), first number – LCZ class number, second number – station's identity number in the given LCZ class).

In Szeged, data collection began on March 23, 2014, and in Novi Sad on June 10, 2014. In this study, the examined period is from June 1 to August 31, while in Novi Sad the analyzed interval is somewhat shorter – lasting from June 10 to August 9 – due to technical issues. In order to overcome the issues around daylight saving time in summer and to be in line with meteorological standards (*WMO*, 2008), time is given in UTC both in the database and in the analyses below.

In this region, summer is generally the most critical season from the viewpoint of health and human comfort. Although with 321 mm precipitation recorded in Szeged, this summer was unusually wet compared to the seasonal average of 169 mm measured in the period of 1901–2000 (*HMS*, 2008). As a consequence, the number of days with favorable weather conditions – conducive to the development of micro- and local climates – was lower than usual.

4. Results and discussion

As we utilize a number of widely known methods during the data evaluation, these methods are mentioned at the beginning of the relevant subsections.

4.1. Sensor performance verification

The Hungarian Meteorological Service's (HMS) SYNOP station 12982 is located next to the urban network's D/1 station in Szeged (*Fig. 1*). Since the station of the HMS is part of the international surface synoptic network, it meets the requirements of the WMO. HMS utilizes Vaisala HMP-35D and HMP-45D temperature and relative humidity sensors and Vaisala MILOS-500 data loggers and transmitters. It records data with 10 minute resolution. As stations 12982 and D/1 are also mounted on the same platform and their radiation shields are the same, the former can be used as a reference for the validation of the latter. The sensor performance verification compared temperature and relative humidity values from the stations and utilized 25,780 pair of data from April 1 to September 29, 2014 in the process. The scatter plots of these values and their differences are presented in *Fig. 3*. We calculated mean absolute error (MAE), root mean square error (RMSE), standard deviation (STDEV), and mean error (MA).

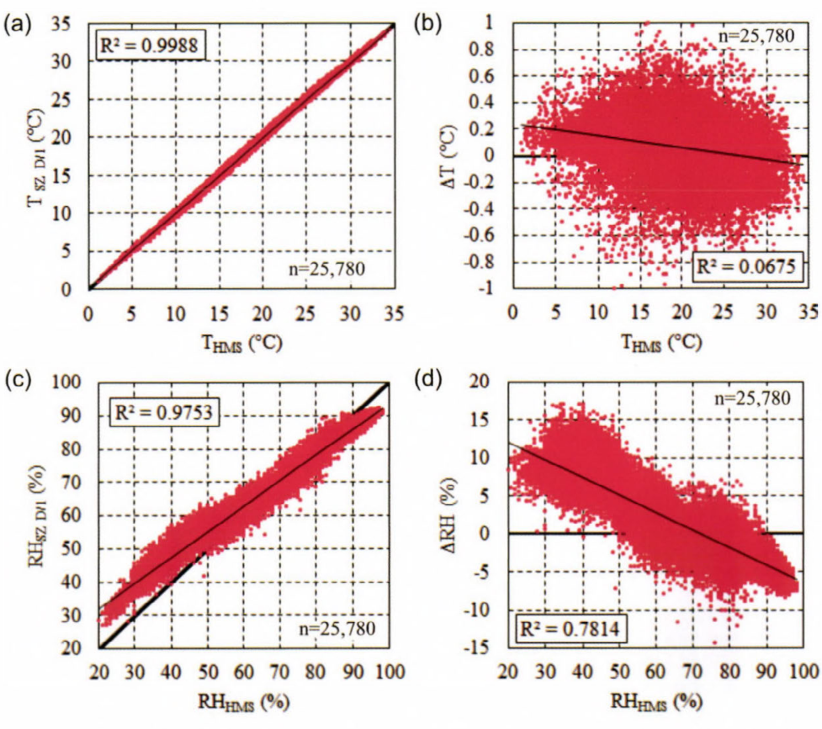

Fig. 3. Scatter plot of temperature (a), relative humidity (c), and their biases (b and d, $\Delta X = X_{SZ\ D/1} - X_{HMS}$) in Szeged.

The performance of the temperature sensor is adequate (*Fig. 3a*). As illustrated in *Fig. 3b*, the errors are small (MAE=0.1745 °C, RMSE=0.2194, while $STDEV_{D/1}$=5.78 °C and $STDEV_{HMS}$=5.83 °C) and almost balanced with a slight overestimation (ME=0.0769 °C). The relative humidity sensor underperforms (ME=0.6044%, MAE=4.2054%, RMSE=5.2277, $STDEV_{D/1}$=15.43%, $STDEV_{HMS}$=19.83%). Although the results shown in *Fig. 3c* do not meet the WMO standards (*WMO*, 2008) – requiring 1% accuracy for high and 5% accuracy for mid-range relative humidity levels –, the sensor was nevertheless deemed adequate for the purpose of the project, as 1–2% difference in RH has little effect on people's thermal comfort sensation in summer (e.g., *Oliveira* and *Andrade*, 2007). In contrast to the temperature sensor where bias is almost independent from its value (*Fig. 3b*), the relative humidity sensor systematically overestimates at lower values and underestimates at higher ones (*Fig. 3d*).

4.2. Intra-urban and inter-urban comparisons

4.2.1. Daily temperature indices

Two temperature indices were determined utilizing daily minimum (T_{min}) and maximum (T_{max}) temperature values: summer days, defined as days with T_{max}>25 °C; and tropical nights, where daily T_{min}>20 °C (*Karl et al.*, 1999). These indices were selected because of their acceptance as reliable indicators of heat stress (e.g., *Gabriel* and *Endlicher*, 2007; *Petralli et al.*, 2011). It was recognized that applying daily minima and maxima causes a kind of time asynchronity, but from the viewpoint of human health and heat stress, these time differences are not significant.

In order to make the daily temperature indices comparable between the two cities, days without data gaps in both locations were selected. The analysis used 48 days that met the criterion. The relative frequencies of these indices for each LCZ class are presented in *Fig. 4*.

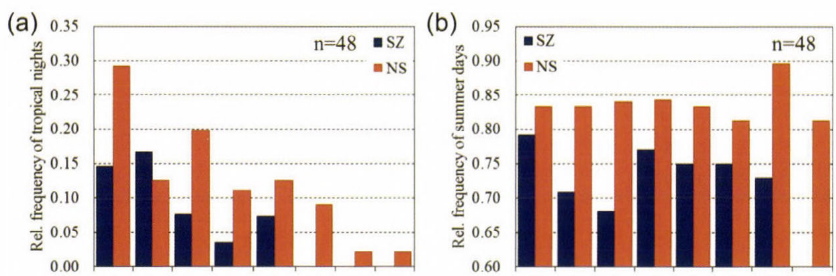

Fig. 4. Relative frequency of tropical nights (a) and summer days (b) by LCZ classes in Szeged and Novi Sad calculated for the selected common set of days.

In the case of tropical nights (Fig. *4a*), the differences between LCZ classes are relatively large, their number varies between 0 (LCZ D and LCZ 9) and 8 days (LCZ 3) in Szeged, while this range is between 1 (LCZ D and LCZ A sites) and 17 (LCZ 2) days in Novi Sad. It is important to note that the highest frequencies of tropical nights occur in the most densely built LCZs (2, 3, and 5). In contrast to tropical nights, the distribution of summer days is relatively even among the different LCZs (*Fig. 4b*). In the case of Novi Sad, LCZ D is an outlier, as it lacks shading from both buildings and taller plants. The cooling effect from shading is the reason behind the lower values recorded at LCZ 3 and 5 in Szeged. In the case of the latter site, the evapotranspiration from the higher amount of vegetation also contributes to this effect.

4.2.2. Diurnal variation of temperature under anticyclonic conditions

For the analysis of the thermal effect of the different LCZs, ideal weather conditions should be examined, because in these conditions the effect of the urban surface for the temperature are undisturbed. In order to eliminate the effects of unfavorable weather conditions and thus to bring forth the characteristic diurnal temperature cycles of various LCZ classes, we applied the average weather factor, Φ_w (*Oke*, 1998) calculated for 3-hour intervals using the data from the HMS SYNOP station 12982. Finally, we selected two time periods with prevailing anticyclonic conditions when Φ_w was greater than 0.7. They run from July 3 to 5, 2014 and from July 19 to 20, 2014 and lasted 72 and 48 hours in length, respectively. *Figs. 5* and *6* present the diurnal variation of absolute and relative temperatures – expressed relative to LCZ D as $T_{LCZ\ X} - T_{LCZ\ D}$.

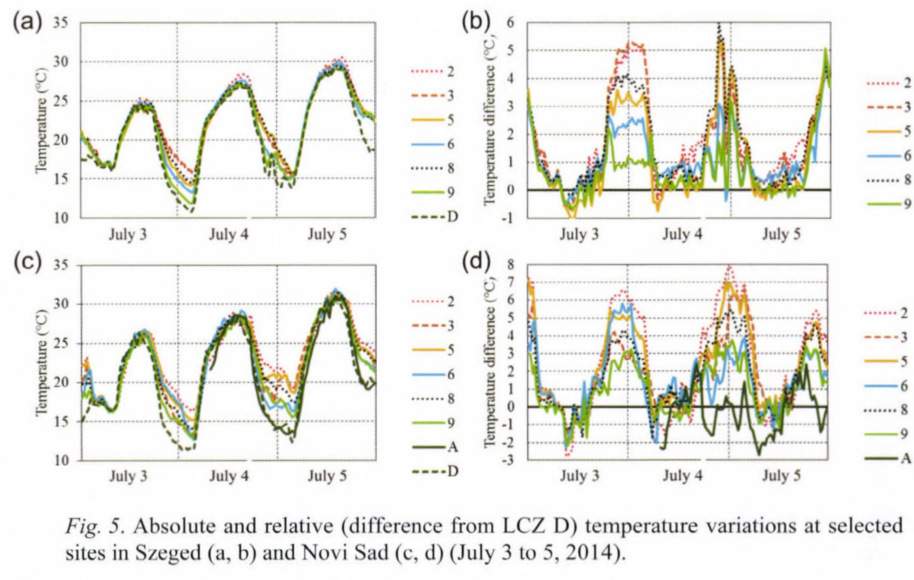

Fig. 5. Absolute and relative (difference from LCZ D) temperature variations at selected sites in Szeged (a, b) and Novi Sad (c, d) (July 3 to 5, 2014).

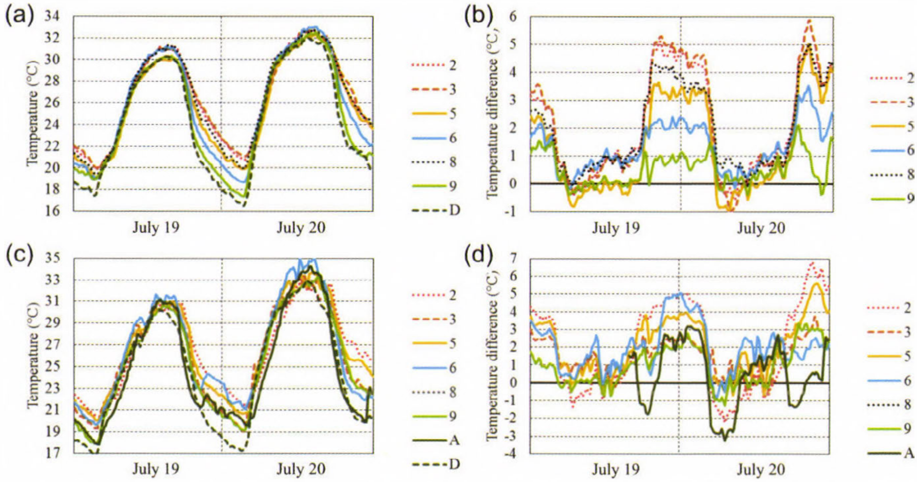

Fig. 6. Absolute and relative (difference from LCZ D) temperature variations at selected sites in Szeged (a, b) and Novi Sad (c, d) (July 19 to 20, 2014).

The measurement sites belonging to various LCZs have distinct daily temperature cycles. The differences between the classes are most pronounced in the case of Szeged, where LCZ 2 and LCZ 3 have an over 5°C temperature surplus at 00:00 UTC, July 4 (*Figs. 5a* and *b*) and at 00:00 UTC, July 20 (*Figs. 6a* and *b*). In the case of LCZ 8, LCZ 5, LCZ 6 and LCZ 9 the largest surplus values are 4 °C, 3.5 °C, 2.5 °C and 1 °C, respectively. In Novi Sad, the temperatures are slightly higher, but the classes differ less. The greatest temperature surpluses occur in LCZ 2 and LCZ 6 (between 5–7 °C), while LCZ 5, LCZ 3. and LCZ 8 remain somewhat cooler. The cycles of LCZ A and LCZ D are similar. The temperature difference between the two types remains within the ±3 °C interval, with the largest values occurring around 00:00 UTC.

Fig. 7 shows the examined sites' characteristic daily temperature cycles, calculated from the selected 'ideal' days as hourly averages relative to the average non-urban reference site (LCZ D). While differences are smaller in Szeged – as it is a smaller city with half the population of Novi Sad –, the diurnal cycle of LCZ's in the two cities indicate similar trends. During daytime, when the insolation is high and convective mixing prevails, temperature differences are below ±1 °C. The only exception is LCZ A in Novi Sad during the morning hours, which is the result of lush vegetation that delays warming through shading and evapotranspiration. During the night, when radiative cooling dominates, the differences are larger and mostly positive. The differences between the LCZ classes are most pronounced during this period due to the unique radiative and thermal properties of the sites. In the case of Szeged, the diurnal cycles of classes are more discernible.

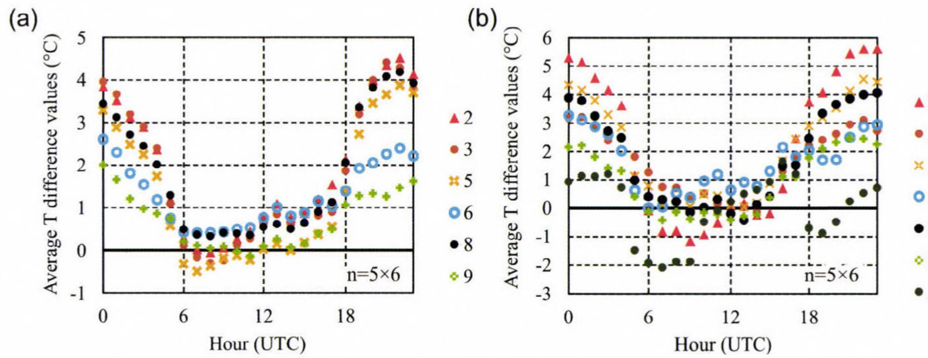

Fig. 7. Average hourly temperature values at selected sites calculated for the five selected days and expressed relative to average LCZ D in Szeged (a) and Novi Sad (b).

4.2.3. Diurnal variation of UHI during summer

This analysis is concerned with the diurnal development of the UHI intensity in the most densely built LCZ areas of Szeged and Novi Sad. Similarly to the conventional heat island studies, the UHI intensity is expressed as the urban conditions relative to non-urban ones. In our case, it was calculated as an average temperature difference between LCZ 2 (urban) and LCZ D (non-urban) sites for half-hour intervals in both cities (*Fig 8*). As noted in Section 3, the investigated period was shorter in Novi Sad due to technical issues.

The shape of isopleths in *Fig. 8* are in line with the general understanding of the thermal behavior of dense urban areas: for the most time, the UHI intensity remains positive with highest values at night, while negative values occur predominantly during the day (urban cool island). The dividing line between these two periods is around 6 UTC and 12 UTC in both cities – see the thick isotherms of 0 °C in *Fig. 8*. The range of UHI intensity is between –1.48 °C and 5.22 °C in Szeged, and between –3.70 °C and 6.85 °C in Novi Sad.

Urban cool island occurs in both cities during the day. It is typically around –1 °C in Szeged and –2 °C in Novi Sad. An exception around 18:00 UTC on July 27 in Szeged (shown in *Fig. 8a*) is caused by the cooling effect of a convective precipitation – 36.4 mm precipitation was measured at the outskirts and 83.0 mm in the inner city. It resulted in large temperature differences between different parts of the city, and produced an outflow with 8.3 ms^{-1} wind speed at the outskirts and 9.3 ms^{-1} in the center. As a consequence, the cooling was much faster in the central area and produced the mentioned anomaly.

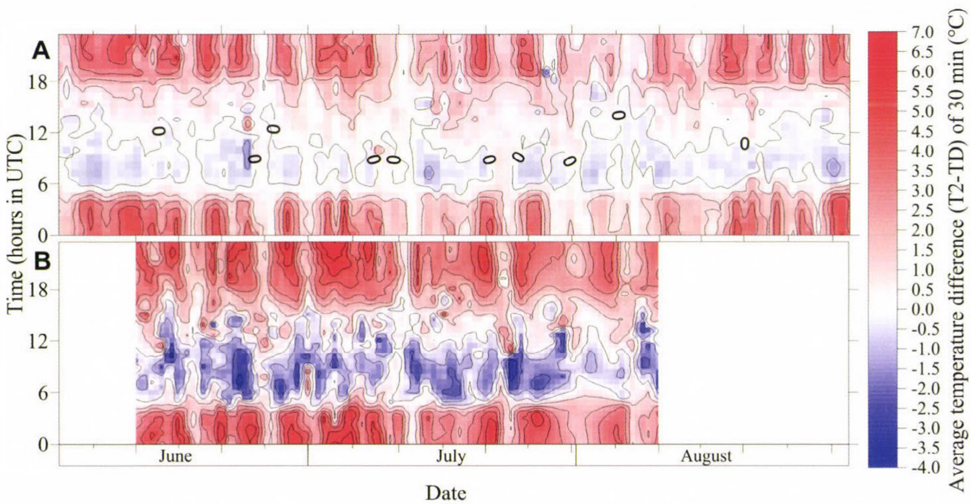

Fig. 8. Average temperature differences [°C] between LCZ 2 and LCZ D (a) in Szeged and (b) Novi Sad (thin isotherms – integer °C, thick isotherms – 0 and 5°C).

5. Conclusions

Monitoring urban temperature patterns is an important task that can assist in formulating adaptation and mitigation strategies to meet the challenges of climate change. The use of automatic weather stations is the most suited method for understanding the spatial and temporal characteristics of the urban climate. Although the global network of AWSs is well developed, their presence in cities is still rather rare. The developed urban climate monitoring systems in Szeged, Hungary and Novi Sad, Serbia visualize the observed temperature and relative humidity data along with calculated human comfort index. The results are freely available online. The selection of measurement sites utilized LCZ maps to ensure a representative number and placement of stations within different LCZs.

This study introduces these monitoring networks through a number of analyses using data from the summer of 2014. The temperature and relative humidity sensors at site D/1 in Szeged were validated against the sensors of the Hungarian Meteorological Service's SYNOP station 12982. In the case of temperature, the sensor performance was found satisfactory with slight underestimation. The relative humidity sensor underperformed, but it was deemed acceptable for the purpose of the project.

The evaluation of the daily temperature indices (summer days and tropical nights) revealed that the highest frequencies of tropical nights occur in the most densely built LCZ classes (2, 3, and 5). Based on these results, the control of building densities or the spatial confinement of dense LCZs could be viable adaptation strategies.

Further, in order to assess the thermal behavior of different LCZs under 'ideal' conditions, two periods with anticyclonic conditions were selected. In the case of Szeged, the distinction between the daily temperature cycles of different LCZ classes was quite pronounced. In contrast, while the nighttime temperature surpluses and the daytime temperature deficits were greater in Novi Sad, the thermal cycle of different LCZs was less distinct. The average daily cycle of each LCZ highlights the differences between day- and nighttime processes.

During summer, the diurnal variation of conventional heat island intensity confirms the general knowledge, that is, it remains positive with highest values at night, while negative values occur predominantly during the day.

Overall, it can be stated that the monitoring networks installed in Szeged and Novi Sad serve their intended purposes – as informing the citizens about the most recent temperature, humidity, and thermal comfort measurements – well. Based on the site visit data of the public display (www.urban-path.hu) of the monitoring system, the daily visitor number is around 200 and the two-thirds of it are new visitors from these two cities. Hopefully, this publicity helps the local authorities to decrease the disadvantageous effects of urban climate. They provide beneficial information about the climate of these cities to the public, moreover, the results (based on a short time period) presented in this paper show that the scientific application of the obtained data is also conductive. The spatial and temporal resolution of the network is adequate, and the accuracy of the sensors is satisfactory. The results indicate that the site selection was appropriate, as the sites belonging to different LCZs exhibit distinct thermal behaviors. The planned operation time of these networks will be over 5 years. Future data series will allow for more detailed and versatile climatological analyses in relation to intra-urban climate variations.

Acknowledgement: The study was supported by the Hungary-Serbia IPA Cross-border Co-operation EU Programme (HUSRB/1203/122/166 – URBAN-PATH), the Hungarian Scientific Research Fund (OTKA K-111768, PD-100352). *Tamás Gál* was supported by the János Bolyai Research Scholarship of the Hungarian Academy of Sciences.

References

Auer, A.H., 1978: Correlation of land use and cover with meteorological anomalies. *J.Appl. Meteorol. 17*, 636–643.

Balázs, B., Unger, J., Gál, T., Sümeghy, Z., Geiger, J. and *Szegedi, S.*, 2009: Simulation of the mean urban heat island using 2D surface parameters: empirical modeling, verification and extension. *Meteorol. Appl. 16*, 275–287.

Balling, R.C. and *Gober, P.*, 2006: Climate variability and residential water use in the City of Phoenix, Arizona. *J. Appl. Meteorol. Climatol. 46*, 1130–1137.

Bartholy, J., Pongrácz, R., Lelovics E., and *Dezső, Z.*, 2009: Comparison of urban heat island effect using ground-based and satellite measurements. *Acta Climatol. Chorol. 42-43*, 7–15.

Basara, J.B., Illston, B.G., Fiebrich, C.A., Browder, P.D., Morgan, C.R., McCombs, A., Bostic, J.P., McPherson, R.A., Schroeder, A.J., and *Crawford, K.C.*, 2011: The Oklahoma City Micronet. *Meteorol. Appl. 18*, 252–261.

Bossard, M., Feranec, J., and *Otahel, J.*, 2000: CORINE land cover technical guide – Addendum 2000. EEA Technical report No 40.

Bottyán, Z., and *Unger, J.*, 2003: A multiple linear statistical model for estimating the mean maximum urban heat island. *Theor. Appl. Climatol. 75*, 233–243.

Chandler, T.J., 1965: *The Climate of London*. London: Hutchinson.

Chapman, L., Muller, C.L., Young, D.T., Cai, X-M., and *Grimmond, C.S.B.*, 2012: An introduction to the Birmingham Urban Climate Laboratory. *8th Int. Conf. on Urban Climate*, Dublin, Ireland, Paper 19.

Chang, B., Wang, H-Y., Peng, T-Y. and *Hsu, Y-S.* 2010: Development and evaluation of a city-wide wireless weather sensor network. *Edu. Technol. Soc. 13*, 270–280.

Chapman, L., Muller, C.L., Young, D.T., Warren, E.L., Grimmond, C.S.B., Cai, X-M., and *Ferranti, E.J.S.*, 2015: The Birmingham Urban Climate Laboratory: An open meteorological testbed and challenges of the smart city. *Bull. Am. Meteorol. Soc. 96*, 1545–1560.

Dabberdt, W., Koistinen, J., Poutiainen, J., Saltikoff, E., and *Turtiainen, H.*, 2005: The Helsinki mesoscale testbed: an invitation to use a new 3-D observation network. *Bull. Am. Meteorol. Soc. 86*, 906–907.

Davies, L., Bell, J.N.B., Bone, J., Head, M., Hill, L., Howard, C., Hobbs, S.J., Jones, D.T., Power, S.A., Rose, N., Ryder, C., Seed, L., Stevens, G., Toumi, R., Voulvoulis, N., and *White, P.C.L.*, 2011: Open air laboratories (OPAL): a community-driven research programme. *Environ. Poll. 159*, 2203–2210.

EEA, 2010: *Urban Atlas*. http://www.eea.europa.eu/data-and-maps/data/urban-atlas, Accessed: 2015-01-28.

Ellefsen, R., 1991: Mapping and measuring buildings in the canopy boundary layer in ten U.S. cities. *Energy and Buildings 15-16*, 1025–1049.

Fenner, D., Meier, F., Scherer, D., and *Polze, A.*, 2014: Spatial and temporal air temperature variability in Berlin, Germany, during the years 2001–2010. *Urban Climate 10*, 308–331.

Gabriel, K.M., and *Endlicher, W.R.*, 2011: Urban and rural mortality rates during heat waves in Berlin and Brandenburg, Germany. *Environ. Poll. 159*, 2044–2050.

Grimmond, C.S.B., Roth, M., Oke, T.R., Au, Y.C., Best, M., Betts, R., Carmichael, G., Cleugh, H., Dabberdt, W., Emmanuel, R., Freitas, E., Fortuniak, K., Hanna, S., Klein, P., Kalkstein, L.S., Liu, C.H., Nickson, A., Pearlmutter, D., Sailor, D., and *Voogt, J.*, 2010: Climate and more sustainable cities: climate information for improved planning and management of cities (producers/capabilities perspective). *Procedia Environ. Sci. 1*, 247–274.

HiTemp, 2014: *High Density Measurements within Urban Environment.* http://www.birmingham.ac.uk/schools/gees/centres/bucl/hitemp/index.aspx Accessed: 2014-08-12.

HMS, 2008: *Climate Data Series of Szeged, 1901-2000. Description of instruments.* http://owww.met.hu/eghajlat/eghajlati_adatsorok/sz/Navig/102_EN.htm, Accessed: 2014-10-01.

Hung, T.K., and *Wo, O.C.*, 2012: Development of a community weather information network (Co-WIN) in Hong Kong. *Weather 67*, 48–50 .

IPCC, 2012: *Managing the Risks of Extreme Events and Disasters to Advance Climate Change Adaptation*, A Special Report of Working Groups I and II of the IPCC. Cambridge, UK and New York, USA: Cambridge University Press.

Karl, T.R., Nicholls, N., and *Ghazi, A.*, 1999: CLIVAR/GCOS/WMO workshop on indices and indicators for climate extremes: Workshop summary. *Climatic Change 42*, 3–7.

Kolokotroni, M., Giannitsaris, I., and *Watkins, R.*, 2006: The effect of the London urban heat island on building summer cooling demand and night ventilation strategies. *Sol. Energy 80*, 383–392.

Kottek, M., Grieser, J., Beck, C., Rudolf, B., and *Rubel, F.*, 2006: World Map of the Köppen-Geiger climate classification updated. Meteorologische Zeitschrift 15, 259-263.

Lelovics, E., Unger, J., Gál, T., Gál, C.V., 2014: Design of an urban monitoring network based on Local Climate Zone mapping and temperature pattern modelling. *Clim. Res. 60*, 51–62.

Lowry, W.P., 1977: Empirical estimation of urban effects on climate: A problem analysis. *J. Appl. Meteorol. 16,* 129–135.

Mikami, T., Ando, H., Morishima, W., Izumi, T., and *Shioda, T.*, 2003: A new urban heat island monitoring system in Tokyo. 5th Int. Conf. on Urban Climate, Lodz, Poland, O.3.5.

Muller, C.L., Chapman, L., Grimmond, C.S.B., Young, D.T., and *Cai, X-M.*, 2013a: Sensors and the city: a review of urban meteorological networks. *Int. J. Climatol. 33*, 1585–1600.

Muller, C.L., Chapman, L., Grimmond, C.S.B., Young, D.T., and *Cai, X-M.*, 2013b: Toward a standardized metadata protocol for urban meteorological networks. *Bull. Am. Meteorol. Soc. 94*, 1161–1185.

Oke, T.R., 1982: The energetic basis of the urban heat island. *Quart. J. Roy. Meteorol. Soc. 108*, 1–24.

Oke, T.R., 1987: *Boundary Layer Climates.* 2nd ed. London–New York: Routledge.

Oke, T.R., 1998: An algorithmic scheme to estimate hourly heat island magnitude. 2nd Urban Environment Symp., Albuquerque, New Mexico, 80–83.

Oke, T.R., 2006: Initial guidance to obtain representative meteorological observations at urban sites. Geneva: WMO/TD No. 1250.

Oliveira, S., and *Andrade, H.*, 2007: An initial assessment of the bioclimatic comfort in an outdoor public space in Lisbon. *Int. J.Biometeorol. 52*, 69–84.

Petralli, M., Massetti, L., and *Orlandini, S.*, 2011: Five years of thermal intra-urban monitoring in Florence (Italy) and application of climatological indices. *Theor. Appl. Climatol. 104*, 349–356.

Petralli, M., Morabito, M., Cecchi, L., Crisci, A., and *Orlandini, S.*, 2012: Urban morbidity in summer: ambulance dispatch data, periodicity and weather. *Central European J. Medicine 7*, 775–782.

Petralli, M., Massetti, L., Brandani, G., and *Orlandini, S.*, 2013: Urban planning indicators: useful tools to measure the effect of urbanization and vegetation on summer air temperatures. *Int. J. Climatol. 34*, 1236–1244.

Pongrácz, R., Bartholy, J., and *Bartha, E.B.*, 2013: Analysis of projected changes in the occurence of heat waves in Hungary. *Adv. in Geosciences 35*, 115–122.

Santamouris, M., Papanikolaou, N., Livada, I., Koronakis, I., Georgakis, C., Argiriou, A., and *Assimakopoulos, D.N.*, 2001: On the impact of urban climate on the energy consumption of buildings. *Sol. Energy 70*, 201–216.

Savić, S., Milošević, D., Lazić, L., Marković, V., Arsenović, D., and *Pavić, D.*, 2013: Classifying urban meteorological stations sites by "Local Climate Zones": Preliminary results for the City of Novi Sad (Serbia). *Geographica Pannonica 17(3)*, 60–68.

Stewart, I.D., 2007: Landscape representation and urban-rural dichotomy in empirical urban heat island literature, 1950-2006. *Acta Climatol. Chorol. 40-41*, 111–121.

Stewart, I.D., 2011: A systematic review and scientific critique of methodology in modern urban heat island literature. *Int. J. Climatol. 31*, 200–217.

*Stewart, I.D.,*and *Oke, T.R.*, 2012: Local Climate Zones for urban temperature studies. *Bull. Am. Meteorol. Soc. 93*, 1879-1900.

Tan, J., Zheng, Y., Tang, X., Guo, C., Li, C., Song, G., Zhen, X., Yuan, D., Kalkstein, A.J., Li, F., and *Chen, H.*, 2010: The urban heat island and its impact on heat waves and human health in Shanghai. *Int. J. Biometeorol. 54*, 75–84.

Tomlinson, C.J., Chapman, L., Thornes, J.E., and *Baker, C.J.*, 2011: Including the urban heat island in spatial heat health risk assessment strategies: a case study for Birmingham, UK. *Int. J. Health Geographics 10*, 1–14.

Unger, J., Savic, S., Gál, T., and *Milosevic, D.*, 2014: Urban climate and monitoring network system in Central European cities. Novi Sad (ISBN: 987-86-7031-341-5), 101 p.

Unger, J., Gál, T., Csépe, Z., Lelovics, E., and *Gulyás, Á.*, 2015: Development, data processing and preliminary results of an urban human comfort monitoring and information system. *Időjárás 119*, 337-354.

URBAN-PATH homepage, 2015: http://www.urban-path.hu, Accessed: 31-01-2015.

Weng, Q., 2009: Thermal infrared remote sensing for urban climate and environmental studies: Methods, applications, and trends. *ISPRS J. Photogramm. Rem. Sens. 64*, 335–344.

WMO, 2008: *Guide to Meteorological Instruments and Methods of Observation.* 8th ed. Geneva, Switzerland: World Meteorological Organization.

Young, D.T., Chapman, L., Muller, C.L., and *Cai, X-M.*, 2014: A low-cost wireless temperature sensor: evaluation for use in environmental monitoring applications. *J. Atmos. Oceanic Tech. 31*, 938–944.

IDŐJÁRÁS
Quarterly Journal of the Hungarian Meteorological Service
Vol. 120, No. 3, July – September, 2016, pp. 301–313

Short-term weather fluctuation and quality assessment of oxbows

János Tamás Kundrát[1*], **Edina Simon**[1], **István Gyulai**[2], **Gyula Lakatos**[1], and **Béla Tóthmérész**[3]

[1]*University of Debrecen, Department of Ecology, Egyetem tér 1, H-4032 Debrecen, Hungary*

[2]*University of Debrecen, Department of Hydrobiology, Egyetem tér 1, H-4032 Debrecen, Hungary*

[3]*MTA-DE Biodiversity and Ecosystem Services Research Group, Egyetem tér 1, H-4032 Debrecen, Hungary*

**Corresponding author E-mails: kundratt@gmail.com*

(Manuscript received in final form December 7, 2015)

Abstract—Our aim was to study the effects of short-term weather fluctuations on the quality of oxbows, based on the physico-chemical parameters of the water. The present study explored the effect of precipitation, temperature, and the water level of the main river on the quality of oxbows. We assessed the quality of four oxbows in the Upper Tisza region (north Hungary) over a two-year period. Water samples were collected in the summer in 2011 and 2012, and 12 physico-chemical parameters were investigated.

We found positive correlations between the dissolved oxygen, water temperature, concentration of hydro carbonate, nitrate, pH, conductivity and the average temperature. Canonical discriminant analysis showed that the studied oxbows were similar in 2011 and 2012, based on physico-chemical parameters. Significant differences were found between the years, in terms of the water temperature, the content of suspended solids, and the concentrations of carbonate and chloride. Our results show that only short-term weather changes such as less precipitation and higher temperature cause the quality of oxbows to deteriorate.

Our results demonstrated that the water quality of oxbows is influenced by the River Tisza, because the decrease in the water level of the Tisza was also responsible for the differences between the years, based on the physical-chemical parameters of the water.

Key-words: physico-chemical parameters of water, weather change, drought index, degradation, emerse vegetation, submerse vegetation

1. Introduction

Conservation of oxbows is of central importance both in Europe and around the world. Although these oxbows are also endangered aquatic habitats, the management and conservation of freshwater resources mainly focuses on running water and larger water bodies (*Oertli et al.,* 2009). Due to their biodiversity, small oxbows are equally significant from a socio-economic and from a conservation biology point of view (*Oertli et al.,* 2009). Many oxbows were found in the Upper Tisza region, which is characterized by abandoned river channels, meanders, and periodical and permanent water marshy areas. Most of the oxbows were created during the regulation of the River Tisza (*Varga et al.,* 2013). There are about 70 oxbows along the Upper Tisza river. They are connected to the river during the floodplain events, when large quantities of suspended particles are transported into the floodplain (*Nguyen et al.,* 2009).

Weather fluctuation has effects on aquatic ecosystems: (i) the temperature increase causes an increase in water temperature which may result in an increase in conductivity that may in turn reduce the level of oxygen and severely stress aquatic fauna (*Bond et al.,* 2008); (ii) the seasonal changes in precipitation alter the hydrological relations existing in aquatic systems (*Georgi* and *Pal*, 2004). Regional patterns in precipitation and temperature predict changes which have the potential to alter natural flow regimes (*Palmer et al.,* 2009). However, the cumulative changes in temperature and precipitation may have both direct and indirect effects on oxbows, because these water bodies have substantial exchanges with atmospheric water in the form of precipitation and evapotranspiration (*Michener et al.,* 1997; *Winter,* 2000). The hydrologic conditions directly affect the chemical and physical processes, and the dynamic of nutrients and suspended solids (*Fink* and *Mitsch,* 2007).

Aquatic macrophytes influence the physical and chemical environment of lakes and oxbows (*Lukács et al.,* 2009, 2011). Macrophytes play a key role in biochemical cycles, organic carbon production, and phosphorus mobilization. They also have a direct influence on hydrology and sediment dynamics (*Bornette* and *Puijalon,* 2011). Numerous studies have demonstrated that they can dramatically alter the material and energy flows between lakes and oxbows (*Frodge et al.,* 1990). Earlier studies have also demonstrated that macrophytes have an influence on the physico-chemical parameters of water on a macro-scale; consequently, the vegetation and the physico-chemical parameters of water are closely related (*Barendregt* and *Bio,* 2003; *Heegaard et al.,* 2001).

The aim of our study was to assess the impact of short-term weather fluctuations, such as reduced precipitation and higher temperature. We also investigated the effect of the water level of the main river and vegetation types on the quality of oxbows, based on the physico-chemical parameters of the water. The physico-chemical parameters of the surface water of oxbows were studied during two years, 2011 and 2012. To compare the studied years a drought index was used, based on the mean temperature and rainfall of the years in question. At the same time, the effect of the water level of the Tisza on the quality of oxbows was also studied. The poor state of oxbows was evident in the field; thus, our hypothesis was that the weather parameters and water level of the Tisza may cause the deterioration of the physico-chemical parameters of the water, which leads to the degradation of the water quality. Thus, the aim of our study was to demonstrate that the precipitation, temperature, and water level of the River Tisza influenced the quality of these oxbows, and that the meteorological parameters and water level affected the oxbow fill up rate, even over a short time period. Our second hypothesis was that the macrophytes also had an effect on the physico-chemical parameters of the water, which may cause a change in the quality of oxbows. The present study explored the factors affecting the quality of oxbows, the precipitation and temperature, the water level, and/or the structure of vegetation.

2. Data and methods

2.1. Study sites

We studied the oxbows in the Upper Tisza region. The area studied covers 95 ha; it is an undisturbed area in the UpperTisza region, in the north part of Hungary. There are many oxbows in this region, and the following four oxbows were studied: the Kis-Zátony oxbow, the Nagy-Zátony oxbow, the Nagy-Pap oxbow, and the Sulymos oxbow (*Fig. 1*). In our study, two vegetation types (submersed and emersed) and open water were studied. The submersed vegetation type was characterized by *Ceratophyllum demersum Nymphaea alba* and *Schoenoplectus lacustris.* The emersed vegetation type was characterized by the following species: *Typha angustifolia, Typha latifolia,* and *Phragmites australis* (*Cook*, 1996). In the open water, there were no macrophytes. In the Kis-Zátony oxbow there were seven sampling points (two open water, four emersed, and one submersed vegetation). In the Nagy-Zátony oxbow, there were three sampling points (one open water, one submersed, and one emersed). In the Nagy-Pap oxbow, there were three sampling points (two emersed and one open water). In the Sulymos oxbow, there were six sampling points (one open water, one submersed, and four emersed vegetation type).

2.2. Water chemistry

We collected surface water samples in 1-liter plastic bottles; the bottles were rinsed out with deionized water three times. Until laboratory processing, samples were stored at 4 °C. We measured the physical and chemical parameters of the water. The following parameters were measured in the field: conductivity, temperature, content of dissolved oxygen (DO) with portable field instruments (WTW cond. 340i), and pH (WTW pH 315i).

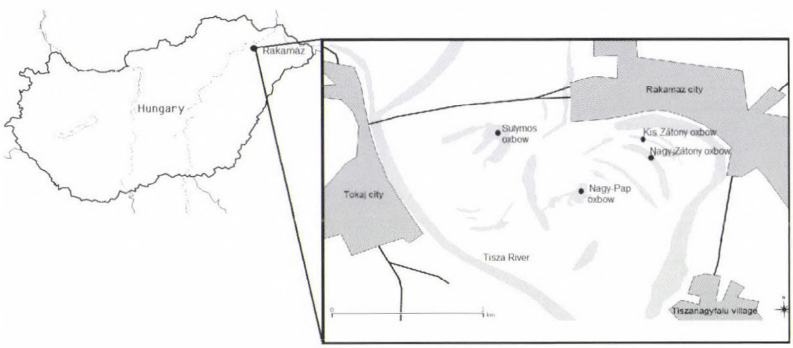

Fig. 1. Locations of oxbows.

We measured suspended solids from the original samples. For nitrite, nitrate, ortho-phosphate, carbonate, hydro-carbonate, carbon-dioxide and chloride concentration we used filtered samples. Water chemistry analysis was performed by the *USEPA* (1983) and *APHA* (2000) methods. For the assessment of quality, the *MSZ 12749* (1993) standard classification was used.

The local meteorological conditions of the study sites were based on the data from the websitwe of the MetNet Association (www.metnet.hu). The following parameters were used: rainfall, number of rainy days, and average temperature (*Table 1*). For our study, the results of four summer months were used. The water level of the Tisza was based on the data of the National Water Warning Service (www.hydroinfo.hu) (*Fig. 2*).

Table 1. Summary of meteorological data from May, June, July, and August (mean ± SE). The average temperature is the mean of the day, and the mean of rainfall is the average of the month

Year	Temperature (°C)	Rainfall (mm)	Number of raining days
2011	20 ± 2	68 ± 26	15 ± 7
2012	22 ± 3	47 ± 3	11 ± 4

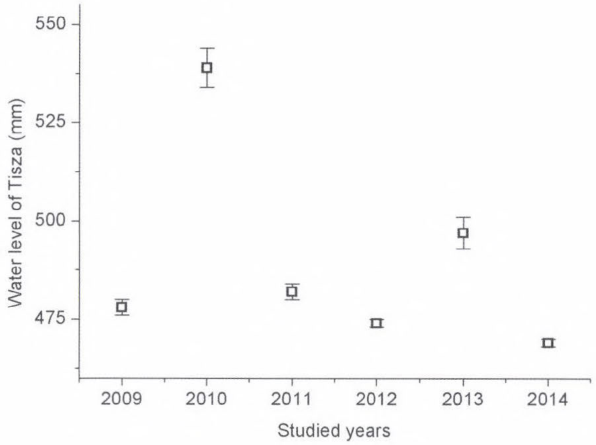

Fig. 2. The water level of the River Tisza (mean ± SE) over the past six years.

2.3. *Drought index*

To compare the years, a drought index (PaDI) was used. This index is a ratio of the mean temperature during the period from April to August and the rainfall from October to August (*Tsakiris* and *Vangelis,* 2004; *Tate* and *Gustard,* 2000). The following drought categories were used: PaDI < 4 represents a drought free year, 4 < PaDI < 6 a slight drought year, 6 < PaDI < 8 a moderate drought year, 8 < PaDI < 10 a medium moderate drought year, 10 < PaDI < 15 a severe drought year, 15 < PaDI < 30 a very severe drought year, and PaDI > 30 an extreme drought year.

2.4. *Statistical analysis*

SPSS/PC+ and Canoco for Windows statistical software packages were used during the calculations. Using redundancy analysis (RDA) we studied the correlation between the physico-chemical parameters of water and precipitation, and the temperature in the studied oxbows. canonical discriminant analysis (CDA) was used to study the physico-chemical parameters of oxbows. The physico-chemical parameters of the oxbows were compared by ANOVA, where the years and vegetation types were fixed factors. In the case of any significant differences, the Tukey's multiple comparison test was used to explore these significant differences.

3. Results

The correlation between the first component (RDA1) of redundancy analysis and the water physico-chemical parameters and weather parameters was 0.955, while for the second component (RDA2), the correlation was 0.562. The cumulative percentage variances were 31.3 (RDA1) and 7.5 (RDA2). In the case of water physico-chemical parameters and weather parameters, the relation was 79.5% (RDA1) and 19.1% (RDA2). For carbon dioxide, suspended solids, and carbonate, a positive correlation was found between concentration and rainfall and the number of rainy days (*Fig. 3*). A positive correlation was found between dissolved oxygen, water temperature, and the concentration of hydro carbonate, nitrate, pH, conductivity, and the average temperature (*Fig. 3*).

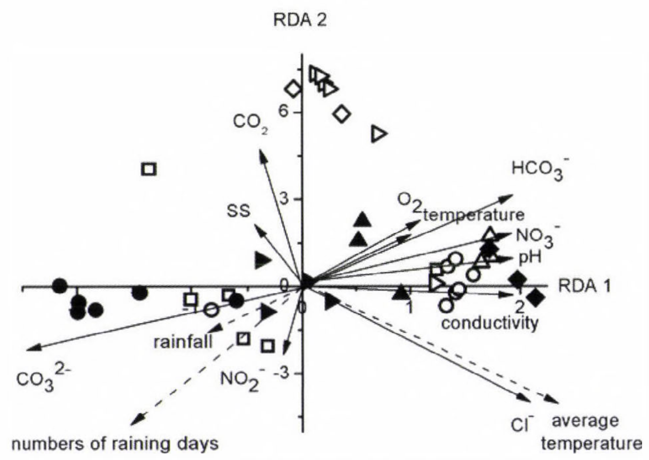

Fig. 3. Redundancy analysis biplot to show the interaction between the physico-chemical parameters of water and the meteorological conditions. Notations: solid arrow – physico-chemical parameters of water, dash arrow – precipitation and temperature.

Based on the physical and chemical parameters of water, the separation of the studied oxbows was similar in 2011 and 2012, based on the canonical discriminant analysis (*Fig. 4A-B*). There were differences between 2011 and 2012 only in the Nagy-Zátony oxbow. The canonical variance percentage was 99.6 in the first and 0.3 in the second axis, based on the 2011 data. The canonical variance percentage was 83.9 in the first and 10.0 in the second axis, based on the 2012 data.

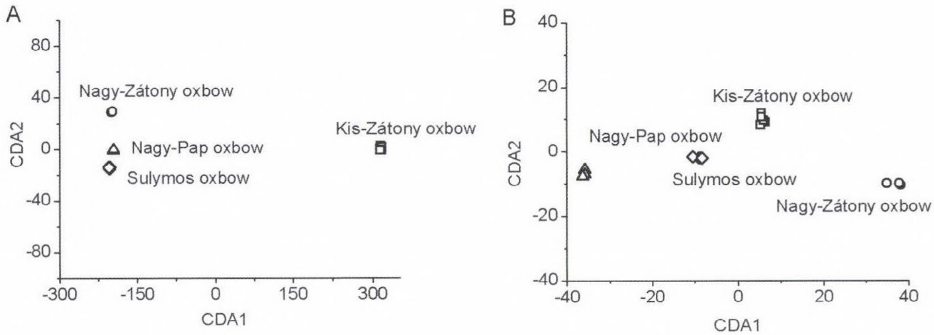

Fig. 4. Canonical discriminant biplot based on the physical and chemical parameters in the studied oxbows in 2011 (A) and 2012 (B).

Based on the vegetation types, the separation was also similar in both years (2011 and 2012). A slight change was found in the case of submersed vegetation types in 2011 and 2012 (*Fig. 5A-B*). The variance percentage was 93.3 in the first and 6.7 in the second axis in 2011. However, in 2012, the variance percentage was 70.8 in the first and 29.2 in the second axis.

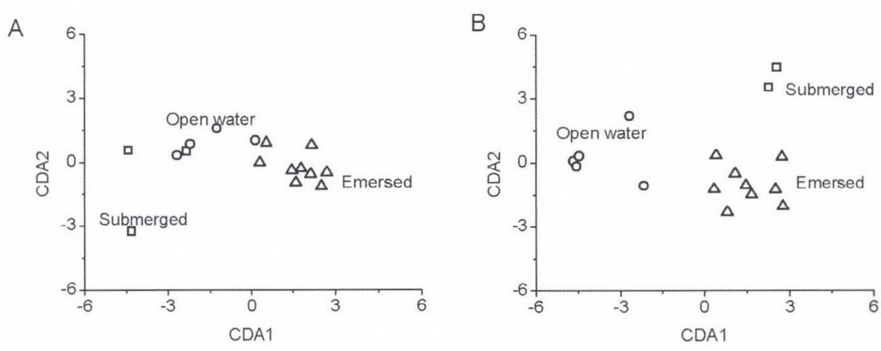

Fig. 5. Canonical discriminant biplot based on the physical and chemical parameters in the vegetation types in 2011 (A) and 2012 (B).

The result for the drought index was similar in the studied years. In 2011 the drought index value was 4.2, while in 2012 the value was 5.9. The index values suggest that each year was a slight drought year. In spite of this, when comparing the water physico-chemical parameters, a difference was found between the years, but differences were not found among vegetation types using two-way ANOVA. There was a significant difference between the years in the water temperature, the suspended solid content, and the concentration of carbonate and chloride (*Table 2*). A significantly higher temperature, suspended solid content, and carbonate and chloride concentration were found in 2012 than in 2011. Significantly higher water temperatures were found in 2011 than in 2012 in the Kis-Zátony oxbow (t_5=–5.413, p=0.003), the Nagy-Pap oxbow (t_3=–52.200, p<0.001), and the Sulymos oxbow (t_8=–26.960, p<0.001). However, the water temperature did not differ between the two years (t_8=–26.960, p<0.001) in the Nagy-Zátony oxbow. The concentration of carbonate was significantly higher in 2012 than in 2011 in the Kis-Zátony oxbow (t_5=–5.541, p=0.003) and the Sulymos oxbow (t_8=–26.960, p<0.001). The concentration of hydro-carbonate was significantly higher in 2011 than in 2012 in the Kis-Zátony oxbows (t_5=7.194, p=0.001). In the Nagy-Zátony oxbow, the concentration of hydro-carbonate was significantly higher in 2012 than in 2011 (t_2=–111.449, p<0.001). Significantly higher concentrations of chloride-ion were observed in 2012 than in 2011 in the Nagy-Pap (t_3=–24.498, p<0.001) and Sulymos oxbows (t_8=–32.680, p<0.001). In the Nagy-Zátony oxbow, the concentration of chloride-ion did not differ between the years (t_2=–2.452, p=0.134) (*Table 3*). There was no significant difference among habitat types in their physical-chemical parameters.

Table 2. Results of ANOVA based on the physical and chemical parameters of years and vegetation types.

	year		**vegetation type**	
	F	*p*	**F**	*p*
temperature (°C)	10.294	0.003	0.232	0.795
pH	2.914	0.099	1.581	0.224
conductivity(μS/cm)	0.239	0.629	0.281	0.757
dissolved oxygen (mg/l)	0.855	0.363	0.526	0.597
suspended solid (mg/l)	11.286	0.002	0.426	0.657
carbonate (mg/l)	11.097	0.002	0.019	0.981
hydro carbonate (mg/l)	2.970	0.096	0.596	0.558
carbon dioxide (mg/l)	0.701	0.409	0.537	0.590
chloride (mg/l)	5.627	0.025	0.202	0.819
orthophosphate (mg/l)	0.109	0.744	0.421	0.661
nitrite (N mg/l)	2.296	0.141	0.630	0.540
nitrate (N mg/l)	1.712	0.201	0.396	0.677

Table 3. Physical and chemical parameters in the surface water of the studied oxbows (mean ± SD). Notations: n.m. means not measured, n.d. means not detected.

	Kis- Zátony oxbow		Nagy- Zátony oxbow		Nagy-Pap oxbow		Sulymos oxbow	
	2011	2012	2011	2012	2011	2012	2011	2012
temperature (°C)	25.1 ± 0.3	27.5 ± 0.2	22.6 ± 0.2	20.7 ± 0.1	18.8 ±0.04	29.7 ± 0.2	18.4 ± 0.2	29.4 ± 0.3
pH	7.2 ± 0.01	7.4 ± 0.1	7.1 ± 0.2	7.1 ± 0.2	7.0 ± 0.1	9.0 ± 0.2	7.0 ± 0.1	7.9 ± 0.2
conductivity(µS/cm)	615 ± 8	699 ± 25	825 ± 7	875 ± 27	694 ± 4	558 ± 7	805 ± 57	621 ± 9
dissolved oxygen (mg/l)	8.2 ± 0.1	4.2 ± 0.4	n.d.	n.d.	2.4 ± 1.6	6.3 ± 0.7	8.2 ± 0.4	5.0 ± 0.5
suspended solid (mg/l)	7.4 ± 1.1	18.9 ± 2.3	10.1 ± 2.8	14.9 ± 4.5	15.4 ± 5.5	54.4 ± 12.9	16.8 ± 5.1	40.7 ± 12.9
carbonate (mg/l)	6.3 ± 3.0	27.1 ± 3.9	n.d.	4.5 ± 0.1	n.d.	n.d.	n.d.	3.8 ± 0.4
hydro carbonate (mg/l)	81 ± 1	5.0 ± 1.7	n.d.	102 ± 3	n.d.	n.d.	n.d.	79.4 ± 0.9
carbon dioxide (mg/l)	28.1 ± 2.4	35.8 ± 4.2	22.5 ± 1.6	42.9 ± 7.4	22.7 ± 2.3	n.d.	13.1 ± 3.1	5.7 ± 1.1
chlorine (mg/l)	25.5 ± 2.2	15.7 ± 1.4	13.6 ± 1.9	18.5 ± 1.0	n.d.	24.3 ± 2.5	n.d.	24.8 ± 2.5
orthophosphate (mg/l)	0.2 ± 0.01	0.1 ± 0.04	0.1 ± 0.01	0.1 ± 0.01	0.1 ± 0.01	0.2 ± 0.04	0.1 ± 0.03	0.2 ± 0.01
nitrite (N mg/l)	0.05 ± 0.03	0.02 ± 0.01	0.01 ± 0.001	0.01 ± 0.01	0.01 ± 0.01	0.03 ± 0.02	0.2 ± 0.1	0.002 ± 0.001
nitrate (N mg/l)	0.2 ± 0.03	0.02 ± 0.01	0.1 ± 0.01	0.05±0.00	0.05±0.01	0.11±0.07	0.02±0.01	0.1 ± 0.01

4. Discussion

The chemical composition of lakes and oxbows is determined by natural and anthropogenic factors; these include geological, climatic, and biological factors (*Moiseenko et al.,* 2013). Many papers have reported the effects of climatic and weather factors on oxbows (*Cullum et al.,* 2006; *Hunyady,* 2010, *Zhao et al.,* 2013). Earlier studies demonstrated that dry seasons and dry years cause worse water quality, similarly to our findings (*Pesce* and *Wunderlin,* 2000, *Vega et al.,* 1998).

The quality of the Kis-Zátony oxbow and the Nagy-Pap oxbow were good, while the Nagy-Zátony oxbow and the Sulymos oxbow were contaminated in 2011, based on the conductivity findings (*MSZ*,1193). A similar conductivity was found in the second year – 2012 – in each oxbow, except for the Sulymos oxbow, where the quality was good in 2012. *Michalska-Hejduk et al.* (2009) found similar conductivity values and the use of their classification shows that the oxbows we studied are ion-rich.

Of the chemical parameters, dissolved oxygen is an important component of the surface water (*Michalska-Hejduk et al.,* 2009). In our study, based on the concentration of dissolved oxygen, the quality of the Kis-Zátony and Sulymos oxbows was excellent in 2011. The quality of the Nagy-Pap oxbow was contaminated in 2011, but in 2012 it was good. Concentrations of dissolved oxygen in the Kis-Zátony and Sulymos oxbows were contaminated in 2012. Anthropogenic activities were not detected in the area of this oxbow; thus, the lower oxygen concentration is probably the result of a decreasing water level. The water level decrease may result in higher organic matter, which has a direct effect on the dissolved oxygen concentration in the water ecosystem (*Michalska-Hejduk et al.,* 2009).

Kröger et al. (2013) found a positive correlation between the concentration of suspended solids and wind speeds. They demonstrated that turbidity has an indirect effect on suspended solid concentrations (*Kröger et al.,* 2013). Similarly to their findings, our results also indicated that weather parameters have an effect on the concentration of suspended solids. We found higher results in 2012 than in 2011 in every oxbow.

The concentrations of anions, including carbonate, hydro carbonate, chloride, nitrite, and nitrate are dependent on atmospheric deposition and conditions, as it is shown in the redundancy analysis. Based on the nitrite concentrations, the quality of the Nagy-Zátony, Nagy-Pap, and Sulymos oxbows was good, while the quality of the Kis-Zátony oxbow was tolerable in 2011. Nevertheless, in 2012, the water quality of the Kis-Zátony oxbow improved to the same level as that of the other oxbows. This could be explained by higher microbial activity, which may have caused the higher temperature and lower water level in this year (*Davidson et al.,* 1998). Similarly to the earlier finding, the conductivity is related to alkalinity which may regulate the aquatic production (*Zablotowicz et al.*, 2010). The concentration of orthophosphate was similar among the oxbows and also between years. Water quality was contaminated in the Kis-Zátony oxbow, based on orthophosphate concentrations in 2011. The other oxbows were tolerable in 2011. In the next year, the quality of water was contaminated in the Nagy-Pap and Sulymos oxbows, while in the Nagy-Zátony and Kis-Zátony oxbows it was tolerable. In spite of earlier findings (*Moiseenko et al.*, 2013), we did not find an increase in the orthophosphate concentration, despite the increase in the daily temperature.

Unlike earlier studies (*Lukács et al.*, 2009, 2011) we did not find any differences between the vegetation types based on the physico-chemical parameters of water. *Lukács et al.* (2009) demonstrated that nitrogen and carbonate were the most important variables for vegetation development. *Lukács et al.* (2011) also observed that among water chemical parameters, calcium, chemical oxygen demand, nitrite, magnesium, and chloride-ion were important in differentiating the vegetation. Our study showed that the physico-chemical parameters of water did not differ among vegetation types, which was probably caused by the low level of the water.

In spite of the poor state of the oxbows which was visible in the field, differences were not found between the weather parameters in the years under investigation. Based on the drought index, each year experienced a slight drought, although with some parameters, such as water temperature, suspended solids content, and the concentration of carbonate and chloride, significant differences between the years were found. Using the water level data for the River Tisza, the results show that in the past years the water level of the river has changed remarkably.

5. Conclusions

We demonstrated that precipitation and temperature influenced the open-water surface area, the water level, and the physico-chemical parameters of oxbows. These oxbows were connected to the main river only during floods; thus, the water level of the main river also had a remarkable effect on the quality of oxbows. The physico-chemical parameters indicated that the anthropogenic activities did not cause the degradation in the state of the oxbows. Our findings suggest that the degradation of the water quality of the oxbows is only slightly influenced by precipitation and temperature. The degradation depends on the water level of the main river, and the frequency and duration of the flooding.

Acknowledgements: This research was supported by the TÁMOP 4.2.1./B-09/1/KONV-2010-0007, and TÁMOP- 274 4.2.2/B-10/1-2010-0024 projects, the European Union and the State of Hungary, co-financed by the European Social Fund. E. Simon was supported by the TÁMOP-4.2.2.A-11/1/KONV. The study was supported by the SROP-4.2.2.B-15/1/KONV20150001 project.

References

APHA, 2000: American Public Health Association, Washington (DC).

Barendregt, A., and *Bio, A.F.M.*, 2003: Relevant variables to predict macrophyte communities in running waters. *Ecol. Modell. 160,* 205–217.

Bond, N.R., Lake, P.S., and *Arthington, A.H.*, 2008: The impacts of drought on freshwater ecosystems: an Australian perspective. *Hydrobiologia 600*, 3–16.

Bornette, G., and *Puijalon, S.*, 2011: Response of aquatic plants to abiotic factors: a review. *Aquat. Sci. 73*, 1-14.

Cook, C.D.K., 1996: Aquatic Plant. Academic Publishing, Amsterdan/New York.

Cullum, R.F., Knight, S.S., Cooper, C.M., and *Smith, S.*, 2006: Combined effects of best management practices on water quality in oxbow lakes from agricultural watersheds. *Soil. Till. Res. 90,* 212–221.

Davidson, E.A., Belk, E., and *Boone, R.D.*, 1998: Soil water content and temperature as independent or confounded factors controlling soil respiration in a temperate mixed hardwood forest. *Glob. Change. Biol. 4,* 217–227.

Fink, D.F., and *Mitsch, W.J.*, 2007: Hydrology and nutrient biogeochemistry in a created river diversion oxbow wetland. *Ecol. Eng. 30*, 93–102.

Frodge, J.D., Thomas, G.L., and *Pauley, G.B.*, 1990: Effects of canopy formation by floating and submergent aquatic macrophytes on the water quality of two shallow Pacific Northwest lakes. *Aquat. Bot. 38*, 231–248.

Georgi, F.X., and *Pal, J.*, 2004: Mean, interannual variability and trends in a regional climate change experiment over Europe. II: climate change scenarios (2071–2100). *Clim. Dynam. 23*, 839–858.

Heegaard, E., Birks, H.H., Gibson, C.E., Smith, S.J., and *Wolfe-Murphy, S.*, 2001: Species–environmental relationships of aquatic macrophytes in Northern Ireland. *Aquat. Bot. 70,* 175–223.

Hunyady, A., 2010: Projected climate change effects on water level of an oxbow. *Phys. Chem. Earth. 35*, 70–75.

Kröger, R., Dibble, E.D., Brandt, J.R., Fleming, J., Huenemann, T.W., Stubbs, R.B., Prevost, J.D., Tietjen, T.E., Littlejohn, K.A., and *Pierce, S.C.*, 2013: Spatial and temporal changes in total suspended sediment concentrations in an Oxbow Lake from implementing agricultural landscape management practices. *River Res. Appl. 29*, 56–64.

Lukács, B.A., Dévai, G., and *Tóthmérész, B.*, 2011: Small scale macrophyte-environment relationship in an oxbow-lake of the Upper-Tisza valley (Hungary). *Community Ecol. 12*, 259–263.

Lukács, B.A., Dévai, Gy., and *Tóthmérész, B.*, 2009: Aquatic macrophytes as bioindicators of water chemistry in nutrient rich backwaters along the Upper-Tisza river (in Hungary). *Phytocoenologia 39*, 287–293.

Michalska-Hejduk, D., Kopeć, D., Drobniewska, A., and *Sumorok, B.*, 2009: Comparison of physical and chemical properties of water and floristic diversity of oxbow lakes under different levels of human pressure: A case study of the lower San River (Poland). *Int. J. Ecohydrol. Hydrobiol. 9*, 183–191.

Michener, W.K., Blood, E.R., Bildstein, K.L., Brinson, M.M., and *Gardner, L.R.*, 1997: Climate change, hurricanes and tropical storms, and rising sea level in coastal wetlands. *Ecol. Appl. 7*, 770–801.

Moiseenko, T.I., Skjelkvale, B.L., Gashkina, N.A., Shalabodov, A.D., and *Khoroshavin, V.Y.*, 2013: Water chemistry in small lakes along a transect from boreal to arid ecoregions in European Russia: Effects of air pollution and climate change. *Appl. Geochem. 28*, 69–79.

MSZ, 1993: MSZ 12749. Hungarian Standard Association.

Nguyen, H.L., Braun, M., Szalóki, I., Baeyens, W., Van Grieken, R., and *Leemarkers, M.* 2009 Tracing the metal pollution history of the Tisza River through the analysis of a sediment depth profile. *Water Air Soil Pollut. 200*, 119–132.

Oertli, B., Céréghino, R., Hull, A., and *Miracle, R.*, 2009 Pond conservation: from science to practice. *Hydrobiologia 634*, 1–9.

Palmer, M.A., Lettenmaier, D.D., Poff, N.L., Postel, S.L., Richter, B., and *Warner, R.*, 2009: Climate Change and River Ecosystems: Protection and Adaptation Options. *Environ. Manage. 44*, 1053–1068.

Pesce, S.F., and *Wunderlin, D.A.*, 2000: Use of water quality indices to verify the impact of Córdoba City (Argentina) on Suquía River. *Water Res. 34*, 2915–2926.
Tate, E.L., and *Gustard, A.*, 2000: Drought definition: A hydrological perspective. In (eds.: *Voght, J.V.*, *Somma, F.*) Drought and drought mitigation in Europe. Kluwer Academic Publishers, Dordrecht.
Tsakiris, G., and *Vangelis, H.*, 2004: Towards drought watch system based on spatial SPI. *Water Resour. Manag. 18*, 1–12.
USEPA, 1983: United States Environmental Protection Agency, Washington (DC).
Varga, K., *Dévai, G.*, and *Tóthmérész, B.*, 2013: Land use history of a floodplain area during the last 200 years in the Upper-Tisza region (Hungary). *Reg. Environ. Change. 13*, 1109–1118.
Vega, M., *Pardo, R.*, *Barrado, E.*, and *Deban, L.*, 1998: Assessment of seasonal and polluting effects on the quality of river water by exploratory data analysis. *Water Res. 32*, 3581–3592.
Winter, T.C., 2000: The vulnerability of wetlands to climate change: a hydrologic landscape perspective. *J. Am. Water Resour. As. 36*, 305–311.
Zablotowicz, R.M., *Zimba, P.V.*, *Locke, M.A.*, *Knight, S.S.*, *Lizotte, R.E.*, and *Gordo, R.E.*, 2010: Effects of land management practices on water quality in Mississippi Delta oxbow lakes: Biochemical and microbiological aspects. *Agr. Ecosyst. Environ. 139*, 214–223.
Zhao, Y., *Xia, X.*, and *Yang, Z.*, 2013: Growth and nutrient accumulation of *Phragmites australis* in relation to water level variation and nutrient loadings in a shallow lake. *J. Environ. Sci. 25*, 16–25.

IDŐJÁRÁS

Quarterly Journal of the Hungarian Meteorological Service
Vol. 120, No. 3, July – September, 2016, pp. 315–329

Comparison of simulated and objectively analyzed distribution patterns of snow water equivalent over the Carpathian Region

Hristo Chervenkov* and **Kiril Slavov**

National Institute of Meteorology and Hydrology – Bulgarian Academy of Sciences
66, Tsarigradsko Shose blvd, Sofia 1784, Bulgaria
E-mails:hristo.tchervenkov@meteo.bg, kiril.slavov@meteo.bg

**Corresponding author*

(Manuscript received in final form February 8, 2016)

Abstract—Snow is a very important component of the climate system which controls surface energy and water balances. Its high albedo, low thermal conductivity, and properties of surface water storage impact regional to global climate. The various properties characterizing snow are highly variable and thus have to be determined as dynamically active components of climate. However, on large spatial scales, the properties of snow are not easily quantified either from numerical modeling or observations. Thus, it is vital to estimate the model performance in comparison with consistent datasets of assimilated data. Snow water equivalent data simulated with four different model configurations of the RegCM climate model over Central Europe for a time window of 10 consecutive winters are compared with the objective analysis data from the high-resolution CARPATCLIM database on monthly and seasonal basis. The CARPATCLIM snow water equivalent data are also modeled, but based on the gridded daily observation of the temperature, precipitation, and relative humidity. The results reveal good commensurability over the bigger, mostly flat part of the domain, however, they show significant discrepancies, mainly overestimation, over the Carpathian Region.

Key-words: *snow water equivalent, numerical simulation, RegCM*

1. Introduction

Snow is a very important component of the climate system which controls surface energy and water balances, and it is the largest transient feature of the land surface according *Yang et al.* (2001). It has an effect on atmospheric circulation through changes to the surface albedo, thermal conductivity, heat capacity, and aerodynamic roughness, as it has been documented in numerous observational and modeling studies (e.g., *Barnet et al.* 1989, *Gong et al.* 2003). The snow properties of the surface water storage control the availability of water in many ecosystems and to a sixth of the world's population (*Clifford,* 2010). Therefore, it is vital that snow is properly represented in geophysical models if we want to understand and make predictions of weather, climate, carbon cycle, flooding, and drought.

The various properties characterizing snow are highly variable and thus have to be determined as dynamically active components of climate. These include the snow depth (h_s) snow water equivalent (*SWE*), density, and snow cover area (*SCA*). To understand global snow water trends in the necessary depth, the most fundamental metric to assess is *SWE*, with h_s as a close second. However, on large spatial scales, the properties of snow are not easily quantified either from modeling or observations. For example, station based snow measurements often lack spatial representativeness, especially in regions, where the topography, vegetation, and overlaying atmosphere produce considerable heterogeneity of the snow-pack distribution (*Liston,* 2004). Thus, despite the weaknesses of the land surface models, the quantitative assessment of the snow properties by the means of the numerical simulation is a pragmatic approach for obtaining of the spatial and temporal continuous distribution of the snow pack. The utilization of regional climate models (RCMs) in the Bulgarian National Institute of Meteorology and Hydrology is within the framework of the common effort for composition of detailed picture of the snow cover and its dynamics over Southeast Europa with focal point to the central part of the Balkan peninsula. So, the latest version of the well-known RegCM regional climate model is applied for quantitative estimation of many surface variables, including *SWE*, for 14 consecutive winters between 2000 and 2013, and the subset 2000–2009 is used in the present study. As in many validation studies, however here even in greater extent, part of the difficulties in exploring the simulation ability issue of the model is rooted in the lack of validation data for small-scale features and reliable measurements. It is clear that datasets as the mentioned model simulation with such time gaps are highly insufficient for any model validation study. Nevertheless, hence such procedure is often treated in similar numerical experiments as a necessary (first) step in verification/model performance evaluation, such comparisons are preformed and the results are described (*Chervenkov et al.,* 2015). Main conclusion from this work is that the comparisons of the measurements with the model output from all runs yield generally similar results. Further, the overall (i.e., over the whole time span) biases are acceptable, but, however, with large discrepancies in the day-by-day comparisons, which is typical for climate modeling studies.

Satellite earth snow observation products have the needed spatial and temporal consistency, which allows comparisons with model output over continuous area and time frames. So, utilizing satellite data is a significant step ahead in the quantitative snow cover assessment. Satellite retrieval estimates, however, require inversion algorithms to relate raw signals recorded at the satellite to physical properties of the land surface, and these inverted estimates can contain errors and biases (*Hancock et al.,* 2013). Although among the other products, *SWE* has been proven to be more problematic (*Hancock et al.,* 2013), especially for wet snow and during melt, which is a typical case in southeast Europe, the common treatment of satellite data and model results has been already performed. The gridded digital maps of the Globsnow SWE product (http://www.globsnow.info/swe/GlobSnow_SWE_product_readme_v1.0a.pdf) are compared with the simulation output for the whole 14-year period on monthly basis (*Chervenkov et al.,* 2016). Certain drawbacks of the Globsnow product can point the absence of data for mountainous regions, which, at least from hydrological point of view, are important.

Another informational sources, suitable for assessment studies are the products of objective analysis of measurements. Depending on the leading physical and mathematical concept, involved data streams and, correspondingly, the incorporated processing methods the can vary greatly. The primary importance feature of these products is the data quality and, second, at least from the end-user point of view, the form of the final product, which is a timely continuous digital map of gridded datasets. The relatively long (in climatological sense, i.e., in order of decades) temporary extend, acceptable horizontal resolution, presence of subsets for various variables, and, not at least, the free-of-charge availability of most of these products make it a preferable tool in many applications, as the presented verification study here. Being typical member of this group, the CARPATCLIM dataset is a motivated choice for testing the model performance, and thus this paper, which, in some extend, is the continuation of *Chervenkov et al.* (2015), is dedicated to the comparison of the simulated values of *SWE* with the analyzed ones.

The paper is organized as follows: Short description of the CARPATCLIM database, the used version of the RCM RegCM, and the methodological approach are placed in the first chapter. The performed calculations and the obtained results are described and visualized in the second chapter. Summarizing remarks and the main conclusions are listed in the last chapter.

2. Concept and methodology

The CARPATCLIM database is the result of the common effort of 10 national institutions from 9 Central European countries as well as the Joint Research Centre and the Institute for Environment and Sustainability to overcome the differences caused by the national specification in the meteorological data sampling and management. According to the product description, the main aim of the project is to improve the basis of climate data in the Carpathian Region for applied regional climatological studies such as a Climate Atlas and/or drought monitoring, to investigate the fine temporal and spatial structure of the climate in the Carpathian Mountains and the Carpathian Basin with unified methods. Manifestation of the success of the project is the freely available, high resolution gridded database for the Larger Carpathian Region (LCR) (see *JRC report* 2010 and the references therein). For ensuring the usage of the largest possible station density, the processing were implemented by the countries themselves using the same methods and software. The commonly used methods were the MASH (Multiple Analysis of Series for Homogenization; *Szentimrey,* 2011) procedure for homogenization, quality control, and completion of the observed daily data series; and the MISH (Meteorological Interpolation based on Surface Homogenized Data Basis; *Szentimrey* and *Bihari,* 2007) for gridding of homogenized daily data series. The harmonization of the datasets was carried out by the exchange of the near border station data of the neighboring countries before and after homogenization.

The evaluation of measured snow cover records at the level of CARPATCLIM area has led to the conclusion that there is a lack of reliable and continuous measured data at the level of the meteorological stations of the region, and it is insufficient for estimating connected variables such as *SWE* and snow depth. This is a chronic problem in many regions of the world, in particular in the Balkan peninsula adjacent to the larger Carpathian Region, as shown in *Chervenkov et al.* (2015). In order to address this gap, a snow cover model employed operationally at the Austrian Central Institute for Meteorology and Geodynamics (ZAMG) was applied to generate a 0.1° latitude/longitude grid of daily mean snow cover and corresponding estimated water equivalent and snow depth simulations. The applied model is based on pre-finished CARPATCLIM grids of mean air temperature, precipitation sum, and relative air humidity. They are processed by the snow cover model regarding three main parts: accumulation of snow cover, ablation of snow cover, and transformation of *SWE* to snow depth. The reader can find more detailed description at http://www.carpatclim-eu.org/docs/computation/SNOW.pdf. The database contains the gridded distributions of 16 variables with horizontal resolution 0.1°×0.1° for domain with longitudinal extent 17 to 27 degrees north and latitudinal extent 44 to 50 degrees east for the period 1961–2010 on diurnal and monthly basis.

RCMs have been developed and extensively applied in the recent decade for dynamically downscaling of the coarse resolution information from different sources, such as global circulation models (GCMs) and reanalysis, for different purposes including past climate simulations and future climate projections. This widely used and productive approach is applied here. The main simulation tool is the freely available latest version of the regional climate model of the International Center of Theoretical Physics in Italy (ICTP). RegCM4 is a 3-dimensional, sigma-coordinate, primitive equation RCM with dynamical core based (version 2 and later) on the hydrostatic version of the NCAR-PSU Mesoscale Model 5 (MM5) (*Grell et al.,* 1994). The radiative transfer package is taken from the Community Climate Model version 3 (CCM3) (*Kiehl et al.,* 1996). The large-scale cloud and precipitation computations are performed by the Subgrid Explicit Moisture Scheme (SUBEX, *Pal et al.,* 2000), and the land surface physics are performed according to the Biosphere-Atmosphere Transfer Scheme (BATS, *Dickinson et al.,* 1993). The adopted convective scheme for the RCM simulations in the present study is the Grell scheme (*Grell,* 1993)) with the Arakawa and Schubert (*Arakawa* and *Schubert,* 1974) closure assumption. Main manifestation of the flexibility of the modern RCMs, including RegCM4, is the possibility for selection among different initial and boundary conditions datasets (ICBC), parameterization schemes/modules within the model, various constants and closure assumptions, etc., combining them in practically countless model setups. Obviously, the simulation output from such model setups will differ from one another, and, more or less, from the "reality". Thus, multiple runs with different model setups/configurations (further: modcons) have to be performed accenting the inspection of the modules that have major role is the proper description of the considered variables. There is overall agreement in the scientific community that the ICBC plays the most important role in the model performance (see *Xue et al.,* 2014 for details). Although there are numerous tests with different reanalysis data, which are considered as better ICBC compared to those produced by GCMs, there is no single reanalysis data set yielding the best results in every region and/or every season. We have performed simulations with the two most popular and widely used reanalysis datasets: the ERA-Interim of the European Centre for Medium-Range Weather Forecasts (ECMWF) (*Dee et al.,* 2011) with horizontal resolution 1.5°×1.5° for RegCM simulations, noted further as EIN15 and the reanalysis 2 of the USA National Centers for Environmental Predictions and the National Center for Atmospheric Research (NCEP/NCAR) (*Kanamitsu et al.,* 2002) with horizontal resolution 2.5°×2.5°, noted further as NNRP2. It is physically reasonable also to expect, that the module, which describes the surface processes and the interactions with the under- and overlaying soil and atmospheric layers, namely the land surface model, plays relevant role especially in the numerical treatment of the snow cover. A major addition to RegCM4 is the option to use the Community Land Model (CLM), version 3.5. Compared to BATS, CLM is a more advanced package (and, as a result, it is computationally heavier), which is described in detail in *Oleson et al.,* (2004, 2008). It uses a series of biogeophysically based parameterizations to describe the land-atmosphere exchanges of energy, momentum, water, and carbon. So, combining the two ICBC datasets with the two land surface models, four modcons are designed: ERAIN/BATS, ERAIN/CLM, NNRP2/BATS, and NNRP2/CLM, noted further as EB, EC, NB, NC.

The model domain is centered over Bulgaria and consists of 72×77 20 km×20 km gridcells and covers the CARPATCLIM one without the most northern latitudinal band in width 1.4° only. The simulation period is from November 1 till March 31 for 14 consecutive years between 2000 and 2014. The row model output is the gridded distribution of the *SWE* on a 6-hourly basis (i.e., at 00, 06, 12, and 18 UTC).

Traditional method to judge the model performance is to assess the degree of agreement between the model output and the analyzed data using well elaborated statistical methods, among them the most frequently applied is the calculation of statistical scores, which is widely used in validation studies.

3. Performed calculations and obtained results

Due to the practical absence of horizontal mixture processes, specific feature of the snow cover is the relatively high heterogeneity (in comparison to the atmospheric lower-level parameters). Thus, even on small distances in order of couple of kilometers, considerable differences in the snow properties can be observed, and the inspection of the CARPATCLIM *SWE* dataset confirms this peculiarity: the differences in some months and regions even for neighboring gridcells can be more than an order of magnitude. Hence, is reasonable to expect that the adequate resolution of the analysis and the model data, and the comparability of both of them is vital. As long as the resolution of the CARPATCLIM (roughly 10 km) is properly selected, the RegCM resolution of 20 km for the current implementation seems insufficient. Additionally, intending initially to obtain the mainly overall picture for a significantly larger domain, the subgridding option was not switched on in the model simulations, which is not applicable for the CLM option. Since interpolation procedures can not reveal smaller scale features than those presented in the original data, and generally all of these leads to smoothing of the field, is methodologically correct to interpolate the finer CARPATCLIM grid to the RegCM one and not vice versa. This is done in the most natural way, by simple spatial averaging of every neighboring 2×2 gridcells with definite values.

Although in some years and gridcells there is already snow cover before the 1st of November, the start of the model simulations at this date ensures generally the practical absence of significant snow pack over the bigger part of the domain. Starting relevantly later would cause systematic underestimations. Ten winters of the period 2000–2009 were taken in consideration in this study.

Usually January is treated as the representative month for the corresponding winter. The inspection of the CARPATCLIM atlas (available at http://www.carpatclim-eu.org/pages/atlas/), however, reveals that the snow cover over the bigger part of the domain for most of the considered years is thicker in February, and thus the average *SWE* for this month is the first considered climate characteristics. The second one is the monthly weighted average *SWE* for the winter, namely December, January, and February. Each month is weighted with the number of days per month.

Hence main aim of this work is to present the comparison between the simulated and analyzed *SWE*, rather than the actual *SWE* climatology, only an indicative sight is given here *Figs. 1* and *2*. It is worth to emphasize, however, its spatial and temporal variation – generally speaking, the *SWE* in the plains is roughly 10–50 mm, when over the Carpathian ridge it is up to 150–200 mm.

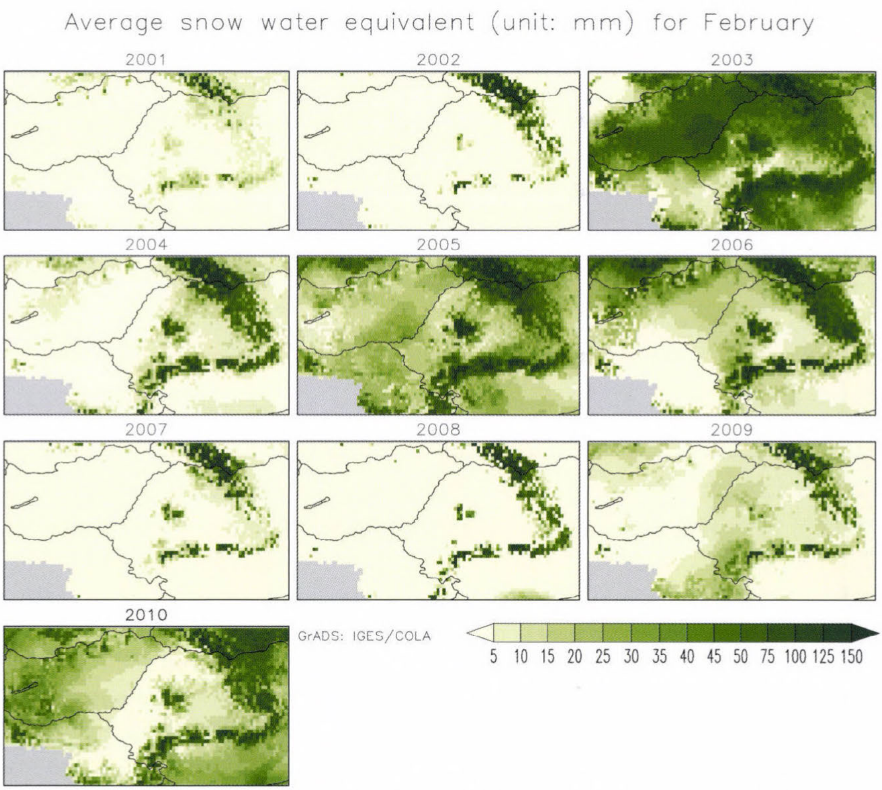

Fig. 1. Monthly average CARPATCLIM *SWE* (unit: mm) distribution for February in the original grid.

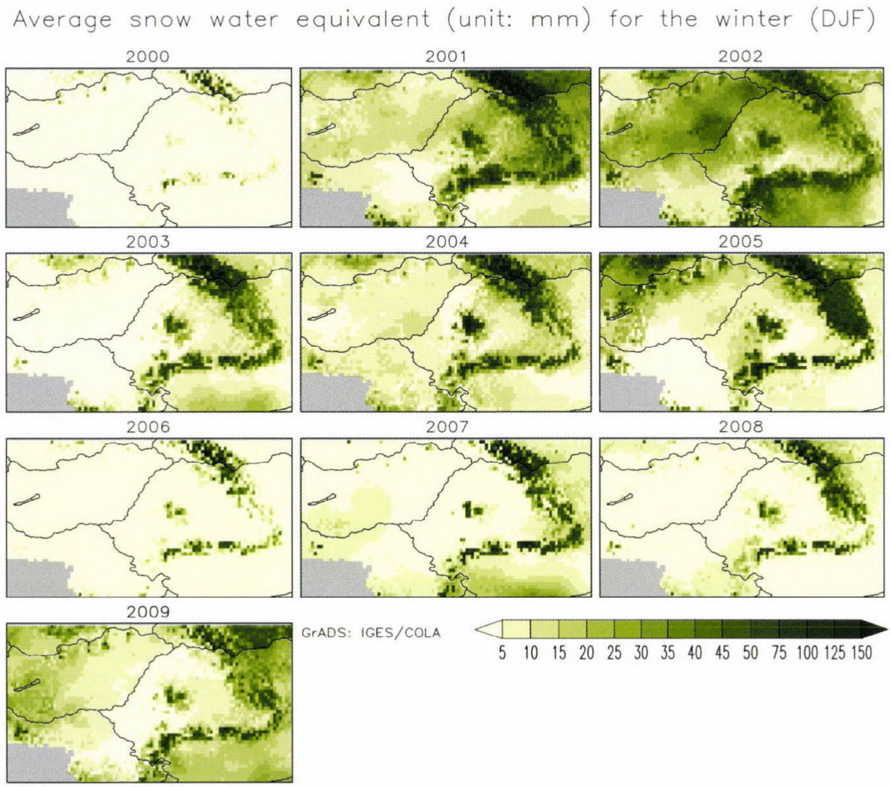

Fig. 2. Winter average (i.e., monthly weighted for December, January, and February) CARPATCLIM *SWE* (unit: mm) distribution in the original grid.

Keeping in mind the above described reasons about the resolution choice and intending to facilitate the comparisons, the modeled data are interpolated to the new, coarser CARPATCLIM 0.2°×0.2° grid. The files with the row RegCM output are handled with the powerful and easy-to-use operator suite climate data operator (*CDO,* 2015). The postprocessing of the model and analysis data is performed with purposely developed own programs, all tasks are automated via Linux bash scripts, and the visualization is done with GrADS scripts.

Most traditional approach for estimation of the departure of the model results from the analysis is applied: the absolute difference between the CARPATCLIM *SWE* and the modeled one (i.e., BIAS) for every winter month and for the monthly weighted winter average are calculated, but, due to the above commented relative importance, only those for February (in *Figs. 3–6*) and for the seasonal mean (in *Figs. 7–10*) are presented.

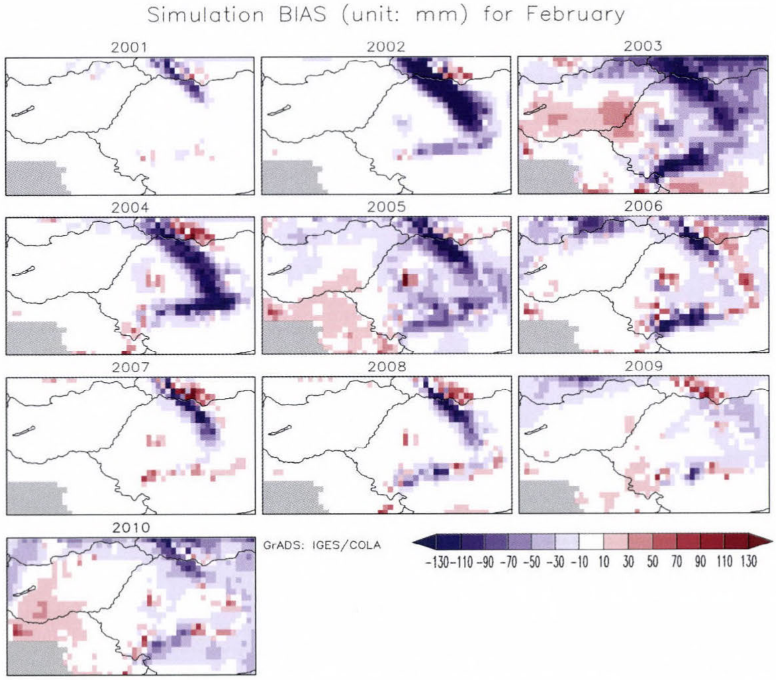

Fig. 3. BIAS (unit: mm) for the modcon 'EB' for February average in the reduced CARPATCLIM grid.

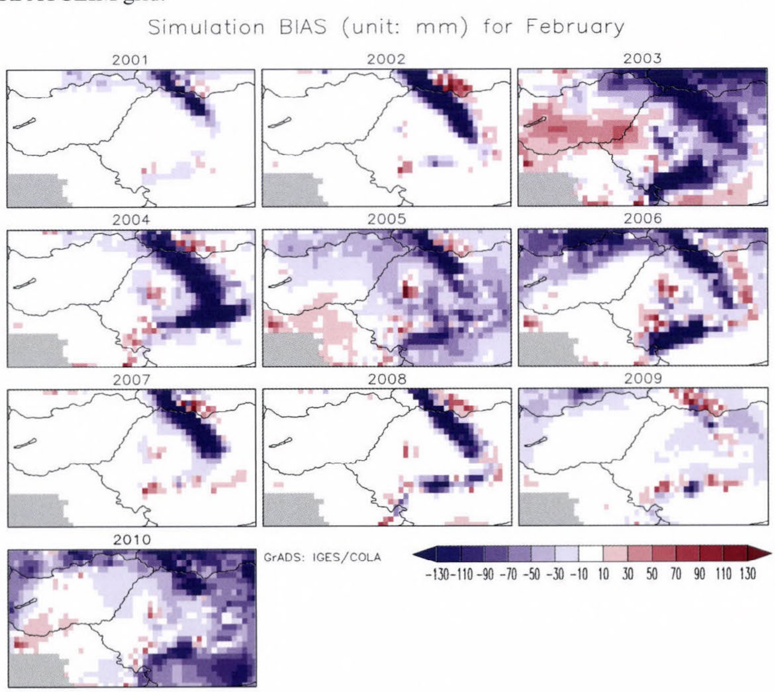

Fig. 4. Same as in *Fig. 3*, but for the modcon 'EC'.

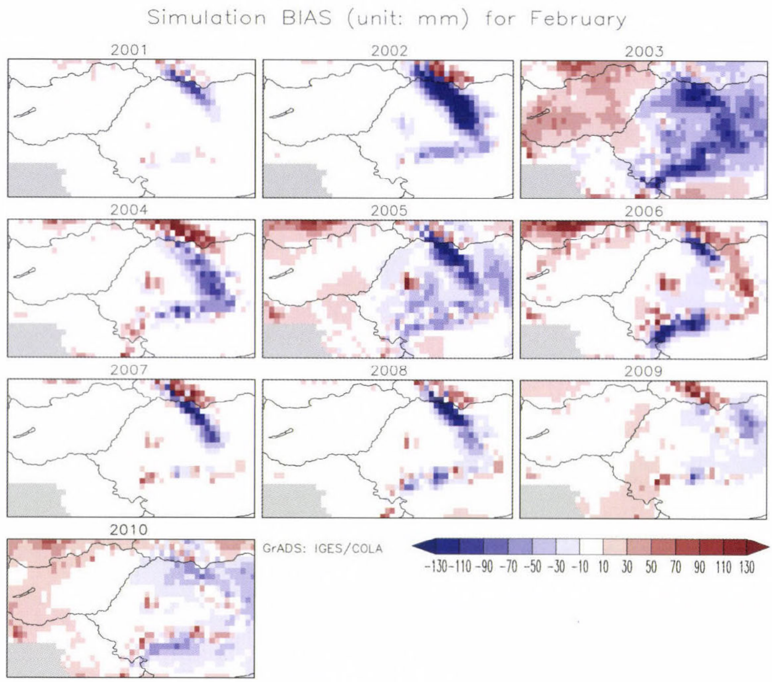

Fig. 5. Same as in *Fig. 3*, but for the modcon 'NB'.

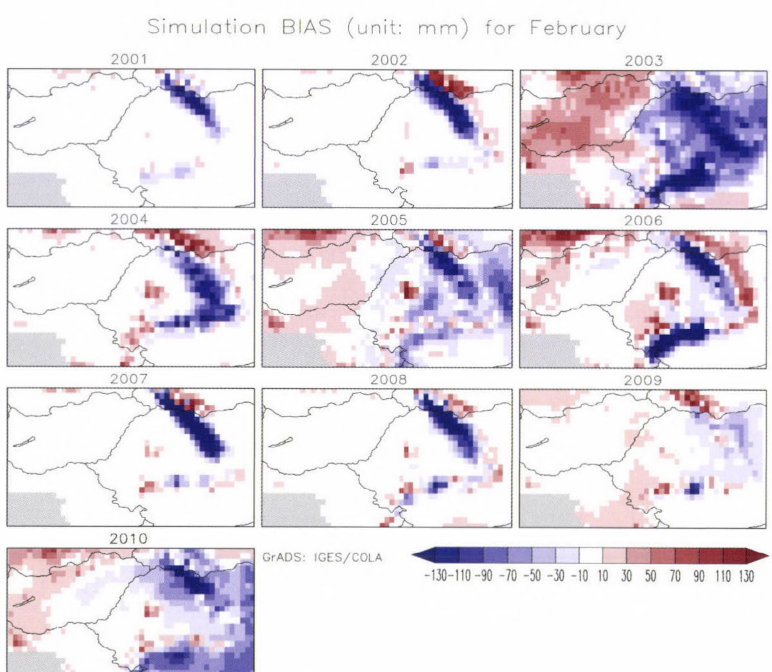

Fig. 6. Same as in *Fig. 3*, but for the modcon 'NC'.

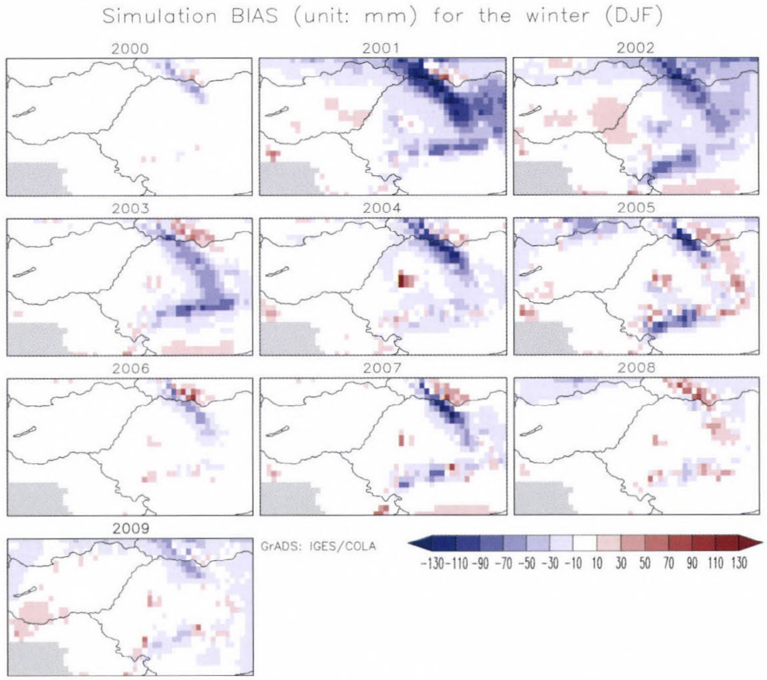

Fig. 7. BIAS (unit: mm) for the modcon 'EB' for the winter average in the reduced CARPATCLIM grid.

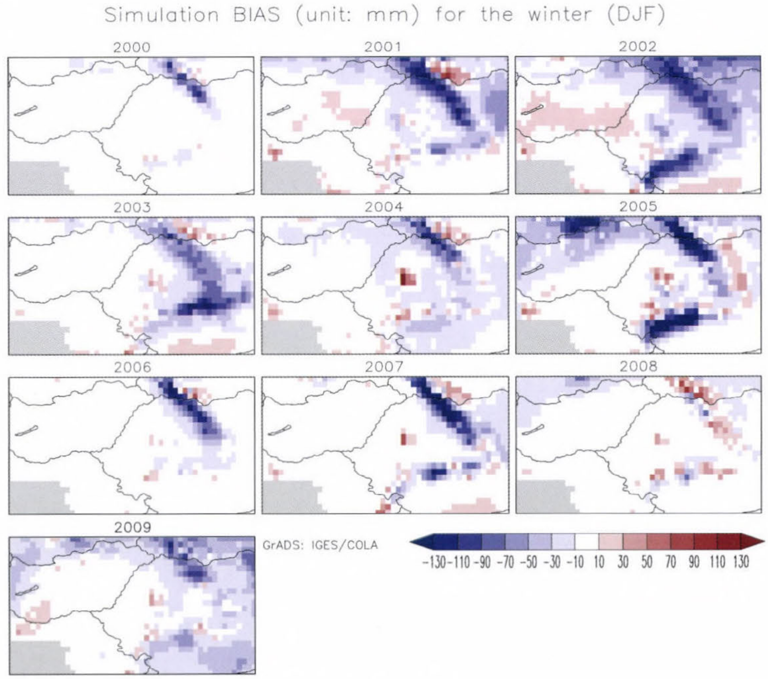

Fig. 8. Same as in *Fig. 7*, but for the modcon 'EC'.

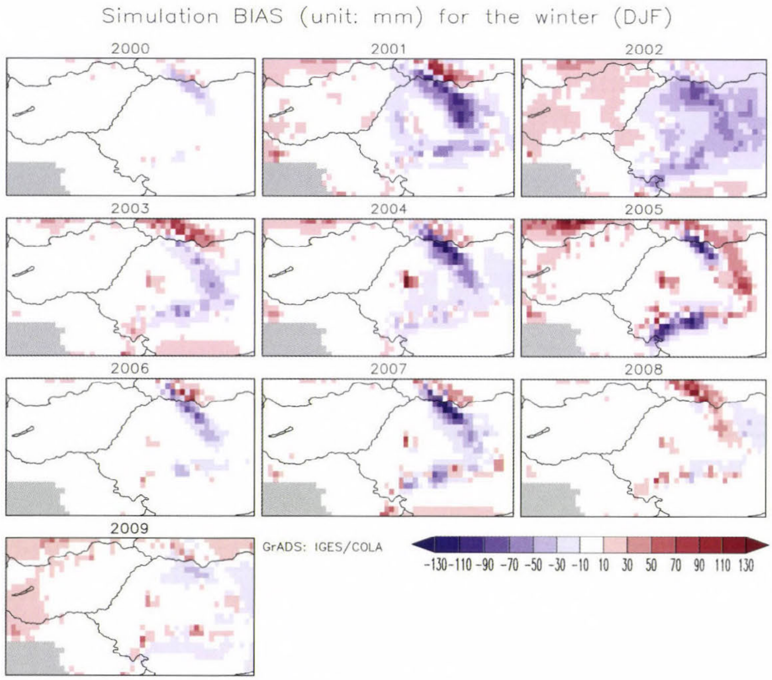

Fig. 9. Same as in *Fig. 7*, but for the modcon 'NB'.

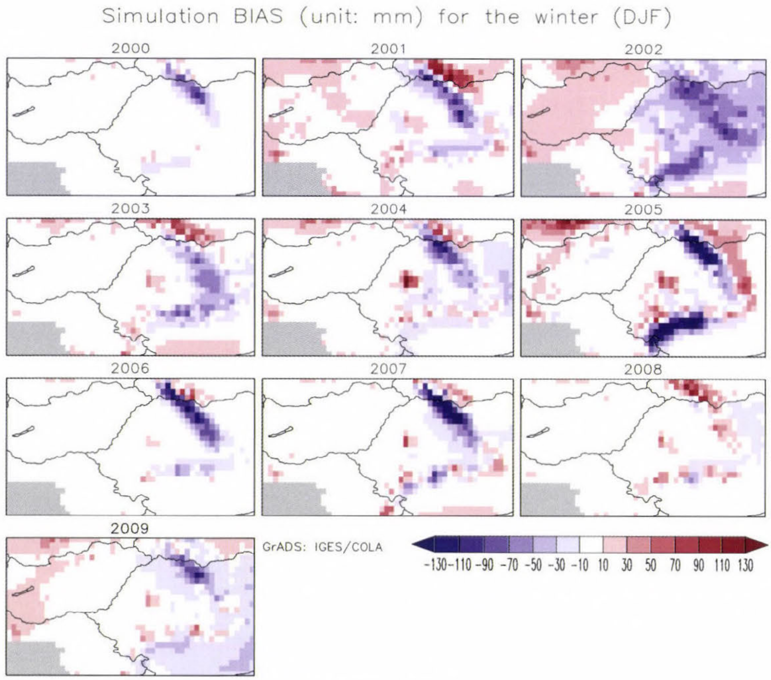

Fig. 10. Same as in *Fig. 7*, but for the modcon 'NC'.

The BIAS is formulated as:

$$BIAS = \frac{1}{N} \cdot \sum_{i=1}^{N} (O_i - M_i), \tag{1}$$

where O_i are the observed, in this case the CARPATCLIM values, M_i are the modeled ones and N is the number of pairs (comparisons).

Hence the spatial variability of the BIAS is significant, it is important to provide also the root mean square error (RMSE) averaged over the domain index, presented in *Table 1*. Using the notation of Eq. (1), the RMSE is equal to:

$$RMSE = \sqrt{\frac{1}{N} \sum_{i=1}^{N} (O_i - M_i)^2} \,. \tag{2}$$

This index can serve for the first (and rough) judgment of the spatially integrated criterion of the model performance. It is not latitudinal weighted, but, due to the relatively small extent of the domain along the meridian, this effect can be neglected.

Table 1. Values of the root mean square error (unit: mm)

Modcon	**EB**				**EC**				**NB**				**NC**			
Winter	**D**	**J**	**F**	**DJF**	**D**	**J**	**F**	**DJF**	**D**	**J**	**F**	**DJF**	**D**	**J**	**F**	**DJF**
2000	2.1	6.3	13.1	6.6	3.3	12.9	25.1	13.1	2.0	5.7	12.2	6.0	2.2	9.5	21.0	10.2
2001	30.0	46.1	45.9	35.9	28.3	41.3	44.1	31.9	15.0	28.8	35.3	22.8	16.2	31.8	31.8	22.4
2002	9.2	31.8	50.4	28.8	12.2	42.1	69.8	38.9	6.5	27.2	44.3	24.3	9.1	34.1	60.2	32.1
2003	5.9	23.7	36.7	20.6	6.3	31.4	52.7	28.0	5.3	18.0	27.2	15.7	5.5	20.4	33.4	18.2
2004	11.0	22.0	35.8	20.9	11.0	22.2	44.6	22.6	10.8	21.7	32.9	20.0	11.0	20.4	37.5	20.2
2005	11.9	26.3	32.9	22.1	20.3	50.7	63.6	42.9	15.0	31.3	33.9	25.8	20.0	43.7	48.8	36.4
2006	3.2	9.0	22.3	10.2	4.8	17.0	45.2	20.4	3.5	11.8	23.0	11.1	5.0	18.2	38.7	18.6
2007	14.5	21.9	22.9	19.1	21.1	31.1	38.1	29.1	13.1	22.0	23.6	18.7	16.3	26.1	33.1	24.1
2008	8.7	13.7	18.6	12.0	9.6	15.5	22.1	13.9	10.6	15.3	19.1	13.4	10.5	15.8	19.8	13.4
2009	6.5	14.9	27.6	14.3	7.7	25.2	58.3	27.8	4.8	14.4	23.4	12.0	5.1	17.5	42.4	18.5
average	**10.3**	**21.6**	**30.6**	**19.1**	**12.5**	**28.9**	**46.4**	**26.9**	**8.7**	**19.6**	**27.5**	**17.0**	**10.1**	**23.8**	**36.7**	**21.4**

4. Summary and conclusions

The interpretation of the results can be specified in many directions, but the most important and obvious conclusions are listed as follows:

- Over the bigger, mostly flat part of the domain, the modeled values of the *SWE* are relatively close to the analysis. The BIAS here shows high spatial and temporal (i.e., from month-to-month and from season-to-season) variability, but generally the BIAS remains in the interval of (–10)–10 mm.

- The most significant discrepancies, mainly in direction overestimation (negative BIAS), are detected clearly over the Carpathian ridge, especially over the northern half.

- For all modcons the absolute value of the BIAS for February is greater than for the winter average, suggesting overall proportionality of the BIAS and the *SWE* values.

- The presented figures and *Table 1* do not outline any model configuration which output is clearly better/worse than the others.

Despite the high variability of the BIAS, even in adjacent gridcells, the detected negative BIAS for all modcons over the Carpathian ridge, especially over its northern part, seems systematic, and this is the main issue of this work. The comparison of the model results with the Globsnow product (*Chervenkov et al.,* 2016) shows significant dispersion of the BIAS, but also with prevailing negative values. Being the "final outcome" of complex atmospheric processes and interactions with the land surface, the snow cover can be influenced in many pathways along the simulation chain. Thus, for example, the relatively poor model performance in 2003 and 2010 can be rooted in the inadequate description of the large scale precipitation over the domain. Finally, the fact that the CARPATCLIM snow products are not pure observations suggests its possible deviation from the "truth state".

The model RegCM is constantly developed and, respectively, its simulation capabilities are steadily increasing. Further numerical experiments have to be performed, in particular including other parameterization schemes. The study confirms, however, that horizontal resolutions over 10 km are highly insufficient for regional snow cover modeling, especially over topographic heterogeneous terrain as the larger Carpathian Region. This fact have to be regarded by selecting the simulation tool and the model configuration. This is very important due to the fact that the mountainous snow covers are, generally speaking, those with the longest duration and thickness, with its all hydrological, ecological, and socio-economical consequences.

Acknowledgments: Deep gratitude to the organizations and institutes (ICTP, CARPATCLIM, ECMWF, NCEP-NCAR, Unidata, MPI-M, and all others), which provides free of charge software and data. Without their innovative data services and tools, this study would be not possible.

References

Arakawa, A. and *Schubert, W.H.*, 1974: Interaction of a cumulus cloud ensemble with the large-scale environment, Part I. *J. Atmos. Sci. 31*, 674–701.

Barnett, T.P., Dumenil, L., Schlese, U., Roechner, E. and *Latif., M.,* 1989: The effect of Eurasian snow cover on regional and global climate variations, *J. Atmos. Sci. 46,* 661–685.

CDO, 2015: Climate Data Operators. Available at: http://www.mpimet.mpg.de/cdo

Chervenkov, H., Todorov, T., and *Slavov, K.,* 2015: Snow Cover Assessment with Regional Climate Model - Problems and Results., Lecture Notes in Computer Science vol. 9374, (Eds. *Lirkov et al.*) Large-Scale Scientific Computing: 10th International Conference, LSSC 2015, Sozopol, Bulgaria, June 8-12, 2015. Springer, 327–334.

Chervenkov, H. and *Slavov, K.*, 2016 Simulated versus Satellite Retrieval Distribution Patterns of the Snow Water Equivalent over Southeast Europe, *Int J Environ. Agricult. Res. 2*, 115–122.

Clifford, D., 2010: Global estimates of snow water equivalent from passive microwave instruments: history, challenges and future developments. *Int. J. Remote Sens. 31*, 3707–3726.

Dee, D.P., Uppala, S.M., Simmons, A.J., Berrisford, P., Poli, P., and *Kobayashi, S.,* 2011: The ERA-Interim reanalysis: Configuration and performance of the data assimilation system. *Q. J. Roy Meteorol. Soc. 137*, 553–597.

Dickinson, R., Henderson-Sellers, A., and *Kennedy, P.J.,* 1993: Biosphere-Atmosphere Transfer Scheme, BATS: version1E as coupled to the NCAR community climate model. NCAR Tech Note, NCAR/TN-387+STR. National Center for Atmospheric Research, Boulder, CO

Gong, G., Entekhabi, D., and *Cohen, J.,* 2003: Modeled Northern Hemisphere winter climate response to realistic Siberian snow anomalies, *J. Clim. 16*, 3917–3931.

Grell, G.A., 1993: Prognostic evaluation of assumptions used by cumulus parametrizations. *Mon. Weather Rev. 121*, 764–787.

Grell, G.A., Dudhia, J, and *Stauer, D.R.,* 1994: A description of the fifth-generation Penn State/NCAR mesoscale model (mm5)., Tech Rep NCAR/TN-398+ STR, National Center for Atmospheric Research, Boulder, CO

Hancock, St., Baxter, R., Evans, J., and *Huntley B.*, 2013: Evaluating global snow water equivalent products for testing land surface models, *Remote Sens. Environ. 128*, 107–117.

JRC, 2010: Climate of the Carpathian Region. Technical Specifications (Contract Notice OJEU 2010 /S 110-166082 dated 9 June 2010)

Kanamitsu, M., Ebisuzaki, W., Woollen, J., Yang, S.K., Hnilo, J.J., Fiorino, M., and *Potter, G.L.,* 2002: NCEP-DOE AMIP- II reanalysis (R-2). *B. Am. Meteorol. Soc. 83*, 1631–1643.

Kiehl, J.T., Hack, J.J., Bonan, G.B., Boville, B.A., Breigleb, B.P., Williamson, D., Rasch, P., 1996: Description of the NCAR community climate model (ccm3). Tech Rep, NCAR/TN-420+ STR. National Center for Atmospheric Research, Boulder, CO.

Liston, G.E., 2004: Representing subgrid snow cover heterogeneities in regional and global models. *J. Clim., 17,* 1381–1397.

Oleson, K.W., Dai, Y., Bonan, G., and *Bosilovich, M.,* 2004: Technical description of the Community Land Model. National Center for Atmospheric Research Tech Note NCAR/TN-461+ STR, NCAR, Boulder CO.

Oleson, K.W., Niu, G.Y., Yang, Z.L., and *Lawrence, D.M.*, 2008: Improvements to the Community Land Model and their impact on the hydrologic cycle. *J. Geophys. Res. 113*, G0102.

Pal, J.S., Small, E.E., and *Eltahir, E.A.B.*, 2000: Simulation of regional-scale water and energy budgets: representation of subgrid cloud and precipitation processes within RegCM. *J Geophys Res, 105,* 29579–29594.

Szentimrey, T., 2011: Manual of homogenization software MASHv3.03, Hungarian Meteorological Service.

Szentimrey, T. and *Bihari, Z.*, 2007: Mathematical background of the spatial interpolation methods and the software MISH (Meteorological Interpolation based on Surface Homogenized Data Basis). Proceedings from the Conference on Spatial Interpolation in Climatology and Meteorology, Budapest, Hungary, 2004, COST Action 719, COST Office, 17 –27.

Yang, F., Kumar, A., Wang, W., Juang, H.-M. H., and *Kanamitsu, M.,* 2001: Snow-albedo feedback and seasonal climate variability over North America. *J. Climate 14,* 4245–4248.

Xue, Y., Janjic, Z., Dudhia, J., Vasic, R., and *De Sales, F.,* 2014: A review on regional dynamical downscaling in intraseasonal to seasonal simulation/prediction and major factors that affect downscaling ability, *Atmos. Res. 147–148*, 68–85.

IDŐJÁRÁS

Quarterly Journal of the Hungarian Meteorological Service
Vol. 120, No. 3, July – September, 2016, pp. 331–351

Climate-based seasonality model of temperate malaria based on the epidemiological data of 1927–1934, Hungary

Attila Trájer[1,2]* and **Tamás Hammer**[1]

[1]*University of Pannonia, Department of Limnology, Egyetem út 10, H-8200, Veszprém, Hungary*

[2]*MTA-PE Limnoecology Research Group, Egyetem út 10, H-8200, Veszprém, Hungary*

**Corresponding author* E-mail: *atrajer@gmail.com*

(Manuscript received in final form October 4, 2015)

Abstract—The potential resurgence of malaria in the temperate areas of Europe due to climate change is an actual topic of epidemiology. Although several ecological forecasting models were built for the prediction of the potential re-emergence of malaria in the recently non-endemic areas of the world, the simulations are mainly based on the recent climatic thresholds of the tropical and subtropical vectors and *Plasmodium* parasites, mainly of *Plasmodium falciparum*. We aimed to reanalyze the primarily *Plasmodium vivax* caused autochthon malaria disease data of the past model period of 1927-1934 in Hungary to gain reliable knowledge about the climatic thresholds and the determinants of the malaria season for a temperate climate in a Central European country. Multivariable and simple linear correlation and regression was performed to analyze the malaria data of 96 months dividing the season a first and a second half parts of the year. Two models were built on the gained correlations using unstandardized and standardized correlation weights. It was found, that both in the first and second halves of the year, the ambient mean temperature was the most important predictor of the relative malaria incidence, while precipitation influenced the first half of the season. Summer sum of precipitation above 200 mm was found as one of the most important determinant of the absolute annual case number of benign tertian malaria. The unstandardized weights-based modeled malaria seasons returned well the observed autochthon malaria seasons.

Key-words: *Plasmodium vivax*, malaria, temperate climate, seasonality, archive data

1. Introduction

Malaria is one of the most important vector-borne diseases in the world affecting at least 3.2 billion people (*World Malaria Report*, 2005) and causing about 700.000 to 2.7 million people deaths per a year (*Patz* and *Olson*, 2006). The disease is caused by different *Plasmodium* species and transmitted by several *Anopheles* mosquitos. About 40% of the mankind live in malaria endemic areas (*Mendis et al.*, 2001). Once in the wide areas of Europe malaria was endemic, however, due to the active eradication programs of the 20th century, malaria became a non-endemic or rare disease in the old continent. Malaria was highly endemic also in Hungary, in the hearth of Central Europe, even to the mid-20th century, when the results of a combination of several actions, malaria became eradicated in the country. For example, in the 1920's, malaria caused six to eight thousand newly acquired cases per year in the continuous regions of the north-east and south-west parts of Hungary (*Lőrincz*, 1981–82). In the territory of the Kingdom of Hungary, the Ministry of the Interior adopted decree against malaria in 1901, but the malaria data was regularly collected from 1927 (*Szénási et al.*, 2003). The year of 1930 was a milestone in the history of the malaria in Hungary indicating the start of the active intervention, although the more intensive epidemiological interventions due to the start of the establishment of the observation stations in the endemic areas started only in 1937 (*Szénási et al.*, 2003). The intent public health efforts, the elimination of the wetland areas and the introduction of DDT led to the eradication of the malaria to 1956 in Hungary, although officially the WHO delivered Hungary to a malaria-free country in 1963.

In contrast to the recent epidemiological situation, the climate models predict the resurgence and worldwide increasing risk of malaria transmission due to the anthropogenic climate change (*Martens et al.*, 1999). It was found that small increases in temperature at low temperatures can increase the risk of malaria transmission substantially (*Lindsay* and *Birley*, 1996), although the potential effect of the changing climatic patterns are strongly influenced by socioeconomic developments and malaria control programs (*Martens et al.*, 1995). For example, in the East African highlands, the warming trend from 1950 to 2002 caused the parallel increases in malaria incidence, too. The rapid response of malaria to the changing temperatures patterns is understandable according to the fact that *Anopheles* mosquitos are highly sensible for the meteorological conditions, particularly to the air temperature. Temperature determines the time of the ontogeny and the questing activity of female mosquitos (*MacDonald*, 1957; *Jetten* and *Takken*, 1994). In addition, the highly complex ontogeny of *Plasmodium* parasites is also the function of the ambient temperature. For example, it is known that the lower temperature threshold of the ontogeny of *Plasmodium vivax* and *Plasmodium falciparum* are 14.5–16 and 18 °C, respectively (*MacDonald*, 1957). Even *Hackett* and *Missiroli* (1935) showed that the pattern of malaria season is in correlation with the latitude of a malaria endemic area, since the latitude essentially determines the annual temperature conditions with other factors, e.g., as the distance from the oceans and the altitude conditions. Before the 20th century, the 15 °C July isotherm appointed the northeast occurrence of the endemic malaria cases (*Menne* and *Ebi*, 2006). Precipitation is also an important factor of the malaria cases determining, with the temperature conditions, the dominance of the *Anopheles* species in Europe (*Kuhn et al.*, 2002). In the Atlantic and continental climate zones of Europe, as the Central European region, *Anopheles atroparvus* van Thiel, in Eastern Europe *Anopheles messeae* Falleroni, and in the Balkan Peninsula *Anopheles superpictus* Grassi are the main potential vectors of the human pathogen *Plasmodium* species. Recently, seven *Anopheles* species are known from Hungary, although the presence of *Anopheles sacharovi* Favre is also possible in the southern border areas (*Tóth* and *Kenyeres*, 2012). The malaria pathogen transmission potential of the different *Anopheles* species are different, the members of the so-called Maculipennis complex (named after the *Anopheles maculipennis* Meigen malaria mosquito) are known to be the most important vector species. In Hungary, *Anopheles atroparvus, Anopheles maculipennis,* and *Anopheles messeae* are the plausible potential vectors of the *Plasmodium* parasites according to the historical data (*Szénási et al.*, 2003). It is also known that before the eradication of the malaria in Hungary, *Plasmodium vivax* caused the 90% and *Plasmodium falciparum* the 10% of the malaria cases.

The resurgence of malaria in Europe is more than a fiction: *Plasmodium*-infected people introduced tropical malaria during the 1997 heat-wave in Germany (*Krüger et al.*, 2001) and Italy (*Baldari et al.,* 1998), when local female *Anopheles* mosquitos bite infected passengers returning from endemic areas. The reverse case is also known, when introduced, infected malaria vectors caused malaria infection in the airport staff or the people living in the neighborhood of the airport (*Giacomini et al.*, 1997). However, the well-developed simulations provide information of the vector potential of the *Anopheles* species in the near future; there are no well-based evidences about the potential seasonality of malaria in the continental areas as the Carpathian Basin. In turn, seasonality and the determinants of the annual run of the disease season can be more important factors of the possibility of reemergence of malaria than the simple presence of the malaria vectors. Since either the tropical vectors or the parasites are not or only partly equivalent to their continental counterparts, the model results require further validation. According to the above described causes, only the historical data of an area in a temperate region can provide a reliable basis and model for the potential near future seasonality of malaria in the temperate regions, even the climate is changing. In contrast to the northern regions of Europe, where malaria spontaneously disappeared in the early 20th century (*Bruce-Chwatt* and *de*

Zulueta, 1980), in Hungary the malaria eradication was the consequence of the joint effort of public health services. Although, autochthon malaria cases were observed in Hungary from the medieval ages to the 1950's, the analyzable period is limited to the start of the regular data collecting activity and the start of the more active public health interventions in the second part of the 1930's.

Our aim was to analyze the autochthon malaria case data of Hungary after the start of the data collection, but before the pre-intervention era in the period of 1927 to 1934. While the threshold of the tropical vectors and parasites is well-known, the threshold of the extinct European strains is still debate (*Menne* and *Ebi*, 2006). We also aimed to gain information about the former seasonality patterns, the effect of the temperature and precipitation on the autochthon malaria cases and to build a phonological malaria seasonality model based on the results. In addition, the re-modeling of the adult female malaria mosquito season was performed for the studied period.

2. Methodology

2.1. Statistics and software

The multivariable and the simple linear correlation and regression were performed by the simple and multiple regression tool of VassarStats on-line statistical program (*Lowry*, 2004). Microsof Office 2010 Excel was used in the visualization of the graphs. ArcGis 10.0 software was used in the performance of the spatial data.

2.2. Climate data

Since the climatic and topographical conditions are very homogenous in the country, Hungary was considered in climatic sense as a homogenous unit. The daily mean temperature data were derived from the European Climate Assessment Dataset (*Haylock et al.*, 2008).

2.2.1. Temperature and precipitation data for the period 1927–1934

We gained the monthly mean temperature and the monthly sum of precipitation data from the dataset of CRU TS3.22 (land) model for 1901–2013. Average values were calculated from the 0.5° grid within the domain including almost the entire Hungary. The latitudinal range was 45.50°N–48.50°N, while the longitudinal was 16.00°E–23.00°E. The monthly mean temperature and the monthly sum of precipitation values were derived from the period of January 1927–December 1934.

2.2.2. Temperature and precipitation data for the period 1970-1999

We gained the mean daily temperature data from the dataset of E-OBS model (1950-now). Average values were calculated from the 0.5° grid within the domain including almost the entire Hungary (*Fig. 1*). The latitudinal range was 45.50°N-48.50°N, while the longitudinal was 16.00°E–23.00°E. The monthly mean temperature values were derived from the period of January 1970–December 1999. The daily data was converted into monthly mean temperature values.

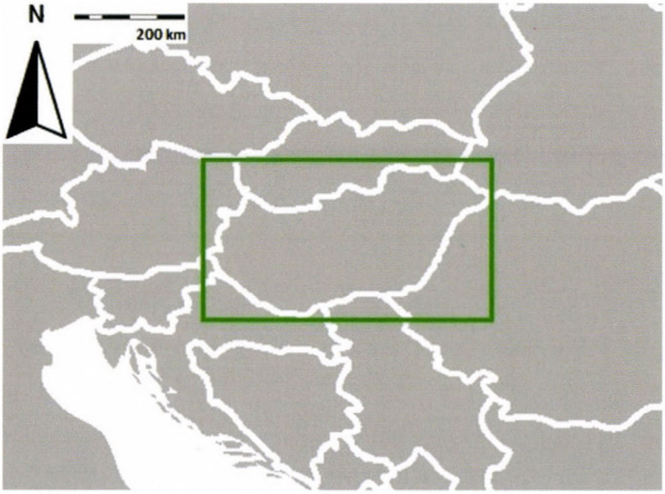

Fig. 1. The domain of Hungary in Central Europe.

2.3. Malaria data

2.3.1. Monthly autochthon malaria data of 1927-1934 in Hungary

The monthly malaria case number of 1927–1934 was based on the article of Zoltán Alföldy (*Alföldy,* 1935). The results of this study are shown in *Fig. 2 left.* Due to the lack of the written data, after the digitalization of the figure, the monthly case numbers were read directly from the figure using a precise covering grid. Although, malaria became a mandatory reportable disease in 1930 in Hungary, the regular collection of the disease started in the autumn of 1926. Since the data of 1926 is incomplete, in the latter analysis we neglected this data. Despite the fact that the studied eight years may seems at first inspect to be a short period, the absolute malaria case number showed a notable fluctuation. While the lowest malaria case number was observed in 1930 with less than 150 cases per year, the highest malaria case number exceeded the 1900 case per year value in 1934. Summer cases formed the most notable part of the annual malaria incidence with a synclinal pattern during the studied period (*Fig. 2 right*).

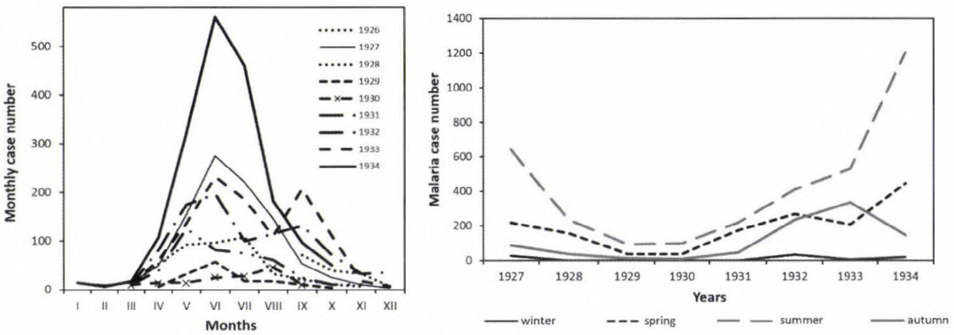

Fig. 2. Left: the autochthon monthly malaria cases in Hungary, in the autumn of 1926 and 1927–1934, *right*: changes of the number of the seasonal autochthon malaria cases in 1927–1934, Hungary.

2.3.2. Spatial data of the malaria cases of 1936 and its georeferencing

To show the former spatial occurrence of malaria in Hungary, the year of 1936 was selected as a characteristic example of the 1930's. In this year the malaria morbidity was 20.8 per 100.000. The spatial distribution data of the malaria cases of 1936 was based on the publication of *Szénási et al.* (2003) (*Fig. 3, Malaria morbidity in Hungary in 1936*). The original spatial data was displayed in the former "járás" (*processus*, the lowest-level administrative unit) system, which corresponds roughly to the present day NUTS4 district areas. We used the site appointing function of Google Earth imagery to mark the central points of the former NUTS4 areas. Each marked points were named after its case number interval. Six intervals of annual case number were used according to the original: the 1 to 5, 6 to 14, 15 to 29, 30 to 59, 60 to 149, and 150 to 284. We converted the designated spatial data into keyhole markup language (*kml*) file format (altitude or gamma intensity data). After opening the *kml* data, we converted them into shape file format in the ArcGIS 10.1 software. To create color images, we linked the points with the mean of the annual case number intervals. The different values were assigned to the referred points and were sorted into attribute table. We interpolated the values of the spatial data by the IDW interpolation function of the spatial analyst tool in the ArcGIS. The aquatic habitats illustrating cut off the second military surveying of the Habsburg Empire were derived from the Mapire homepage (*Mapire,* 2015), which is a digitized and georeferenced raster mosaic of the original individual sheets (*Molnár* and *Timár,* 2009).

2.4. Mosquito data

The relative abundance, *RA* (in %), value of the female imago individuals of *Anopheles messeae*, a member of the *Anopheles maculipennis* complex was gained from the three decades (1970's, 1980's, and 1990's) covering countrywide mosquito collecting data of *Tóth* (2004). We assorted the number of collected female mosquitos according to the months of the year and used the summarized monthly female mosquitos in the model. The number of the collected number of the mosquitos was termed as a relative abundance (*RA*). Since the monthly value of *RA* depends on the number of monthly trapping occasions, we used the quotient of *RA* and the number of the trapping occasions (termed as the normalized relative abundance value, *NRA*):

$$NRA = \frac{RA_i}{N_t}, \tag{1}$$

where *NRA* is the normalized relative abundance, RA_i is the the normalized relative abundance of the *i*th month of the year, and $N_t$is the the number of trapping occasions in the ith month of the year.

Since this number is based on the summarized amount of collected mosquitos, this data was utilized to build only a relative model predicting the seasonal run of the malaria mosquito season.

2.5. Modeling approaches

To analyze the phenology of the malaria season, two different approaches were used: a climate-based model and a vector (*Anopheles messeae*)-based model. In the first approach, we also used the temperature and precipitation data to predict, at first, the annual relative incidence (*RI*, in %) and after the percentage of the malaria case number according to the whole period's case number (*R*). Since, in contrast to the past malaria data, we used the 30 years summarized monthly number of the mosquitos, in the vector-based model only the temperature and the annual normalized relative abundance of the potential vectors (*NRA*, in %) were used. Both *NRA* and *RI* values mean the percentage of the monthly cases or number according to the annuals'. The *R* value was calculated according to the incidence values of the period of 1927–1934.

2.5.1. The first approach

The model was built to analyze the determinant climatic factors of the former run of the annual malaria case curve in Hungary and to reconstruct the curve in the studied period. At first, we calculated the relative case number values form the monthly cases, as in the period of 1927 to 1934. The case number of malaria showed the above described high variance, and the relative case number (relative malaria incidence, RI_m) values were used instead of absolute incidence or case number values as the basis of the model. The model was constructed to calculate the RI_m values of a certain month based on the monthly mean temperature (T_m) and the monthly sum of precipitation (P_m). Since RI_m may be related to the abundance of the actual questing, hungry active female *Anopheles* population, we hypothesized that malaria can positively correlate with the outdoor temperature and the precipitation. Our approach was that the annual RI is the amount of the monthly values of the temperature and precipitation dependent abundance related relative monthly malaria case numbers in the first (RI_{m1}; from the 1st to the 6th months) and second part of the year (RI_{m2}; from the 7th to the 12th months). Although the correlation between the relative monthly malaria incidence and the sum of the monthly precipitation values was negligible in case of the second part of the season, keeping the consistency of the model, precipitation was involved. RI is the product of the following equation:

$$RI = \sum_{i=1}^{6} RI_{m1} + \sum_{i=7}^{12} RI_{m2}, \tag{2}$$

where RI is the relative annual malaria incidence ,RI_{m1} is the relative malaria incidence (%) of the months of first half part of the year, and RI_{m2} is the relative malaria incidence (%) of the months of second half part of the year.

The monthly relative malaria incidence was described as a multivariable linear regression function of the T_m and P_m according to the gained coefficients of the multiple linear regression analyses in Eq.(3):

$$RI_m = a + \beta_1 T_m + \beta_2 P_m, \tag{3}$$

where RI_m is the relative monthly malaria incidence, a is a constant, $_{1,2}$ are correlation weights, T_m is the mean monthly temperature, and P_m is the sum of the monthly precipitation (mm).

Since the multiple linear regression analyses gave unstandardized and standardized coefficients, two groups of the models were built according to the used coefficients. $Model_a$ was built on the unstandardized, $Model_b$ on the standardized coefficients.

At the second step, we aimed to converse the output (the RI) of the relative annual model into the relative (R) values of the whole period. The conversation of the case numbers into incidence values was not considered to be necessary due to the relatively short period. Since the summer cases formed the more than 50% of the cases, the correlation between the summer precipitation and the summer malaria case number was analyzed. It was hypothesized that the ratio of the modeled summer case number according to the mean can be used as the multiplier of the annual case number:

$$R = RI_m \frac{N_{modeled\,summer\,malaria}}{N_{mean\,summer\,malaria}}. \tag{4}$$

2.5.2. The second approach

We used a simple linear model to gain correlation between the *NRA* values of the two *Anopheles* species and the mean monthly temperature of the period 1970–1999. Since the domain of the two sources of the temperature data was the same, we calculated the *NRA* values of the malaria mosquitos for the months of the period of 1927–1934. Finally, we compared the *RI* and *NRA* values for the studied period.

3. Results

3.1. The spatial occurrence of malaria in the 1930's

The historical malaria case data of 1936 shows that the former autochthon malaria cases in Hungary had three main focuses, the Upper Tisza region the northeast (*Fig. 3.*1), the river Drava in the southwest (*Fig. 3.*2a), and the south area of Zala hills, adjacent to the Drava valley (*Fig. 3.*2b). The endemic malaria focus in the Upper Tisza valley was partly related to the great Ecsed marsh. The central and northern parts of Hungary were malaria-free areas in 1936. The elevation of the Upper Tisza region focus is 101–118 m above sea level, in case of the southwestern former malaria focuses the topography is very heterogenic, the mean elevation is about 85–170 m, respectively (*Fig. 3,* upper map).The lower maps of *Fig. 3* show the most influenced autochthon malaria regions in 1936 according to the second military survey of the Habsburg Empire. Although the survey itself was carried out in the period from 1853 to 1873, the coverage with wetlands, oxbows, and marches did not differ notably from the conditions of the 1920's and 1930's. In the southern part of the Upper Tisza valley, the marshes formed the dominant potential aquatic habitats of *Anopheles* species, while in the northern part of the Upper Tisza and the Drava valley, these habitats were the oxbows and flood puddles.

3.2. The phenology of the autochthon malaria seasons from 1927 to 1934 in Hungary

The incidence of the autochthon malaria cases was the following: 1.17 (1927), 0.53 (1928), 0.25 (1929), 0.16 (1930), 0.53 (1931), 1.11 (1932), 1.33 (1933), and 2.29 (1934) per 10,000 inhabitants calculating with the population of Hungary according to the census of 1930 (8685109 inhabitants), respectively. The mean of the incidence values was 0.92, the variance was 0.4675, and the standard deviation was 0.7053 per 10,000 inhabitants. In the studied period, the malaria season in 6 cases had unimodal patterns (in 1927, 1928, 1929, 1930, 1931, and 1934), in 2 cases the season had bimodal feature (in 1932 and 1933). The maximum monthly case numbers were observed in May in 1 case (1931), in June in 5 cases (1927, 1928, 1929, 1930, and 1934), in August in 2 cases (1932 and 1933). In case of 1932, and 1933, a second seasonal peak was observed in September (*Fig. 4*).

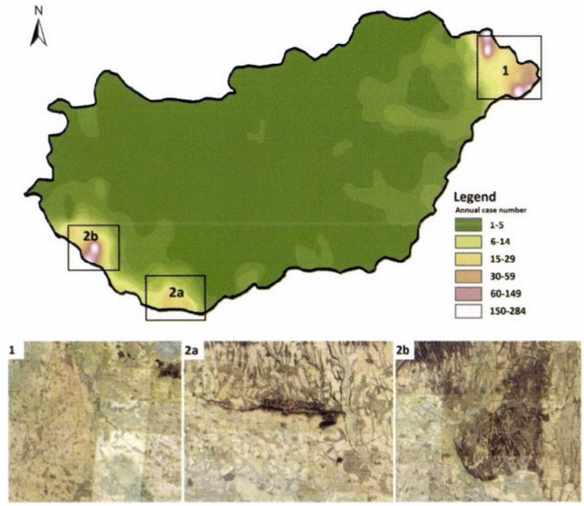

Fig. 3. Spatial distribution of the malaria cases in 1936. 1: Szatmár-Bereg plain, 2a: Drava Plain, and 2b: south Zala hills (upper map) are the most influenced autochthon malaria regions in the 1930's in the maps of the second military survey of the Habsburg Empire. Blue colors refer to the wetlands and rivers of the areas. **1**: the upper Tisza, **2a**: the Drava, and **2b**: the south area of Zala hills, adjacent to the Drava valley (lower maps).

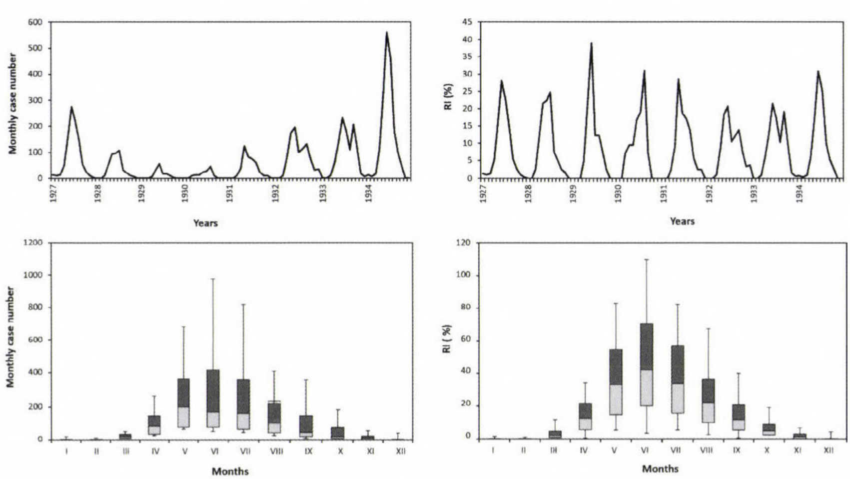

Fig. 4. Upper left: absolute monthly autochton malaria case numbers. *Left*: box and whiskers plots of the monthly case numbers of the years. *Upper right*: relative malaria incidence values. *Lower right*: box and whiskers plots of the annual proportion of the monthly case numbers of the years of 1927–1934 in Hungary.

The season started in March in general, although in 1929 and 1930, the malaria season started in April and May. The summer proportion of the cases according to the annual total case number were the following in the studied years: 1927: 65.69%, 1928: 54.54%, 1929: 63.41%, 1930: 66.66%, 1931: 49.59%, 1932: 43.23%, 1933: 49.00%, 1934: 66.21%. In general, the 57.29% of the annual cases occurred during the summer months in 1927–1934. The seasonal run of the malaria seasons show that the season started when the portion of the monthly malaria case number reached about the 5% of the annual cases. According to this criterion, the malaria season started in April except the year 1930, when the season started in March. The monthly mean temperatures, of the starting months were the following: 9.6 (1927), 10.3 (1928), 6.1 (1929), 6.2 (1930), 7.5 (1931), 9.5 (1932), 7.2 (1933) and 13.0 °C (1934). In general the start of the season occurred at 8.7 °C monthly mean temperature (SD: 2.37 °C). Using the same criterion for the end, the season ended in September in 1927–31 and 1934 and in October in 1932-33. The monthly mean temperatures of the last months were the following: 16.6 (1927), 15.9 (1928), 15.6 (1929), 16.8 (1930), 12.0 (1931), 11.9 (1932), 10.4 (1933), and 16.7 °C (1934). In general the end of the season occurred in 14.5 °C monthly mean temperature (SD: 2.6 °C). The absolute minimum temperature threshold of malaria in the begining and the end and of the season was about 5 °C mean monthly temperature (*Fig. 5 left)*. The peak season month occurred at the following mean temperature and monthly sum of precipitation conditions: 19.0 °C –76.7 mm (1927), 22.3 °C –21.3 mm (1928), 17.2 °C –79.0 mm (1929), 18.8 °C –92.7 mm (1930), 17.5 °C –42.1 mm (1931), 17.0 °C –52.5 mm (1932), 15.6 °C –102.4 mm (1933), and 17.7 °C –116.6 mm (1934) with a mean of 18.1°C (SD: 2 °C) and 72.9 mm (SD: 32.2 mm; *Fig. 5 right*).

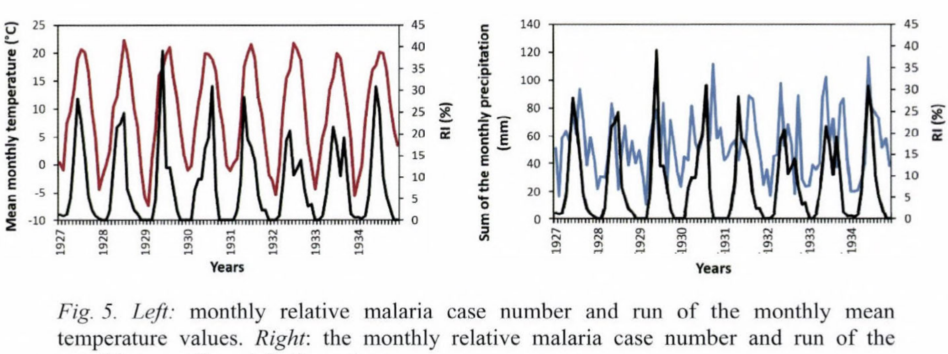

Fig. 5. Left: monthly relative malaria case number and run of the monthly mean temperature values. *Right*: the monthly relative malaria case number and run of the monthly sum of precipitation values.

3.3. Modeling approach 1

3.3.1. The first part of the year

Strong correlation was found between the *RI* and the mean monthly temperature values (r^2=0.75). We also found notable correlation (r^2=0.5) between the *RI* and the sum of the monthly precipitation in the first part of the year. The multiple r^2 of the regression was 0.78; the adjusted r^2 was 0.77 with a standard error of 4.7901. The value of the intercept is –2.5895. The correlation matrix and the gained regression coefficients can be seen in *Tables 1* and *2*.

Table 1. Correlation matrix of the results of the multiple regression in case of the months of the first half of the year; RI_{m1}: relative incidence of the months of first half in the year, T_m: mean monthly temperature, P_m: sum of the monthly precipitation

	T_m	P_m	RI_{m1}
T_m	1	0.656	0.866
P_m	0.656	1	0.71
RI_{m1}	0.866	0.71	1

Table 2. The gained regression coefficients; T_m: mean monthly temperature, P_m: sum of the monthly precipitation, *b*: unstandardized regression weights, *B*: standardized regression weights

	b	*B*	$B \times r_{TmPm}$
T_m	0.8904	0.7025	0.6081
P_m	0.1067	0.2487	0.1765

For the relative malaria incidence of the first six months of the year, RI_{m1}, the following equations can be written:

$$RI_{\mathrm{m1}} = -2.5895 + 0.8904T_m + 0.1067P_m, if\ T_{monthly}^{1927-1934} > 5\ °\mathrm{C} \quad (5.a)$$

$$RI_{\mathrm{m1}} = -2.5895 + 0.7025T_m + 0.2487P_m, if\ T_{monthly}^{1927-1934} > 5\ °\mathrm{C} \quad (5.b)$$

Eq. (5.a) is based on the unstandardized, while Eq. (5.b) is based on the standardized weights, where T_m is the mean monthly temperature and P_m is the sum of the monthly precipitation.

3.3.2. *The second part of the year*

Notable correlation was found between the *RI* and the mean monthly temperature values ($r^2 = 0.57$; *Fig.6 upper part*). In contrast, the correlation between the *RI* and the sum of the monthly precipitation was negligible in the second part of the season ($r^2 = 0.03$, *Fig. 6 lower part*). The multiple r^2 of the regression was 0.58; the adjusted r^2 was 0.56 with a standard error of 5.1746. The value of the intercept is 0.2607. The correlation matrix and the gained regression coefficients can be seen in *Tables 3* and *4*.

Table 3. Correlation matrix of the results of the multiple regression in case of the months of the second half of the year; RI_{m2}: relative incidence of the months of first half in the year, T_m: mean monthly temperature, P_m: sum of the monthly precipitation.

	T_m	P_m	RI_{m2}
T_m	1	0.313	0.758
P_m	0.313	1	0.168
RI_{m2}	0.758	0.168	1

Table 4. The gained regression coefficients; T_m: mean monthly temperature, P_m: sum of the monthly precipitation, *b*: unstandardized regression weights, *B*: standardized regression weights

	b	*B*	$B \times r_{TmPm}$
T_m	0.7727	0.7818	0.5924
P_m	–0.028	–0.0771	–0.0129

For the relative malaria incidence of the first six months of the year, RI_{m1}, the following equations can be written:

$$RI_{\mathrm{m1}} = 0.2607 + 0.7727T_m - 0.0280P_m, if\ T_{monthly}^{1927-1934} > 5\ °\mathrm{C} \quad (6.a)$$

$$RI_{\mathrm{m1}} = 0.2607 + 0.7818T_m - 0.0771P_m, if\ T_{monthly}^{1927-1934} > 5\ °\mathrm{C} \quad (6.b)$$

Eq. (6a) is based on the unstandardized, while Eq. (6b) is based on the standardized weights, where T_m is the mean monthly temperature and P_m is the sum of the monthly precipitation.

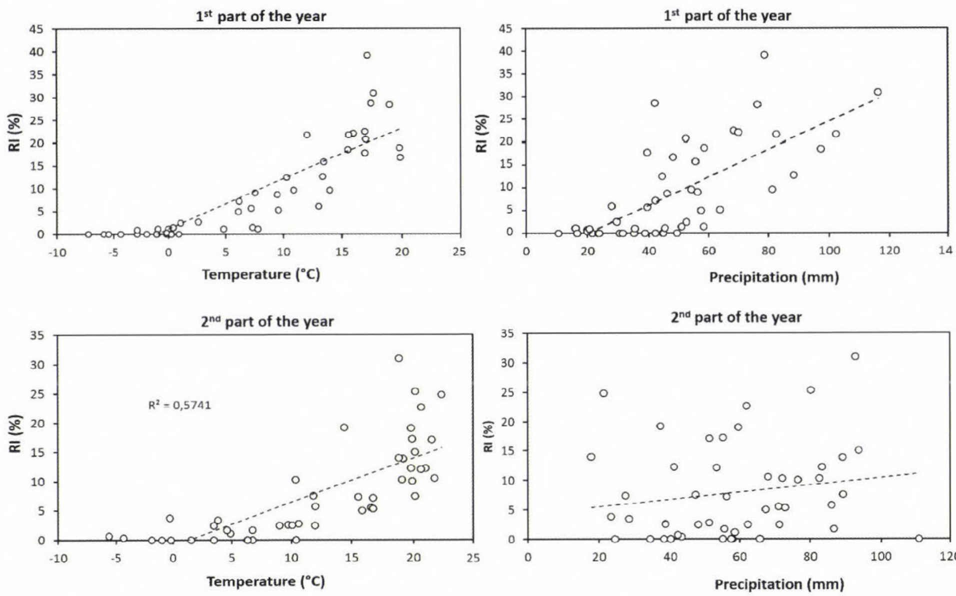

Fig. 6. Upper left: correlation between the monthly relative malaria case number and the run of the monthly mean temperature values in the first part of the year. *Upper right*: correlation between the monthly relative malaria case number and the run of the monthly sum of precipitation values. *Lower left*: correlation between the monthly relative malaria case number and the run of the monthly mean temperature values in the second part of the year. *Lower right*: correlation between the monthly relative malaria case number and the run of the monthly sum of precipitation values.

3.4. Modeled relative seasons

3.4.1. Correlation between the summer precipitation and the number of the summer malaria morbidity

Significant correlation was found between the sum of the summer precipitation and the summer malaria case number:

$$N_{malaria} = 23.437e^{0.0125\times P_{\Sigma ms}}, \qquad (7)$$

where r^2=0.58 and p=0.3557. Results of the Eq. (7) are drawn in *Fig. 7.*

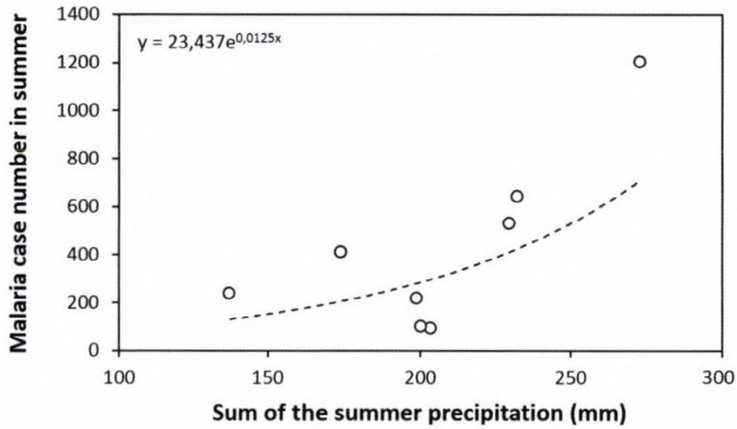

Fig.7. Correlation between the sum of the summer precipitation and the malaria case number in summer

Using unstandardized weights, the sum of the absolute errors is 3.7109, in case of standardized weights it is 4.3859 (*Fig.8 top*). The 12.5% of the malaria case numbers of the period of 1926–1934 occurred in a given year. The ratio of the real case number and the mean of the period were the following: 1927: 1.24, 1928: 0.38, 1929: 0.86, 1930: 0.83, 1931: 0.82, 1932: 0.60, 1933: 1.20, 1934: 2.06. The correlation of the relative malaria cases and the results of the model using unstandardized weights according to the linear and polynomial approximations are $r^2 = 0.6487$and $r^2 = 0.7247$, while in case of standardized weights these values are $r^2 = 0.311$ and $r^2 = 0.341$, respectively. The sum of the absolute errors in case of unstandardized weights was 70.78, in case of standardized weights 82.55, respectively. Although the model somewhat overestimate the relative case number of 1929 and 1930, it predicts the higher season peak values well in case of 1927, 1933, and 1934 (*Fig. 8* bottom).

3.5. The second modeling approach

3.5.1. The temperature dependent seasonality of Anopheles messeae in Hungary

The main part of the mosquito seasons of *Anopheles messeae* started in April and ended in October, however, a few numbers of individuals were collected also in March and November. The main parts (91%) of the female Anopheles maculipennis complex individuals were collected in months with more than 12 °C average temperature (*Fig. 9*).

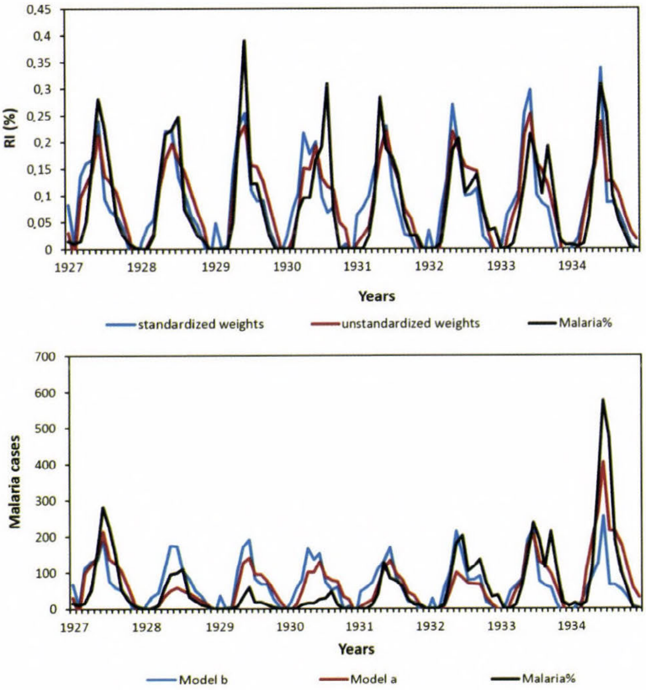

Fig. 8. Top: The observed and modeled relative autochthon malaria seasons according to the unstandardized and standardized weights. *Bottom*: the observed and modeled absolute autochthon malaria seasons according to the unstandardized and standardized weights.

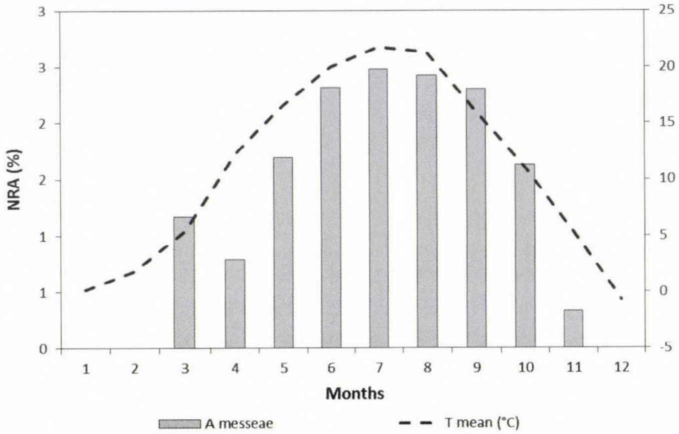

Fig. 9. Seasonality of *Anopheles messeae* and the monthly mean air temperature in the period of 1970–1999.

In case of the normalized relative annual numbers of *Anopheles messeae*, strong significant correlation were found with the monthly mean temperature ($r^2 = 0.89$, $p < 0.0001$). According to the correlation between the monthly mean temperature and the summarized relative (%) number of the collected female individuals of *Anopheles messeae* the following equation was gained:

$$NRA = 0.1147T_m + 0.0117, \qquad (8)$$

where NRA is the normalized relative abundance (%) and T_m is the monthly mean temperature (°C).

3.5.2. *The reconstructed Anopheles messeae seasonality in 1927–1934*

Eq. (7) was replayed for the monthly temperature values of 1927–1934 and it was depicted with the relative (%) number of the observed autochthon malaria cases (*Fig. 10*).

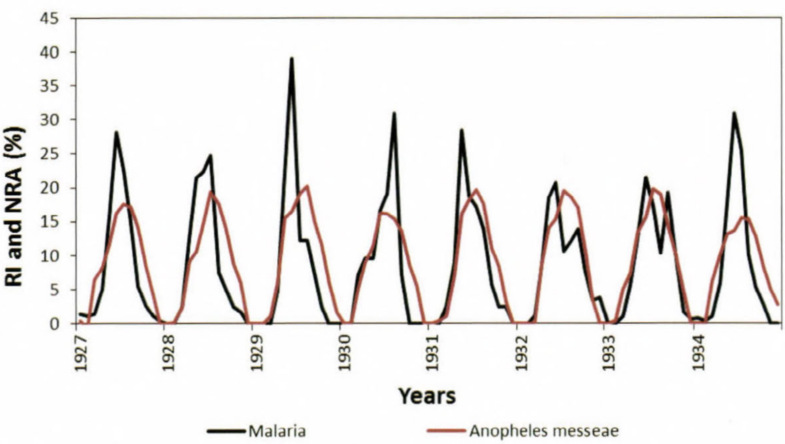

Fig. 10. The observed normalized relative malaria incidences and the modeled relative mean abundance values of *Anopheles messeae.*

4. Discussion

The reanalysis of the historical malaria data in the central part of Europecountry provides a unique feasibility to gain confident data about the former seasonality of the autochthon malaria in a temperate region of Europe. Historical maps show that the autochthon malaria cases occurred primarily in wetland areas or river basins and not at lakes as lake Balaton. The spatial occurrence of the cases was linked to two major aquatic habitats: marshes and the floodplain of the river valleys. It can be stated that the cases are accumulated in the water collecting area of medium-sized rivers as river Tisza, Drava, or river Körös. The salt lakes of the Danube-Tisza interfluve, the rivers and creeks of the Transdanubian mountain range were not affected by malaria in the studied period. It is plausible that areas with the extent presence of barely or not regulated river sections had the greatest risk for malaria endemicity. Although, the most notable focus in 1926–1934 were linked into south-western and north-eastern parts of Hungary, a major malaria endemic focus is plausible according to the historical records and the FY A Duffy blood group allele in the great plain of Hungary and the south parts of the Carpathian Basin. The recent presence of the local low FY A allele frequency in south Hungary, north Serbia, Vojvodina, and south western Romania (see *Howes et al.,* 2011) may refer to the former presence of a long-persistent malaria endemic area in the south-eastern part of the Carpathian Basin, since malaria resistance is linked to the Duffy-negative phenotype against *Plasmodium vivax* infection. In contrast, the recent distribution of sickle haemoglobin (HbS) allele frequency shows that *Plasmodium falciparum* caused malaria was endemic only in the South Balkan in the historical times (see *Piel et al.,* 2010) and it lacked from the Carpathian Basin which is consistent with the known sensibility of the parasite for cold conditions.

In the historical times, up to the middle of the 20th century, *Plasmodium vivax* was the predominant cause of malaria in the temperate parts of Europe, and *Plasmodium falciparum* persisted only in the Mediterranean coastal regions of the old continent (*de Zulueta,* 1994). The possibility of the overwintering of *Anopheles* mosquitos is not theoretical, since the lethal temperature for some members of the genus is below –15 °C (*Wallace* and *Grimstad,* 2002). It is plausible that relatively cold-resistant *Plasmodium vivax* was the main infectious agent of malaria in Hungary (*Szénási et al.*, 2003), which *Plasmodium* species outside of Africa recently accounts for more than 50% of all human malaria cases (*Mendis et al.*, 2001). *Plasmodium vivax* infection is a re-emerging malaria disease in the eastern part of the Mediterranean basin (*Andriopoulos et al.*, 2013). The occurrence of malaria is strictly limited by precipitation and temperature thresholds. For example, the temperature threshold of the digestion of blood meal in case of *Anopheles maculipennis* is 9.9°C, while the threshold temperature of the extrinsic incubation cycle of *Plasmodium vivax* is 14.5-15°C (*Martens et al.,* 1995).

The absolute minimum limits of the start and the end of the malaria season were about at the 5 °C mean monthly temperature values which are lower than the recent known, at least 14.5 °C ontogeny threshold of the *Plasmodium* species (*MacDonald,* 1957). It is in accordance with the gained, also about 5 °C minimum activity threshold of adult female *Anopheles messeae* individuals. These observations raise the possibility that the former malaria strains were much cold tolerant in the temperate regions of Europe – similarly to the vectors - than in case of the recent genetic lines of the tropical/subtropical regions.

In contrast to the recent tropical and subtropical examples, malaria in the temperate, continental climate of Hungary had mainly unimodal seasonality with a 3 to 4 months winter diapause. It is also notable that the also mosquito-transmitted, in Hungary recently endemic West Nile fever has a late summer - early autumn peak season with a very low and negligible case number in June (*Trájer et al.*, 2014). The clear difference of the seasonality of the two mosquito-borne diseases could be explained by the different reservoirs, which are birds in case of West Nile fever and humans in case of malaria. While active mosquitos can transmit malaria directly from human to human, West Nile fever epidemics can only break out after that the amount of the circulating virus reaches a given threshold prevalence level in the mosquito population. It should be added, that West Nile virus can overwinter in their mosquito vectors (*Nasci et al.*, 2001). It is somewhat surprising that while the mosquito population could increase during the summer season, the malaria incidence reached its annual peak already in early summer in most of the years. It is possible that infected mosquitos could overwinter in an increased number within the population, since *Plasmodium* infected mosquitos have increased longevity (*Vézilier et al.*, 2012).The observed June maximum in the majority of the years and the early and fast increase of the former malaria season support the hypothesis, that the infected overwintering female imago malaria mosquitos played a notable role in the transmission in the studied former autochthon malaria cases. Another possible interpretation of the former early outbreak and peak of malaria is the role of humans as reservoirs living in wetland areas, since the incubation period varies between 7 and 15 days in general, and the long incubation period can take several months (sometimes years) in case of *Plasmodium vivax* caused malaria without any effective treatment (*ECDC Epidemiological update,* 2013).

The found, 3 to 4 months winter diapause period of the potential vector mosquitos in the cold half of the year led the public health services to the successful intervention. *Szénási et al.* (2003) described that the infected people were re-treated in the spring of the next year, which practice was one of the most important cause of the eradication of malaria in Hungary.

Bismil'din et al. (2000) and *Kuhn et al.* (2003) concluded that there are strong link between the re-emergence of malaria and non-climatic factors. Climate change alone can be insufficient to trigger the reappearance of the autochthon malaria in an area. We found that precipitation is an important determinant factor of the relative incidence in the first half part of the year, and it influences significantly the summer incidence. This finding is in accordance with that rainfall has significant effect on the number of Anopheline vectors as e.g. *Anopheles gambiae* (*Koenraadt et al.*, 2004). We found that in the second half of the year, precipitation had no notable effect on the malaria incidence. Temperature played important role in the determination of the notable points (the start and the end) of the season although the absolute case number or the possible bimodality of the season was rather determined by the summer precipitation patterns. The effect of the summer precipitation sum above about 200 mm increased rapidly the summer, and consequently, the annual incidence of malaria. The gained similarity of the observed relative malaria and the modeled relative vector seasons confirms the former observations and hypotheses that the native members of Maculipennis complex, e.g., *Anopheles messeae* were the vectors of the malaria in Hungary. It can be concluded that our seasonality model can be well-adapted for the recent *Plasmodium vivax* malaria endemic areas of the world.

Acknowledgement: This study was supported by TÁMOP-4.2.2B-15/1/KONV-2015-0004.

References

Alföldy, Z., 1935: A malária járványgörbéjének évszakos változásáról 1934. *Népegészségügy 16*, 68–75. (In Hungarian)

Andriopoulos P., Economopoulou A., Spanakos, G., and *Assimakopoulos, G.*, 2013: A local outbreak of autochthonous Plasmodium vivax malaria in Laconia, Greece –a re-emerging infection in the southern borders of Europe? *Int. J. Infect. Dis. 17,* e125–e128.

Baldari, M., Tamburro, A., Sabatinelli, G., Romi, R., Severini, C., Cuccagna, G., Fiorilli, G., Allegri, M.P., Buriani, C. and *Toti, M.*, 1998: Malaria in Maremma, Italy. *The Lancet. 351,* 1246–1247.

Bismil'din, F.B., Shapieva, Z., and *Anpilova, E.N.*, 2000: Current malaria situation in the Republic of Kazakhstan. *Med Parazitol (Mosk). 2001*, 24–33.

Bruce-Chwatt, L.J. and *De Zulueta, J.*, 1980: The rise and fall of malaria in Europe: a historico-epidemiological study. Oxford: Oxford University Press, Walton Street.

De Zulueta, J., 1994: Malaria and ecosystems: from prehistory to posteradication. *Parassitologia. 36,* 7–15.

ECDC Epidemiological update: Local cases of malaria in Greece, September- October 2013 25 Nov. Website http://ecdc.europa.eu/en/press/news/_layouts/forms/News_DispForm.aspx? List=8db7286c-fe2d-476c-9133-18ff4cb1b568&ID=912.

Giacomini, T., Axler, O., Mouchet, J., Lebrin P., Carlioz R., Paugam, B., Brassier D., Donetti L., Giacomini, F., and *Vachon, F.* 1997: Pitfalls in the diagnosis of airport malaria. Seven cases observed in the Paris area in 1994. *Scand. J. Infect. Dis. 29*, 433–435.

Hackett, L.W. and *Missiroli, A.*, 1935: The varieties of Anopheles maculipennis and their relation to the distribution of malaria in Europe. *Riv. Malariol. 14*, 1.

Haylock, M.R., Hofstra, N., Klein, Tank, A.M.G., Klok, E.J., Jones, P.D. and *New, M.*, 2008: A European daily high-resolution gridded dataset of surface temperature and precipitation. *J. Geophys. Res (Atmospheres). 113(D20)*,119.

Howes, R.E., Patil, A.P., Piel, F.B., Nyangiri, O.A., Kabaria, C.W., Gething, P.W., Zimmermann, P.A., Barnadas, C., Beall, C.M., Gebremedhin, A., Ménard, D., Williams, T.N., Weatherall, D.J., and *Hay, S.I.*, 2011: The global distribution of the Duffy blood group. *Nat. Commun. 2*, 266.

Jetten, T.H. and *Takken, W., 1994:* Anophelism without malaria in Europe. A review of the ecology and distribution of the genus Anopheles in Europe. Landbouwuniversiteit Wageningen (Wageningen Agricultural University), Wageningen.

Koenraadt, C.J.M., Githeko, A.K., and Takken, W., 2004: The effects of rainfall and evapotranspiration on the temporal dynamics of Anopheles gambiae ss and Anopheles arabiensis in a Kenyan village. *Acta Trop. 90,* 141–153.
Krüger, A., Rech, A., Su, X.Z., and *Tannich, E.*, 2001: Two cases of autochthonous Plasmodium falciparum malaria in Germany with evidence for local transmission by indigenous Anopheles plumbeus. *Trop. Med. Int. Health. 6,* 983–985.
Kuhn, K.G., Campbell-Lendrum, D.H., Armstrong, B., and *Davies, C.R.*, 2003: Malaria in Britain: past, present, and future. *Proc. Natl. Acad. Sci. 100,* 9997–10001.
Kuhn, K.G., Campbell-Lendrum, D.H., and *Davies, C.R.*, 2002: A continental risk map for malaria mosquito (Diptera: Culicidae) vectors in Europe. *J. Med. Entomol. 39,* 621–630.
Lindsay, S.W., and *Birley, M.H.*, 1996: Climate change and malaria transmission. *Ann. Trop. Med. Parasit. 90,* 573–588.
Lowry, R., 2004: VassarStats: Website for statistical computation. Vassar College. Accessed: 30 04 2015. Website http://vassarstats.net/
Lőrincz, F., 1981–82: Malária Magyarországon régen és ma. Visszaemlékezés. *Parasit Hung. 14*, 13–16. (In Hungsarian)
MacDonald, G., 1957: The epidemiology and control of malaria. London: Oxford Univ. Pr., Oxford.
Mapire, 2015: The Historical maps of the Habsburg Empire. Website http://mapire.eu/hu/
Martens, P., Kovats, R.S., Nijhof, S., De Vries, P., Livermore, M.T.J., Bradley, D.J., Cox, J., and *McMichael, A.J.*, 1999: Climate Change and Future Populations At Risk Of Malaria. *Global Environ. Chang. 9(Suppl 1)*,89–107.
Martens, W.J., Niessen, L.W., Rotmans, J., Jetten, T.H., and *McMichael, A.J.*, 1995: Potential impact of global climate change on malaria risk. *Environ. Health Persp. 103:* 458.
Mendis, K., Sina, B.J., Marchesini, P., and *Carter, R.*, 2001: The neglected burden of Plasmodium vivax malaria. *Am. J. Trop. Med. Hyg. 64(Suppl 1),* 97–106.
Menne, B. and *Ebi, K.L. (Eds.)*, 2006: Climate change and adaptation strategies for human health. Steinkopff Verlag/Springer, Darmstad.
Molnár, G. and *Timár, G.*, 2009: Mosaicking of the 1: 75 000 sheets of the Third Military Survey of the Habsburg Empire. *Acta. Geod. Geophys. Hu. 44:*115–120.
Nasci, R.S., Savage, H.M., White, D.J., Miller, J.R., Cropp, B.C., Godsey, M.S., Kerst, A.J., Bennett, P., Gottfried, K., and *Lanciotti, R.S.*, 2001: West Nile virus in overwintering Culex mosquitoes, New York City. *Emerg. Infect. Dis. 7:* 742.
Patz, J.A. and *Olson, S.H.*, 2006: Malaria risk and temperature: Influences from global climate change and local land use practices. *Proc. Natl. Acad. Sci. 103,* 5635–5636.
Piel, F.B., Patil, A.P., Howes, R.E., Nyangiri, O.A., Gething, P.W., Williams, T.N., and *Hay, S.I.*, 2010: Global distribution of the sickle cell gene and geographical confirmation of the malaria hypothesis. *Nat. Commun. 1,* 104.
Szénási, Z., Vass, A., Melles, M., Kucsera, I., Danka, J., Csohán, A., and *Krisztalovics, K.*, 2003: MaláriaMagyarországon: aktuális állapot és védekezési elvek. [Malaria in Hungary: origin, current state and principles of prevention]. *Orvosi hetilap 144,* 1011–1018.(In Hungarian)
Tóth S. and *Kenyeres Z.*, 2012: Revised checklist and distribution maps of mosquitoes (Diptera, Culicidae) of Hungary. *Eur Mosq Bull. 30,* 30–65.
Tóth, S., 2004: Magyarország csípőszúnyog-faunája (Diptera: Culicidae). [Mosquito Fauna of Hungary]. Natura Somogyiensis, Kaposvár. (In Hungarian)
Trájer, A.J., Bede-Fazekas, Á., Bobvos, J., and *Páldy, A.*, 2014: Seasonality and geographical occurrence of West Nile fever and distribution of Asian tiger mosquito. *Időjárás 118:* 19–40.
Vézilier, J., Nicot, A., Gandon, S., and *Rivero, A.*, 2012: Plasmodium infection decreases fecundity and increases survival of mosquitoes. *Proc. R. Soc. B. 279:* 4033–4041.
Wallace, J.R. and *Grimstad, P.R.*, 2002: A preliminary characterization of the physiological ecology of overwintering Anopheles mosquitoes in the midwestern USA. *J. Am. Mosq. Control. Assoc. 18,* 126–127.
World malaria report, 2005: In:World Health Organization and UNICEF. Website: http://www.unicef.fr/sites/default/files/documents/admin/unicef/929-2.pdf. Accessed April 30, 2015.

INSTRUCTIONS TO AUTHORS OF *IDŐJÁRÁS*

The purpose of the journal is to publish papers in any field of meteorology and atmosphere related scientific areas. These may be

- research papers on new results of scientific investigations,
- critical review articles summarizing the current state of art of a certain topic,
- short contributions dealing with a particular question.

Some issues contain "News" and "Book review", therefore, such contributions are also welcome. The papers must be in American English and should be checked by a native speaker if necessary.

Authors are requested to send their manuscripts to

Editor-in Chief of IDŐJÁRÁS
P.O. Box 38, H-1525 Budapest, Hungary
E-mail: journal.idojaras@met.hu

including all illustrations. MS Word format is preferred in electronic submission. Papers will then be reviewed normally by two independent referees, who remain unidentified for the author(s). The Editor-in-Chief will inform the author(s) whether or not the paper is acceptable for publication, and what modifications, if any, are necessary.

Please, follow the order given below when typing manuscripts.

Title page: should consist of the title, the name(s) of the author(s), their affiliation(s) including full postal and e-mail address(es). In case of more than one author, the corresponding author must be identified.

Abstract: should contain the purpose, the applied data and methods as well as the basic conclusion(s) of the paper.

Key-words: must be included (from 5 to 10) to help to classify the topic.

Text: has to be typed in single spacing on an A4 size paper using 14 pt Times New Roman font if possible. Use of S.I. units are expected, and the use of negative exponent is preferred to fractional sign. Mathematical formulae are expected to be as simple as possible and numbered in parentheses at the right margin.

All publications cited in the text should be presented in the *list of references*, arranged in alphabetical order. For an article: name(s) of author(s) in Italics, year, title of article, name of journal, volume, number (the latter two in Italics) and pages. E.g., *Nathan, K.K.,* 1986: A note on the relationship between photosynthetically active radiation and cloud amount. *Időjárás 90,* 10-13. For a book: name(s) of author(s), year, title of the book (all in Italics except the year), publisher and place of publication. E.g., *Junge, C.E.,* 1963: *Air Chemistry and Radioactivity.* Academic Press, New York and London. Reference in the text should contain the name(s) of the author(s) in Italics and year of publication. E.g., in the case of one author: *Miller* (1989); in the case of two authors: *Gamov* and *Cleveland* (1973); and if there are more than two authors: *Smith et al.* (1990). If the name of the author cannot be fitted into the text: *(Miller,* 1989); etc. When referring papers published in the same year by the same author, letters a, b, c, etc. should follow the year of publication.

Tables should be marked by Arabic numbers and printed in separate sheets with their numbers and legends given below them. Avoid too lengthy or complicated tables, or tables duplicating results given in other form in the manuscript (e.g., graphs).

Figures should also be marked with Arabic numbers and printed in black and white or color (under special arrangement) in separate sheets with their numbers and captions given below them. JPG, TIF, GIF, BMP or PNG formats should be used for electronic artwork submission.

More information for authors is available: journal.idojaras@met.hu

Published by the Hungarian Meteorological Service

Budapest, Hungary

INDEX 26 361

HU ISSN 0324-6329

IDŐJÁRÁS

QUARTERLY JOURNAL
OF THE HUNGARIAN METEOROLOGICAL SERVICE

CONTENTS

VOL. 120 * NO. 4 * OCTOBER – DECEMBER 2016

IDŐJÁRÁS

Quarterly Journal of the Hungarian Meteorological Service

Editor-in-Chief
LÁSZLÓ BOZÓ

Executive Editor
MÁRTA T. PUSKÁS

Editorial Office: *Kitaibel P.u. 1, H-1024 Budapest, Hungary*
P.O. Box 38, H-1525 Budapest, Hungary
E-mail: journal.idojaras@met.hu
Fax: (36-1) 346-4669

Indexed and abstracted in Science Citation Index Expanded™ and Journal Citation Reports/Science Edition

Covered in the abstract and citation database SCOPUS®

Included in EBSCO's databases

Subscription by mail:
IDŐJÁRÁS, P.O. Box 38, H-1525 Budapest, Hungary
E-mail: journal.idojaras@met.hu

IDŐJÁRÁS
Quarterly Journal of the Hungarian Meteorological Service
Vol. 120, No. 4, October – December, 2016, pp. 353–364

An interpretation of the measured planetary radiation imbalance

György Major

Hungarian Meteorological Service
P.O.Box 38, H-1525 Budapest, Hungary
E-mail: major.gy@met.hu

(Manuscript received in final form May 31, 2016)

Abstract—Some time variation properties of the planetary imbalance are shown by using satellite measured radiation budget data. The covered period is 1962–2014. The data have been collected from publications and data bases. The solar incom part of the budget has been homogenized using new total solar irradiance (TSI) values. The positive imbalance increases as well as the time delay between the incoming and outgoing radiation.

Key-words: planetary imbalance, radiation budget, satellite measurements, TSI, response time

1. Introduction

The radiation budget of the planet Earth is

$$\text{NET} = \text{TSI}/4 - \text{REF} - \text{OUT}, \tag{1}$$

where:

- NET is the result of all radiation processes.
- TSI is the total solar irradiance, the number 4 is the ratio of the surface of the sphere to the cross section of the sphere perpendicular to the solar rays, this way TSI/4 is the planetary (global) average solar irradiation at the top of the atmosphere (incoming solar radiation: ICO). The shape of the Earth is not

exactly spherical, the rotational ellipsoid approximation gives 4.002 yearly ratio. *Loeb et al.* (2009) calculated 4.0034. In this work the spherical value is used. It is worth to mention that the few tenth of a percent correction is near to the uncertainity of recently measured TSI values.

- REF is the solar radiation reflected to the interplanetary space by the planet.
- OUT is the longwave radiation emitted to the interplanetary space by the planet. Its value is not a simple response to the incoming/absorbed one.

Eq. (1) does not contain the energy of cosmic rays and radio waves arriving to the Earth from the space, since their energy is negligible to the named ones.

If the climate of the planet is in equilibrium, the yearly average net radiation should be zero, that is the incoming and outgoing radiation is balanced, the possible imbalance should be short living small variations around zero.

To check the actual state of the radiation budget of the Earth, several experts have made serious efforts to construct instruments, develop data processing procedure, estimate the error of the received data, and analyze the received data provided by satellite-born instrumentation since the begining of the 1960's. Some early results directed to the global net radiation are the followings: *Ardanuy et al.* (1992), *Arking* and *Vemury* (1984), *Arking* (1996), *Ellis* and *VonderHaar* (1976), *Gruber* and *Winston* (1978), *Harrison et al.* (1993), *Jacobowitz et al.* (1984), *Kandel et al.* (1994), *Kyle et al.* (1985), *Kyle et al.* (1993), *Loeb et al.* (2009), *MacDonald* (1970), *Ohring* and *Gruber* (1983), *Randel* and *VonderHaar* (1990), *Raschke et al* (1973), *Raschke* (1968), *Spänkuch* (1995), *Stephens et al.* (1981), *VonderHaar* and *Raschke* (1972), *Winston* (1970). The latest global net radiation data are provided by the CERES (Cloud and the Earth's Radiatiant Energy System) project since March of 2000 (*Loeb,* 2015). This project uses all the previous experiences in instrument building, data processing, and personal knowledge, moreover, the data sampling is the best in the history of radiation budget measurements.

The values of yearly global net radiation provided by the above mentioned data sources are between +0.9 and + 5 W/m^2, that is during the past 5 decades, negative radiation imbalance did not exist according to the measured data series. The series were produced by several projects, and there were significant interruptions between the periods covered by different projects. Since the uncertainity of these net radiation data is equal or even larger than the values itself, climate scientists could not use these data series. According to the energy budget investigations of the full Earth system, these values do not fit the system, they are too high.

Using the GISS (Goddard Institut for Space Science) climate model *Hansen et al.* (2005) calculated the planetary radiative imbalance for the period of 1880–2005. From the begining the imbalance generally increases from zero to the order of 1 W/m^2, the increase interrupted by the volcanic eruption for 2–3 years, when the imbalance falls below even –2 W/m^2. The increase is slow until 1960, afterward it is more significant. These results are in good agreement with the ocean heat content data. The heat capacity of oceans gives 93 percent of the planetary heat capacity, therefore, the planetary energy imbalance is almost equal to the change of the heat balance of the oceans.

Loeb et al. (2009) modified the original CERES data series creating the CERES EBAF (Energy Balanced And Filled) data series to eliminate the deviation between the satellite measured radiation imbalance and the ocean heat content data, moreover, they stated that the probable reason of the deviation is some kind of systematic calibration error of the satellite-born radiometers. This EBAF series has been constructed to serve the purposes of the climate system science.

In this work, the trends in both the EBAF and the previous satellite radiation budget data series are looked for.

2. Data

2.1. TSI

The TSI is not identical to the solar constant (the first solar constant measurement was made by Pouillet in 1838 from the surface), it contains the variations of incoming solar radiation that are due to variations in the solar activity. TSI measurements have been and are made separately from the measurement of other components of the radiation budget. Continuous satellite based TSI measurements are made from November 1978. The first group of modern (cavity) absolute pyrheliometers were constructed by the Eppley Laboratory (J. Hickey), the Jet Propulsion Laboratory (JPL, R. Willson), the Physical Meteorological Observatory Davos (PMOD, C. Frőhlich), and the Royal Meteorological Institut of Belgium (RMIB, D. Crommelynck). From these instruments a standard group is selected that defines the World Radiometric Reference (WRR), the recently official radiometric scale of the World Meteorological Organization (WMO). In 2003, the National Institut of Standards and Technology of USA (NIST) developed a corrected absolute pyrheliometer named Total Irradiance Monitor (TIM), that measures the TSI approximately by 6 W/m^2 lower than the previously mentioned first group. Recently, Finsterle (PMOD) and several collaborators develop the Cryogenic Solar Absolute Radiometer (CSAR) (*Finsterle,* 2015), that is an essentially different new absolute pyrheliometer in development phase. It seems that after 2018, the WMO shall have to decide amongst the above mentioned 3 pyrheliometric scales. Recently, most of TSI users accepts the NIST scale. In the time period of satellite-based planetary radiation budget measurements, only the development of the TSI measuring instrumentation is known precisely.

Some solar physicists groups connected the satellite-measured TSI data to solar models, and this way they constructed TSI data series backward to some hundred years. For the period 1700–2000, *Dewitte* (2014) presented a TSI series. From this series we use the 1950–2000 section, but the values are decreased by 2.5 W/m^2 to transform them to the NIST scale. For the period 2000–2014 we accept the CERES Edition 4 TSI values (*Kratz et al.,* 2015), these are somewhat higher than the Edition 3A ones. In *Fig. 1,* the yearly mean TSI values are shown from 1950 to 2014.

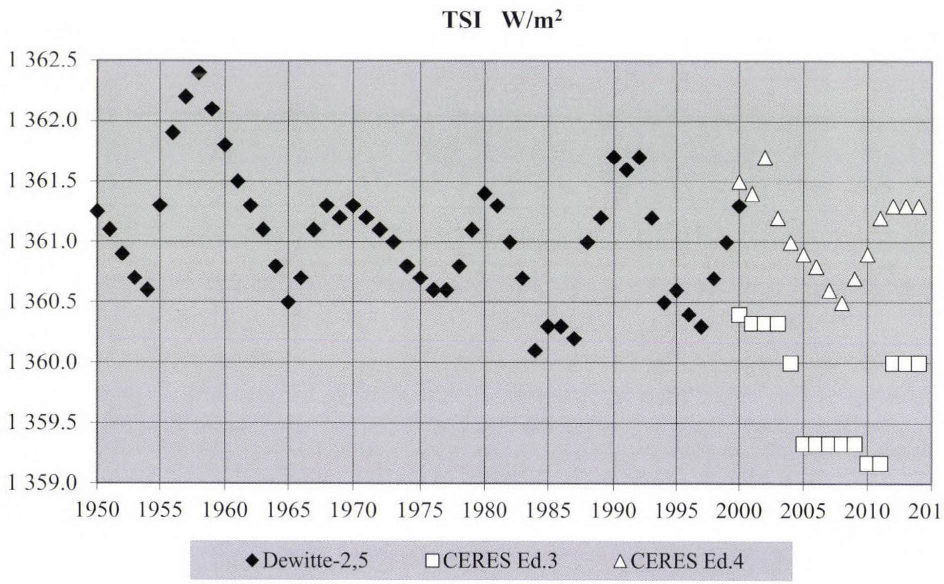

Fig. 1. The yearly TSI values used in this work. The 11 years sunspot cycle is seen clearly.

2.2. *Radiation budget of 1962–1995*

In *Table 1,* yearly or several yearly net radiation budget data are listed as they available from the named publications or data bases. This way, these data eliminate the variations arising from the yearly change of the Sun-Earth distance. Those published values that belong to period longer than 1 year has been composed from several monthly measured ones to represent the „mean" value of the period.

Table 1. Original data taken from publications and data bases. The numbers in parentheses are calculated from the original ones. Where not written, the unit is W/m^2. Earlier used unit: ly = langley = cal /cm^2.

Time period	Experiment	TSI	Reflected	Albedo	Absorbed	OUT	NET	ICO	Source
1962–1966 33 months	TIROS Nimbus-2 ESSA-7	1.95 ly/min		30.0%		0.34 ly/min	0.00 ($0.9 W/m^2$)		*VonderHaar-Raschke*, 1972
1964–1971 29 months	TIROS Nimbus-2,3 ESSA-7 ITOS-1 NOAA-1	1360.0	103.3	32.4%	236.7	235.8	0.9	340.0	*Ellis-VonderHaar*, 1976
1964–1977 48 months	TIROS Nimbus-2,3,6 ESSA-3,7	1376.0		30.0%		232	9		*Stephens et al.*, 1981
1979	ERB	1372.7	(101.4)			235.8	6.0	(343.2)	*Ardanuy et al.*, 1992
1980	”	1373.3	(101.2)			236.3	5.8	(343.3)	”
1981	”	1372.0	(100.6)			236.4	6.0	(343.0)	”
1982	”	1371.7	(101.5)			235.4	6.0	(342.9)	”
1983	”	1371.7	(101.5)			235.9	5.5	(342.9)	”
1984	”	1371.3	(100.8)			235.4	6.6	(342.8)	”
1985	”	1371.5	(101.4)			234.9	6.6	(342.88)	”
1986	”	1371.4	(101.1)			235.2	6.6	(342.85)	”
1985	ERBE	(1362.4)		29.8%		234.0	5.1	(340.6)	Larc NASA S4G data
1986	”	(1362.8)		29.7%		234.0	5.5	(340.7)	”
1987	”	(1363.6)		29.5%		236.0	4.3	(340.9)	”
1988	”	(1368.4)		29.5%		237.0	4.2	(342.1)	”
1989	”	(1361.6)		29.7%		236.0	4.0	(340.4)	”
Mar-Sep, 1994 Nov-Dec, 1994 Jan-Feb,1995.	ScaRaB	(1366.0)		29.9%		237.0	2.4	(341.5)	ScaRaB CDs

In this work, the original radiation budget data have been corrected by substituting the original ICO or TSI data by using the TSI data shown in *Fig. 1*. The reflected solar radiation and the outgoing longwave radiation values are kept as in the original series. The corrected yearly imbalance data series is seen in *Fig. 2*. As a try of correcting the reflected and outgoing radiation data, *Shrestha et al* (2015) presented an improved ERBE series, but it is restricted to the 60N – 60S part of the globe.

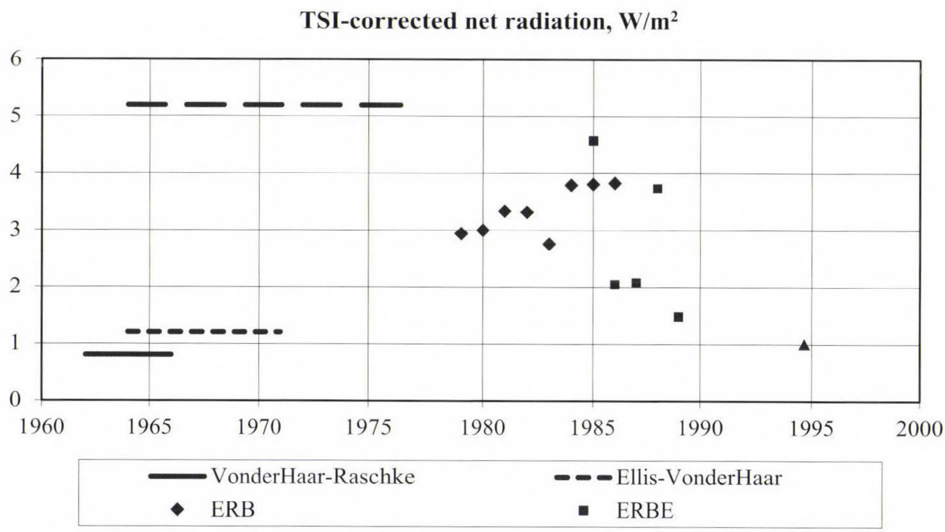

Fig. 2. The used imbalance data for 1964 – 1995. They are corrected to the TSI values seen in *Fig. 1*. The horizontal lines are characteristic to the covered period written in *Table 1*, the dots are calendar year means, except the ScaRaB point that is the mean of March 1994 –Febr 1995. The missing October is filled by interpolation.

2.3. Radiation budget of 2000–2014

Since the March of 2000, continuous high quality annual radiation budget data are available from the CERES Project (*https://ceres.larc.nasa.gov/products*). In this work, the CERES Ed.3A radiation data are used, except that the ICO of Ed.3A is changed to ICO of Ed.4 as mentioned in Section 2.1. The yearly (March-February) values are seen in *Fig. 3* altogether with the EBAF values. These Ed. 2.8 EBAF data are not corrected to the newer TSI (that is they contain the original Ed.3A ICO values), since the EBAF is fitted to the whole energy budget data of the climate system.

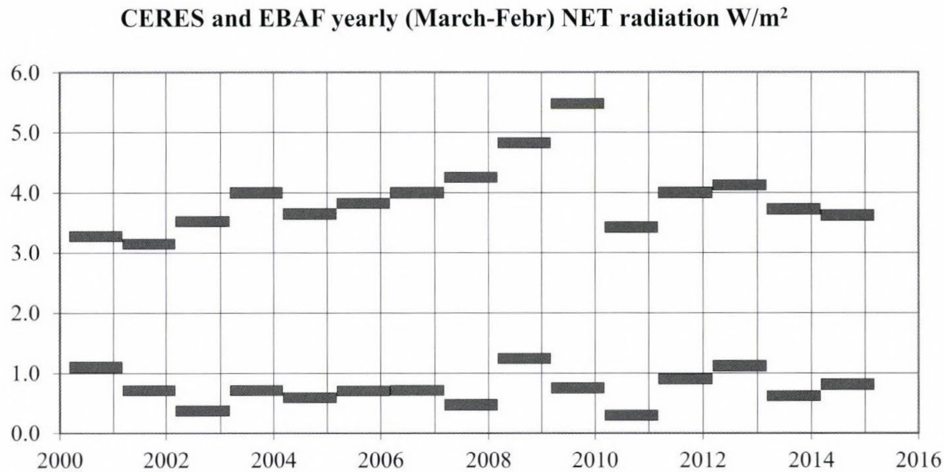

Fig. 3. The radiation balance data for the period of March 2000 – February 2015.

3. *Time variations*

3.1. The time period of March of 2000 – February 2014

This time period is covered the latest satellite-measured radiation budget data. Looking at *Fig. 3,* the most significant feature in the original CERES data series is the inreasing imbalance between 2000 and 2009, then a sudden decrease in 2010 and a weak increase afterward. The EBAF data do not show such strong variability, however, the year-to-year change is significant compared to the imbalance values itself. The basic statistics of the two series are printed in *Table 2*. Both linear trend coefficients show a slight (compared to the year-to-year variations) increase of the imbalance. In the increase of imbalance, the incoming solar radiation does not play important role, it is decreasing weakly, while the reflected and outgoing radiation are decreasing more significantly. Accordig to the standard deviations, the reflected solar and outgoing longwave radiation are not independent of each other.

Table 2. Basic characteristics of the March 2000 – February 2015 period according to the CERES and EBAF data series.

	EBAF			CERES		
	Mean W/m²	**Standard deviation W/m²**	**Trend Wm⁻²year⁻¹**	**Mean W/m²**	**Standard deviation W/m²**	**Trend Wm⁻²year⁻¹**
ICO	340.0	0.08	–0.0043	340.2	0.09	–0.0045
REF	99.7	0.20	–0.0083	97.9	0.51	–0.0486
OUT	239.6	0.24	–0.0019	238.8	0.24	0
NET	0.7	0.27	0.0059	3.5	0.60	0.0441

3.2. The time period of 1962 – 2014

The data seen in *Fig. 2* plus the original CERES data seen in *Fig. 3* are the satellite-measured yearly radiation imbalance of the last 5 decades. Taking them as one data series its basic statistical parameters are shown in *Table 3*. The trend parameters were calculated using the middle time point of the years or of the time periods the radiation values belong to. The planetary imbalance is increasing during this half century, while the year-to-year variation is much more significant similarly to the 2000 – 2014 period. If the idea of constant systematic calibration error of the satellite-born radiometers measuring the reflected solar and the outgoing longwave values is accepted for the whole period, then according to the high value of the regression coefficient of NET radiation, this error is not a simple additive one.

Table 3. Basic statistics for the period of 1962 – 2014

	Mean W/m²	**Standard deviation W/m²**	**Trend Wm⁻²year⁻¹**
ICO	340.2	0.106	0.0017
REF	99.7	2.126	–0.1328
OUT	237.1	1.802	0.1006
NET	3.4	1.135	0.0339

4. *Time delay between incoming and outgoing radiation*

Fig. 4 shows the monthly CERES values of absorbed solar (short wave) and emitted longwave radiation. As it is expected, the yearly variations of the absorbed radiation (~ 15 W/m^2) exceed that of the emitted (long wave) ones (~ 8 W/m^2). The phase shift (response time) between the two waves is approximately a half year. The time delay between the absorbed and outgoing radiation depends not only on the thermal inertia of the planet but on the longwave transmissivity and emissivity properties of the atmosphere. The positive imbalance is seen clearly, the shortwave curve goes higher than the longwave one. Similar figure were prepaered by *Ardanuy et al.* (1992) for the period of 1979 – 1986.

The time delay (phase shift) between two waves could be measured by the time difference between the maxima and minima. Since the EBAF data fits better to the climate system than the original CERES ones, to quantify the response time between the planetary radiation income and outcome the differences of the dates of EBAF OUT yearly max and the yearly Perihelion, as well as that of EBAF OUT yearly min and the yearly Aphelion are taken. The astronomical dates have been obtained from http://aa.usno.navy.mil/data/EarthSeasons.php.

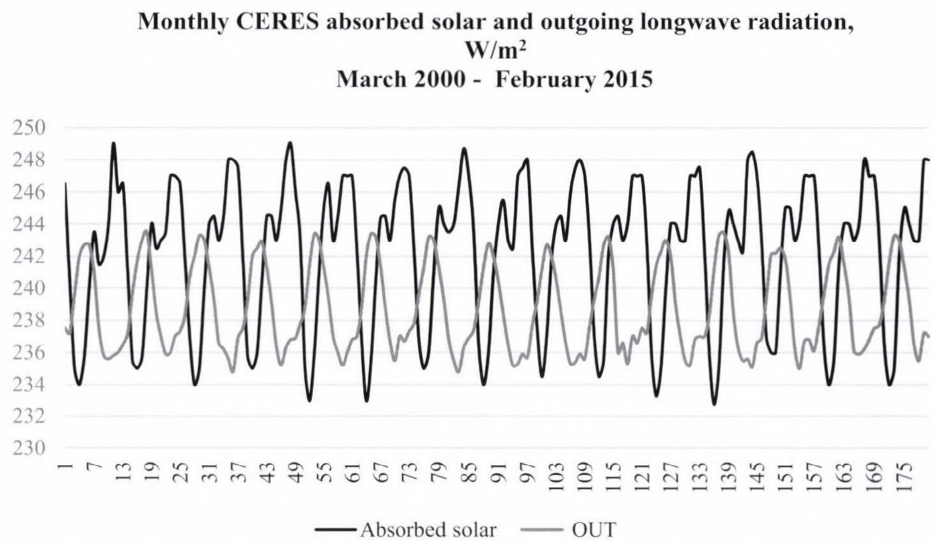

Fig. 4. Monthly global absorbed solar radiation and outgoing emitted radiation from the CERES data series.

Since the date of the peak values of OUT data are not well defined, two kinds of smoothing have been applied:

- the monthly values were taken into account instead of daily ones,
- a second order polinom were fitted to 5 monthly values around the expected dates, the dates of peak values of these polinoms were taken as peak dates of outgoing radiation.

In the outgoing radiation the dates of max peaks vary between July 23 and 31, while those of min peaks between December 29 and January 25. The first derived time difference between the max peaks has been established between the date of max OUT in July 2000 and the date of Perihelion in January 2000. The first one between min peaks has been derived from the date of min OUT in January 2001 and the date of Aphelion in July 2000. *Fig. 5* shows separately the 15 – 15 values between the maxima and minima. The linear trend gives a slight increase in both cases.

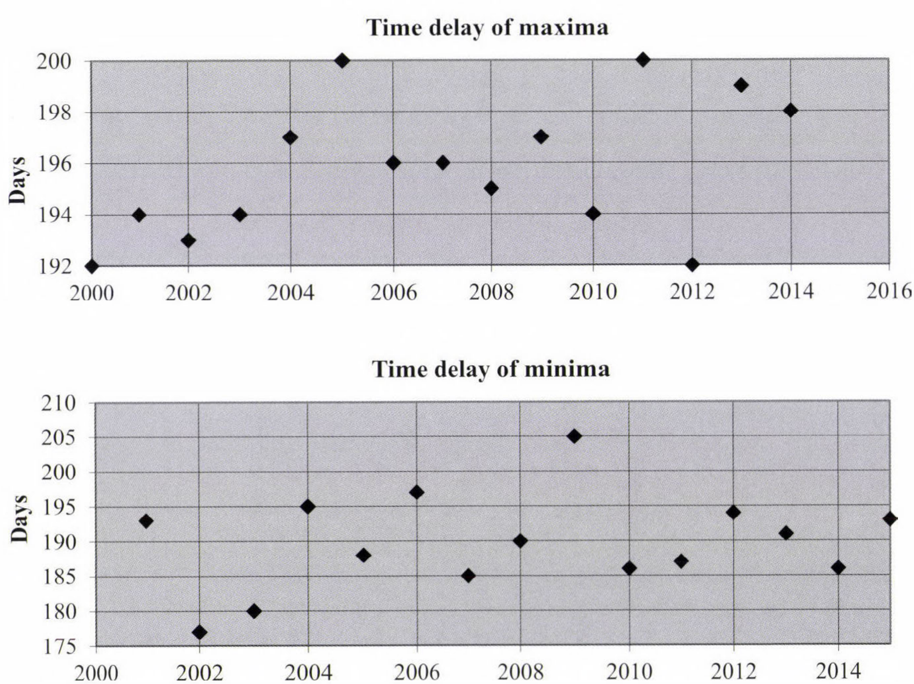

Fig. 5. Time difference (days) between the incoming solar radiation and the EBAF outgoing radiation. Upper panel: difference of max peaks, lower panel: that of min peaks.

5. Conclusion

More efforts would be necessary to correct the REF and OUT components of the radiation budget data measured by satellites before 2000 to better connect the planetary radiation imbalance to the global climate processes.

References

Ardanuy, P.E., Kyle, H.L. and *Hoyt, D.*, 1992: Global Relationship among the Eart's Radiation Budget, Cloudiness, Volvcanic Aerosols and Surface Temperature. *J. Climate 5*, 1120–1139.

Arking, A., 1996: Absorption of Solar Energy in the Atmosphere: Discrepancy Between Models and Observations. *Science 273*, 779–782.

Arking, A. and *Vemury, S.*, 1984: The Nimbus-7 ERB Data Set: A Critical Analysis. *J.Geophys Res. 89*, D4, 5089–5097.

Dewitte, S. 2014: The RMIB space odissey from Total Solar Irradiance to the Sun-earth IMBAlance (SIMBA). 23rd Science Team Meeting, October 6–10 2014, Toulouse ceres.larc.nasa.gov/science-team-meetings.

Ellis, J.S. and *VonderHaar, T.H.*, 1976: Zonal Average Earth Radiation Budget Measurements from Satellites for Climate Studies. Dept. Atm. Sci. CSU Paper No 240.

Finsterle, W. 2015: Status and future of the WRR in the SI. IPC-XII, 2015, PMOD/WRC Davos.

Gruber A. and *Winston J.S.* 1978: Earth-atmosphere radiative heating based on NOAA Scanning Radiometer measurements. *B. Am. Meteorol. Soc. 59*, 1570–1573.

Hansen, J., Nazarenko, L., Ruedy, R., Sato, M., Willis, J., Del Genio, A., Koch, D., Lacis, A., Lo, K., Menon, S., Novakov, T., Perlwitz, J., Russel, G., Schmidt, G.A., and *Tausnev, N.* 2005: Earth's energy imbalance: Confirmation and implications. *Science 308,* 1431–1435.

Harrison E.F., Minnis, P., Barkstrom B.R,. and *Gibson G.G.*, 1993: Radiation Budget at the Top of the Atmosphere. In: Atlas of Satellite Observations Related to Global Change. Cambridge University Press, London, 1993, CD Edition by NASA LARC. 19–38.

Jacobowitz H., Soule H.V., Kyle H.L., House F.B., and *the Nimbus-7 ERB Experiment Team,* 1984: The Earth Radiation Budget (ERB) Experiment: An Overview. *J.Geophys. Res. 89*, D4, 5021–5038.

Kandel R.S., Monge J.-L., Viollier M., Pakhomov L.A., Adasko V.I., Reitenbach R.G., Raschke E., and *Stuhlmann R.* 1994: The SCARAB Project: Earth Radiation Budget Observations from METEOR Satellites. *Adv. Space Res. 14.* 147–154.

Kratz, D.P., Gupta, S.K., Wilber, A.C., and *Sothcott, V.E.*, 2015: Status of the SOFA Validation and TSI Data. 24th Science Team Meeting, 4–9 May 2015, Hampton, Virginia, ceres.larc.nasa.gov/science-team-meetings.

Kyle, H.L, Ardanuy, P.E., and *Hurley, E.J.*, 1985: The Status of the Nimbus-7 Earth-Radiation-Budget Data Set. *B. Am. Meteorol. Soc. 66*, 1378–1387.

Kyle, H.L., Hickey, J.R., Ardanuy, P.E., Jacobowitz, H., Arking, A., Campbell, G.G., House, F.B., Maschhoff, R., Smith, G.L., Stowe, S.S., and *VonderHaar, T.H.*, 1993: The Nimbus Earth Radiation Budget (ERB) Experiment 1975 to 1992. *B. Am. Meteorol. Soc. 74*, 815–830.

Loeb, N.G., Wielicki, B.A., Doelling, D.R., Smith, G.L., Keyes, D.F., Kato, S., Manalo-Smith, N., and *Wong, T.*, 2009: Toward Optimal Closure of the Earth's. Top-of-Atmosphere Radiation Budget. *J. Climate 22*, 748–766.

Loeb, N.G., 2015: State of CERES. CERES Science Team Meeting, May 5–7, 2015, ceres.larc.nasa.gov/science-team-meetings2.php.

MacDonald, T.H., 1970: ESSA-7 Radiation Budget Data October 1968 – April 1969. Personal Communication.

Ohring, G. and *Gruber, A.*, 1983: Satellite radiation observations and climate theory. *Advan. Gerophys. 25*, 237–301.

Randel, D.L. and *VonderHaar, T.H.* 1990: On the Interannual Variation of the Earth Radiation Balance. *J. Climate 3*, 1168–1173.

Raschke E., 1968: The Radiation Balance of the Earth-Atmosphere System from Radiation Measurements of the Nimbus-2 Meteorological Satellite. NASA TN D-4589.

Raschke, E., VonderHaar T.H., Pasternak M., and *Bandeen, W.R.* 1973: The Radiation Balance of the Earth-Atmosphere System from Nimbus-3 Radiation Measurements. NASA TN D-7249.

Shrestha, A.K., Kato, S., Wong, T., Stackhouse, P.W., Rose, F., Miller, W.F., Bush, K., Rutan, D.A., Minnis, P. and *Doelling, D.*, 2015: Modeling ERBE WFOV Nonscanner dome degradation and reprocessing its radiation budget data from 1985 to 1998. CERES Science Team Meeting, September 1–3, 2015, ceres.larc.nasa.gov/science-team-meetings2.php.

Spänkuch, D., 1995: Die Strahlungseigenschaften der Erdamosphäre. *Sitzungberichte der Leibniz-Sozietät* 7(7). (In Deutsch)

Stephens, G.L., Campbell, G.G., and *VonderHaar, T.H.,* 1981: Earth Radiation Budgets. *J. Geoph. Res. 86,* 9739–9760.

VonderHaar, T.H. and Raschke, E. 1972: Measurements of the Energy Exchange Between Earth and Space from Satellites During the 1960's. Dept. Atm. Sci. CSU Paper No 184.

Winston, J.S. 1970: Radiation budget graphs March 1967 – February 1968. P*ersonal communication.*

IDŐJÁRÁS

Quarterly Journal of the Hungarian Meteorological Service
Vol. 120, No. 4, October – December, 2016, pp. 365–381

Changes in the structure of days with precipitation in Southern Poland in 1971-2010

Barbara Skowera[1]*, **Joanna Kopcińska J.**[2], and **Anita Bokwa**[3]

[1]*Department of Ecology, Climatology and Air Protection,*
Faculty of Environmental Engineering and Land Surveying,
University of Agriculture in Krakow,
24/28 Mickiewicza Av., 30-059 Krakow, Poland
E-mail: barbara196@interia.pl

[2] *Department of Applied Mathematics,*
Faculty of Environmental Engineering and Land Surveying,
University of Agriculture in Krakow,
253C Balicka St., 31-149 Krakow, Poland
E-mail:rmkopcin@cyf-kr.edu.pl

[3]*Institute of Geography and Spatial Management,*
Jagiellonian University,
7 Gronostajowa St., 30-387 Krakow, Poland
E-mail:anita.bokwa@uj.edu.pl

**Corresponding author*

(Manuscript received in final form January 13, 2016)

Abstract— In Poland, no clear tendencies have been detected in multi-year trends in precipitation sums. However, the number of days with precipitation has increased significantly. Therefore, we analyzed changes in the structure of days with precipitation, i.e., trends in the percentage of days with different ranges of daily precipitation sums. The precipitation data were from 1971–2010, from four stations in Southern Poland representing agricultural areas (Stare Olesno, Glubczyce, Lapanow, and Tuchow). Statistically significant upward trends (1–9 days per 10 years) and low variability were found for the number of days with daily precipitation sums up to 5 mm, mainly in the cold half of the year, and downward trends were found for days with 20–30 mm of precipitation (1 day per 10 years), with high variability. Comparison with the results of previous studies shows that the increase in the number of days with precipitation is not linked to a significant increase in precipitation sums.

Key-words: precipitation, Poland, trends, water resources, agriculture

1. Introduction

Changes in precipitation observed worldwide in recent decades are much more diversified regionally than changes in air temperature. The results presented in the Fifth Assessment Report of the IPCC *(Hartmann et al.,* 2013*)* show an overall increase in precipitation in the mid-latitudes of the Northern Hemisphere (30°N to 60°N) from 1901 to 2008, with statistically significant trends for each dataset used. For all other zones, due to data sparsity, poor data quality, and/or a lack of quantitative agreement among available estimates, characterization of such long-term trends in zonally averaged precipitation may be unreliable. Analyses of annual precipitation sums in Europe in the period 1960–2014, provided by the European Environmental Agency (*European Environmental Agency,* 2014*)*, show a decrease in Southern Europe (–37.07 mm per decade) and an increase in Northern Europe (20.64 mm per decade), both statistically significant. These tendencies were also found in earlier studies *(Schönwiese et al.,* 1997*; Brunetti et al.,* 2000*;, Førland* and *Hanssen-Bauer,* 1995*; Degirmendžić et al.,* 2004*; Klein Tank* and *Können,* 2003*; Bartholy et al.,* 2015*)*. Central Europe is located in a transitional zone. A study by *Niedźwiedź et al.* (2009) showed that precipitation in Central Europe fluctuates greatly in both time and space. No changing trend was found in any of the precipitation series studied, but a certain spatial regularity could be discerned. The test statistics change from a strongly negative value in Budapest to positive values that increase north-eastwards. These results are consistent with other studies covering smaller areas in Central Europe *(Domonkos* and *Tar,* 2003, *Kürbis et al,* 2009*; Tošić et al.,* 2016).

Previous studies of precipitation sums in Poland have not shown statistically significant changes *(Czarnecka and Nidzgorska-Lencewicz,* 2012*; Degirmendžić et al.,* 2004*)*. The authors of studies devoted to characteristics of the precipitation regime in Poland emphasize long-term fluctuations in the number of days with precipitation $\geq$0.1mm (*Degirmendžić et al.,* 2004*; Podstawczyńska,* 2007*; Wibig* and *Fortuniak,* 1998*; Bochenek,* 2012*; Skowera et al.,* 2014*)* and statistically significant upward trends in the number of days with precipitation *(Bochenek,* 2012*; Skowera et al.,* 2014*; Twardosz,* 2000). Therefore, the objective of this study was to analyze the multi-year variability in the structure of the number of days with precipitation, trends in the number of days with precipitation, and the role of days in particular classes of precipitation in determining the precipitation sum in the years 1971–2010, at stations representing agricultural areas in four regions of southern Poland. Regional aspects of both the structure of and trends in the number of days with precipitation are important in terms of formation of underground water resources and securing the precipitation needs of crop plants. Therefore, in this study we have considered all classes of precipitation sums. Agricultural regions of southern Poland, unlike in central and northern Poland, are located on diverse terrain, which in the case of atmospheric precipitation is an additional significant factor determining the spatial variability of this element.

Hence, in this study long-term changes in characteristics of the number of days with precipitation were considered with respect to the role of terrain relief.

2. Study areas

The data analyzed come from four meteorological stations, representing agricultural areas located in four mesoregions (following the division by *Kondracki* (2011)) belonging to two voivodeships (administrative regions) of southern Poland (*Fig. 1*). *Table 1* presents basic data on each station.

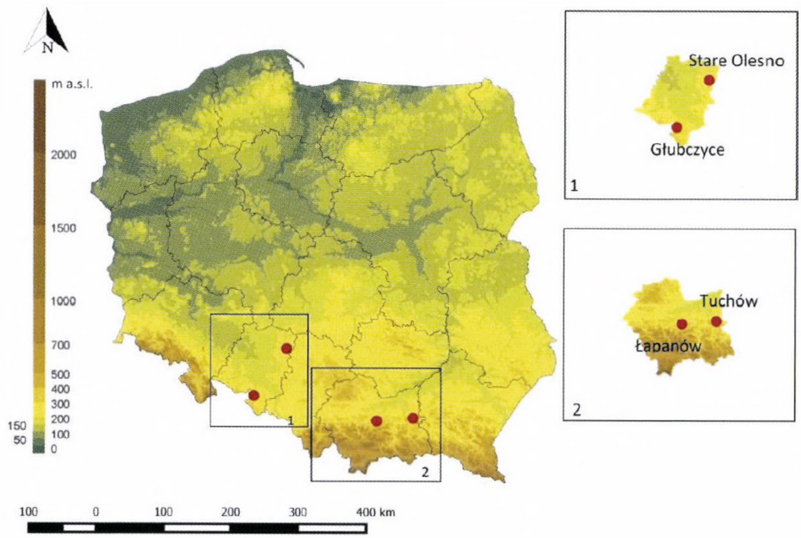

Fig. 1. Location of the Stare Olesno and Glubczyce in Opole Voivodeship (1) and Lapanow and Tuchow in Lesser Poland Voivodeship (1).

Table 1. Meteorological stations used in the study

Station	Voivodeship	Region	Coordinates	Altitude (m a.s.l.)
Stare Olesno	Opole	Woznicki cuesta	50°54′N 18°21E′	230
Glubczyce		Glubczyce Plateau	50°12′N 17°49′E	290
Lapanow	Lesser Poland	Wisnicz Foothills	49°52′N 20°19′E	236
Tuchow		Ciezkowice Foothills	49°54′N 21°03′E	235

As the spatial distribution of precipitation is highly dependent on the impact of land forms, both on a regional and a local scale, a short description of each mesoregion is provided. Woznicki cuesta, where the Stare Olesno station is located, is a low ridge running NW to SE. The mesoregion is located on the western border of the Woznicki-Wielun Upland. The neighboring region to the west and south is the Opole Lowland, and the difference in altitude between the regions is about 60 m. Glubczyce Plateau, where the Glubczyce station is located, is surrounded to the west by the Sudety Mountains. (altitude difference between the regions is about 1,000 m), and the neighboring region to the east is the Raciborz Basin (altitude difference is about 90 m). Lapanow and Tuchow are located in two foothill mesoregions belonging to the Carpathian Foothills, but Lapanow represents its western part and Tuchow its central part. Both stations are situated in river valleys (of the Stradomka River and the Biala River, respectively) which run south to north and are surrounded by hills (altitude about 400 m and 500 m a.s.l., respectively). Both mesoregions are surrounded by the Beskidy Mountains. to the south (altitude difference between the regions is about 1,000 m) and by the Sandomierz Basin to the north (altitude difference about 200 and 300 m, respectively). All four stations are located so as to represent the climatic conditions of the agricultural areas on a mesoregional scale. A factor contributing to the origin of precipitation in all study areas is the domination of western winds in Poland. As humid air masses bringing precipitation come from the west, the local land forms can enhance precipitation sums, acting as orographic barriers, or, conversely, can reduce precipitation sums in comparison to neighboring regions, i.e., create a rain shadow effect.

3. Materials and methods

In the study, we used the daily precipitation sums from 1971–2010 from the four meteorological stations described in Section 2. A day with precipitation was defined as a day with a daily precipitation sum $\geq$ 0.1mm. The structure of days with precipitation was presented according to the criterion proposed by *Olechnowicz–Bobrowska* (1970). This method classifies days with precipitation according to daily precipitation sums in 6 classes:

0.1–1.0 mm: day with very light precipitation,

1.1–5.0 mm: day with light precipitation,

5.1–10.0 mm: day with moderate precipitation,

10.1–20.0 mm: day with moderately heavy precipitation,

20.1–30.0 mm: day with heavy precipitation,

> 30.0 mm: day with very heavy precipitation.

The number of days with precipitation was calculated in each class in successive months and half-years, i.e., the cold half of the year (October-March) and the warm half (April-September), and mean values were calculated for the period 1971–2010. The structure of days with precipitation was based on successive decades of the period 1971–2010 and presented as the percentage share of the number of days with precipitation of a given class during the year and for the warm and cold halves of the year. The warm half of the year is the growing season for plants and the time of work in the fields, and the cold half is the period of dormancy for crop plants. Coefficient of variation V (%) was calculated for days with a daily precipitation sum ≥ 0.1 mm and separately for each class of days with precipitation.

Trends in the number of days with precipitation were analyzed for each month and half-year. The Mann-Kendall test *(Kendall,* 1975*)* was used to verify whether we could reject the null hypothesis, that there is no trend in the sequence of data in favor of the alternative hypothesis of an upward or downward trend in the data y_i. The test determines whether the difference between a given element of the data sequence and a previous element is a positive or a negative value ($y_j - y_i$, where $j > i$) and assigns a value of 1 if the difference is positive, –1 if it is negative and 0 if it is 0. The statistic S was calculated as the sum of the integers according to the following formula:

$$S = \sum_{i=1}^{n-1} \sum_{j=i+1}^{n} \operatorname{sgn}(y_j - y_i), \qquad (1)$$

where n is the total number of data.

The null hypothesis, that there is no trend in the data sequence, is rejected when the value of statistic S is significantly different from zero. We verify the null hypothesis on the basis of a normal Gaussian distribution, standardizing the statistic S according to the following formula:

$$Z = \begin{cases} \dfrac{S-1}{\sqrt{VAR(S)}} & S > 0 \\ 0 & S = 0, \\ \dfrac{S+1}{\sqrt{VAR(S)}} & S < 0 \end{cases} \qquad VAR(S) = \sqrt{\frac{n(n-1)(2n+5)}{18}}. \qquad (2)$$

We reject the null hypothesis when the absolute value of statistic Z is greater than the theoretical value of the normal distribution $Z_{1-\frac{\alpha}{2}}$, where α is the level of significance. We adopted the values α=0.05 and α=0.1. The Z values are

$Z_{1-\frac{\alpha}{2}} = 1.95$ for $\alpha = 0.05$ and $Z_{1-\frac{\alpha}{2}} = 1.28$ for $\alpha = 0.1$. For data for which an upward or downward trend was found, the magnitude of the changes was estimated by calculating the Sen's slope estimator *(Hirsch et al.,* 1982) according to the following formula:

$$\beta = median\left(\frac{y_j - y_I}{j - i}\right), \qquad \text{for } i < j\,;\, i = 1, 2, \ldots, n\text{-}1, \qquad j = 2, 3, \ldots, n. \tag{3}$$

Monthly, annual and semi-annual precipitation sums were also calculated, and then Spearman's rank coefficients were calculated between these sums and the number of days with precipitation in particular classes.

4. Results

Analysis of the structure of the number of days with precipitation in four regions of southern Poland in 1971–2010 revealed temporal and spatial variation in this characteristic of the precipitation regime. The highest mean annual number of days with precipitation was noted at the Stare Olesno station, with 171.3 days, and the lowest at the Glubczyce station, with 155.7 days (*Table 2*).

Table 2. Average number of days with precipitation per year and half-year in each precipitation class in 1971–2010.

	Stare Olesno			Glubczyce			Lapanow			Tuchow		
Sum (mm)	**Year**	**Oct-Mar**	**Apr-Sep**	**Year**	**Oct-Mar**	**Apr-Sep**	**Year**	**Oct-Mar**	**Apr-Sep**	**Year**	**Oct-Mar**	**Apr-Sep**
> 0.1	171.3	79.4	91.8	155.7	79.2	76.2	160.9	80.9	79.9	166.2	78.8	87.4
0.1 – 1.0	64.2	24.1	40.1	66.0	26.5	39.6	51.2	20.3	30.7	58.3	22.2	36.1
1.1 – 5.0	66.8	30.1	36.7	55.0	27.9	27.0	64.6	29.8	34.7	64.7	28.7	36.0
5.1 – 10.0	24.1	13.1	11.0	19.4	13.2	6.1	23.8	14.4	9.4	24.0	14.3	9.7
10.1 – 20.0	12.0	8.4	3.6	10.6	7.6	3.0	14.9	10.8	4.1	13.7	10.1	3.5
20.1 - 30.0	2.6	2.3	0.3	3.3	2.8	0.5	3.7	3.0	0.7	3.3	2.9	0.5
> 30.0	1.5	1.4	0.05	1.4	1.4	0.02	2.7	2.6	0.1	2.2	0.6	1.7

These differences can be attributed to the location of Glubczyce leeward of the Sudety Mountains., at their eastern foot. These mountains form an orographic barrier for moist polar air masses from the west. Precipitation is much lower to the east of the mountain range than to the west *(Kondracki,* 2011*).* Stare Olesno is situated on a convex landform, where the precipitation is determined mainly by atmospheric circulation processes. The average annual number of days with precipitation at all stations during the study period was about 10-20 days higher than those reported by *Olechnowicz-Bobrowska* (1970) for the period 1951–1960. According to the *Atlas of the climate in Poland* (2005), in 1971–2000 the average annual number of days with precipitation >0.1 mm in the regions discussed was about 170, which was similar to the results obtained in our study. The number of days with precipitation >10 mm was also comparable. On an annual scale, light precipitation (class 1.1–5.0 mm) had the largest share in the structure of days with precipitation, with the exception of Glubczyce, where days with very light precipitation (0.1–1.0 mm) were dominant. In the warm half of the year, days with precipitation in the 0.1-1.0 mm class were dominant (except for Lapanow, with the greatest number of days in the 1.1–5.0 mm class), while in the colder half of the year, days with 1.1–5.0 mm dominated.

The structure of days with precipitation in successive decades of the study period is presented in *Figs. 2.1* and *2.2* for classes 0.1–1.0, 1.1–5.0, 5.1–10, and >10.0 mm (the class of days with precipitation >10.0 mm was introduced because the number of days in higher classes was small). Notable in this structure are the upward trends primarily in classes of days with very light and light precipitation in the cold half of the year and the variation in the number of days with precipitation between different meteorological stations in each decade.

The parametric Mann-Kendall test was used to verify whether the tendencies observed in changes in the structure of days with precipitation were statistically significant (significant trends $\alpha \leq 0.05$ and weak trends $0.05 < \alpha \leq 0.1$) (*Table 3.a*). Significant changes in very light precipitation (0.1–1.0 mm) were noted in Lapanow and Tuchow in both half-years and for the year, and in Glubczyce for the year and for the cold half of the year, while in Stare Olesno no trend coefficients were statistically insignificant. In Glubczyce, Lapanow, and Tuchow statistically significant trends were also noted in certain months, mainly in the cold half of the year. All statistically significant trends were upward; according to the Sen estimator, the number of days with precipitation in class 0.1–1.0 mm increased by about 1–9 per decade. In the case of higher classes, no significant trends were found in individual months and, therefore, for these classes the trends for the year and for each half-year are presented (*Table 3.b*). Statistically significant trends were noted only for classes 1.1–5.0 mm and 20.1–30 mm. In the case of class 1.1–5.0 mm these were upward trends, affecting only the number of days with such precipitation sums in Stare Olesno and Tuchow; for the year and the cold half-year they were about 2–3 days per decade. In the case of class 20.1–30.0 mm in Stare Olesno and Tuchow in the warm half of the year, a decrease was noted of about 1 day per 10 years. In successive months of the warm half-year, no significant trends were found in the total number of days with precipitation (daily sum ≥0.1 mm) (*Table 4*).

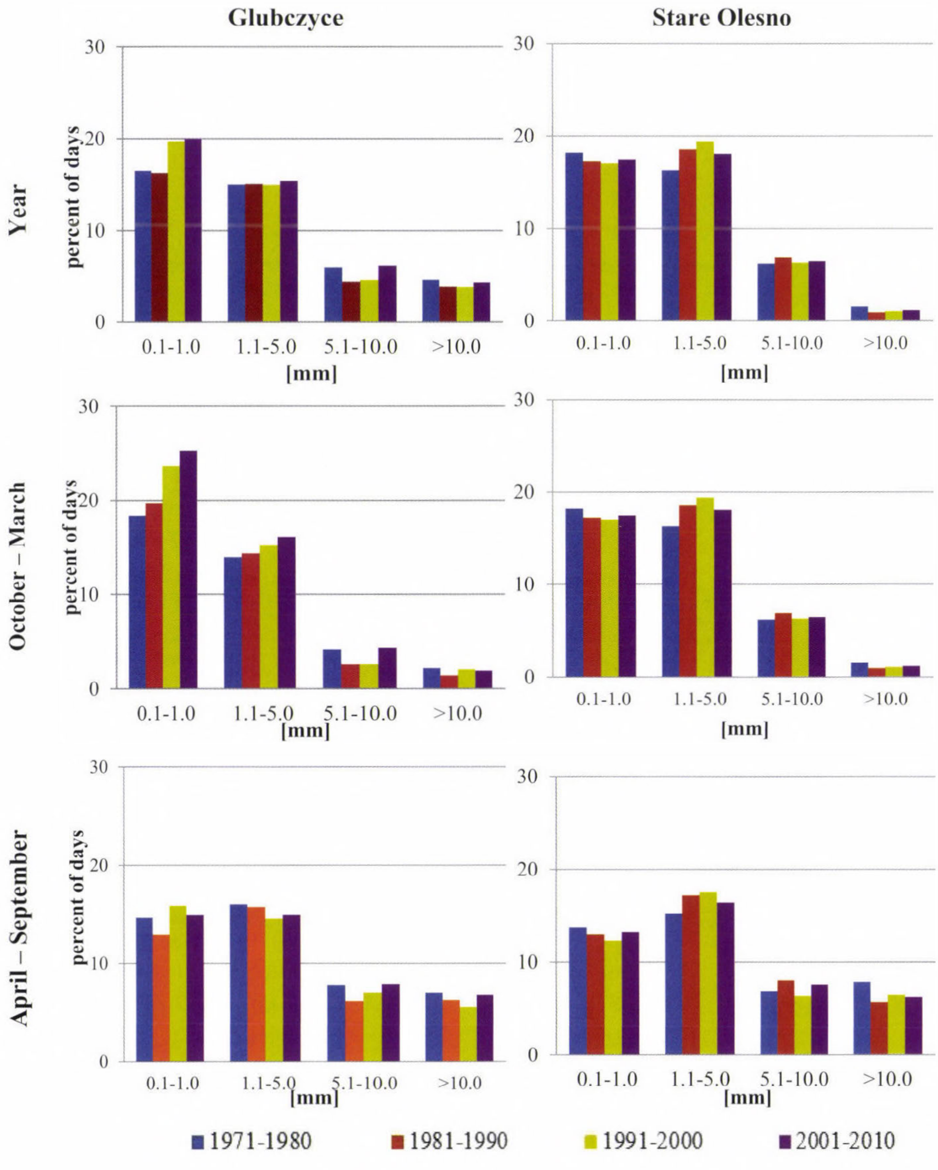

Fig. 2.1. Structure of days with precipitation (in successive decades) at selected stations in Opole Voivodeship in southern Poland (1971–2010).

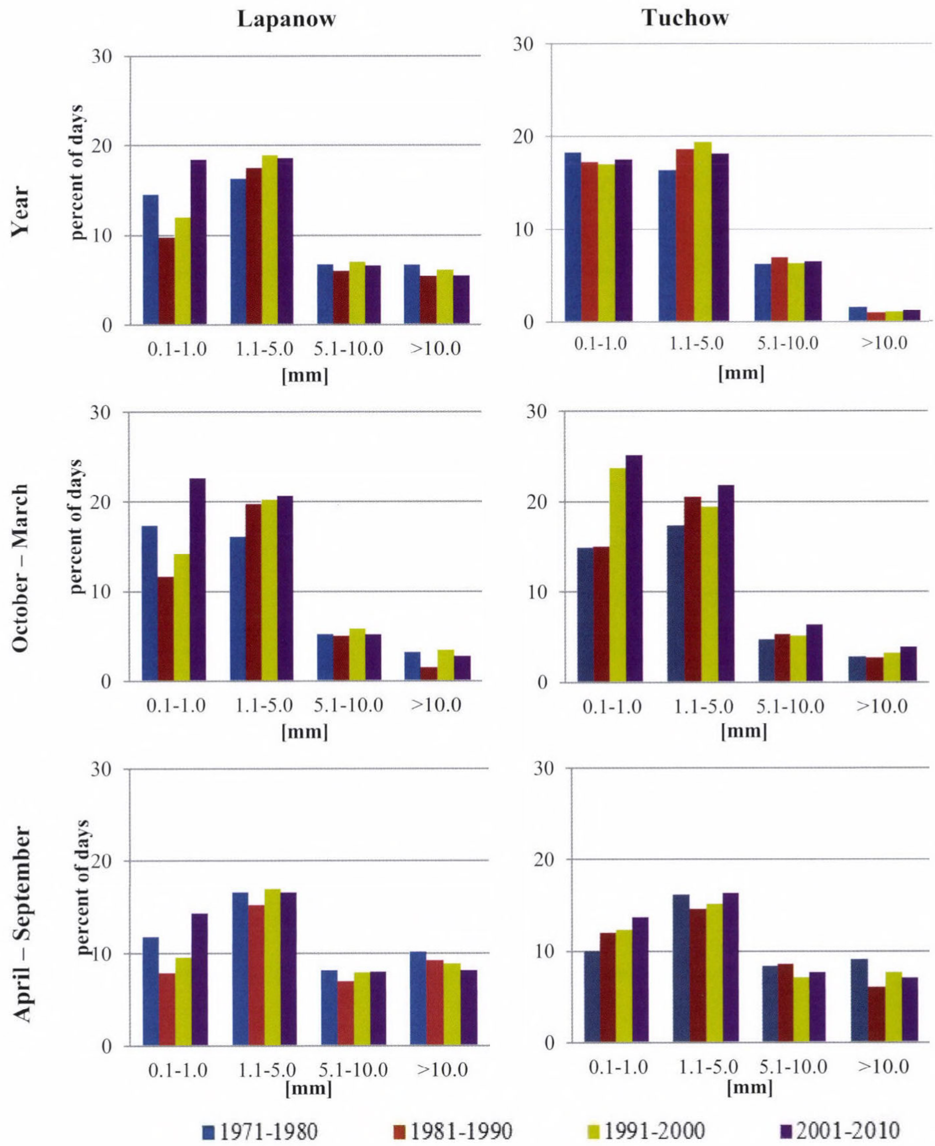

Fig. 2.b. Structure of days with precipitation (in successive decades) at selected stations in Lesser Poland Voivodeship in southern Poland (1971–2010).

Table 3.a. Trend coefficients for the number of days with precipitation |z| in 1971-2010: class 0.1–1.0 mm (individual months, half-years, and year)

Meteorological station	January	February	March	April	May	June	July	August	September	October	November	December	Year	Oct-Mar	Apr-Sep
Stare Olesno	0.53	0.20	-0.03	-1.47*	1.06	0.85	0.00	1.20	-1.05	0.47	-1.15	-0.24	0.52	-0.35	-0.05
Increase in days/10 years	-	-	-	-	-	-	-	-	-	-	-	-	-	-	-
Glubczyce	1.72*	3.40**	1.28	-0.30	-0.35	0.01	1.31*	0.34	-0.48	1.47*	2.88**	1.31*	2.81**	2.96**	1.41*
Increase in days/10 years	-	1.3	-	-	-	-	-	-	-	-	1.2	-	5.2	4.5	-
Lapanow	0.12	3.92**	0.66	2.07**	0.16	2.32**	0.79	1.02	0.76	0.76	2.11**	2.43**	2.74**	2.79**	2.16**
Increase in days/10 years	-	1.3	-	0.6	-	0.5	-	-	-	-	0.8	1.1	7.3	4.7	2.5
Tuchow	2.63**	2.92**	2.57**	0.17	1.59*	1.25	0.13	3.24**	1.28	3.01**	3.54**	2.63**	4.80**	4.57**	2.75**
Increase in days/10 years	2.69	1.0	0.8	-	-	-	-	1.4	-	1.4	1.3	0.8	8.2	6.3	2.0

Table 3.b. Trend coefficients for the number of days with precipitation |z| in 1971–2010: remaining classes of precipitation sums (half-years and year).

	1.1-5.0			5.1-10.0			10.1-20.0			20.1-30.0			>30.0		
Meteorological station	Year	Oct-Mar	Apr-Sep	Year	Oct-Mar	Apr-Sep	Year	Oct-Mar	Apr-Sep	Year	Oct-Mar	Apr-Sep	Year	Oct-Mar	Apr-Sep
Stare Olesno	2.54**	2.38**	0.42	0.23	0.54	-0.70	0.34	0.26	-0.13	-2.82**	0.08	-3.48**	1.09	0.00	0.00
Increase in days/10 years	3.3	2.5	-	-	-	-	-	-	-	-0.6	-	-0.6	-	-	-
Glubczyce	0.36	1.05	-0.60	0.04	-0.44	0.15	0.31	-0.21	0.49	-0.77	-0.27	-0.63	0.54	0.00	0.00
Increase in days/10 years	-	-	-	-	-	-	-	-	-	-	-	-	-	-	-
Lapanow	1.60*	1.66*	0.18	-0.38	-1.12	0.35	-0.61	0.17	-1.29*	-1.65*	-0.02	-2.30**	-0.05	0.00	0.00
Increase in days/10 years	-	-	-	-	-	-	-	-	-	-	-	-0.7	-	-	-
Tuchow	2.61**	2.30**	0.43	-0.36	1.28	-1.44*	-0.68	0.48	-0.67	-0.76	0.31	-0.48	_1.80*_	_3.70**_	_-2.27**_
Increase in days/10 years	2.9	2.3	-	-	-	-	-	-	-	-	-	-	-	_0.5_	_0_

Statistical significance: ** - for $\alpha = 0.05$ with $|z| > 1.95$; * - for $\alpha = 0.1$ with $|z| > 1.28$

Italics indicate values, which due to the small number of cases of days with precipitation >30mm (despite significant values for statistic |z|) can not be treated as reliable

Table 4. Trend coefficients for the number of days with precipitation >0.1mm in 1971–2010

Meteorological station	January	February	March	April	May	June	July	August	September	October	November	December	Year	Oct-Mar	Apr-Sep
Stare Olesno	1.38*	1.61*	1.29*	–1.61*	0.98	-0.21	0.13	1.72*	–1.37*	0.29	–0.16	–0.39	1.06	1.14	–0.31
Glubczyce	0.81	2.93**	1.53*	–0.64	0.75	–0.50	0.96	–0.16	–0.62	1.24	2.32**	0.23	2.68**	2.67**	–0.07
Lapanow	1.34*	2.58**	2.53**	0.52	0.88	0.70	0.63	–0.47	0.16	0.79	0.76	0.85	2.58**	2.62**	0.81
Tuchow	2.71**	2.86**	2.47**	1.01	1.04	0.09	0.08	1.71*	–0.01	1.74*	2.34**	1.08	4.80**	4.83**	1.04

Statistical significance: ** for $\alpha = 0.05$ for $|z| > 1.95$; * for $\alpha = 0.1$ for $|z| > 1.28$

A characteristic feature of the precipitation sums and the number of days with precipitation in the regions studied is the considerable variability from year to year. As in the case of the trends, the coefficient of variation in each precipitation class was calculated for the year and for both half-years-warm and cold. Following *Sobczyk* (2009): a value >20% was taken to mean that a given population is significantly varied in terms of the trait analyzed. The coefficient of variation of the annual number of days with precipitation (daily sum ≥0.1 mm) ranged from 10% at the stations located in the Opole Voivodeship to 11–12% in the Lesser Poland Voivodeship. In the warm half-year at all stations, the variability of this characteristics ranged from 13% to 15% and was somewhat lower than in the colder half of the year, i.e., from 15% to 19%, which means small variation in annual and semi-annual numbers of days with precipitation. However, the variability in monthly numbers of days with precipitation was much greater. The highest variation in the number of days with precipitation at all stations was noted for October (38–44%), while the lowest variation for this trait (about 26–27%) occurred in different months at different stations. The lowest variation was found for the number of days with light precipitation (1.1–5.0 mm: 11–25%), followed by very light (0.1–1.0 mm: 16–31%) and moderate (5.1–10.0 mm: 21–42%) precipitation. In the higher classes (>10 mm), the variation in the number of days was much greater, at 25–67%, and in the case of these classes, greater variation between seasons can be seen. In the cold half of the year, the coefficient of variation reached a value of 45–67%, and in the warm half, 29–33% (*Table 5*).

Table 5. Coefficient of variation for mean annual and seasonal numbers of days with precipitation (%) in the classes distinguished, in the period 1971-2010 at the stations studied

Sum (mm)	**Stare Olesno**			**Glubczyce**			**Lapanow**			**Tuchow**		
	Year	**Apr -Sep**	**Oct-Mar**	**Year**	**Apr-Sep**	**Oct-Mar**	**Year**	**Apr-Sep**	**Oct-Mar**	**Year**	**Apr-Sep**	**Oct-Mar**
>0.1	10	13	15	10	14	18	12	15	17	11	13	19
1.1–1.0	16	20	20	17	20	25	27	31	31	24	23	30
1.1–5.0	14	20	22	13	20	22	14	25	22	11	17	21
5.1–10.0	21	33	29	29	34	38	27	28	42	22	28	36
>10.0	58	31	66	28	33	62	25	29	67	28	32	45

Table 6 presents correlations between the number of days with precipitation in individual classes and annual and semi-annual precipitation sums. At all stations, the precipitation sum in both seasons was significantly influenced by the number of days with precipitation in classes > 10 mm, and in the cold half of the year, the precipitation sum was also significantly influenced by the number of days with precipitation in lower classes.

Table 6. Correlations between the number of days with precipitation in a given class (mm) and the precipitation sum in the year and half-years in 1971-2010

Meteorological station	Period	>0.1	0.1-1.0	1.1-5.0	5.1-10.0	10.0-20.0	20.1-30.0	>30.0
Stare Olesno	Year	0.47*	0.02	0.12	0.11	0.62*	0.39*	0.61*
	Apr-Sep	0.57*	0.28	0.01	0.30	0.56*	0.51*	0.56*
	Oct-Mar	0.56*	-0.04	0.58*	0.61*	0.72*	0.34*	0.34*
Glubczyce	Year	0.46*	0.09	0.22	0.47*	0.22	0.63*	0.59*
	Apr-Sep	0.46*	0.01	0.32*	0.29	0.34*	0.55*	0.60*
	Oct-Mar	0.32*	0.04	0.43*	0.23	0.35*	0.48*	-0.05
Lapanow	Year	0.51*	0.25	0.20	0.48*	0.34*	0.40*	0.74*
	Apr-Sep	0.53*	0.11	0.15	0.28	0.54*	0.47*	0.72*
	Oct-Mar	0.72*	0.36*	0.38*	0.49*	0.64*	0.46*	0.22
Tuchow	Year	0.51*	0.09	0.26	0.59*	0.50*	0.63*	0.63*
	Apr-Sep	0.63*	0.07	0.34*	0.32*	0.57*	0.56*	0.31*
	Oct-Mar	0.51*	0.15	0.46*	0.63*	0.72*	0.33*	0.17

* significant correlation coefficient (α=0.05)

5. 5. Discussion

The results presented show that in all the regions similar tendencies were observed in changes in the structure of the number of days with precipitation, with certain aspects of these tendencies modified by local environmental conditions. In the structure of the number of days with precipitation, days with precipitation sums < 5 mm, i.e., very light and light, are dominant. They show a statistically significant upward trend and, at the same time, little variation over the long term. This increase is observed mainly in the cold half of the year, both in the entire half-year and in some of its months. Moreover, the number of days with daily precipitation sums < 5 mm has a significant role in determining the precipitation sum, mainly in the cold half of the year. For days with higher daily precipitation sums, including for extreme precipitation, either no statistically significant trends in changes are observed or the trends are downward. *Lupikasza* (2010) summed up studies of changes in extreme precipitation in Europe and in Poland and found that 'during summer time, any positive trends in extreme precipitation observed in Europe are much weaker than those found in winter time and are mostly statistically insignificant. Indeed, significant negative trends have been identified in many areas of Europe in summer time' and 'during 1951–2006, decreasing trends in extreme precipitation indices dominated in both the warm and cool halves of the year and in the seasons in Poland.' The results of our study in southern Poland are thus consistent with the tendencies observed in *Lupikasza's* study (2010), as well as with results obtained by *Bartholy et al.* (2015) for Hungary, *Moberg et al.* (2006) and *Rodrigo* (2010) for Europe. At all stations, the number of days with precipitation > 10 mm showed either no statistically significant trends in changes or downward trends, and at the same time, the highest long-term variation. Moreover, days with precipitation > 10 mm have a significant role in determining the precipitation sums in the year and in half-years. In terms of water resources for agriculture, the tendencies presented indicate a direction of changes in the precipitation regime that can be considered unfavorable. The climate scenarios presented in the IPCC report *(Kirtman et al.,* 2013*)* suggest that in 2016–2035, in comparison with 1986–2005, seasonal precipitation sums in the regions studied in Poland will be about 5% lower in the summer and 5% higher in the winter. A significant factor is the considerably greater long-term variability in the number of days with precipitation > 10 mm than in the number of days with precipitation < 5 mm. In the cold half of the year, which covers the beginning and end of the growing season, we can expect the precipitation demands of crop plants to be met, while during most of the growing season we can expect a shortage, due to the lower number of days with precipitation, high variability in the frequency of days with high and extreme precipitation, and lower precipitation sums. Previous studies have shown that due to increased air temperature, in some mesoregions of Poland, rainfall deficits in the spring have been more frequent than the excessive rainfall for crops (*Skowera et al.,* 2014). The number of days with precipitation determines the distribution of precipitation supply over time. In the years 1971–2010, a downward tendency was observed in the number of precipitation spells in the warm half of the year (Glubczyce) and an increase in the cold half of the year (Lapanow and Tuchow) (*Skowera* and *Wojkowski,* 2015). Given that in the cold half of the year the number of days with very light precipitation increased while no increase was observed in the precipitation sum, we can conclude that the observed change in the structure of the number of days with precipitation did not translate to an increase in post-winter water resources for crop plants.

6. Conclusion

Most studies of the number of days with precipitation focus on extreme precipitation, while precipitation with lower daily sums is overlooked.

The results presented regarding the structure of the number of days with precipitation in southern Poland demonstrate the significant role of the number of days with very light (0.1–1.0 mm) and light precipitation (1.1–5.0 mm) in determining precipitation sums (particularly in the cold half of the year) and water resources for agriculture. In the period 1971–2010, changes in precipitation sums showed no significant tendencies, but an increase was observed in the number of days with very light and light precipitation and a decrease in the number of days with 20.1–30.0 mm of precipitation. The magnitude of these changes varied between stations. In light of the anticipated climate changes in Europe, precipitation in southern Poland will undergo slight changes in the next few decades, similar to those observed until now, but with a tendency towards a decrease in precipitation in the summer and an increase in the winter. If the tendency in the change in the number of days with precipitation does not change, we can expect a further increase in the number of days with very light and light precipitation, particularly in the cold half of the year, and a decrease in the number of days with 20–30 mm of precipitation in the summer period.

Acknowledgements–Research was supported by the Ministry of Science and Higher Education of Republic of Poland through the core funding for statutory R&D activities

References

Bartholy, J., Pongrácz, R., and *Kis, A.,* 2015: Projected changes of extreme precipitation using multi-model approach. *Időjárás 119*, 129–142.

Bochenek, W., 2012: Ocena zmian warunków opadowych na Stacji naukowo-badawczej IGIPZ PAN w Szymbarku w okresie 40 lat obserwacji (1971–2010) i ich wpływ na zmienność odpływu wody ze zlewni Bystrzanki. *Water-Environment-Rural Areas 12*, 2(38), 29–44 (in Polish)..

Brunetti, M.; Maugeri, M., and *Nanni, .T,* 2000: Variations of temperature and precipitation in Italy from 1866–1995. *Theor. Appl. Climatol. 65*, 165–174.

Czarnecka, M. and *Nidzgorska-Lencewicz J.,* 2012: Wieloletnia zmienność sezonowych opadów w Polsce, *Water-Environment-Rural areas*, 12, 2 (38), 45–60 (in Polish).

Degirmendžić, J., Kożuchowski, K. and *Żmudzka, E.,* 2004: Changes of air temperature and precipitation in Poland in the period 1951–2000 and their relationship to atmospheric circulation. *Int. J. Climatol.*, 24, 291–310.

Domonkos, P., and *Tar, K.,* 2003: Long-term changes in observed temperature and precipitation series 1901–1998 from Hungary and their relations to larger scale changes, *Theor. Appl. Climatol. 75*, 131–147.

European Environment Agency, 2014. Trends in annual precipitation across Europe. www.eea.europa.eu/data-and-maps/figures/observed-changes-in-annual-precipitation-1961-4.

Førland, E.J., and *Hanssen-Bauer, J.,* 1995: Changes in "normal" precipitation in Norway and the North Atlantic region. In: (Ed.: *Heikinheimo P.*) International conference on past, present and future climate. Proceedings of the SILMU conference held in Helsinki, Finland, 22–25 August. Academy of Finland, Helsinki, 228–232

Hartmann, D.L.; Klein Tank, A.M.G.; Rusticucci, M.; Alexander, L.V., Brönnimann, S., Charabi, Y., Dentener, F.J., Dlugokencky, E.J., Easterling, D.R., Kaplan, A., Soden, B.J., Thorne, M.P.W., and *Zhai, Wild P.M.*, 2013: Observations: Atmosphere and Surface. In: Climate Change 2013: The Physical Science Basis. In (Eds.: *Stocker, T.F., D. Qin, G.-K. Plattner, M. Tignor, S.K. Allen, J. Boschung, A. Nauels, Y. Xia, V. Bex and P.M. Midgley*) Contribution of Working Group I to the Fifth Assessment Report of the Intergovernmental Panel on Climate Change. Cambridge University Press, Cambridge, United Kingdom and New York, NY, USA.

Hirsch, R.M.; Slack, J.R. and *Smith, R.A.*, 1982 Techniques of trend analysis for monthly water quality data. *Water Resour. Res. 18*,107–121.

Kendall, M.G., 1975: Rank Correlation Methods. Charless Griffin, London.

Kirtman, B., Power, S.B., Adedoyin, J.A., Boer, G.J., Bojariu, R., Camilloni, I., Doblas-Reyes, F.J., Fiore, A.M., Kimoto, M., Meehl, G.A., Prather, M., Sarr, A., Schär, C., Sutton, R., van Oldenborgh, G.J., Vecchi, G. and Wang, H.J., 2013:. Near-term climate change: projections and predictability. In (Eds.: *Stocker, T.F., D. Qin, G.-K., Plattner, M., Tignor, S.K., Allen, J., Boschung, A,. Nauels, Y., Xia, V. Bex* and *P.M. Midgley*) Climate Change: The Physical Science Basis. Contribution of Working Group I to the Fifth Assessment Report of the Intergovernmental Panel on Climate Change. Cambridge University Press, Cambridge, United Kingdom and New York, NY, USA.

Klein Tank, A.M.G. and *Können, G.P.*, 2003: Trends in Indices of Daily Temperature and Precipitation Extremes in Europe, 1946–99. *J. Climate 16*, 3665–3681.

Kondracki, J., 2011: Geografia regionalna Polski, PWN, Warszawa, (in Polish).

Kürbis, K.; Mudelsee, M.; Tetzlaff, G. and Brázdil, R., 2009: Trends in extremes of temperature, dew point, and precipitation from long instrumental series from central Europe, *Theor. Appl. Climatol*, 98, 187–195.

Lupikasza, E., 2010: Spatial and temporal variability of extreme precipitation in Poland in the period 1951–2006. *Int. J. Climatol.*, 30: 991–1007.

Moberg, A; Jones, P.D., Lister, D., Walther, A., Brunet, M., Jacobeit, J., Alexander, L.V., Della-Marta, P.M., Luterbacher, J., Yiou, P., Chen, D., Klein Tank A. M. G., Saladie', O., Sigró, J,, Aguilar, E., Alexandersson, H., Almarza, C., Auer, I., Barriendos, M., Begert, M., Bergström, H., Böhm, R., Butler, C. J., Caesar, J, Drebs, A,, Founda, D., Gerstengarbe, F.-W., Micela, G., Maugeri, M., Österle, H., Pandzic, K., Petrakis, M., Srnec, L., Tolasz, R., Tuomenvirta, H., Werner, Peter C., Linderholm, H., Philipp, A., Wanner, H., and *Xoplak, E.*, 2006: Indices for daily temperature and precipitation extremes in Europe analyzed for the period 1901–2000, *J. Geoph. Res. 111*, D22106.

Niedźwiedź, T., and *Twardosz, R., Walanus, A.*, 2009: Long-term variability of precipitation series in east central Europe in relation to circulation patterns, *Theor. Appl. Climatol. 98*, 337–350.

Olechnowicz-Bobrowska, B., 1970: Częstość dni z opadem w Polsce. Instytut Geografii Polskiej Akademii Nauk, *Prace Geograficzne. 86*, PWN, Warszawa. 75 (in Polish).

Podstawczyńska, A., 2007: Dry and wet periods in Łódź in the XX[th] Century. *Acta Univ. Lodzensis Folia Geog. Physica 8*, 9–25.

Rodrigo, F.S., 2010: Changes in the probability of extreme daily precipitation observed from 1951 to 2002 in the Iberian Peninsula. *Int. J. Climatol. 30*, 1512–1525.

Schönwiese, C.D., and *Rapp, J.*, 1997: Climate Trend Atlas of Europe Based on Observations 1891–1990. Kluwer Academic Publishers, Dordrecht.

Skowera, B., Kopcińska, J., and *Kopeć, B.*, 2014: Changes in thermal and precipitation conditions in Poland in 1971-2010. *Ann. Warsaw Univ. of Life Sci. - SGGW, Land Reclam. 46*, 153–162.

Skowera, B., and Wojkowski, J., 2015: Ciągi dni z opadem w wybranych mezoregionach Polski Południowej w latach 1971–2010. *Acta Agrophisica, 22*, 435–447. (in Polish).

Sobczyk, M., 2009: Statystyka. Podstawy teoretyczne. Przykłady. Zadania. Wyd. UMCS, Lublin. (in Polish).

Tošić, I., Zorn, M., Ortar, J., Unkaševic, M., Gavrilov, M. B., and *Markovic, S. B.*, 2016: Annual and seasonal variability of precipitation and temperatures in Slovenia from 1961 to 2011, *Atmos. Res.*, 168, 220-233.

Twardosz, R., 2000: Wieloletnia zmienność sum dobowych opadów w Krakowie w powiązaniu z sytuacjami synoptycznymi. [W:] Studies in Physical Geography, Red. B. Obrębska-Starklowa, *Prace Geograficzne Instytutu Geografii UJ 105*, 19–71 (in Polish).

Wibig, J. and *Fortuniak, K.*, 1998: The extreme precipitation conditions in Łódź in the period 1931-1995. *Acta Univ. Lodzensis Folia Geog. Physica*, *3*, 241–249.

IDŐJÁRÁS
Quarterly Journal of the Hungarian Meteorological Service
Vol. 120, No. 4, October – December, 2016, pp. 383–394

Potential benefit of the ensemble forecasts in case of heavy convective weather situations

Dóra Lázár[1] and **István Ihász**[2*]

[1]*Department of Meteorology, Eötvös Loránd University,*
P.O. Box 32, H-1518 Budapest, Hungary
E-mail: ldora1989@gmail.com

[2]*Hungarian Meteorological Service,*
H-1675 Budapest, P.O.Box 39.
E-mail: ihasz.i@met.hu

**Corresponding author*

(Manuscript received in final form November 15, 2016)

Abstract— Nowadays, early warning and alarm for high impact weather situations becomes more and more important. Besides deterministic model forecasts, using ensemble forecasts gets increasing attention, but in case of the convective events, probabilistic forecasts have not been widely used. Due to the fact that convective events are very changeable in space and time, probabilistic approach can have a lot of advantages. Current horizontal resolution of the global ensemble models is around 30 km, so we cannot aim to focus on small scale convective events, but focusing on frontal zones and extended squall lines can be possible. We attempt pioneering steps to develop new methods and tools to support early warning based on ensemble (ENS) forecasts of the European Centre for Medium-Range Weather Forecast (ECMWF). We focus on the forecast probabilities of three main components generating convection.

Key-words: convection, convective available potential energy, ensemble timeline diagram, ensemble vertical profile, probability charts, relative humidity, statistical and case studies, wind shear

1. Introduction

Protection of life and property is one of the most important tasks of weather forecasts. Heavy convective events quite often cause heavy rainfall, hail, or extremely strong wind causing severe damages. The European unified warning system, the so-called Meteoalarm collects the alert information coming from member states of EUMETNET. It provides real time warning on its website: www.meteoalarm.eu. The Hungarian Meteorological Service has been maintaining a warning system for counties and alert system for subregional areas since August 1, 2011. This system provides warnings for up to maximum 48 hours (current day and one day ahead) and alerts for ultra short-range (0.5 – 3 hours). The warning system is mostly based on forecasts coming from different models, for this purpose mainly deterministic models were used in the past. The alert system is mostly based on radar and satellite information besides ultra short-range model forecasts. Even nowadays, usage of the global and regional ensemble models gets increasing attention (*Molteni et al.*, 1996, *Palmer*, 2006; *Persson* and *Riddaway*, 2011, *Barkmeijer et al.,* 2012).

Every five years ECMWF makes a strategic plan covering the forthcoming 10 years. In the current ECMWF's Strategic Plan covering the period 2016–2025, developing methods for early warning up to 4–5 days is among the key elements of the strategy (ECMWF, 2016). During our work, we developed a few new objective methods supporting warnings based on ensemble forecasts.

For the development of heavy convective events, three components are needed: atmospheric vertical instability, adequate moisture, and vertical wind shear (*Horváth* and *Geresdi*, 2001; *Craven* and *Brooks,* 2002).

The atmospheric vertical instability is often characterized by the so-called instability index. One of the most popular and often used indexes is the convective available potential energy (short name is CAPE). CAPE is computed according to the following formula:

$$CAPE = \int_{LFC}^{EL} g \frac{T'_v - T_v}{T_v} dz , \tag{1}$$

where *EL* is the equilibrium level (the height at which a rising parcel of air is at the same temperature as its environment), *LFC* is the level of free convection (the height at which the relative humidity of an air parcel will reach 100% when it is cooled by dry adiabatic lifting), g is the gravity, and T_v is the virtual temperature (the temperature at which a theoretical dry air parcel would have a total pressure and density equal to the moist parcel of air).

Vertical wind shear is also a critical factor in the development of the thunderstorms. Vertical wind shear, or the change of winds with height, interacts dynamically with thunderstorms to either enhance or diminish vertical upwelling. So we used the CAPE index, relative humidity, and vertical wind shear (*Horváth*, 2007).

Focusing on these three meteorological parameters, we examined benefits of the usage of ensemble forecasts. To support this, a comprehensive set of tools has been developed.

Our study provides a summary of the newly developed methods based on ECMWF ensemble forecasts (ENS) to assist successful prediction of the convective weather situations. In the first part of the study, key elements of the new approach are presented and illustrated by a few examples. In the second part, result of the statistical investigation is summarized. In the third part, only one selected case study is presented due to some space constraints. Finally, we summarize the benefits of this new system and we have a short outlook too.

2. Statistical studies

Statistical studies of these three parameters were based on a ten-year period of a 51-member ensemble forecasting model for the convective summer season (*Fig. 1*). Relationships between the rate of the convective and total precipitation and the aforementioned three parameters were studied by different statistical methods. On the histogram of CAPE, the values decreased exponentially. On the histograms of the wind shear and relative humidity, the distributions were lognormal.

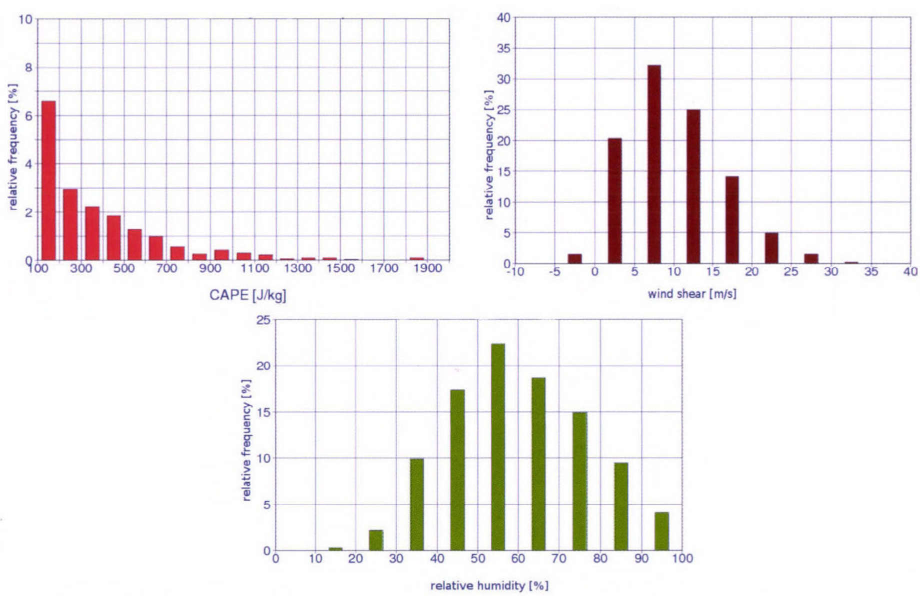

Fig. 1. Histograms of CAPE (J/kg), wind shear (m/s), and relative humidity (%) in summer seasons for Budapest between 2004 and 2013.

We studied whether high rate of convective precipitation was associated with high CAPE values in convective weather situations. Convective/total precipitation rate was calculated and the relationship of these two parameters was studied with crossdiagrams (*Fig. 2*). The thresholds of the CAPE were 0, 500, 1000, 1500, 2000, and 2500 J/kg, and the comparison of the convective/total precipitation rate and CAPE was made for selected thresholds of total precipitation (0, 1, 5, 10, 15, 20, and 25 mm). In the most typical situation, low convective/total precipitation rate was connected with low CAPE values. In case of the extreme values, this relationship was not so strong, thus strong convection was connected not only with CAPE, some other meteorological variables could be quite important too.

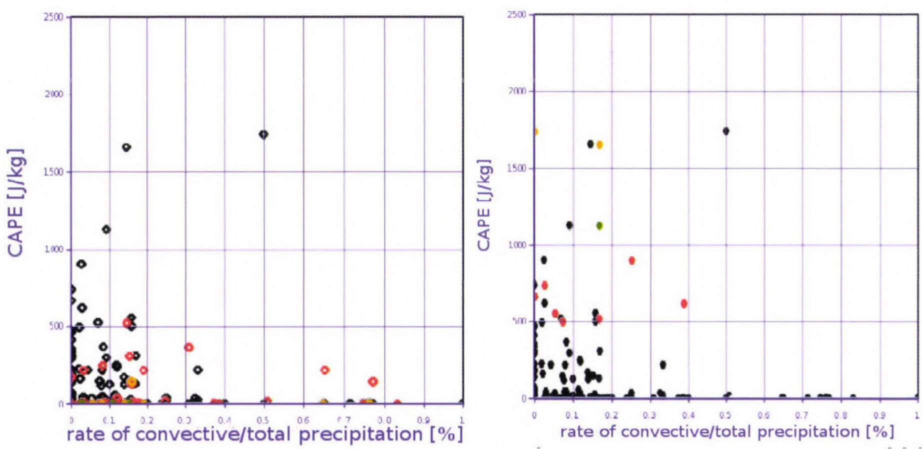

Fig. 2. Crossdiagrams of CP/TP precipitation rate and CAPE values: (left) threshold of CAPE: 0 J/kg, thresholds of precipitation (with quantity): black dot: 0 – 5 mm (125 cases), red dot: 5 – 15 mm (38 cases), orange dot: 15 – 20 mm (3 cases), green dot: above 20 mm (2 cases) for Budapest, (right) threshold of precipitation: 0 mm, thresholds of CAPE (with quantity): black dot: 0 – 500 J/kg (163 cases), red dot: 500 – 1000 J/kg (7 cases), orange dot: 1000 – 1500 J/kg (1 cases), green dot: above 1500 J/kg (1 case) for Budapest

We studied the characteristics of the convective/total precipitation rate forecasts based on different model runs. As the most intensive convective activity typically occurs in the early afternoon, it seemed to be useful to study the similarities and differences of the 00 and 12 UTC model runs. On the histogram *(Fig. 3)*, the total 24-hour sum of the precipitation can be seen, 00 and 12 UTC ENS and control models associated with different thresholds (1, 5, 10, 15, 20, and 25 mm) were plotted. Generally, the 12 UTC model runs produced less number of heavy convective cases than the 00 UTC model runs, but with increasing CP/TP ratio to the proportion of the former grows. At the thresholds of 1 and 5 mm, the relative frequency of the CP/TP ratio extends from 10 to a maximum of 15%. At 15 mm, another column of 75–85% appeared (not shown). At 20 and 25 mm, due to the low number of cases, comparing distributions was not possible.

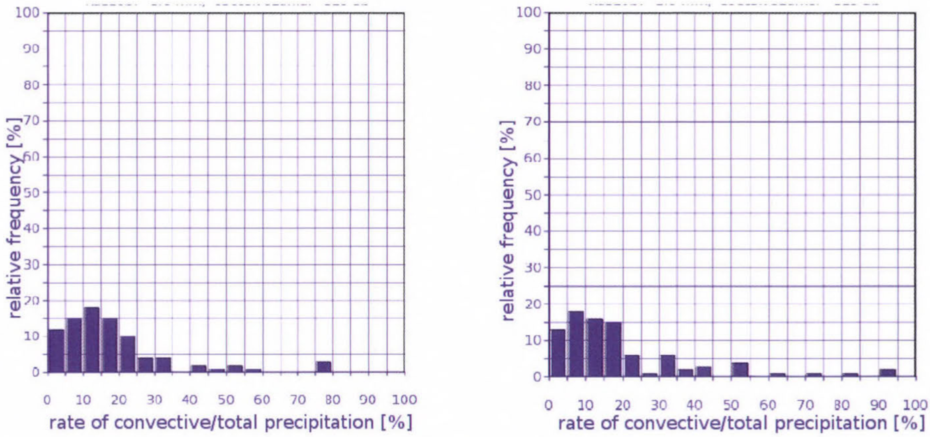

Fig. 3. Histograms for rate of the convective and total precipitation with 1 mm threshold for Budapest: (left) 00 UTC (116 cases), (right) 12 UTC (115 cases)

We also examined the similarity of the distribution curves with the help of the two-sample Kolmogorov-Smirnov test. We checked the condition whether the distribution functions of random examined variable corresponds to a specific distribution function. Consider the (ξ, η) as a random variable pair and ξ, η, n_1 and n_2 as thereof derived independent element patterns. Mark the distribution function of ξ as $F(x)$, the empirical distribution function calculated from the sample as $F_{n1}(x)$, and using the same method for the random variable η, mark its distribution function and empirical distribution function as $G(x)$ and $G_{n2}(x)$. Chosen probe attached to the probe test statistic:

$$D_{1,2} = \sqrt{\frac{n_1 - n_2}{n_1 + n_2}} \left(\sup \left| F_{n_1}(x) - G_{n_2}(x) \right| \right), \tag{2}$$

whereof (*Kolmogorov*, 1933, *Smirnov*, 1936):

$$P(D_{1,2} < x) = K(x), \tag{3}$$

where $K(x)$ is the limit distribution function. To define the range of acceptance, it is necessary to assign x_α values for the most important levels of significance (*Table 1*).

Table 1. x_α values for the most important levels of significance

A	0.1	0.05	0.001
x_α	1.23	1.36	1.63

We take the x_α values from the table of $K(x)$ distribution function, $K(x_\alpha) = 1-\alpha$. Our acceptance range of $(0, x_\alpha)$ interval is on the level of α significance. Thus, the null hypothesis is kept $0 \leq D_n < x_\alpha$. The null hypothesis is rejected when $D_n \geq x_\alpha$ (*Dévényi* and *Gulyás,* 1988).

As our value was about 2.1, it was found that in a 95% hypothesis test the distribution of the convective/total precipitation rates for 24 hours based on 00 and 12 UTC model runs are different. In both cases of the visual and statistical methods, the same conclusion was made.

In this chapter, three parameters (CAPE, wind shear, relative humidity) were examined with statistical methods which revealed their physical features. Long-period investigations showed the most frequent values and revealed the attributes of the above-mentioned parameters. Using these data in the case studies, the threshold values can be easily chosen. We studied the relationship between the CAPE values and the convective/total precipitation rate, therefore, the convective/total precipitation rate parameter was added to the examination. Thereafter, features of the convective/total precipitation rate were examined with various time and threshold values on histograms and with the Kolmogorov-Smirnov test too.

3. New comprehensive probabilistic approach to forecast convective events

As it has been mentioned, CAPE index, relative humidity, and vertical wind shear were investigated. Focusing on these three meteorological parameters, we studied potential opportunities of the ensemble forecasts with four newly developed graphical tools.

Two of the four visualization methods, the ensemble meteogram and the ensemble vertical profiles (*Ihász* and *Tajti,* 2011) were available at the beginning of our work. These two point forecast products have been operationally available at the Unit of Methodology Development of Hungarian Meteorological Service since 2011. Both methods show probability distributions of the meteorological parameters for the selected location.

On the ensemble meteogram you can see the probability of the CAPE index, the wind shear between 10 m and the 500 hPa level, and the average relative humidity between 850 and 500 hPa levels. The ensemble vertical profile is based on temperature, dew point, wind direction and speed at 91 ensemble model levels.

Additionally, we developed two new methods for studying convective events. The first method provides probability map of the event exceeding predefined thresholds. Probability of CAPE, wind shear, and relative humidity with other parameters are studied. Other parameters are the 500 hPa geopotential height, 300 hPa potential vorticity, and convective precipitation. Applying this approach we can study weather situations in more details. Intensity of the dangerous weather conditions can be well estimated. Intensive convective periods are clearly marked during the forecasting period. Another new visualization tool shows time evolution of predefined multiple thresholds in graphical form for any selected location. In our case studies, CAPE and wind shear with different thresholds were examined.

First of all, our aim was to study the probability maps, so we could identify the time and spatial location of the convective weather situation. Then we used multiple thresholds timeline diagrams in selected points, so we could see when the most extreme values of these parameters were predicted and how they changed in time. In the third part of our study we investigated the evolution of the vertical properties of the atmosphere in time. In the end, we studied the relationships among these three parameters with ensemble meteograms. We studied the day-to-day consistency of the forecasts too, so the analyzed period was between day –4 and day –1 before the event.

Horizontal resolution of the numerical models are regularly increased (*Horányi et al.,* 2011, *Szintai et al.,* 2015). In spring 2016, ECMWF increased the horizontal resolution of the high resolution (deterministic) model from 16 km to 9 km. At the same time, the horizontal resolution of the ensemble model changed from 32 km to 18 km. After 2020 running of global non-hydrostatic models would be necessary (*Wedi* and *Malardel*, 2010). These developments will likely cause increasing reliability of the forecasts in heavy convective situations too.

In this chapter, new applied visualization tools were presented. We intended to explore their applicability in forecast situations, therefore case studies were investigated. A selected case study is presented in the next chapter.

4. Case study of heavy convective events

During our former studies (*Lázár,* 2013), comprehensive case studies were done. Weather situations representing different type of convective events were selected in summer 2012. In this paper, weather situation of July 29, 2013 is presented, this event followed the hottest period of summer 2013. On July 29, 2013 lots of thunderstorms were observed in Hungary (*Horváth* and *Kolhmann*, 2013).

It was a really hot weather situation when new record maximum temperatures were registered before a thunderstorm line reached Hungary. In front of the cold front, the temperature had been increasing and 23 °C appeared at the 850 hPa level. In Western Europe, intense thunderstorms connected to the cold front were erupted. Around 20 UTC, the upper air cold front with stormy winds (60–80 km/h) reached the Transdanubian Region from southwest direction. In the early hours of July 29, the northwestern cold front arrived in the lowest levels.

During our study, first the probability maps were examined, forecasts of day –4 to day –1 were used (*Fig. 4*). The investigated time was July 29, 2013, 21 UTC, so the studied forecasts were made on the following three consecutive days: July 26, 27, 28, 2013, 00 UTC. High probability of high CAPE values could be seen in the northwestern part of the country. The local maximum of the potential vorticity was located northwest to this area. A pair of ridge and trough was connected to this region too, the latest forecast showed stronger contrast between the ridge and trough.

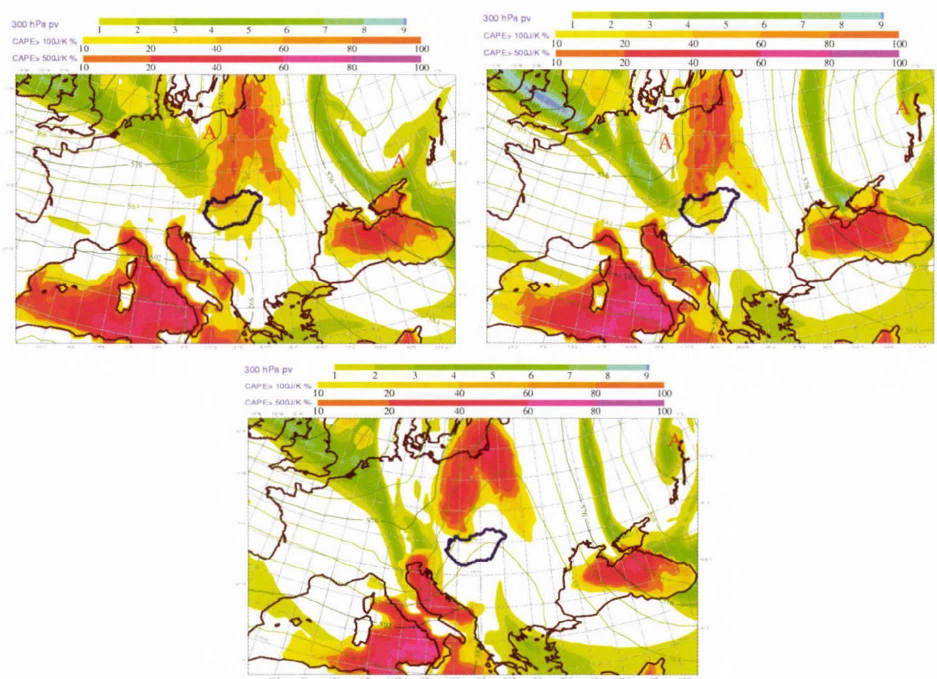

Fig. 4. Forecast of the CAPE probability (shaded yellow to pink), potential vorticity values (shaded green to blue), and 500 hPa height fields (green lines) at July 29, 2013, 21 UTC (by forecast of July 26, 2013, 00 UTC + 93 hours, July 27, 2013, 00 UTC +69 hours, and July 28, 2013, 00 UTC +45 hours)

At the second step, particular locations, like Szombathely were selected, where the time evolution of the predefined multiple thresholds of CAPE values was studied. The most dangerous time period, early late afternoon was predicted in every model run. Intensity of the probabilities was changed from model run to model run (*Fig. 5*).

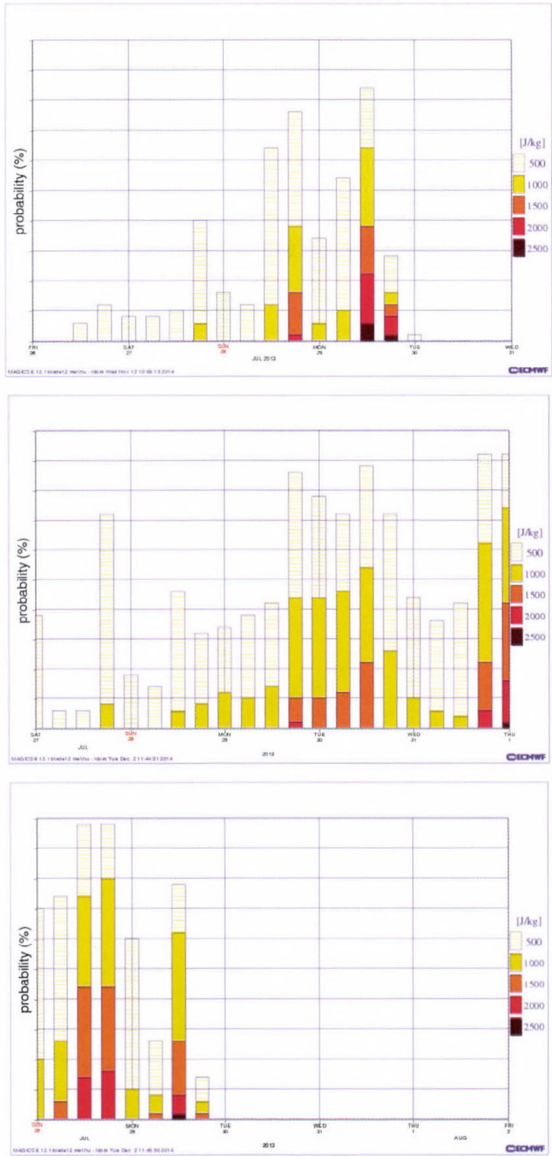

Fig. 5. Time evolution of predefined multiple thresholds of CAPE values (the thresholds: 500 (yellow dot), 1000 (yellow), 1500 (orange), 2000 (red) and 2500 (brown) J/kg) based on modeled values of July 26, 27, 28, 2013 for Szombathely.

The third studied diagram was the ensemble vertical profile for the selected location (*Fig. 6*). It can be clearly seen, that the lower troposphere was relatively dry, and between 700 and 300 hPa an extended wet layer could be found which supported the possibility of severe convective events.

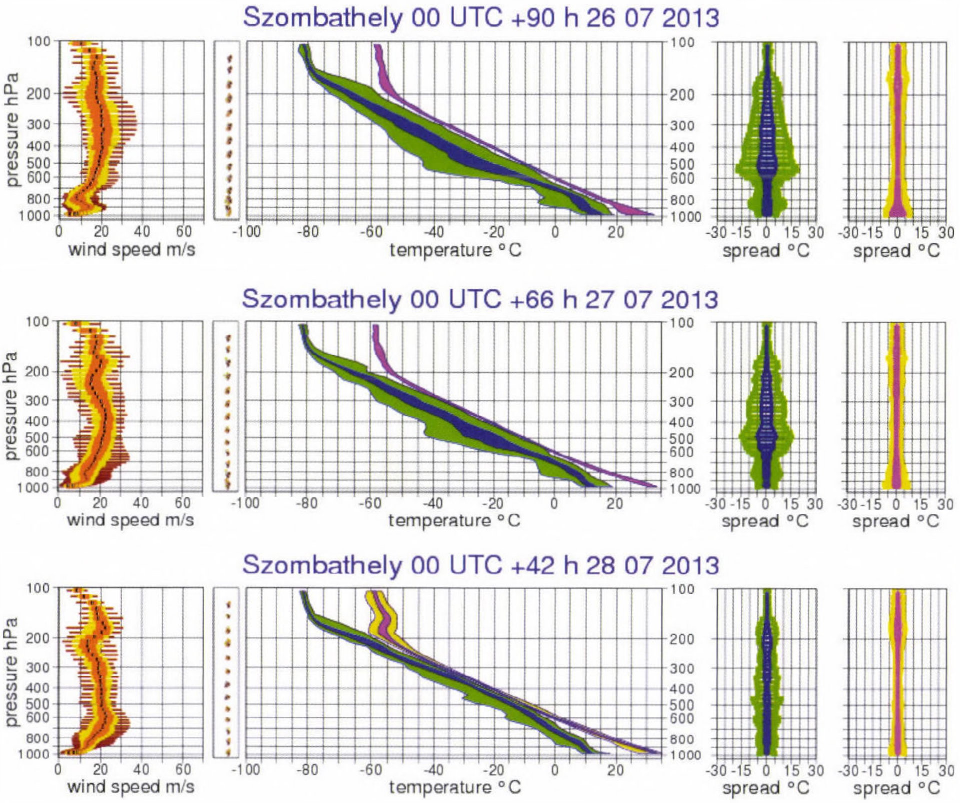

Fig. 6. Ensemble vertical profiles based on model runs of 00 UTC July 26, 27, 28, 2013 for Szombathely

Finally, we studied the ensemble meteograms of these three parameters (*Fig. 7*). In the forecast of July 27, 00 UTC, it could be seen that the probabilities of the CAPE and wind shear were increasing gradually until the evening of July 29. Probabilities of the relative humidity were decreasing gradually until the evening of July 29. After July 30, the CAPE values were near to zero, the intensity of the wind shear decreased, and the relative humidity increased. This statement could be seen in the forecast of July 28, 00 UTC, but it was not so much strong as in the forecast of July 27, 00 UTC.

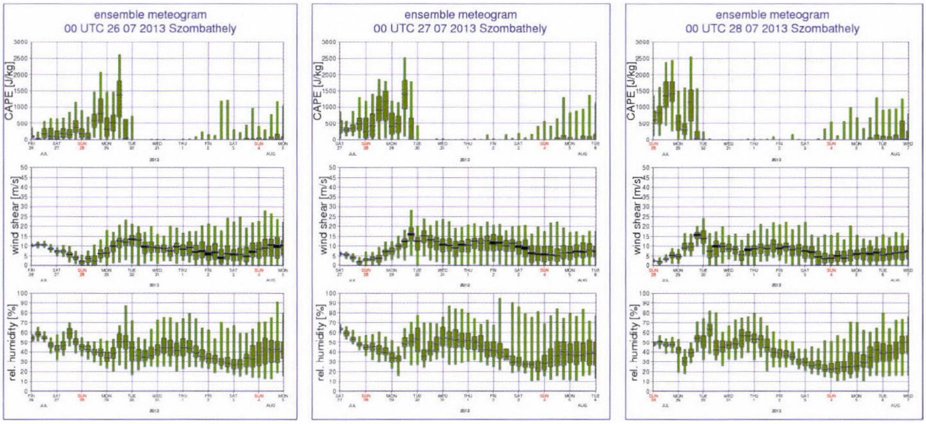

Fig. 7. Ensemble meteograms of CAPE (top), wind shear (middle), relative humidity (bottom) of July 26, 27, 28, 2013 for Szombathely.

5. Summary and conclusions

In this paper, it was shown how important it is to forecast the probability of the dangerous weather situations as precisely as possible. We attempted to provide a combination of new probabilistic tools for supporting successful forecasts of dangerous weather situations. Four graphical probabilistic methods were applied for three meteorological parameters, which are CAPE, wind shear, and relative humidity. It can be stated that wind shear is the most predictable parameter. Relative humidity has more uncertainty, but mostly it can be characterized as a respectable parameter. The medium-term forecast of CAPE index is not always successful, but with other fields it can provide useful extra information in the operational forecast. In the future, this new complex approach can be used for high resolution hydrostatic and nonhydrostatic ensemble models, as ALADIN and AROME.

References

Barkmeijer, J, Buizza, R., Kallen, E., Molteni, E., Mureau, R., Palmer, T., Tibaldi, S., and *Tribia, J.,* 2012: 20 years of ensemble prediction at ECMWF. *ECMWF Newsletter 134*, 16–32.

Craven, J.P. and *Brooks, H.E*, 2002: Baseline climatology of sounding derived parameters associated with deep moist convection. Proceeding of The 21st Conference on Severe Local Storms and 19th Conference on Weather Analysis and Forecasting/15th Conference on Numerical Weather Prediction. San Antonio, TX, 11-16 August 2002.

ECMWF, 2016: The ECMWF Strategy, 2016-2025, Reading, United Kingdom, 13.

Dévényi, D. and *Gulyás, O.*, 1988: Matematikai statisztikai módszerek a meteorológiában. Tankönyvkiadó, Budapest, 235-236. (in Hungarian)

Horányi, A., Mile, M., and *Szűcs, M.,* 2011: Latest developments around the ALADIN operational short-range ensemble prediction system in Hungary, *Tellus 63A*, 642–651.

Horváth, Á. and *Geresdi, I.*, 2001: Severe convective storms and associated phenomena in Hungary. *Atmos. Res. 56*, 127–146.

Horváth, Á., 2007: The ingredients of atmospheric convection. *In A légköri konvekció.* Hungarian Meteorological Service. Budapest, 4–17. (in Hungarian)

Horváth, Á. and *Kohlmann, M.*, 2013: Egy forró periódus vége. Hungarian Meteorological Service. July 31. 2013. (http://www.met.hu). (in Hungarian)

Ihász, I. and Tajti, D., 2011: Use of ECMWF's ensemble vertical profiles at the Hungarian Meteorological Service. *ECMWF Newsletter 129,* 25–29.

Kolmogorov, A.N., 1933: Sulla determininazione empirica di una legge, *Giornale dell' Instituto Italiano degli Attuari 4*, 83–91. (in Italian)

Molteni, F.R., Buizza, T.N., Palmer, T.N., and *Petroliagis*, 1996: The ECMWF ensemble prediction system: methodology and validation. *Q.J.Roy. Meteorol. Soc. 122*, 37–119.

Smirnov, N.V., 1936: Sui la distribution w2 (Criterium de M.R.v Mises), *Comptes Rendus*, Paris, 202, pp. 449-452. (in French)

Palmer, T.N., 2006, Predictability of Weather and Climate from theory to practice. In (*Eds.: Palmer, T.N. and Hagedorn, R.*) Predictability of Weather and Climate, Palmer and Hagedorn, Cambridge Univ, Press, 1–29.

Persson, A. and *Riddaway, B.*, 2011: Increasing trust in medium-range weather forecasts. *ECMWF Newsletter 129,* 8–12.

Lázár, D., 2012: Valószínűségi előrejelzések alkalmazhatósága a nyári konvektív időjárási helyzetekben. Master Thesis, Eötvös Loránd University, Budapest. (in Hungarian)

Szintai, B., Szűcs, M., Randriamampianina, R., and *Kullmann, L.*, 2015: Application of the AROME non-hydrostatic model at the Hungarian Meteorological Service: physical parameterizations and ensemble forecasting. *Időjárás 119*, 215–241.

Wedi, N. and *Malardel, S.*, 2010: Non-hydrostatic modelling at ECMWF. *ECMWF Newsletter 125,* 17–21.

IDŐJÁRÁS

Quarterly Journal of the Hungarian Meteorological Service
Vol. 120, No. 4, October – December, 2016, pp. 395–414

Impact of atmospheric circulation on the occurrence of heat waves in southeastern Europe

Arkadiusz M. Tomczyk

Department of Climatology, Adam Mickiewicz University in Poznań,
Dzięlgielowa 27, 61-680 Poznań, Poland
E-mail: atomczyk@amu.edu.pl

(Manuscript received in final form May 31, 2016)

Abstract—The main objective of this article is to identify the pressure conditions conducive to the occurrence of heat waves in southeastern Europe. Before this objective could be achieved, the spatial and temporal variability of the occurrence of heat waves in the region were determined. This article defines a hot day as a day of maximum temperature (Tmax) above the 95th annual percentile, and a heat wave is considered to be a sequence of at least 5 such days. The study is based on the data of 21 stations from the period 1973–2010. In the discussed period, at all stations, a statistically significant increase in Tmax and the number of hot days were observed. The total number of heat waves fluctuated from 25 in Burgas to 48 in Drobeta-Turnu Severin, Skopje, and Split, while the sum durations of heat waves ranged between 173 days in Botosani and 414 in Split. Heat waves in southeastern Europe occurred most often when a ridge of high pressure lay over Europe. This system caused the inflow of continental air masses from the northeast or east. An alternative source of air masses causing heat waves was advection from the south.

Key-words: heat waves, atmospheric circulation, climate change, southeastern Europe

1. Introduction

One of the most important factors determining weather and climate conditions is atmospheric circulation (*Chromow,* 1952; *Niedźwiedź,* 1981; *Yarnal,* 1993). In particular, high pressure systems and blocking situations, which determine the meteorological conditions of a particular region by breaking zonal circulation, are of great importance (*Bielec-Bąkowska,* 2014). The consequence of such patterns is the occurrence of heat waves in summer and frost waves in winter

(*Porębska* and *Zdunek,* 2013; *Bielec-Bąkowska,* 2014). The impact of atmospheric circulation on thermal conditions and the occurrence of thermal extremes has been the subject of many studies (*Founda* and *Giannakopoulos,* 2009; *Avotniece et al.,* 2010; *Ustrnul et al.,* 2010; *Kažys et al.,* 2011; *Porębska* and *Zdunek,* 2013; *Tomczyk* and *Bednorz,* 2014; *Unkašević* and *Tošić,* 2015; *Tomczyk* and *Bednorz,* 2016). Further and more detailed research is required into the importance of circulation, and above all its changes, both global and local, as well as from both a holistic perspective and a perspective taking its particular elements into consideration (*Bielec-Bąkowska,* 2014).

According to the authors of the Fifth IPCC Assessment Report (2013), in each of the last three decades, at the Earth's surface temperature was higher than in the preceding decade and, simultaneously, higher than in any previous decade since 1850; in the Northern Hemisphere, the period of 1983–2012 was probably the warmest 30-year period in the last 1400 years. One manifestation of the observed warming is the increasing frequency of extremely hot days and heat waves (*Avotniece et al.,* 2010; *Kyselý,* 2010; *Shevchenko et al.,* 2014; *Keggenhoff et al.,* 2015; *Unkašević* and *Tošić,* 2015; *Tomczyk* and *Bednorz,* 2016; *Tomczyk et al.,* 2016), with the simultaneous decrease in frost days and frost waves (*Kejna et al.,* 2009; *Avotniece et al.,* 2010; *Bednorz,* 2011; *Mužíková et al.* 2011; *Niedźwiedź et al.,* 2012; *Krzyżewska,* 2014; *Migała et al.,* 2016). The heat waves from 2003 to 2010, defined as "mega heat waves," caused more than 500-year records for seasonal air temperatures across approximately 50% of the area of Europe (*Barriopedro et al.,* 2011).

In recent years, there has been an increase in the number of publications concerning extreme weather phenomena, including heat waves. These publications have largely focused on determining the influence of heat waves on the number of deaths caused by biometeorological conditions affecting human body systems (*Johnson et al.,* 2005; *Poumadere et al.,* 2005; *Paldy* and *Bobvos,* 2009; *Shaposhnikov et al.,* 2014; *Bobvos et al.,* 2015; *Revich et al.,* 2015). Despite these numerous scientific works, there is still a noticeable deficiency of scientific papers analyzing the occurrence of heat waves on the basis of long and uniform data series for the different regions of Europe. Therefore, the objective of this article was to determine the spatial and temporal variability of the occurrence of heat waves in southeastern Europe. However, the main emphasis of this article was to identify the atmospheric conditions conducive to the occurrence of heat waves in this part of Europe. The undertaking of this subject is especially relevant in light of forecasts which show that heat waves in the 21st century are going to be not only more frequent, but also longer and more intensive (*Meehl* and *Tebaldi,* 2004; *Beniston et al.,* 2007; *Koffi* and *Koffi,* 2008; *Kürbis et. al.,* 2009; *Kyselý,* 2010; *Pongracz et al.,* 2013; *Zacharias et al.,* 2015).

2. *Methods and data*

This article used daily values of the maximum (Tmax), minimum (Tmin), and mean air temperature (T) for 21 stations located in eight countries: Bulgaria, Croatia, Greece, Macedonia, Romania, Serbia, Slovenia, and Hungary (*Fig. 1*). The article defined this area simply as southeastern Europe. The data were obtained for the period of 1973–2010 from the freely accessible databases of the National Oceanic and Atmospheric Administration (NOAA).

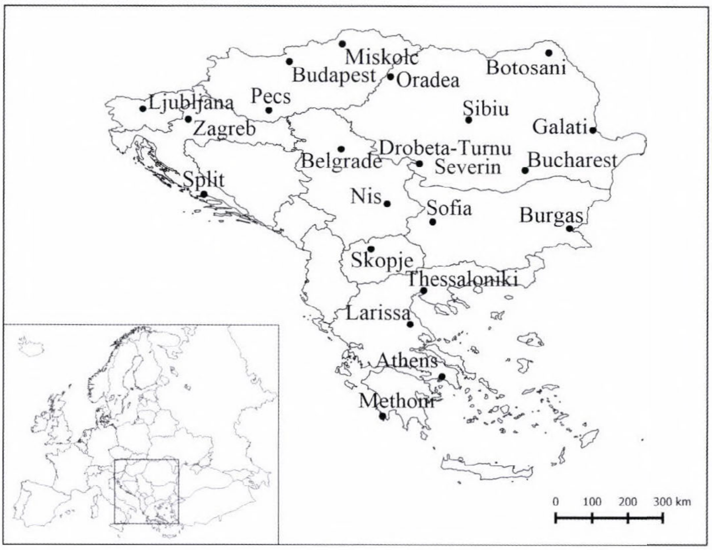

Fig. 1. Locations of the meteorological stations.

This article defines a hot day as a day with Tmax above the 95th annual percentile (*Fig. 2a*), and a heat wave (HW) is considered to be a sequence of at least 5 hot days. This assumption is based on the definition of an extreme weather event included in the IPCC reports (2007), according to which, a weather phenomenon is defined as an extreme weather event if it is so rare within a particular area and in a particular season that it lies within the range of the 10th or 90th percentile of an observed probability density function, or rarer. This definition of a HW has been used in articles concerning, among others, the occurrence of HWs in central Europe (*Tomczyk* and *Bednorz,* 2016) and northern Europe (*Tomczyk et al.,* 2016).

The literature offers equal definitions of HWs which differ in methodological assumptions. According to *Krzyżewska* (2010), this results from the fact that distinguishing HWs is most of all dependent on local climatic conditions, which change with latitude, height above sea level, and direction of air mass inflow. HWs are defined as, among others: (1) a several-day period with the maximum or mean daily temperature above a specific threshold value (*Kyselý,* 2002; *Kosowska-Cezak,* 2010; *Bobvos et al.,* 2015); (2) a period with apparent temperature (AT) above the 95th percentile which starts with a minimum 2.0°C increase in relation to the preceding day (*Kuchcik* and *Degórski,* 2009); (3) a period >5 consecutive days with Tmax >5 °C above the 1961–1990 daily Tmax norm (*Frich et al.,* 2002; *Unkašević* and *Tošić,* 2009).

On the basis of the data, the mean Tmax of the particular months and summer seasons (June–August) was calculated, and hot days were selected to distinguish HWs. Additionally, Pearson's correlation coefficient was calculated between the mean Tmax in summer and the number of hot days. Subsequently, variability within the multiannual period and statistical significance ($p \leq 0.05$) were determined for the distinguished climatological characteristics.

In order to define pressure conditions conducive to the occurrence of HWs, daily values of atmospheric pressure at sea level (SLP), the height of the isobaric surface 500 hPa (z500 hPa), and the temperature on the isobaric surface 850 hPa (T850) were used. The data were obtained from the records of the National Center for Environmental Prediction/National Center for Atmospheric Research (NCEP/NCAR) Reanalysis (*Kalnay et al.,* 1996), which are available in Climate Research Unit resources. In the study, values of SLP and z500 hPa in 120 geographical grid points 2.5°×2.5° for the area of 25°–75°N latitude, 35°W–65°E longitude were used. On the basis of the above-mentioned data, the SLP, z500 hPa, and T850 maps for the summer season (June–August), as well as a collective map for hot days forming HWs were drawn up. The description was supplemented with the drawing up of maps of anomalies. Anomalies were calculated as differences between the mean SLP, z500 hPa, and T850 values for HWs and the mean summer values of these characteristics in the analyzed multiannual period. Only days on which the temperature met the criterion of a hot day in at least five stations were selected for analysis. The circulation types which cause the occurrence of HWs were distinguished by clustering days according to their values of sea-level pressure, using the minimum variance method known as Ward's method (1963). This method is based on Euclidean distances, and in essence involves merging the pair of clusters A and B which, after merging, provide the minimum sum of squares of all objects' deviations from the newly-created cluster's centre of gravity (*Ward,* 1963; *Wilks,* 1995). In order to achieve that, standardized SLP values were used. The standardization was made to deseasonalize the observations, while keeping the intensity of pressure field (*Esteban et al.,* 2005). Clustering methods (among others, Ward's method) are often applied in climatology, e.g., in distinguishing seasons and climatic regions, and identifying weather types (*Bednorz,* 2008; *Tomczyk* and *Bednorz,* 2016). The maps of SLP, z500 hPa, and T850, as well as maps of anomalies were drawn up for the identified circulation types. Additionally, for the selected days in the distinguished circulation types, there were 48-hour back trajectories of air particles traced by means of the NOAA HYSPLIT model (http://ready.arl.noaa.gov/HYSPLIT.php). Back trajectory analysis enables one to determine the area of origin of air masses on selected days, which constitutes a supplement to the information displayed by weather maps.

3. *Results*

3.1. Maximum temperature in the summer

In southeastern Europe, between 1973 and 2010, the mean Tmax in summer was 27.8 °C and ranged from 25.0 °C in Ljubljana to 32.4 °C in Larissa (*Fig. 2b*). In the analyzed period, at all stations the lowest mean Tmax was recorded for the years 1973–1980, and varied then from 23.6 °C in Sibiu to 31.8 °C in Larissa. Meanwhile, in 90% of the stations the highest mean Tmax was observed for the years 2001–2010, and ranged from 25.7 °C in Ljubljana to 33.0 °C in Larissa. Analysing the particular summer seasons, at 67% of the stations, the coldest summer season occurred in 1976, and at 24% of the stations it was in 1978. On the other hand, the warmest season at 52% of the stations was recorded in 2007, and at 43% of them in 2003. Deviation of the mean Tmax in the particular seasons from the mean for the analyzed multiannual period ranged from –4.1 °C in 1976 (Sofia, Skopje) to 4.5 °C in 2007 (Galati). The course of the mean Tmax in the analyzed years shows considerable year-to-year fluctuations. Within the majority of the area, the variability of the mean Tmax was similar, which is proven by its barely-diversified standard deviation values, falling within a range of 0.9–1.5 at 86% of stations. In the analyzed period, at all stations, a statistically significant increase in Tmax in summer was observed. These changes ranged from 0.4 °C/10 years in Thessaloniki to 1.2 °C/10 years in Sofia and Niš (*Fig. 2c*). The aforementioned changes were considerably influenced by an increase in Tmax in the first decade of the 21st century, when Tmax generally exceeded the norm for the 1973–2010 multiannual period. In summer, the highest increase in Tmax was observed in August and, on average, it was 0.9°C/10 years for the analyzed area. In that month, the highest increase was recorded in Sofia, and it was 1.5 °C/10 years.

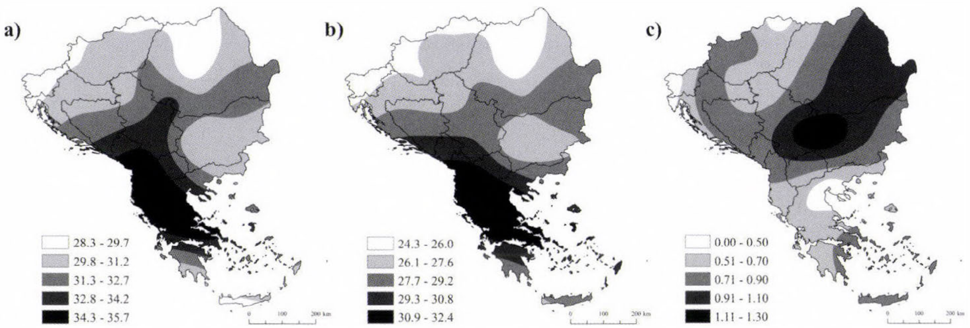

Fig. 2. The value of the 95th annual percentile of the Tmax (°C) (a); the mean Tmax (°C) in the summer (June–August) (b); and changes in the mean summer Tmax in °C/10 years during the period 1973-2010 (c).

3.2. Hot days

In southeastern Europe, the observed increase in Tmax translated into an increase in the number of hot days and, consequently, into an increase in the frequency of occurrence of HWs. At all stations, the coefficient of correlation between the mean Tmax in summer and the number of hot days fluctuated around 0.84–0.93. The average number of hot days in the summer season in the analyzed area was 18. At 95% of the stations, the lowest number of days of the aforementioned category was recorded in the 1973–1980 multiannual period, and their average number ranged from 4 days in Niš to 14 days in Thessaloniki. On the other hand, at 90% of the stations the highest number of hot days occurred in the first decade of the 21st century—then, the average number of hot days varied from 18 days in Oradea to 30 days in Bucharest and Split. When analyzing the particular summer seasons, it was found that at 80% of the stations, the lowest number of hot days—or even zero hot days—were recorded in 1976 or 1978. On the other hand, the highest number of days of the analyzed category was specific for 2003 and 2007, at 33% and 29% of the stations, respectively. In the analyzed period, the maximum number of the days recorded in one year was 57, and it was observed in 2003 in Zagreb and Methoni (*Fig. 3*). In the analyzed period, in southeastern Europe, there was an average increase in observed hot days, which was 6.2 days per 10 years, and it was statistically significant. This increase was not uniform across the analyzed area; changes ranged from 3.5 days/10 years in Miskolc and Larissa, to 8.4 days/10 years in Bucharest, and were statistically significant in all stations (*Fig. 3*). Hot days were recorded from April to November; still, the highest number of those days occurred in July and August, with 38.6% and 38.2% of all hot days, respectively. At 57% of the stations, the highest number of the above-mentioned days was found in July, while at the rest of the stations it was August. The earliest occurrence of a hot day was as early as 6 April (1998, Bucharest, Galati), and the latest one was November 5 (1980, Methoni); therefore, for the whole analyzed area, the potential period of the occurrence of hot days was 214 days.

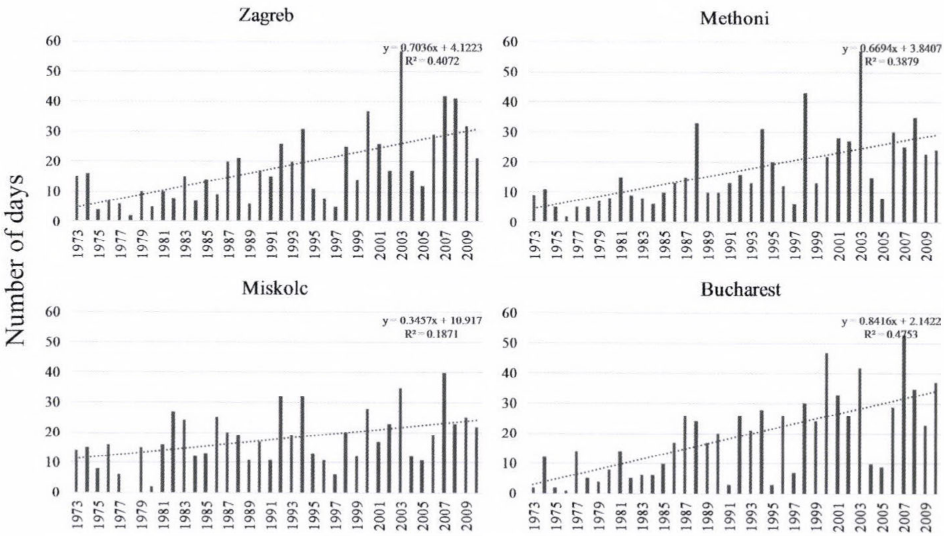

Fig. 3. Multi–year series of the annual number of hot days with the trend line and regression equation at selected stations.

3.3. *Heat waves*

In southeastern Europe, in the analyzed multiannual period, the total number of HWs ranged from 25 in Burgas to 48 in Drobeta-Turnu Severin, Skopje, and Split. On the other hand, the total duration of HWs ranged from 173 days in Botosani to 414 in Split. In 90% of stations, the fewest—or even zero—HWs were recorded between 1973 and 1980. Within this period, there were no HWs observed in four stations (that is, Botosani, Burgas, Galati, and Methoni), whereas the most waves were observed in Thessaloniki (seven waves), and their total duration was 39 days (*Fig. 4*). On the other hand, at 62% of the stations, the highest number of HWs was recorded between 2001 and 2010. At that multiannual period, the number varied between 7 (Oradea) and 23 (Split). In

14% of stations, the same number of waves was found both in the 1991–2000 period and the 2001–2010 period; still, in the first decade of the 21st century the waves were longer.

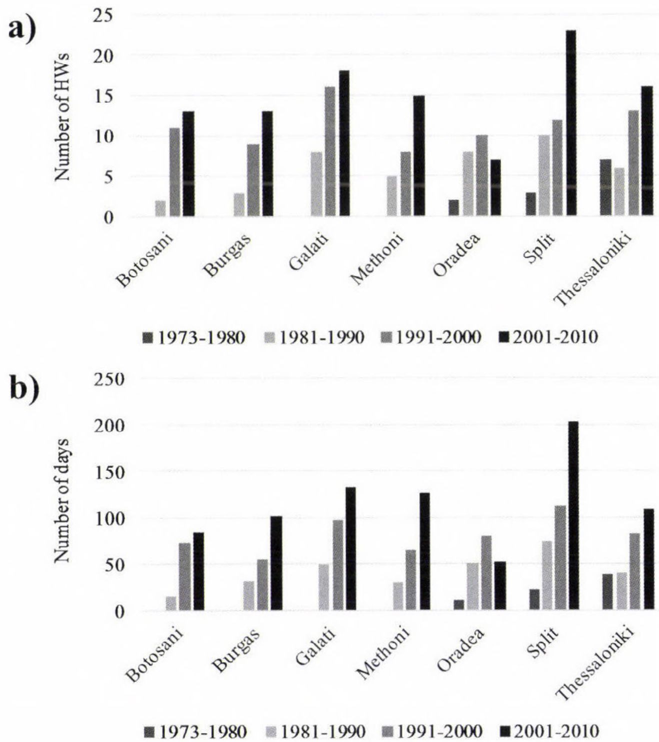

Fig. 4. The number of HWs (a) and the duration of HWs (b) in 1973–2010 at selected stations.

In the analyzed multiannual period in southeastern Europe, HWs occurred from May to September. At 62% of the stations, the highest number of HWs was recorded in August; in the case of two stations, the same number of waves was found in July and August. May HWs (four cases) only occurred in the last decade of the analyzed multiannual period. The earliest HW was recorded in Sibiu on May 7–13, 2003, while the latest, in Sofia and Skopje, were recorded on September 7–15, 1994 and September 9–15, 1994, respectively. The above-mentioned data show that the potential period of the occurrence of HWs within the particular area was 133 days, from May 7 to September 15. In the particular stations, the duration of this period ranged from 64 days in Burgas (from June 22 to August 24) to 125 days in Sibiu (from May 7 to September 8).

At 81% of the stations, the most HWs were 5-day-long, while at 9% of the stations, there were 6-day waves. 7-day waves were most numerous only in Botosani. Meanwhile, in Sofia, 5- and 6-day waves had a similar frequency. Apart from three stations (Botosani, Burgas, Split), 5- and 6-day waves constituted over 50% of all the recorded waves, and at three stations (Belgrade, Miskolc, Niš), they even constituted over 70%. The longest HW was observed in Methoni, and lasted as long as 38 days, from July 28 to September 3, 2003.

The mean Tmax during the analyzed HWs was 34 °C, while Tmin was 18.8 °C. The highest average Tmax was observed during HWs in Larissa (July 3–9, 2000) and was 40.6 °C. Moreover, at that station, there were four HWs found with a mean Tmax above 40 °C; namely, in 1982, 1987, 1998, and 2007 (*Table 1*). HWs with a mean Tmax above 40 °C were also observed in Niš and Skopje. On the other hand, the highest mean Tmin was found in Athens (July 5–10, 1988), and was 27.1 °C, while the lowest was in Ljubljana (13–17 August 1993) with an average of only 10.7 °C. In the analyzed multiannual period, a statistically significant increase in Tmax during HWs was found at only two stations, while in the case of Tmin, these changes were recorded at seven stations.

Table 1. Occurrence of heat waves with a mean Tmax above 40 °C (their duration and average Tmax) in southeastern Europe between 1973 and 2010

Station	Date	Tmax
Larissa	July 3–9, 2000	40.6 °C
	June 24–28, 1982	40.4 °C
	July 18–27, 1987	40.3 °C
	June 30–July 4, 1998	40.1 °C
	June 19–28, 2007	40.1 °C
Niš	July 15–24, 2007	40.2 °C
Skopje	July 18–26, 1987	40.1 °C

3.4. *Impact of circulation on the occurrence of heat waves*

The occurrence of HWs (424 days) in southeastern Europe in the analyzed period was connected, on average, with an extensive ridge of high pressure lying across the continent and reaching as far as eastern Europe. Over the analyzed area, SLP ranged from approximately 1008 to 1016 hPa (*Fig. 5a*). Apart from the northwestern and southern part of the analyzed area, positive anomalies up to > 1 hPa were recorded in the east (*Fig. 5b*). The described system caused an inflow of air masses from the northeast and east. Contour lines of the isobaric surface 500 hPa over southeastern Europe bent northeastward, creating its elevation over the analyzed area, which confirms the settling of warm air masses over this part of the continent. The pattern of z500 hPa contour lines shows western and southwestern air flow in the middle troposphere layer. The described conditions were accompanied by T850 positive anomalies, which fluctuated from 2 to >4 °C over the analyzed area (*Fig. 5c*).

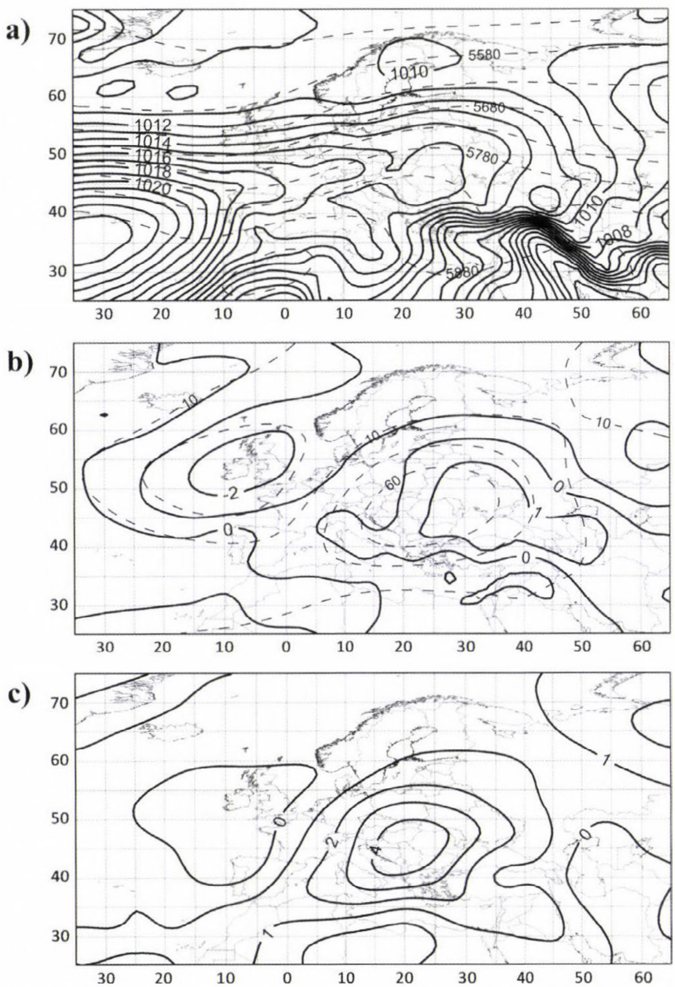

Fig. 5. SLP and z500 hPa (a), SLP and z500 hPa anomalies (b), and anomalies of T850 (c) for the HWs days.

The above-mentioned maps only display pressure conditions which cause the occurrence of HWs in southeastern Europe. However, individual HWs might be caused by different synoptic situations; therefore, the next step consisted in clustering HWs days by SLP, in order to distinguish circulation types. On this basis, two circulation types conducive to the occurrence of HWs within the analyzed area were distinguished. 324 hot days were classified as type 1. On those days, there was a ridge of high pressure settled over Europe, within which, there was a local high-pressure area (>1017 hPa) over the eastern part of the analyzed area (*Fig. 6a*). SLP positive anomalies occurred over the majority of the continent. Over the analyzed area, SLP was higher than the summer average, from approximately 0 to over 2 hPa in the east (*Fig. 6b*). The centre of anomalies was located over central Ukraine, and these exceeded 3 hPa. The described conditions were accompanied by z500 hPa positive anomalies, which fluctuated from 20 to over 90 gpm over southeastern Europe. The presence of warm air masses is also confirmed by T850 positive anomalies, which were from 1 to >4 °C over this part of the continent (*Fig. 6c*). The described system caused an inflow of dry, continental air masses from the northeast and east. This direction of air inflow was also shown by the traced 48-hour back trajectories of air particles for the selected days of this type (*Fig. 7*). All the trajectories showed settlement of air masses, which is typical of high pressure systems.

There were 100 days classified as type 2. The composite maps drawn up for these days show two main pressure systems over Europe, that is, a well-developed Azores High and a low with its centre over southern Scandinavia and Denmark (*Fig. 8a*). A weak pressure gradient occurred over the analyzed area. SLP negative anomalies were recorded over the continent, which ranged between –5 and –2 hPa over the analyzed area (*Fig 8b*). The presence of warm air masses was confirmed by z500 hPa positive anomalies. The settling air masses were warmer than in type 1, which is shown by T850 anomalies. The temperature on the isobaric surface 850 hPa was higher than the summer average by 1 to >6 °C (*Fig. 8c*). The described system caused an inflow of air masses from the southwest, from over northern Africa. This direction of air mass advection was confirmed by the traced back trajectories of air particles (*Fig. 9*). Most of the trajectories show rising air masses, which is typical for low-pressure systems.

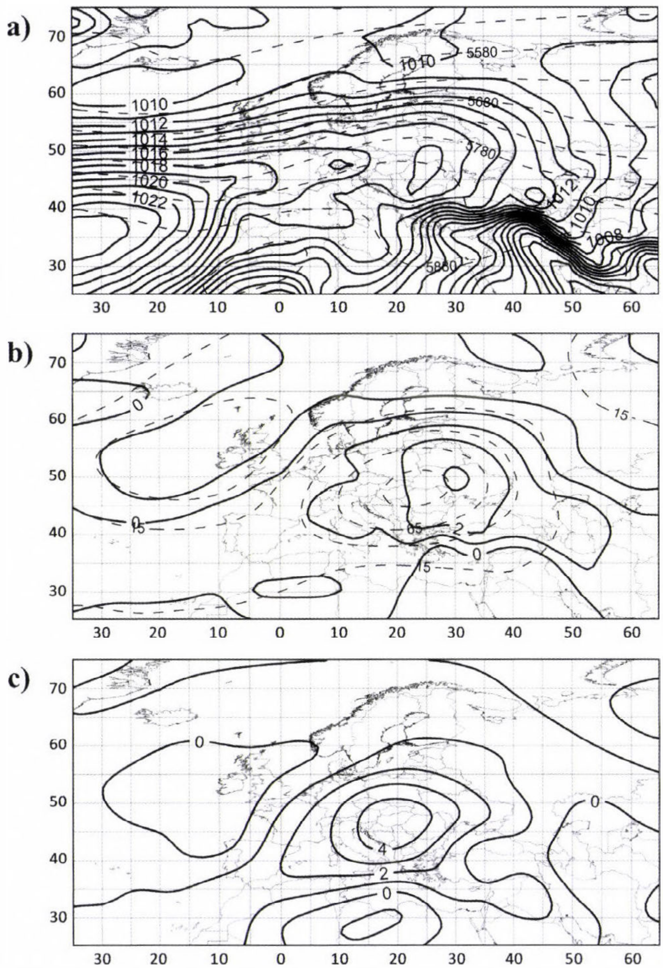

Fig. 6. Mean SLP and z500 hPa (a), SLP and z500 hPa anomalies (b), and anomalies of T850 (c) for the synoptic type 1 causing HWs.

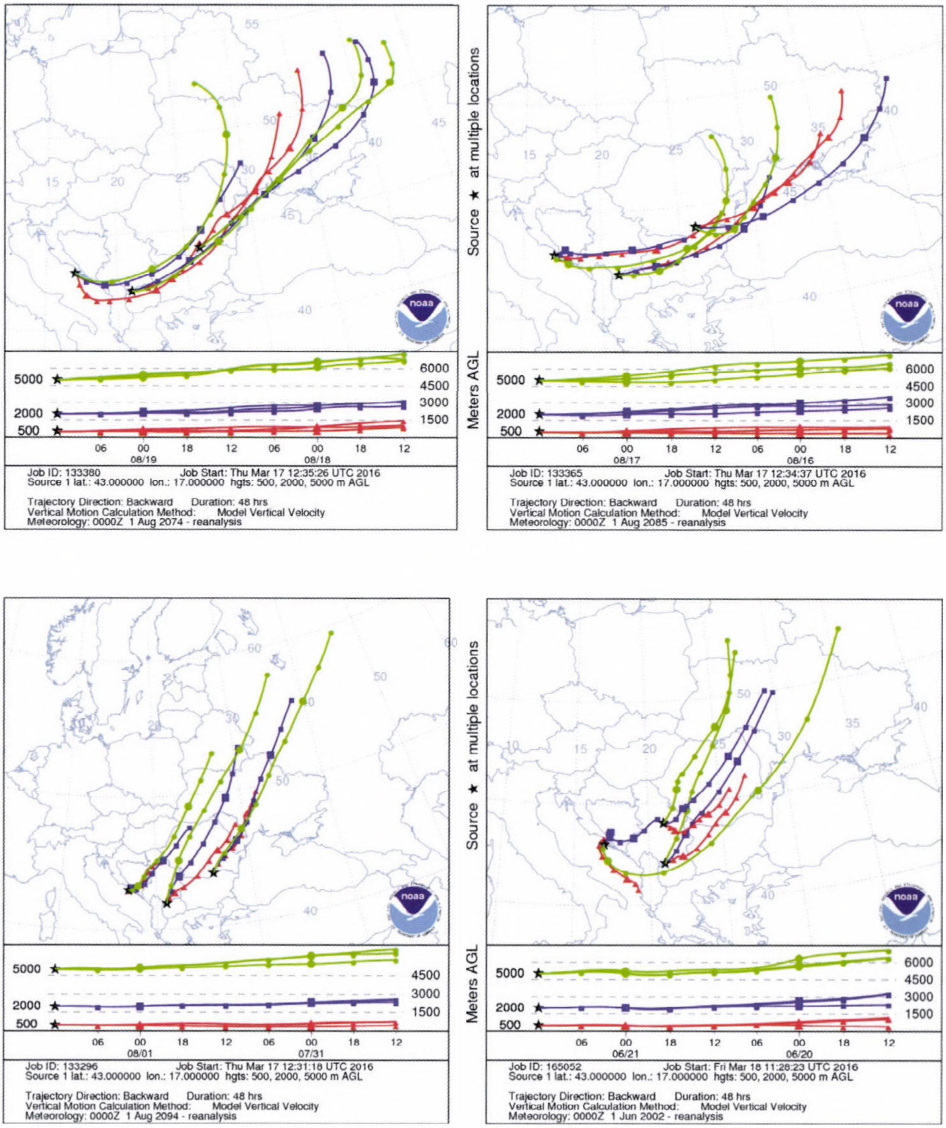

Fig. 7. 48-hour backward trajectories for the selected days in the synoptic type 1 causing HWs based on the reanalyses of the NOAA HYSPLIT model.

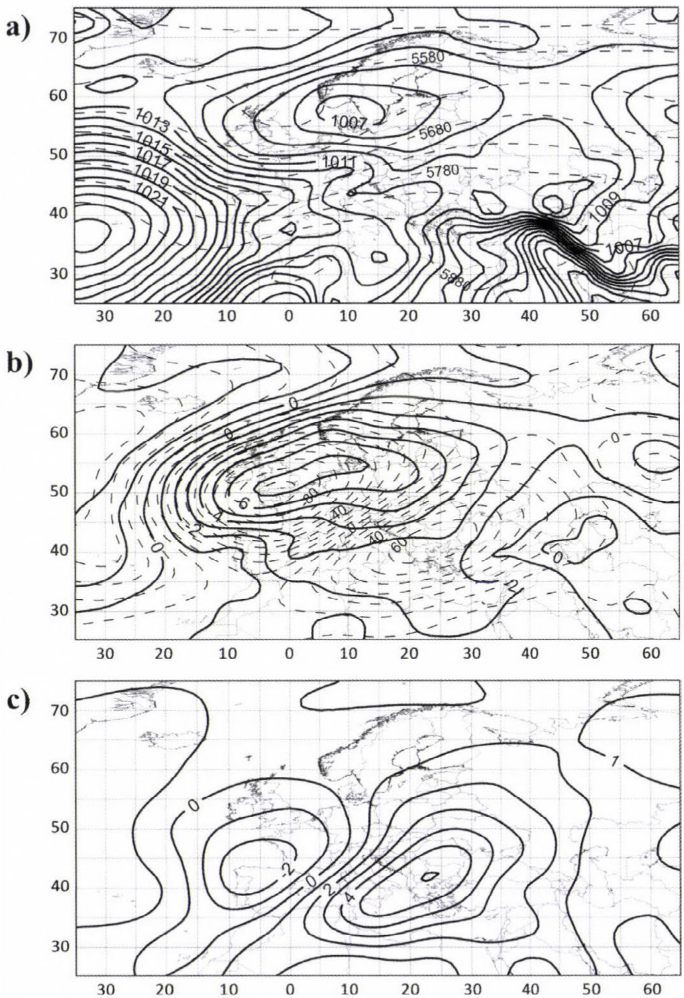

Fig. 8. Mean SLP and z500 hPa (a), SLP and z500 hPa anomalies (b), and anomalies of T850 (c) for the synoptic type 2 causing HWs.

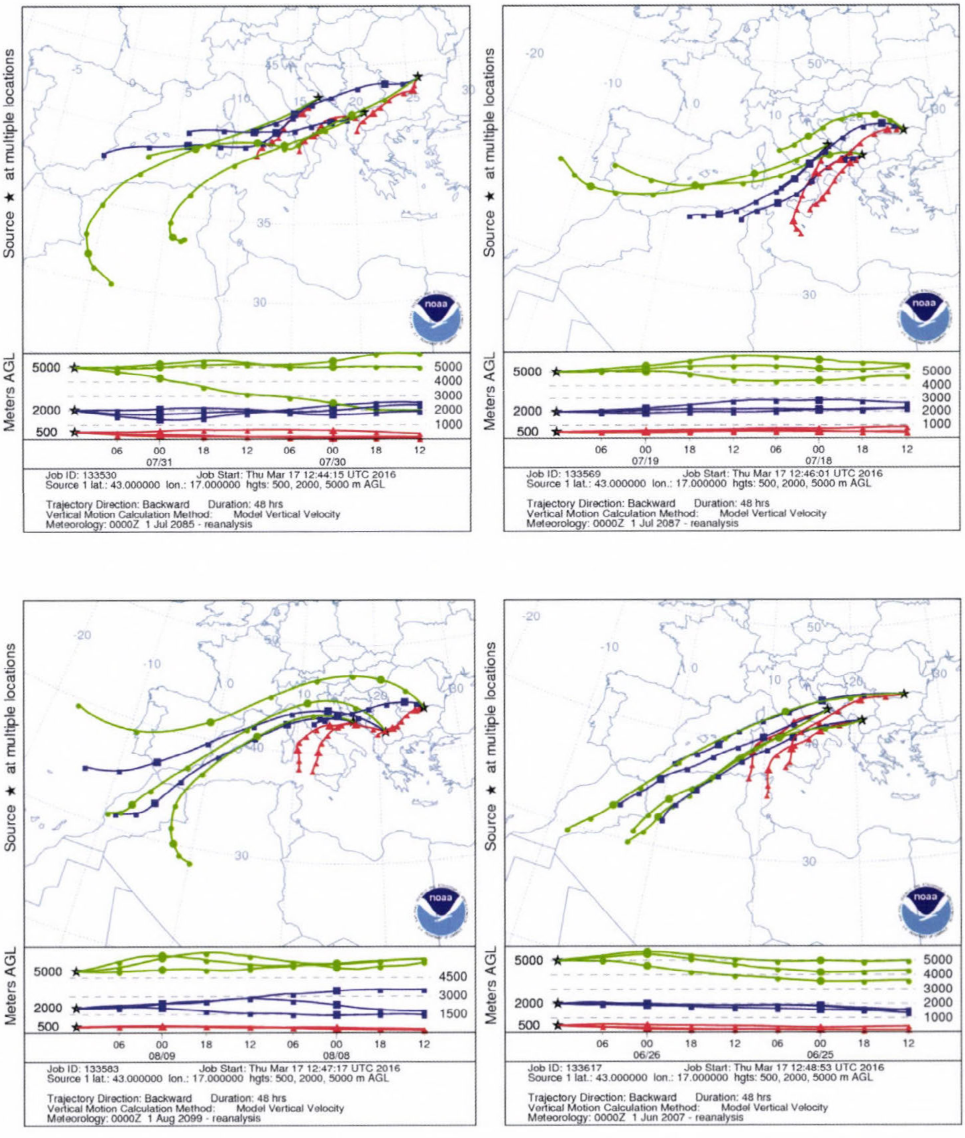

Fig. 9. 48-hour backward trajectories for the selected days in the synoptic type 2 causing HWs based on the reanalyses of the NOAA HYSPLIT model.

4. *Discussion and summary*

According to the research, in southeastern Europe between 1973 and 2010, there was an increase in Tmax in summer, which, averaged for the whole area, was 0.78 °C/10 years. A similar trend of changes in Tmax was also observed in central Europe (0.52 °C/10 years; *Tomczyk* and *Bednorz,* 2016) and northern Europe (0.38 °C/10 years; *Tomczyk et al.,* 2016). Within the analyzed area, similarly to other regions of Europe, the recorded increase was considerably influenced by changes in Tmax in the first decade of the 21st century, when Tmax generally exceeded the norm of the 1973–2010 multiannual period. The obtained results are consistent with previous research concerning air temperature changes in, among others, Greece (*Philandras et al.,* 2008; *Founda* and *Giannakopoulos,* 2009), Moldova (*Corobov et al.,* 2010), Romania (*Ionita et al.,* 2013), Serbia (*Bajat et al.,* 2015; *Unkašević and Tošić,* 2009), Slovenia (*de Luis et al.,* 2014; *Tošić et al.,* 2016), and the Mediterranean (*Efthymiadis et al.,* 2011).

The consequence of the increase in Tmax was an increasingly frequent occurrence of hot days and HWs. In the analyzed period, the rate of change in the number of hot days was 6.2 days/10 years. The observed changes are much more intensive than in central Europe (2.9 days/10 years; *Tomczyk* and *Bednorz,* 2016) and northern Europe (1.7 days/10 years; *Tomczyk et al.,* 2016). In the analyzed multiannual period, at most of the stations, both hot days and HWs were most numerous in the first decade of the 21st century. The obtained results are consistent with trends of changes found in Europe (*Gocheva et al.*, 2006; *Kyselý,* 2010; *Efthymiadis et al,* 2011; *Papanastasiou et al,* 2014; *Shevchenko et al.,* 2014; *Spinoni et al.,* 2015; *Unkašević* and *Tošić,* 2015; *Lakatos et al.,* 2016) and worldwide (*Batima et al.,* 2005; *Ding et al.,* 2010; *Pai et al.,* 2013; *Peterson et al.,* 2013; *Keggenhoff et al.,* 2015).

The occurrence of HWs in southeastern Europe was mostly connected with a well-developed ridge of high pressure settling over Europe, which caused an inflow of air masses from the northeast and east. Similar results were obtained by *Unkašević* and *Tošić* (2009) when they were analysing the occurrence of HWs in Serbia. The authors showed that HWs occurred most frequently during BM type according to the Grosswetterlagen (GWL) classification; therefore, with the presence of a ridge of high pressure over central Europe. Summer advection of continental air masses from the eastern sector also causes the occurrence of high temperatures and HWs in central Europe (*Wibig,* 2007; *Ustrnul et al.,* 2010; *Porębska* and *Zdunek,* 2013; *Tomczyk* and *Bednorz,* 2016).

The second circulation type conducive to the occurrence of HWs in southeastern Europe is connected with the occurrence of the Azores High over the continent and a low with its centre spreading from the North Sea to the Baltic Sea. Then, there was a weak pressure gradient recorded over the analyzed area. This situation was conducive to the advection of warm air masses from the south and southwest. A similar circulation type was identified by *Unkašević* and *Tošić* (2011), who investigated the HW of 2007 in Serbia. During HWs, T850 positive anomalies were also observed, which were higher in type 2, and this confirms that advection of air masses from the southern sector is related to higher temperatures within the analyzed area than to advection from the northeast and east. The obtained results are consistent with previous research studies which have proven that the occurrence of extreme temperatures in southern Europe is caused by the inflow of air masses from over North Africa (*Domonkos et al.*, 2003; *Gocheva et al.*, 2006; *Unkašević* and *Tošić*, 2009).

Acknowledgements: This work was supported by the Polish National Science Centre under grant number: UMO-2014/15/N/ST10/00717.

References

Avotniece, Z., Rodinov, V., Lizuma, L., Briede, A., and *Kļaviņš, M.,* 2010: Trends in the frequency of extreme climate events in Latvia. *Baltica 23,* 135–148.

Bajat, B., Blagojević, D., Kilibarda, M., Luković J., and *Tošić I.,* 2015: Spatial analysis of the temperature trends in Serbia during the period 1961–2010. *Theor. Appl. Climatol. 121*, 289–301.

Barriopedro, D., Fischer, E.M., Luterbacher, J., Trigo, R.M., and *García-Herrera R.,* 2011: The hot summer of 2010: redrawing the temperature record map of Europe. *Science 332*, 220–224.

Batima, P., Natsagdorj, L., Gomboluudev, P., and *Erdenetsetseg B.,* 2005: Observed climate change in Mongolia. *AIACC Working Paper 13*, 4–25.

Bednorz, E., 2008: Synoptic conditions of snow occurrence in Budapest. *Meteorologische Zeit. 17,* 39–45.

Bednorz, E., 2011: Occurrence of winter air temperature extremes in Central Spitsbergen. *Theor. and Appl. Climatol. 106*, 547–556.

Bielec-Bąkowska, Z., 2014: Silne wyże nad Europą (1951-2010). *Wydawnictwo Uniwersytetu Śląskiego*, Katowice, 219. (in Polish)

Beniston, M., Stephenson, D.B., Christensen, O.B., Ferro, C.A.T., Frei, C., Goyette, S., Halsnaes, K., Holt, T., Jylha, K., Koffi, B., Palutikof, J., Scholl, R., Semmler, T., and *Woth, K.,* 2007: Future extreme events in European Climate: An exploration of regional climate model projections. *Climatic Change 81*, 81–95.

Bobvos, J., Fazekas, B., and *Páldy, A.,* 2015: Assessment of heat-related mortality in Budapest from 2000 to 2010 by different indicators. *Időjárás 119, 2*, 143–158.

Chromow, S.P., 1952: Meteorologia i klimatologia, Warszawa, *PWN*, 488. (in Polish)

Corobov, R., Sheridan, S., Overcenco, A., and *Terinte, N.,* 2010: Air temperature trends and extremes in Chisinau (Moldova) as evidence of climate change. *Climate Res. 42*, 247–256.

Ding, T., Qian, W.H., and *Yan Z.W.,* 2010: Changes of hot days and heat waves in China during 1961–2007. *Int. J. Climatol. 30*, 1452–1462.

de Luis, M., Čufar, K., Saz, M.A., Longares, L.A., Ceglar, A., and *Kajfež-Bogataj, L.,* 2014: Trends in seasonal precipitation and temperature in Slovenia during 1951–2007. *Regional Environmental Change 14*, 1801–1810.

Domonkos, P., Kyselý J., Piotrowicz, K., Petrovic, P., and *Likso, T.,* 2003: Variability of extreme temperature events in south-central Europe during the 20th century and its relationship with large-scale circulation. *Int. J. Climatol. 23*, 987–1010.

Efthymiadis, D., Goodess, C.M., and *Jones, P.D.,* 2011: Trends in Mediterranean gridded temperature extremes and large-scale circulation influences. *Nat. Haz. Earth Sys. Sci. 11*, 2199–2214.

Esteban, P., Jones, P.D., Martin–Vide, J., and *Mases, M.,* 2005: Atmospheric circulation patterns related to heavy snowfall days in Andorra, Pyrenees. *Int. J. Climatol. 25*, 319–329.

Frich, P., Alexander, L.V., Della-Marta, P., Gleason, B., Haylock, M., Klein Tank, A.M.G., and *Peterson T.,* 2002: Observed coherent changes in climatic extremes during 2nd half of the 20th century. *Climate Res. 19,* 193–212.

Founda, D., and *Giannakopoulos, C.,* 2009: The exceptionally hot summer of 2007 in Athens, Greece–a typical summer in the future climate? *Glob. Planet. Change 67,* 227–236.

Gocheva, A., Trifonova, L., Marinova, T. and *Bocheva, L.,* 2006: Extreme Hot Spells and Heat Waves on the Territory of Bulgaria. Paper presented in Water Observation and Information System for Decision Support, 23 - 26 May 2006, Ohrid, Republic of Macedonia.

Ionita, M., Rimbu, N., Chelcea, S., and *Patrut, S.,* 2013: Multidecadal variability of summer temperature over Romania and its relation with Atlantic Multidecadal Oscillation. *Theor. Appl. Climatol. 113,* 305–315.

IPCC (2007) Climate change: The physical science basis. Contribution of Working Group I to the Fourth Assessment Report of the Intergovernmental Panel in Climate Change. Cambridge University Press, Cambridge.

IPCC (2013), Climate change: The physical science basis. Contribution of Working Group I to the Fifth Assessment Report of the Intergovernmental Panel in Climate Change, Cambridge University Press, Cambridge.

Johnson, H., Kovats, R.S., McGregor, G., Stedman, J., Gibbs, M., and *Walton, H.,* 2005: The impact of the 2003 heat wave on daily mortality in England and Wales and the use of Rapid Weekly Mortality Estimates. *Eurosurveillance 10, 7-9,* 168–171.

Kalnay, E., Kanamistu, M., Kistler, R., Collins, W., Deaven, D., Gandin, L., Iredell, M., Saha, S., White, G., Woollen, J., Zhu, Y., Leetmaa, A., Reynolds, R., Chelliah, M., Ebisuzaki, W., Higgins, W., Janowiak, J., Mo, K.C., Ropelewski, C., Wang, J., Jenne, R. and *Joseph D.,* 1996: The NMC/NCAR 40–Year Reanalysis Project. *Bull. Amer. Met. Soc. 77,* 437–471.

Každys, J., Stankūnavičius, G., Rimkus, E., Bukantis, A., and *Valiukas D.,* 2011: Long–range alternation of extreme high day and night temperatures in Lithuania. *Baltica 24, 2,* 71–82.

Keggenhoff, I., Elizbarashvili, M., and King, L., 2015: Heat Wave Events over Georgia since 1961: Climatology, Changes and Severity. *Climate 3,* 308–328.

Kejna, M., Araźny, A., Maszewski, R., Przybylak, R., Uscka-Kowalowska, J., and *Vizi, Z.,* 2009: Daily minimum and maximum air temperature in Poland in the years 1951–2005. *Bull. Geography – Physical Geography, Ser. 2/2009,* 35–56.

Koffi, B, and *Koffi, E.,* 2008: Heat waves across Europe by the end of the 21st century: multiregional climate simulations. *Climate Research 36,* 153–168.

Kossowska-Cezak, U., 2010: Fale upałów i okresy upalne - metody ich wyróżniania i wyniki zastosowania. *Prace Geograficzne 123,* 143–149. (in Polish)

Krzyżewska, A., 2010: Fale upałów jako zjawisko ograniczające turystykę w dużych miastach świata. *Krajobrazy rekreacyjne – kształtowanie, wykorzystanie, transformacja. Problemy Ekologii Krajobrazu XXVII,* 239–244. (in Polish)

Krzyżewska A., 2014: Warm and cold waves in South-Eastern (V) bioclimatic region in years 1981-2010. *Annales UMCS, Geographia, Geologia, Mineralogia et Petrographia 69, 2,* 143–154.

Kuchcik, M., and *Degórski, M.,* 2009: Heat– and cold–related mortality in the north–east of Poland as an example of the socio–economic effects of extreme hydrometeorological events in the Polish Lowland. *Geographia Polonica 82,* 1, 69–78.

Kürbis, K., Mudelsee, M., Tetzlaff, G., and *Brázdil R.,* 2009: Trends in extremes of temperature, dew point, and precipitation from long instrumental series from Central Europe. *Theor. Appl. Climatol. 98,* 187–195.

Kyselý, J., 2002: Temporal fluctuations in heat waves at Prague–Klementinum, the Czech Republic, from 1901–1997 and their relationships to atmospheric circulation. *Int. J. Climatol. 22,* 33–50.

Kyselý, J., 2010: Recent severe heat waves in central Europe: how to view them in a long–term prospect? *Int. J. Climatol. 30,* 89–109.

Lakatos, M., Bihari, Z., Szentimrey, T., Spinoni, J., Szalai, S., 2016: Analyses of temperature extremes in the Carpathian Region in the period 1961–2010. *Időjárás 120,* 41-51.

Meehl, G.A., and *Tebaldi C.,* 2004: More intense, more frequent, and longer lasting heat waves in the 21st century. *Science 305,* 994–997.

Migała, K., Urban, G., and *Tomczyński, K.*, 2016: Long-term air temperature variation in the Karkonosze mountains according to atmospheric circulation. *Theoretical and Applied Climatology125,* 337–351.
Mužíková, B., Vlček, V., and *Středa, T.*, 2011: Tendencies of climatic extremes occurrence in diff erent Moravian regions and landscape types. *ACTA Universitatis Agriculturae et Silviculturae Mendelianae Brunensis LIX, 5,* 169–178.
Niedźwiedź, T., 1981: Sytuacje synoptyczne i ich wpływ na zróżnicowanie przestrzenne wybranych elementów klimatu w dorzeczu górnej Wisły. *Rozprawy Habilitacyjne Uniwersytetu Jagiellońskiego* 58, Kraków. (in Polish)
Niedźwiedź, T., Łupikasza, E., and *Małarzewski, Ł.*, 2012 Wpływ cyrkulacji atmosfery na występowanie dni mroźnych w Hornsundzie (Spitsbergen). *Problemy Klimatologii Polarnej 22,* 17–26. (in Polish)
Pai D.S., Nair, S.A, and *Ramanathan, A.N.*, 2013: Long term climatology and trends of heat waves over India during the recent 50 years (1961–2010). *Mausam 64*, 4, 585–604.
Paldy, A. and *Bobvos, J.*, 2009: Impact of the Unusual Heatwave of 2007 on Mortality in Hungary. *Epidemiology 20, 6*, 126–127.
Papanastasious, D.K., Melas, D., and *Kambezidis, H.D.*, 2014: Heat waves characteristics and their relation to air quality in Athens. *Global Nest J. 16,* 919–928.
Peterson, T.C Heim, R.R., Hirsch, R., Kaiser, D.P., Brooks, H., Diffenbaugh, N.S., Dole, R.M., Giovannettone, J. P., Guirguis K.,. Karl, T.R., Katz, R.W., Kunkel, K., Lettenmaier, D., McCabe, G.J., Paciorek, C.J., Ryberg, K.R., Schubert, S., Silva, V.B.S., Stewart, B.C., Vecchia, A.V., Villarini, G., Vose, R.S., Walsh, J., Wehner, M., Wolock, D., Wolter, K., Woodhouse, C.A., and *Wuebbles, D.*, 2013: Monitoring and understanding changes in heat waves, cold waves, floods, and droughts in the United States: State of knowledge. *Bull. Amer. Met. Soc. 94,* 821–834.
Philandras, C., Nastos, P., and *Repapis, C.*, 2008: Air temperature variability and trends over Greece. *Global Nest J. 10*, 273–285.
Pongrácz, R., Bartholy, J., and *Bartha, E.B.*, 2013: Analysis of projected changes in the occurrence of heat waves in Hungary. *Adv. Geosci. 35*, 115–122.
Porębska, M., and *Zdune M.*, 2013: Analysis of extreme temperature events in Central Europe related to high pressure blocking situations in 2001–2011. *Met. Zeit. 22,* 533–540.
Poumadere, M., Mays, C., Le Mer, S., and *Blong, R.*, 2005: The 2003 Heat Waves in France: Dongerous Climate Change Here and Now. *Risk Analysis 25,* 1483–1494.
Revich, B.A., Shaposhnikov, D.A., Podol'naya, M.A., Khor'kova, T.L., and *Kvasha E.A.*, 2015: Heat Waves in Southern Cities of European Russia as a Risk Factor for Premature Mortality. *Studies on Russian Economic Development 26, 2,* 142–150.
Shaposhnikov, D., Revich, B., Bellander, T., Bedada, G.B., Bottai, M., Kharkova, T., and *et al.*, 2014: Mortality related to air pollution with the Moscow heat wave and wildfire of 2010. *Epidemiology 25,* 359–364.
Shevchenko, O., Lee, H., Snizhko, S., and *Mayer H.*, 2014: Long–term analysis of heat waves in Ukraine. *International J. Climatol. 34*, 1642–1650.
Spinoni, J., Lakatos, M., Szentimrey, T., Bihari, Z., Szalai, S., Vogt, J., and *Antofie T.*, 2015: Heat and cold waves trends in the Carpathian Region from 1961 to 2010. *Int. J. Climatol. 35,* 4197–4209.
Tomczyk, A.M., and *Bednorz, E.*, 2014: Heat and cold waves on the southern coast of the Baltic Sea. *Baltica 27,* 45–53.
Tomczyk, A.M., and *Bednorz, E.*, 2016: Heat waves in Central Europe and their circulation conditions. *Int. J. Climatol. 36,* 770–782.
Tomczyk, A.M., Piotrowski, P., and *Bednorz, E.*, 2016: Warm spells in Northern Europe in relation to atmospheric circulation. *Theor. Appl. Climatol.* DOI 10.1007/s00704-015-1727-0
Tošić, I., Zorn, M., Ortar, J., Unkašević, M., Gavrilov, M.B., and *Marković, S.B.*, 2016: Annual and seasonal variability of precipitation and temperatures in Slovenia from 1961 to 2011. *Atmos. Res. 168*, 220–233.
Unkašević, M., and *Tošić, I.*, 2009: An analysis of heat waves in Serbia, *Glob. Planetary Change 65*, 17–26.
Unkašević, M., and *Tošić, I.*, 2011: The maximum temperatures and heat waves in Serbia during the summer of 2007. *Climatic Change 108*, 207–223.

Unkašević, M., and *Tošić, I.*, 2015: Seasonal analysis of cold and heat waves in Serbia during the period 1949-2012. *Theor. Appl. Climatol. 120*, 29–40.

Ustrnul, Z., *Czekierda, D.*, and *Wypych A.*, 2010: Extreme values of air temperature in Poland according to different atmospheric circulation classifications. *Physics Chemistry Earth 35*, 429–436.

Ward, J.H., 1963: Hierarchical grouping to optimize an objective function. *J. Amer. Statistical Assoc. 58*, 236–244.

Wibig, J., 2007: Fale ciepła i chłodu w środkowej Polsce na przykładzie Łodzi. *Acta Universitatis Lodziensis, Folia Geographica Physica 8*, 27–61. (in Polish)

Wilks, D.S., 1995: Statistical methods in the atmospheric sciences: an introduction. International geophysics series, vol. 59. Academic, New York, 464 pp.

Yarnal, B., 1993: Synoptic Climatology in Environmental Analysis. Belhaven Press, London.

Zacharias, S., *Koppe, Ch.*, and *Mücke, H–G.*, 2015: Climate change effects on heat waves and future heat wave–associated IHD mortality in Germany. *Climate 3*, 100–117.

IDŐJÁRÁS
Quarterly Journal of the Hungarian Meteorological Service
Vol. 121, No. 1, January – March, 2017, pp. 415–430

Energy performance of the cooled amorphous silicon photovoltaic (PV) technology

Henrik Zsiborács[1*], **Béla Pályi**[1], **Hegedűsné Nóra Baranyai**[1], **Mihály Veszelka**[1], **István Farkas**[2], and **Gábor Pintér**[1]

[1] *University of Pannonia, Georgikon Faculty, Deák Ferenc Street 16, 8360 Keszthely, Hungary*

[2] *Szent Istvan University, Páter Károly Street 1, 2103 Gödöllő, Hungary*

**Corresponding author E-mail: ifj.zsiboracs.henrik@gmail.com*

(Manuscript received in final form February 1, 2016)

Abstract—In this paper, the effect of two types of water based cooling methods of amorphous silicon (a-Si) modules and a panel was studied in the summer period. One new (unused) and some 11-year-old a-Si modules and a panel with two different cooling techniques (sprinkling and flowing water cooling) were examined. Our reference for the evaluation was an unused a-Si module without any cooling. The results were analyzed from both statistical and technical aspects.
Key-words: solar energy, temperature dependence, water cooling, Z-test

1. *Introduction*

Renewable energies have an increasing role in the process of energy production (*Szabó et al.*, 2015, *Horváth et al.*, 2015). Besides numerous other benefits, energy production based on solar performances can significantly contribute to sustainable energy management. By a one-time investment in solar PV technology it is possible to produce CO_2-free, green energy for free without producing any waste for several decades (*Hosenuzzaman et al.*, 2015, *Aman et al.*, 2015).

The quantity of energy which can be produced by a solar PV module depends primarily on its type and composition and the joint effects of the location and the current natural factors. Modules are tested and certified under laboratory conditions under which their nominal performances are established (STC-Standard Test Conditions, AM = 1.5 air pollution, 1000 W/m^2 solar radiation, and 25 °C module temperature). However, these conditions are not given during operation, so PV modules hardly ever produce their nominal performance (TÜV SÜD America Inc, 2015).

Due to their reliability, the market share of crystalline silicon PV modules is 85–90%, and their efficiency can reach 25.6% ± 0.5% in the case of monocrystalline modules and 20.8% ± 0.6% in the case of polycrystalline ones (*Green et al.*, 2015; IEA, 2014; *Cosme et al.*, 2015; Panasonic Corporation, 2014; *Verlinden et al.*, 2014).

The amorphous silicon solar module is a type of thin film PV solar module with an efficiency of up to 10.2% ± 0.3%. The market share of all thin film PV modules is 10–15%, but that of amorphous silicon solar modules within that is difficult to determine (*Green et al.*, 2015; IEA, 2014; *Matsui et al.*, 2013).

The temperature coefficient of thin film solar modules is better than that of crystalline ones. Thus, their use is favorable primarily in very hot, desert environments and in power stations (*Fábián,* 2015).

Several factors may influence the efficiency of the utilization of solar energy coming to the Earth. In the case of solar PV technologies, the fluctuation of module temperatures due to the change of air temperature and global radiation is one of the important factors (*Skoplaki* and *Palyvos,* 2009; *Hai Alami,* 2014). Under Hungarian climatic conditions, the temperature of solar PV modules can reach 60–70 °C on warm days, which results in a decrease of power generation in the module. For this problem, various cooling technologies may offer solutions.

According to *Bahaidarah et al.,* (2013), the performance of PV modules strongly depends on the actual module temperature. Generally it can be said that most of the incoming energy turns into thermal energy in the PV modules and is not utilized (*Chandrasekar et at.,* 2013). The arising quantity of heat gets lost, on the one hand, and causes additional losses in the short and long term, on the other hand, since the increase in the temperature of the modules reduces the efficiency of the system, and, thus, it reduces the quantity of electric energy produced, while, in the long run, they also accelerate the ageing of the PV modules (*Ndiaye et al.,* 2014; *Kahoul et al.*, 2014). The decrease in efficiency may vary depending on the type of the PV module. In the case of crystalline silicon PV modules, the efficiency characteristically decreases by 0.5%, while in the case of a-Si modules by 0.3% as a result of a 1 °C temperature rise (*Radziemska* and *Klugmann*, 2002).

Various active and passive cooling procedures are used in solar PV technology for controlling the operating temperatures of the modules (*Chandrasekar et al.*, 2015; *Elnozahy et al.*, 2015; *Du et al.,* 2012). Four groups of the cooling techniques can be distinguished (*Chandrasekar et al.,* 2015; *Ji et al.*, 2008):

- air-based,
- water-based,
- refrigerant-based,
- heat pipe-based.

In the present study, the water-based (water spraying and water flow over the front) procedures are discussed. In the course of spraying with water, the temperature of cooled PV modules decreases significantly compared to modules without cooling (under identical circumstances) due to the phenomenon of evaporation (*Abdolzadeh* and *Ameri,* 2009).

2. Measurement site

In the present experiment, cooled and uncooled Kaneka amorphous silicon PV modules were examined under real meteorological circumstances. The measurements took place in the same location on 8 different days in August 2015 with 4 different settings:

- A: ground-mounted, unused PV module without cooling as control,
- B: ground-mounted, unused PV module with cooling (sprayed),
- C: ground-mounted, 11-year-old PV modules with cooling by flowing water over the module front,
- D: roof-mounted, 11-year-old PV panel (with 6 modules) with cooling by flowing water over the module front connected to the grid with an inverter (*Fig. 1*).

Long-term global radiation data were not available for our research. Thus, the economic data related to cooling the PV modules were calculated on the basis of the above-mentioned days.

The unused amorphous silicon PV modules were facing south with a tilt angle of 35°. For the measurements, two PicoLog data acquisition systems were used, one with 12 and one with 16 input channels. These instruments allowed second-based, continuous data recording by a personal computer. The advantage of the data acquisition devices used for this research is that several units can be connected to one computer and its software is flexible. Consequently, the incoming signs are simultaneously visible (*Zsiborács et al.*, 2015).

In the case of the control module – besides the voltage and the current –, the surface temperature was measured at one point (in the middle of the top third of the module).

Table 1. The parameters of the solar modules examined

Specifications	Amorphous silicon PVmodule (unused)	Amorphous silicon PVmodule (11-year-old)
Country of origin	Japan	Japan
Manufacturer/Distributor	Kaneka	Kaneka
Model	G-EA050	K54
Nominal output (Pm) (W)	50	54
Power output tolerance (%)	±10%	±10%
Maximum power voltage (Vmp) (V)	67	62
Maximum power current (Imp) (A)	0.75	0.87
Open circuit voltage (Voc) (V)	91.8	85
Short circuit current (Isc) (A)	1.19	1.14
Module dimensions (mm)	960×990×40	920×920×40

Fig. 1. The measurement site in Keszthely (*Zsiborács et al.*, 2015).

In the case of the sprayed amorphous PV module, the temperature was measured at two places. One sensor was placed in the middle of the top third of the a-Si module, and the other one was on the left side of the bottom third of the a-Si module. This article uses the data from the first sensor. The temperature of the sprayed water, the voltage, and the current were measured. The automation of the cooling system was controlled by a thermostat, which was connected to the surface of the middle of the top third of the PV module.

In order to save water, the spray heads sprinkled the unused amorphous silicon modules intermittently, using exactly the amount of water needed to replace the water evaporated (*Zsiborács et al.*, 2015). However, the location of the 11-year-old a-Si modules did not allow the application of the spraying method. That is why the technique of flowing water over the module front was used, creating a homogeneous water film.

The water got to the spray head through an ion-exchange resin water-softening appliance The water needed for the cooling of the a-Si modules was supplied by a domestic waterworks from a garden well with filtered groundwater (*Fig. 2*) (*Zsiborács et al.*, 2015).

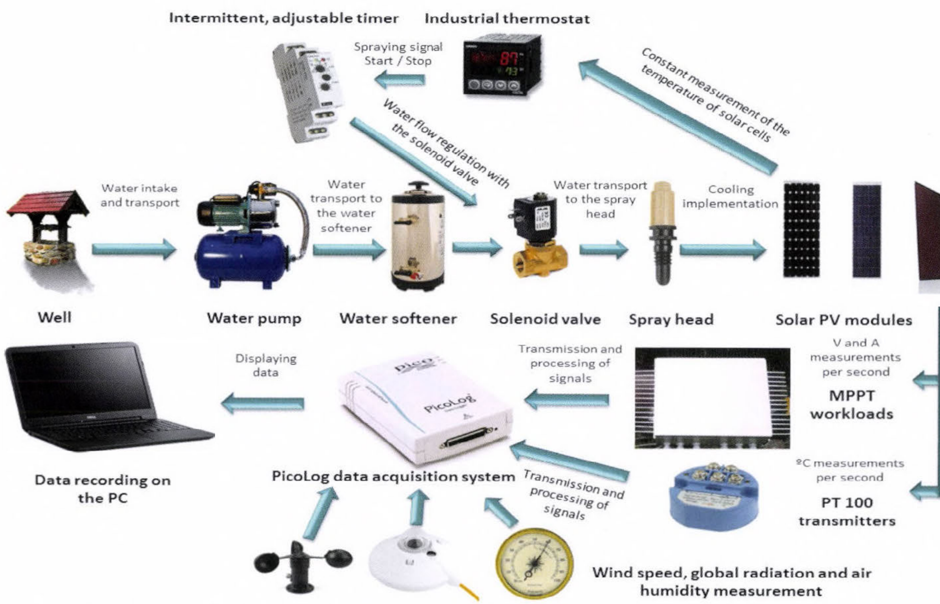

Fig. 2. Schematic diagram of PV modules measuring point (*Zsiborács et al.*, 2015).

For measuring the temperatures, Pt 100 sensors were used with the help of the PicoLog devices (*Zsiborács et al.*, 2015). The calibration of the whole temperature measurement system was done using an LM 35 digital thermometer with a linear voltage change (+ 10.0 mV/°C, 0.1 V = 1 °C, 1 V = 100 °C) and an accuracy of ± 1/4 °C at room temperature and that of ± 3/4 °C between –55 and + 150 °C.

A Voltcraft VC607 professional multimeter, which was checked by an LT1021 device (10,000 V +–5 mV), was used for the calibration of the voltage and the current.

The humidity of the air was measured by a HYTE-ANA-1735 device. The global radiation was measured by a pyranometer (an Eppley Black and White Model 4–48, certified by the Hungarian Meteorological Service). The wind speed was measured by a JL-FS2, 4–20 mA, 3-spoon aluminium device. The electric signs from the measurements were transmitted to the PicoLog device (*Zsiborács et al.*, 2015). The pyranometer was placed next to the PV modules at a 35° angle (same as the PV modules). The air humidity and wind speed measurements took place at the side of the PV modules at a height of 80 cm (*Fig. 3*).

A True Maximum Point Seeking (TMPS) device, which maintained the maximum power point (MPP) was used for the measurements. The schematic diagram of the measurement point is shown in *Figs. 2, 3,* and *4*.

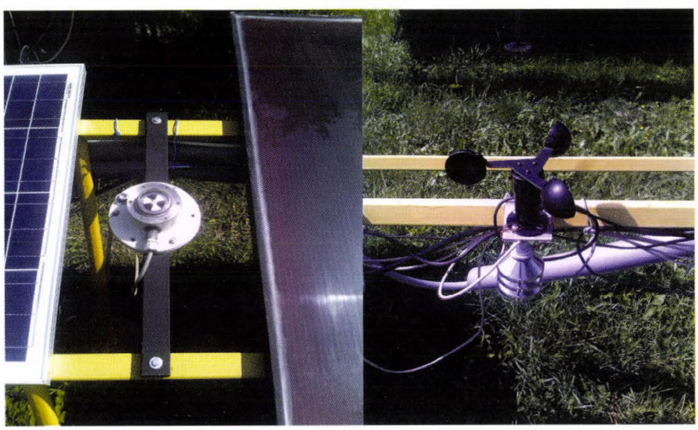

Fig. 3. The pyranometer, the wind speed sensor anemometer, and the humidity module.

Fig. 4. The unused amorphous silicon solar module measurement site in Keszthely.

A solar field consisting of 84 thin-film modules were used for the measurements of the 11-year-old a-Si modules, which had a nominal power of 4.5 kW. This system was set up at the same angle and location as the system above (*Fig. 5*). A Fronius Ig Tl inverter was used for the solar PV system.

Protection against TCO (transparent conductive oxide) corrosion, which can be caused by the chemical reaction of the water and the a-Si module if water gets under the glass, is important. If this problem is not prevented, the PV modules might go wrong in a couple of years (SMA Solar Technology AG, 2010). Grounding was impossible through the Tl inverter. However, the problem was solved by using a three-position switch. Silicone sealant was also applied to protect the PV modules between the glass and the frame.

The data from the 11-year-old modules were transmitted either to the PicoLog device or to the Fronius inverter. The control PV module was again an unused a-Si module.

The water needed for the PV module came from a domestic waterworks from a garden well with filtered underground water, after water softening.

For measuring the temperature of the 11-year-old amorphous silicon solar modules, a Lux Tools laser thermometer, which had been calibrated by a Pt100 sensor, was used. It was necessary to use the thermometer, since Pt100 sensors could not be used at the a-Si modules due to the limited number of channels of the measurement data collecting device.

The oscillation True Maximum Point Seeking device was suitable for receiving the data, because the voltage and current values were not far from each other. The a-Si modules examined are shown in *Fig. 5*, the first two columns on the left.

Fig. 5. The 11-year-old amorphous silicon solar panels

First the reaction of the six ground-mounted modules to cooling with flowing water over the module front was investigated one by one compared to that of the unused ones between 11.00 am – 12.15 pm on August 16, 2015. Each solar PV module examined was separated from the PV system and the parameters of the cooling were recorded one by one.

In the second phase the PV panel (with six a-Si modules) was studied (*Fig. 6*) in a way that only the panel was connected to the inverter. The other modules were disconnected at this time. That way the power surplus resulting from the cooling process could be measured. Here the TMPS solution, which was used in the first phase, could not be used. Thus, the data were supplied by the inverter.

Fig. 6. Amorphous silicon solar panel on the roof.

It is possible that the power changes in the control a-Si module due to natural effects during the period of the cooling process of the test modules. These changes have to be deducted from the power of the cooled amorphous silicon solar module.

The data were sampled hourly while spraying during sunny periods. The duration of cooling varied between 10 and 20 minutes depending on the measurement settings.

The surplus power was measured in the periods examined:

- before switching on spraying,
- at the end of the cooling period in a given hour.

Ten-minute cooling periods were sufficient for investigating the method of flowing water over the module.

The surplus power was measured in the periods examined:

- before switching on spraying,
- at the end of the cooling period in a given hour.

During the research, two-sample Z-tests were used to establish if there were any significant percentage differences in the performances of the cooled and the control PV modules.

3. *Measured data and statistical analysis*

In this chapter, the following issues are dealt with:

- regulation of the spraying water,
- the extra power produced by the unused and the 11-year-old amorphous silicon solar modules and panel,
- the actual daily energy production,
- hard water treatment.

3.1. The regulation of the spraying water at the unused a-Si module

The daily water consumption under operating conditions was examined on August 8, 2015.

In order to reduce water consumption, the spray heads were operated intermittently, thereby the system used minimal energy and only the amount of water necessary for evaporation. This way the efficiency of the spraying method could be determined for the amorphous silicon solar module.

By using the digital thermostat, a temperature regulating method that – depending on the temperature of the control module – can reduce the temperature of the surface of the cooled module by the average value of temperature reduction achievable in the given hour of the day was tested manually. Thus, the daily cooling period was maximally exploited.

In the case of the 50-W unused amorphous silicon solar module, 3 nozzles placed at a distance of 32 centimeters from each other were used. Depending on the weather, this system created a nearly homogenous sprayed surface (100 cm wide, 100 to 120 cm long) at 2 psi. From 9:00 am to 05:00 pm the water consumption was 4.2 l.

3.2. *Detecting extra performance produced by the sprayed unused amorphous silicon PV module*

The unused, test, and control PV modules were the same type and capacity according to the manufacturer's specifications. The relative changes in their performances were compared on August 7, 2015 (01:00 pm – 05:00 pm). The data were recorded every second. The two-sample Z-test established that the relative changes in the performances of the two unused modules were the same (P= 0.634).

Depending on the weather conditions (sunny weather), the measurements took place every hour between 09:00 am and 05:00 pm. This experiment involved 21 measurements. The average measurement data are shown in *Table 2*. By this test, the extra performance and temperature decrease of the PV module achievable by the sprinkling method were determined. It can be seen that the daily average extra performance increase of the unused amorphous silicon solar module was + 3.6% compared to the control a-Si module. Our tests support the results of *Skoplaki* and *Palyvos* of 2009, since in the case of the cooled a-Si module, an average performance increase of 0.3% for every 1-°C decrease in module temperature was observed.

Table 2. Data of the unused PV modules during spray cooling in August

Time (h)	**Average global radiation (W/m²)**	**Average wind speed (m/s)**	**Average air temperature (°C)**	**Average air humidity (%)**	**Sprayed a-Si module average temperatures decrease (°C)**	**Observed average extra power during spray cooling (%)**
9–10	455.45	0.2	28.0	38.0	7.3	2.6
10–11	679.3	0.2	27.2	37.0	12.7	4.0
11–12	771.5	0.1	30.5	37.0	13.5	3.4
12–13	904.8	0.3	29.0	37.0	14.4	4.1
13–14	925.7	0.4	32.9	35.8	17.4	4.8
14–15	928.5	0.2	32.6	36.4	15.1	3.3
15–16	816.3	0.0	29.4	37.8	15.1	3.6
16–17	641.8	0.5	28.3	37.5	12.4	3.0
Average						**3.6**
CV (%)						17.9

3.3. *Detecting extra performance produced by the 11-year-old, ground-mounted a-Si modules cooled by water flow over the front*

The testing of the 11-year-old a-Si modules took place on August 26, 2015 from 11:00 am to 12:15 pm.

In the first phase of the test, the relative change in the performance of the ground-mounted PV modules was examined over time without cooling compared to the unused module. Before the cooling experiment, all six a-Si modules were examined for 30 seconds each, one by one. The two-sample Z-test established that the relative change in the performance of the modules was the same ($P = 0.759$).

The cooling was done by water flow over the front. The averaged measurement data are shown in *Table 3*. In this test, the achievable extra performance and temperature decrease of the PV modules were determined. It can be seen that compared to the control a-Si module, the average performance increase of the 6 modules was 3.8% during the measurements. For the unused a-Si module this value was + 3.6%, meaning that the reaction to cooling was almost the same after 11 years of use.

Table 3. Data of the 11-year-old a-Si modules cooled by water flow over the front on August 26, 2015 (11:00-12:15)

Module	**Average global radiation (W/m^2)**	**Average wind speed (m/s)**	**Average air temperature (°C)**	**Average air humidity (%)**	**Sprayed a-Si module average temperatures decrease (°C)**	**Observed average extra power during cooling (%)**
1.	748.2	0.6	24.7	35.8	11.1	4.3
2.	767.7	0.5	25.5	36.0	14.1	3.4
3.	787.7	0.5	25.8	35.4	15.0	3.4
4.	816.3	0.3	26.6	35.0	12.5	4.0
5.	830.5	0.5	26.5	34.7	16.8	3.5
6.	844.1	0.5	26.2	35.5	14.3	4.3
Average						**3.8**
CV (%)						10.1

3.4. Detecting extra performance produced by the 11-year-old a-Si panel connected to a grid-connected inverter

The testing of the amorphous silicon panel took place on August 26, 2015 from 11:00 am to 2:00 pm. During the experiment only 6 a-Si modules were connected to the inverter. Thus, the extra power resulting from the water cooling effect could be detected more easily. During the experiment three tests were carried out, but the last measurement was not reliable due to changes in global radiation.

The Fronius inverter constantly checks the MPP and shows the changes in performance every 2 seconds. To establish the amount of extra performance during the first measurement, the average performance of the 1 minute before the start of cooling and the average performance in the last 1 minute of the cooling were used. The first test lasted for 8 minutes, during which the temperature of the a-Si module decreased by 18.3°C and the performance increased by 5.2% (*Table 4*).

During the second measurement, the average performance of the last 30 seconds before the start of cooling and the average performance in the last 1 minute of the testing process were used to establish the quantity of extra performance. The duration of the second measurement was 6 minutes, since the global radiation changed after that. During the test, the temperature of the amorphous silicon solar PV module decreased by 15.3 °C and the performance increased 3.8% (*Table 4*).

The grid-connected PV system tests showed that increases in power were detectable not only in PV modules but also in the inverter-connected 11-year-old amorphous silicon panel.

Table 4. Data of the 11-year-old a-Si panel cooled by water flow over the front on August 26, 2015 (13:00 – 14:00)

a-Si panel number of measurements	Average global radiation (W/m^2)	Average wind speed (m/s)	Average air temperature (°C)	Average air humidity (%)	Sprayed a-Si module average temperatures decrease (°C)	Observed average extra power during cooling (%)
1	887.5	0.2	27.5	36.3	18.3	5.2
2	880.4	0.2	26.9	36.9	15.3	3.8

3.5. The actually achievable daily energy production

The average extra performance data detected during the investigation of the unused a-Si module were projected onto an a-Si system (4.6 kW) located in Balatonudvari, since the measurement site in Keszthely undergoes two shady periods in the early morning and in the late afternoon, which could have distorted the results. On the two ideal summer days the examined PV system in Balatonudvari reached a peak performance of 3.4 kW and 3.3 kW between 1 pm. and 2 pm. That means that the actual performance was between 71.7% and 73.9% of the maximum performance theoretically achievable. Consequently, the inverter capacity was not completely utilized, which could provide an opportunity for increasing the performance by cooling (SZALONTAI Rendszerintegrátor Kft., 2015).

As seen above, the average performance increase of the unused cooled a-Si module was + 3.6% between 9 am and 5 pm. compared to the control amorphous silicon PV module, which means 3.6% more energy output during that period.

In the experiment, a domestic waterworks consuming 750 Wh energy (1800 l/hour, 30 l/min) was used. The pump did not have to operate all the time, since as a pressure tank, it also belonged to the system. For one a-Si module, 4.2 l of water and 1.75 Wh pump energy were used (from 9:00 am – 5:00 pm) during the cooling period.

For determining the daily energy actually produced the above-mentioned 4.6-kW a-Si PV system in Balatonudvari was used. The plant, situated at a distance of 44.6 km from Keszthely, is equipped with an online monitoring station with production data. In order to calculate the average daily production three ideal days were selected in August (August 01, 10, 28, 2015).

In *Table 5*, the energy production of the PV system determined for the given days on the basis of the available hourly actual energy production data series is shown. It was established that 6.5% of the average daily energy produced could not be used for cooling due to the characteristics of the cooling method, since no reaction to cooling was detectable before 09:00 am and after 05:00 pm. According to our measurements, a minimum global radiation of 450 W/m^2 at an air temperature of 20 °C and 390 W/m^2 at an air temperature of 30 °C is necessary to operate the cooling system. For this reason, the actual significance of water cooling for energy generation decreased from 3.6% to 3.4% on a daily basis. If the 1.75 Wh energy necessary for the pump is deducted from the energy produced daily, the actual energy gain decreases to 2.7%.

Table 5. Daily production data of the 4.6-kW PV field in Balatonudvari

Time (day)	Actual daily energy production (7-20) (kWh)	Energy produced during the cooling period (9-17) (kWh)	Released 3,6% extra energy during cooling period (9-17) (kWh)	Total energy production with cooling (kWh)	Actual extra energy during cooling period (kWh)	Daily amount of energy that cannot be used for cooling (%)	Actual daily extra energy (%)	Average daily extra energy (%)
Aug 1, 2015	25.0	23.3	24.2	25.9	0.8	7.3	3.4	
Aug 10, 2015	23.1	21.5	22.3	23.9	0.8	7.3	3.4	3.4
Aug 28, 2015	23.5	22.4	23.2	24.3	0.8	4.9	3.4	

3.6. Hard water treatment

The protection against limescale is necessary for the applied cooling method, since limescale is deposited on the glass surface of the PV modules. Ion-exchange polymers do not solve the problem completely. Therefore, it is advisable to apply a reverse osmosis water purifier.

4. Summary

Two different techniques (sprinkling and flowing water cooling) for cooling a-Si modules and a panel were examined in the summer period to establish their average extra performance increase thanks to the cooling process. The performance increase in the case of the cooled unused amorphous silicon solar module was +3.6% compared to the control a-Si module. Our experiments confirmed the results of *Skoplaki* and *Palyvos* of 2009, since in the case of the cooled a-Si module, an average performance increase of 0.3% for every 1-°C decrease in module temperature was observed.

It was found that compared to the control a-Si module, the average performance of the six cooled, 11-year-old, ground-mounted a-Si modules was 3.8% higher during the measurements. For the unused a-Si module this value was + 3.6%, meaning that the reaction to cooling was almost the same after 11 years of use.

The grid-connected PV system tests showed that increases in power were detectable not only in PV modules but also in the inverter-connected 11-year-old amorphous silicon panel.

Based on data from the PV system in Balatonudvari it was established, that 6.5% of the average daily energy produced could not be used for cooling due to the characteristics of the cooling method, since no reaction to cooling was detectable before 09:00 am and after 05:00 pm. According to our measurements, a minimum global radiation of 450 W/m^2 at an air temperature of 20 °C and 390 W/m^2 at an air temperature of 30 °C is necessary to operate the cooling system. For this reason, the actual significance of water cooling for energy generation decreased from 3.6% to 3.4% on a daily basis. If the 1.75 Wh energy necessary for the pump is deducted from the energy produced daily, the actual energy gain decreases to 2.7%.

References

Abdolzadeh, M. and *Ameri, M.*, 2009: Improving the effectiveness of a photovoltaic water pumping system by spraying water over the front of photovoltaic cells. *Renew. Energ. 34,* 91–96.

Aman, M.M., Solangi, K.H., Hossain, M.S., Badarudin, A., Jasmon G.B., and *Mokhlis H.*, 2015: A review of Safety. Health and Environmental (SHE) issues of solar energy system. *Renew. Sustain. Energy Rev. 41*, 1190–1204.

Bahaidarah, H., Subhan, A., Gandhidasan, P., and *Rehman S.*, 2013: Performance evaluation of a PV (photovoltaic) module by back surface water cooling for hot climatic conditions. *Energy 59*, 445–453.

Chandrasekar, M., Rajkumar, S., and *Valavan, D.*, 2015: A review on the thermal regulation techniques for non integrated flat PV modules mounted on building top. *Energy Buildings 86*, 692–7.

Chandrasekar, M., Suresh, S., Senthilkumar, T., Ganesh Karthikeyan, M., 2013: Passive cooling of standalone flat PV module with cotton wick structures. *Energ. Convers. Manage. 71*, 43–50.

Cosme, I., Cariou, R., Chen, W., Foldyna, M., Boukhicha, R., Cabarrocas, P.R.I., Lee, K.D., Trornpoukis, C., and *Depauw, V.*, 2015: Lifetime assessment in crystalline silicon: From nanopatterned wafer to ultra-thin crystalline films for solar cells. *Solar Energ. Materials Solar Cells 135*, 93–98.

Du, B., Hu, E., and *Kolhe, M.*, 2012: Performance analysis of water cooled concentrated photovoltaic (Cphotovoltaic) system. *Renew. Sustain. Energy Rev. 16*, 6732–6736.

Elnozahy, A., Rahman, A.K.A., Ali, A.H.H., Abdel-Salam, M., and *Ookawara, S.*, 2015: Performance of a PV module integrated with standalone building in hot arid areas as enhanced by surface cooling and cleaning. *Energy Buildings 88*, 100–109.

Fábián, T., 2015: A Rádiótechnika Évkönyve 2015. *Rádióvilág Kft.* HU-ISSN 0557-6229, 101–107.

Green, M.A., Emery, K., Hishikawa, Y, Warta, W., and *Dunlop, E.D.*, 2015: Solar cell efficiency Tables (Version 45). *Progr. Photovoltaics Res Appl. 23*, 1–9.

Hai Alami, A., 2014: Effects of evaporative cooling on efficiency of photovoltaic modules. *Energy Conv. Manage. 77*, 668–679.

Horváth, M., Kassai-Szoó, D., and *Csoknyai, T.*, 2016: Solar energy potential of roofs on urban level based on building typology. *Energy Buildings 111*, 278–289.

Hosenuzzaman, M., Rahim, N.A., Selvaraj, J., Hasanuzzaman, M., Malek, A.B.M.A., and *Nahar, A.*, 2015: Global prospects. progress policies and environmental impact of solar photovoltaic power generation. . *Renew. Sustain. Energy Rev. 41*, 284–97

Ji, J., Pei, G., Chow, T.T., Liu, K., He, H., Lu, J., and *Han, C.*, 2008: Experimental study of photovoltaic solar assisted heat pump system. *Solar Energy 82*, 43–52.

Kahoul, N., Houabes, M., and *Sadok, M.*, 2014: Assessing the early degradation of photovoltaic modules performance in the Saharan region. *Energy Conv. Manage. 82*, 320–326.

Matsui, T., Sai, H., Suezaki, T., Matsumoto, M., Saito, K., Yoshida, I., and *Kondo M.*, 2013: Development of highly Stable and efficient amorphous silicon based solar cells. Proc. 28th European Photovoltaic Solar Energy Conference. 2213–2217.

Ndiaye, A., Kebe, C.M.F., Charki, A., Ndiaye, P.A., Sambou, V., and *Kobi A.*, 2014: Degradation evaluation of crystalline-silicon photovoltaic modules after a few operation years in a tropical environment. *Solar Energy 103,* 70–77.

Panasonic Corporation, 2014: Panasonic HIT® Solar Cell Achieves World's Highest Energy Conversion Efficiency of 25.6% at Research Level Available at: news.panasonic.com/ press/news/official.,data/data.dir/2014/04/en140410-4/en140410-4.html.Downloaded: 21.11.2015

Radziemska, E. and *Klugmann, E.*, 2002: Thermally affected parameters of the current–voltage characteristics of silicon photocell. *Energy Conv. Manage. 43*, 1889–1900.

Skoplaki, E. and *Palyvos, J.A.*, 2009: On the temperature dependence of photovoltaic module electrical performance: A review of efficiency/power correlations. *Solar Energy 83*, 614–624.

Skoplaki, E. and *Palyvos, J.A.*, 2009: Operating temperature of photovoltaic modules: A survey of pertinent correlations. *Renew Energy 34*, 23–29.

SMA Solar Technology AG., 2010. Module Technology - SMA inverters provide the optimum solution for every module. Duennschicht-TI-UEN114630|Version 3.0. 1–7. Available at: files.sma.de/dl/7418/Duennschicht-TI-UEN114630.pdf. Downloaded: 21.11.2015

Szabó, Sz., Enyedi, P., Horváth, M., Kovács, Z., Burai, P., Csoknyai, T., and *Szabó, G.*, 2015: Automated registration of potential locations for solar energy production with Light Detection And Ranging (LiDAR) and small format photogrammetry. *J. Cleaner Product 112,* 3820–3829.

SZALONTAI Rendszerintegrátor Kft. Balatonudvari PV system. 2015: Available at: www.sunnyportal.,com/Templates/PublicPageOverview.aspx?page=294cb041-aece-4668-93e3-fa9a4c89fbcc&plant=152c508b-dca1-48b7-9258-3f32e8574bfa&splang=en-US.Downloaded: 21.11.2015

TÜV SÜD America Inc., 2015. Basic Understanding of IEC Standard Testing For Photovoltaic Panels. Regan Arndt and Dr. Ing Robert Puto TÜV SÜD Product Service. 1–15. Available at: www.tuvamerica.com/services/photovoltaics/articlebasicunderstandingphotovoltaic.pdf. Downloaded: 21.11.2015

Verlinden, P., Deng, W., Zhang, X., Yang, Y., Xu, J., Shu, Y., Quan, P., Sheng, J., Zhang, S., and *Bao, J.*, 2014: Strategy, development and mass production of high-efficiency crystalline Si PV modules, in: 6th World Conference on Photovoltaic Energy Conversion, Kioto, Japan, 2014.

Zsiborács, H., Pályi, B., and *Pintér, G.*, 2015: Permetezett monokristályos napelemek vizsgálata. LVII. Georgikon Napok. 505–514.

IDŐJÁRÁS

VOLUME 120 * 2016

BUDAPEST, HUNGARY

AUTHOR INDEX

TABLE OF CONTENTS

I. Papers

II. News

SUBJECT INDEX

INSTRUCTIONS TO AUTHORS OF *IDŐJÁRÁS*

The purpose of the journal is to publish papers in any field of meteorology and atmosphere related scientific areas. These may be

- research papers on new results of scientific investigations,
- critical review articles summarizing the current state of art of a certain topic,
- short contributions dealing with a particular question.

Some issues contain "News" and "Book review", therefore, such contributions are also welcome. The papers must be in American English and should be checked by a native speaker if necessary.

Authors are requested to send their manuscripts to

Editor-in Chief of IDŐJÁRÁS
P.O. Box 38, H-1525 Budapest, Hungary
E-mail: journal.idojaras@met.hu

including all illustrations. MS Word format is preferred in electronic submission. Papers will then be reviewed normally by two independent referees, who remain unidentified for the author(s). The Editor-in-Chief will inform the author(s) whether or not the paper is acceptable for publication, and what modifications, if any, are necessary.

Please, follow the order given below when typing manuscripts.

Title page: should consist of the title, the name(s) of the author(s), their affiliation(s) including full postal and e-mail address(es). In case of more than one author, the corresponding author must be identified.

Abstract: should contain the purpose, the applied data and methods as well as the basic conclusion(s) of the paper.

Key-words: must be included (from 5 to 10) to help to classify the topic.

Text: has to be typed in single spacing on an A4 size paper using 14 pt Times New Roman font if possible. Use of S.I. units are expected, and the use of negative exponent is preferred to fractional sign. Mathematical formulae are expected to be as simple as possible and numbered in parentheses at the right margin.

All publications cited in the text should be presented in the *list of references*, arranged in alphabetical order. For an article: name(s) of author(s) in Italics, year, title of article, name of journal, volume, number (the latter two in Italics) and pages. E.g., *Nathan, K.K.,* 1986: A note on the relationship between photosynthetically active radiation and cloud amount. *Időjárás 90,* 10-13. For a book: name(s) of author(s), year, title of the book (all in Italics except the year), publisher and place of publication. E.g., *Junge, C.E.,* 1963: *Air Chemistry and Radioactivity.* Academic Press, New York and London. Reference in the text should contain the name(s) of the author(s) in Italics and year of publication. E.g., in the case of one author: *Miller* (1989); in the case of two authors: *Gamov* and *Cleveland* (1973); and if there are more than two authors: *Smith et al.* (1990). If the name of the author cannot be fitted into the text: (*Miller,* 1989); etc. When referring papers published in the same year by the same author, letters a, b, c, etc. should follow the year of publication.

Tables should be marked by Arabic numbers and printed in separate sheets with their numbers and legends given below them. Avoid too lengthy or complicated tables, or tables duplicating results given in other form in the manuscript (e.g., graphs).

Figures should also be marked with Arabic numbers and printed in black and white or color (under special arrangement) in separate sheets with their numbers and captions given below them. JPG, TIF, GIF, BMP or PNG formats should be used for electronic artwork submission.

More information for authors is available: journal.idojaras@met.hu

Published by the Hungarian Meteorological Service

Budapest, Hungary

INDEX 26 361

HU ISSN 0324-6329